CONFERENCE

ON

CLOUD PHYSICS

AUGUST 24-27, 1970
FT. COLLINS, COLORADO

The manuscripts reproduced in this collection of preprints are unrefereed papers presented at the Conference on Cloud Physics; their appearance in this collection does not constitute formal publication.

CLOUDS

Down the blue night the unending columns press
In noiseless tumult, break and wave and flow,
Now tread the far South, or lift rounds of snow
Up to the white moon's hidden loveliness.
Some pause in their grave wandering comradeless,
And turn with profound gesture vague and slow,
As who would pray good for the world, but know
Their benediction empty as they bless.

They say that the Dead die not, but remain
Near to the rich heirs of their grief and mirth.
I think they ride the calm mid-heaven, as these,
In wise magestic melancholy train,
And watch the moon, and the still-raging seas,
And men, coming and going on the earth.

Rupert Brooke
THE PACIFIC, Oct. 1913

Clouds, the eerie mists, the gentle rains, the dynamic bubbles, the lightning glow, the violence and devastation, the abating wind, the fading thunderoll and the sun's glowing rays pouring through the broken canopy -- we see and know them all. Some we know well; others we know little.

We welcome you to this Cloud Physics Conference, a forum for discussions on the most recent contributions to this important part of the science of our environment.

The response to the call for papers for this conference has been almost overwhelming. Many new and exciting fields of interest are developing. We see a tightening of the scientific relationships between Cloud Physics and the physics and mathematics of other dimensions of the environment. Both the Cloud Physics Committee and the Program Committee for the conference trust that you find the program a stimulating one.

Colorado State University was chosen by the Cloud Physics Committee of the American Meteorological Society for this conference, for two very important reasons -- firstly in support of C.S.U.'s Centenary Year celebrations, and secondly in recognition of the many excellent scientific contributions which this University's Department of Atmospheric Sciences has made to the field of Cloud Physics.

On behalf of the Committees, I wish to express sincere appreciation of the untiring efforts of Dr. Bernice Ackerman under whose chairmanship this conference originated. To Professor Lewis Grant and the Fort Collins Local Arrangements Committee, we give our heartiest thanks as we do also to Dr. Kenneth Spengler and Miss Evelyn Mazur of the American Meteorological Society.

Joseph A. Warburton

Joseph A. Warburton, Chairman
Program Committee

Conference Program Committee:

Lewis O. Grant
Harold D. Orville
John Hallett
Paul B. MacCready
Joseph A. Warburton

Cloud Physics Committee:

Bernice Ackerman
Lewis O. Grant
John Hallett
Peter V. Hobbs
Charles A. Knight
Byron B. Phillips
Richard G. Semonin

CONTENTS

*To be presented by title only.

*To be presented by title only.

*To be presented by title only.

*To be presented by title only.

*To be presented by title only.

*To be presented by title only.

AN EVALUATION OF THE RAPID EXPANSION TECHNIQUE FOR MEASURING ICE NUCLEUS CONCENTRATIONS

Roger F. Reinking
Colorado State University
Fort Collins, Colorado

ANALYSIS

All current techniques for routine field measurements of nucleus concentrations have many limitations as well as advantages. No existing instrument meets the requirements necessary to be an absolute reference unit. Precision (consistency) and accuracy (representation of nature) of the various devices must be known to interpret the measurements correctly. In this study previous and new observations have been combined to establish the advantages and limitations of the rapid expansion instrument (1) (2) in relation to the collection and activation of the ice nuclei, and the growth, detection and counting of the nucleated ice crystals. Some of the principal results of this study are outlined here in terms of eight criteria for ice nucleus counter evaluation:

1. Mechanical reliability and convenience of operation are strong points of the instrument. Simplicity is emphasized in in construction and operating procedures.

2. Time continuity of measurements. The expansion unit is the only device which can be used to obtain successive counts at different nucleating temperatures at 10-12 minute intervals. The expansion-produced temperatures do not require changing and stabilizing the (constant) wall temperature. Measurements are immediately available for interpretation in the field.

3. Pre-nucleation effects on particles. Pump heating of sampled air will destroy the activity of preactivated or preconditioned ice nuclei. Stokes law computations indicate that particles larger than about 2-3μ will settle out during a 5-minute pre-expansion period allowed to stabilize temperature and humidity of the air sample. Computations with standard diffusive deposition equations show that roughly 10% of particles with $d \leq 0.01\mu$ will be lost by diffusion to the walls. Theories of size effect on nucleation indicate that the sedimentation loss of nuclei is most significant. On the other hand, in an aged aerosol population, few particles larger than 2-3μ will remain.

4. Pressure characteristics. Pressure transducer measurements show that any particular overpressure is repeatable to at least ± 2 mb (±0.05C). The air is overpressured from ambient pressure. Variations of the latter can cause a maximum deviation of ±0.5C and a normal deviation of ±0.1C from the theoretical nucleation temperature. Expansion rate is the same for all overpressures (Fig. 1). Observer effects on decompression time from a given overpressure are negligible (Fig. 1) and are not expected to affect nucleation temperatures.

5. Temperature and moisture characteristics and the nucleation process. A 5 minute preconditioning period is necessary to bring the air sample to a steady state temperature. The moisture level at the end of this period regulates the cloud formed on expansion. Cambridge hygrometer measurements of dew point up to this time using initially dry air (T_d = -8.8C, e/e_w = 0.11) and initially extremely moist air (T_d = +25.8C, e/e_w = 1.0) show that moisture diffusion to the walls and evaporation from the sugar solution greatly reduce initial moisture differences (Fig. 2). In almost all situations the final pre-expansion saturation ratio will be between 0.7 and 0.8.

Temperature uniformity in the chamber after expansion is shown in Fig. 3 for a theoretical T = -20C. Without compensation, a count underestimate of 4.5, 8 and 18% for T = -14, -20, and -26C, respectively, would result from portions of the chamber being warmer than T. Supersaturations (SS's), droplet nucleation and growth, and cloud duration during and after expansions also influence ice nucleation and the nucleus count. Cloud durations in the chamber are not extremely different for moist and dry air (Fig. 4). This is due to the equalization of moisture content during preconditioning of the air sample. The cloud persists for a time substantially longer than the maintenance of the minimum nucleation temperature (5s). SS's greater than in natural clouds do occur in the chamber, but the following evidence shows that their effects on nucleus count are less influential than often assumed. The expansion proceeds at a finite rate; it is not instantaneous (Fig. 1). Natural condensation nuclei are present in the air sample. Droplets form at very low SS's and continue to grow throughout the expansion, thus reducing the SS and keeping it well below dry adiabatic values. A realistic estimate of maximum peak SS is roughly 50%. Mossop and Jayarweera (3) found that SS has little effect on freezing (AgI-NaI) nuclei, whereas a significant effect on sublimation (AgI) nuclei was observed for T > -15C but not for colder temperatures. Alkezweeny (4) observed that at -18C an increase of SS from 1% to 22% increases the count by 1.5-3x, but SS's above 22% in the 22-60% range produce little increase in (sublimation) nucleus count. These observations apply to the expansion count. A further factor that will cause the SS to play a subordinate role is the short persistence time of SS's in the chamber. The nucleus count is influenced by the duration of SS (4) (5). The post-expansion duration of SS is < 1/10 the time that the cloud remains within 1C of the minimum nucleation temperature T_f. (Determined by measuring time to completion of cloud development in the chamber as revealed by lasar beam extinction.) The measured post-expansion supersaturation durations of 0.1 to 0.3 sec agree with estimates by Mason (6). A further experiment has shown that the time lag in nucleation leads to activation of a significant number of "post-expansion nuclei." These activate in the absence of supersaturations.

The net effect of SS, temperature and the resulting cloud may be examined by comparing mean expansion and mixing chamber spectra. In both types of chambers, SS's exist and increase toward colder temperatures. This increase is somewhat greater in expansion units at least at the colder temperatures. The expected relative position and slope of the nucleus-temperature spectra if SS's were the dominant factor, and the supersaturation in the expansion chamber were greater for larger expansions and greater than in the mixing chamber is illustrated in Figure 5a. The expected relative spectra if persistence of both minimum temperature and cloud are the dominant factors (both are less in expansion than in mixing chambers) is shown in Fig. 5b. An extensive series of comparisons by Kline and Brier (2) resulted in mean spectra as in Fig. 4b. The mixing curve-expansion curve separation varies with mixing technique, but mixing chambers generally read about 2-5x higher. The evidence is that SS in the expansion unit partially compensates for the temperature nonuniformity effect but is not the dominant factor in determining the nucleus count.

6. Detection of nucleated ice crystals. Computations of crystal growth and evaporation times related to settling velocity and cloud durations show that crystals nucleated when $T_f \leq$ -20C will definitely survive for a time sufficient to settle into the sugar solution for detection. For $T_f \leq$ -17C, detection will be marginal for crystals other than those formed and settling from relatively near the chamber base. Thus, at -14C as few as 1/3 of the crystals may be detected. Partial compensation is provided by the facts that (1) due to the temperature distribution in the chamber, a greater fraction of crystals will be produced in the lower part, (2) the average natural nucleus concentration at -14C is below the counter's minimum detectable level ($0.1/\ell$), so when average-or-below conditions apply no crystals will be detected with or without the undercount, and (3) the calculations were made assuming crystal evaporation rate was equal to growth rate; actually the evaporation is slower.

7. Contamination of the air pump without nucleating material will occasionally occur. It is estimated that observed contamination has occurred at the level of about 10^{-10} particles of which only a minute fraction is released with any one measurement. Maximum possible contamination due to an upwind seeding operation is estimated at 10^6 nuclei, assuming all nuclei passing through the pump are collected. Even with this impossible collection "efficiency", the 10^6 level is 10^4 lower than observed. In a great number of field seeding cases, the measured nucleus count has been observed to quickly retreat to levels comparable to the pre-seeding background concentrations after seeding has been stopped. It is very unlikely that the observed

contamination is due to pump collection of seeding material dispersed upwind. All evidence indicates that the pump contaminates only when a quite active nucleant is handled in large quantities in the immediate vicinity of the instrument. This means that contamination may be controlled with precautions. The contamination factor must be watched very carefully.

8. Comparisons. Intercomparisons of several rapid expansion counters resulted in count correlation coefficients ≥ 0.95 for paired series (2). The natural cloud is the one absolute reference available for calibrating ice nucleus counters. Observed ratios of natural cloud-produced ice crystal concentrations to ice nucleus concentrations measured by the expansion method at corresponding temperatures for individual unseeded cases were 1.3, 3.3, 1.7, 0.5 and 0.33. For cases seeded with AgI, ratios were 1.0, 0.8, 1.0 and 0.2. Cloud top temperatures for the various cases ranged from -15 to -26C (7) (8) (9). The agreement is good. Counts obtained with the expansion unit are certainly within a range of magnitudes that have direct physical meaning in terms of cloud processes.

CONCLUDING REMARKS

A more comprehensive version of this evaluation is complete and forthcoming. The study reveals that the expansion technique is reliable. The results allow one to distinguish between instrument effects and natural effects on nucleus count. As with all current ice nucleus measuring devices, improvements are in order. A number of improvements have been incorporated in a new CSU Expansion Counter. Professor Lewis O. Grant is thanked for his helpful suggestions throughout this study. The Research was supported by NSF Grant No. GA-1553.

References

(1) Warner, J., 1957: An instrument for the measurement of freezing nucleus concentrations. Bull. L'Obs. Puy de Dome, 2, 33-46.

(2) Kline, D. B., and G. W. Brier, 1961: Some experiments on measurements of natural ice nuclei. Mon. Wea. Rev., 89, 263-272.

(3) Mossop, S. C. and K. Jayaweera, 1969: AgI-NaI aerosols as ice nuclei. J. Appl. Meteor., 8, 241-248.

(4) Alkezweeney, A. J., 1970: Evaluation of the millipore filter technique for ice nuclei measurements. Meteorology Research, Inc. Report MR170 FR-909, 16 pp.

(5) Fletcher, N. H., 1962: The Physics of Rainclouds, Cambridge, 386 pp.

(6) Mason, B. J., 1951: Spontaneous condensation of water vapor in expansion chamber experiments. Proc. Phys. Soc. London, 64B:773-779.

(7) Hindman, E. E. II, 1967: Snow crystal and ice nuclei concentrations in orographic snowfall. Colo. State Univ., Atmospheric Science Paper No. 109, 83 pp.

(8) Grant, L. O., 1968: The atmosphere as a standard for the calibration of ice nuclei counters. J. Rech. Atmos., 3, 179-180.

(9) Reinking, R. F. and L. O. Grant, 1968: The advection of artificial ice nuclei to mountain clouds from ground-based generators. Proc. First Nat'l. Conf. Wea. Modif., Albany, 433-445.

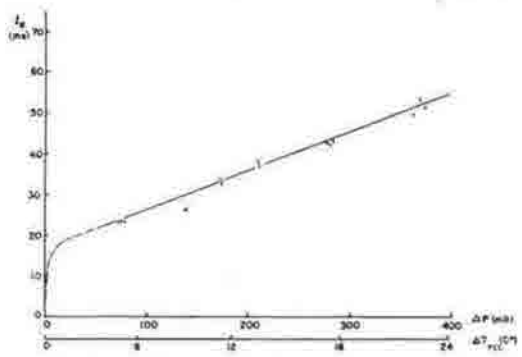

Fig. 1. Total air sample decompression time, t_R, as a function of overpressure, and of corresponding temperature drop for a pressure elevation of 840 mb.

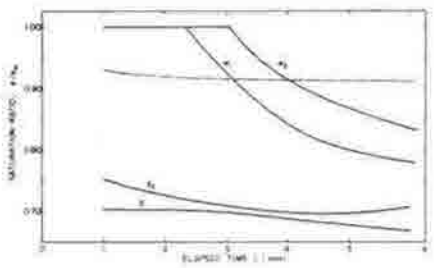

Fig. 2. Saturation ratio with respect to water as a function of time elapsed during the preconditioning period. Wet air cases are indicated by w, dry by d. Dashed curve = ice saturation.

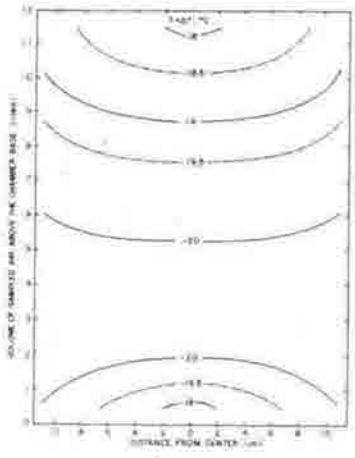

Fig. 3. Cross-sectional chamber map of nucleation temperatures actually attained on expansion to a theoretical temperature of -20C.

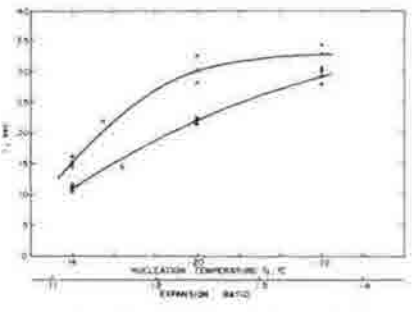

Fig. 4. Cloud duration t in the expansion chamber. (a) Very moist intake air, T_d = +23C. (b) Dry air, T_d = 4C (P = 840 mb).

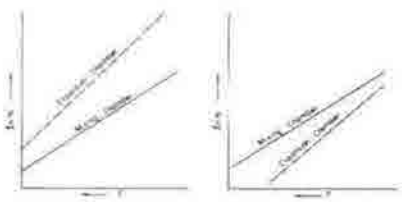

Fig. 5. (a) left, and (b) right. Expected nucleus temperature spectra under conditions specified in the text.

A DILUTION-CHAMBER FOR COUNTING HIGH CONCENTRATIONS OF ICE CRYSTALS

by M. ANDRO and R. SERPOLAY

Faculté des Sciences - 29 N Brest - France

I - Introduction

The ice-nuclei counters are generally designed for counting ice-crystals in concentrations not so high as 1,000 per liter. The use of such counters for studying the capability of various ice-nucleating agents implies a previous dilution of the active aerosol.

When the ice-nuclei or ice-crystals are directly injected from the source into the supercooled cloud, it is necessary to perform the dilution at the stage of the ice-cloud.

For such studies, the following device is proposed.

II - Description of the device

The device includes a cloud-chamber against which is soldered a dilution-chamber. This set is adjusted in a home freezer. The counting of the ice-crystals is performed by the sugar solution method (1) at the bottom of the dilution-chamber.

1°) The cloud-chamber is a parallelepipedic brass vat of about 100 liters. An opening through which the nucleating agent is injected and the visual observation of the cloud is made has been contrived on the lid of the vat. The upper part of the chamber is covered with an insulating material.

2°) The dilution-chamber in an air-tight box of about 18.5 liters. By the mean of an adequate system of tap and syringe it is possible to operate a slight depression inside the box or to realize the communication with the outside. A sensitive pressure gauge recorder (2) is also connected to the dilution-chamber. By the mean of a window on the upper wall and a light inside it is possible to observe or to photograph the plate containing the sugar solution at the bottom. The temperature of the sugar solution is controled independantly by a cooling plate.

3°) In the middle of the common wall of the chambers a small hole which can be closed by an air-tight shutter has been drilled. By this hole a small volume of the air of the cloud-chamber can be sucked into the dilution-chamber.

III - Working up of the device

Before cooling, the chambers are carefully dried and prepared in order to prevent rime formation against the walls. Then the sugar solution is introduced at the bottom of the dilution-chamber, the supercooled cloud is produced by introducing a stream of satured warm air (25° C). Before turning off the supply of moist air, a part of the stream is directed towards the dilution-chamber just for providing to the latter a sufficient moisture. Then the supercooled cloud is seeded with the ice-nucleating agent and a light depression is performed in the dilution-chamber. Immediately after, the shutter is opened. Because of the depression and the possible change of temperature in the dilution-chamber, a small volume of air is passing from the seeded cloud-chamber into the other. This volume "v" is easily calculated from the pressure change Δp read on the recorder. Supposing adiabatic the compression of the volume V_o of the dilution-chamber, we obtain :

$$v = \frac{V_o}{\gamma P_o} \Delta p$$

where : P_o is the atmospheric pressure

γ equals 1.4

On the last stage of the dilution, a supplementary and brief supply of moist air is provided to the chamber in order to produce a light turbulence which makes the ice-crystals spatial distribution more homogeneous. After falling in sugar solution, the ice-crystals are growing and can be photographed and counted.

IV - Conclusion

The device has been used for comparing the capability of ice-crystal formation with the various nucleating agents, namely different cold-producing liquids

directly sprayed in the supercooled clouds.

With this method it has been possible to count ice-crystals concentrations as high as 2×10^6 per liter.

V - Acknowledgment

The most part of this work was supported by the Airport of Paris under the convention n° 286.308.

VI - Références

(1) Bigg E.K. : A new technique for counting ice forming nuclei in aerosols. Tellus, 9 (1957), 3, pp. 394-400.

(2) Paugam J.Y., Serpolay R. et Mazé R. : Un barographe différentiel pour l'enregistrement des faibles variations de pression. J.R.A., 1970, sous presse.

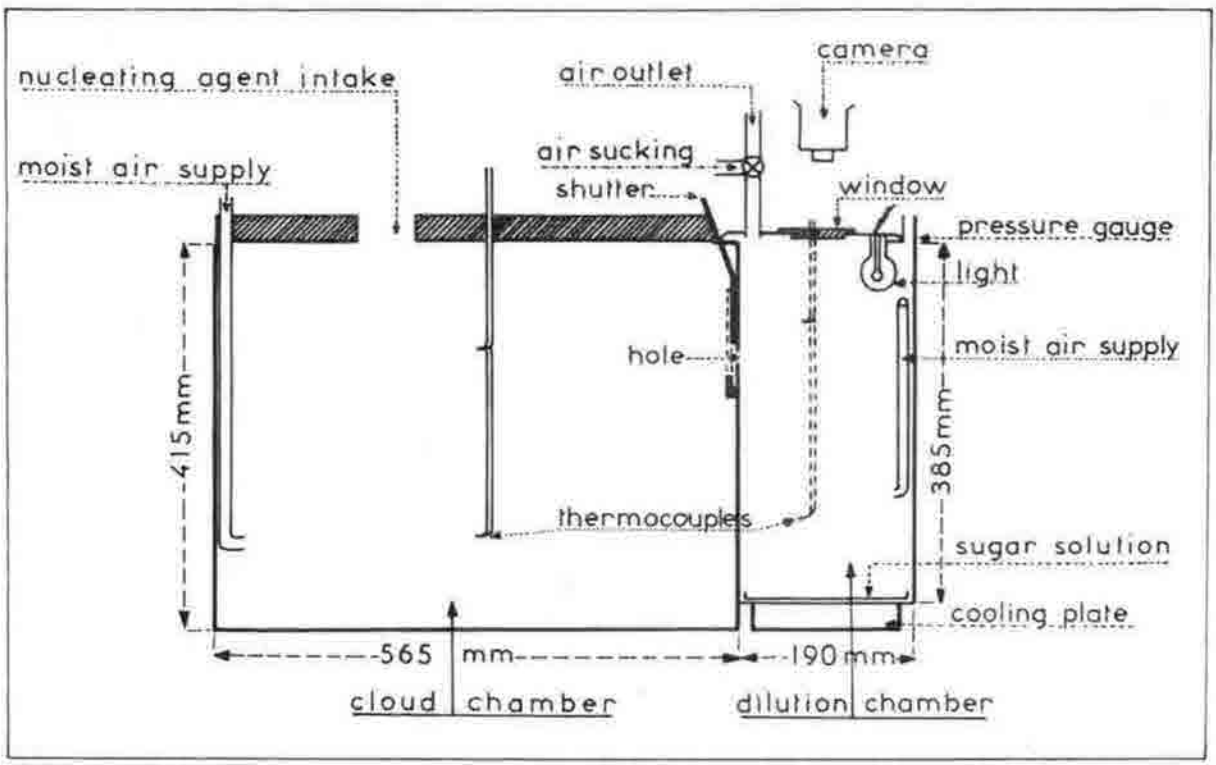

Sketch of the device

AEROSOL SIZE DISTRIBUTIONS FROM LIGHT SCATTERING MEASUREMENTS

Franklin S. Harris, Jr., Physical Electronics Laboratory

Aerospace Corporation, P.O. Box 95085, Los Angeles, Calif 90045

INTRODUCTION

The aerosol content in the atmosphere is an important factor in radiation transfer, visibility, air pollution and many meteorological processes. Aerosols can serve as a valuable tool in understanding and following dynamical processes, if correlated with meteorological variables such as wind, temperature, humidity, pollution sources, inversion layers, solar radiation, mixing, Aitken nuclei, and precipitation. The determination of the nature of the aerosols as specified by size distribution, composition, shape, and changes in these characteristics in time and space, is an important measurement task.

AEROSOL SIZE MEASUREMENTS

Aerosol sizes can be measured by collecting individual particles such as by using aerodynamical or electrical characteristics which are size dependent, or by measuring them one at a time as they pass through a light-scattering photometer. Attractive, but not yet available, is the method of sizing individual particles,with also obtaining the index of refraction, by measuring the scattering simultaneously at several angles for each individual particle, and processing the measurements with the help of a computer. Useful though these techniques are they permit sampling only at the equipment location, though the equipment may be mobile. More flexible and versatile techniques need to be employed to obtain the needed measurements to study the aerosols throughout a volume extended in geography.

Another approach is to characterize the general nature of a polydisperse aerosol at the instrument, or remotely, by measuring the scattering intensity simultaneously at several angles for various polarization parameters at suitable, and preferably, several wavelengths.

The inversion from scattering measurements to obtain the size distribution does not, in general, give a rigorous solution. (1) But by experience, trial and error, and using computers to simplify the calculations the general type of size distribution can be obtained. Some reasonable assumptions have to be made about the shape and material of the particles, or they must be measured independently. It should be observed first of all that model aerosol size distributions such as those of Junge and Deirmendjian are helpful, but in nature there are wide variations in the shape of the size distribution, for example,in the recent work of Blifford(2), and Harris. (3)

THREE ANGLE METHOD

Though some useful information on the size distribution can be gained by using only the variation in transparency with the aerosols, or by using several small scattering angles, a wider range of angles gives more information to deal with a greater diversity of distribution types. Barteneva,et al (4) have measured the angular scattering intensity as a function of the visibility, showing the characteristic change expected as the distribution changes from small Rayleigh to cloud-type particles. The scattered radiation angular intensity varies as a function of the shape of the size distribution and the complex index of refraction as noted, for example, by Rozenberg (5) and Harris. (6) By choosing three angular regions carefully the simultaneous measurement of intensity and polarization gives a good characterization of the aerosol size distribution and the index of refraction. The most useful three angles for discrimination and characterization of the aerosol depend on the particular aerosol, and how wide a range of possible distribution types are to be considered. For example, aerosols with many large particles scatter most of the energy in the near-forward direction, and angles in the near-forward direction (corona) would be useful. For a wide range of aerosol types a wider range of angles would be chosen. A suitable choice of angles would be one in the 30° to 40° scattering angle region, one at 90°, and one in the range from 140° to 150°, with the measurement of both polarizations. From the two measured polarizations(perpendicular and parallel to the plane of observation), the Stokes parameters of polarization can be obtained, and hence the polarization ratio, the polarization, the ellipticity and the angle of inclination of the polarization ellipse. This gives then six parameters for expressing the angular variation of the scattered radiation.

APPLICATION OF THE THREE-ANGLE METHOD

To assess the usefulness of measuring the scattering at three angles simultaneously to determine the nature of an aerosol size distribution a group of ideal and actual size distributions have been studied. The method involves calculating, by means of Mie theory and a computer, the expected angular distribution of intensity for the various polydispersed groups of particles. Three angles were used and the ratios of the parameter values at the three angles determined. Actual measured values of Los Angeles aerosols were used, but smoothed for purposes of calculation. Eleven quite varied types were chosen and calculations made for eleven different combinations of wavelength and indices of refraction, for each of the six parameters. Deirmendjian's haze and cloud model data (7) were also used for varied indices of refraction and both polarizations and polarization ratio to illustrate the three-angle method.

With perpendicular polarization, for example, the small particle Rayleigh scattering (or large sizes with still longer wavelengths to give the same ratio) gives the intensity at all three angles about the same. As the particle sizes become large the 30-40° intensity becomes much greater with the 90° intensity less than the 130-140° angle intensity. For still larger particles there is a fog-bow region at 130-140° which is much greater than the 90° intensity, taking into consideration the marked polarization effects the fog-bow (or rainbow for large water droplets) region is very useful. From these values of the angular intensity and polarization parameters the usefulness, and limitations, of measuring three angle intensities to obtain size distribution and index of refraction can be seen.

REFERENCES

(1) Kerker, Milton, 1969: The Scattering of Light and Other Electromagnetic Radiation, Academic Press, New York, p. 449f.

(2) Blifford, Irving H., Jr., and Lynn D. Ringer, 1969; "The Size and Number Distribution of Aerosols in the Continental Troposphere," J. Atmos. Sci., 26, 716-726.

(3) Harris, Franklin S., Jr., 1970: "Aerosols and Air Pollution in Los Angeles," Air Pollution Control Association Meeting, St. Louis, June 15-18, 1970, Paper 70-146.

(4) Barteneva, O. D., E. N. Dovgiallo, and E. A. Poliakova, 1967: "Experimental Studies of Optical Properties of the Surface Layer of the Atmosphere," Leningrad. Glav. Geofiz. Obs. Trudy, No. 220, 243pp.

(5) Rozenberg, G. V., 1968: "Optical Investigations of Atmospheric Aerosol," Soviet Physics, Uspekhi, 11, 353-380.

(6) Harris, Franklin S., Jr., 1970: "Calculated Laser Scattering of Typical Los Angeles Aerosols," J. Opt. Soc. Am., 60, 732.

(7) Deirmendjian, D., 1969: Electromagnetic Scattering on Spherical Polydispersions, Elsevier, New York, 290pp.

FIELD AND LABORATORY MEASUREMENTS WITH AN IMPROVED AUTOMATIC CLOUD CONDENSATION NUCLEUS COUNTER

by
Lawrence F. Radke
Cloud Physics Group, Atmospheric Sciences Department
University of Washington, Seattle, Washington

INTRODUCTION

The operating characteristics of the original automatic cloud condensation nucleus counter (Radke and Hobbs[1])somewhat restricted its application in aircraft measurements. These limitations have been largely overcome in the second generation instrument. The sample processing rate has been increased 500% to 5 samples per minute; moreover we have made substantial reductions in the total size, weight, and the height+width aspect ratio.

Recently, Fitzgerald[2] and Saxena, et al[3] predicted theoretically that under certain conditions of sample and chamber temperature and sample relative humidity, it was possible to have transient supersaturations in a thermal diffusion chamber which are larger than the steady state value. For our instrumental configuration, their results predicted possible large errors at, or near, a sample relative humidity of 100%. This would then preclude making accurate measurements in or near clouds without extensive sample conditioning. However, contrary to these predictions, experiments using a controlled humidity aerosol of either natural CCN or nebulized NaCl nuclei show that only a negligible counting error occurs as 100% relative humidity is approached.

With these constraints on aircraft measurements removed, an experiment was designed to examine further the observation that evaporating clouds appear to release more CCN (active at a given supersaturation) than were present when the cloud formed (Radke and Hobbs[4]; Saxena, et al.[3]).

EXPERIMENTAL DESCRIPTION

Because previous observations of cumulus and stratus clouds apparently creating CCN were complicated by the possible presence of precipitation accumulation zones as well as vertical transport of air from lower levels, it was decided to make the observations on a time-stable mountain wave cloud. Such clouds form frequently over the major peaks in western Washington State and often remain stationary long enough to repeat a given sequence of measurements several times. The measuring sequence generally consisted of: (1) a vertical profile in the region of the cloud; (2) a measurement in the clear air near the condensing leading edge of the cloud; and (3) a traverse over or under the cloud to the evaporating trailing edge.

The NCAR Queen Air aircraft which was used in this study was instrumented with standard sensors (total temperature, dew point, altitude, and airspeed). The experimental payload consisted of the automatic CCN counter, a sodium-containing particle detector, an ice crystal counter (under development in this lab), and an integrating nephelometer for measuring the light scattering coefficient (Charlson, et al.[5]).

PRELIMINARY RESULTS

A partial analysis of results provides dramatic confirmation of the earlier observations. Fig. 1 shows two traverses of a long lee wave cloud (23 km), one traverse under (A) and the other above the cloud (B). The concentration of CCN (measured at 0.5% supersaturation) in the air following out of the wave cloud was about a factor of 3 larger than the air flowing into the cloud. Fig. 2 shows an effect of the same magnitude from a cap cloud which formed later the same day. Fig. 3 depicts similar results with a lower wind speed, northerly air flow, and somewhat cleaner air. Measurements were made in several other wave clouds in the Olympic Range with results similar to those shown in Fig. 3.

CONCLUSIONS

These measurements show in-cloud production of active CCN to be a potentially major source of CCN. The production mechanism is still unclear. A major effort involving a detailed analysis of the aerosol size distribution and composition as well as trace gas constituents will probably be necessary to understand this mechanism.

ACKNOWLEDGMENTS

Thanks are due to Professors P. V. Hobbs and A. B. Fraser, and to L. B. Engel, F. M. Turner, J. Covington, and the NCAR aviation facility for assistance during this study.

This research was supported by Grant GA-17381 from the Atmospheric Sciences Section of the National Science Foundation.

REFERENCES

1. Radke, L. F., and P. V. Hobbs, 1969: "An automatic cloud condensation nuclei counter," J. App. Meteor. 8, 105-109.
2. Fitzgerald, J. W., 1970: "Non-steady-state supersaturations in thermal diffusion chambers," J. Atmos. Sci., 27, 70-72.
3. Saxena, V. K., J. N. Burford and J. L. Kassner, 1970: "Operation of a thermal diffusion chamber for measurements on cloud condensation nuclei," J. Atmos. Sci., 27, 73-80.
4. Radke, L. F. and P. V. Hobbs, 1969: "Measurement of cloud condensation nuclei, light scattering coefficient, sodium-containing particles, and Aitken nuclei in the Olympic Mountains of Washington," J. Atmos. Sci., 26, 281-288.
5. Charlson, R. J., H. Horvath, and R. F. Pueschel, 1967: "The direct measurement of atmospheric light scattering coefficient for studies of visibility and air pollution," Atmos. Environ., 1, 469-478.

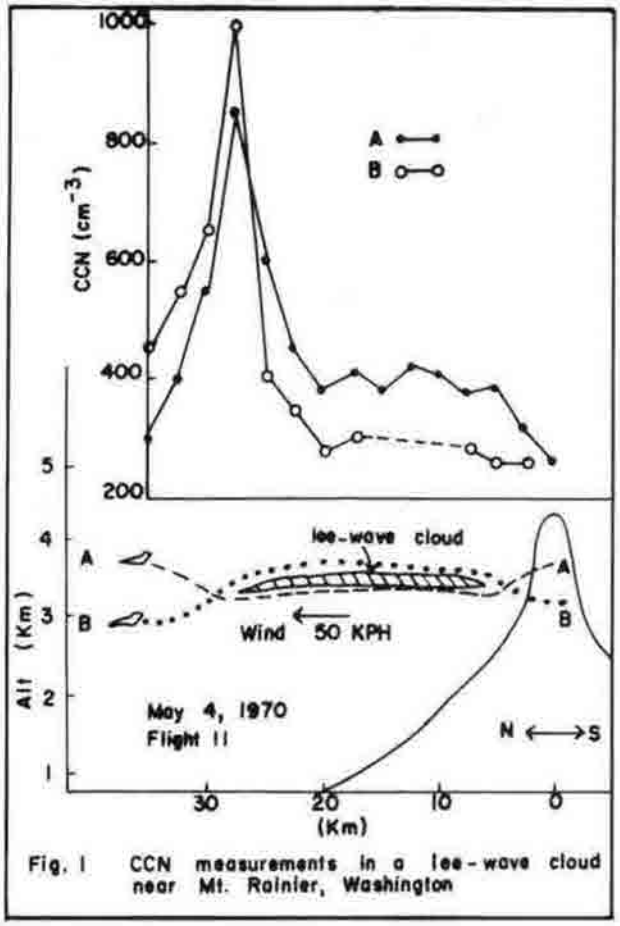

Fig. 1 CCN measurements in a lee-wave cloud near Mt. Rainier, Washington

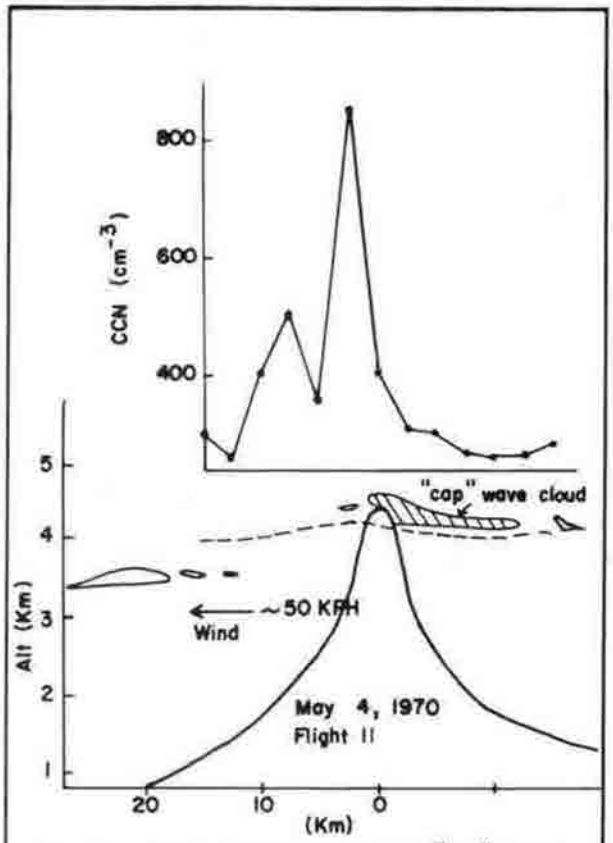

Fig. 2 CCN measurements in a "cap" wave cloud over Mt. Rainier, Washington

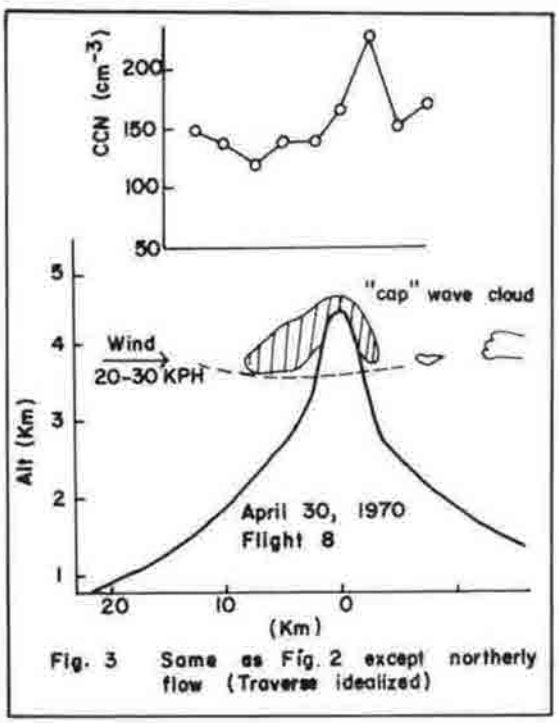

Fig. 3 Same as Fig. 2 except northerly flow (Traverse idealized)

DECAY AND SUPERSATURATION DISTRIBUTION OF NATURAL AEROSOL

V. K. Saxena, A. H. Biermann and J. L. Kassner, Jr.
Graduate Center for Cloud Physics Research
University of Missouri-Rolla

INTRODUCTION

This laboratory has been struggling hard lately to improve the performance of cloud[1,2] and Aitken[3,4,5] nuclei counters. In summer 1968 a joint effort in collaboration with ESSA and NAPCA was undertaken to intercompare four Aitken nuclei counters[6] in order to assess their performance. These counters were a Pollak and a Gardner counter supplied by Mr. Paul Allee of ESSA and a Pollak and a G.E. counter supplied by Mr. Norman White of NAPCA. The results of these comparisons were rather surprising for individual counters sampling the same air differed often by 50%. Since the time of this effort, an absolute Aitken nuclei counter[5] has been put into operation in this laboratory. Measurements taken on the absolute counter are described here which help provide a plausible explanation for these unexpected differences.

The concentration of room aerosol, stored in a doubly aluminized Mylar bag of 851 liter capacity, was measured as a function of time. In one of the attempts, this was done at five different operating supersaturations. From these data are derived the supersaturation distribution and size distribution for the test aerosol which furnish some remarkable features.

EXPERIMENTAL

The details of our absolute nuclei counter are described elsewhere[5] which essentially is an expansion cloud chamber. This chamber is capable of being operated at eight different supersaturations, thus covering the whole range of interest for Aitken nuclei. The sample dilution is a special feature in this chamber which helps in reducing the experimental error that mainly arises due to uncertainty in drop counts. One centimeter thick light beam obtained from two well collimated and matched flash tubes, one on each side of the chamber, is used for direct photography of the sensitive region at right angles to the beam. The natural room aerosol was stored in a nuclei reservoir[6].

The chamber is capable of measuring aerosol concentration after every 5 min interval. While taking data at five different supersaturations, the highest was operated first, and then the others were operated in successive decreasing order. Thus at a given supersaturation, the concentration could be recorded after each 25 min interval.

The overall rate of change in the number of nuclei, $\dot{N}$, may be expressed by a differential equation involving the sum of two terms[7,8] as

$$\dot{N} = -\lambda N - \gamma N^2, \tag{1}$$

where λ takes account of the diffusion to the container-walls and by sedimentation and γ is related to the loss of nuclei by coagulation. Obviously, the second term is dominant in Eq. (1) when N is large. On analysing our data we found that they could be well correlated by considering only the first term of Eq. (1). This amounts to representing the decay of the test nuclei as

$$N = N_o \exp(-\lambda t). \tag{2}$$

Eq. (2) was fitted to our data by the method of least squares and the values of N_o and t are displayed in Table 1. In the last column of this table are recorded the percent absolute average deviation (%AAD) which indicate that Eq. (2) represents our data within experimental error[5], which is about 10%. In this table, S stands for the operating supersaturation. It seems reasonable to infer that in the concentration range of our experiments, the decay process is dominated by diffusion phenomenon as sedimentation for these sizes of Aitken nuclei is relatively small.

TABLE 1: Values of N_o and λ, Eq. (2).

Date	S	N_o	$10^5\ \lambda$, sec^{-1}	% AAD
2 Jan 1969	3.20	16,681	5.24	10
5 Feb 1969	3.24	31,271	6.49	4.9
9 Jun 1969	3.78	8,393	2.58	4.4
9 Jun 1969	3.05	8,000	2.00	5.6
9 Jun 1969	2.56	6,936	1.74	3.6
9 Jun 1969	1.92	6,227	1.91	8.0
9 Jun 1969	1.43	5,446	2.29	8.2

TABLE 2: Values of k and α, Eq. (3).

t, min	k	α	% AAD
30	2,036	0.46	1.7
90	1,870	0.45	2.1
150	1,716	0.44	2.9
330	1,326	0.42	5.9

DISCUSSION

Supersaturation Distribution: The data of 9 Jun 1969 are used to derive the critical supersaturation spectrum of the test aerosol. The following equation is found to represent the data satisfactorily:

$$dN/d(\ln S^*) = k(S^*)^{\alpha}, \tag{3}$$

where S^* is the critical supersaturation for dN nuclei of the total population. The values of k and α at four different times are recorded in Table 2. The total change in α over a period of 5.5 hr is only about 9%. The exponential decay of aerosol exhibited by Eq. (2) has been theoretically predicted by Shapiro and Erickson[9]. Eq. (3) seems analogous to log radius-number distribution of Junge[10].

Calibration of Aitken Nuclei Counters: In Fig. 1, the differential supersaturation spectrum is shown which is derived from Eq. (3) and Table 2. As an example, consider a counter B calibrated against an absolute counter A at S = 3.4 using the test aerosol at t=30 min. Let ΔS be supersaturation decrement in B due to its non-ideal conditions[3,4,6]. This corresponds to dN_1 nuclei at t=30 min while at t=330 min, it corresponds to dN_4 nuclei such that $dN_4=\frac{3}{5}\, dN_1$ (Fig. 1). Thus, if the counter B is used to measure the concentration of the same aerosol at t=330 min, it is likely to produce counts off by 40% of the value of dN_1. If the supersaturation spectra of the test aerosol and the aerosol used for calibration are widely different, obviously this error would become still large depending on the value of ΔS and the nuclei concentration.

Assuming the test nuclei as hygroscopic, the log radius-number distribution due to Junge[10] is calculated for the test aerosol on the basis of data in Table 2 and is shown plotted in Fig. 2. The bi-modal feature of the distribution is readily apparent which supports the findings of Twomey and Severynse[11]. It seems that the qualitative features of the size distribution are preserved. This is what Shapiro and Erickson found as a result of their theoretical analysis[9].

ACKNOWLEDGMENTS: This work was supported through grants under contract No. N00014-68A-0497 from the Office of Naval Research and GA-1501 from National Science Foundation.

REFERENCES

1. Saxena, V. K., J. N. Burford and J. L. Kassner, Jr., 1970: Operation of a thermal diffusion chamber for measurements on cloud condensation nuclei. J. Atmos. Sci., 27, 73-80.
2. Saxena, V. K. and J. L. Kassner, Jr., 1970: Performance of thermal diffusion chambers as cloud nuclei counters. Proc. 1970 Precipitation Scavenging Meeting, AEC Symposium Series, June 1-5, 1970, Richland, Wn.
3. Kassner, Jr., J. L., J. C. Carstens and L. B. Allen, 1968: The myth concerning the condensation nucleus counters. J. Rech. Atmos., 3, 25-31.
4. Kassner, Jr., J. L., J. C. Carstens and L. B. Allen, 1968: Analysis of the heat and vapor propagation from the walls of the Nolan, Pollak and Gardner type condensation nucleus counters. J. Atmos. Sci., 25, 919-926.
5. Kassner, Jr., J. L. et. al., 1968: Expansion cloud chamber technique for absolute Aitken nuclei counting. J. Rech. Atmos., 3, 45-51.
6. Mansell, J. W., 1969: An experimental comparison of various nuclei counters. M.S. thesis, University of Missouri-Rolla. See also J.W. Mansell, J.F. Stampfer, Jr., P. Allee, N. White and J. L. Kassner, Jr., ibid, to be published.
7. Davis, C. N., 1966: Aerosol Science. New York, Academic Press, 31-58.
8. Pollak, L. W., T. Murphy and T. C. O'Connor, 1956: The uncertainties in measurements of concentration of condensation nuclei with photoelectric counters and the decay of nuclei in large vessels. London, Butterworth, Scientific Proceedings I.U.G.G. Association of Meteorology, 369-373.
9. Shapiro, A. H. and A. J. Erickson, 1957: On the changing size spectrum of particle clouds undergoing evaporation, combustion, or acceleration. Trans. ASME, 79, 775-788.
10. Junge, C. E., 1963: Air Chemistry and Radioactivity. New York, Academic Press, 113-123.
11. Twomey, S. and G. T. Severynse, 1964: Size distributions of natural aerosol below 0.1 micron. J. Atmos. Sci., 21, 558-564.

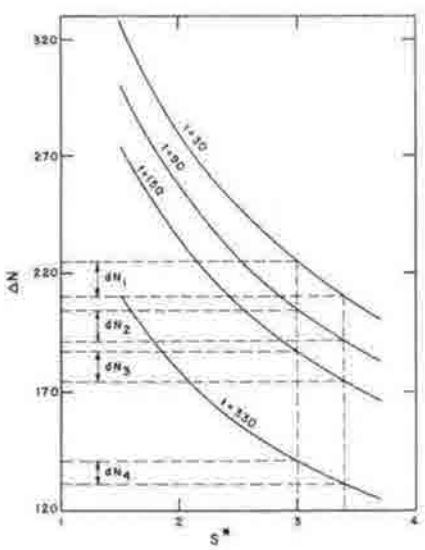

Fig. 1: Differential supersaturation spectrum at different times (t, min)

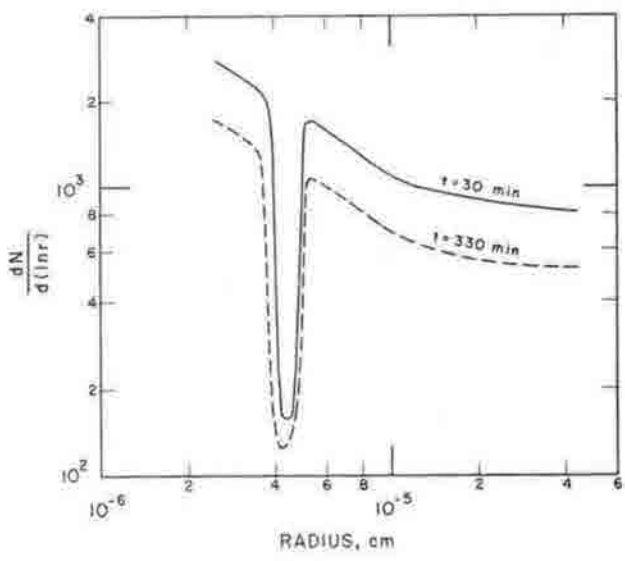

FIG. 2: Log radius-number distribution

SOME COMPARISON MEASUREMENTS OF CLOUD DROPLET AND PARTICLE DISTRIBUTIONS IN CLOUDS USING AIRBORNE SENSORS

by

Theodore W. Cannon

and

J. Doyne Sartor

National Center for Atmospheric Research
Boulder, Colorado 80302

Several cloud study flights were made by NCAR aircraft during the period 8 January, 1970 to 5 March, 1970 on the eastern side of the Rocky Mountains in Colorado and Wyoming. The studies were performed using instrumentation mounted on a Beech Queen Air twin propeller aircraft and on a Schweizer 2-32 sailplane.

Cloud droplet and particle size distribution measurements were made using two types of probes. One of these, a MIT-AFCRL electrostatic probe, was used to gather data which were recorded on either tape or strip charts. Histograms of droplet and particle size distributions could be obtained within a few hours after conclusion of a flight from analysis of the tapes or charts. This probe was located on top of the nose and forward of the canopy on the Queen Air and on the end of a boom projecting from the nose of the sailplane.

The second type of probe was a slide gun which was an NCAR modification of one used by the University of Chicago Atmospheric Physics Group. This unit exposes 10 mm x 45 mm glass slides to the airstream within the cloud with an exposure time of about 15 milliseconds. The slides were coated with either magnesium oxide on Dri-Film or 3-4% Formvar in ethylene dichloride solution. A slide is mounted near the end of a spring-loaded rod. When released by a trigger, the rod travels in a tube which extends through the top or the side of the aircraft. The exposure is made through an opening in the tube about 39 cm from the outer surface of the aircraft. Data taken with the slide gun were used to make comparisons with the distribution measurements taken with the electrostatic probe, to identify the presence of ice or water in the cloud, and to cloud droplet and particle distributions for cloud physics studies.

Nine histograms displaying distributions taken from magnesium oxide slides are shown. Two histograms showing distributions taken from the electrostatic probe data taken on 19 January are also shown in Figs. 1 and 2. They indicate a favorable correlation with the magnesium oxide method.

The 19 January histograms, which were obtained for large wave clouds (about 25 miles wide by 50 miles long) show the broadest spectra, lowest number of drops per unit volume (average 35.9 drops cm^{-3}) and highest liquid water content (average 1.67 gm m^{-3}) of any of the distributions shown. The bimodal distribution is evident in both of these distributions. This cloud was warmer (T = -7°C) than the other clouds studied which ranged from -25.2°C to -14.5°C. The small cumulus cloud distributions shown in Figs. 3-5 show more narrow spectra, but a larger number of particles per unit volume (range 82-117 cm^{-3}) and lower liquid water content (range 0.191-0.619 gm m^{-3}) than the large wave cloud. The narrowest spectra were obtained from the small wave clouds, Figs. 6-9. These clouds exhibited a somewhat higher particle count per unit volume (range 107-175 particles cm^{-3}) than the other clouds studied, but a wider range of liquid water contents (0.108-1.10 gm m^{-3}) .

By using a 3-4% Formvar solution it was possible to make some ice replicas with the slide gun at airplane speed (about 60 meters sec^{-1}). Some good crystal replicas 10-80 microns in size were obtained in the cumulus cloud sampled on 2 March. Better resolution of ice crystal structure is obtained by making Formvar replicas instead of impressions in magnesium oxide. The chief disadvantage is that the solution and slides must be kept at approximately -10°C until all water has evaporated from the ice replicas. Using the Formvar slide technique, it is possible to make positive identification of the presence of ice crystals in the cloud. This information supplements data from the electrostatic probe which cannot distinguish between water and ice particles.

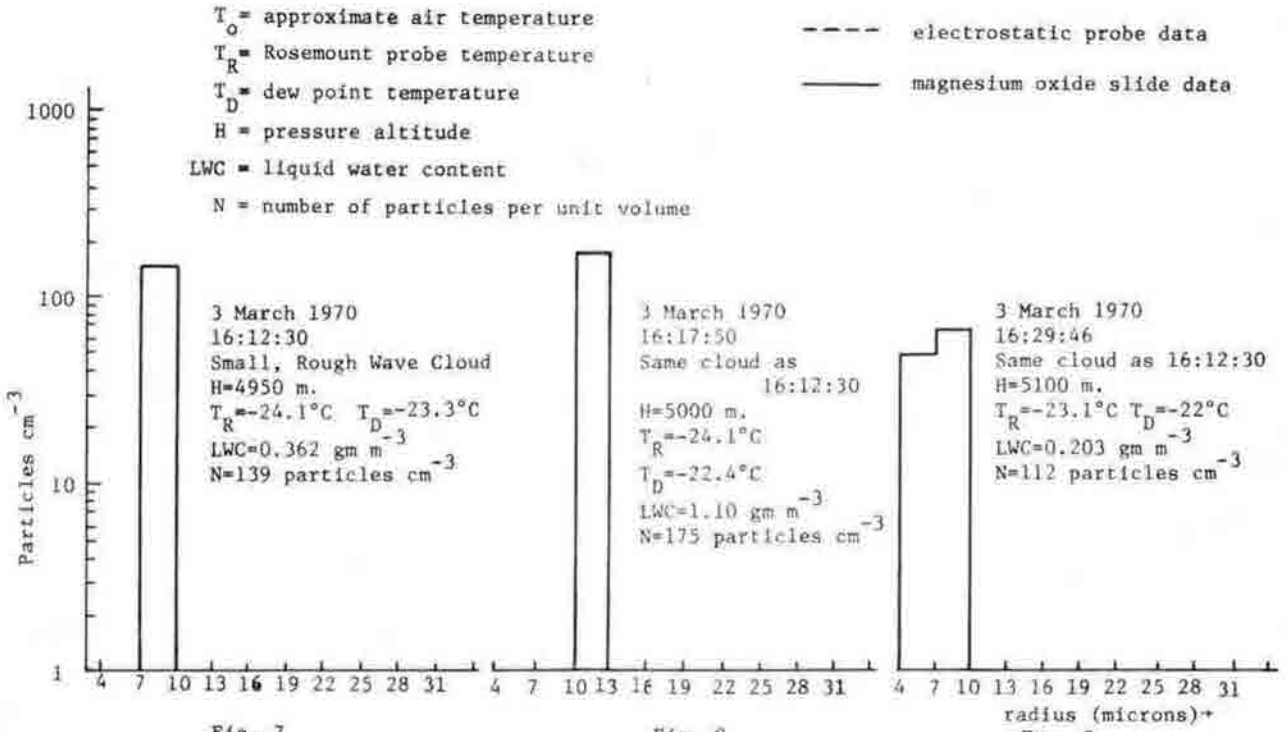

Fig. 7 Fig. 8 Fig. 9

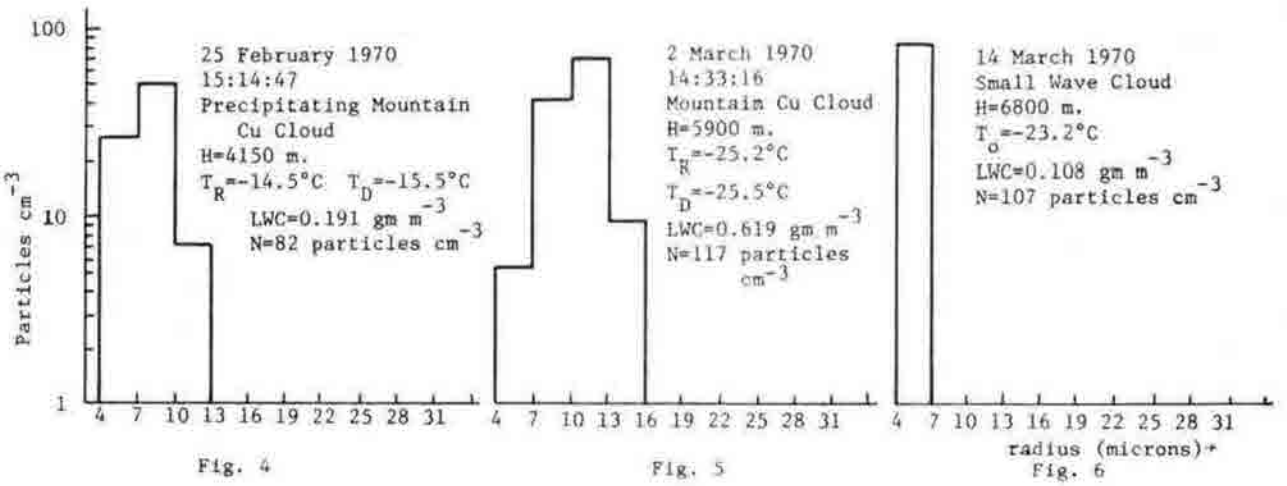

Fig. 4 Fig. 5 Fig. 6

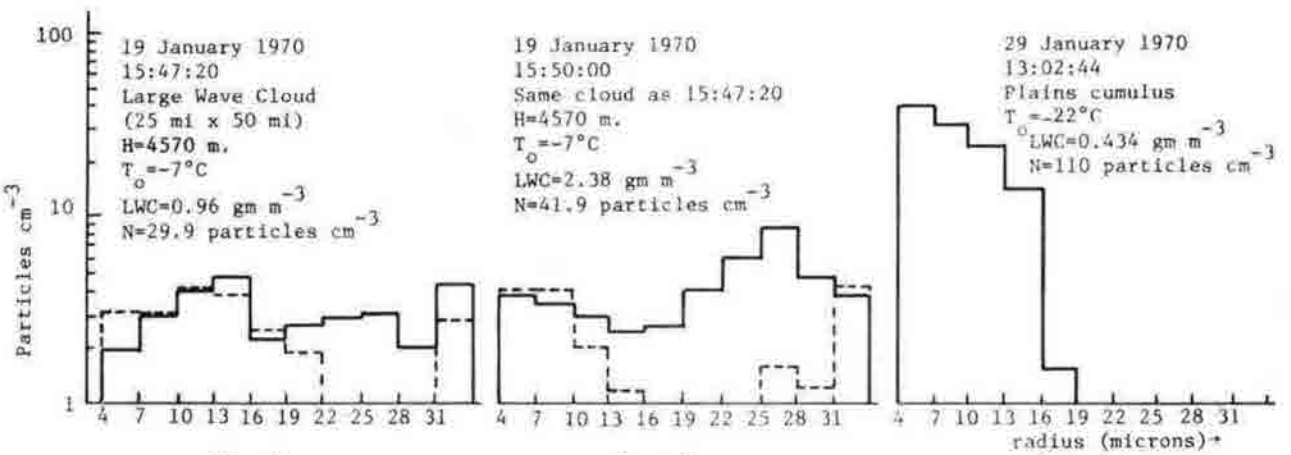

Fig. 1 Fig. 2 Fig. 3

CONTRIBUTION TO THE PROBLEM OF THE COLLECTION EFFICIENCY OF THE FALLING ICE CRYSTAL

J. Podzimek
Atmospheric Sciences Research Center
State University of New York at Albany
Albany, New York 12203

The paper deals with the calculation of the collection efficiency of the falling ice crystals in a supercooled water cloud using the evaluation of the number and of the position of the droplets frozen on the surface of individual ice crystals.

In order to express the collection efficiency A_{2l} of ice crystals falling in a population of cloud droplets having the size spectrum distribution function $f(r_l)$, we assume that, for a given size of collector (ice crystal), it can be expressed in the form

$$A_{2l} = \frac{\int g(r_l)dr_l}{\int f(r_l)dr_l}$$

$g(r_l)$ signifies the "disturbed" size spectrum distribution function corresponding to the droplets caught on the frontal and rear sides of a falling crystal of a known geometry. The case of $g(r_l) = f(r_l)$ corresponds to the removal of all cloud droplets in the volume defined by the cross section of an ice crystal and its path in a unit of time.

The evaluation of the droplet position patterns on the surface of plate-like, sector plate-like, star-like and star (with a central plate)-like crystals (in the figure denoted as D, SD, H, DH) showed that we can always find for a certain range of the sizes of the ice crystals some characteristic function $g(r_l)$ enabling us to calculate A_{2l}. A characteristic example is presented in the attached figure. Relating the "disturbed" size spectrum curve $g(r_l)$ to the normal size spectrum distribution curve [assuming $f(r_l) = Ar_l^2 e^{-Br_l^n}$ - n is usually near to 1] on a semilogarithmic paper, we get immediately the information of the catching efficiency of the ice crystals of a certain type.

Other, very useful information about the general collection efficiency of different parts of an ice crystal gives us the detailed analysis of the location of the droplets on different parts (arms, central plate) of an ice crystal. Some characteristic "catching" efficiencies were found in relation to the typical forms of simple ice crystals. The features of these characteristics can be explained on the basis of the corresponding Stokes' number. The sophistications mentioned are valid mostly for the case of a layer mixed cloud with low intensity of turbulent flow and low degree of riming on ice crystals.

There are some other (of course limited) possibilities of the use of the procedure mentioned in the case of the growth of an ice crystal through collision with smaller ice crystals. Some other interesting conclusions can be made comparing the number and size of the droplets caught on the frontal and rear sides of falling ice crystals. The number of droplets frozen on the rear side of a crystal is not negligible and surpasses in the domain of the smallest droplets ($r_l < 10$ u) the number caught on the frontal side. However, the contribution to the total change of liquid water of such a cloud by the catching of the droplets on the rear side of falling crystals is small.

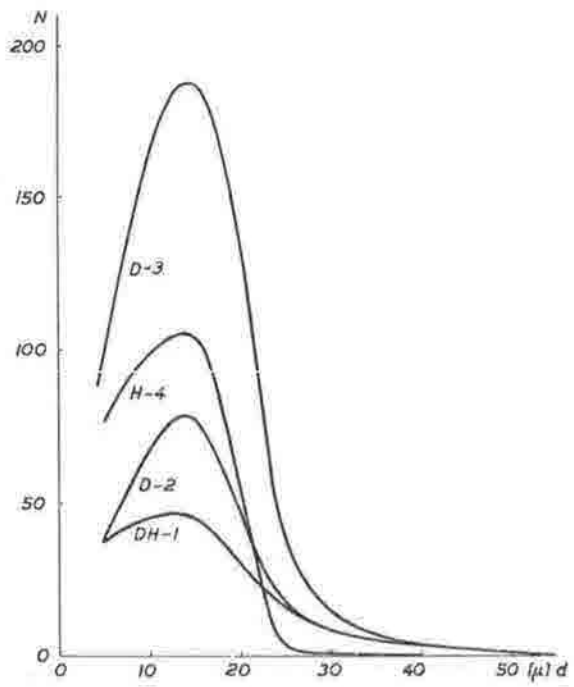

THE ROLE OF THE ADSORBED LAYER IN ICE NUCLEATION

L. F. Evans
Division of Applied Chemistry
C.S.I.R.O., Melbourne, Australia

The current theory of ice nucleation is at present undergoing profound modification in order to bring the theory into line with the better experimental data which is now available.(1) One of the factors which is receiving increasing attention is the role played by the layer of water adsorbed on the ice nucleating substrate. For example, from experiments conducted at high pressure it has been shown that the adsorbed layer exists in at least two states--an ordered state, called 2D-ice, stable below the two-dimensional (2D) melting point, and a disordered state, stable above the 2D-melting point.(2,3) The ice nucleation properties of the substrate are completely dependent on the state of the adsorbed layer, the 2D-ice state imparting the better ice nucleation ability. By taking into account the hysteresis which accompanies the transformation from one 2D-state to the other, it has been possible to account for the pre-activation which is observed when a particle is allowed to nucleate ice after being exposed to cold, moist conditions.(4)

It is the purpose of this paper to draw attention to the fact that the properties of the adsorbed layer can also explain the mechanical nucleation of ice, i.e., nucleation by direct mechanical movement,(5) shock waves,(6) cavitation,(7,8) or ultrasonics.(9) All these phenomena have in common the rapid movement of water over a previously dry hydrophobic surface, and the essence of the present proposal is that it is the rapid formation of an interface between water and a hydrophobic substrate which induces ice nucleation.

The basis of this proposal is the fact that around non-polar molecules, water is known to adopt a strongly bonded structure which often results in clathrate formation.(10) Similarly, at the interface between water and a non-polar (hydrophobic) surface, the structure of the adsorbed layer is a laterally bonded structure which we may term 2D-clathrate. At supercooled temperatures the stable state of the adsorbed layer is 2D-ice, but the transformation from 2D-clathrate to 2D-ice requires considerable supercooling as evidenced by the poor ice-nucleating properties of materials such as polyethylene.

When water freshly wets a non-polar surface the initial state of the adsorbed layer is disordered, a situation which prevails for a time probably comparable to the rotational period of a water molecule. During this time, if the adsorbed layer is supercooled, 2D-ice has the opportunity to nucleate from the high-energy transient disordered phase. It is proposed that the higher free energy change associated with this process accounts for the ease with which ice nucleates under the influence of mechanical movement.

The same mechanism may account for the nucleation observed by Pruppacher,(11) when a supercooled drop resting on a hydrophobic surface is caused to wet the adjacent surface by applying an electric field.

References

(1) Fletcher, N. H., 1970: Physical basis of ice crystal nucleation: Developments since 1960. Proc. Second Nat. Conf. Weather Modification, Santa Barbara, p. 320.
(2) Evans, L. F., 1967: Nucleation under pressure and in salt solution. Trans. Faraday Soc., 63, 1.
(3) Edwards, G. R., L. F. Evans, and A. F. Zipper, 1970: Two-dimensional phase changes in water adsorbed on ice-nucleating substrates. Trans. Faraday Soc., 66, 220.
(4) Roberts, P., and J. Hallett, 1968: A laboratory study of the ice nucleating properties of some material particulates. Quart. J. Roy. Meteorol. Soc., 94, 25.
(5) Dorsey, N. E., 1948: The freezing of supercooled water. Trans. Amer. Phil. Soc., 38, 247.
(6) Edwards, G. R., L. F. Evans, and S. D. Hamann, 1968: Nucleation of Ice by Mechanical Shock. Nature, 223, 390.
(7) Hunt, J. D. and K. A. Jackson, 1966: Nucleation of solid in an undercooled liquid by cavitation. J. Appl. Phys., 37, 254.
(8) Gitlin, S. N., and S. Lin, 1969: Dynamic nucleation of the ice phase in supercooled water. J. Appl. Phys., 40, 4761.
(9) Turner, C. F. and A. Van Hook, 1950: The effect of ultrasonic irridiation on the formation of colloidal sulfur and ice. J. Colloid Sci., 5, 315.
(10) Nemethy, G., and H. A. Scheraga, 1962: Structure of water and hydrophobic bonding in proteins. II Model for the thermodynamic properties of aqueous solutions of hydrocarbons. J. Chem. Phys., 36, 3401.
(11) Pruppacher, H. R., 1963: The effect of electric field on the supercooling of water drops. J. Geophys. Res., 68, 4463.

TIME DEPENDENCE OF SOME NUCLEATION PHENOMENA

Thomas E Hoffer

Desert Research Institute
Lab. of Atmospheric Physics
University of Nevada
Reno, Nevada 89506

The effect of cloud processes on the nucleation of water droplets is of primary importance to cloud physics. The recution or enhancement of the nucleating ability of a particle as it undergoes modification due to its changing environment should be further elucidated.

Roberts and Hallett (1968) have shown that preactivation is dependent upon the time history of the particle. Hoffer (1967) and Hoffer and Ogne (1965) have shown that this is also true when the particle goes through a stage when there is liquid on the nucleating particle.

This paper is concerned with changes in the nucleating ability of AgI and phloroglucinol particles as a function of the time they are subjected to a fixed vapor pressure greater than that necessary for saturation.

The equipment used in the research is a plate covered with Teflon whose temperature is controlled. The plate was on the bottom of a chamber in which the dew point was controlled.

The dew point was controlled in a constant temperature system where moisture was always taken from the air by means of a radiator. All the peripheral equipment was automated to insure duplication of experimental conditions.

The experimental procedure was as follows: 1. Particles of the nucleating agent under study were placed on an inert Teflon surface by means of a fall column. 2. The plate temperature was held constant at 10C as was the dew point. 3. After a predetermined length of time the temperature of the plate was decreased at the at the rate of .25C/minute. 4. The drop freezing temperature was determined by examining photographs taken each minute (black and white with polarized light). 5. Adjustment was made if two drops were in contact.

The results of the study show (as indicated on Figures 2 and 3) that there is a time dependency in the nucleation. Note that for the phloroglucinol that the high solubility accounts for the abrupt fall off as the particle goes into solution. For AgI the changes in the curve may be attributable to reforming of sites after an equilibrium is approached in the diffusion. Simple calculation of diffusion in water shows this to be not unrealistic.

It is apparent that for these size particles in contact with water that the dissolution process takes a relatively long time. The ratio of droplet size to particle size is roughly that encountered in the atmosphere. Thus, it appears that for even the soluble particles that they will be effective, if released at cloud base before dissolving.

In other experiments a mixture of NaI, AgI was used. In this case also the time to nucleation was long and the particles acted. In order to activate the nuclei apparently require sufficient water to reduce the concentration of the solution surrounding the AgI to less than 1/1000 molal.

REFERENCES

Hoffer, T.E., 1967: Some aspects of nucleation on lead iodide. Skywater Conference on Nucleation. Proc. pp. 232-246.

Hoffer, T.E., and Marshall L. Ogne, 1965: A difference in the behavior of phloroglucinol and silver iodide nuclei. J. Geophys. Sci., 70, No. 16. Pp. 3857-3860.

Roberts, P., and J. Hallett, 1968: A laboratory study of the ice nucleating properties of some mineral particulates. Quart. J. Roy. Meteor. Soc., 94, No. 399, pp.25-34.

ACKNOWLEDGMENTS

This research was made possible by National Science Foundation Grant GA 11131.

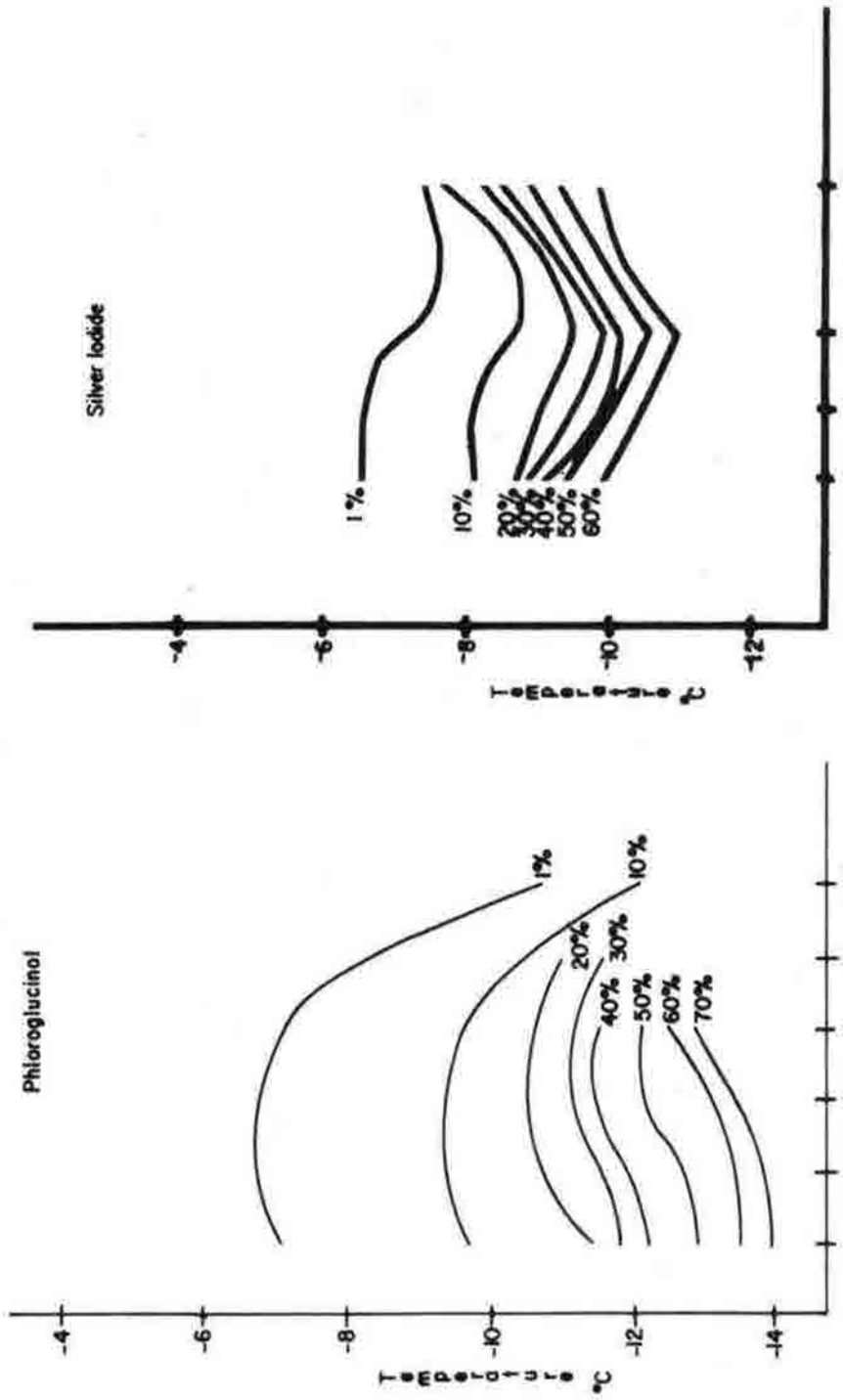

FIGURE 1. Time dependency of phloroglucinol particles in contact with water droplets growing on the particles from the vapor.

FIGURE 2. Time dependency of silver iodide particles in contact with water droplets growing on the particles from the vapor.

SOME SIZE DISTRIBUTION MEASUREMENTS OF AgI NUCLEI WITH AN AEROSOL SPECTROMETER

H. Gerber*, P. Allee**, H. Weickmann**, U. Katz+, C. Davis+, and L. Grant+

* Atmospheric Sciences Laboratory, U.S. Army, Ft. Monmouth, New Jersey
** Atmospheric Physics and Chemistry Laboratory, E.S.S.A., Boulder, Colorado
\+ Atmospheric Science Department, Colorado State University, Ft. Collins, Colorado

INTRODUCTION

Recently a method was developed which promises to meet the need for a practical ice nuclei sizing technique (1), (2). Essentially, the Göetz Aerosol Spectrometer (AS; (3)), a high speed centrifuge, is used to deposit the nuclei along a polished chrome foil according to their Stokes diameters. Upon removal from the AS, the foil is exposed to a saturated environment at the desired sub-freezing temperature, and the active nuclei grow into visible ice crystals. To find the diameters of the nuclei only the locations of the corresponding ice crystals need be determined since the coordinates of the foil are related to particle size by Stokes law after calibration of the AS.

Before describing some AgI ice nuclei measurements, it is first necessary to place the utilization of the AS on a firmer basis since the scientific community currently questions the ability of the instrument to size atmospheric particulates accurately (e.g., (4)).

PERFORMANCE OF THE GOETZ AEROSOL SPECTROMETER

The reputation of the AS is largely a result of a theoretical study of the aerosol dynamics inside the centrifuge channels (5) and of subsequent attempts to verify the theoretical predictions (5), (6), (7). Theory and experiment did not agree except in demonstrating that the AS did not operate in the required manner of a horizontal elutriator. In contrast, a recent comprehensive calibration of the AS showed proper operation for a limited number of the instrument's operating modes (different combinations of flow rate and centrifuge rotor rpm) and for particle sizes ranging from 0.1 μm to 2.0 μm (8). Also, the inconsistencies of the earlier work were explained.

Since a large portion of the particles from AgI generators usually is smaller than 0.1 μm, it was also necessary to test the AS for these sizes. The AS was calibrated with AgI particles generated by evaporating AgI-isopropyl amine (0.2% AgI by weight) at about 1000C in a stream of nitrogen. The operating mode used to collect the particles was 0.25 L min^{-1} and 18,000 rpm. The projected diameters of about 3500 particles were measured with an electron microscope at eight different distances along the foil (A-J, Fig. 1). At the longer distances, size cutoffs in the projected diameter size distributions existed for smaller particles. This is consistent with the proper operation of the AS and provided the calibration curve for the coordinates of the foil (l_D) vs particle projected diameter. Fig. 1 shows that under the specified operating mode, the size of the smallest particles which can be 100% captured is 200A. The size analysis also gave the shape of the entire AgI size distribution as being approximately log-normal with a geometric mean of 145A and geometric standard deviation of 1.59 (curve A in Fig. 2).

SIZE DISTRIBUTION OF ACTIVE AgI PARTICLES

"Pure" Laboratory AgI Particles

The AgI generator and the AS were operated in exactly the same manner as before. One deposit was exposed to water saturation at -20C and two others were exposed at -15C. The size distributions of the active particles is given in Fig. 2. The results of the -15C tests agreed closely and are combined. The values of all the distributions are relative hence, the shapes of the curves are absolute although their proper positions with respect to the ordinate are unknown.

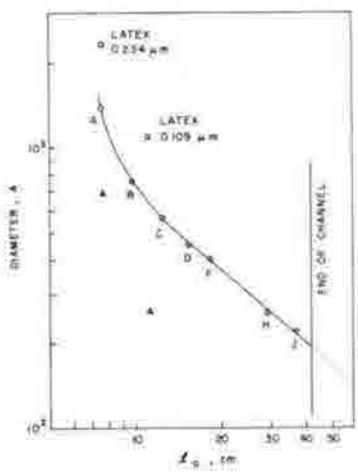

The outstanding difference between the curves in Fig. 2 is the lack of activity for small particles in the measured distributions of active particles. Below 400A for the -15C curve and below 320A for the -20 curve, the activities initiate a sharp decrease. Within a 30% reduction in each of these particle sizes, a 95% decrease takes place in the activity of the AgI particles.

It is customary to compare the activity of ice nuclei to the classical theory of Fletcher (9). At temperatures of -15C and -20C, his computations show a particle size threshold of 85A and 20A respectively for freezing and 500A and 300A for sublimation. Comparison of these values with Fig. 2 shows reasonable agreement if the active AgI particles are assumed to

Fig. 1 - The maximum deposit length l_D of AgI particles as a function of their projected diameters ( ). The latex particle calibration points ( ) are used to find the Stokes diameters of spherical AgI particles ( ) as well as the effective density 2.06 gm cm^{-3} and shape factor 2.17 of the generated AgI particles.

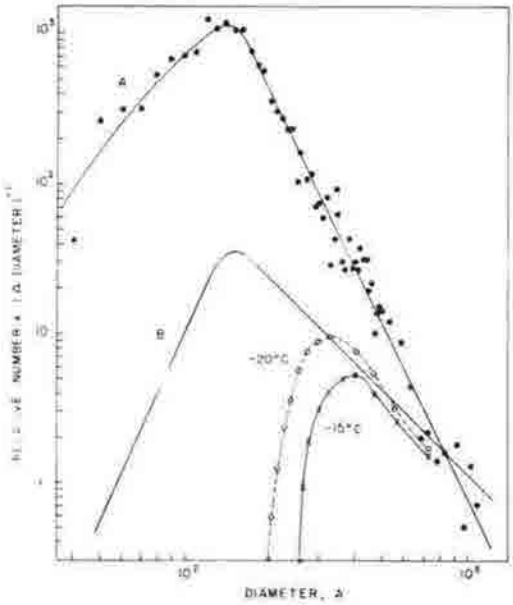

Fig. 2- The size distributions of active AgI particles (-15C, -20C), of the AgI particles sized by electron microscopy (A), and of the active AgI particles according to the "surface area rule" (B).

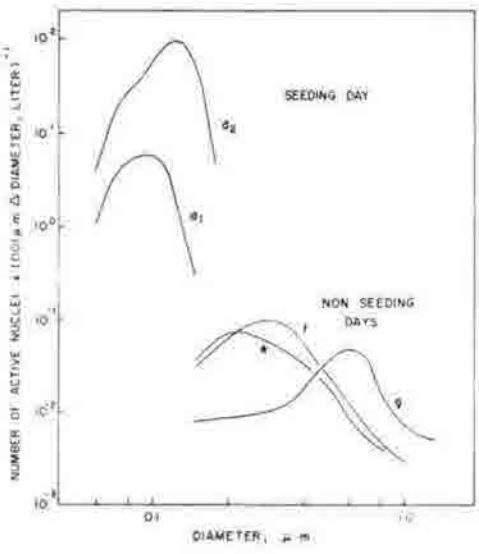

Fig. 3- The size distributions of ice nuclei (active at -20C) measured on Chalk Mt. with the AS on a seeding day (d_1, d_2, 9/11/69) and on non-seeding days (e, 9/12/69); f, 9/16/69; g, 9/17/69).

nucleate ice by sublimation. The slight shift in the activity threshold in Fig. 2 from Fletcher's values might indicate that the AgI particles behaved more nearly like ideal sublimation nuclei. Or perhaps, this deviation and the lack of a sharp cutoff in the activity, as specified by the theory, are related to the uncertain relationship between the projected diameters used in Fig. 2 and the spherical particles in the theory. However, the basic agreement between experiment and Fletcher's theory suggests the appropriateness of the assumptions in his derivation. Therefore, contrary to some of the other currently popular nucleation theories (e.g., water cluster theory (10) and the two dimensional crystalization theory (11)), it is necessary to conclude that ice embryos in the shape of spherical caps form on the active sites of AgI when nucleation occurs by sublimation.

AgI Particles Generated With An Acetone Generator In The Field

Over a two week period (Sept. 1969), ten size distributions of atmospheric ice nuclei were measured on Chalk Mt. which is the seeding target area for the Colorado State University cloud seeding project (12). On two days at least two modified Skyfire AgI-NaI ground generators were operated for 12 hours in valleys at least six miles upwind. The foils were evaluated at -20C. On each seeding day the size distribution was typically narrow, was centered at 0.1 μm (at 0.07 μm if the effective density of the nuclei is assumed to be 2.0 gm cm^{-3} instead of 1.0 gm cm^{-3}), and integrated to an average concentration of 105 nuclei L^{-1} for a total sampling time of eight hrs. The background distributions were much broader, were centered at about 0.5 μm, and gave an average concentration of 1.1 nuclei L^{-1} for 18 hrs. (Fig. 3). These findings are in good agreement with a large volume of ice nuclei counts at the same site (13) and clearly demonstrate that the AgI particles actually advected to the summit of Chalk Mt., that little if any coagulation occured in the aerosol during its trajectory, and that the measurement of particle size is a good indicator of the presence of the seeding agent.

REFERENCES

1. Allee, P., H. Gerber, and H. Weickmann, 1968: J. Rech. Atmos., 1-2, 167.
2. Allee, P., H. Gerber, and H. Weickmann, 1969: Proc. VII Intern. Conf. Condensation and Ice Nuclei, Prague and Vienna, 262-267.
3. Goetz, A., H. Stevenson, and O. Preining, 1960: J. Air Pollut. Control Ass., 10, 378-383.
4. Green, H., and W. Lane, 1966: Particulate Clouds., Spon, London, 471 pp.
5. Stöber, W., 1964: Staub, 24, 295-305.
6. Baust, E., 1967: Staub, 27, 16-23. (Engl. Translation)
7. Rabbe, O., 1966: Ph. D. thesis, University of Rochester.
8. Gerber, H., 1970: Submitted for publication in Atmospheric Environment.
9. Fletcher, N., 1958: J. Chem. Phys., 29, 572-576.
10. Zettlemoyer, A., A. Tcheurekdjian, and J. Chessick, 1961: Nature, 192, 653.
11. Edwards, G., and L. Evans, 1968: J. Atmos. Sci., 25, 249-256.
12. Grant, L., and P. Mielke, Jr., 1967: Proc. V Berkeley Sympo. Math. Stat. and Prob., 5, 115-131.
13. Reinking, R., and L. Grant, 1968: Proc. I Nat. Conf. Weather Modification, 433-445.

NATURAL ICE-FORMING NUCLEI IN SEVERE STORMS

J. Rosinski, G. Langer, C. T. Nagamoto, F. Prodi and T. C. Kerrigan
National Center for Atmospheric Research*
Boulder, Colorado

There are two populations of aerosol particles in severe storms: normal background aerosol and aerosolized soil particles. Concentration of the latter, which depends on the wind velocity and soil conditions, may be orders of magnitude higher than those of the former source. Condensation nuclei are derived principally from the first source. Ice forming and freezing nuclei, which derive from the soil particles, increase in concentration during storms up to 100 times the pre-storm value. This concentration increase is less than that of the aerosol population, indicating that only a fraction of soil particles exhibit ice nucleating properties.

The fraction of soil particles active as ice forming nuclei in a given particle size range increases with particle size; however, the concentration of ice forming nuclei in air is counteracted by a decrease in the concentration of aerosol particles with size. A concentration peak of ice-forming nuclei derived from soil particles and active at warmer temperatures occurred in the 7.5-11.5μ diameter size range. In addition to nucleation of supercooled water drops by hydrosol particles, the water soluble soil compounds, upon recrystalization during supercooling, nucleate ice at temperatures as high as -5.3C.

The quantity of water vapor released during the freezing of supercooled water drops was determined experimentally and was also calculated. This value depends primarily on the size of water drops and, to a lesser degree, on the temperature of supercooling. The released water vapor equal to 0.03 to 3.5 mg/l-5 mm diameter drop produces more than a 2% supersaturation with respect to water at the temperature of the environment in a volume of 300 to 10^5 cm^3, respectively. The water vapor recondenses on cloud droplets and aerosol particles acting as condensation nuclei at higher supersaturation. Some of the aerosol particles acting as freezing nuclei will form ice crystals in the water vapor recondensation zone, and these particles will propagate the ice phase within an updraft. This mechanism of ice phase propagation is especially applicable to severe storms where large water drops are formed around giant aerosol particles. These giant particles, after becoming hydrosol particles, are the most effective freezing nuclei derived from the soil and should be responsible for the appearance of ice at the lowest altitude (warmest temperature).

A water drop freezing technique was used to determine the warmest freezing temperature of different hydrosols made of various ices separated from natural hailstones. It was found that this temperature value was not necessarily associated with hailstone embryos. This indicates that many hailstone embryos form at higher altitudes (lower temperature zones) rather than forming at freezing level corresponding to the temperature at which the warmest ice forming nuclei are active.

---

*The National Center for Atmospheric Research is sponsored by the National Science Foundation.

ICE FOG AND ITS NUCLEATION PROCESS*,**

Takeshi Ohtake***
Colorado State University
Fort Collins, Colorado

INTRODUCTION

Ice fogs, which seriously restrict visibility and thus hamper aircraft operation, have become an increasing problem during mid-winter in the interior of Alaska. The ice fog is believed to be composed of many minute ice crystals without water phase particles except very near the sources of fogs (1). The shapes of ice fog crystals are mostly spherical, some hexagonal columns, and irregular crystals, with the sizes 2 to 20μ. The shapes and sizes of crystals vary with temperature as does the concentration of crystals (200 p. cm^{-3} in average)(1). Under humidity conditions of slightly higher than ice saturation, these ice crystals are considered to be aerosols which are produced by discharge of large amounts of water vapor into cold stable air.

Although earlier studies (2, 3, 4) have suggested that the mechanism of ice fog formation is the freezing of water droplets resulting from moisture of car exhaust or open water, they showed neither verifications nor considerations based upon observations for the purpose. Furthermore, in spite of the suggestion, there was no explanation or observation on the relationship between the concentrations of ice fog crystals and ice or freezing nuclei. In the present paper, we studied the problem by considering ice nuclei, condensation nuclei, temperature profiles over open water, which results from power plants cooling water and observations of humidity and evaporation rate under low temperature conditions.

ELECTRON MICROSCOPE STUDY OF ICE FOG NUCLEI

To find out what kind of materials acted as nuclei of ice fog crystals, an electron microscope with a diffraction device was used. To prepare the ice crystal specimens, formvar replications of crystals using the vapor method were made. Many specimens of ice fog crystals were collected at different places and conditions for the study. The sizes of ice fog nuclei are in range of 0.01 to 1μ, which are almost in agreement with Kumai's (3) result. Even though we tried to make the films on blank sheet mesh as clean as possible, sometimes minute particles could be found outside and inside the replicas of crystals. Since identification was difficult in some cases, we measured the most probable and the largest particle inside the replica. If any small particle was found in the crystal we assumed it was a nucleus. However any particles outside of the replicas of ice fog crystals were disregarded as contamination or as dusts which co-existed with ice fog in the air. Nevertheless, we found many ice fog crystals containing no particles inside the crystal replica. It shows that the crystals were frozen spontaneously from supercooled water droplets which had homogeneously condensed from water vapor.

Seventy-one (71) out of 713 crystals inspected by the electron microscope did not have any nucleus in the crystal replicas. Most of these were found in ice fog at Chena and Manley Hot Springs away from the city, at temperatures below -40C. At the IAP site which is located near the open water in Fairbanks, we found no nuclei in about 12% of 110 ice fog crystals we collected when the temperature was -39C. At the center of the city only 2% of 236 ice fog crystals had no nuclei, and a few ice fog crystals had many particles inside of the replicas and few or none outside. These crystals were probably frozen from dirty droplets formed directly from some kind of exhaust such as car exhaust. On the other hand many ice fog crystals even in the center of the city did not have large dust particles. These ice fog crystals must have formed initially from the process of water vapor condensation under conditions of high supersaturation which are available from car, power and heating plant exhausts and from steam coming from open water.

Although we tried to identify the composition of the nuclei by use of the electron microscope and electron diffraction, we could not determine the composition very well, especially for the smallest size nuclei. Some nuclei were presumed to be only carbon black resulting from combustion. Using a morphological determination which was essentially the same as Yamamoto and Ohtake's (5), we found that most (more than 90%) of the ice fog nuclei were classified as combustion by-products.

CONCENTRATION OF ICE NUCLEI AT LOW TEMPERATURES

Since ice fog crystals normally appear in higher temperatures than those of spontaneous freezing corresponding to the particle sizes, it is necessary to measure ice nuclei concentrations in the area. We have had little information about ice nuclei concentrations at temperatures lower than -30C.

Temperature spectrums of ice nuclei concentration were obtained at the Ester Dome (10 miles west from Fairbanks) and at the HAO station, Climax, Colorado, using an NCAR acoustical counter and an expansion counter, respectively. Ice nuclei concentrations obtained by both counters were 100 and 300 nuclei per liter for -35C, respectively. These numbers are very small compared to the

*Full paper is given in "Studies on Ice Fog", Univ. of Alaska Rpt. UAG R-211 (June 1970).

**Supported by the National Center for Air Pollution Administration, P.H.S. under Grant No. AP00449 and partially by NSF Grant GA-1553.

***On leave from the Geophysical Institute, University of Alaska.

concentration of the ice fog crystals. Also 300 n. per liter is the maximum detectable number by the expansion type counter. The concentrations of ice nuclei for various effective temperatures varied by a factor of 10 per 4C in the temperature range between -20C and -35C in the case of the expansion chamber. Assuming that this relation is valid to -39C, we may expect 3,000 n. per liter for a temperature of -39C, which is still almost negligible in comparison to observed ice crystal concentrations in ice fog at a temperature of -39C.

However, these observations were made at places where the air is relatively clean (where condensation nuclei numbers are 200 to 2,000 n. cm^{-3}) and it is expected that the air which contains a lot of condensation nuclei might produce many more ice crystals in the expansion chamber, because the condensation nuclei which made water droplets in the chamber may act as freezing nuclei in the water droplets under such low temperature conditions. In fact, adding some combustion by-products to the air to be tested before the expansion obviously resulted in the formation of many more ice crystals in the chamber under the same temperature conditions. In the chamber of the expansion counter, the degree of supersaturation appears to be very high, even though only momentarily. Thus it is suggested such condensation nuclei are very important for the formation of many ice crystals in a high supersaturation environment in the temperature range between -20C and -37C. In other words, many condensation nuclei in the air must act as freezing nuclei under ice fog conditions.

In the air at temperatures lower than ≈ -37C (diameter of water droplets is assumed about 10μ) some droplets would freeze spontaneously. In clean air with a very high moisture content, a combination of homogeneous condensation and spontaneous freezing must result in a threshold temperature between -37 and -40C. In polluted air in the same temperature range, such a threshold would not be recognized because the crystals can be formed by both homogeneous and heterogeneous nucleation on pure and polluted water droplets.

MECHANISM OF ICE FOG FORMATION

In the present research we have shown that: 1) Large amounts of steam (small droplets), formed in the layer very close to the water surface and disperse into the atmosphere. The evaporation rate of water vapor from the surface and production rate of water droplets were also estimated, based upon the observations. 2) Aerial photographs showed steam or water clouds, which are important sources of ice fog moisture, coming from the open water of the river and cooling ponds, power plants and private heating systems. 3) Such water droplets will freeze in several seconds within a distance of 3 to 5 m from open water under low temperature conditions (1). This was confirmed by the observations of the time required for droplets to freeze, and temperature profiles above water surfaces. Also it was supported by calculation of conductive cooling and radiative cooling, which were also directly measured by means of a radiometer for various objects in ice fog (6). Auto exhausts supplement water droplets and they will be changed to ice fog crystals in the same way. So running cars are sprinkling ice crystals rather than adding moisture as vapor into the atmosphere. 4) The humidity in ice fog lies slightly higher than ice saturation, allowing minor ice crystal growth. This results in ice fog crystals having the smallest size of ice crystals and being suspended in the air for a long time. 5) The most important factor in the formation of steam or water droplets is not the concentration of condensation nuclei in the case of steam from open water, heating plants and car exhausts under ice fog conditions but rather the temperature differences between water (not ice) and ambient air temperature. However, condensation nuclei or other particles contained in the water droplets accelerate the freezing of water droplets at a higher temperature than the spontaneous freezing. The onset temperature of ice fog formation is higher in inhabited areas than in unpolluted areas due to the greater numbers of condensation nuclei and effective freezing nuclei in the city, as well as the difference of moisture supply between in-city and out-of-city sites. However, at temperatures lower than about -37C, the homogeneous nucleation of condensation and successive spontaneous freezing of water droplets are quite possible even in contaminated areas. 6) The lowering of air temperature increases the rate of evaporation from consistent moisture sources, i.e. rate of water-droplet formation, speed of the droplet freezing, suppression of the ice-crystal growth, and formation of more numbers of smaller crystals. Thus, denser ice fog can be seen at lower temperatures. So the low temperatures are essential for dense ice fog, providing constant moisture sources are available.

REFERENCES

(1) Ohtake, T., 1970: Studies on Ice Fog, Univ. of Alaska Rpt. UAG R-211, 179 pp.

(2) Robinson, E., and collaborators, 1954: An Investigation of the Ice Fog Phenomena in the Alaskan Area. Final Rpt., Contract No. AF19(122)-634, Stanford Research Institute, 65 pp.

(3) Kumai, M., 1964: A Study of Ice Fog and Ice Fog Nuclei at Fairbanks, Alaska, Part I, CRREL Rpt. 150, 27 pp.

(4) Benson, C.S., 1965: Ice Fog: Low Temperature Air Pollution, U. of Alaska Rpt. UAG R-173, 78 pp.

(5) Yamamoto, G. and T. Ohtake, 1953: Electron Microscope Study of Cloud and Fog Nuclei. Sci. Rpt. Tohoku Univ., Ser. 5, Geophy. 5, 141-159.

(6) Ohtake, T., 1968: Freezing of Water Droplets and Ice Fog Phenomena, Proc. Intn. Conf. Cloud Phys., Aug. 1968, Toronto, 285-289.

ICE NUCLEI ACTIVE AT LOW TEMPERATURES AND HUMIDITIES

E.K. Bigg and R.T. Meade

Division of Radiophysics, C.S.I.R.O., Sydney, Australia

Ice crystals are usually plentiful in clouds at temperatures below -25°C so that initiation of the ice phase in the atmosphere has generally been studied at warmer temperatures where the presence or absence of ice nuclei may be crucial to the efficiency of the precipitation process.

However, high level clouds may also be important to the development of weather systems, for they alter very considerably the radiation budget of the ground beneath them and they may also seed lower clouds with ice crystals. They commonly arise from air undergoing gradual and widespread lifting, and to understand their mode of formation we must examine at low temperatures the way in which the number of ice crystals formed varies with humidity.

Membrane filters, which are so useful at warmer temperatures for capturing and detecting ice nuclei, contain many nucleation sites active at low humidities at temperatures below -30°C. They are useful only for studying the onset of nucleation by aerosols as the humidity is lowered, for the large number of "background" crystals depresses the actual humidity in a thermal diffusion chamber. Significant differences between crystal totals on exposed and unexposed filters are first found at humidities approximately half-way between ice and water saturation at temperatures below -30°C. This is at about 85% humidity relative to water.

In order to find the full curve of number of ice crystals as a function of humidity it is necessary to find a supporting surface which is relatively inactive. So far our most successful method has been to coat a metal disc with a thin layer of "Teflon" (polytetrafluorethylene) sprayed on from solution in a clean room. The metal disc is then used as the cold plate of a thermal precipitator. The aerosols present in samples of a few liters of air are precipitated and the ice crystals "developed" in a thermal diffusion chamber. Figure 1 shows the appearance of the ice crystals formed at -30°C and a humidity nominally at water saturation. The patch of higher concentration is located immediately below the air inlet.

We find that the first ice crystals (one per 10 ℓ) appear at humidities between 80% and 90% (relative to water) and that their concentration increases to about 10 ℓ^{-1} to 100 ℓ^{-1} at water saturation. However, the large number of crystals formed at higher humidities obviously reduces the true humidity at the surface in the diffusion chamber which we use. We have not yet discovered a surface which is sufficiently clean to allow smaller air samples to be used. Concentrations of crystals vary rapidly with humidity at a given temperature but not very rapidly with temperature at a given (low) humidity.

The implication of these results is that where the atmosphere is undergoing steady uplift there should first occur ice-supersaturated layers almost totally devoid of ice crystals. As uplift continues, some ice crystals will form and continue to grow as they fall through the ice-supersaturated layer below but may not become large enough or be numerous enough to form a visible cloud. The maximum depth of this layer if the temperature is near -40°C is likely to be about 200 m, for the temperature difference between ice and water saturation is then about 3.6°C. The final stage will be reached when the humidity becomes high enough to activate sufficient nuclei to form a visible cloud.

A direct test of the existence of such supersaturated layers is to release a small meteorological balloon carrying a few hundred grams of dry ice. Wherever an ice-supersaturated layer is encountered the ice crystals left in its wake grow rapidly and are readily visible from the ground. Figure 2 shows such a cloud, which had a vertical extent of about 200 m at a height of 8000 m and a temperature of -35°C. Thin altocumulus and cirrus formed in the vicinity about an hour later when this cloud was still visible.

Aircraft condensation trails are a familiar sight, but because the aircraft engines introduce additional water vapour are not proof of natural supersaturation. Inadvertent weather modification caused by these trails may become a major problem, and to understand it we must know the frequency of occurrence and the depth and degree of supersaturation of ice-supersaturated layers. We suggest that the simple balloon experiment which we have described could be widely applied with relatively little effort in order to provide this information.

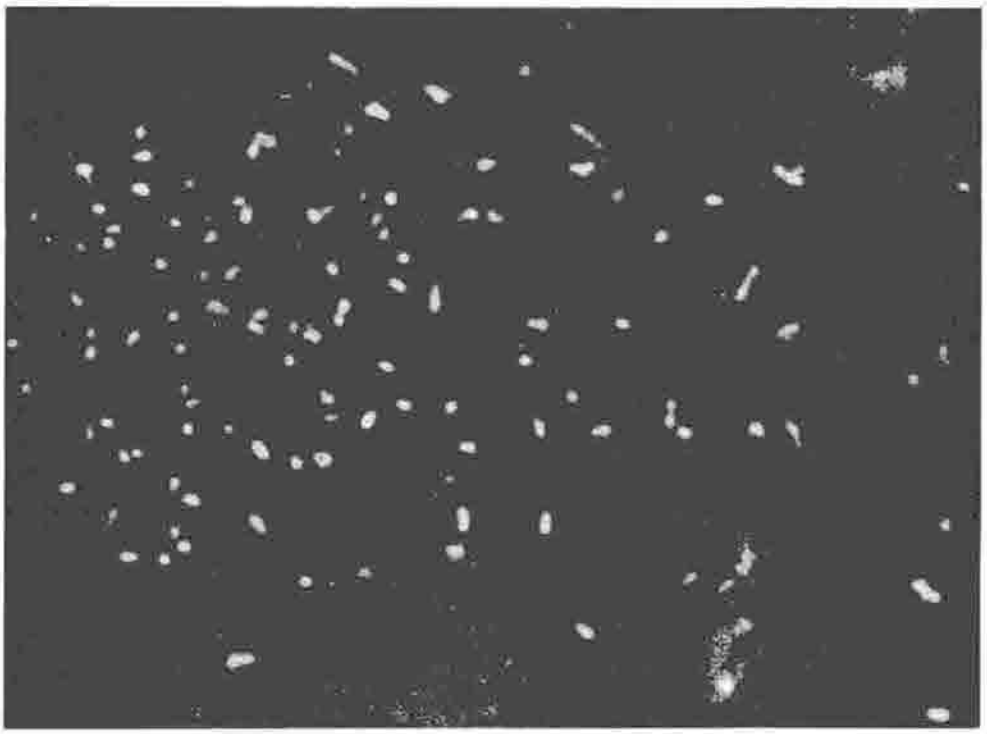

Fig. 1 Ice crystals grown from nuclei thermally deposited on a Teflon-coated metal plate. Temperature -30°C, water saturation.

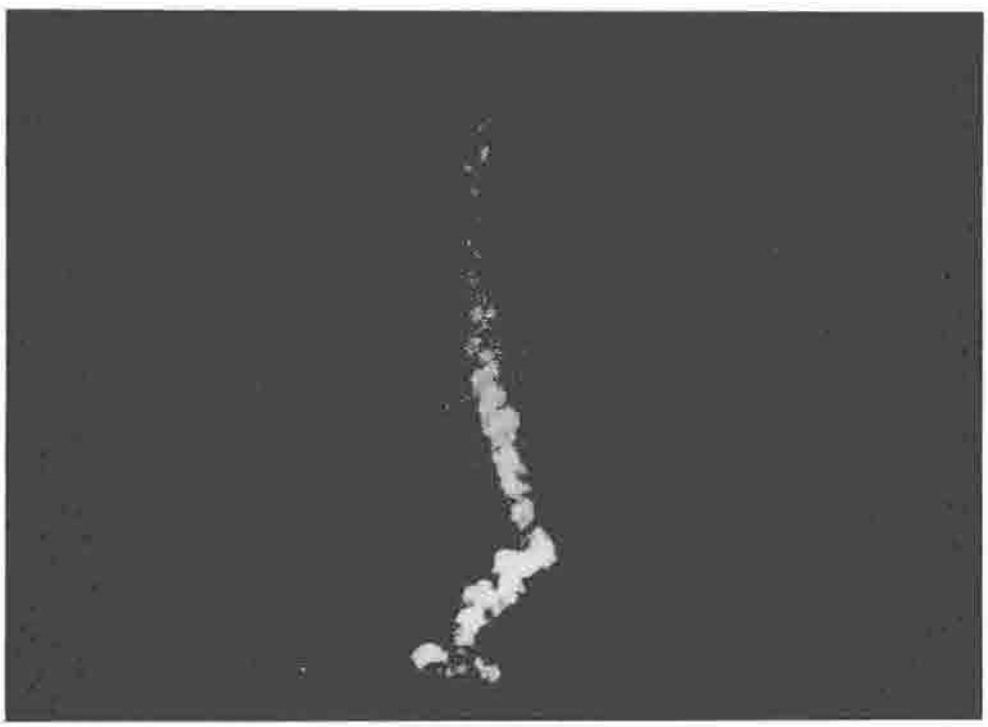

Fig. 2 Cloud formed at 8000 m in a clear sky by a small balloon carrying dry ice.

INTERACTION BETWEEN SILVER IODIDE AND WATER VAPOR AT HIGH RELATIVE PRESSURES

M. L. Corrin and W. R. Barchet
Atmospheric Science Department
Colorado State University
Fort Collins, Colorado 80521

INTRODUCTION

Measurements of the adsorption of water vapor on silver iodide at high relative pressures are noticeably lacking. Volumetric adsorption techniques limited the studies of previous investigators to relative pressures less than 0.9. These low relative pressure measurements on both pure and hygroscopically contaminated silver iodide powders demonstrate the hydrophobic character of the silver iodide surface with adsorption occuring primarily on hydrophilic sites. Gravimetric adsorption techniques circumvent the high relative pressure corrections required in volumetric approaches. The region near ice and liquid water saturation is of prime interest in this work.

MATERIALS AND METHOD

Silver iodide prepared by the method of Corrin, Nelson, Cooley and Rosenthal (1) is used for all adsorption measurements. Distilled, degassed water transferred by distillation into an adsorbate reservoir provides the water vapor.

A Cahn Electrobalance is used to detect the increase in weight of a tared sample of silver iodide as water vapor is adsorbed. Separate constant temperature baths around the sample and adsorbate reservoir specify the saturation vapor pressure (sample temperature) and vapor pressure respectively.

The sample weight in equilibrium with a given adsorbate reservoir temperature gives a point on an adsorption isotherm. Stepwise increases in the adsorbate reservoir temperature produces the isotherm. All temperatures are determined to ± .01°C. Isotherms at -3, -6.5, and -10.0C were measured.

THEORY

Adsorption thermodynamics makes direct use of adsorption isotherms in computing the heat of adsorption and the change in surface free energy of the adsorbent. The Gibbs equation allows the computation of the latter:

$$\pi_x = \gamma_o - \gamma_x = RT \int_o^x \Gamma \, d\ln x' = RT \int_o^x \frac{\Gamma}{x'} \, dx' \qquad (1)$$

where π_x = spreading pressure or change in surface free energy, γ, due to the presence of the adsorbate in equilibrium with a relative pressure x; T = absolute temperature; Γ = surface excess or amount of vapor adsorbed; R = gas constant; and x = relative pressure p/p_o.

The isosteric heat of adsorption is found from isotherms at different temperatures using a Clausius-Clapeyron equation:

$$\left(\frac{d\ln x}{dt}\right)_\Gamma = \frac{\Delta\tilde{s}_{vl} - \bar{s}_\sigma}{RT} = \frac{\Delta\tilde{h}_{vl} - \bar{h}_\sigma}{RT^2} = \frac{q_{st}}{RT^2} \qquad (2)$$

where $\Delta\tilde{s}_{vl}$ = molar entropy change in vapor to liquid transition; $\bar{s}_\sigma$ = partial molar entropy of absorbate; $\Delta\tilde{h}_{vl}$ = heat of vaporization; $\bar{h}_\sigma$ = partial molar heat of adsorption; and q_{st} = isosteric (constant Γ) heat of adsorption.

RESULTS

Low pressure adsorption isotherms of Corrin and Nelson (2) were interpolated to the sample temperatures used here using equation (2). Integration of the Gibbs equation was extrapolated to zero with the Dubinin-Radushkevich model. At higher relative pressures a numerical integration was used.

The isosteric heats of adsorption showed a maximum at low relative pressures and a tendency to approach the heat of condensation as the relative pressure increased. This indicates a transition of the adsorbed film to a liquid-like state. For the film to become ice-like, an increase in the heat of adsorption at higher relative pressures must occur.

The spreading pressure gives the minimum surface free energy of the "bare" adsorbent at which wetting will not occur. This minimum increases rapidly as saturation is approached requiring, in effect, the contact angle to increase also.

The decrease of the surface free energy of the adsorbent and the trend of the heat of adsorption toward the heat of condensation with increasing relative pressure substantiates the clustering model of adsorption and provides some insight into the mechanism of heterogeneous nucleation on silver iodide.

1. M. L. Corrin, J. A. Nelson, B. Cooley, and B. Rosenthal; The Preparation of "Pure" Silver Iodide for Nucleation Studies. J. Atmos. Sc., 24, 1967, (594).

2. M. L. Corrin and J. A. Nelson; Energetics of the Adsorption of Water Vapor on "Pure" Silver Iodide. J. Phys. Chem., 72, 1968, (643).

DETERMINATION OF CRYSTALLITE SIZE AND ANELASTIC STRAIN IN VARIOUS TYPES OF GENERATOR EFFLUENT

Ronald L. Petersen and Briant L. Davis
Institute of Atmospheric Sciences, South Dakota School of Mines and Technology
Rapid City, South Dakota 57701

INTRODUCTION

This paper is concerned with certain physical characteristics of AgI aerosols, namely, the "apparent particle size" and anelastic strain. With these quantities the physical state of aggregation of AgI-NaI aerosols and the amount of strain energy stored in the crystallites can be surmised.

THEORY AND EQUATIONS

The determination of the strain and "apparent particle size" of the AgI and NaI aerosol particles generated by the combustion of various solutions of the two components was accomplished by determining the integral breadth of the pure x-ray diffraction profile, f(x), that profile with broadening due to strain and/or particle size alone. This involves the Stokes Fourier analysis[1] of the unbroadened profile, g(x), or that profile due to instrumental effects alone, and a profile, h(x), which has broadening due to strain and/or particle size and instrumental effects. The convolution equation relating these profiles is given by

$$h(x) = \int_{-\infty}^{\infty} f(y)\, g(x-y)\, dy. \tag{1}$$

The equation for calculating f(x) derived from (1) was found to be

$$f(x) = \sum F_r(t) \cos(2\pi xt/a)\Delta t + \sum F_i(t) \sin(2\pi xt/a)\Delta t, \tag{2}$$

where

$$F_r = [H_r G_r + H_i G_i]/[G_r^2 + G_i^2]$$
$$F_i = [H_i G_r - H_r G_i]/[G_r^2 + G_i^2]$$

and H_r, H_i, G_r, and G_i are the real and imaginary Fourier coefficients of h(x) and g(x) respectively.

The integral breadth, β, of f(x) is then calculated for use in the following equation[2]

$$\beta^* = \xi d^* + 1/D, \tag{3}$$

where $\beta^* = \beta \cos(\theta)/\lambda$, and $d^* = 1/d$ where d is the interplanar spacing, ξ the root-mean-square strain, D the "apparent particle size" and θ the Bragg angle. From Eq. (3) it can be seen that if plots of β^* versus d^* are made, the slope of the line will give ξ and the β^* intercept the reciprocal of D.

The stress, P, was calculated by making use of a relation due to Stokes and Wilson[3]

$$P = \xi/[2(A + BH)], \tag{4}$$

where $A = S_{12}$, $B = -2(S_{11} - S_{12} - \frac{1}{2}S_{44})$, and $H = (k^2\ell^2 + \ell^2h^2 + h^2k^2)/[(h^2 + k^2 + \ell^2)^2]$. The S_{ij} are the elastic compliances of the crystal; the $(hk\ell)$ represent the Miller indices of the parallel planes which are perpendicular to the direction of the normal stress.

The strain energy was calculated from

$$W = P_{hk\ell}\xi/2 \tag{5}$$

and the mean value for the sample was defined by

$$\overline{W} = (W_{max} + W_{min})_{hk\ell}/2 \tag{6}$$

EXPERIMENTAL METHOD

The test samples (samples with stored strain and small particle size) were prepared by the combustion of various solutions of AgI and/or NaI. The control samples (samples with large particle size and negligible strain) were prepared by grinding AgI under liquid nitrogen and by precipitating a nearly saturated solution of NaI onto filter paper. The samples were then analyzed using x-ray diffraction techniques.

The experiment consisted of four different series of runs. The test samples for Series I were obtained by burning a 3% by weight solution of NaI in acetone, Series II by burning a 6% by weight solution of AgI in isopropylamine (IPA), Series III a 3% AgI by weight, 2:1 molar AgI to NaI, acetone solution, and Series IV the same solution as for Series III only the NaI was washed from the filter paper before the x-ray analysis.

RESULTS

A summary of the results of the analysis can be seen in Table I and Fig. 1. Due to space limitations only the results involving the AgI will be discussed.

For Series II, runs 1a, 2a, and 3, and 1b and 2b designate the results before and after annealing respectively. No annealing was involved in the Series IV experiment.

The decrease in strain with annealing can be noticed along with the decrease in strain energy. The greater residual strain energy of AgI-IPA as compared with the AgI-NaI-acetone (washed) generated aerosols can also be seen. Previous work[4] would tend to indicate that the former are more effective as ice nuclei than the latter. It can also be noticed that the strain energy values all fall below the theoretical maximum of 4×10^4 ergs/gm[4].

Table I

A summary of the results for each series of runs, where ξ is the root-mean-square strain, D the "apparent particle size," and $\overline{W}$ the average strain energy.

	Run No.	ξ	D(μ)	$\overline{W}$(ergs/gm)
Series I (NaI-acetone)	1a	.00116	.1272	1.988×10^4
	1b	.00112	.1068	1.977×10^4
	2	.00031	.0773	$.153 \times 10^4$
	3	.00059	.0931	$.512 \times 10^4$
Series II (AgI-IPA)	1a	.00188	.0819	2.567×10^4
	1b	.00097	.0757	$.683 \times 10^4$
	2a	.00159	.0816	1.821×10^4
	2b	.00066	.0719	$.318 \times 10^4$
	3	.00129	.0840	1.198×10^4
Series III (AgI-NaI-acetone)	1	.00015	.0866	$.324 \times 10^3$
	2a	.00019	.0837	$.526 \times 10^3$
	2b	.00051	.0913	3.845×10^3
	3	.00020	.0975	$.603 \times 10^3$
Series IV (AgI-NaI-acetone washed)	1	.00040	.0816	1.161×10^3
	2	.00021	.0529	$.317 \times 10^3$
	3	.00053	.0730	1.918×10^3

The average particle sizes for Series I thru IV respectively were 0.1011, 0.0790, 0.0898, and 0.0692 microns. The composite average was 0.0847 microns. The extreme values of 0.1272 and 0.053 microns can be explained by variables in the sample preparation technique.

SUMMARY

1. The composite "apparent particle size" for all series of runs was 0.0847 microns, a result that compared favorably with the results of another worker in the field.(5)

2. The physical state of aggregation of the AgI-NaI aerosols was deduced to be that of distinct particles instead of shell-core composite particles.

3. The stored strain energy of the washed AgI-NaI aerosols was significantly lower than the stored strain energy of the AgI aerosols generated from an IPA solution.

4. The effect of annealing was noticed in the AgI aerosols generated from the IPA solution but the effect would be insignificant for cloud seeding operations. The effect of annealing on the AgI-NaI aerosols would not be noticed due to the already low strain energy values for the unannealed samples.

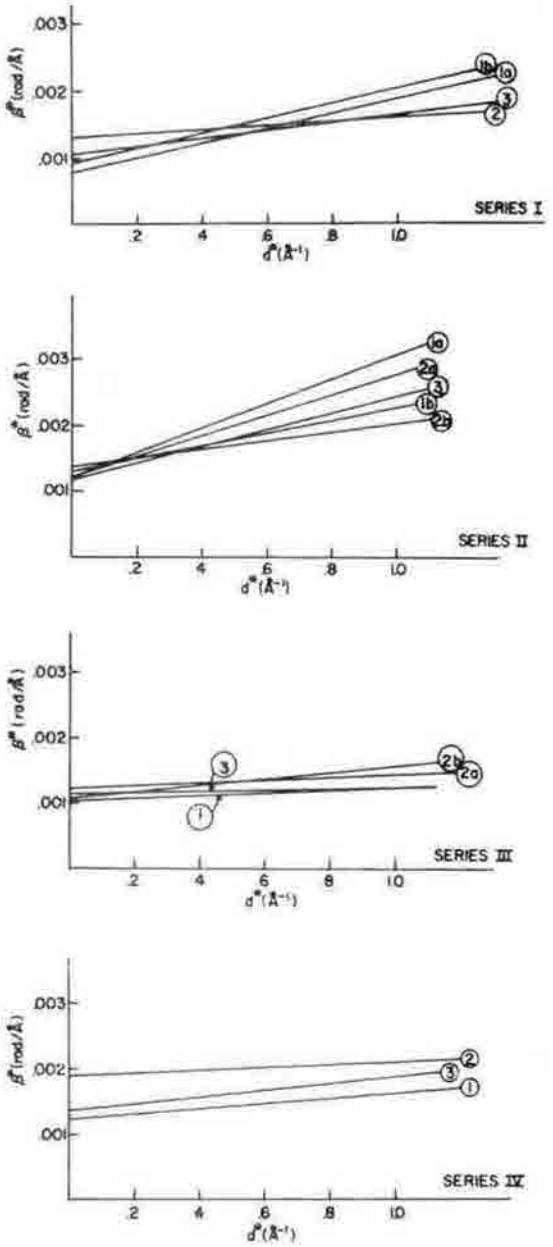

Fig. 1. Summary of the β^*-d^* plots for each series of runs.

ACKNOWLEDGMENTS

This research was carried out under the sponsorship of the Office of Atmospheric Water Resources, Bureau of Reclamation, U. S. Department of the Interior, Contract No. 14-06-D-6796.

REFERENCES

(1) Stokes, A. R., 1948: A numerical Fourier-analysis method for the correction of widths and shapes of lines on x-ray powder photographs. Proc. Phys. Soc., 61, 382-391.

(2) Williamson, G. K., and W. H. Hall, 1953: X-ray line broadening from filed aluminum and wolfram. Acta. Met., 1, 22-31.

(3) Stokes, A. R., and A. J. C. Wilson, 1944: The diffraction of x-ray by distorted crystal aggregates. Proc. Phys. Soc., 56, 174-181.

(4) Davis, B. L., and D. N. Blair, 1969: Role of substrate strain in ice nucleation. J. Geophys. Res., 74, 4571-4580.

(5) Mossop, S. C., and C. Tuck-Lee, 1968: The composition and size distribution of aerosols produced by burning solutions of AgI and NaI in acetone. J. Appl. Meteor., 7, 234-240.

FREEZING NUCLEATION BY SILVER IODIDE COMPLEXES

by

Gabor Vali
University of Wyoming
Laramie, Wyoming

and

William G. Finnegan
Naval Weapons Center
China Lake, California

A great deal of effort has gone into comparing the ice nucleating activity of pure silver iodide with aerosols produced by methods which use sodium iodide or potassium iodide as solubilizers. These comparisons have been extremely beneficial not only from the practical point of view but also in helping to elucidate the modes of ice nucleation for silver iodide. St. Amand et al., (1968) pointed out the possible importance of the complexes that form from the silver and alkali iodides and postulated that due to their hygroscopic nature, the complexes condense water from which silver iodide precipitates upon further dilution and acts as a freezing nucleus. Burkardt et al., (1970) has shown that the activities of wide varieties of complexes in a cloud chamber were higher than that of pure silver iodide. Mossop and Jayaweera (1969) have also argued that AgI-NaI aerosols act as freezing nuclei.

Various silver iodide complexes were tested by the drop freezing technique: this method detects the freezing nucleating ability of the suspended material in bulk water. For each sample approximately 200 drops of 2.7 mm diameter were frozen and the freezing temperature recorded with 0.25C resolution. The result of a typical experiment is shown in Figure 1: Various dilutions of a 3KI·AgI suspension were used to determine the nucleus concentrations over a wide range, and original nucleus concentrations with respect to volume of water have been converted to nuclei per gram of silver iodide on the bases of the dilution factors. There is a characteristic break in the curve such that the rapid increase in concentrations between -5C and -10C is followed by very little increase until -20C is reached, beyond which the nucleus concentrations again increase rapidly. The relatively low numerical efficiency for silver iodide in this sample as compared to aerosols is due to the larger particle sizes used. The results of a series of experiments, in which the proportions of the silver iodide to alkali iodides were altered, is shown in Table 1. Here the nucleation activity is characterized by the average freezing temperature of the drops which corresponds to approximately 10^6 nuclei per gram of AgI. For each series shown in Table 1 finely ground solid, whose composition is given by the first line for each series, was introduced into the water and subsequently further amounts of potassium iodide or sodium iodide were added to alter the composition. The large change in freezing temperatures due to the addition of potassium iodide (Series A) seem significant. The changes in freezing temperature for sodium iodide (Series B and C are relatively small and it is unclear why the shifts occur in opposite directions in the two tests. Regarding the applicability of these results to aerosols produced by the burning of solutions of different compositions it remains to be established whether the addition of further amounts of alkali iodides to a suspension is equivalent or not to changing the composition of the solid material before it is introduced into the water. The dependence of solubility on particle size may also need to be considered. It is in these directions that an explanation will have to be sought for the lack of activity found by Vali (1968) for an AgI-NaI aerosol.

For another series of experiments, 0.4 mole AgI was dissolved in a 4 molal solution of KI which was then diluted with varying amounts of water. The concentrate was found to be a true solution by the lack of Tyndall-scattering of a laser beam, in agreement with the solubility found by Mills et al., (1970). The experimental results are shown in Figure 2. The vertical bars for each sample indicate the range of freezing temperatures of the drops and correspond to the range in which the nucleus content increases from 1 to 10^3 per gram of solution. Precipitation from the solution was visually observed when the KI molality was reduced to below 1.2. Some nucleation activity was, however, observed for even more concentrated solutions; the nucleation activity increased gradually with increasing dilution and leveled off in the neighborhood of 0.07 mole AgI and 0.7 mole KI. The melting points of the concentrated solutions were noted in two cases as indicated by circles in Figure 2 and calculated from standard formula for dilute solutions as shown by crosses in Figure 2. The parallel trend between the melting point curve and the temperatures of activity is quite striking. The gradual increase in nucleation temperature with greater dilutions is due to reductions in the melting point depressions and to increased precipitation of AgI from the solution. The latter effect, if isolated, may perhaps be related to the sizes of the particles.

One of the interesting features of the freezing nucleation experiments with AgI complexes is the alteration of activity with successive cycles of freezing and melting. Figure 3 shows an example of a gradual rise in nucleation temperature for a drop containing 10^{-3} parts by weight of 3KI·AgI. The average freezing temperature for 80 drops rose from -8C to -3.9C after 18 cycles of freezing and melting The warmest freezing temperature at the end of the sequence for an individual drop was -2.8C. Increasing nucleation temperatures is with recycling were found for the majority of the samples. The increases cannot be accounted for on the basis of a time effect since additional periods of 10 to 20 minutes at -4C to -6C have not resulted in warmer nucleation temperatures. This behavior for the AgI complexes is quite different from the patterns obtained for other substances which showed essentially unchanged nucleation temperatures when repeatedly frozen and melted. It is thought that the increasing effectiveness (ripening) of the complexes indicates a lack of stability of the particles or of the nucleation sites on their surface. Recrystallization is probably occurring due to changes in solubilities with temperature (Mills et al., 1970) and a change in particle sizes may also be involved with the larger particles growing at the expense of the smaller ones. Apparently the new surfaces created in the process have improved abilities to nucleate ice.

The sizes of the particles involved in these tests are of obvious importance. It was found that filtering any of the samples with 0.02 micron pore diameter filters removed essentially all nucleation activity. Filtration with 1.2 micron pore filters on the other hand resulted in only a relatively small reduction in nucleation activity. An example of ripening mentioned in the previous paragraph is shown in Figure 4. Unfiltered and filtered samples were processed simultaneously with approximately 1 degree colder freezing temperatures for the filtered sample initially. This difference gradually disappeared as the samples were refrozen several times until the average freezing temperatures for the filtered sample became qual to and even exceeded the temperatures for the unfiltered sample.

It is evident from the results presented above that the silver iodide complexes are indeed effective sources of freezing nuclei under the circumstances of these tests. Extensions of the work to smaller particle sizes will assure greater transferability of the results to problems of cloud nucleation. Explanation of many of the facts observed will require a better understanding of the physical state of the silver iodide complex/water system.

REFERENCES

Burkardt, L. A., W. G. Finnegan, F. Kirk Odencrantz and Pierre St. Amand, 1970: Pyrotechnic production of nucleants for cloud modification - Part IV -- Compositional effects on ice nuclei activity. J. Weather Modification, 2(1), 65-76.

Mills, D. R., C. M. Perrott and N. H. Fletcher, 1970: The production of single crystals of AgI. Journal of Crystal Growth, 6, 266-268.

Mossop, S. C. and K. O. L. F. Jayaweera, 1969: AgI-NaI aerosols as ice nuclei. J. A. M., 8, 241.

St. Amand, P., W. G. Finnegan, L. Burkardt and F. K. Odencrantz, 1968: Effects of the type of nucleant on modification of clouds for the stimulation of rainfall. Paper presented at First National Conference on Weather Modification, Albany, New York.

Vali, G., 1968: Filter elutrition experiments for the measurement of airborne freezing nuclei. J. Rech. Atmos., III(2), 175-177.

TABLE 1

SERIES	COMPOSITION	AVG. FREEZING TEMP.	
A	3KI·AgI	-7.2	1.5×10^{-4}m AgI
	6KI·AgI	-8.5	
	12KI·AgI	-11.0	
	48KI·AgI	-11.0	
B	0.7 NaI·AgI	-6.5	2.2×10^{-3}m AgI
	4 NaI·AgI	-5.8	
	8 NaI·AgI	-5.4	
C	0.5 NaI·AgI	-7.5	1.6×10^{-3}m AgI
	2 NaI·AgI	-7.9	
	24 NaI·AgI	-8.4	
D	AgI	-6.4	4.1 x 10-3m

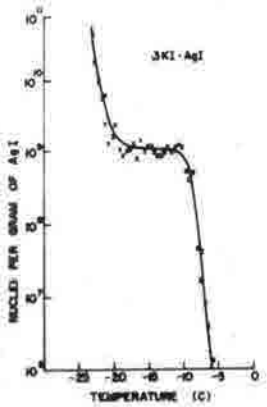

Figure 1

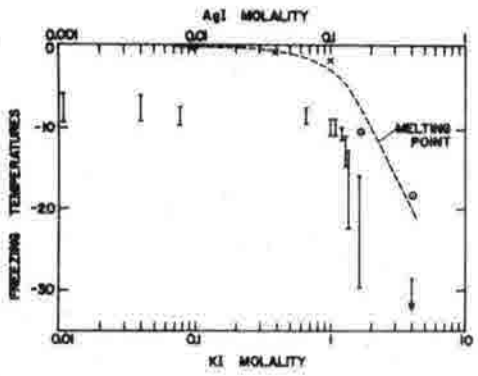

Figure 2

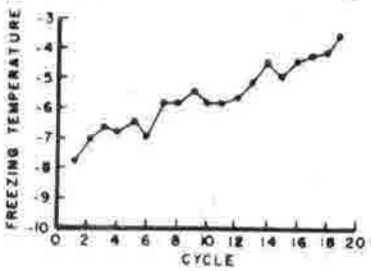

Figure 3

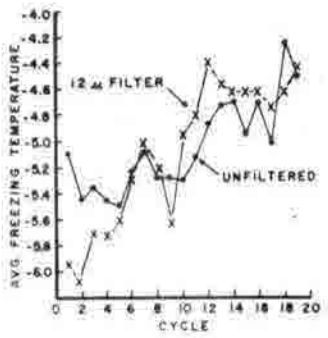

Figure 4

This research was made possible by the U.S. Department of the Interior, Bureau of Reclamation, OAWR, under contract No. 14-06-D-6801 (July 1, 1969) and by the Naval Weapons Center under contract No. N66001-70-C-0639 to the NRRI, University of Wyoming.

RELATION BETWEEN ICE FORMING ABILITY AND CONDITIONS OF FORMATION OF SILVER IODIDE NUCLEI

by

H. Isaka, R. Pejoux and G. Soulage
(Faculté des Sciences de Clermont-Fd - France)

Since the discovery of the effects of AgI nuclei on supercooled clouds various devices to produce these nuclei have been investigated but very often empirically or incompletely. In the past, some authors (Dessens (1) , Steele (2), (3), ...) have partly studied the problem under its thermodynamical aspect.

In this paper, we reexamine it under the same aspect for a "Skyfire" generator burning an acetone solution of AgI and NaI. We study successively :

- the spraying and the combustion of acetone droplets ;
- the vaporization of AgI in the flame of the burner ;
- the size spectrum of the produced nuclei in various conditions ;
- the ice forming properties of the same nuclei as a fonction of the size spectrum.

Then we try to explain the results theoretically.

For this work, we have built an experimental "Skyfire" burner and a device (fig. 1) enabling us to control each parameter (stoichiometric ratio of combustion, temperature, dilution, ...) governing the production of nuclei.

A first result that we have obtained concerns the positive effect of an auxiliary combustible (propane) on the output of a generator burning an acetone solution of AgI. Auxiliary combustible raises the temperature of flame and favors the complete evaporation and combustion of solution droplets as well as the complete vaporization of AgI.

Stoichiometric ratio	Distribution parameters		Median radius
	Median ($\log_{10}$ R)	Standard deviation	
0.5	2.71	0.21	510
1	2.54	0.31	350
1.5	2.75	0.24	560

Tab. 1

A second result is relative to the variation of the size spectrum of the produced nuclei (tab. 1) and, consequently, the variation of the ice forming ability of the same nuclei (fig. 2) as a fonction of the stoichiometric ratio of combustion. The radius of nuclei decreases as the stoichiometric ratio varies from 0.5 to 1, then increases as the stoichiometric ratio varies from 1 to 1.5. At the same time, the number of nuclei effective below -8°C increases when the stoichiometric ratio changes from 0.5 to 1, then increases when it changes from 1 to 1.5. For a temperature above -8°C, the number of effective nuclei increases, not only when the stoichiometric ratio increases from 0.5 to 1, but also when it increases from 1 to 1.5. This result shows one must use a stoichiometric ratio of 1.5 to get a greater output of nuclei effective at high temperature.

At last we have experimentally found that the acetone vapor deactivates the AgI ice nuclei at high temperatures. This fact might explain the decrease of effective ice nuclei observed above -8°C for a stoichiometric ratio of 0.5.

The above results are discussed from the point of view of ice nucleation theories : kinetic theory of ice nucleation and theory of "ice nucleation site" proposed by Katz (4). The first of these theories explains our experimental results better than the second.

REFERENCES

(1) Dessens, H., 1961 : "Le générateur de noyaux d'iodure d'argent de l'Association d'Etudes", Bull. Obs. Puy de Dôme, 1, p. 23.

(2) Steele, R.L. and Sciacca, F.W., 1966 : "Characteristics of silver iodide ice nuclei originating from anhydrous amonia - silver iodide complexes : Part II - Thermal systems", J. R. Atm., 2, p. 315.

(3) Davis, C.I. and Steele, R.L., 1968 : "Performance characteristics of various artificial ice nuclei source", J. Appl. Meteor., 7, p. 667.

(4) Katz, U., 1962 : "Wolkenkammeruntersuchungen der Eiskeimbildungsaktivität einiger ausgewählter Stoffe", ZAMP. 13, p. 333.

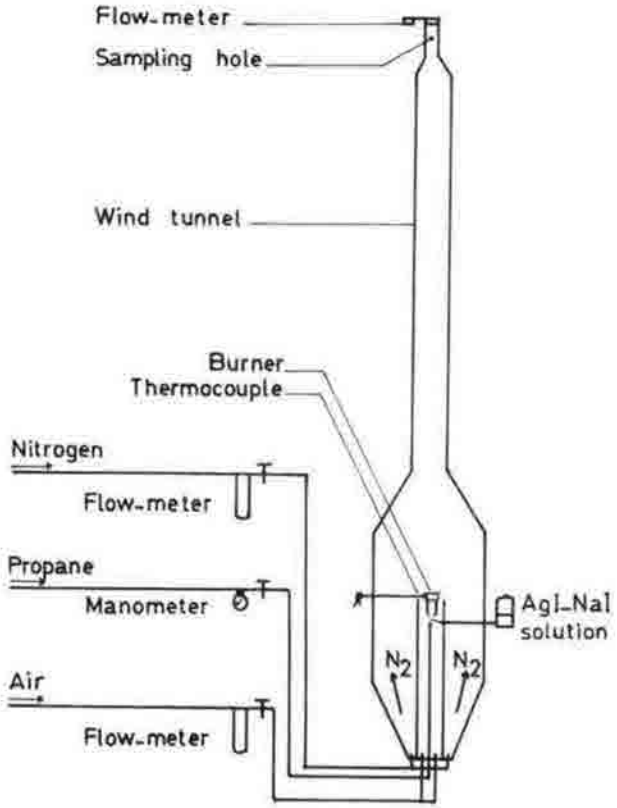

Fig. 1

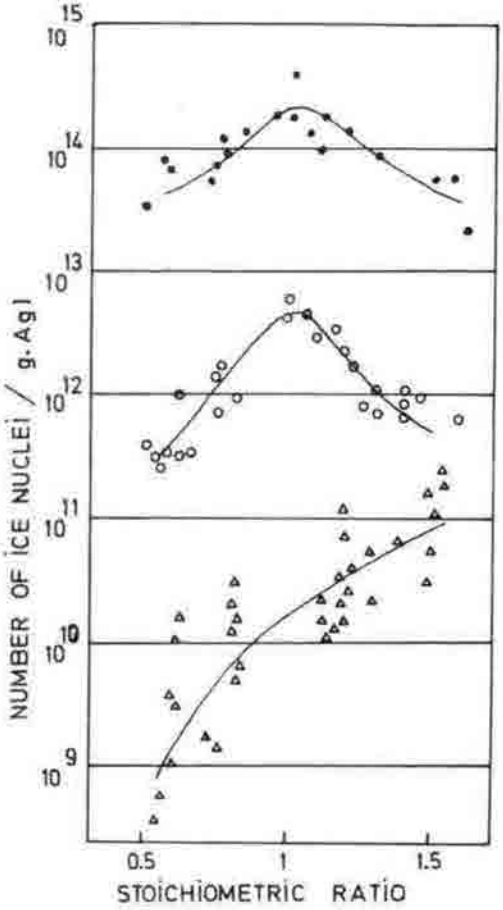

Fig. 2

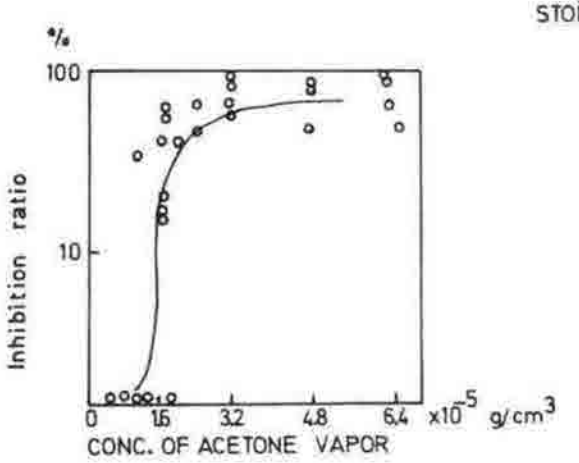

Fig. 3

EVALUATION OF THE FILTER TECHNIQUE FOR ICE NUCLEI MEASUREMENT

A. J. Alkezweeny
Meteorology Research, Inc., Altadena, California

INTRODUCTION

One of the difficult problems in cloud physics today is the design of an instrument by which the ice nuclei concentration in the air can be measured precisely. All the available nuclei counters lack precise control of temperature and supersaturation, effect of frost forming on the inner walls of the counter, and the limitation of detection technique. Therefore, they do not reproduce atmospheric conditions (1, 2).

The millipore filter technique which was introduced by Bigg et al. (3), and later improved considerably (4, 5, 6) has shown promising results. This paper discusses some aspects of the technique and compares the results with other nuclei counters.

THE EFFECT OF SUPERSATURATION

Two filters were exposed at the top of the MRI building. Sampling volume of air was 100 and 200 liters for filters (a) and (b), respectively. The two filters were processed in the same diffusion chamber at a temperature of -18C, and different supersaturation values. The results are shown in Table I. The number of active nuclei increased with increasing supersaturation. However, the rate of increase of the nuclei was not the same for both filters. Furthermore, no increase was detected between 22 and 60 percent supersaturation.

Table I
THE EFFECT OF SUPERSATURATION ON THE ICE NUCLEI CONCENTRATION

No. of Ice Crystals Grown on the Filter Surface		Supersaturation (%)
Filter (a)	Filter (b)	
13	27	1
25	35	6
30	36	11
31	39	22
31	41	33
31	41	46
31	41	60

Table II
ICE NUCLEI COUNTS USING DIFFERENT PORE SIZE

Pore Diameter (μm)	Total Count at Temperature of			
	-15C	-18C	-20C	-23C
0.025	8	18	31	38
0.05	0	3	8	12
0.10	5	12	17	20
0.30	2	8	18	19
0.45	2	7	10	15

EFFECT OF PORE SIZE

Five millipore filters of different pore sizes were exposed to 100 liters of air at the top of the MRI building and processed at four different temperatures, and the results are shown in Table II. The highest counts at each temperature were obtained with the small pore size filters. With one exception, the 0.05 μm size, the trend at each temperature is for higher counts with smaller pore size. Before attaching much significance to the pore size effect, it must be emphasized that the maximum range at any temperature was only approximately a factor of three. For almost any practical application, a factor of three changes in ice nuclei count has no importance. Considering potential experimental error and practical importance, variation in ice nuclei concentrations should be greater than an order of magnitude before it is considered significant. On the basis of Table II, one must conclude that the filter's pore size is not of vital importance when measuring ice nuclei in air.

COMPARISON OF THE MRI ICE NUCLEI COUNTER AND THE MILLIPORE FILTER

A primary result in the comparison between the fast-response MRI ice nuclei counter and the millipore filter technique is presented in Table III. The procedure here was to sample the air with the filter at the same location and time where the MRI counter was also counting the ice nuclei concentration. Later the filters were processed at a temperature of -20C (which was the same temperature as the MRI counter) and at both 1 and 70 percent supersaturation. It is seen from the table that there is good agreement between the two techniques when the supersaturation was at 70 percent.

Table III
COMPARISON OF THE MRI COUNTER AND THE MILLIPORE FILTER

Run No.		No. Ice Nuclei per liter	Supersaturation (%)
1	Filter	1.8	1
		5	70
	MRI Counter	5	?
2	Filter	4	1
		>100	70
	MRI Counter	130-30	?

Table IV
ICE NUCLEI COUNTS IN 1.5 cc OF RAINWATER COLLECTED ON THE ROOF OF MRI

Temp. (°C)	Relative Humidity During Cooling (%)	16 January 1970 Moderate Rain 1330 MST	1415 MST
- 5	30	0	0
-10	30	0	0
-15	30	1	0
-18	30	1	3
-20	30	10	11
- 5	100	0	0
-10	100	0	0
-15	100	6	6
-18	100	18	8
-20	100	67	26

ICE NUCLEI COUNTS IN RAINWATER

Rainwater, 1.5 cc per sample, was collected at 1330 and 1415 PST on 16 January from moderate rain. Each sample was filtered through a millipore filter of 0.45 μm pore size. After drying, the filters were processed at one-percent supersaturation and different temperatures. Two runs were made. In the first run, the relative humidity was maintained at 30 percent before the filters reached the required temperature. In the second run, the relative humidity maintained at 100 percent. The results of this nuclei count are shown in Table IV.

The concentration derived from the counts in Table IV are lower by an order of magnitude or more than Vali found in Canadian rain (7). A possible experimental explanation for the discrepancy between Table IV and Vali's results can be found in the observing technique. Vali collected his rain, made it into drops, subjected the drops to progressively colder temperatures, and counted the number of drops that froze per degree of cooling. If the nuclei that he observed were smaller than 0.45 μm diameter, they would pass through the filters.

Another important result of Table IV is that the count would be higher if the filters were subject to 100 percent relative humidity during the cooling period. A possible explanation is that, in the first run, only sublimation nuclei were detected, while in the second run, condensation was taking place forming water droplets and then freezing them.

CONCLUSIONS

From the previous sections we can conclude that: (1) supersaturation influences the nuclei count, (2) filter pore size is not vitally important when measuring ice nuclei in air, (3) filter technique compares well with the MRI fast-response counter if the filter is processed at high supersaturation, and (4) the relative humidity during cooling influences the final nuclei count.

ACKNOWLEDGMENT

This work was supported by the Bureau of Reclamation under Contract 14-06-D-6581 and 10-D-1187.

REFERENCES

1. Mason, B. J., 1968: Initiation of the ice phase in the atmosphere. Proc. Intl. Conf. on Cloud Physics, Toronto, Canada, August 26-30, 162-173.
2. Alkezweeny, A. J., 1970: Technique for detecting ice nuclei in the atmosphere. J. Weather Modification Association, 2, 1, 132-135.
3. Bigg, E. K., G. T. Miles, and K. J. Heffernan, 1961: Stratospheric ice nuclei. J. Meteor., 18, 804-806.
4. Stevenson, C. M., 1968: An improved millipore technique for measuring the concentration of freezing nuclei in the atmosphere. Quart. J. Roy. Meteor. Soc., 94, 35-43.
5. Alkezweeny, A. J., 1970: The use of millipore filters for ice nuclei measurement. Second Conf. on Weather Modification, Santa Barbara, Calif., April 6-9, 357-360.
6. Langer, G., 1970: Modification of the membrane technique to efficiently detect and study silver iodide in nuclei. Ibid., 352-356.
7. Vali, G., 1968: The freezing nucleus content of precipitation and its relation to the formation of ice in the clouds. Proc. Intl. Conf. on Cloud Physics, Toronto, Canada, August 26-30, 232-237.

SOME ORIGINS AND SINKS OF ICE NUCLEI IN THE ATMOSPHERE

by
Peter V. Hobbs and J. D. Locatelli
Cloud Physics Group, Atmospheric Sciences Department
University of Washington, Seattle, Washington

CONTINENTAL, MARITIME AND CITY SOURCES OF ICE NUCLEI

For a period of four months simultaneous measurements were made, using an acoustical ice nucleus counter, of the concentrations of ice nuclei in the air at three sites in Washington State. The sites were Quillayute (on the Pacific Coast), the University of Washington (in northeast Seattle), and Stampede Pass (in the Cascade Mountains). The mean concentrations of ice nuclei at the three sites for various wind directions are shown in Fig. 1.

The following conclusions can be drawn from Fig. 1:

(a) The concentrations of ice nuclei in the city of Seattle were much greater than those at the two non-city sites.

(b) When the wind at the University of Washington was from a southwesterly direction (i.e. from the downtown and main industrial areas of Seattle), the concentrations of ice nuclei were much higher than for other wind directions.

(c) At Quillayute the concentrations of ice nuclei were greater when the winds were from the continent (north through east to south) than when they were from the Pacific Ocean (north through west to south).

(d) At the inland station (Stampede Pass), which was remote from any centers of population or industry, the concentrations of ice nuclei were relatively independent of the directions of the wind.

The high concentrations of ice nuclei at the University of Washington is attributed to a source of ice nuclei in the city of Seattle. The source, however, appears to be widespread and we have not, as yet, been able to identify it with any particular industry. Schaefer[1] pointed out that lead particles in the exhaust of automobiles are a potential source of ice nuclei if they react with iodine to form lead iodide. However, free iodine in the atmosphere is quite rare; the main natural source is probably the ocean. Since Seattle is adjacent to the Puget Sound and close to the Pacific Ocean, it is possible that the high ice nucleus counts measured in the city are due to the reaction of lead particles from automobiles with iodine from the ocean to form lead iodide. Further studies are being carried out to check this possibility.

SOME EFFECTS OF RAIN AND FOG ON ICE NUCLEI

Hobbs et al.[2] observed that the concentrations of ice nuclei in the air sometimes increase for a short period of time following the onset of rain. Further evidence for this effect was found in the present study. For example, Fig. 2 shows the variation in ice nucleus count at Quillayute over a period of two days (October 29 and 30, 1968). At 2130 hours on October 29 a rain shower started and the ice nucleus count increased by about a factor of 50 for a short period of time. It should be emphasized that the ice nucleus count does not always increase in rain showers. On those occasions when we have observed an increase, fairly strong mixing was taking place between cloud base and ground. It is postulated that under these conditions some of the ice nuclei released into the air due to the evaporation of raindrops below cloud base are transferred down to the ground.

We have observed also, on a number of occasions, increases in the concentrations of ice nuclei in the air during the dissipation of fogs. Two such cases are illustrated by the results shown in Fig. 3. In order for a fog to increase the concentration of ice nuclei in the air when it dissipates, it is necessary for the fog to either concentrate the existing ice nuclei in the air (i.e. to act as a sink for ice nuclei) or for it to increase the effectiveness of those ice nuclei which it captures. An analogous effect was observed by Radke and Hobbs[3] who observed that, in addition to storing cloud condensation nuclei, some clouds also "generate" these particles so that when the cloud dissipates the concentration of cloud condensation nuclei in the air increases.

For a detailed account of the work summarized here the reader is referred to Hobbs and Locatelli[4]

ACKNOWLEDGEMENTS

This research was supported by the Atmospheric Sciences Section of the National Science Foundation under Grant GA-780 and the Cascade Atmospheric Water Resources Program, State of Washington, Dept. of Water Resources, under Contract No. 14-06D-5970 with the U.S. Dept. of Interior, Bureau of Reclamations.

REFERENCES

1. Schaefer, V. J., 1968: "Ice nuclei from auto exhausts and organic vapors." J. App. Meteor., 7, 148-149.
2. Hobbs, P. V., W. D. Scott, D. A. Burrows, L. F. Radke, and J. D. Locatelli, 1968: "Field research in cloud physics in the Olympic Mountains, winter 1967-68." Cont. from the Cloud Physics Lab. Research Rpt. 2, University of Washington.
3. Radke, L. F. and P. V. Hobbs, 1969: "Measurements of cloud condensation nuclei, light scattering coefficient, sodium-containing particles, and Aitken nuclei in the Olympic Mountains of Washington." J. Atmos. Sci., 26, 281-288.
4. Hobbs, P. V. and J. D. Locatelli, 1970: "Ice nuclei measurements at three sites in Western Washington." J. Atmos. Sci., 27, 90-100.

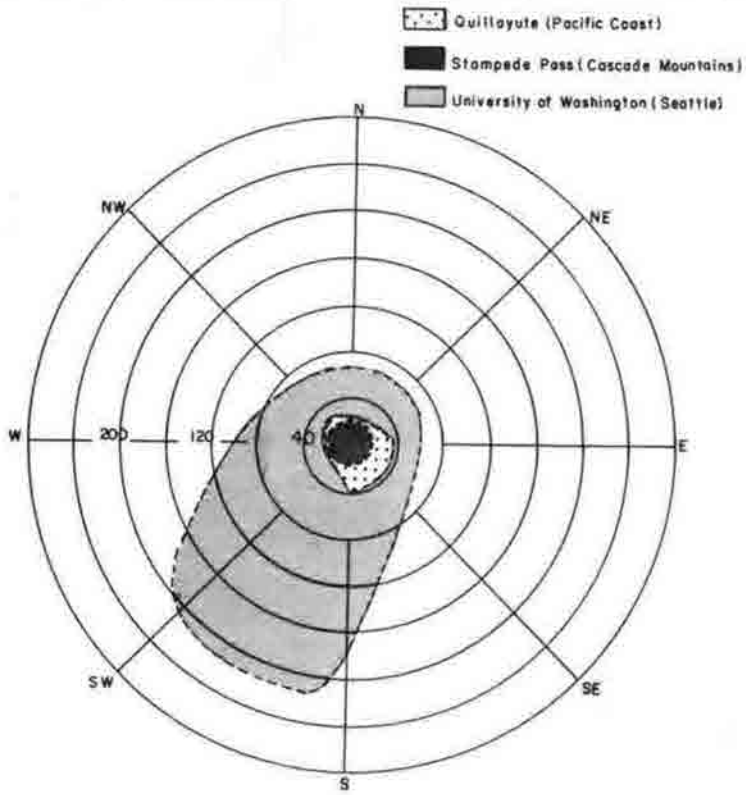

Fig. 1 Wind roses of ice nucleus concentrations at Quillayute, Stampede Pass, and University of Washington (Scale gives number of ice nuclei for 300 liters of air active at -21° C).

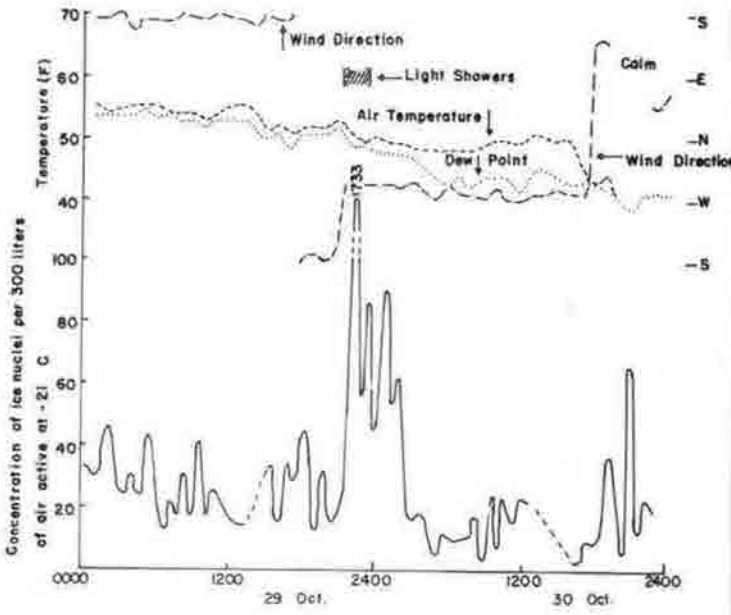

Fig. 2 Increase in ice nucleus count during a rain shower at Quillayute on 29 October, 1968.

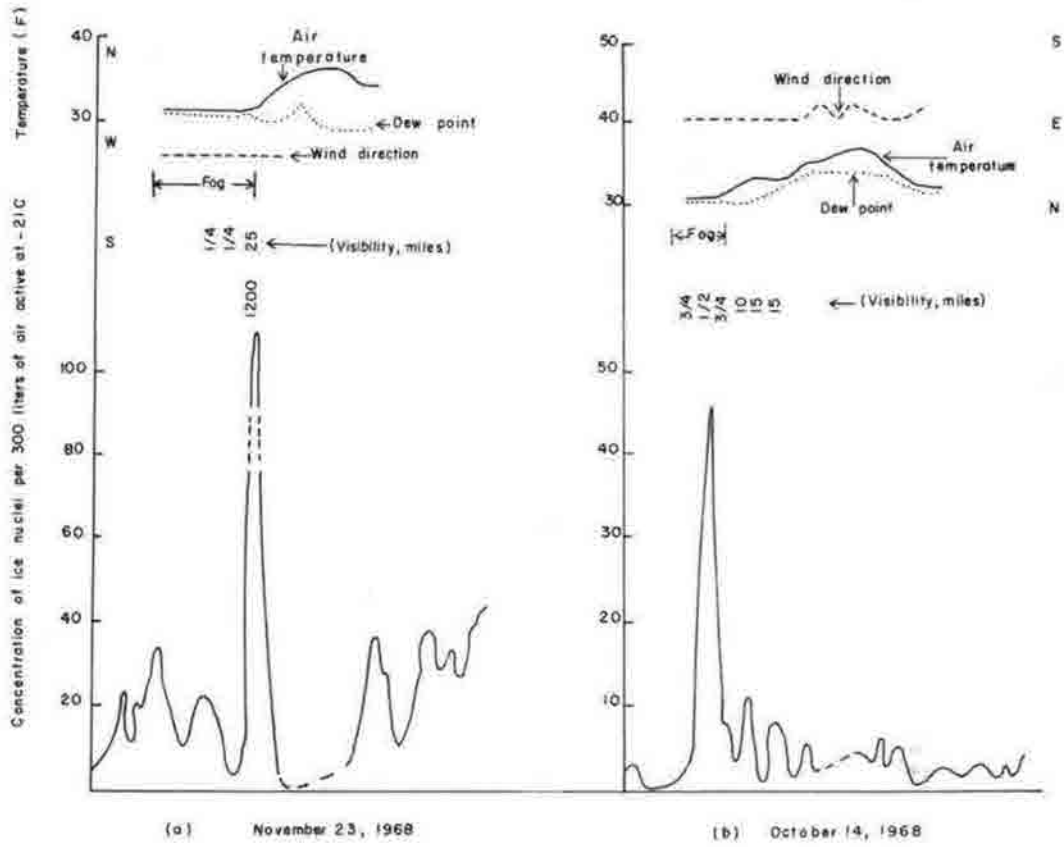

Fig. 3 Increases in ice nucleus count during the evaporation of fogs at Stampede Pass.

ICE NUCLEUS CONCENTRATIONS DURING PRECIPITATION WEATHER

Roger F. Reinking
Colorado State University
Fort Collins, Colorado

INTRODUCTION

Cloud seeding to increase precipitation from winter orogenic clouds has been demonstrated as effective under particular temperature, moisture and wind conditions (1). However, a potential for positive modification does not always exist. Cloud treatment with artificial nucleants has to be tailored for existing conditions. Seeding is founded on the presumption that the background nucleus level is so low as to be ineffective in initiating precipitation except at relatively cold temperatures, but background nucleus concentrations fluctuate by orders of magnitude. This investigation establishes the frequency distributions of ice nuclei active in the -14 to -28C temperature range for the nucleus populations which occur during precipitation weather (PW) in the mountain atmosphere, suggests possible explanations for the features of the distributions, and physically relates the characteristics of these distributions to the nucleus concentrations which would cause mountain clouds to precipitate at optimum efficiency. The PW nucleus distributions are taken from control cases of randomized cloud seeding in the Colorado Rocky Mountains. The nucleus concentrations (total sample, approximately 21,000 measurements) were measured with a USWB-modified Bigg-Warner expansion chamber (2) (3) (4) at the High Altitude Observatory (HAO, elev. 3.7 km msl) on the continental divide near Climax, Colorado.

PRECIPITATION WEATHER ICE NUCLEUS DISTRIBUTIONS

The frequency distributions for background ice nucleus concentrations measured during PW at HAO are presented in Fig. 1. Corresponding mean, median and extreme spectra are represented by the curves in Fig. 2. A measure of precision of sample means at specific nucleation temperatures as estimates of population means is given by $\sigma' = \frac{\sigma}{\sqrt{n}}$ (σ' and σ are standard deviations of the mean and the whole sample; n is sample size.) The σ' is illustrated by the bars on curve a, Fig. 2. In general the PW spectrum follows the typical ln N-T pattern. The irregularities provide clues to the nucleus sources; these and the extremes are suspected to be significant in regulating the precipitation process. In Fig. 3, for comparison, the PW spectrum is presented along with the background nucleus spectrum representing all weather conditions at HAO and the approximate world-wide average background spectrum (5). The volumetric, mainly sea-level world-wide measurements, were adjusted to the HAO pressure level (663 mb).

INTERPRETATIONS

The lowest ice nucleus concentration measurable with the expansion counter is $0.1/\ell$, so the PW means are slightly biased toward lower than actual concentrations for temperatures where populations below the $0.1/\ell$ level occur frequently. The rapid dropoff in concentration from -14 to -12C is partially attributable to expansions insufficient to produce saturation or clouds of sufficient density and duration. Even with this effect the mean measured concentration at -12C is twice the world-wide mean. Instrument effects are not responsible for the other major features of the PW spectrum. A critical analysis on the basis of the instrument evaluation by Reinking (4 and unpublished) revealed that the -14 to -16C plateau and the differing slope relative to the world-wide spectrum slope represent the real nucleus population.

A combination of the effects of station remoteness, elevation and combustion products may explain the lower than world-wide average concentrations in the PW spectrum at the colder temperatures, especially -26 and -28C. At these temperatures only, an occasional buildup of nucleus concentrations overnight and a decrease through the course of the morning occurs at HAO. These possibly indicate a nocturnal accumulation of cold-temperature-active local combustion-product nuclei under inversions forming near the cold mountain surface, and a morning release with solar heating. On the average, the high elevation, remote HAO site is freer of such pollutants than the majority of other nucleus measuring stations around the world.

Residuals of artificial nuclei from cloud seeding may at least partially account for the high PW concentrations relative to world-wide concentrations at temperatures warmer than about -21C. Nucleus distributions on each of the 1st through the 8th days after seeding, compared by a nonparametric statistical test (5) to a control sample, revealed that a residual does occur on the 1st and 2nd post-seeding days, with a significance at the 0.00% and 0.60% confidence levels, respectively. Timewise, a number of the individual randomized control cases occurred immediately after seeding cases. An effect of residual nuclei on the spectrum is therefore probable. AgI Generator efficiencies dictate that residual nucleus populations will be masked by natural nuclei for temperatures colder than about -20C, but could be significant for warmer temperatures, as indicated by the mean PW spectrum. The mean all-weather spectrum, which includes the PW data but is diluted by much more no-seed data without possible residual effects, lies below the PW spectrum for T>-22C as expected if residuals exist.

The residuals cannot entirely explain the -14 to -16C plateau. An influence of warm-temperature-active organics (e.g. turpenes) is possible. The reality of the plateau is possibly reflected in the mean daily snowfall recorded at Climax (Fig. 4) which also shows a plateau over the -14 to -16C range. Ice crystal multiplication by fracture of dendritic crystals could also explain this snowfall characteristic.

PRECIPITATION WEATHER CONCENTRATIONS RELATIVE TO OPTIMUM

Maximum utilization of cloud water through the cold cloud process is expected to occur when the integrated growth rate of ice crystals per unit volume (N_c) proceeds at the same rate that cloud water is supplied to each unit volume by condensation. The optimum crystal concentration can then be expressed (6) as

$$N_c = -7.7(10^{-11})(\omega/r)(q_{s_{700}} - q_{s_{500}})/F(T)$$

where ω is the upward air motion in mb/hr, r is the crystal radius in microns, q_s is the saturation mixing ratio in g/kg at 500 or 700 mb, and F(T) is a crystal growth parameter (7).

If one ice nucleus leads to formation of one ice crystal, then the excess or deficit in available nuclei/unit volume is given by $N = N(T) - N_c$ where N(T) is the actual nucleus concentration at T (1). Excesses and deficits for the mean, 95th percentile and 5th percentile spectra from the PW nucleus distributions are shown in Figure 5, a, b, and c. Optimum conditions are tabulated with each figure (cloud top levels correspond approximately to the 500 mb level). The 15 cm/sec upward motion is most applicable in the Climax Area. For the mean, the optimum conditions are 1-2C colder than those calculated by Grant, et al (1) who assumed the world-wide mean was applicable at Climax. On the average a few more storms than previously realized may be seeded to produce precipitation increases. For high extreme nucleus levels, optimum temperatures are about 3C warmer than for mean conditions; warmer clouds precipitate efficiently without seeding. When low extreme nucleus populations occur, there are deficits and clouds are seedable for all $T \geq -28C$.

The mean nucleus spectrum for seeded conditions (curve d, Fig. 3) is well above background for all temperatures. Assuming the released AgI reaches the cloud in these concentrations, seeding is sufficient to increase optimum temperatures by 5 to 8C on the average, thus optimizing precipitation for storms with cloud top temperatures in the -15 to -22C range. If it is assumed that ice crystal multiplication occurs in this cloud at such a rate that 10 crystals are produced for each ice nucleus, so $N = 10\,N(T) - N_c$, then optimum conditions occur for T>-13C. This means that on the average over-seeding would

result at least for clouds colder than about -15C. However, significant positive seeding results have been found at Climax for clouds in the -15 to -20C range. The combined evidence is strongly against the occurrence of a significant multiplication effect for those temperatures. The one nucleus-one crystal assumption made above is certainly valid in the first approximation.

CONCLUDING REMARKS

The PW ice nucleus spectrum presented here is based on a very large and long-term data sample. It is considered to be representative of real nucleus populations. Consideration of the residual nucleus effect and the extremes of the precipitation weather nucleus distribution make it clear that field monitoring of nuclei before and during seeding operations can be very advantageous in determining what generator outputs should be used, which individual cloud systems should be seeded, and which systems will precipitate most efficiently without modification. Professor L. O. Grant is acknowledged for his helpful discussions of this work. The research was supported by NSF Grant No. GA-1553.

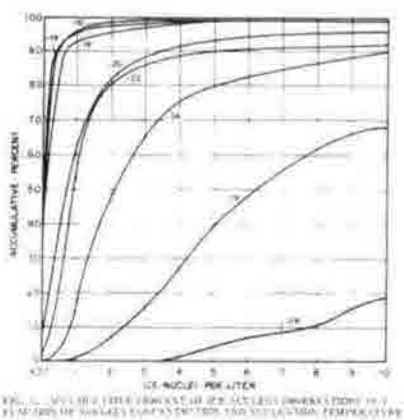

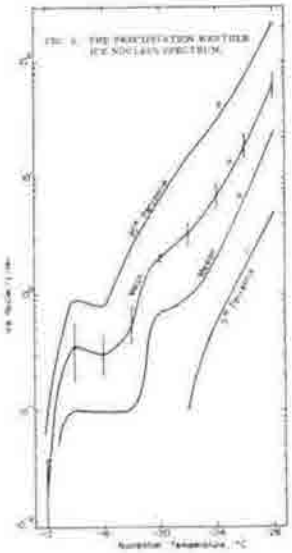

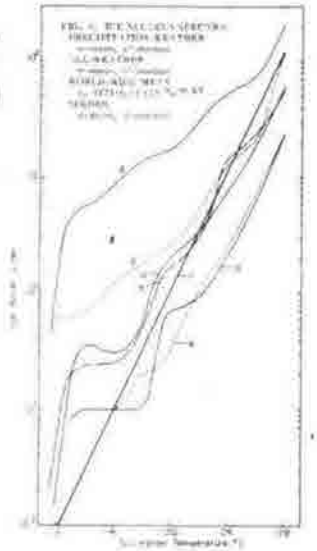

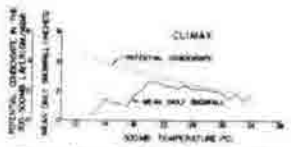

Fig. 4. Mean Daily Snowfall as a function of the cloud top temperature (500 mb), the adiabatic condensate from lifting a parcel through a saturated 700-500 mb layer (Grant, et al, 1969).

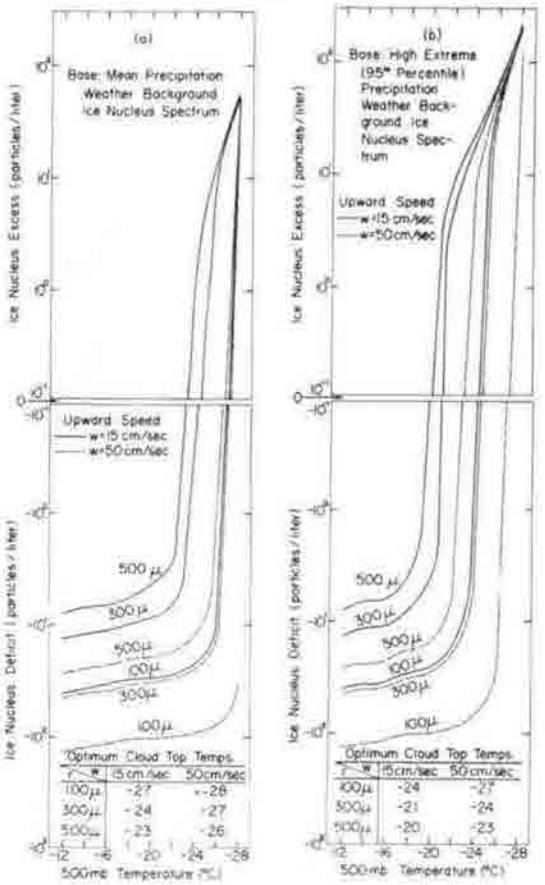

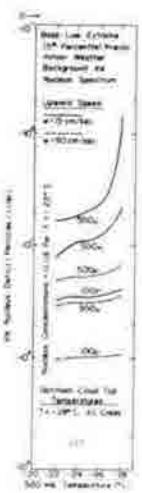

FIG. 5. THE DEFICIT AND EXCESS IN EFFECTIVE ICE NUCLEUS CONCENTRATION REQUIRED TO OPTIMIZE THE PRECIPITATION EFFICIENCY FOR VARIOUS CRYSTAL SIZES r AND UPWARD SPEEDS w AS A FUNCTION OF THE CLOUD TOP TEMPERATURE.

REFERENCES

(1) Grant, L. O., et al, 1969: An operational adaptation program of weather modification for the Colorado River Basin. Interim Report to the Bureau of Reclamation, Colo. State Univ., 97 pp.

(2) Warner, J., 1957: An instrument for the measurement of freezing nucleus concentrations. Bull. L'Obs. Puy de Dome, 2, 33-48.

(3) Kline, D. B. and G. W. Brier, 1961: Some experiments on measurements of natural ice nuclei. Mon. Wea. Rev., 89, 263-272.

(4) Reinking, R. F., 1970: An evaluation of the rapid expansion technique for measuring ice nucleus concentrations. Pre-prints of papers - Conf. Cloud Phys., Aug. 24-26, Ft. Collins, Colo.

(5) Mason, B. J., 1968: Initiation of the ice phase in the atmosphere. Proc. Int'l. Conf. Cloud Phys., Toronto, 162-173.

(6) Mielke, P. W., Jr., 1967: Note on some squared-rank tests with existing ties. Technometrics, Vol. 9, 312-314.

(7) Chappell, C. F., 1970: Ph.D. Dissertation, Colo. State Univ., to be published.

(8) Mason, B. J., 1953: The growth of ice crystals in a supercooled water cloud. Quart. J. Roy. Meteor. Soc., 79, 104-112.

THE CLOUD SEEDING POTENTIAL OF SALT LAKE VALLEY AIR POLLUTION - COLD SEASON*

George W. Reynolds, Utah State University, Logan, Utah

There are a number of reports in the literature which indicate that cloud seeding, and even over seeding, by air pollution is a very real possibility. (The two-page limitation on this document prevents proper acknowledgement of the various authors.) Possible ice nuclei sources in the Salt Lake Valley include copper smelters, steel mills, refineries, the Great Salt Lake, a population concentration, an unusually large number of wood burning fireplaces, and moderately dense freeway traffic, all within 20 miles of the Wasatch Front. The prevailing westerly component of the winds during seedable conditions may very well force the pollution to rise into the clouds when it meets the nearly continuous, NNW-SSE oriented Wasatch Front, which rises to 4,000'-5,000' above the east side of the Valley floor.

Provisions were made for airborne nuclei counting by Atmospherics, Incorporated, during whatever time was not utilized under a contract for airborne seeding. Both ice nuclei and condensation nuclei were counted, but only ice nuclei are discussed in this paper. The numbers of ice nuclei were estimated by visual counting, using a modified MRI cold box. The airborne sampling was supplemented by ice nuclei counting at the ground.** This is a tentative summary of the results of the ice nuclei phase of the airborne experiment. There were 21 air sampling flights on 11 days. Flight durations ranged from 1/2 to 3 1/2 hours. All 21 flights included sampling along a horizontal path, and for each of 13 flights, samples were also collected, at intervals of 1,000', from 5,000' to 10,000' (MSL) or higher above a selected location. All counts were at 20 Centigrade.

The following statistical summary should give a general idea of ice nuclei concentrations, over the inspected portion of the Salt Lake Valley, during the experimental period.

Highest count--6,000/liter. Lowest count--zero/liter. Number of flights with at least one count: $\geq$ 100/liter--17; $\geq$ 250/liter--16; $\geq$ 500/liter--16; $\geq$ 1,000/liter--15; $\geq$ 2,000/liter--12; $\geq$ 3,000/liter--9; $\geq$ 4,000/liter--6; $\geq$ 5,000/liter--2; $\geq$ 6,000/liter--1. Number of flights with no count as high as: 100/liter--4; 10/liter--3. Altitude of the highest count--5,000'; altitude with the highest average count--7,000'.

In general, the air sampling flights were made during periods when conditions were unsuitable for seeding operations. With these sampling conditions, a diurnal effect on contamination dispersal would not be surprising. Comparisons were made between morning and afternoon counts which were taken at the same altitude and location on the same day. Compared pairs were limited to those of which at least one member had counts of at least 100/liter.

There were 14 comparisons of data collected on 3 days during horizontal profile flights, and 14 comparisons of data collected on 4 days during vertical profile flights over the Garfield smelter. There was no clear indication that the time of day was a consistent control factor on the number of ice nuclei over the Garfield smelter during the daytime, in February or March. However, the data suggest that future experiments should provide data for further consideration of the diurnal influence problem. Even with more conclusive statistics, one could hardly have drawn generalizations from samples collected during 14 flights on 7 days.

Flight No.	MSL Alt. (Ft)	March 3, 1970		March 10, 1970		March 19, 1970		March 20, 1970	
		11	12	15	16	17	18	19	20
		a.m.	p.m.	a.m.	p.m.	a.m.	p.m.	a.m.	p.m.
	14,000	—	1	—	—	—	—	—	—
	13,000	—	7	—	—	—	—	—	—
	12,000	0	4	—	—	—	5	200	4
	11,000	3	3	1	1	—	25	7	2
	10,000	1,500	200	1	2	1	10	5	9
	9,000	750	300	2	3	3	500	8	1,000
	8,000	1,000	250	2	2	5	200	26	2,000
	7,000	5,000	500	500	200	1,000	1,000	4,000	1,500
	6,000	3	14	3	5	0	1,000	3,000	1,000
	5,000	5	15	2	1	1	500	5	1

TABLE 1: Observed Ice Nuclei Concentrations During 8 Flights Over the Garfield Smelter

*Funded by the Office of Atmospheric Water Resources of the Office of Chief Engineer, U.S. Bureau of Reclamation, under contract No. 14-06-D-6820 with Utah State University.

**The ground counting was done by William Slusser using an NCAR counter.

The evidence leaves no doubt that the Garfield Copper smelters were a primary source of ice-forming nuclei. One might reasonably ask whether the proximity of the Great Salt Lake and the salt flats had any influence on the effectiveness of this source. The highest reading of all, 6,000 nuclei/-liter was observed here. The highest reading of each flight was most frequently observed over this smelter. For 13 of the 19 flights during which observations were made over the smelter, the highest reading per flight ranged from 1,000 to 6,000 nuclei/liter. Mr. Slusser's observations at the ground, using the NCAR counter, supported the declaration that the Garfield smelter was a primary ice nuclei source.

The steel mill also appears to be a source of ice nuclei. For 3 of the 7 flights during which counts were made over this plant, the readings were 2,000, 1,000, and 500 nuclei/liter respectively.

Counts of 1,000 or more nuclei/liter were observed over the Salt Lake City-Bountiful path for 4 of the 20 flights over this route. This is the region of heaviest automobile traffic and includes the refineries. Accompanying counts suggest the possibility that these concentrations may have come from the smelter and/or steel mills, but this is by no means certain. The decision as to whether or not there was an ice nuclei source within this locale is deferred, pending further study of the wind patterns in the area and the checking of refinery operations. Again, possible contributions of the Great Salt Lake and the salt flats to the effectiveness of this source makes this aspect interesting.

As indicated in Table 1, vertical profile data were recorded at intervals of 1,000', at MSL heights from 5,000' to 16,000' on 7 days. The elevation of the Great Salt Lake surface is about 4,200 feet. The highest counts reported were at least 100/liter for 11 of the 15 vertical profiles (6 days); 1,000/liter for 8 of these flights (5 days); 3,000/liter for 5 of the flights (4 days).

These high counts occurred in layers which were 1,000' to 4,000' thick. The highest counts were at the lowest reporting level (5,000') for only two of the 11 flights for which counts in excess of 100 nuclei/liter were reported. For 4 of the flights the high count layers ($\geq$100/liter) started at 5,000'. (They may have started below this level.) For 5 of the flights the base of the high count layer was at 7,000', which was also the level of the highest average count.

An attempt to relate the observed thicknesses and altitudes of the high count layers to lapse rate conditions produced no consistent relationship. Part of the reason could, of course, lie in the selection of the path for the vertical profile. Another factor could be the differences between the times of the soundings and the respective times of the vertical profiling. This phase is to receive further attention, since vertical nuclei distributions might provide valuable evidence concerning atmospheric behavior-stability relationships.

In summary, this was a pilot study, so all conclusions must be regarded as tentative. Horizontal and/or vertical samplings of the number of ice nuclei were conducted during 21 flights on 11 days during February and March, 1970. The highest count was 6,000 per liter, and counts of at least 1,000 per liter were noted at one or more levels on 70% (15) of the flights. There was no clear indication that the time of day exerts a consistent control on the number of ice nuclei in the Salt Lake Valley, during daylight hours, in February and March.

There is no doubt that the operation of the Garfield copper smelter was a primary source of ice nuclei in the immediate area. There was a strong indication that the steel mills were an ice nuclei source under at least some circumstances. There was some indication that the contributions of the large refineries and/or heavy traffic near Salt Lake City may be significant under some conditions but this needs more consideration before drawing even tentative conclusions.

The high concentrations definitely tended to occur in layers which were 1,000' to 4,000' thick. The bases of these layers were generally, but not always at more than 1,000' above the valley floor. Comparisons between ice nuclei layer characteristics and lapse rate conditions failed to produce consistent relationships.

The data are to be submitted to further analysis and reported in a project technical report.

Acknowledgments: This investigation is indebted to Gary Langer (NCAR) and Tom Henderson (Atmospherics, Inc.) for counsel on nuclei counting and analysis. The loan of the NCAR counter by NCAR, which is sponsored by the National Science Foundation, is also appreciated.

CONTRIBUTION OF NATURAL FREEZING NUCLEI TO PRECIPITATION DEVELOPMENT

by
Gabor Vali and Russell Schnell
University of Wyoming, Laramie, Wyoming

With present knowledge it is still difficult to assess what the major mechanisms of precipitation formation may have been under individual circumstances. It is difficult to determine what contribution are made by warm rain processes or by mechanisms involving the ice phase; it is even more difficult to estimate the relative contributions made by different ice nucleating mechanisms. The in-cloud observations of droplet and ice particle concentrations and sizes, which are now being made with increasing frequency, can provide some basis for determining the dominant processes. One major finding of such investigations was the discrepancy between the concentrations of ice crystals in the cloud and the concentrations of ice forming nuclei as detected by cloud chamber devices. Another approach to the problem is to examine the individual precipitation elements and reproduce its method of formation. Soulage (1957) and Hoffer and Braham (1962) have examined snow crystals and graupel particles from summer cumuli respectively and found that ice could be re-formed only at temperatures much colder than those that occurred in the clouds. In this paper, some further observational data will be reported, on the relation of individual precipitation elements to their freezing nucleus contents.

Freezing nucleus content was determined by drop freezing experiments, the nuclei detected are therefore those that are capable of ice formation while suspended in bulk water. The drops examined were formed by subdividing the rain samples which were collected in polyethylene bags, or by allowing individual graupel particles to melt. For the rain samples, the data are presented in the form of cumulative nucleus spectra, giving the concentrations of nuclei per gram of water which are active above the indicated temperatures. Details of the technique were given by Vali (1968). The technique used for the freezing of the graupel particles was described by Vali, et al. (1970). Coincident with the collection of rain samples, dyed filter papers were exposed to obtain drop-size distributions and to determine the numbers of drops of different sizes that were collected with each gram of rain sample.

The data displayed in Figure 1 relate to a thunderstorm which occurred on August 3, 1969 in Central Alberta. Two consecutive rain samples were collected and drop-size distributions recorded at three instants dispersed throughout the period of rain collection. The freezing nucleus contents of the two samples were essentially identical and only moderately high for summer storms. The drop sizes were fairly large, such that there were approximately ten drops over 4 mm in diameter for each gram of rain water. Although the actual drop-size distributions and the rainfall rates varied quite widely for the three records the contributions of different drop-size ranges to the water mass appear to be conservative. The results of another set of observations (July 20, 1969, Alberta) are shown in Figure 2. Rain samples were collected at three different locations (B, C, D) along a twelve mile line. Three, two and three records of drop size distributions were obtained at the three sites; the averages of these distributions are shown in Figure 2. From a comparison of the three sets of data it appears that higher nucleus content in the rain is coupled with relatively smaller proportions of large raindrops. On the other hand, the larger the number of raindrops is (per gram of rain water) the larger is the concentrations of nuclei active at the warmer temperatures.

From the proportions of different sized drops in the rain and from the nucleus content it is possible to deduce the average numbers of nuclei for each drop of given size at several temperatures. This, in other words, means the probability of finding a nucleus active above a certain temperature for each of the drops that are greater than the chosen size. Figure 3 shows the results of such a computation for a thunderstorm in which several samples and several size distributions were obtained, all very closely the same. As can be seen from Figure 3, there is a freezing nucleus active above -15C for each of the raindrops greater than 1 mm diameter, and similarly on the average there is a freezing nucleus active at -10C for each of the drops that are greater than 3.3 mm diameter. Extending this line of thought a little further and asserting that the temperature at which the numbers of nuclei match the numbers of drops above a certain size is the temperature at which those drops froze in the atmosphere and thus began preferentially accelerated growth the relation shown in Figure 4 can be derived. The two curves in this figure are for two different sampling occasions; on August 3, 1969 cloud droplets nucleated at the same temperature grew on the average 1.5 millimeter greater than on July 17.

In thunderstorms the cloud elements are likely to traverse all temperatures between cloud base and cloud top and incipient precipitation elements form in continually increasing numbers as the temperature falls in the rising air. Ice particles that form at a warmer temperature will have a longer growth time and consequently are likely to be larger at the end of their growth than ice particles that were nucleated at colder temperatures. This is the picture underlying the analysis given above and the reasonableness of the temperature regimes that are obtained for the nucleation of the large raindrops lends at least some credence to this picture. Detailed calculations of the rates of growth (from the vapor and by riming) and trajectories of the graupel particles will be required to ascertain whether this idea can be upheld or not.

It is interesting to compare the findings for thunderstorms with similar observations for wintertime orographic cap clouds. It was found (Vali, et al., 1970) that only about 15 percent of the snow particles which developed in the cap cloud re-froze at temperatures warmer than the temperature at the top of the cloud. Initiation of ice growth by droplet nucleation can thus not account for the total number of precipitation elements in these wintertime clouds. It is possible that it will be found that in the thunderstorms also, the numbers of ice particles will be greater than what can be accounted for on the basis of the freezing nucleus content (as was in fact found by Hoffer and Braham (1962) for cumuli) in which case the one-to-one relation between nuclei and drops which was postulated above will have to be abandoned. In the meantime, the results can be considered to represent an estimate of how precipitation development can be accounted for on the basis of ice formation by freezing nucleation.

REFERENCES

Hoffer, T. E. and R. R. Braham, Jr., 1962: A laboratory study of atmospheric ice particles. J. Atmos. Sci., 19, 232-235.

Soulage, G., 1957: Les noyaux de congelation de l'atmosphere. Ann. Geophys., 13(2), 103-134.

Vali, G., 1968: Ice nucleation relevant to formation of hail, McGill University Stormy Weather. Gr. Sci. Rep. MW-58, 51 pp.

Vali G., D. L. Veal, A. H. Auer, Jr. and D. J. Knowlton, 1970: Reactivation of nuclei in crystals from cap cloud. Preprints of Papers Presented at the Second National Conference on Weather Modification, American Meteorological Society, Santa Barbara, California, 366-369.

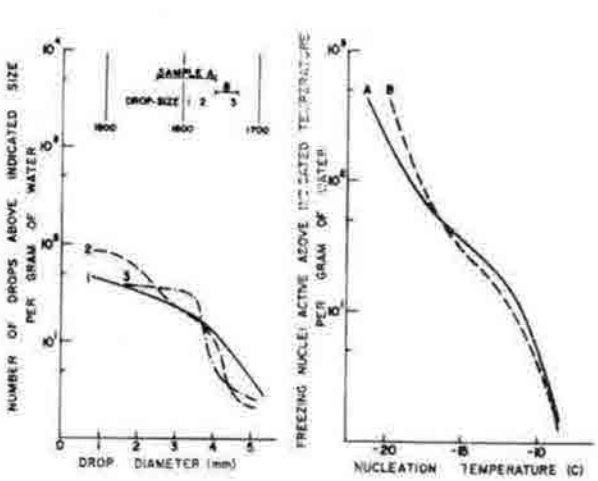

Figure 1

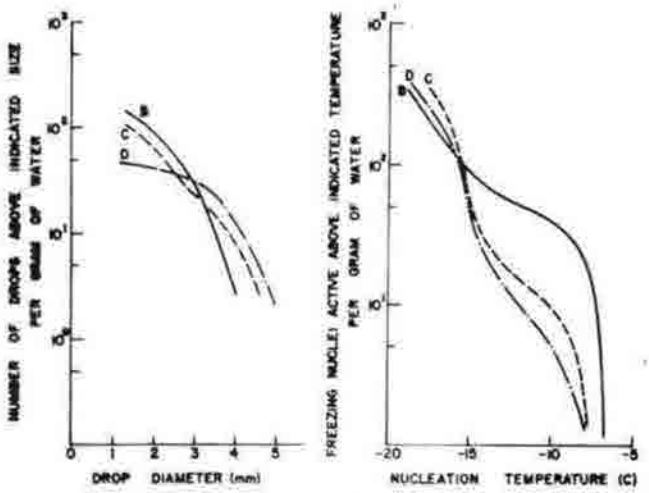

Figure 2

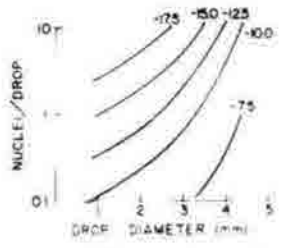

Figure 3

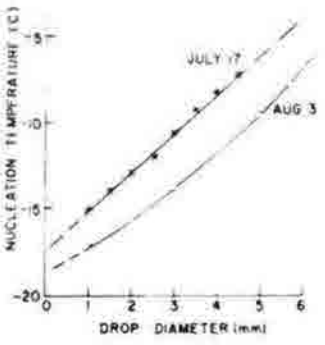

Figure 4

This research is made possible by the National Science Foundation, under grant GA-1527 to the Natural Resources Research Institute and by the Research Council of Alberta under contract P.O. 10278-A.

OBSERVATIONS OF ICE CRYSTAL NUCLEATION BY DROPLET FREEZING IN NATURAL CLOUDS

by
August H. Auer, Jr. and Donald L. Veal
University of Wyoming, Laramie, Wyoming

INTRODUCTION

Early studies of ice crystal shapes (1, 2) described observations of dendritic crystals of double forms, oftentimes exhibiting an asymmetric structure. Weickmann (3, 4) noted that in each case these "double crystals" possessed a circle in their center resembling a cloud droplet; he, therefore, premised that small droplets, upon freezing, could become tiny monocrystalline prisms whose two base planes then grow into a hexagonal or dendritic crystal form.

Expanding on these implications (4), the deposition and droplet freezing modes of nucleation were observed within orographic cap clouds during natural and seeded conditions. This paper will discuss the results of these observations and suggest possible implications concerning various modes (deposition or droplet freezing) of nucleation.

PROCEDURES

The ice crystal replicas were inspected under a microscope (100-400X) to determine the crystal type (5); measure the dimensions of the double crystals asymmetries, if any; and check for the presence of the circular (droplet) center.

The crystal types studied were limited to hexagonal plates, thick plates, stellars, and dendrites since the structural patterns of interest are most easily ascertained from such crystal types.

RESULTS

Figures 1-3 illustrate some representative crystal replicas with circular (droplet) centers and corresponding double or asymmetric structures found in the untreated orographic cap cloud. In particular, Figures 2-3 show how clearly the crystal with circular (droplet) centers can be delineated from their neighbors without such a structure. The circular (droplet) center is always accompanied by the double or asymmetric structure of plate family crystals. The relationship shown in Figure 4 is generated from observations of the circle (droplet) diameter d within the observed ice crystal and separation h (including crystal thicknesses) between the double or asymmetrical crystal faces. Figure 5 is a comparison between the average observed cloud droplet spectrum for Elk Mountain cap clouds and the observed circle (droplet) center spectrum from double or asymmetric ice crystals found within the same clouds.

An inspection, then, of Figures 1-5 indicates that the circular centers of the double or asymmetric ice crystals possess nearly spherical shape and arise from the population of cloud droplets commonly observed within the cap cloud. These observations, when combined with the evidence from (4) for single crystalline structure of frozen cloud droplets, clearly imply that ice crystals having a center circle and possessing double or asymmetric structures have their genesis from frozen cloud droplets.

Figure 6 shows the relationship between the observed cap cloud limit temperatures and the corresponding total ice crystal concentration, "frozen droplet" crystal percentage and "frozen droplet" crystal concentration. For a given temperature regime in untreated cap clouds, it appears that there is a predictable percentage of ice crystals having their origin from cloud droplet freezing.

Figure 7 illustrates a representative sample of ice crystal replicas acquired during ice supersaturation but water subsaturation conditions atop Elk Mountain. Frozen cloud droplet centers were never found in ice crystals nucleated during water subsaturation conditions. Hence, ice crystals found in ice supersaturated but water subsaturated conditions are presumably the result of growth by deposition. Similar results were also to be expected during periods of seeding with dry ice, since dry ice does not act by heterogeneous but rather homogeneous nucleation. Indeed, ice crystals formed in such a manner did not possess frozen droplet centers and/or asymmetric structures as shown in Figure 8.

It may be suggested that the respective concentrations of the frozen droplet crystals and of the balance of the ice crystal population may be considered as representative estimates of the freezing and deposition nucleus concentrations, disregarding ice multiplication processes.

IMPLICATION

Ice crystal replicas were also obtained during cap cloud seeding with an acetone generator for the purpose of detecting any possible changes in the percentage of frozen droplet crystals during seeding intervals as implied from cloud chamber nucleation studies (4). Throughout the single seeding experiment discussed herein, the height of the cloud base (2900m msl), cloud base temperature (-17C), and Observatory (3300m msl) temperature (-20C) remained steady. The seeding agent was injected into the cloud from below cloud base; at all times during the experiment water saturated conditions were maintained through the treated cloud depth.

During background conditions, the percentage of frozen droplet crystals lay near 27%, a value to be expected from other independent data shown in Figure 6. Following the arrival of the silver iodide detected by the NCAR acoustical counter, there was a corresponding increase in the total ice crystal concentrations, and especially in the percentage and concentration of the frozen droplet crystals, similar to those shown in Figures 1-3. Throughout the seeding interval, the droplet freezing and deposition nucleation modes appeared responsible for nearly equal numbers (168 liter^{-1} and 179 liter^{-1}, respectively of crystals but the increases in the concentration of the respective nuclei (droplet freezing vs deposition) over background concentrations (27 liter^{-1} and 73 liter^{-1}, respectively) seemed to slightly favor the freezing nucleus. It may thus be concluded that the droplet freezing and deposition nucleation activities of silver iodide produced from a generator burning an acetone solution of silver iodide (2.5%) and sodium iodide yield equal numbers of observed ice crystals in orographic cap clouds for the case of cloud activating temperatures between -17 and -20C.

Further research concerning the relevance of the findings in this paper and those, for example from (6) concerning the role of silver iodide in the drop freeezing process in natural clouds are forthcoming.

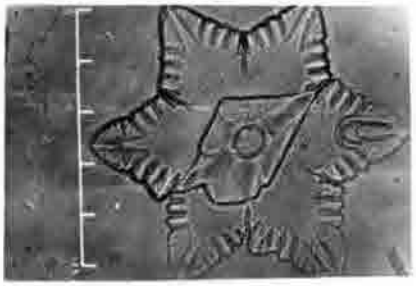

Figure 1

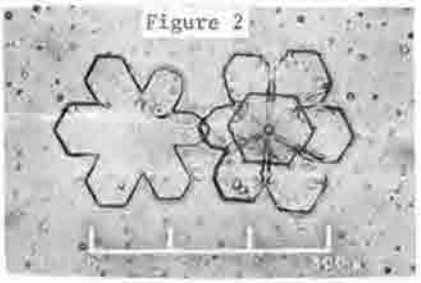

Figure 2

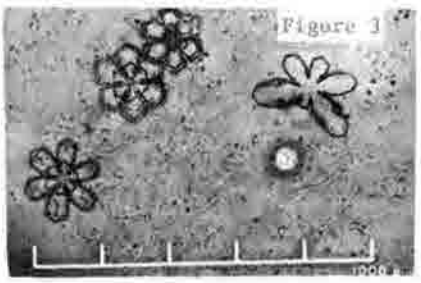

Figure 3

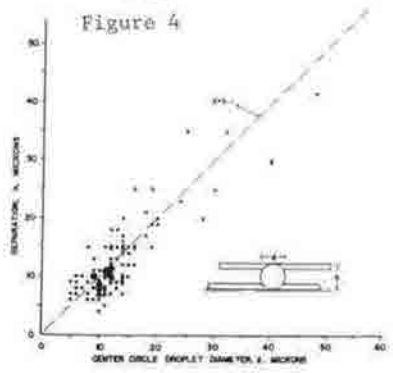

Figure 4

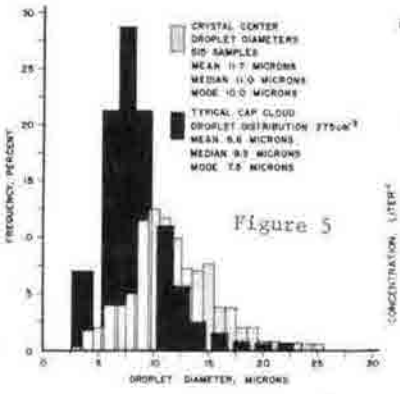

Figure 5

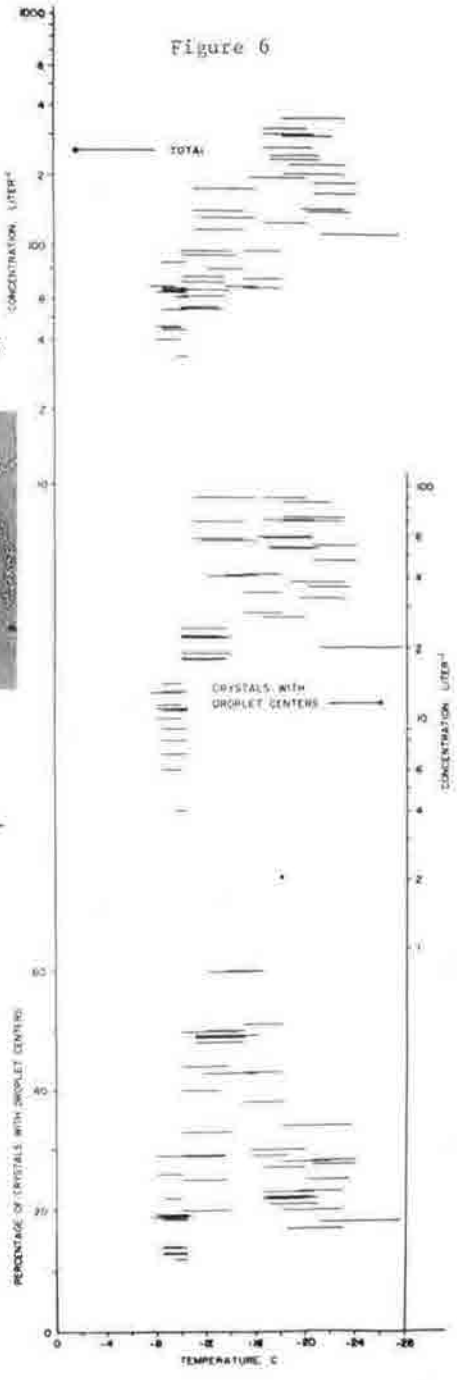

Figure 6

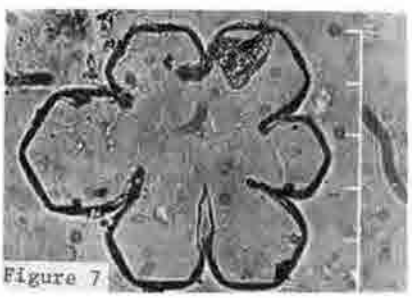

Figure 7

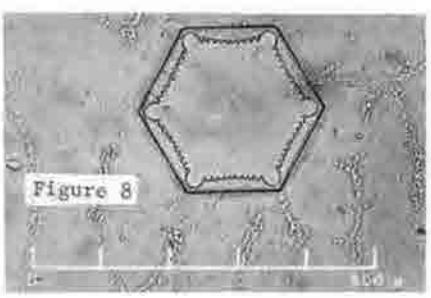

Figure 8

REFERENCES

(1) Nakaya, U., Y. Sekido and M. Tada., 1936: Notes on irregular snow crystals and snow pellets. J. Fac. Sci., Hokkaido University, Series II, Physics, 1(3), p. 215.

(2) Nakaya, U., 1954: Snow crystals: Natural and artificial. Harvard University Press, Cambridge, 510 pp.

(3) Weickmann, H., 1947: The ice phase in the atmosphere. Rep. and Trans., 716(Volkenrode), Ministry of Supply, London, 154 pp.

(4) Weickmann, H., U. Katz and R. Steele, 1970: AgI-sublimation or contact nucleus? Preprints of the papers presented at the Second National Conference on Weather Modification, Santa Barbara, California, 332-336.

(5) Magono, C. and C. W. Lee, 1966: Meteorological classification of natural snow crystals. J. Fac. Sci., Hokkaido University, Series VII, 2(4), 321-362.

(6) Edwards, G. R. and L. F. Evans, 1968: Ice nucleation by silver iodide: III. The nature of the nucleation site. J. Atmos. Sci., 25(2), 249-256.

This research was made possible by the U.S. Department of the Interior, Bureau of Reclamation, OAWR, under contract No. 14-06-D-6002 (July 1, 1966) and No. 14-06-D-6801 (July 1, 1969 and by the Naval Weapons Center under contract No. N66001-70-C-0639 to the NRRI, University of Wyoming.

DEPOLARIZATION OF MICROWAVES BY HYDROMETEORS IN A THUNDERSTORM*

Louis J. Battan and John B. Theiss
The University of Arizona
Tucson, Arizona 85721

During the past decade, relatively little has been done to extend the theory of the scattering of microwaves by non-spherical hydrometeors. Harper (6) and Atlas and Wexler (1) made laboratory measurements of the backscattering from large ice and plastic spheroids. Scientists at the Central Aerological Observatory in Moscow have been actively investigating various aspects of the depolarization of microwaves. Minervin, Morgunov and Shupiatskii (9) discussed depolarization of 3-cm radiation by the hydrometeors in cumulonimbus clouds. They showed that the depolarization ratio varies from more than -10 db to less than -20 db. Large variations occur over distances of about 1 km.

Observations of depolarization have been made in convective clouds in southeastern Arizona by means of vertically pointing 3.2-cm radar equipment. A pulsed-Doppler radar, already described by Battan and Theiss (3), was used for transmitting and receiving the backscattered signals in one plane. A second antenna (0.8 m in diameter) and receiver were used for detecting the power backscattered in a plane perpendicular to the plane of transmission [see Lofgren and Battan (7)]. The output of both receivers was displayed on a dual beam A-scope and photographed.

Figure 1 shows the vertical profile of depolarization ΔP_1 in decibels, where $\Delta P_1 = 10 \log P_c/P_p$ and P_p and P_c are the backscattered powers in the plane of polarization of the radar and in the cross-polarized plane, respectively. The pattern of ΔP_1, in a thunderstorm on Aug. 7, 1967, is based on a grid of points 152 m apart in altitude and about 54 sec apart in time. It is evident that the depolarization varied greatly over distances of about 0.5 to 1 km. Minervin and Shupiatskii (8) also found large variability in depolarization in cumulonimbus clouds, but the small scale "eddies" shown in Fig. 1 do not appear in their illustrations. Perhaps the grid scale used to construct their diagrams was such as to mask perturbations several hundred meters in diameter.

The depolarization shown in Fig. 1 ranges from about -12 to -24 db, the latter being essentially the smallest quantity which can be measured with this radar system. Minervin and Shupiatskii (8) observed about the same range of depolarizations. On the basis of ground-based radar observations and flight observations of the hydrometeors they advanced the following conclusions. When $\Delta P_1 < -17.5$ the hydrometeors can only be raindrops; when $\Delta P_1 > -9$ only ice particles exist. Most of the time, at intermediate values of ΔP_1, mixtures of water and ice would be expected.

It is seen in Fig. 1, that depolarizations exceeding -14 db were observed at altitudes below about 3.5 km (MSL) between 1426 and 1432 MST. Doppler radar data [Battan and Theiss (4)] show that this was a region of downdrafts exceeding 4 m/sec where the radar reflectivity factor was as high as 3.2×10^3 mm^6 m^{-3}.

If it is assumed that turbulence spreading of the Doppler spectrum is negligibly small, the spread of Doppler velocity can be taken as the terminal velocities of the largest detectible particles, W_{max}. In the region of $\Delta P_1 > -14$ db, W_{max} was 8 to 10 m sec^{-1}. At the indicated altitudes, these terminal velocities correspond to raindrops having diameters between about 2.3 and 3.7 mm [Foote and du Toit (5)].

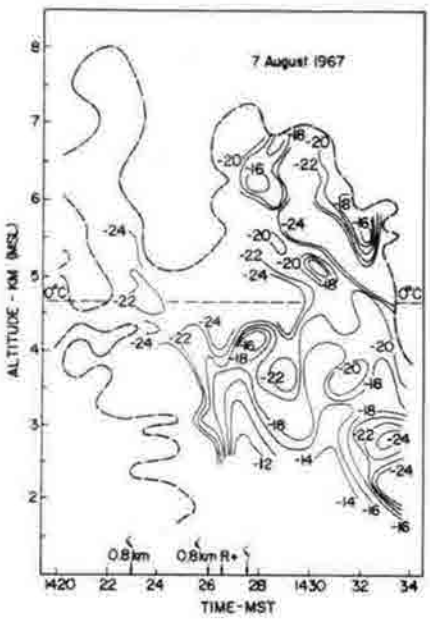

Figure 1

The fact that the Doppler spectra were some 8 to 10 m sec^{-1} broad, indicates a spectrum of raindrop sizes ranging from the barely detectable, perhaps a few hundred microns to the sizes just cited. If all the scattering particles were raindrops which were small with respect to the wavelength and were randomly oriented with respect to the plane of polarization of the radar set, a depolarization of -14 db could be produced by oblate spheroids having an axis to diameter ratio of about 0.4 [Atlas, Kerker and Hitschfeld (2)]. It is difficult to believe that even large raindrops, i.e., those approaching 4 mm in diameter could be so distorted except for brief instants of time.

*The research reported in this paper was supported by the Atmospheric Sciences Section of NSF under Grant Nc. GA 1431.

The measurements were made with the antenna pointing vertically. If the particles were falling oblate spheroids, it would be expected that the axial ratios would be close to unity. It seems impossible if one accepts the measurements, to accept the notion of oblate scatterers.

It appears that the measured depolarizations can be explained if the scatterers were assumed to be prolate spheroids composed of water. If they were randomly oriented, they would need an axis to diameter ratio of about 1.8 according to Atlas, Kerker and Hitschfeld (2). This distortion does not appear to be as extreme as in the case of oblate spheroids. Nevertheless, it is difficult to imagine all-water, randomly oriented prolate spheroids. In order to satisfy the requirements, it is necessary to assume that the particles were composed of ice surrounded by water. If this were the case, the result is in agreement with the results published by Minervin and Shupiatskii (8).

Figure 1 shows regions of depolarization larger than -18 db above the 0°C level between about 1427 and 1433 MST. Doppler radar data show that they were mostly associated with updrafts and low radar reflectivities. In these regions, the maximum terminal velocities were relatively high, between 10 and 15 m/sec. According to Foote and du Toit (5), at a pressure of 500 mb and temperature of -10°C, the maximum terminal velocities of water drops is 12 m sec^{-1}. It seems reasonable therefore, to assume that the particles producing the velocities greater than 12 m sec^{-1} in the upper part of the cloud were composed of ice at least in part. If they consisted of ice having a density of 0.9 g/cm^3, a sphere 5 mm in diameter would have a terminal velocity of 12 m sec^{-1}.

Depolarizations of -18 db and -16 db correspond to depolarization ratios of 1.6 and 2.5 percent, respectively. According to Atlas, Kerker and Hitschfeld (2) the smaller of these quantities can be produced by particles having the axial ratios listed in Table 1.

Table 1. Axis to diameter ratios of small particles which can produce a depolarization of -18 db on a 3-cm radar.

Shape	Composition	
	Ice	Water
Oblate	0.30	0.62
Prolate	3.3	1.5

It seems unreasonable that a vertically pointing radar set would measure such large cross polarizations from oblate spheroids. On the other hand, it is possible to imagine prolate spheroids having an axial ratio of 1.5. An axial ratio exceeding about 3.3 appears to be extreme and unlikely. Thus, it seems that the observations may be explained by assuming the presence of wet ice particles resembling prolate spheroids. This result agrees with the conclusion of Minervin and Shupiatskii (8) which would indicate that a depolarization of -16 to -18 db would be associated largely with a mixture of water and ice.

REFERENCES

1. Atlas, D. and R. Wexler, 1963: Backscatter by oblate ice spheroids. J. Atmos. Sci., 20, 48-61.
2. Atlas, D., M. Kerker and W. Hitschfeld, 1953: Scattering and attenuation by non-spherical atmospheric particles. J. Atmos. Terr. Phys., 3, 108-119.
3. Battan, L. J. and J. B. Theiss, 1966: Observations of vertical motions and particle sizes in a thunderstorm. J. Appl. Meteor., 23, 78-87.
4. Battan, L. J. and J. B. Theiss, 1970: Measurements of vertical velocities in convective clouds by means of pulsed Doppler radar. J. Atmos. Sci., 27, 293-298.
5. Foote, G. B. and P. S. du Toit, 1969: Terminal velocity of raindrops aloft. J. Appl. Meteor., 8, 249-253.
6. Harper, W. G., 1962: Radar backscattering from oblate spheroids. Nubila, Anno V, 60-72.
7. Lofgren, G. R. and L. J. Battan, 1969: Polarization and vertical velocities of dot angel echoes. J. Appl. Meteor., 8, 948-951.
8. Minervin, V. E. and A. B. Shupiatskii, 1968: Investigations of Cb phase structure by means of radar signal polarization characteristics. Proc. Thirteenth Radar Meteor. Conf., Amer. Meteor. Soc., August, 1968, 20-23.
9. Minervin, V. E., S. P. Morgunov and A. B. Shupiatskii, 1968: Proc. Third All Union Conf. on Radar Meteor., Gidrometeoizdat, Moscow, 54-62.

THE TERMINAL VELOCITIES OF ICE CRYSTALS

Stanley R. Brown
Colorado State University
Fort Collins, Colorado

INTRODUCTION

The terminal velocities of several individual crystal types have been studied by Nakaya (1). His work is generally regarded as the standard for ice crystal terminal velocities. Several other studies, (2) and (3), have been reported on individual crystals, but these have not substantially altered Nakaya's results. Unfortunately, however, Nakaya did not have a large data sample. In addition, more refined techniques than Nakaya used are now available for measurement. For those crystal types not studied by Nakaya, the terminal velocities are not well known.

A study has been carried out to measure the terminal velocities of the crystal types studied by Nakaya using a more refined technique and to establish values for the terminal velocities as a function of size for some of the crystal types not previously reported.

PROCEDURE

The procedure used consisted of photographing a falling crystal using a strobe light for illumination. To shield the camera from the strobe a 9 cm x 27 cm x 15 cm box was constructed. The box contained at one end a vertical slit with a 1 cm^2 grid on the back. At the other end, a 35 mm camera was mounted. A glass window in the slit side allowed illumination. To prevent drafts a plastic tube was placed on top of the slit and the bottom could be closed. The crystals were photographed as they fell through the slit and since they were illuminated by the strobe at 6000 c. p. m. a series of images for each crystal was produced. Image clarity was quite good and in most cases natural crystals could be readily identified from the film. The distance between images was determined from the grid on the slit and thus only a simple calculation was necessary to find the fall velocity of the crystal. One distinct advantage of this method was that any accelerations of the crystals were apparent by a variation in separation of the crystal images. If the distance was constant it was assumed that the crystal had reached terminal velocity.

Two sources of crystals were used. Natural plane dendrites were collected and preserved in the cold chamber for later use. Other crystal types discussed in the study were photographed as they fell in natural snowfall.

RESULTS AND DISCUSSION

When a crystal reaches terminal velocity, its weight is balanced by an aerodynamical drag force. Thus

$$\frac{1}{2} C_D A \rho_a U^2 = g(\rho_c - \rho_a) V$$

where C_D is the drag coefficient, A is the cross sectional area of the crystal normal to the direction of fall, ρ_a is the density of air, U is the velocity of the crystal of density ρ_c and volume V, and g is gravitational acceleration. Solving for U:

$$U = \sqrt{\frac{2g\rho_c V}{C_D \rho_a A}}$$

where buoyancy effects have been neglected.

It has been found by Magono and in the author's work that plane crystals fall with their basal plane horizontal. This includes both plates and dendrites. Thus the cross sectional area is simply the area of the basal plane and V/A reduces to h, the crystal thickness. This leads to the fact that U is a function of the crystal thickness h.

Ono (4) has reported that plane crystals show an increase in thickness to about 50 to 60μ as the diameter increases and remain constant thereafter. The thickness reaches 50 to 60μ at a diameter of about 1600μ. From these results and the above discussion one would expect the terminal velocity of plane crystals of greater than 1600μ diameter to be constant. This, of course, is what Nakaya found and it should be pointed out that the smallest dendrite that he included in his fall velocity measurements was about 1600μ diameter. Likewise, the terminal velocity of dendrites whose diameter is less than 1600μ should show a functional dependence on their diameter. Although the data is meager in this size range the present study tends to confirm this, as shown in Fig. 1.

Also evident in Fig. 1 is the fact that the values for the terminal velocity of crystals larger than 1600μ differ by about 20 cm/sec between Nakaya's results and the present study. Nakaya performed his work at an elevation of 1030 m whereas this investigation was performed at an elevation of 1525 m. Thus the difference in density would account for approximately 2-3 cm/sec. Of more significance is the experimental design that Nakaya used. If it can be assumed that the diagram depicting the apparatus used by Nakaya is drawn to scale, then it appears that the crystals only fell approximately 20 cm before timing began. It is doubtful that crystals would reach their terminal velocity in this distance, and this would result in a value less than terminal velocity being computed.

When spacial dendrites are considered, the problem becomes more complex. Because of the random orientation and number of arms occurring it is not possible to define cross sectional area and volume as simply as for plane crystals. To overcome this difficulty in reaching a theoretical expression for terminal velocity the following approach was taken: The spacial dendrites were considered in terms of a sphere which would just enclose them and it was assumed that the volume of the sphere would contain x percent ice and the remaining volume, air. Likewise, for a cross section, a certain percent of the area would be ice. This would vary, depending on the cross section, so a mean percentage $\bar{y}$ was assumed for each crystal. x and $\bar{y}$ would be constants for a given crystal. We can now write the expression for terminal velocities of spacial dendrites as:

$$U = \left[\frac{2g\rho_c(x\frac{4}{3}\pi r^3)}{C_D\rho_a(\bar{y}\pi r^2)}\right]^{\frac{1}{2}}$$

where r is the radius of the sphere just enclosing the spacial dendrite. This reduces to:

$$U = \left[\frac{8g\rho_c xr}{3C_D\rho_a\bar{y}}\right]^{\frac{1}{2}}$$

This gives u as a function of r and this result was found experimentally as is shown in Fig. 2. Once again this varies from Nakaya's findings. It is difficult to understand why Nakaya did not find a size dependence for dendrites. A possible explanation is the wide variety of form occurring in crystals classified as spacial dendrites. Perhaps the crystals studied by Nakaya were basically plane dendrites with only small appendages radiating off of the basal plane and consequently behaved much like a simple plane dendrite. The spacial dendrites used in the present study could more appropriately be called spacial stellars since they consisted of long, thin, non-branched arms radiating in all directions. Results for needles and capped columns are shown in Figs. 3 and 4.

CONCLUSIONS

This study on the terminal velocities of ice crystals was performed using a more refined method than Nakaya used. Results show some disagreement but these can be satisfactorily accounted for from a theoretical standpoint. Prof. Lewis O. Grant and Dr. Takeshi Ohtake are acknowledged for their helpful discussions. The research was supported by NSF Grant No. GA-1553.

REFERENCES

1. Nakaya, U., 1954: Snow Crystals. Harvard University Press, Cambridge, 510 pp.
2. Schaefer, V. J., 1947: Properties of particles of snow and the electrical effects they produce in storms. Trans. Amer. Geophys. Un., 28, 587.
3. Magono, C., 1953: On the growth of snowflake and graupel. Sci. Rpt., Yokohama Nat'l. U., Sec. I, 3.
4. Ono, A., 1969: The shape and riming properties of ice crystals in natural clouds. J. Atmos. Sci., 26, 138-147.

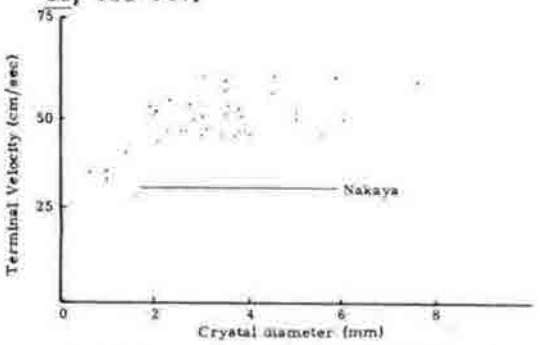

Fig. 1. Relationship between terminal velocity and crystal diameter of unrimed plane dendrites. Solid line is Nakaya's results.

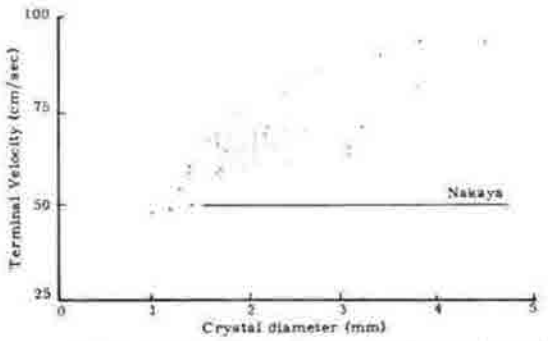

Fig. 2. Relationship between terminal velocity and crystal diameter of spacial dendrites.

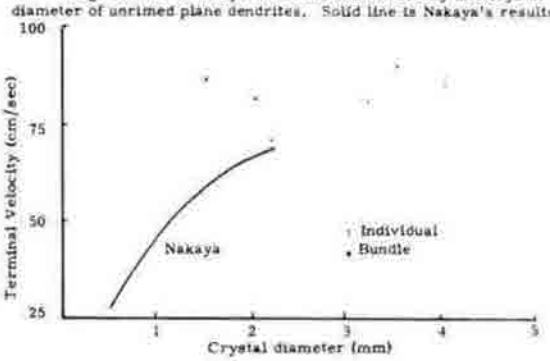

Fig. 3. Relationship between terminal velocity and crystal length of needles and needle bundles.

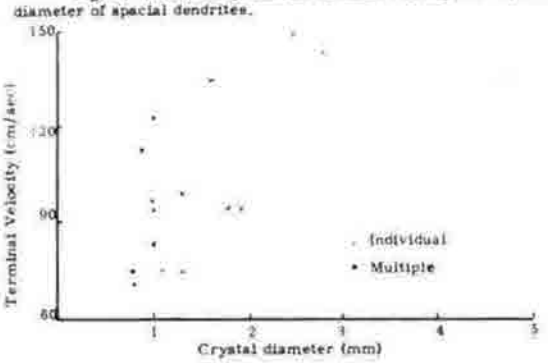

Fig. 4. Relationship between terminal velocity and dimension of capped columns.

SNOW CRYSTAL RIMING RELATED TO CLOUD SYSTEM CHARACTERISTICS

C. F. Chappell
Colorado State University
Fort Collins, Colorado

The growth of snow crystals by accretion of supercooled drops is generally considered to be a time dependent process. The usual procedure for incorporating accretional growth of snow crystals into microphysical models of cold orographic clouds consists of assuming a cloud liquid water content, a collection efficiency for the falling crystal, and initiating accretional growth after a specific size is attained by a given crystal habit. This approach usually shows that accretional growth of snow crystals rapidly becomes the dominant mode of growth. However, observations taken at Climax, Colorado indicate diffusional growth of crystals predominates in most cases. These observations also show that crystal dimensions associated with riming onset are variable from case to case. This suggests other factors may play an important role in controlling accretional growth within the cold orographic cloud system. It is possible through an expression for the supersaturation of a mixed phase cloud to draw theoretical inferences concerning possible contributions of accretion to overall crystal growth.

The time rate of change of cloud supersaturation may be written

$$\frac{dSi}{dt} = Q_1 \frac{dz}{dt} - Q_2(4\pi G)\sum_{1}^{N_d} r_d\left(S_w - \frac{a}{r_d} + \frac{b}{r_d^3}\right) - Q_3(4\pi F_2 S_i G')\sum_{1}^{N_c} CF_1 - Q_3(\pi Q_\ell)\sum_{1}^{N_c} r^2 EV_c \qquad (1)$$

where Q_1, Q_2, Q_3, G, G' are thermodynamic functions
S_i, the supersaturation relative to a plane ice surface
S_w, the supersaturation relative to a plane water surface
z, the distance measured in the vertical
r_d, the cloud droplet radius
r, the snow crystal radius
Q_ℓ, the liquid water content
E, the collection efficiency of the falling crystal
F_1, the ventilation factor of the crystal in the airflow
F_2, the vapor factor that corrects the vapor field to that of a supercooled cloud.
C, the electrostatic capacity factor of the crystal
V_c, the crystal fall speed relative to the environment
a, a function of temperature
b, a function of the solute contained in the droplet
N_d, the cloud droplet concentration
N_c, the snow crystal concentration

Equation (1) shows the time rate of change in cloud supersaturation is due to imbalances between the cooling rate associated with the updraft speed, rate of droplet growth, and the rates of crystal growth by vapor diffusion and accretion. The droplet growth rate term acts as a stabilizing influence on cloud supersaturation since it takes on both negative (evaporation) and positive (growth) values. If the magnitude of the diffusional growth rate term is greater than the cooling rate term, then the droplet growth rate term becomes negative and droplet evaporation tends to maintain the cloud supersaturation at the level of water saturation. Eventually, the reservoir of liquid droplets is depleted and cloud supersaturation begins to fall. However, as cloud supersaturation decreases the diffusional growth rate also falls and the cloud supersaturation attains steady state at some value in excess of ice saturation but below water saturation.

In contrast, if the magnitude of the diffusional growth rate term is smaller than the cooling rate term, then the droplet growth rate term is positive and droplet growth tends to relieve the cloud supersaturation. Under this condition droplets grow within the cloud system, and this production of liquid water ($Q_\ell > 0$) now brings about the possibility that the accretional growth rate term may also assume importance in controlling cloud supersaturation. Depending upon the many complex factors which determine accretional growth rates (crystal habit, collection efficiency, etc.), cloud supersaturation under these conditions attains steady state at some value in excess of water saturation. Juisto and Schmitt (1) have demonstrated some of the above relations by numerical integration of an equation similar to (1). From the above theoretical discussion the following inferences appear valid for cold orographic clouds: Significant accretional growth of snow crystals is to be expected under conditions of steady state cloud supersaturation only when the diffusional growth rate term is less than the cooling rate term. In other words, the occurrence of significant numbers of rimed crystals reflects an inefficiency in the diffusional ice growth process within the cloud system. Normally, the accretional growth rate will fail to make up the total deficit between the supply rate of condensate and the growth rate of ice. Therefore, one may assume that a weather modification potential exists when significant numbers of rimed crystals are observed. Thus, it is possible to crudely recognize cold orographic cloud seeding potential by defining those meteorological conditions for which significant accretion is observed.

This possibility is now investigated using observed crystal data from the Climax experiment.

Figure 1 shows the precipitation measured at the High Altitude Observatory (HAO) near Climax, Colorado on non-seeded days during the 1960-65 years of the Climax experiment plotted as a function of cloud system temperature. The abrupt decrease in precipitation at a 500 mb temperature of -20C probably reflects the temperature at which the diffusional ice growth process is rapidly becoming inefficient. Assuming this to be true, a time averaged vertical motion of 12 cm/sec and a time averaged cloud top height of 460 mb give an average condensation rate and an average diffusional growth rate of ice which reasonably approximate the observed precipitation rate as a function of cloud system temperature. It can be inferred from figure 1 therefore, that no significant accretional growth should be present in the Climax cloud system at 500 mb temperatures colder than about -20C since the rate of crystal growth by vapor diffusion equals or exceeds the rate of vapor supplied. On the other hand, at 500 mb temperatures warmer than -20C where the diffusional ice growth process becomes inefficient, the growth of larger cloud droplets (Q_l becomes relatively large) should increase the probability of observing a significant percentage of rimed crystals.

Figure 2 shows the percentage of total crystals rimed as a function of cloud system temperature. The crystal replication was accomplished on a total of 16 seed and non-seeded days at HAO and nearby Chalk Mountain. It is seen that the percentage of crystals rimed on both seeded and non-seeded days is negligibly small in the colder cloud systems but increases rapidly as temperatures become warmer than about -22C to -21C for unseeded events and about -18C for seeded events. Thus, seeding appears to have the effect of reducing the amount of riming at all temperatures and translates the onset of significant riming toward warmer cloud systems. The onset of significant riming on non-seeded days at 500 mb temperatures around -22C to -21C is in good agreement with observed cloud seeding results at Climax, which show precipitation increases of over 100% for temperatures of -20C and warmer (2) (3). This is consistent with the inference that weather modification potential might be crudely delineated by those meteorological conditions associated with significant numbers of rimed crystals. The translation toward warmer temperatures of the appearance of significant numbers of rimed crystals on seeded days, is consistent with the Climax model (3), and apparently is due to a more efficient diffusional ice growth process in this temperature range. The theory and observed data therefore suggests that the specification of riming onset by crystal type and size in cold orographic clouds is rather meaningless without concurrent knowledge of cloud supersaturation. Ice crystal growth by accretion is a time dependent process only after it is determined that there are any collectable droplets at all. The real control on the onset of riming under conditions of steady state cloud supersaturation is in the interplay between the cooling rate term and the diffusional growth rate term. It is therefore mainly dependent upon updraft speeds and cloud system temperatures.

REFERENCES

1. Juisto, James E. and Richard K. Schmitt, 1970: A model of supercooled cloud microphysics, Preprint of Second Nat'l Conf. on Weather Modif., Santa Barbara, Calif., Apr. 6-9, 41-43.
2. Chappell, C. F., 1967: Cloud seeding opportunity recognition. Atmospheric Sci. Tech. Paper 118, Dept. of Atmos. Sci., Colorado State Univ.
3. Grant, L. O., C. F. Chappell and P. W. Mielke, Jr., 1968: The recognition of cloud seeding opportunity. Proc. of First Nat'l Conf. on Weather Modif., Albany, N.Y.

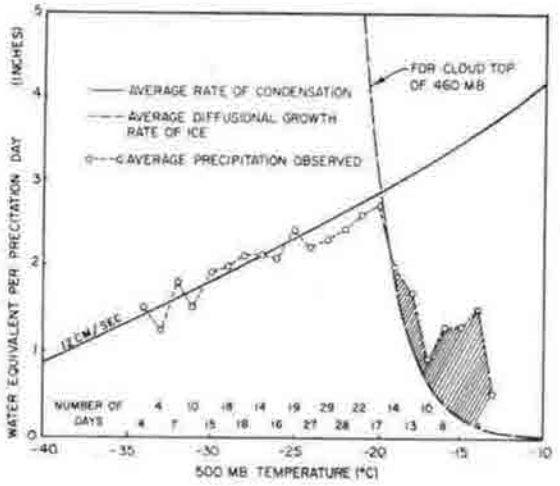

FIG. 1. THE DISTRIBUTION OF OBSERVED PRECIPITATION INTENSITY AT CLIMAX COMPARED TO A THEORETICAL DISTRIBUTION COMPUTED ASSUMING ONLY DIFFUSIONAL GROWTH OF ICE CRYSTALS. CROSS-HATCHED AREA PROBABLY REPRESENTS AN ADDITIONAL PRECIPITATION INTENSITY ARISING FROM ACCRETIONAL GROWTH AND POSSIBLY ICE CRYSTAL MULTIPLICATION IN THE CLOUD SYSTEM.

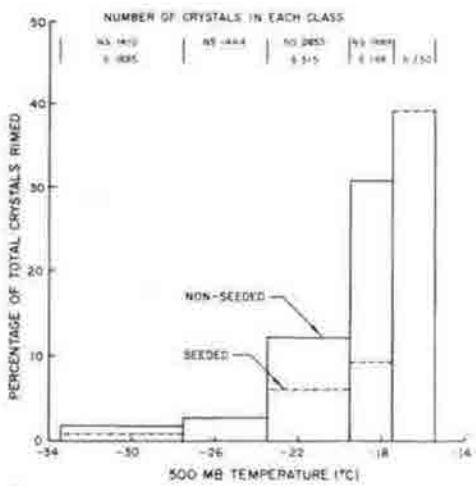

FIG. 2. RELATIONSHIP BETWEEN THE ONSET OF SIGNIFICANT ACCRETIONAL GROWTH IN THE CLIMAX CLOUD (MEASURED BY THE PERCENTAGE OF TOTAL CRYSTALS RIMED) AS A FUNCTION OF CLOUD SYSTEM TEMPERATURE.

ON THE NUMBER DISTRIBUTIONS OF HAIL GROWING IN UPDRAFTS

R.B. Charlton and Roland List

Dept. of Physics, University of Toronto
Toronto, Canada

The formation of hail in a convective updraft causes liquid water depletion and imposes a body force on the updraft's air parcels. Conversely, the growth of hailstones is dependent on their ability to compete for the available liquid water and on the updraft field's reaction to their presence.

When Iribarne and de Pena (2) and List et al. (3) modelled hail growth with hail embryos of a single size injected into an updraft, they were able to increase the embryo number to a critical value which caused nearly all of the cloud's liquid water to be depleted. This situation results in hail accumulation zones which are highly populated and which represent an unrealistic force on the updraft. If these critical numbers are spread over several closely-spaced embryo sizes the unrealistic situations in terms of water depletion and energy balance are no longer encountered.

The new model is based on hail embryos injected continuously in known numbers and sizes at the 0C level of a non-divergent (cloud air density times updraft velocity equals constant at all levels) and pre-determined updraft. The only cloud parameter directly influenced by the growing hailstones is the liquid water content (LWC). The hailstones move at terminal velocity (drag coefficient 0.5) and accrete (with 100% efficiency) the LWC which moves at updraft speed.

Two types of growth from an embryo size spectrum are considered, both of which are steady-state. The first grows hail as it ascends from the input level. The LWC depletion by stones of each size group is no longer considered when their balance levels has been attained. This solution represents hail growth conditions at a certain time after the first embryos entered the updraft and just before the descent begins. The second type considers hailstones ascending to their balance levels and also growing while descending back to the input level.

Taking numerical values for the updraft air parcels and the cloud environment from an average Denver 'hail day' sounding allows comparison of the upward thermal buoyant force to the downward drag force of the hailstones plus the LWC. Since the updraft velocity increases with height as the air density decreases, the kinetic energy for this acceleration from the cloud's 0C level can be compared to the energy available from the integrated thermal buoyant force and the hydrometeor weight.

Figures 1-5 show the results of injecting 0.3, 0.4, 0.5, 0.6, and 0.7 cm spherical embryos simultaneously and continuously in numbers of 0.2, 0.6, 1.4, 0.6, and 0.2/m^3 respectively into an 18 m/s updraft at the 0C level. (The updraft increases to 27 m/s at 4 km). The values of forces, energies, total hailstone number and hailstone size distributions (Figs. 3-7) are calculated by standard smoothing techniques.

The example from Charlton, 1970 (1), shows that during growth on ascent the LWC depletion (Fig. 2) is significant (20%) and occurs in the region where the most numerous embryos reach their balance levels. The hydrometeor forces of the ascent case are not large enough to greatly influence the updraft's energy balance (Fig. 4). When ascent and descent growth occurs there is much more depletion ($\sim$ 70%) and the cloud's force and energy balance is upset.

All examples calculated to date have shown that hail mass accumulation zones can only be equivalent to 2 to 4 times the natural LWC, and that moderate LWC depletion (20-40%) is usually sufficient to considerably influence the cloud's energy balance. The growth curves (Fig. 1) show how the rejection of smaller stones towards the cloud's top, as liquid water is depleted by hail growing at lower levels, tends to impede the formation of accumulation zones. The model has also shown how 5 to 10 hail size classes at a given level are sufficient to describe a smoothed number distribution (Fig. 6 and 7). In connection with these studies, Charlton (1) also found that when no individual hailstone size is capable of depleting more than about 40% of the LWC then only realistic conditions are encountered.

Acknowledgements. This study was sponsored by the Environmental Science Services Administration, U.S. Department of Commerce through the National Severe Storms Laboratories, Norman, Oklahoma. One of the authors (R.B.C.) gratefully acknowledges receipt of a Burton Scholarship from the University of Toronto.

REFERENCES

(1) Charlton, R.B., 1970: Hail formation and its effect on a model updraft. Ph.D. thesis, University of Toronto, pp. 136.

(2) Iribarne, J.V., and R.G. de Pena, 1960: The influence of particle concentrations on the evolution of hailstones. Nubila, 5, 7-30.

(3) List, R., R.B. Charlton, and P. Buttuls, 1968: A numerical experiment in the growth and feedback mechanisms in a one-dimensional steady-state model cloud. J. Atmos. Sci., 25, 1061-1074.

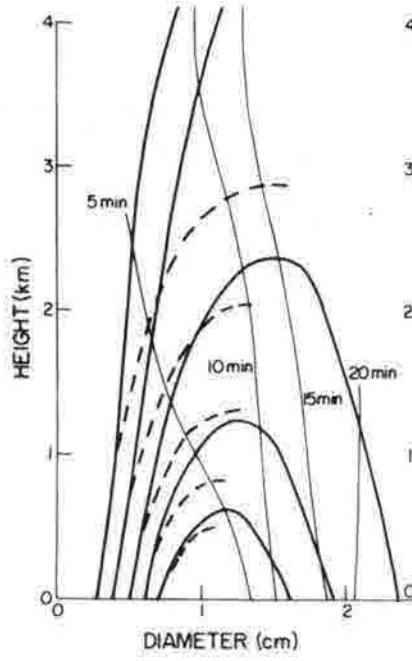

Figure 1

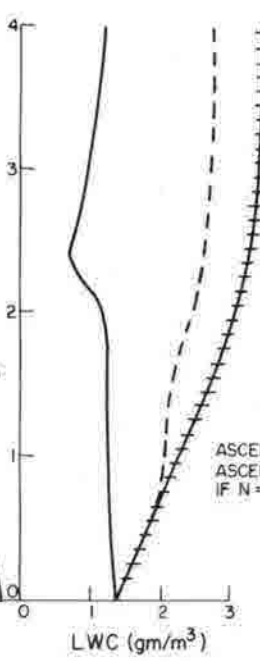

Figure 2

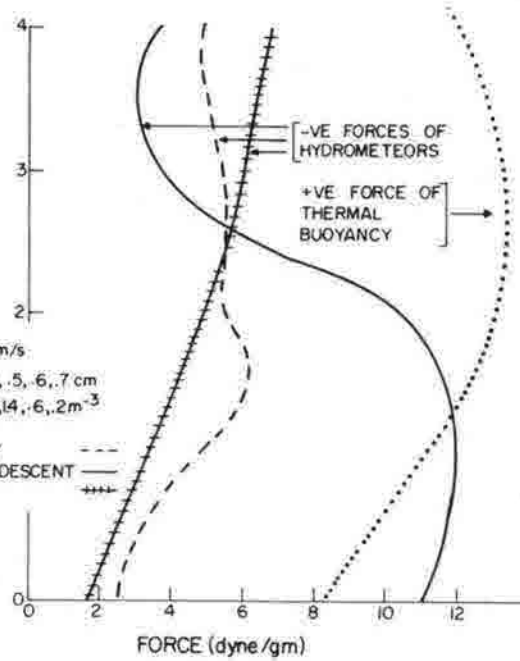

Figure 3

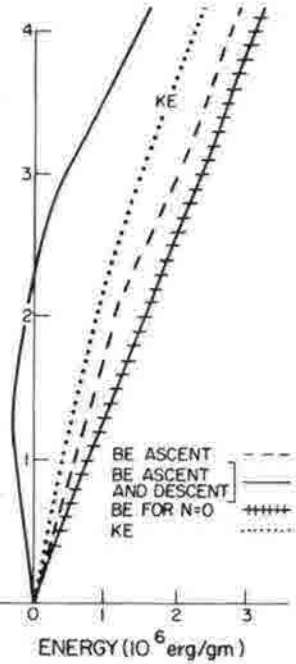

Figure 4

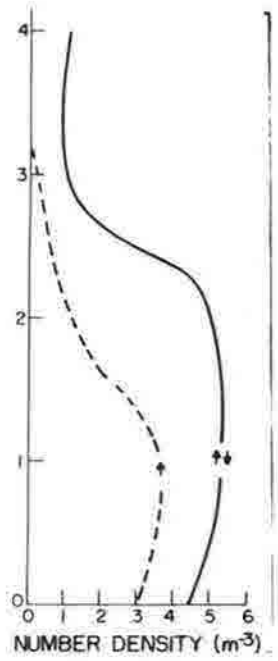

Figure 5

Figures 1 and 2 - Hail growth curves and liquid water content as functions of height above embryo injection level. A 'Gaussian' type embryo size distribution centered about 0.5 cm diameter is injected into an 18 m/s updraft. Figure 1 also shows growth times for the ascent and descent case. Figure 3 compares the downward force of hail and liquid water (or liquid water only in the case of no hailstones) to the upward thermal buoyant force which was calculated from an actual 'hail day' sounding. In Figure 4 the buoyant energy BE, which is the buoyant force plus hydrometeor force integrated from the input level, is compared to the cloud parcel's kinetic energy increase KE from the input level. Figure 5 shows total hailstone number density. Figures 6 and 7 show smoothed hailstone number density distributions for various heights, mostly at balance levels.

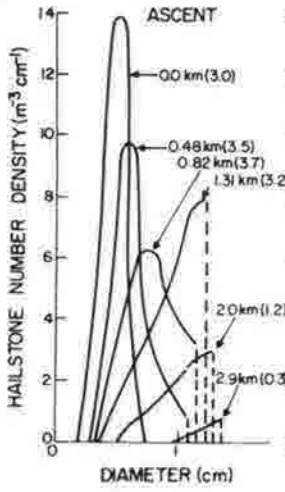

Figure 6

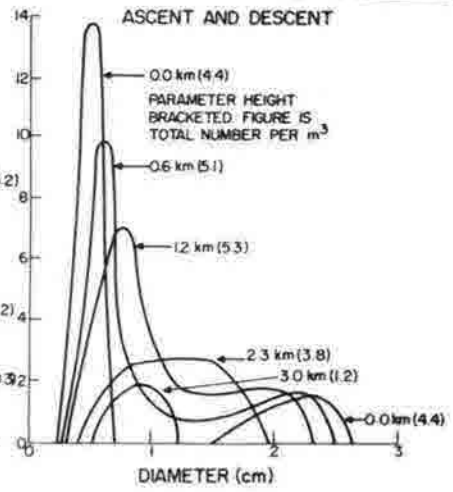

Figure 7

GENERATION OF MICRO-DROPLETS BY FREEZING A SUPERCOOLED WATER DROP

Roger J. Cheng

Atmospheric Sciences Research Center
State University of New York at Albany
Albany, New York

INTRODUCTION

The ejection of micro-droplets from the surface of a supercooled water drop has been observed and photographed. The fragmentation of a freezing drop in the forms of splintering, shattering or bursting has been known for some time. This new phenomena of ejection of micro-droplets, with numerous droplets ejected, the duration of their ejection and the electrical properties of these droplets suggest a possible mechanism of charge generation in thunderstorms.

EXPERIMENTAL

A water drop of 1 mm in diameter, placed on a microslide, was supercooled inside a temperature controlled chamber located under a high power microscope. Observations of the freezing of the drop were made by using cinephotomicrographic technique. The chamber and drop were cooled. At the moment the freezing started, a thin ice shell formed immediately on the surface of the water drop and its temperature, monitored by a small thermocouple, jumped to 0° C. Then, a large number of small water droplets, ranging from <1μ to 20μ, were ejected from the surface of the freezing water drop. These droplets fell on to the microslide. The small droplets were ejected continuously for an average of 50 seconds, depending on environmental conditions. During this period, the small droplets on the slide near the freezing drop grew more rapidly than the ones farther away. The concentration of small droplets on the microslide also increased rapidly and the interior temperature of the freezing drop remained about 0° C. After completion of freezing, the growth of the small droplets terminated and the temperature of the frozen drop decreased rapidly to the environmental temperature. Then all of the small droplets began to diminish in size. Those farthest from the frozen drop gradually disappeared. Some of the small droplets froze by contact with spicules from the frozen drop, as shown in Figure 1. Similar experiments were also performed with a water drop suspended on a fine fiber. After freezing started, a stream of small water droplets were ejected continuously from the surface of the freezing drop during the entire freezing period. This phenomenon terminated after completion of freezing.

Electric measurements were made in three ways; (1) by placing the probe of a sensitive electrometer into the stream of ejected small droplets, (2) by placing the probe into the freezing water drop, and (3) by observing the deflection of the stream of ejected small droplets in an electric field. The results indicated that the ejected small droplets carried net positive charge and net negative charge was left on the residual frozen drop.

DISCUSSION

Experimental evidence has shown that positive charged droplets were generated by the freezing of a supercooled water drop. The possible mechanisms for their generation are:

1. Due to increase of interior pressure, unfrozen water in the form of small droplets was excreted from numerous pores which appeared to be weak spots found in cracks on the ice surface. Small spicules formed later at these same weak spots as shown in Figure 1.

2. Condensation of water vapor, sublimated from the ice surface of the freezing drop, also contributed a large number of small droplets. The temperature of the freezing drop was higher than that of the surrounding environment.

3. Formation of small droplets by bursting of air bubbles, which were observed under the ice surface on the drop and in the interior of spicules. The air bubbles were formed due to the decrease of solubility of air in water when the temperature of the drop increased upon freezing.

Based on the observations of sequences of photomicrographs of the drop freezing and of the temperature curve shown in Figure 2, it is noted that the vapor pressure gradient reversed direction twice during the freezing period. These reversals occurred when the freezing started and when the freezing was completed, and the water vapor molecules moved outward from the surface of the freezing drop during the entire freezing period. A definite radial temperature gradient was maintained within the drop during the freezing period, with the colder region at the surface and the warmer region at the interior. A concentration of positive charge was found in the outer layer of the freezing drop (1, 2) when the small droplets were ejected from the surface, they carried net positive charge with them, while negative charge was left on the residual frozen drop.

CONCLUSION

It is suggested that this newly observed phenomenon of the ejection of droplets is an important process which occurs under natural conditions in thunderclouds near the freezing level and where the water drops, carried from the base of the thundercloud by updrafts, are freezing.

It is also possible that these ejected small droplets will also freeze after being carried upward to the higher and colder region of the thundercloud. Also it is widely accepted that the charge generation and separation processes in a thundercloud are closely associated with the development of precipitation and the main charge centers that appear above the freezing level. It is natural to associate their generation with the ice phase.

Previous attention has been given to the fragmentation of a freezing water drop (1, 2, 3, 4, 5) in the forms of shattering, splintering or bursting, which has occurred occasionally during the freezing period. This present observation suggests that the ejection of small droplets by freezing a supercooled water drop may play an important role in the studies of thundercloud dynamics and in the generation of thunderstorm electricity.

REFERENCES

(1) Mason, B. J. and Maybank, J., 1960: "The Fragmentation and Electrification of Freezing Water Drop", Quart. J. R. Met. Soc., 86, 176-186.

(2) Latham, J. and Mason, B. J., 1961: "Generation of Electric Charge Associated with the Formation of Soft Hail in Thunderclouds", Proc. Roy. Soc. A, 260, 523-536.

(3) Johnson, D. A., 1968: "An Experimental Investigation of Charge Separation Due to the Fracture of Freezing Water Drops", Proc. Inter. Conf. Cloud Physics, 624-628.

(4) Johnson, D. A. and Hallett, J., 1968: "Freezing and Shattering of Supercooled Water Drops", Quart. J. R. Met. Soc., 94, 468-482.

(5) Dye, J. E. and Hobbs, P. V., 1968: "The Influence of Environmental Parameters on the Freezing and Fragmentation of Suspended Water Drop", J. Atmos. Sci., 25, 82-96.

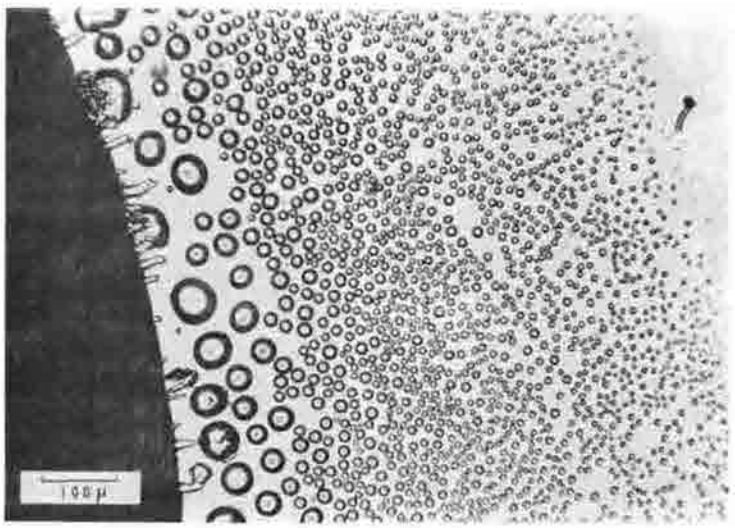

FIGURE 1. EJECTION OF MICRO-DROPLETS BY FREEZING A SUPERCOOLED WATER DROP.

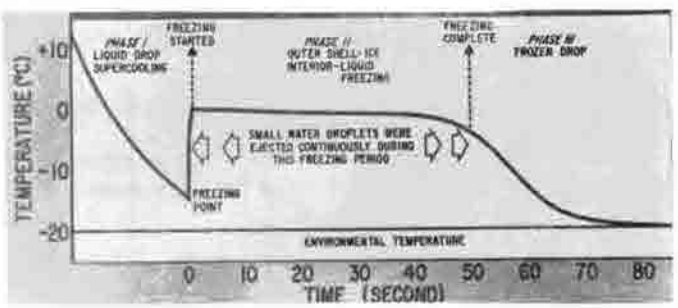

FIGURE 2. TIME-TEMPERATURE CURVE FOR THE FREEZING OF A SUPERCOOLED WATER DROP.

THE INFLUENCE OF THE LATENT HEAT RELEASED DURING ICE CRYSTAL RIMING ON VAPOR DEPOSITION GROWTH

by William R. Cotton[1]
Pennsylvania State University
Univeristy Park, Pennsylvania

Assuming that an ice crystal is in thermodynamic equilibrium, the rate of mass growth of an ice crystal by vapor deposition can be shown to be

$$\left(\frac{dM}{dt}\right)_s = \frac{4\pi C(S-1)}{\underbrace{\frac{m_w L_s^2}{KRT^2}}_{A_K} + \underbrace{\frac{R\,T}{m_w D e_s(T)}}_{B_K}} - \frac{\frac{m_w}{R} L_s L_f \left.\frac{dM}{dt}\right|_R}{KT^2 (A_K + B_K)} \qquad (1)$$

where C represents the crystal capacitance,
S is the supersaturation with respect to ice,
m_w is the molecular weight of water,
K^w is the molecular thermal conductivity,
R is the gas constant of air,
T is the cloud temperature,
$e_s(T)$ is the saturation vapor pressure with respect to ice,
D^s is the diffusivity of water vapor in air
L_s is the latent heat of sublimation,
L_f is the latent heat of fusion, and
$dM/dt)_R$ is the rate of mass growth of an ice crystal by riming of supercooled cloud droplets. The derivation of Equation 1 is similar to the development by Byers (1965) with the addition of the heat released by riming growth. The effect of the second term of the right hand side of Equation 1 on the predicted rate of mass growth of a dendrite is considered in this study. The dendrite is assumed to nucleate on a sublimation nucleus, grow by vapor deposition as a hexagonal plate until it becomes 30 μm thick and then grow two-dimensionally by vapor deposition in the geometric configuration determined by Nakaya (1954). Crystal ventilation is treated similarly to the method of Shiskin (1965). Following a 60-second analytic initialization, crystal-riming growth is also simulated. The rate of growth of a dendrite by riming is

$$\left.\frac{dM}{dt}\right)_R = \frac{\pi a^2}{4} (V_c - V_D)\, E\, w, \qquad (2)$$

where a is the length of the crystal basal plane axis,
V_c is the crystal terminal velocity
V_D is the terminal velocity of the droplet contributing the most to the liquid water content,
E is the average collection efficiency, and
w is the cloud liquid water content. Rimed water mass is deposited only in the direction of the crystal c-axis (prism-plane axis). Following initialization, all growth equations are integrated numerically by centered differences.

Figures 1 and 2 illustrate the predicted rate of vapor deposition growth of a dendrite with the rime-heating term neglected and included, respectively. Figure 3 shows the percentage difference in the predicted total mass of a dendrite with and without the rime-heating term. The greatest percentage difference occurs with a liquid water content of 0.8 g/m^3 because there is a considerable time delay in the onset of graupel formation when the term is neglected. Figure 4 illustrates the predicted total mass of a dendrite grown by vapor deposition and riming with the rime-heating term included in Equation 1. For further details, see Cotton (1970).

REFERENCES

Byers, H. R., 1965: Elements of Cloud Physics. The University of Chicago Press, 109-127.

Cotton, W. R., 1970: Numerical Simulation of Precipitation Development in Supercooled Cumulus. Ph.D. Dissertation, Department of Meteorology, Pennsylvania State University.

Nakaya, U., 1965: Snow Crystals. Harvard University Press, Cambridge, Massachusetts.

Shiskin, N. S., 1965: On snow crystal growth in clouds. Supplement to Proc. of Int. Conf. on Cloud Physics, Tokyo, Japan.

ACKNOWLEDGMENTS

This work was supported by Contract No. E22-103-68(N) with ESSA, Atmospheric Physics and Chemistry Laboratory and by Grant No. GA 138/8 from the National Science Foundation.

[1]Present affiliation: EMB, Atmos. Physics and Chem. Lab., ESSA, Coral Gables, Florida.

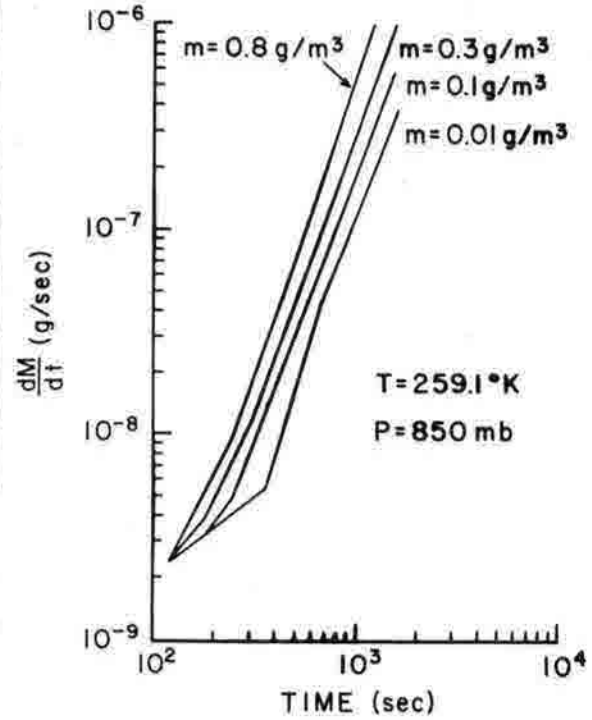

Figure 1. Rate of vapor deposition growth of a dendrite with the rime heating term neglected in Equation 1.

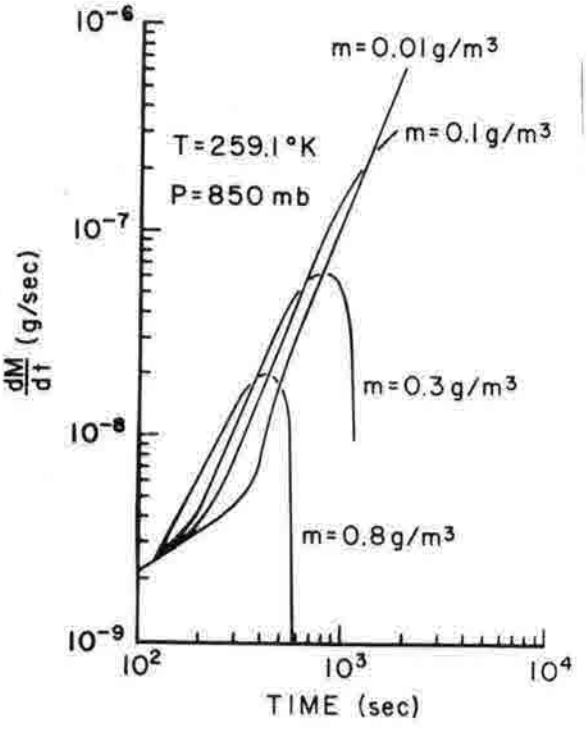

Figure 2. Rate of vapor deposition growth of a dendrite with the rime heating term included in Equation 1.

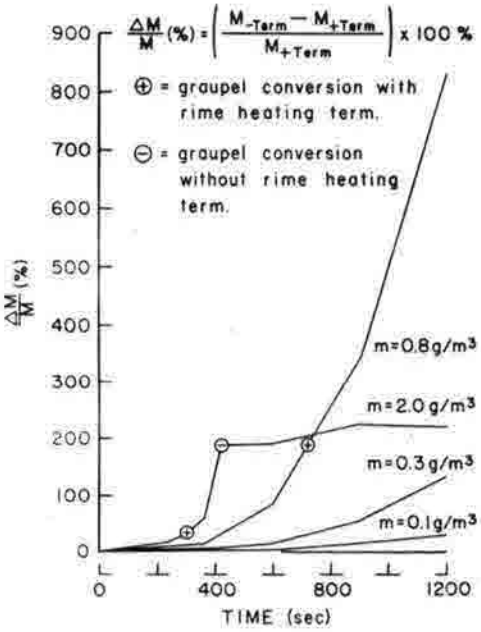

Figure 3. Percentage difference between the predicted total mass of a dendrite, grown by vapor deposition and riming, with the second term in Equation 1 neglected and with the term included.

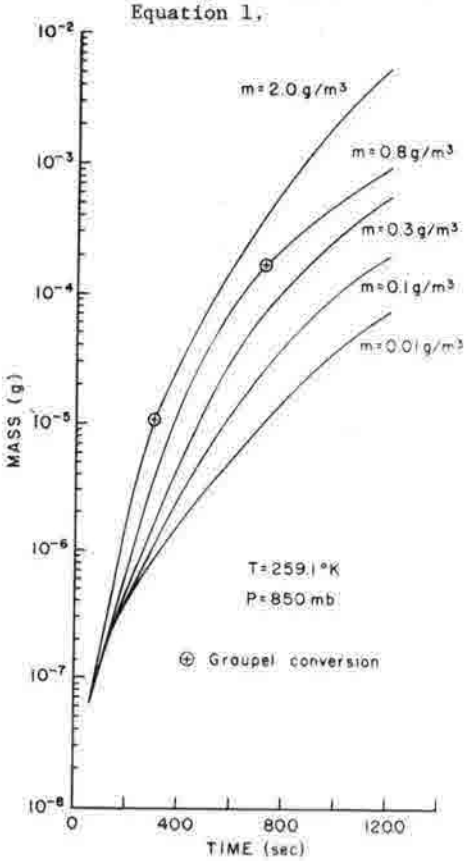

Figure 4. Predicted total mass of a dendrite grown by vapor deposition and riming with the rime heating term included in Equation 1.

OBSERVATIONS AND THEORY OF A MONTREAL HAILSTORM

Marianne English and Charles Warner
McGill University, Montreal, Canada

The Montreal storm of 1 August 1969 developed within widespread air mass convection in the warm sector of an occluding low centred over James Bay. This relatively short-lived cell penetrated the tropopause at 11.2 km between 1500 and 1615 EDT and produced hail over a swath more than 20 km long and 6 km wide. With a slowly veering direction of motion, the storm moved at about 29 kt from 209°, to the left of all wind directions above cloud base. The wind was about 47 kt from 234° at 12.2 km altitude. The hail swath, rainfall isohyets and the passage of the precipitation core are shown in Fig. 1. The storm produced its heaviest hail (with largest dimensions up to 7.5 cm and masses up to 70 g) over about a 4 km distance and a period of 15 mins.

The McGill FPS-18 radar, operating at 10 cm and having a 1° conical beam and a pulse width of 1 μ sec, showed the presence of a marked overhang with strong reflectivity gradients, which was detected between about 1505 and 1540 EDT. The storm at the peak of its development is shown in a HARPI (Height-Azimuth and Range display, reconstructed from PPI information), Fig. 2 and in the 2.8° PPI of Fig. 3.

14 raingauges, 8 instrumented stations and many citizens' reports provided surface data on the storm. These confirmed the implication of the radar data that the storm fed on its left front side. Four anemograms from stations in the path of the storm showed a pattern of confluence occurring ahead of the region of marked difluence (with gusts up to 50 knots) which accompanied the precipitation. These data, and reports of cloud cover from citizens and from the Observer at Dorval Airport, on the north-west side of the precipitation area, indicated that the updraft area was about 9 km across.

A simple two-dimensional model of the updraft region of this storm has been extracted from the above data; using as a guide the successful model for the Alberta Hail Storm of 29 June 1967 (1). The present model has been improved by developing a method for calculating the slope of the updraft and by adopting a more realistic updraft profile.

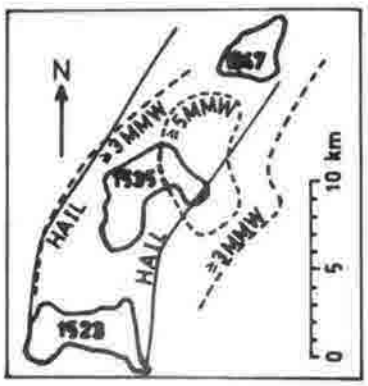

Fig. 1: The hail swath, rainfall isohyets (--), and contours of reflectivity 60 dBz at 2.8° elevation and at three times. The storm reached a maximum height close to 12.3 km at about 1523 EDT, dropped the largest hail at 1535, and began to dissipate at 1547.

The adiabatic profile for this storm yielded a maximum updraft speed of 34 m sec^{-1} at 9 km and a cloud top at 12.3 km. This implied unrealistically large horizontal divergence in the upper cloud. Following Fujita and Grandoso (2) the updraft maximum was lowered to 7.8 km, and 32 m sec^{-1}, the adiabatic value at that level, was taken as the maximum.

To calculate the geometry of the storm circulation, an equation based on work by F.C. Bates (3) was used. The change in horizontal velocity $\bar{V}$ with height z of an element of updraft rising with vertical velocity $\bar{w}$ and embedded in a horizontal flow of velocity $\bar{V}$ was determined as $\bar{w}\frac{d\bar{v}}{dz} = \frac{C}{\pi}\left|\bar{V} - \bar{v}\right|(\bar{V} - \bar{v})$.

C was held constant at 7 km^{-1} after calibration using two well documented Alberta storms. $\bar{V}$ as a function of height was obtained, and thus the updraft geometry (assumed approximately steady). The calculation was not sensitive to the assumptions made, and showed that at 3 km, where the adiabatic L.W.C first reached 4 g kg^{-1} the draft was sloping away from direction 340° (± 10°): Fig. 3 shows the precipitation core and downdraft displaced from the updraft in this

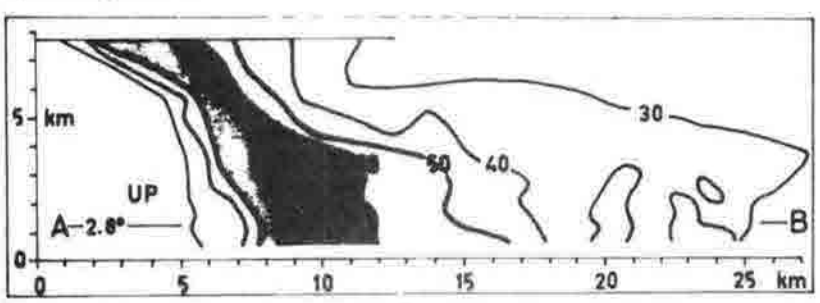

Fig. 2: "HARPI", 1526 EDT 23.3 km slant range, along line AB in Fig. 3. Reflectivities on the contours in dBz. Note the overhang to the north-west (at left), at about 6.5 km above ground. Up- and down-draft regions are separated by strong reflectivity gradients. The adjacent mass to the south (to the right) is dissipating.

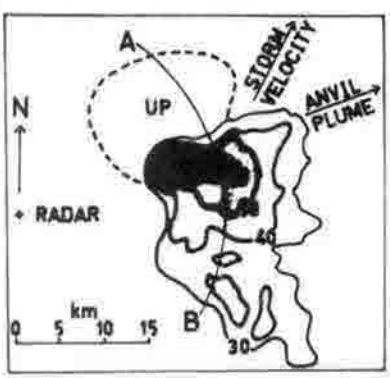

Fig. 3: 2.8° PPI, 1526 EDT, and major storm features. AB is the HARPI section at 23.3 km range shown in Fig. 2. Downdrafts occurred with heavy precipitation. Updraft area indicated by dashed outline.

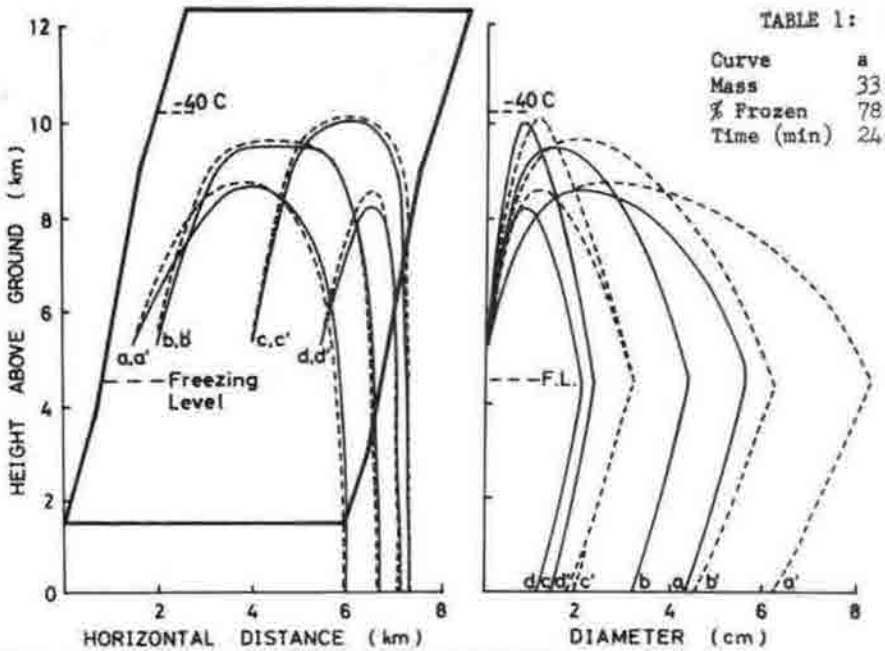

TABLE 1: HAIL PARAMETERS AT GROUND

Curve	a	a'	b	b'	c	c'	d	d'
Mass	33	93	15	36	1.4	2.5	0.7	2.1
% Frozen	78	69	93	86	100	99	100	94
Time (min)	24	23	20	20	17	17	15	15

Fig. 5: Hail trajectories (left) and growth curves (right). Pairs of curves (a and a' etc.) are shown for each of four initial horizontal positions. The solid-line curves (a, b, etc.) are for rough spherical stones and the dashed, (a', b', etc.) are for rough oblate stones with axial ratio of 0.8. The initial diameter of the hail embryo is 1 mm at a height of 5.3 km (-5C) (The change in slope in the growth curves at the F.L. is due to melting.)

direction. The minimum slope from the vertical of the updraft axis was calculated to be $8^{o} \pm 2^{o}$.

The non-sphericity of the hailstones was striking. Maximum and minimum diameters of 115 hailstones were measured, and the diameter ratios of these stones are shown as a function of mass in Fig. 4. The median diameter ratio is 0.61. Note that all large stones have diameter ratios in the range 0.54 to 0.8, i.e. relatively close to the median value.

In the hail growth calculations, the effects of hail shape and surface irregularities have been considered. The hail shape has been approximated by that of an oblate spheroid. Following List (4) and others, the crucial assumption that the hailstones fall with their minor axis vertical has been made. A constant axial ratio of 0.8 has been used. This value is somewhat higher than the median value to allow for the effect of melting on shape (5). The principal effect of surface irregularities is to increase the heat transfer between air and stone; the results of Bailey and Macklin (6) have been used here.

Results of the hail growth calculations are shown in Fig. 5 and in Table 1. (The results seem to be insensitive to initial height and diameter; initial levels of -10C and -15C and an initial diameter of 2 mm were tried.) Comparing curves a and a', b and b', etc. we note that there is little difference in the trajectories of spherical and oblate stones but the oblate stones grow to much bigger sizes. The largest spherical stone, a, has a mass of only 33 g at ground, while our measurements indicate that about one-fifth of the stones exceeded this. Thus to account for the largest stones, we must invoke the oblate stone model; the largest calculated oblate stone being 93 g at ground. This is in good agreement with our measurements, since none of the spherical stones (diameter ratio 0.9 or greater) weighed more than 30 g. The time required to grow the calculated hailstones, 15 to 24 min, is consistent with radar evidence and citizens' reports. The heights of the trajectory peaks and the fall of the largest hail closest to the updraft core are also consistent with the radar observations. Thus this model of hail growth yields results in satisfactory agreement with observations.

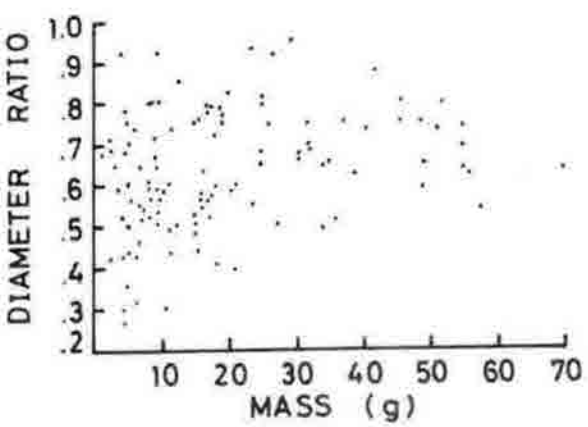

Fig. 4: Diameter ratio vs mass for 115 hailstones selected from a sample of about 300.

References and acknowledgements

1. Warner, C., M. English, A.J. Chisholm and W. Hitschfeld, 1969: The pattern of an Alberta Hailstorm. Preprints 6th Conf. on Severe Local Storms, Chicago, 290-295.
2. Fujita, T. and H. Grandoso, 1969: Split of a thunderstorm into anticyclonic and cyclonic storms and their motion as determined from numerical model experiments. J.Atmos.Sci.25.
3. Newton, C.W., 1968: Convective cloud dynamics. Proc. Int. Conf. on Cloud Phys. Toronto.
4. List, R.,1959: Zur Aerodynamik von Hagelkoerner. Z. Angew. Math. Phys., 10, 143-159
5. Macklin, W.C., 1964: Factors affecting the heat transfer from hailstones. Quart. J. Roy. Met. Soc., 90, p.84.
6. Bailey, I.H. and W.C. Macklin, 1968: Heat transfer from artificial hailstones. Quart. J. Roy. Met. Soc., 94, p.93.

This work was supported by the Meteorological Service and the National Research Council of Canada.

ESTIMATION OF THE OCCURRENCE OF HAIL AND HAILSTONE SIZES

Narayan R. Gokhale and K. M. Rao
State University of New York at Albany
Albany, New York 12203

INTRODUCTION

Many earlier investigators with some success correlated the occurrence of hail and their sizes to different meteorological parameters such as (a) instability, (b) height of the wet bulb freezing, (c) wind shear at high altitudes, (d) maximum height of the radar echo, (e) intensity of radar echo. All these parameters may indicate the occurrence of a severe thunderstorm but cannot be used in all cases to distinguish thunderstorms from hailstorms. Instability is a factor in causing hail but the presently published data show that one cannot identify the stability which will produce hail. Fawbush and Miller (1) with some success correlated the occurrence of hail with height of the wet bulb freezing and to large positive areas on the tephigram between the environmental dry bulb curve and the parcel adiabat. But other workers like Douglas and Hitschfeld (2), Longley and Thompson (3) could not get the same correlation for their Alberta data. Though the maximum height of the radar echo was reported to correlate well with hail occurrence [Douglas and Hitschfeld (2)], Geotis (4) concludes from his radar data in New England hailstorms that there is no clear dependence of either hail size or hail echo duration upon the height of the storm. Whereas the intensity of radar echo is a good indicator of heavy precipitation, it cannot distinguish between heavy rain and hail. The Gokhale and Rao (5) theory of hail growth indicated that not all of the above mentioned parameters are important. On the other hand, few other parameters which were not considered earlier are important for the formation and occurrence of hail. These parameters are (a) cloud base height and temperature, (b) height (Z_1 to Z_2) of the -4°C to -30°C temperature region, (c) duration for which the intensity of the radar echo exceeded 55 db (10 cm radar) in the region, Z_1 to Z_2. The curves (a) and (c) in Fig. 1 border the temperature range within which the freezing of different size supercooled drops occurs for the model cloud. The warmest is -4°C and the coldest temperature is -30°C for the diameter range of 5.75 mm and 0.1 mm. In Fig. 2, the region A indicates where the hydrometeors of diameter up to 6.0 mm originate, and the lower region, B, the region of hail growth.

NOMOGRAM TO ESTIMATE HAILSTONE SIZES

Prediction of the maximum size of hailstone that can occur in a hailstorm is as important as predicting the occurrence of hail itself. A nomogram is developed relating the size of hailstone with cloud base temperature, radar reflectivity and duration. The nomogram in Fig. 3 corresponds to a cloud base height of 1.5 km. For different cloud base heights appropriate nomograms can be developed.

The nomogram is essentially a graph which consists of hail growth curves for different values of effective LWC and duration. For these calculations, the growth of the hailstone during its fall,

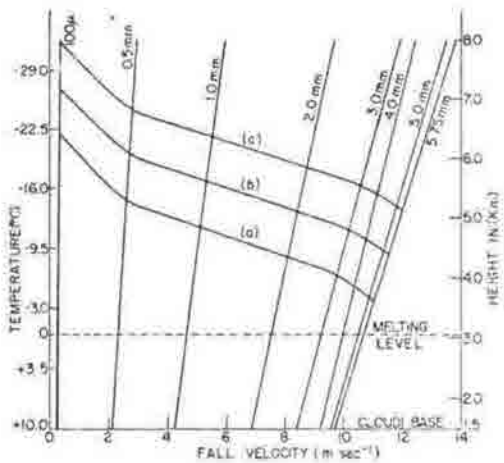

FIG. 1. Characteristics of the model cloud. The cloud base temperature is +10°C and height is 1.5 km. The slant lines indicate the fall velocities of the indicated drop sizes at different heights. Curves (a), (b) and (c) indicate the freezing temperatures of few drops, 50% of drops and all drops respectively. (after Gokhale and Rao, 1969).

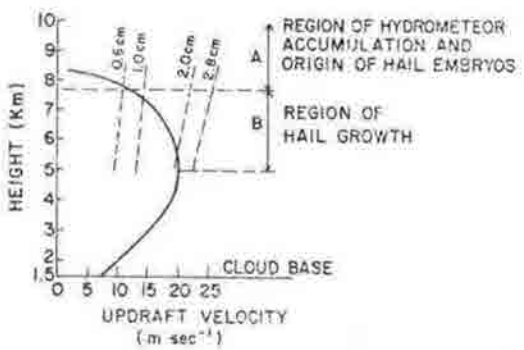

FIG. 2. Regions of hail embryos and hail growth in a typical well developed steady updraft. (after Gokhale and Rao, 1969).

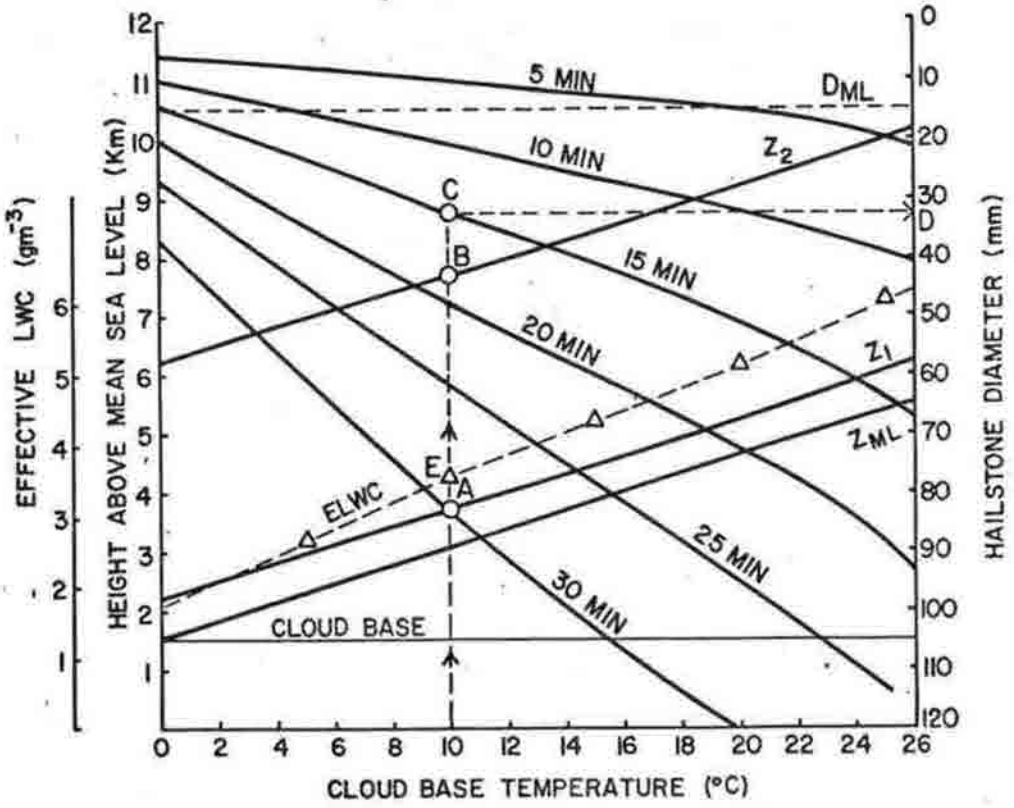

FIG. 3. Nomogram for determining hailstone size.

its reduction in size due to melting and evaporation in subcloud layer are not considered. The use of the nomogram is described with an example. To calculate the maximum size of the hailstones for a cloud base temperature +10°C and for 15 minutes duration, proceed as indicated by dashed line, in Fig. 3.

OCCURRENCE OF HAIL

Atlas (6) reviewed the earlier work on radar reflectivity factor and hail. The duration and the region of occurrence of this high reflectivity was not considered. Gokhale and Rao (5) have shown that the region of hail growth mainly lies between temperature range -4°C and -30°C, the region between the lines Z_1 and Z_2 in Fig. 3. If the radar reflectivity higher than 55 db (10 cm radar) persists for a duration greater than say 10 minutes in this region, it seems the probability of occurrence of hail is rather high. If this high reflectivity value occurs below the height Z_1 or above the height Z_2, it does not indicate the formation of hail. Thus not only the intensity of the radar echo, but its duration in the region bounded by the lines Z_1 and Z_2 needs to be considered. This particular technique of forecasting hail limits the forecast time to 10 to 15 minutes and may not be of much importance for forecasting well in advance, but still it may be adequate for hail suppression work.

ACKNOWLEDGMENTS

The research reported in the paper was sponsored by the Air Force Cambridge Research Laboratories, Office of Aerospace Research, under Contract Number F19628-68-C-0057.

REFERENCES

1. Fawbush, E. J. and R. C. Miller, 1953: A method for forecasting hailstone size at the earth's surface, Bull. Amer. Met. Soc., 34, pp. 235-244.
2. Douglas, R. H. and W. Hitschfeld, 1959: Patterns of hailstorms in Alberta, Quart. J. R. Met. Soc., 85, pp. 105-119.
3. Longley, R. W. and C. E. Thompson, 1965: A study of the causes of hail, J. Appl. Meteor., 4, pp. 69-82.
4. Geotis, S. G., 1963: Some radar measurements of hailstorms, J. Appl. Meteor., 2, pp. 270-275.
5. Gokhale, N. R. and Rao K. M., 1969: Theory of hail growth, Journal de Recherches Atmospheriques, Vol. IV, No. 4, pp. 153-178.
6. Atlas, D., 1964: Advances in Radar Meteorology, Advances in Geophysics, Vol. 10, Academic Press, New York, pp. 318-468.

SNOW CRYSTAL STUDY OF A LAKE ERIE SNOW SQUALL

Andrew J. Heymsfield
The University of Chicago Cloud Physics Laboratory
and
R. G. Layton
Northern Arizona University, Flagstaff, Arizona

Lake effect snow squalls are localized areas of intense snowfall which occur over and to the lee of the Great Lakes. During the winter of 1968, a project was initiated by ESSA to seed the squalls originating over Lake Erie in an attempt to redistribute the snowfall away from the populous areas.

One of the goals of this project was to decrease riming of the crystals so that the resulting lighter crystals would advect further inland from Lake Erie.

Five continuously operating snow crystal replicators were designed for the project by Andrew and Gerald Heymsfield. They were placed in a network near the shore line and further inland. This network is shown in Figure I.

Though replicas were obtained from many seeded squalls, a particularly interesting day to analyze the effectiveness of seeding was December 14, 1968 (1). Four snow crystal replicators were operating in the seeded regions. Some of these results are shown in the space-time conversion in Figure II. The band of snow was assumed moving at 25 mph at 310°. The results indicate that an intense squall was successfully seeded, resulting in plane dendrites, plates and aggregates of plates and dendrites near the shore line, instead of heavily rimed crystals. The lighter crystals advected further inland to Charlotte Center and Randolph, where no snow occurred before and after the passage of this seeded area. Following passage of the seeded area, crystals near the lake shore returned to heavily rimed stellars and graupel, whereas further inland there was a decrease in snowfall. The second seeding area resulted in a pulse of snowfall at Charlotte Center and later on at Randolph, with no change in snow crystal types at the lake shore. A silver analysis of the snow was made by Warburton (4) in the regions shown in Figure II. Silver content above background level is indicated. The snow crystal analysis agrees quite well with the results obtained by Warburton.

A snow crystal analysis of the reduced data was performed in an attempt to verify whether the growth equation was valid in the temperature range -7 to -12C. No ventilation of crystals is assumed. Also, when a crystal was only lightly rimed, no change in terminal velocity from the unrimed form was assumed. The factor K is a constant determined at the 1000 mb level. The equations to be used are:

A plot of h vs. D is shown in Figure III. The mean snow crystal size for each ten-minute interval obtained from replica data was used to determine the altitude at which the mean size was nucleated. This altitude is plotted in Figure IV. The time required to grow this size crystal was also computed and the mean crystal size was traced back in time. This is also indicated in Figure III. The 95% confidence limits on the mean siz for each ten-minute interval are indicated. The crystal nucleation altitude and time agree quite well with the seeding time and altitude.

REFERENCES

1. Heymsfield, A.J., 1969: Snow crystal analysis of the effectiveness of seeding a Lake Erie snow squall on December 14,1968, State University College,Fredonia, New York.
2. Hindman,E. E., II, 1967: Snow crystal and ice nuclei concentrations in orographic snowfall. Master's Thesis,Atmospheric Science Paper 109, Colorado State University.
3. Marwitz, J. and A. Auer, 1968: Ice crystal growth by diffusion and accretion. Proceedings of the International Conference on Cloud Physics, Toronto, August 26-30, 1968, pp 249-254.
4. Warburton, J. and M. Owens, 1969. Silver analysis on lake effect studies, 1968. Desert Research Institute.

ACKNOWLEDGEMENTS

Mr. Gerald Heymsfield at State University of New York at Fredonia for his help in designing and constructing the replicators and drafting figures. Mr. Stephan Nelson at The University of Chicago for computer programming the equations. Finally, Roscoe R. Braham, Jr., at The University of Chicago, and Dr. James Jiusto at the State University of New York at Albany for their suggestions.

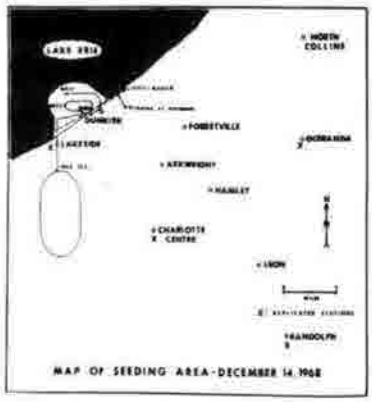

Figure I. Seeding area.

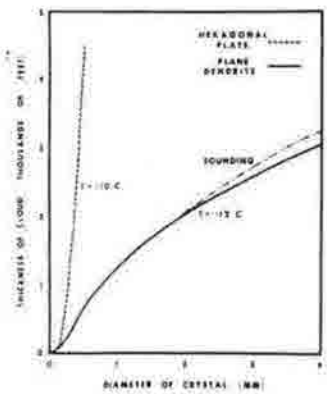

Figure III. Thickness of cloud required to grow size D crystal at water saturation and mean updraft zero.

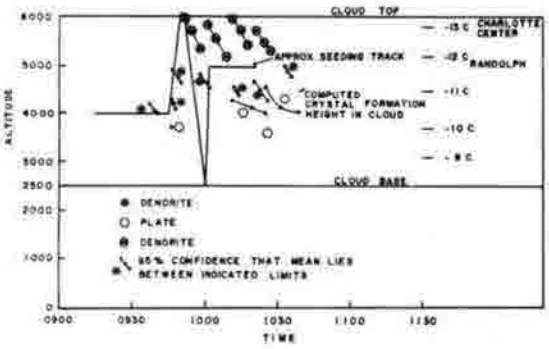

Figure IV. Predicted nucleation site and time using growth equation. Seeding altitude and time are indicated. Flaking of crystals is assumed at cloud base.

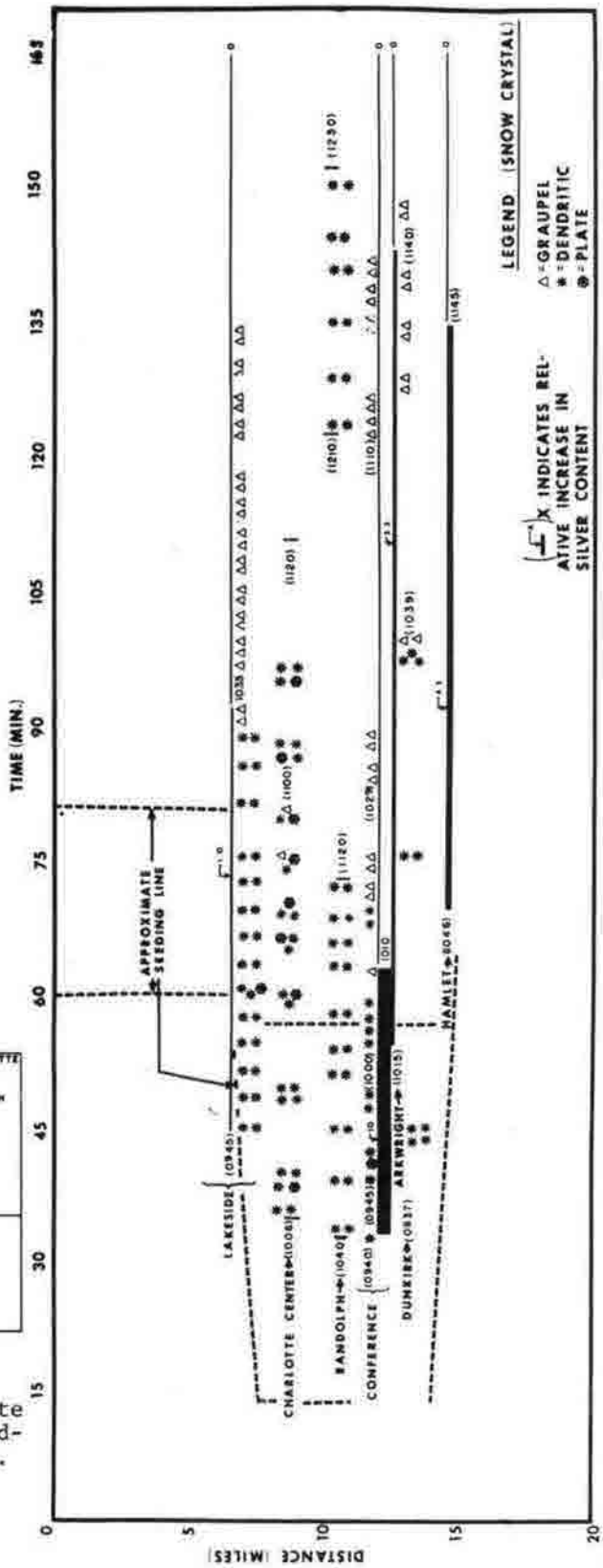

Figure II. Space-time conversion of snow line. The line is assumed moving 310° at 25 mph. The first plume passed over the lake shore areas reducing riming. Lighter crystals advected inland. The second seeding, inland, resulted in crystals at Charlotte Center and Randolph, but no change at the lake shore above background levels of silver are indicated.

NUMERICAL SIMULATION OF ICE HYDROMETEOR DEVELOPMENT

by

Edward E. Hindman, II and Ensign David B. JOHNSON
U. S. Navy Weather Research Facility
Norfolk, Virginia

INTRODUCTION

Numerical methods have been developed to simulate the growth of ice hydrometeors by diffusion and accretion. The classical diffusion growth equation relating the rate of change of mass to ice supersaturation, diffusivity, and geometrical shape factors is widely used. This approach requires the use of empirical mass-dimension relations to transform the crystal mass into tangible crystaline shapes. Simulations of accretion growth of falling crystals by continuous collection of supercooled droplets are in general use. This paper summarizes an empirical approach to the simulation of crystal diffusion growth which appears more flexible than the classical equation. An expanded form of the continuous collection method for accretion is included. Both growth mechanisms are combined to describe the growth of ice hydrometeors from ice crystals to rimed crystals, to graupel, and finally to hailstones.

DIFFUSION GROWTH

The following basic relation is used to express the increase in crystal mass by diffusion:

$$dm/dt = \rho\, dv/dt = \rho\, d(0.649\ a^2 c)/dt \qquad (1)$$

The density of deposited ice (ρ) is assumed solely a function of temperature. Density data from Fukuta [1] are used. The term v is the volume of a hexagonal prism or plate (depending on the temperature); a is the a-axis dimension, and c is the c-axis dimension. The axis growth was parameterized from measurements of crystal growth in several water saturated, constant temperature environments. The measurements were from data compiled by Todd [6] and from recent laboratory data taken by Fukuta [1]. The axis dimensions are expressed as a function of time:

$$a = K_a(t/t_o)^{\alpha} \qquad \text{and} \qquad c = K_c(t/t_o)^{\beta} \qquad (2)$$

where t_o equals one minute and K_a, K_c, α, and β are functions of temperature.

The parameterization has sufficient flexibility to allow for varying conditions of temperature and humidity. The basic equations (2) are differentiated with respect to time to give the incremental growth of the crystaline axes:

$$\Delta a = \alpha a(a/K_a)^{-1/\alpha}\Delta t \qquad \text{and} \qquad \Delta c = \beta c(c/K_c)^{-1/\beta}\Delta t \qquad (3)$$

The increments Δa and Δc are summed over a series of time steps while the terms in equation (3) are continually updated to reflect both the changing crystal dimensions and temperature conditions. The growing crystal will thus change its shape as the environment temperature is varied. Deviations of the growth environment from water saturation are approximated by multiplying the growth rate from equation (1) by a scale factor. This factor is equal to the quotient of the actual supersaturation with respect to ice, and the ice supersaturation corresponding to water saturated conditions.

ACCRETION GROWTH

The growth of ice hydrometeors by accretion is approximated by the following expression:

$$dm/dt = \rho\, dv/dt = E \cdot S \cdot \Delta V \cdot Q \qquad (4)$$

The density (ρ) of the accreted mass is expanded to be a function of the cloud liquid water and hydrometeor surface temperature. The density is derived from Macklin's [3] empirical density relation which is coupled with List's [2] formula for determining the surface temperature. The volume (v) is initially the same as in equation (1). This term is replaced with the volume of a sphere when the rimed crystal becomes spherical. The remaining terms in equation (4) describe the accretion process: E is the collection efficiency of the type of ice hydrometeor, S is its collecting cross-section, ΔV is the fall velocity differential between the ice hydrometeor and the supercooled droplets, and Q is the liquid water content.

SUMMARY OF NUMERICAL SIMULATIONS

A preliminary numerical model simulated ice hydrometeors growing in a steady-state supercooled cloud with constant temperature and liquid water content. Initially crystals grow by diffusion until large enough to begin growth by accretion. The smaller axis grows by both mechanisms while the larger grows only by diffusion. If the smaller axis grows rapidly and overtakes the larger, the particle is assumed to become spherical graupel. The onset of hail is assumed to occur when the hydrometeor diameter reaches one centimeter. When the surface temperature of the hail reaches 0°C, the unfrozen portion of the accreted mass is assumed to be shed.

The times required for the development of crystal growth by accretion, the onset of graupel, and the onset of hail were computed for a range of temperatures and liquid water contents. Specific results are listed in the accompanying table. The uniformity of the onset time for accretion suggests that variations in temperature and water content have little effect. Accretion onset times adapted from measurements at -5C compare favorably with the modeled results [4]. At low liquid water contents (0.1 g m^{-3}), graupel onset apparently is dependent upon temperature. Graupel did not form at -5 and -15C but it did form at -10 and -20C. These graupel particles, however, did not reach hail size within one hour. The onset of hail was observed to depend more on liquid water content than on temperature. As the water content increased, the hail onset time decreased. Warner [7] has estimated that one centimeter hail could develop in roughly twenty minutes. This is within the range of hail onset times presented in the accompanying table.

Temperature (°C)	-5			-10			-15			-20		
Liquid Water (g m^{-3})	.1	1	10	.1	1	10	.1	1	10	.1	1	10
Accretion Onset (min)	2	2	2	1	1	2	2	1	2	3	3	6
Graupel Onset (min)	-	12	10	11	3	7	-	5	5	15	6	9
Hail Onset (min)	-	53	17	-	50	10	-	34	8	-	54	11

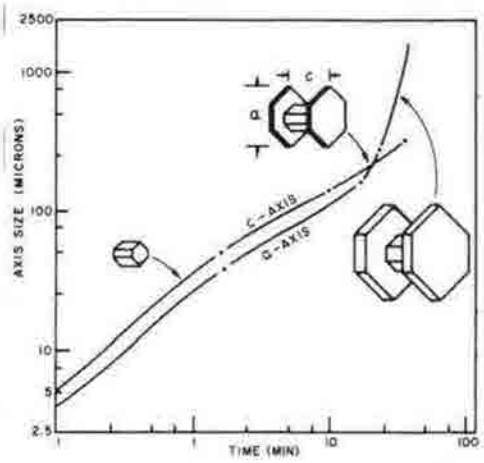

EVOLUTION OF A CAPPED COLUMN

A separate model simulated the growth of capped columns and spatial dendrites by applying simple limitations to the diffusion growth parameterization. The evolution of a capped column is illustrated in the accompanying figure. The column grew for 20 minutes at approximately -20C. By this time, it had accumulated enough mass to settle into a plate growth region where the rapid growth of the a-axis was limited to the ends of the column.

The diffusion growth parameterization was used in a supercooled-fog clearing model. In this model ice crystals grow at the expense of the fog liquid water in conditions of varying supersaturation. The model results were found to agree favorably with several documented fog-clearing operations [5].

REFERENCES

1. FUKUTA, N., 1969: Experimental Studies on the Growth of Small Ice Crystals. J. Atmos. Sci., 3, 522-531.

2. LIST, R., R. B. CHARLTON, and P. I. BUTTULS, 1968: A Numerical Experiment on the Growth and Feedback Mechanisms of Hailstones in a One-Dimensional Steady-State Model Cloud. J. Atmos. Sci., 6, 1061-1074.

3. MACKLIN, W. C., 1962: The Density and Structure of Ice Formed By Accretion. Quart. J. Royal Meteor. Soc., 88, 30-50.

4. ONO, A., 1969: The Shape and Riming Properties of Ice Crystals in Natural Clouds. J. Atmos. Sci., 1, 138-147.

5. TAG, P. M., D. B. JOHNSON, and E. E. HINDMAN II, 1970: Engineering Fog-Modification Experiments By Computer Modelling. Preprints - 2nd Nat. Conf. Wea. Mod., Am. Meteor. Soc., Boston, 97-102.

6. TODD, C. J., 1964: A System For Computing Ice Phase Hydrometeor Development. On file at Meteorology Research, Inc., Report No. ARG 64 Pa-121, 30 pp.

7. WARNER, C., M. ENGLISH, A. J. CHISHOLM, and W. HITSCHFELD, 1969: The Pattern of an Alberta Hailstorm. Preprints - 6th Conf. Severe Local Storms, Am. Meteor. Soc., Boston, 290-295.

GROWTH RATES OF ICE CRYSTALS GROWN FROM THE VAPOR

by
Dennis Lamb
Cloud Physics Group, Atmospheric Sciences Department
University of Washington, Seattle, Washington

INTRODUCTION

The growth of ice in the free atmosphere is known to be important to the initiation of precipitation by the Wegener-Bergeron mechanism. The rates at which vapor molecules are incorporated into the lattice of a given ice crystal governs the rate of accumulation of mass and also the growth habit. The interdependence of the habit and the mass growth rate then determines the intensity of the instability implied by the Wegener-Bergeron mechanism and the fall speed of the individual crystals. These factors ultimately depend upon the rates of advance of individual crystalline faces which are limited both by the processes occurring in the environment and those taking place on the growing surface itself. In order to better understand the microphysics of cold cloud precipitation, an attempt is made to separate the relative importance of the various transfer processes.

EXPERIMENTAL APPARATUS AND PROCEDURES

A laboratory study of the linear growth rates* of the prism and basal faces of ice has been carried out. Ice was grown on the stage of an optical microscope in the vacuum chamber shown in Fig. 1. The chamber was machined as a unit of stainless steel and immersed in a circulating bath of methanol. Two o-rings sealed the glass plate and a connection plate to the chamber. A small semiconductor thermoelectric element was sandwiched between two copper plates. The bottom plate made thermal contact with the bath and the upper cylinder distributed the heat evenly over the area of the growth substrate. The electrical current through the thermoelectric element was controlled electronically to maintain the temperature of the substrate constant to within $\pm 0.001^{\circ}C$ relative to a reference chamber mounted in the primary bath. An independent control of the chamber pressure was effected by measuring the pressure relative to the same reference chamber containing ice and controlling the current through a stainless steel heater tape imbedded in the moat ice. Such a "double differential" control could provide a net control of the excess pressure to about 10%.

Initially the chamber was evacuated to an estimated pressure of 1μ-Hg (about 1μb) with a mechanical oil pump applied to the vacuum system. After outgassing at about $100^{\circ}C$ overnight, the bath temperature was lowered to about $0^{\circ}C$ and water distilled into the chamber under vacuum from a source of previously distilled water. When enough water had been collected in the moat, the temperature was lowered further and the liquid frozen. Crystals could then be grown on the center stage by suitably controlling the differential temperature and pressure.

The linear rates of advance of individual crystal faces were measured by following the edge of the face where it intersected the substrate. The orientation of the face was determined by noting the angle at which the incident light beam was reflected specularly into the microscope. This allowed the calculation of linear growth rates normal to the crystal surface.

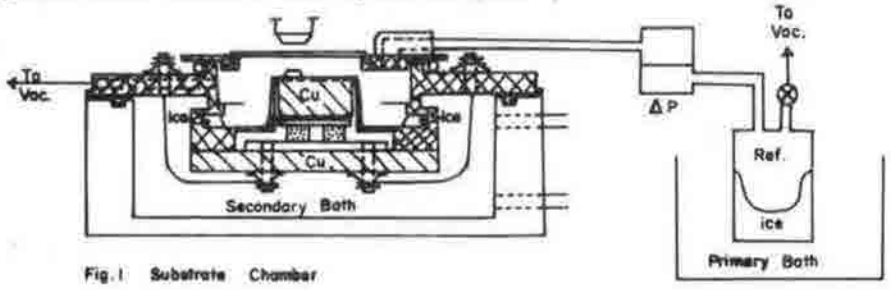

Fig. 1 Substrate Chamber

RESULTS

By introducing air into the chamber at various partial pressures below 1 atmosphere, it was found (Fig. 2) that the growth rates tend to follow a 1/P relationship (solid line) on the average, although the individual curves are consistently concave upward at pressures higher than about 10 mm-Hg. The essential features of the data may be explained qualitatively as follows. At very low pressures, where the inactive constituent (air) makes up only a small fraction of the vapor phase, the growth rate is largely controlled by surface kinetics and heat transfer and is not greatly dependent on pressure. As the partial pressure of the inactive gas is increased, diffusive resistance increases and progressively diminishes the net flux of molecules to the growing surface causing a 1/P dependence of the growth rate on pressure. This behavior is consistent with the pressure dependence of the vapor diffusivity. At still higher pressures convection currents within the chamber tend to offset further decreases of mass fluxes due to molecular diffusion, leading to a more gradual fall off of the growth rate with pressure. At least to a first approximation then the environmental air seems to modify the growth rates by merely reducing the net flux of vapor molecules which impinge on the surface. Interactions with surface kinetics can probably be ignored.

Measurements of the linear growth rates in pure vapor as a function of temperature between $-4^{\circ}C$ and $-18^{\circ}C$ are shown in Fig. 3. The measurements were made on individual crystal faces at constant excess vapor pressure as the temperature was changed linearly with time. This technique preserves the

*The term "linear growth rates" refers, as in many works on crystallization, simply to the time rate of change of the position of the interface. Linear rates are to be distinguished from mass growth rates.

identity of the crystal face and tends to minimize the scatter in the data. The thin solid lines represent smoothed averages of the various data runs and indicate the likely temperature trends of the "inherent" growth rates of prism and basal faces. (The "inherent" rates refer to growth governed by surface kinetics and not by vapor or thermal diffusion.)

Direct extrapolation of these data to atmospheric conditions may not be justified on several counts, but it is interesting to apply the results to growth of an ideal hexagonal prism. A simple integration of the growth rates of prism and basal faces at a particular temperature over the area of the prism yields a value for the total rate of mass accumulation. Repeating this spacial integration at different temperatures, one obtains the "inherent" temperature dependence of the mass growth rate which is shown by the heavy solid line in Fig. 3.

If this hypothetical crystal were to grow in stationary air by diffusive fluxes of vapor, the growth rates of all faces would be reduced in accord with a reduced mass transfer coefficient. At the same time, however, the non-uniform distribution of molecular fluxes that would be set up over the different faces would lead to enhancements in the crystal habit. That is, if at a particular temperature the "inherent" habit were "plate-like," then, the growth habit in a diffusion field would become even more "plate-like"; likewise, inherently columnar crystals would become relatively longer in the diffusion field. Considering a range of temperature the effect would be to intensify the temperature dependence of the habit. Similarly, the overall mass growth rate would be greatly reduced by growth in a diffusion field, but, because of the intimate link that exists between the crystal habit and the distribution of vapor fluxes, it is very likely that the temperature dependence of the mass growth rates would be enhanced as well.

The concept of such enhancements of habit and mass rate peaks seems necessary to bridge the gap between surface kinetic processes and environmental interactions. A significant point, of course, is that the kinetics need only account for a fraction of the total effects observed with crystals grown in a diffusion field. It may be enough, for instance, that the "inherent" growth rates of a prism face exceed that of a basal face at a given temperature by only a factor of two in order that the primary habit of an ice crystal grown in air have a length to width ratio of 10 to 1.

The ideas expressed here have been purposely simplified by considering the most basic geometry applicable to vapor grown ice crystals. The enhancement factors would become very complicated with other crystal geometries, but very likely larger and of greater significance. It is not claimed that the growth rate data used here are strictly applicable to the real atmosphere, but the analysis does show that inherent mass growth peaks do very likely exist at some temperatures and that these peaks, as well as the crystal habits, should be enhanced. Relatively small differences in kinetic parameters on different faces can thus lead to the profound variations in the crystals with temperature and supersaturation that are observed in the real atmosphere.

ACKNOWLEDGMENTS

This research was supported by Grants GA-11250 and GA-17381 from the Atmospheric Sciences Section, National Science Foundation (Principal Investigator: Prof. P. V. Hobbs).

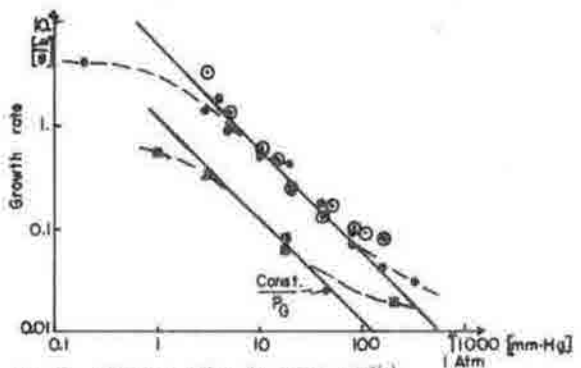

Fig. 2 Linear growth rate versus partial pressure of gas

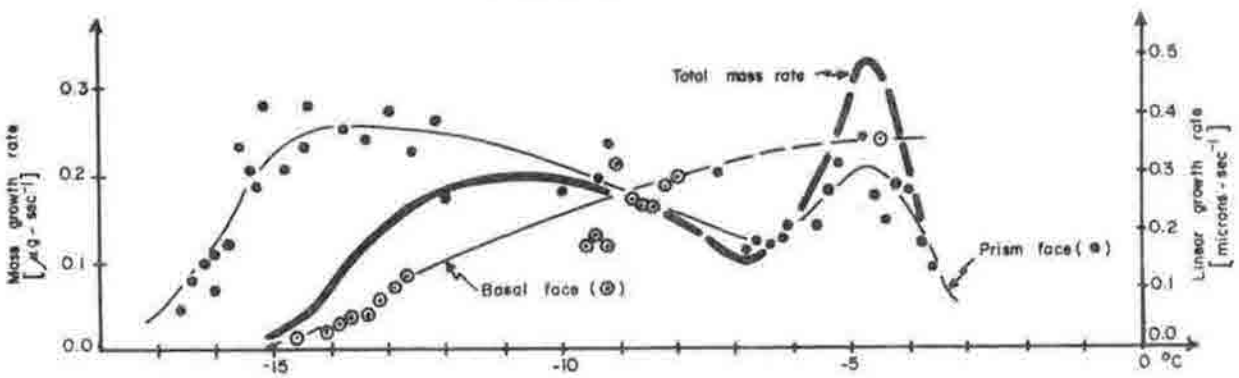

Fig. 3 "Inherent" growth rates versus temperature (results to date)

ON THE TUMBLING OF SPHEROIDAL HAILSTONES

Roland List, P. R. Kry and U. W. Rentsch
Department of Physics, University of Toronto
Toronto, Canada

1. INTRODUCTION

The most commonly observed hailstones can be described as oblate spheroids although their two major axes may differ somewhat. Simple free fall experiments in water tanks (List, 1959) have shown that these hydrometeors fall in the direction of the minor axis. The question now arises: why do they have a symmetry plane perpendicular to their fall direction? What makes the hailstone turn over and over again to achieve this symmetry?

This led to experiments by Lozowski (1967) and Byram (1969) on the drag and lift forces and stabilizing torques of spheroidal particles in a wind tunnel. But nothing was inferred about tumbling, mainly because the models were not given rotational freedom. Therefore, spheroidal hailstone models with this freedom about a vertical major axes were tested in a horizontal wind tunnel.

The following parameters might determine the resultant rotational motion: magnitude of Reynolds number, Re; turbulence caused by shadowing due to other similar bodies; turbulence as such; spheroid axis ratio; particle roughness; asymmetric protrusions and collisions with other hailstones. The last factor might be the only mechanism for turning over hailstones at lower Reynolds numbers.

The experiments described in this paper deal only with angular motions in free flow and with the effects of the wake of a disk (shadowing) on this motion.

2. EXPERIMENTAL SETUP

The model was a smooth 17.8 cm diameter wooden spheroid with axis ratio 1:0.67 which was mounted in a wind tunnel with a velocity range 0-50 m/sec and a cross section of the measuring section of 60 x 60 cm. The disk used for shadowing was 17.8 cm in diameter and placed 3 diameters in front of the sphere in three positions: full shadowing (center of disk and model on axis of tunnel), half shadowing (center of disk displaced one radius to the side), and edge shadowing (center of disk displaced one diameter to the side). Fig. 1 shows the velocity and turbulence profiles three diameters behind the disk for full shadowing. The profiles are normalized to the free stream velocity from which the corresponding Reynolds number was calculated.

3. TYPES OF MOTION

If left undisturbed, the model maintained its stable equilibrium except in the cases of shadowing where small amplitude oscillations (20° peak to peak) occasionally occurred spontaneously for $Re > 4 \times 10^5$. Therefore, to initiate motion, the model was deflected by a known angle and released. Three types of motion could be observed: uni-directional rotation, interrupted rotations, or damped or continuous oscillations. In uni-directional rotation, the model either rotated (a rotation is a turning through at least 180°), or oscillated with increasing amplitude until it rotated. In the final phase it either stopped rotating and oscillated to equilibrium or continued to rotate, apparently indefinitely. In interrupted rotations, the model rotated at least once and then oscillated before rotating again, in the same or opposite sense. It then either stopped rotating and oscillated to equilibrium or continued to carry on its interrupted rotating. The third class of motion was only oscillation, either damped to equilibrium or to the small amplitude oscillations which occurred spontaneously.

The physical difference between these three motions is the magnitude of the difference between the amplifying forces and the damping forces which control the motion. In uni-directional rotation this difference is at its greatest.

The frequencies measured for the oscillations and rotations varied from 0.5 to 4 hz, but it is difficult to assess the friction and bending of the suspension system and to extrapolate the frequency range to natural hailstones. From movies taken by parachutists when following freely falling model hailstones, it is known that tumbling frequencies in a similar Re range are of the order of 15-20 hz (private communications by Dr. Charles Knight, NCAR).

4. MOTIONS IN FREE STREAM

Fig. 2 gives the results of the measurements of the relative occurrence of two classes of motion as a function of Reynolds number for various deflection angles in the free stream. Initial deflections of 25° always led to damped oscillations. In more than 75% of the cases initial deflection angles $\geq 45^{\circ}$ initiated uni-directional rotation in the range $1.5 \times 10^5 < Re < 4 \times 10^5$. At the lowest Reynolds numbers the rotations ceased after one turn, while at the high Reynolds numbers ($Re > 3.5 \times 10^5$) effects due to the support may have stabilized the spheroid.

5. EFFECT OF SHADOWING ON MOTION

Fig. 3 demonstrates the effect of shadowing. Although the motion for edge shadowing and half shadowing is sustained, the motion for full shadowing ended in small amplitude oscillations, which also occurred spontaneously. The rotation in the case of half shadowing and edge shadowing was caused by the difference in velocities on each side of the model. The shift to higher Reynolds numbers of the curve for full shadowing is due to the fact that the Reynolds number was based on the free stream velocity and not on the actual reduced velocity the model was exposed to because of the shadowing. The chief conclusion to be drawn from Fig. 3 is that shadowing and associated turbulence damps out any rotational motion.

6. CONCLUSIONS

Static torques on fixed spheroids do suggest that the spheroid has one position of stable equilibrium. However, when the spheroid has a rotational degree of freedom, there are processes which can cause spontaneous oscillations or amplification of oscillations leading to rotations. Rotations tend to be damped by shadowing and the associated turbulence. In the free stream, rotations are quite likely for sufficient initial deflection and $1.5 \times 10^5 < Re < 4 \times 10^5$. Collisions with other hailstones are a likely cause of the initial deflections, but there are considerable problems in trying to calculate realistic collision rates.

In summary, it can be said that very large spheroidal hailstones can tumble in a continuous fashion. To what extent this is caused by a 'spring' effect of the wake is not known at present. But there is no way yet to explain why small ellipsoidal hailstones also do exhibit a symmetry requiring tumbling. It may be that surface roughness, eccentric protrusions or different positions of rotation axes could explain tumbling at Reynolds numbers as low as 2×10^4. Concerning the validity of wind tunnel experiments for the explanation of the free fall behaviour, it is our feeling that an improved suspension system would provide data not too different from free fall.

ACKNOWLEDGEMENT

This work was carried out within a research program sponsored by the National Research Council of Canada. One of the authors (P.R.K.) gratefully acknowledges receipt of a Centennial NRC Scholarship.

REFERENCES

Byram, A.C.,: The Aerodynamics of oblate spheroidal hailstone models, M.Sc. Thesis, University of Toronto, pp. 91. (1)

List, R., 1959: Zur Aerodynamik von Hagelkörnern. Z. angew. Math. Phys., 10, 143-159. (2)

Lozowski, E. P., 1967: Wind tunnel measurements of the drag and lift forces and the restoring moment acting on oblate spheroids, M.Sc. Thesis, University of Toronto, pp. 94. (3)

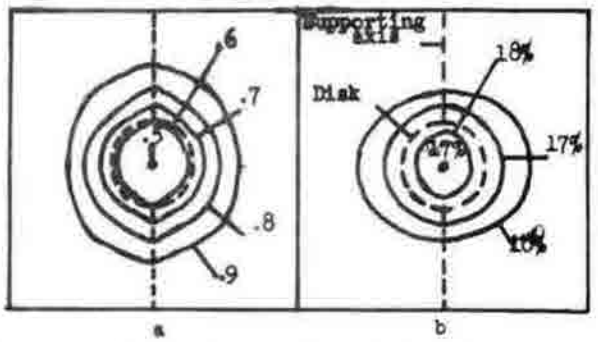

Figure 1. a) Velocity profile relative to a free stream velocity of 25.3 m/sec three diameters behind disk for full shadowing. b) Turbulence profile for same conditions.

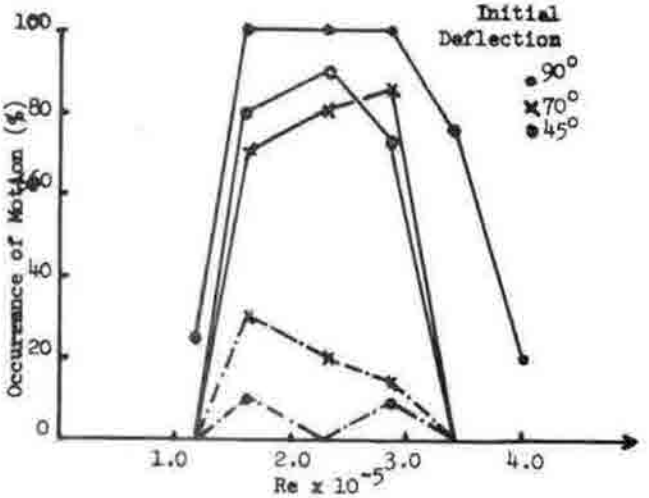

Figure 2. Percent occurrence of the two types of rotational motion under free stream conditions as a function of Reynolds number, for various initial deflection angles of the model; solid lines for unidirectional rotation, broken lines for interrupted rotations.

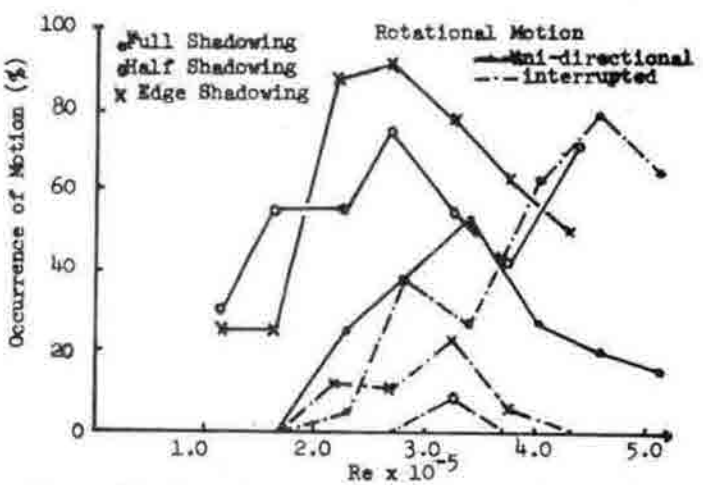

Figure 3. Percent occurrence of the two types of rotational motion as a function of Reynolds number, for various degrees of shadowing of a disk; initial deflection angle 90°.

THE ELECTRIFICATION OF SEEDED AND UNSEEDED CLOUDS

Paul B. MacCready, Jr., and Donald M. Takeuchi
Meteorology Research, Inc., Altadena, California

INTRODUCTION

A summary of dominant electrification mechanisms, with special application to Flagstaff clouds, is given by Latham and Stow (1969). They concluded that of the various existent theories, there are only two which are not inconsistent with the data obtained in field investigations at Flagstaff. Both these mechanisms are related to the development of precipitation. One mechanism is the Reynolds-Brook process. In this, the development of charged hydrometeors and hence potential gradients is found greatest when three types of particles co-exist: supercooled droplets, ice crystals, and larger ice hydrometeors. The other mechanism, proposed by Müller-Hillebrand, provides enhancement of a field as small ice crystals bounce off the bottom of falling larger ice hydrometeors. Seeding, by directly altering the cloud particle situation, would be expected to alter the buildup of electrification.

In the summer of 1969 data on particle types, charges, and potential gradients were obtained during sequential traverses at about the -10C level for various unseeded and seeded convective clouds at Flagstaff, Arizona. Interpretation of these data sheds further light on the mechanisms of electrification of these clouds. The results are consistent with the conclusions of Latham and Stow and add more information to support inferences about the possible effects of seeding. More details about instruments, observations, and interpretation are given in the report to the sponsor (MacCready, P. B, Jr., and D. M. Takeuchi, Cloud Electrification at Flagstaff, 1969, MRI 70 FR-901, MRI Final Report to U. S. Forest Service on Cont. No. 26-2298, January 29, 1970).

A SUMMARY VIEW

Figure 1 provides an overall look at observations in all the eight clouds for which the data are reasonably complete. The electrification plotted is the maximum vertical gradient over any 300-m section of the traverse. When lightning is observed, the trace is erratic; then the data points on Fig. 1 are arbitrarily put at 1000 volts/cm. The precipitation factor (CR) is the integrated ice phase precipitation as ascertained from the aluminum foil impactor on the Aztec aircraft, totalized from the start of precipitation. The precipitation was primarily graupel. The techniques of handling this hydrometeor sampler data are given by Takeuchi (1969). CR is derived from (mass)× (still air falling speed) of the ice particles, with diameters exceeding 200 μm, at the traverse altitude, for a circular cloud of the observed cross section dimension. These ice particles have grown by riming and most are falling, and so CR can be deemed an approximate measure of the total riming above the flight altitude. All-water precipitation was sometimes present but was relatively rare in the cloud studied.

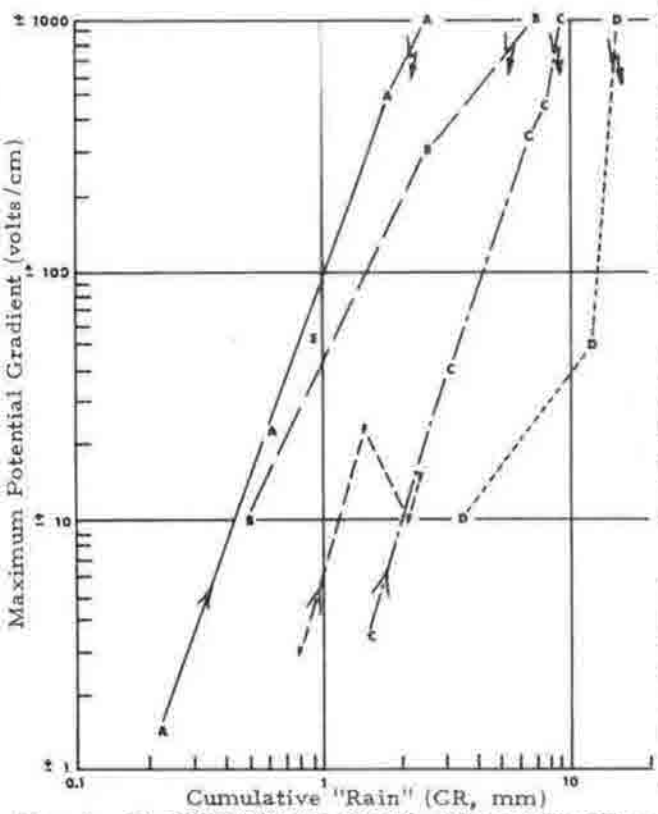

Fig. 1. ELECTRIFICATION VS. PRECIPITATION FACTOR
Cloud G CR < 0.7 mm, PG < 1 volt/cm
Cloud H CR < 0.07 mm, PG < 1 volt/cm

Of the four clouds giving lightning, two experienced negative fields. Once lightning was observed, each showed a sign reversal. In all these clouds, the locations and strengths of hydrometeor charging were closely related to precipitation regions and precipitation intensity. The liquid water content of these four clouds was appreciable, averaging 0.4 gm/m^3.

The main message conveyed by Fig. 1 is that the electrification correlates rather well with the integrated precipitation, CR, with the suggestion of a trend along a slope of 3 for the curves for the various cases. Based on the limited data in Fig. 1, if CR exceeds 2.5 mm, there is lightning. If CR is tiny, say below 0.2 mm, the gradients are only of the order of the fair weather field.

ELECTRIFICATION MECHANISM

Figure 1 shows that certain clouds required larger CR values than others in order to develop the same strong electrification. Many cloud physics and cloud evolution variables were examined in an effort to see if there was some obvious factor to explain this: liquid water content, size of ice hydrometeors, number of small ice particles, initial cloud diameter, timing between first ice and lightning, etc. Of all the factors studied, only R', the ratio of the number of small ice crystals (180 to 250 μm dia.) to large ice hydrometeors (>250 μm dia.), seemed to be capable of explaining the horizontal spread on Fig. 1 of the four lightning clouds A, B. C, and D. By the Reynolds-Brook or Müller-Hillebrand theory, the possibility of good electrification would require a big CR value (lots of riming to permit hydrometeor growth, and a good fall of hydrometeors to separate charge areas); then, if this possibility for electrification exists, the presence of many small crystals would serve to produce strong electrification. Of the four clouds with large CR values, Cloud A had the largest R' ratio (54), while D had the lowest R' ratio (2.1), and B and C were intermediate (18 and 19). Although R' was large for clouds E, F, G, and H, CR for these was low.

The observations do not permit deciding whether the Reynolds-Brook or the Müller-Hillebrand mechanism is the more likely. Each requires the coexistence of large ice particles and small ice particles, plus the presence of supercooled droplets at some stage in the precipitation development.

Order of magnitude calculations suggest that an ice hydrometeor-related mechanism of potential gradient development may be adequate to explain the electrification required for causing lightning. The charges on the hydrometeors on the average are 5 or 10 percent of the maximum such hydrometeors can carry (see Latham and Stow, 1969, for measurements, and MacCready, 1959, for calculations), and although both signs are usually found in the same region, there is ordinarily a preponderance of one sign or the other. A net charge of about 0.35 coulombs will be transported per km^2 by 1 mm of precipitation. For a 20-km^2 cloud and 5 mm of cumulative precipitation, with a 3-km spacing assumed between dipole centers, an electrical dipole of over 100 C km will be established, which is average for lightning discharges. In the real cloud system, some charge centers which are initially separated by hydrometeor gravity-fall can be expected then to be more rapidly separated by the faster relative convective motions, and influence charges collected at boundaries will be stirred into the cloud system. Thus a simple precipitation-based hypothesis cannot be expected to give the whole picture with accuracy, but our evidence argues that a dominant role in the initial strong electrification is played by a mechanism related to the growth and fall of ice hydrometeors in regions with small ice crystals.

SEEDING CONSEQUENCES

Even assuming a Reynolds-Brook or a Müller-Hillebrand mechanism to be the only significant electrification mechanism, the effects of seeding on the electrification should not be simple to summarize. There are many factors which are involved in determining CR and R' -- environmental stability, cloud size, stage of cloud development, characteristics and efficiency of seeding technique, natural nuclei, etc. Six of the eight clouds studied were seeded (A, B, C, D, G, H), and they demonstrated the expected complexity of effect. Some of the seeding was too limited and/or too late to cause appreciable artificial effects (C, D, G), while some of the seeding caused overseeding and almost complete glaciation (B, H). In the overseeding cases, the electrification was weak in the overseeded region, but was strong in cells at the edge of this region (B), or strong in subsequent peripheral cells (H).

We conclude that in almost any circumstances, the initial effect of seeding is likely to be an increase of electrification, as ice crystals and hydrometeors are developed earlier than without seeding. If the seeding is continued in such a way as to overseed the cloud and decrease the amount of supercooled water to well below the natural quantity, then the development of strong electrification (as well as precipitation) should be inhibited in that area.

ACKNOWLEDGMENTS

The data were obtained under contract with the U.S. Forest Service, Northern Forest Fire Laboratory. Facilities and data reduction were aided by a concurrent contract with the Bureau of Reclamation, Office of Atmospheric Water Resources, PROJECT SKYWATER.

REFERENCES

Latham, J., and C. D. Stow, 1969: Airborne studies of the electrical properties of large convective clouds. Quart. J. Roy. Meteor. Soc., 95, 486-500.

MacCready, P. B., Jr., 1959: The lightning mechanism and its relation to natural and artificial freezing nuclei. Recent Advances in Atmospheric Electricity, New York, Pergamon Press, 369-381.

Takeuchi, D. M., 1969: Analyses of hydrometeor sampler data for ESSA cumulus experiments, Miami, Florida, May 1968. Final Rept. to Experimental Meteorology Branch, ESSA, University of Miami, Cont. E22-28-69(n).

THE ANALYSIS OF A HAILSTONE

W.C. Macklin[1], L. Merlivat[2] and C.M. Stevenson[3]

[1]Department of Physics, University of Western Australia, Nedlands, Western Australia.
[2]Meteorological Office, Bracknell, Berks., England.
[3]Centre d'Etudes Nucleaires de Saclay, Saclay, France.

INTRODUCTION

On 1 July 1968 a severe thunderstorm developed near Cardiff, Wales and produced hailstones whose maximum dimension exceeded 7cm. One of these hailstones was cut into thin sections and two adjacent sections on either side of the growth centre were analysed. One section was used to obtain records of the air bubble and crystallographic structure, and the isotopic composition of the other was determined as a function of radius. From the available meteorological data a sounding was constructed and from this the pressure and temperature of the cloud base were estimated to be 870 mb and 15.5° C.

RESULTS and DISCUSSION

A schematic diagram of the air bubble structure of the hailstone section is shown in the top right of Fig. 1. Outside the central core the stone is divided into five main layers of alternately clear and opaque (bubbly) ice. The first opaque layer is quite thin while the second is much thicker and denser. The crystal layers, as indicated by crystal size, coincided exactly with the bubble layers and there was a change in size from a few mm to a few tenths of a millimetre as the ice changed from clear to opaque.

The deuterium and O^{18} composition of the adjacent hailstone section was measured using the techniques described by Merlivat et al.(1). The results of the deuterium analysis are shown in Fig. 1. The deuterium values relative to Standard Mean Ocean Water, δD , are given in parts per thousand and the standard error is ±0.7 °/oo .

Because of the relatively large number of variables involved (droplet temperature, size, concentration and impact speed) it is possible to give only rather broad interpretations of the bubble and crystalline structures. However, the isotopic data does permit a unique interpretation if it is assumed that the ascent is adiabatic. There is then conservation of each molecular species and it is possible to show that

$$\delta D_L = \frac{\delta D_v^i + \varepsilon m_v/m_o}{1 - \varepsilon m_v/m_o} \qquad (1)$$

where δD_L is the deuterium value in the droplets at a given height, δD_v^i that in the initial water vapour before condensation, α is the isotopic separation factor, $\varepsilon = \alpha - 1$, m_v is the mass of vapour condensed and m_o the total mass of water substance in the ascending air. α is known as a function of temperature and m_v and m_o can be obtained from the sounding.

To construct a curve of δD_L versus height it was assumed that the lowest δD value measured was produced at an air temperature of -35° C. From the data in Fig. 1 a trajectory for the hailstone was then determined. This is shown in Fig. 2 and it is evident that the stone underwent at least two ascents in cloud. From the trajectory the rate of rise of the stone was ascertained and updraught profiles calculated assuming that the cloud water concentration was adiabatic (Fig. 3). For comparison theoretical updraught profiles deduced from the sounding using the extended parcel method are also shown.

The bubble and crystalline structures of the hailstone can be broadly fitted into the growth history outlined above and are consistent with Brownscombe and Hallett's(2) scheme for the opacity of accreted ice and with Levi and Aufdermaur's(3) experimental data on crystal size. Brownscombe and Hallett suggest that the transition from clear to opaque ice occurs slightly in the wet growth regime at a temperature of about -22°C. This is close to the temperatures at which the ice became opaque in the first and second ascents. Near the wet growth limit Levi and Aufdermaur find that the transition from large (> 2mm) to medium (between 0.5 and 2mm) or small (< 0.5mm) crystals occurs at an ambient temperature of about -18°C. This temperature is not appreciably different from that inferred for the growth of the first opaque larger (-21° C). The change from medium to small crystals in the second ascent also occurs at about this temperature.

The present analysis has shown that from the isotopic composition of a hailstone it is possible to infer the air temperature, updraught speeds and approximate cloud water concentrations experienced by the stone during its growth and hence obtain a trajectory compatible with its internal bubble and crystalline structures. The advantage of the isotopic method of analysis is that the ambient temperature is virtually the only variable involved in the interpretation of the data. The analysis confirms a recycling process of the nature envisaged in the severe storm model of Browning and Ludlam(4) and the calculated updraught profiles are in reasonable agreement with those inferred from the extended parcel theory.

REFERENCES

1. Merlivat, L., Nief, G. and Roth, E. Abhandhungen der Deutschen Akademie der Wissenschaften zu Berlin, 7, p. 839, 1965.
2. Brownscombe, J.L. and Hallett, J. Quart. J. Roy. Met. Soc., 93, p. 455, 1967.
3. Levi, L. and Aufdermaur, A.N. Manuscript submitted to J. Atmos. Sci.
4. Browning, K.A. and Ludlam, F.H. Quart. J. Roy. Met. Soc., 88, p. 117, 1962.

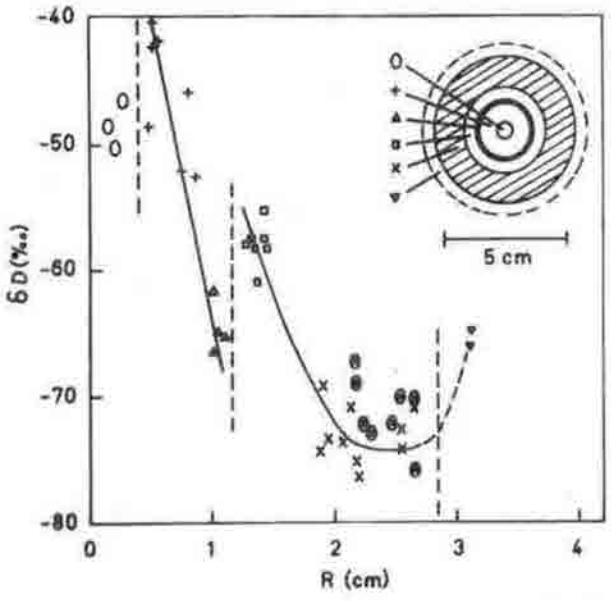

Fig. 1.

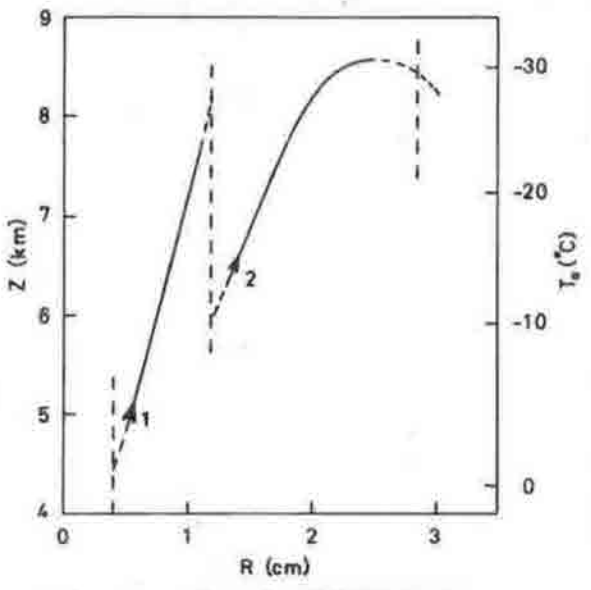

Fig. 2.

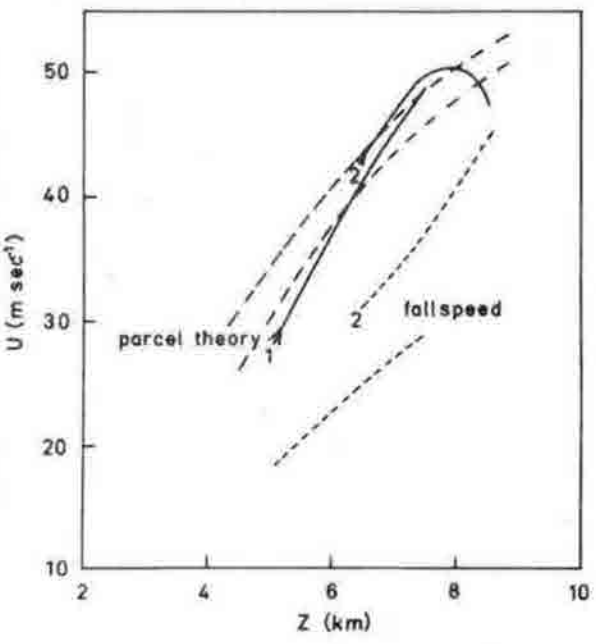

Fig. 3.

LEGENDS TO FIGURES

Fig. 1. The measured values of δD as a function of hailstone radius. A spherical model of the stone is shown in the top right corner and the symbols used for samples from the various layers are as indicated. The opaque layers are hatched.

Fig. 2. The height of the hailstone as a function of radius showing the two ascents.

Fig. 3. Updraught profiles deduced for the two hailstone ascents. Included are updraughts deduced from the parcel method. In the lower of the two latter curves no account has been taken of the kinetic energy of the inflow while in the upper curve the average speed of the inflow has been taken to the 15 m sec^{-1}. The fallspeed of the stone at various heights is shown for the two ascents.

ON THE ELECTRIC CHARGE OF LOW SNOW CLOUDS

By Choji Magono, Tatsuo Endo and Tadashi Shigeno
Dept. Geophysics, Hokkaido University, Sapporo, Japan

Although snow clouds in the winter season in Hokkaido are fairly low and steady, they sometimes bring out local thunderstorms. It was, therefore considered that the observation of charge distribution of the low snow clouds would give us some information about the charge generation mechanism in thunderclouds.

Because it was expected that not only charge distribution but other accompanying properties of the clouds were important to discuss the result of the observation, low snow clouds were observed by the use of many methods, e.g. by releasing electric charge sondes, electric field sondes, snow crystal sondes and usual radio sondes, simultaneously with taking photographs of the clouds and with various kinds of surface observations at a seashore of Japan Sea, Ishikari Town. A weather radar in the Sapporo Meteorological Observatory was also available.

Steady snow clouds as shown in Fig.1 were landing at the Ishikari Plain through 30 Jan. 1969. According to the radar observation, the clouds were of single band type and were steadily over the observation point. Sometimes showerly snowfall occurred.

The four kinds of the sondes were released from Ishikari Town in the afternoon around 1400 (JST) within one hour. The results obtained are shown in Fig.2. As seen in the left end of the figure, a temperature inversion was existed near 2000 m altitude which coincided with the top of the lower humid layer. Therefore the height of the cloud top was estimated as 2000 m. The vertical distribution of snow crystal type is shown in the center of the figure. It is seen that snow crystals of bullet type were predominant in the upper layer, and plane dendritic snow crystals were predominant in the lower half of the cloud. Although graupels were not recorded in the snow crystal sonde, a showerly graupel fall was observed at the surface about 40 minutes before the releasing the snow crystal sonde.

The vertical distribution of charge on individual snow crystals are shown to the right side of the crystal distribution. White and black dots mean positive and negative charges respectively. It is seen that positive charge was distributed in the layer lower than 800 m altitude, and negative charge ranged from 750 to 1600 m altitude. A vertical distribution of electric field obtained by an Altielectrograph of Simpson type[1] is shown in the right hand of the figure, where white and black areas on the curves mean positive and negative field respectively. A vertical distribution of space charge was estimated from the field distribution which are shown by + and - marks in the figure. It may be accepted that the distribution of space charge estimated from the field distribution agreeded very well with that obtained directly by the electric charge sonde.

At the surface, positive graupels (o) were observed in the period 13^h46^m and 14^h04^m, then negative snow crystals (•) were predominant between 14^h13^m and 15^h00^m, as shown at the bottom of Fig.3. Assuming that the fall velocity of the graupels and snow crystals was 1.3 and 0.6 $m \cdot sec^{-1}$ respectively, the correspondence of electric structure of the cloud to the time change in the precipitation charges and the electric field at the surface are shown in Fig.3. It is seen that a local positive was generated on graupels in the layer warmer than -10°C by colliding with snow crystals which were negative, and the positive graupels fell down to the ground at first, then the negative snow crystals reached the ground surface.

It is also seen that the mirror image relation held between the electric charge and the surface field. At first 13^h40^m when positive graupels were approaching the surface, a positive field was observed. Then negative field was established because positive space charge was removed from the air. This forms the mirror image relation, then as negative snow crystals fell to the ground, in other words negative space charge was removed, a positive field was established at the surface.

Reference

(1) Simpson, G.C. and F.J. Scrase, 1937: The distribution of electricity in thunderclouds. Proc. Roy. Met. Soc., A, 85, pp.309-352.

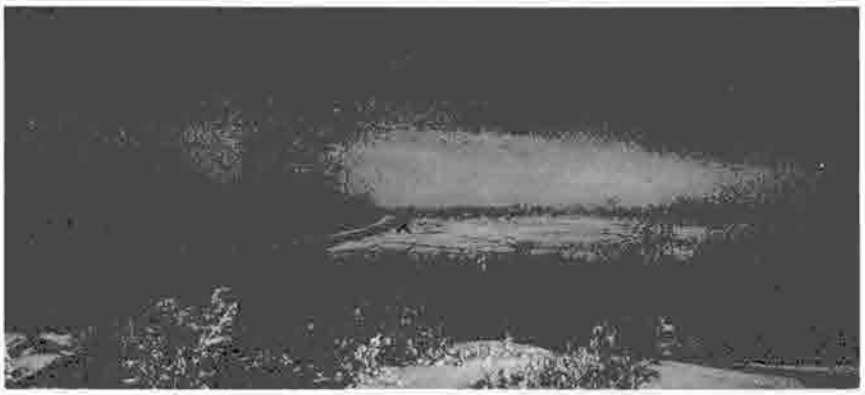

Fig.1 Side view of a typical low snow cloud which measured. X mark : observation point, Ishikari Town.

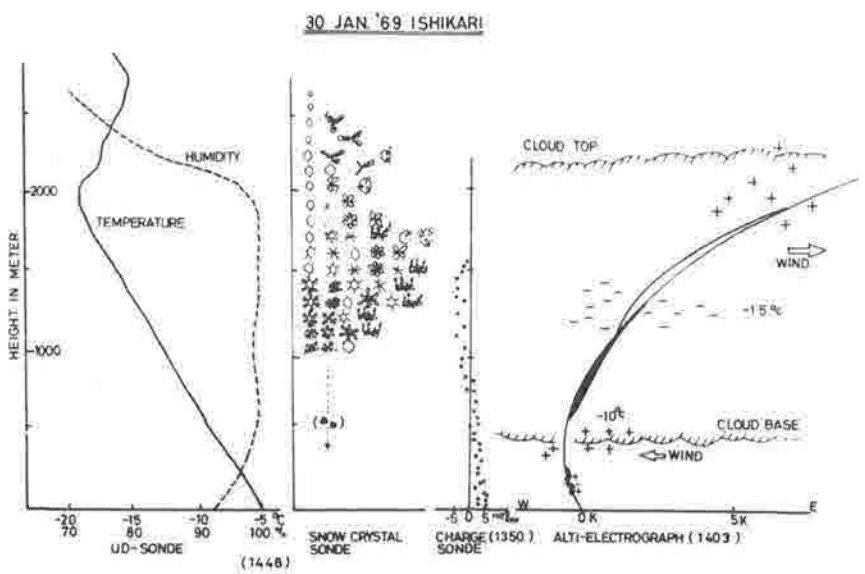

Fig.2 Vertical distribution of air temperature, relative humidity, snow crystal shape, electric charge and electric field of a low snow cloud.

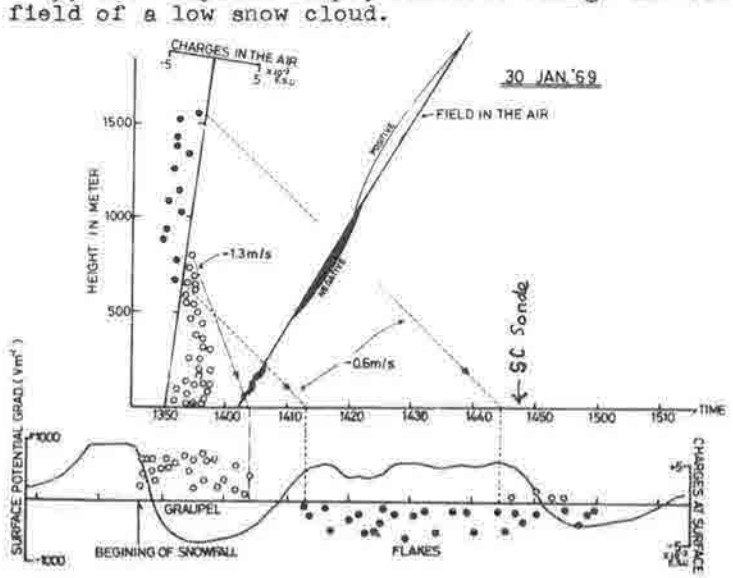

Fig.3 Electric structure of the snow cloud and corresponding time change in precipitation charge and electric field on the ground surface.

ON THE CRYSTAL SHAPE OF SNOW AND ICE CRYSTALS IN THE COLD TEMPERATURE REGION, PART I

By Choji Magono
Dept. Geophysics, Hokkaido University, Sapporo, Japan

It is frequently observed that snow and ice crystals do not grow into single crystals but into polycrystals, e.g. combination of columns or bullets, irregular combination of columns and plates, and side plane in the temperature region colder than -20°C. Among them, the snow crystal of side plane type as shown in Fig.1 is the most interesting. Recently Dr. Kikuchi(1) found snow crystals of strange types which were considered to be a kind of side plane type, as shown in the upper half of Fig.2.

As a first step of study on snow crystals of the complicate polycrystalline in the colder temperature region, it was undertaken to determine the optical axis (c-axis) of individual plates of snow crystals of side plane type, utilizing various methods as follows.

1. Polarization microscope.
2. Shape of thermal etching pits on the plate.
3. Apparent shape of the plate.
4. Crystal type of branches which extend from the plate.

As a result, it was found that there were two types in the snow crystal of so called side plane. One is composed of crossed plates whose c-axes are always perpendicular to the plane of the plates, as shown in Fig.3. In this case, the snow crystal is polycrystalline. The snow crystal of this type will be named as "crossed plates" in this paper. The other is composed of a columnar crystal and a side plane which extends from the prism plane of the columnar crystal. In this case, the snow crystal is a single crystal, because the c-axis of the extended side plane is the same as that of the columnar crystal, as shown in Fig.4. The snow crystal of this type will be named as "extended side plane".

About the formation mechanism of snow crystals of those two types, following consideration was made. If a snow crystal is composed of two single crystals of different c-axes in its early stage, plates develope along a-axes plane (basal plane), then "crossed plates" is formed, as shown in Fig.3. The plates cross each other with about a right angle. If a prism plane of a columnar crystals extends from the column, a "extended side plane" is formed. When the snow crystal is composed of two scrolls in its early stage, the developed shape will be as shown in Fig.4. In this case, the snow crystal of course is a polycrystal.

When Dr. Nakaya(2) found snow crystals of so called side plane type, he considered that the side plane was a extension of a prism plane of a column, therefore he named this type as extended side plane. However, as the example of this type, he showed snow crystals of "crossed plates type" in the present paper, as shown in Fig.1. According to the result of determing c-axes, snow crystals of side plane which extended from prism planes had the shape as shown in the upper half of Fig.2 or in Fig.4.

Natural snow crystals of crossed plate type or extended side plane type are observed together with columns or bullets. In case of the laboratory experiment also, snow crystals of those types are formed on a rabbit hair common to columns or bullets. It is, therefore considered that the formation condition for the crossed plates or extended side plane is near the same as those of columns and bullets, meteorologically. Very local but unknown factors may be related to the formation of crossed plates or extended side plane.

References

(1) Kikuchi, K., 1969: Unknown and peculiar shape of snow crystals observed at Syowa Station, Antarctica. Jour. Fac. Sci., Hokkaido Univ., Ser.VII, 3, pp.99-116.
(2) Nakaya, U., 1954: Snow Crystals, natural and artificial. Harvard Univ. Press, p.63.

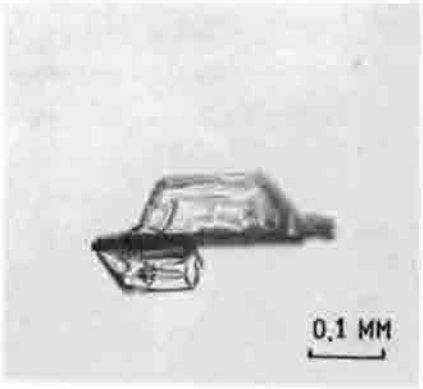

Fig.1 Snow crystal with crossed plates.

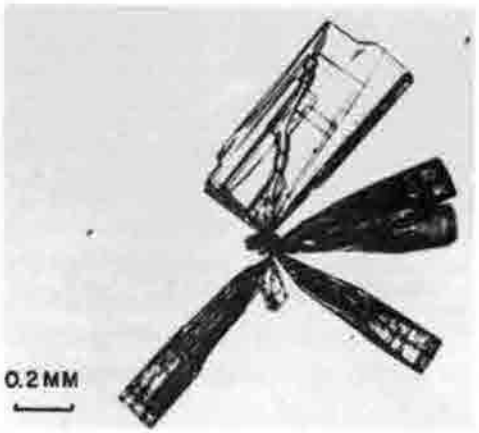

Fig.2 Snow crystal with extended side planes which is combined with bullets.

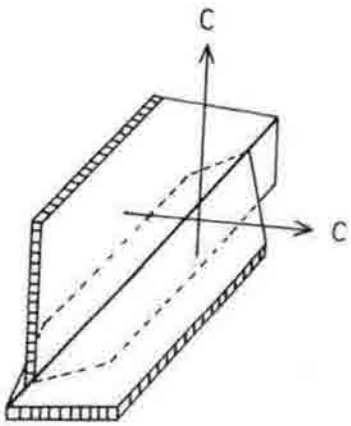

Fig.3 C-axes of a snow crystal of crossed plate type.

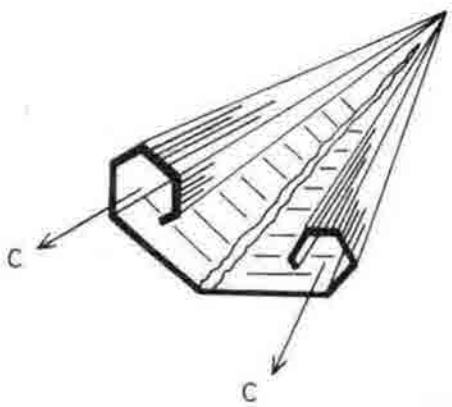

Fig.4 C-axes of a snow crystal of extended side plane type.

NUMERICAL MODELING OF HAILSTONE GROWTH

by

D. J. Musil and A. S. Dennis
Institute of Atmospheric Sciences
South Dakota School of Mines and Technology
Rapid City, South Dakota

1. INTRODUCTION

This paper considers hailstone growth with the aid of three numerical models describing microphysical processes. The models do not account for possible feedbacks of microphysical processes upon cumulus dynamics; nevertheless, they shed light upon several aspects of hailstone growth. They also permit an assessment of a simple conceptual approach to hail suppression, namely, the glaciation of supercooled cloud water at higher temperatures than normal for hail-producing clouds.

The three models in order of increasing complexity are: 1) the growth equations model, 2) the feeder cloud model, and 3) the hailstone screen model. These models are discussed briefly in the following three sections.

2. GROWTH EQUATIONS MODEL

Musil has derived equations governing hailstone growth in the presence of supercooled cloud water and ice crystals[2]. As long as a hailstone is able to dispel all the latent heat of fusion associated with accreting cloud droplets or raindrops and maintain a temperature below 0C, growth occurs in the dry state and all accreted water is incorporated into the hailstone. If the hailstone is colliding with many liquid droplets and the ambient temperature is not far below 0C, the temperature of the stone may rise to 0C and a film of water appear on its surface. This is the wet growth condition. It is assumed in the present model that excess water is shed and that no spongy lattice is formed. In that case the wet growth rate is dependent solely upon the rate at which heat can be transferred from the hailstone to the environment and is independent of the liquid water concentration in the environment. Hailstone growth in a mixture of ice crystals and supercooled cloud droplets is faster than in a cloud consisting entirely of supercooled water, other things being equal, because some of the latent heat of fusion released by the accreting cloud water is used to warm the ice crystals from the ambient temperature up to 0C.

The growth equations yield the growth rate for a hailstone of any size in environmental conditions. Both wet and dry growth rates are computed and the smaller of the two is assumed to apply. The maximum growth rate occurs at the transition point from dry to wet growth.

The model has been applied to an "unseeded" cloud in which the water content follows the adiabatic values for a day on which hail was observed at Rapid City and in which the cloud water freezes between -20 and -40C in a nonlinear fashion suggested by Vali[3]. The maximum growth rate occurs at temperatures around -25 to -28C, the exact value depending slightly upon hailstone diameter. The temperature at which the maximum growth occurs falls as the concentration of supercooled water increases, so that in some hail-producing clouds it may occur at temperatures below -30C.

Howell has suggested one simple conceptual model (among others) for hail suppression in which suppression is achieved by glaciating the supercooled cloud water, thereby slowing hailstone growth[1]. Weickmann* has argued conversely that the conversion of droplets to ice crystals might speed the growth of hailstones, for reasons noted above. Some insight into the relative merits of the two points of view can be obtained by comparing results of the growth equations model for a "seeded" cloud glaciated between -5 and -25C to those for the unseeded cloud. The seeded cloud shows three important changes with respect to the unseeded cloud:

1) The region of maximum hailstone growth rate is moved to near -15C, i.e., downward in the cloud.

2) Maximum hailstone growth rate is smaller in the seeded cloud than in the unseeded cloud.

3) Appreciable hailstone growth rates are limited to a region of smaller vertical extent.

These results suggest that the concept of hail suppression through cloud glaciation has some merit.

3. FEEDER CLOUD MODEL

It is impossible to calculate from the growth equations model how much a hailstone will grow in passing upward or downward through a cloud without taking into account updraft speeds and hailstone terminal velocities to determine the time spent at the various levels. This has been done with a one-dimensional time-dependent model of a feeder cloud. A feeder cloud begins as a small cumulus cloud

*Private communication.

in the vicinity of a hailstorm and grows rapidly as it approaches and merges with the main storm. Musil has traced the history of hail embryos ranging from 40 to 1000 microns diameter introduced into the feeder cloud model at different elevations and at different times[2].

The feeder cloud model can be considered as defining the environment experienced by a hailstone along its trajectory rather than as a description of a cloud. It is equally applicable to embryos carried inward toward the core of a three-dimensional hail cloud and, therefore, subjected to increasing updrafts with time. Inward motion occurs below the level of maximum updraft in all convective clouds and might also occur on the upshear side above the level of maximum updraft.

Musil considered glaciation of cloud water to occur between -20 and -40C (an unseeded cloud). We have investigated hypothetical effects of seeding by assuming glaciation to occur between -5 and -25C. Comparing the hailstones produced in this case with those produced in the unseeded cloud confirms expectations based on the growth equations model. Embryos of most sizes introduced at a majority of points in the seeded version of the feeder cloud model result in smaller hailstones falling from the cloud base than they would produce if introduced at the corresponding point in the unseeded cloud model. Some exceptions occur in the case of embryos reaching the upper limit of their trajectories near the -10C level in the seeded cloud.

4. HAILSTONE SCREEN MODEL

To this point we have taken no account of competition among hailstone embryos or hailstones. This lack is less serious than might at first appear. The growth rate of a hailstone is not affected by those above it nor by those located to one side, but only by those located below it. The hailstones below make their presence felt by removing some of the supercooled cloud water blowing upward past them so that their effect upon a particular hailstone under consideration is completely expressed in the ice and water budgets.

Consider a screen of hailstones balanced near the top of a cloud with the largest ones at the bottom of the screen. The decrease of the updraft with height implies horizontal divergence of the air, which must be shared by the precipitation and the cloud particles present. However, as the hailstones are balanced by the updraft they do not share in the vertical convergence of the air motion. In a steady state situation, the only factor offsetting the horizontal divergence is accretional growth.

One can determine under what conditions accretional growth offsets the horizontal divergence. Neglecting the presence of cloud ice and assuming dry growth, this requires

$$(DIV)_{XY} \cdot N \cdot \frac{\pi \rho D^3}{6} = N \cdot \frac{\pi D^2}{4} \cdot V_t \cdot X \qquad (1)$$

where $(DIV)_{XY}$ is the horizontal divergence, N is the hailstone concentration, ρ is hailstone density, D is hailstone diameter, V_t is hailstone fall speed, which in this case equals the local updraft speed, and X is the cloud water content. Examination of (1) shows that the balance between accretion and horizontal divergence depends on hailstone diameter and cloud water content, but is independent of hailstone concentration. For typical conditions, increases in mass concentration with time are possible only for stones under 1 cm diameter, and concentrations of larger hailstones decrease with time. This reduces the possibility of competition among the largest hailstones growing in the updraft, although stones moving upward from below the updraft maximum could offset this tendency to some extent.

Competition enters when conditions at more than one level are considered, because the concentration of hailstones at one level controls the cloud water content at higher levels. The situation has been modeled in a computer with hailstones making their way downward through the updraft as they grow by accretion but subjected all the while to horizontal divergence. After each time step, a fraction of the hailstones at each level are moved downward to the next level as a result of growth and the concentrations of hailstones are adjusted for horizontal divergence. Cloud water concentrations are adjusted for condensation, horizontal divergence, vertical convergence and losses by accretion. The results show that in a cloud with adiabatic water content most of the hailstones would exit from the updraft with diameters around 1 cm. This agrees with the median diameter observed in many hailstorms. Of course, a few stones would make their way downward near the storm core so that the maximum updraft still provides an indication of maximum hailstone diameter to be observed in a storm.

Work is in progress on the effects of artificial glaciation of the cloud water upon the ultimate hailstone sizes achieved in this model.

REFERENCES

1. Howell, W. E., 1966: Conceptual models that guide applied cloud seeding. Bull. Amer. Meteor. Soc., 47, 397-400.

2. Musil, D. J., 1970: Computer modeling of hailstone growth in feeder clouds. J. Atmos. Sci., 27, 474-482.

3. Vali, G., 1968: Ice nucleation relevant to formation of hail. Sci. Report MW-58, Montreal, McGill University, 51 pp.

EXPERIMENTAL STUDIES OF FREEZING, WAKE EFFECT, AND BREAKUP OF FREELY SUSPENDED SUPERCOOLED WATER DROPS

John D. Spengler and Narayan R. Gokhale
State University of New York at Albany
Albany, New York 12203

INTRODUCTION

A large vertical wind tunnel (1) was used to suspend 2mm to 5mm size water drops. The interaction of these suspended drops and their freezing were studied at ambient air temperatures from +3°C to -27°C. Thousands of drops have been observed freezing and interacting with drops of the same size or impacted by smaller droplets. Some of the resulting ice pellets were collected, photographed and measured. Approximately 10,000 feet of high speed movies were taken at framing rates from 500 frames per second to 2,000 frames per second.

FREEZING OF SUPERCOOLED DROPS

Type of freezing

There are essentially three distinct types of temperature dependent freezing (2).

1. Upon slow freezing in the temperature range 0 to -5°C, an ice shell forms around a drop. Starting with a frozen disc on the bottom of a drop an ice layer slowly envelopes the entire drop. However, there is a finite time when the drop has a frozen bottom and a liquid top. During this period a difference in the manner of oscillations can be observed. The liquid has the appearance of sloshing back and forth across the ice disc. The maximum amplitudes of oscillations do not occur along the horizontal and vertical axes as in the case of liquid drops; but, rather, they occur at about 45 degrees from the vertical axis. These ice-liquid drops may encounter heavy turbulence such as the wake of another drop and shed the liquid portion of the partially frozen drop. This results in an ice disc which accelerates upward in a zig-zagging manner.
2. At temperatures between -5 and -10°C drops can obtain a frozen shell of clear ice which completely encloses a liquid center. While the interior of the pellet is still liquid, the outer ice shell may be easily cracked upon contact with a hard surface.
3. Rapid freezing occurring at temperatures colder than -10°C results in opaque ice pellets. Deliberate nucleation by sand, clay, dust or ice crystals produces opaque ice pellets at temperatures as warm as -5°C.

Shapes and terminal velocities

Similar to liquid drops, the terminal velocities of ice pellets are determined by their shape. (Fig. 1 and 2) Upon freezing the resulting ice pellet would either remain suspended at the same terminal velocity (even 10mm diameter ice pellets), or increase its terminal velocity and fall to the Hexcel on top of the tunnel or decrease the terminal velocity and accelerate vertically and be thrown out of the updraft. Whether the frozen pellet would change its velocity or not depended on the type of freezing and its resulting shape. During opaque freezing, drops often froze in a state of large amplitude of oscillation. A frozen oblate ellipsoid would have a larger surface area and hence a lower terminal velocity than a drop in its mean shape. All the frozen ice pellets which rapidly accelerated upwards in the wind tunnel were opaque and had an oblate ellipsoidal shape.

The ice pellets which either remained at the same terminal velocity or increased their terminal velocity can be characterized by having a shape similar to the mean shape of a liquid drop. The pellets were observed to be either very stable, or to rock back and forth, or to fall inverted to the drop shape with the flat side up and the rounded side down. (Fig. 2) This inverted position of fall was anticipated by McDonald (3) and Blanchard (2). The center of drag forces for a liquid drop is below the center of gravity. Upon freezing the shape of the drop is fixed and it may no longer adjust to this coupled force and it is possible to invert the drop to a more stable fall position.

Coagulation of two frozen drops

Two ice pellets frozen together were observed many times at various degrees of supercooling. (Fig. 3) The actual mechanism of fusing two ice pellets has not been determined. However, visual observation and high speed film give some insight. Frozen pellets have been photographed coalescing with supercooled drops forming a liquid layer on the surface of the ice pellet. Such an ice pellet contacting another "dryer" ice pellet at a colder temperature could cause freezing at the point of contact and fuse the pellets together. Close inspection of figure 3 gives this appearance.

On two occasions supercooled drops of millimeter sizes made contact with a larger ice object fixed in the updraft and froze immediately. The result was a protuberance in the shape of the frozen drop. (Fig. 4) With this mechanism it should be possible for two freely suspended hydrometeors to fuse together.

A third possible mechanism involves the cracking of the thin ice shell shortly after the commencement of freezing. This could provide the water necessary to freeze the pellets together.

Nucleation with ice crystals

The wind tunnel was operated several times during or shortly after a snowstorm. Consequently, a great number of ice crystals were introduced into the updraft. At other times, ice crystals were deliberately introduced to test their effect on the ability to supercool. At -2°C ice bulb temperatures, ice crystals were 100% effective in freezing the drops. At -0.5°C ice crystals had a 50% efficiency.

Fig. 1.

Ice pellets frozen at -17°C. Dimension of center pellet ≃ 11.85mm diameter

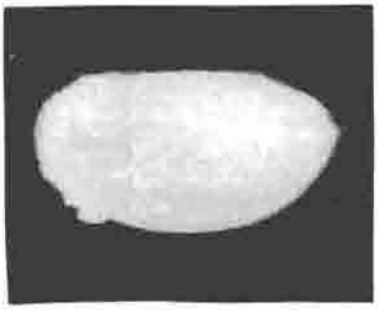

Fig. 2.

Falling position of many ice pellets. Dimensions 10.5mm x 5.85mm Temperature = -16°C

Fig. 3.

Two ice pellets frozen together. Dimension 19mm length Temperature = -16°C

Fig. 4.

Protuberance on artificial stone - note similarity to supercooled 5mm drop nearby.

Ice crystals were introduced to initiate freezing for high speed movies and produced an interesting effect. The resulting ice pellets had ice crystals protruding from the bottom indicating collection of crystals by the frozen pellets. Under the proper conditions, probably with the surface temperature of the ice pellet near 0°C, ice pellets may increase in mass by accretion of ice crystals.

BREAKUP

It is well known that drop breakup is important for drop diameters greater than 5.5mm. These studies with the vertical wind tunnel show that wake effect interactions and small drop impactions on larger drops are two important additional mechanisms in determining drop size distributions.

Wake effects

Over 200 wake interactions between 4.5mm sized drops were analyzed from high speed films. During wake interactions drops which were brought into contact exhibited three distinct types of behavior. They were said to coalesce when the oscillations produced during contact appeared to be damped out. Coalescence occurred in 33% of the wake collisions. For 20% of the collisions the drops bounced off each other. 44% resulted in breakup. Because of the positions of the drops in the field of view, the remaining 3% could not be accurately labeled as either bounce off or breakup or as no contact. The drops that broke up can be subdivided into 20% bag breakup and 30% fragmentation into several millimeter size droplets. For 50% of the wake breakups, the drops pulled out a filament producing several small droplets while maintaining most of their original mass.

Small drop impaction

Initial reviewing of our films indicates that small droplet impaction on suspended larger drops is an important process in drop breakup. Smaller drops in the size range 500 μ to 1.5mm striking a 5mm drop near the edge pull out a filament of very small droplets while decreasing only slightly in their velocity. Impactions near the stagnation point of a 5mm drop produce a crown-like splash pattern with the points of the crown breaking into smaller droplets.

ACKNOWLEDGMENTS

We wish to thank James Goold, Jr., Research Associate of the Atmospheric Science Department of the State University of New York for his assistance in performing these experiments.

The research reported in the paper was sponsored by the Air Force Cambridge Research Laboratories, Office of Aerospace Research, under Contract Number F19628-68-C-0057. The photographic equipment was procured with support from the Atmospheric Sciences Section of the National Science Foundation under Grant Number GA 1568.

REFERENCES

1. Spengler, J. D. and N. R. Gokhale, 1970: Large vertical wind tunnel for hydrometeor studies, Second National Conference on Weather Modification, April 6-9, 1970, Santa Barbara, California, pp. 289-293.
2. Blanchard, D. C., 1957: The supercooling, freezing and melting of giant waterdrops at terminal velocity in air, Artificial Stimulation of Rain, Pergamon Press, pp. 233-248.
3. McDonald, J. E., 1954: The shape and aerodynamics of large raindrops, Journal of Meteorology, 11, pp. 478-494.

RIMING PROPERTIES OF HEXAGONAL ICE CRYSTALS

by
Robert D. Wilkins and August H. Auer, Jr.
University of Wyoming, Laramie, Wyoming

INTRODUCTION

Information concerning the collection efficiencies of ice crystals between 100 and 1000μ, riming thresholds, and droplet deposition characteristics is important in studies of cloud water transport mechanisms; e.g., graupel and/or hail formation. Since 1967 replication, classification and analysis of ice crystals has been carried out at the Elk Mountain Observatory (3300m msl); this location afforded an excellent opportunity for studying the full spectrum of ice crystals produced by both large general storm situations as well as those ice crystals resulting from the isolated cap cloud.

Observations of the minimum dimensions of hexagonal plate crystals necessary for riming to be possible have been reported (1). In a further attempt to isolate some features of the riming process within natural clouds, this paper will compare the theoretical and observed minimum threshold dimensions of hexagonal plate crystal size necessary for riming to be possible; in addition, comparisons will also be made between the observed and theoretical sizes of the collected cloud droplets. The deposition characteristics of the accreted cloud droplets will also be discussed.

THEORY

Estimations of collection efficiencies for hexagonal plates have been obtained utilizing the inertial collection theories developed for thin discs (2, 3). Since inertial collection efficiencies are a function of Stokes numbers (2), these Stokes numbers have been calculated for various combinations of crystal sizes and cloud droplet diameters. The resulting theoretical collection efficiencies are plotted in Figure 1. It may be predicted from Figure 1 that a 200μ diameter crystal might selectively rime cloud droplets in the 20μ range. For this crystal size, cloud droplets smaller than 15μ in diameter cannot be collected due to inertial considerations; for cloud droplets approaching 25μ in diameter, the negligible differences between the terminal fall velocities of the ice crystal and the droplet accounts for the declining collection efficiency. Furthermore, crystals of 300-400μ in diameter show an increasing tendency to collect 15μ and larger cloud droplets. Also from Figure 1 it should be noted that a 10μ cloud droplet is close to the theoretical minimum size which can be collected by ice crystals between 100 and 1000μ in diameter. This prediction is further supported by Ranz and Wong (2), who suggest no collection of such cloud droplets by hexagonal plates is possible since the respective Stokes numbers are less than or equal to the critical value, 0.196 (3).

OBSERVATIONS

Ice crystals observed within the cap cloud were captured and replicated on Formvar coated slides. Ice crystals within the cap cloud may be replicated at very slow impact speed; and, therefore, the breakage of even the most fragile of crystals is not found. The replicas were then inspected under a microscope to determine the riming characteristics. Magnifications of 100-400X were required to insure sufficient resolutions.

Figures 2-8 illustrate representative hexagonal plate replicas possessing various degrees of riming. These data suggest a riming threshold size for hexagonal plates to lie between 200-299μ. Ono (1) reported the onset of riming was on plane ice crystals greater than 400μ in diameter but not on crystals less than 300μ. The implication to be made is that 200-300μ crystals must be carefully inspected for accreted droplets while the riming on 300-400μ crystals is more obvious due to the higher collection efficiencies.

Figure 9 presents the mean accreted droplet spectra for various size ranges of hexagonal plate crystals. For the range of crystal diameters between 200 and 1000μ, the average number of droplets per crystal reaches a maximum for accreted droplet diameters near 20μ, regardless of the degree of riming. Since all ice crystal replications were made in a water cloud, the potential for riming due to the availability of water droplets existed; nevertheless, hexagonal plate crystals less than 200μ in diameter were not found to exhibit any accreted droplets (as demonstrated in Figure 10). Furthermore, no accreted droplets less than 10μ in diameter were found on any size hexagonal plate; however, as the collector crystal size increases, there is a tendency for the accreted droplet spectrum to broaden towards larger droplet sizes. These observations appear to be in reasonable agreement with the predictions from the theoretical collection efficiencies outlined in Figure 1; in particular, the selectivity of 20μ droplets by 200μ crystals and the predicted absence of accreted droplets less than 10μ in diameter. The apparent absence of rimed droplets with diameters greater than 30μ appears inconsistent with the predictions from the collection efficiencies of Figure 1. This inconsistency can be explained by the lack of available droplets within this size range in orographic cloud systems. It should be noted that for these droplet spectra, no adjustment was made for the measured droplet diameter for the possible deformation due to impaction. Figure 11 indicates an obvious sphericity and lack of deformation of accreted droplets; this is in agreement with Brownscombe and Hallett (4).

A further inspection of Figures 2-8 indicates that droplet deposition is most pronounced at the perimeter of the crystal in the initial stages of the riming process. As the degree of riming increases, the droplets may be distributed across the entire face of the crystal; however, the principle accretional growth still continues at the perimeter of the crystal, as illustrated in Figures 6-8.

REFERENCES

(1) Ono, A., 1969: The shape and riming properties of ice crystals in natural clouds. J. Atmos. Sci., 26(1), 138-147.

(2) Ranz, W. E. and J. B. Wong, 1952: Impaction of dust and smoke particles. Ind. Eng. Chem., 44(6), 1371-1380.

(3) Fuchs, N. A., 1964: The mechanics of aerosols. Pergamon Press, London, England, 408 pp.

References cont. next page.

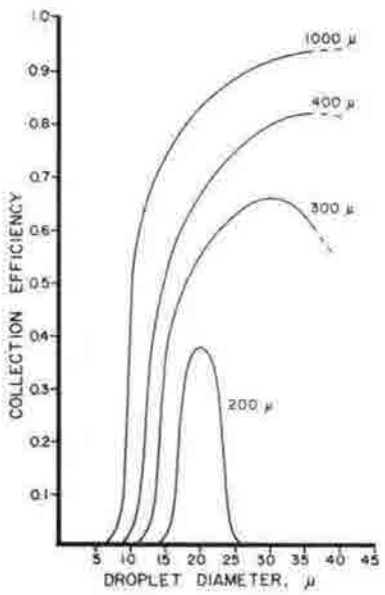

Figure 1: Hexplate Collection Efficiencies

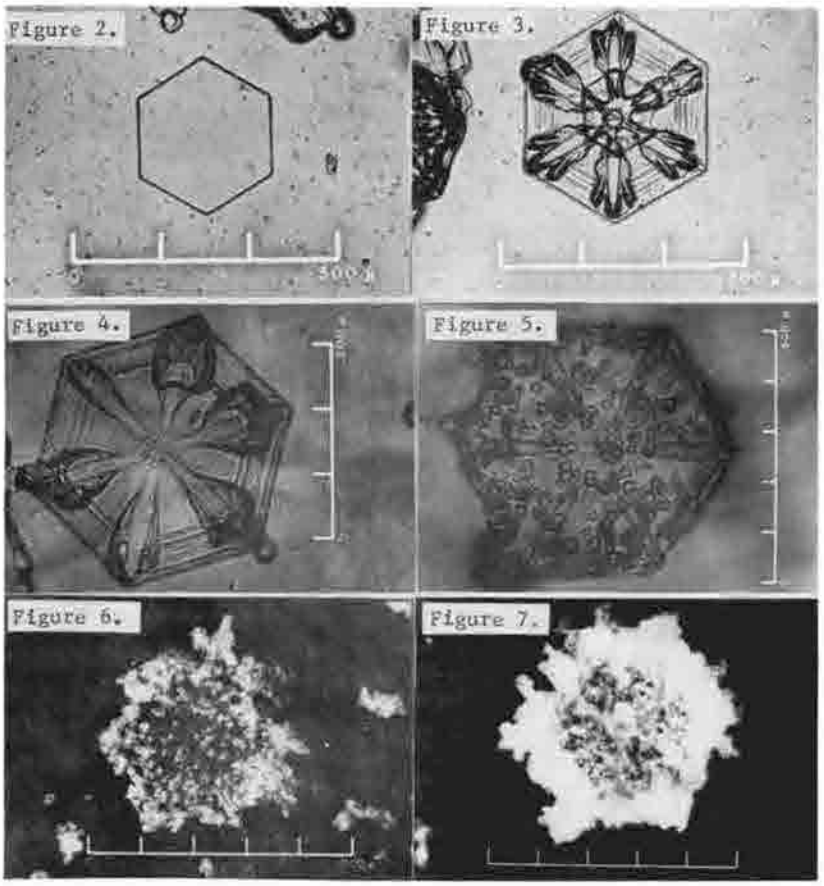

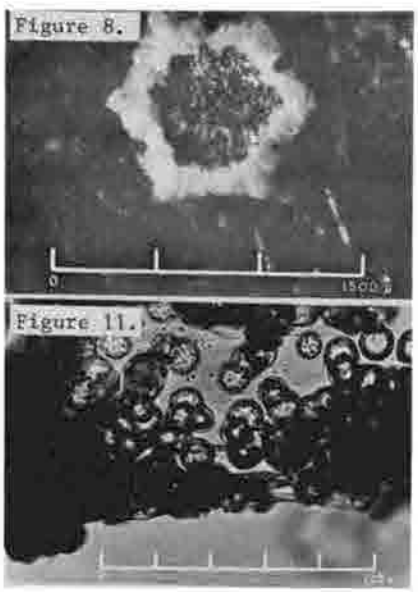

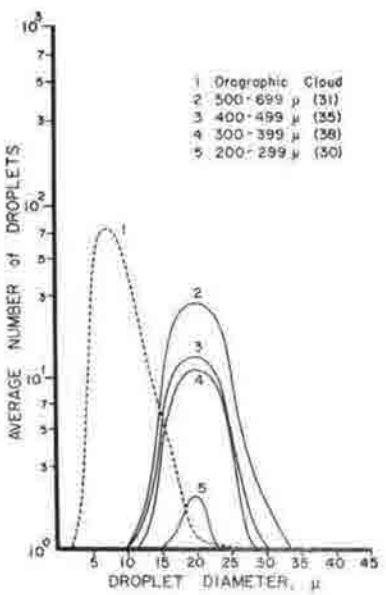

Figure 9: Hexplate Droplet Spectra.

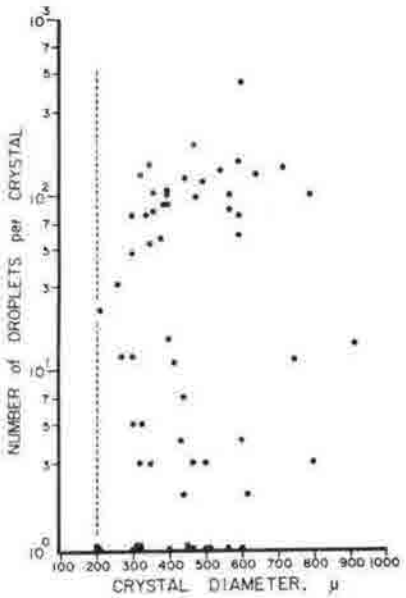

Figure 10: Hexplate Riming Threshold.

(4) Brownscombe, J. L. and J. Hallett, 1967: Experimental and field studies of precipitation particles formed by the freezing of supercooled water. Quart. J. Roy. Met. Soc., 93(396), 455-473.

This research was made possible by the U.S. Department of the Interior, Bureau of Reclamation, Office of the Atmospheric Water Resources, under contract No. 14-06-D-6002 (July 1, 1966) and No. 14-06-D-6801 (July 1, 1969) to the Natural Resources Research Institute, University of Wyoming.

SHAPE, SIZE AND SURFACE CHARACTERISTICS OF HAILSTONES COLLECTED IN ALBERTA

Brian L. Barge and George A. Isaac
McGill University
Montreal, Canada

Introduction

Shape measurements of 1915 hailstones have been obtained from 99 hail samples collected on 8 days during the summer of 1969. The measurements were made to determine hailstone distributions with shape for use in weather radar depolarization studies. Knowledge of the physical properties of hailstones is also useful for the development and verification of hail growth models.

Most of the hail was gathered by volunteer observers who provide data as part of the hail surveillance program of the Alberta Hail Studies. Precipitation sampling vehicles also collected hail when directed into suspected hail regions detected by the Alberta Hail Studies radar. To minimize the effects of melting, hail which remained on the ground longer than 10 minutes was not included in the analysis.

Method of Analysis

Each hailstone was visually classified according to its shape and surface structure into one of the seven following categories: oblate and prolate ellipsoids, spheres, cones, acorns, raspberries, and irregulars. Hailstones resembling acorns were bell-shaped with a small tip or protrusion at the end opposite the apex. Those similar to raspberries possessed small surface roughness features or bumps with an indentation at the base. "Apples" observed by Carte and Kidder (1) (see their Fig. 5h) are similar to those in the raspberry classification. Artificial hailstones produced by Bailey and Macklin (2) and shown in their Figs. 3 and 4 resemble raspberries and acorns respectively. Whenever classification of hailstones on the basis of shape and surface structure became difficult, observations of opacity influenced the classification decision. For example, many cone shaped hailstones were opaque at the apex and clear at the base. Hailstones with similar shape and surface roughness characteristics as raspberries were often opaque at the base (in which a small indentation was always observed) and clear at the apex.

The hailstone dimensions were measured with a vernier caliper according to the shape classification. Ideally all the shapes in the classification scheme should have axial symmetry. In reality, hailstones are rarely axially symmetric, necessitating two base measurements and a height measurement for the cones, acorns, and raspberries, while triaxial measurements were required for the ellipsoids and spheres. Only the minimum and maximum dimensions of irregularly shaped hailstones were measured.

Results

The ratio of the minimum dimension to the maximum dimension, hereafter designated by MIN/MAX, has been chosen to describe hailstone shape. A distribution of all hailstones with MIN/MAX is shown in Fig. 1. The minimum value of MIN/MAX was found to be 0.30; the modal value 0.80.

All the hailstones with maximum dimensions between 0.75 and 3.75 cm were grouped into three intervals: 0.75-1.75 cm, 1.75-2.75 cm, and 2.75-3.75 cm. Distributions with MIN/MAX for each of these intervals are shown in Fig. 2. It is noteworthy that the modal value of MIN/MAX decreases slightly with increasing maximum dimension.

Fig. 3 shows the distribution for cones, acorns, and raspberries to be remarkably similar. However, ratios of the average base dimension to the height (B/H) show that 82% of cones in contrast to 14% of acorns and 4% of raspberries have a B/H less than 1.0. Consequently, the height of cones is generally the maximum dimension while for raspberries and acorns, the base tends to be the maximum.

A distribution of hailstones with the ratio of the figure axis to the diameter is presented in Fig. 4. It was assumed that this ratio, figure axis/diameter, was equivalent to MIN/MAX for oblate ellipsoids, while for prolates it was MAX/MIN. Notice that the modal value of the distribution is at a MIN/MAX (or figure axis/diameter) of 0.69, which indicates that oblates are more deformed than any other category (see Fig. 3).

Table 1 shows the percentage of hailstones within each 0.50 cm size interval for every category of the classification. The most common value of the maximum dimension of all hailstones analyzed occurs between 1.50 and 1.75 cm. Also presented is the distribution of all hailstones with respect to the classification category and the maximum dimension. Of all the hailstones analyzed, 71% were ellipsoids or cones. From Fig. 2 one would expect oblate ellipsoids to be the most deformed type of hailstone since Table 1 indicates the fractional percentage of oblates generally increases with hailstone size. This is corroborated by Fig. 4. The increase in the fractional percentage of ellipsoids and raspberries with size, and the decrease in the percentage of cones is in broad agreement with the results of Carte and Kidder (1).

Summary

Of the 1915 hailstones analyzed, the most common value of the ratio of minimum dimension to maximum dimension was 0.80; the minimum ratio 0.30. Hailstones classified as cones, acorns, or raspberries had similar distribution with shape. Those classified as oblate ellipsoids were usually the most deformed. Distributions of hailstones with shape indicate that larger hailstones tend to be more deformed than smaller hailstones.

Acknowledgements

The authors wish to thank members of the Stormy Weather Group, especially Profs. R.H. Douglas and R.R. Rogers, for their helpful comments. We also gratefully acknowledge the many members of the Alberta Hail Studies who made the hail collection possible.

References

1. Carte, A.E., and R.E. Kidder, 1966: Transvaal hailstones. Quart. J. Roy. Met. Soc., 92, 388-392.
2. Bailey, I.H. and W.C. Macklin, 1968: The surface configuration and internal structure of artificial hailstones. Quart. J. Roy. Met. Soc., 94, 1-12.

Category of Classification	Maximum dimension (cm)									Total No. of Stones
	0.50-0.99	1.00-1.49	1.50-1.99	2.00-2.49	2.50-2.99	3.00-3.49	3.50-3.99	4.00-4.49	4.50-5.99	
Oblates	34	39	33	41	52	52	68	64	37	794
Cones	30	29	30	13	8	8	4	14	13	404
Spheres	14	15	10	9	4	7	4	9		193
Prolates	17	7	6	11	8	8	4	4		153
Irregulars	1	6	13	10	6	3	4	9	13	153
Acorns	3	2	3	10	11	14	7		25	118
Raspberries	1	2	5	6	11	8	9		12	100
Total No.	110	473	535	272	261	159	75	22	8	1915

Table 1. Percentages of the number of hailstones within each size interval.

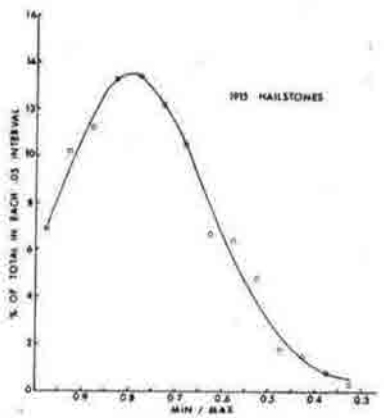

Fig. 1 Distribution of all hailstones with MIN/MAX

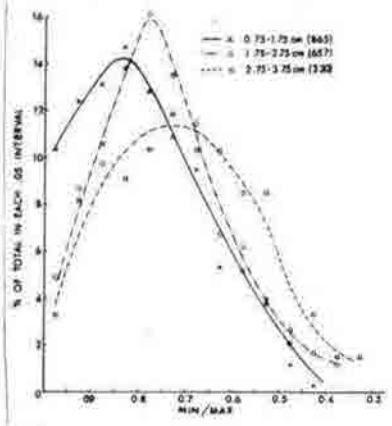

Fig. 2 Distributions with MIN/MAX for three maximum dimension intervals

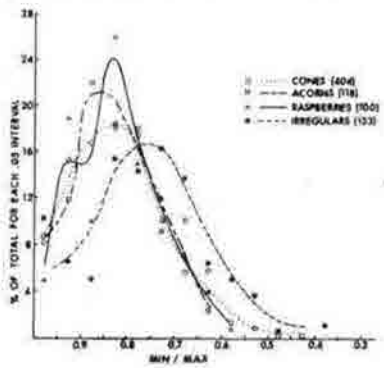

Fig. 3 Distributions of cones, acorns, and raspberries with MIN/MAX

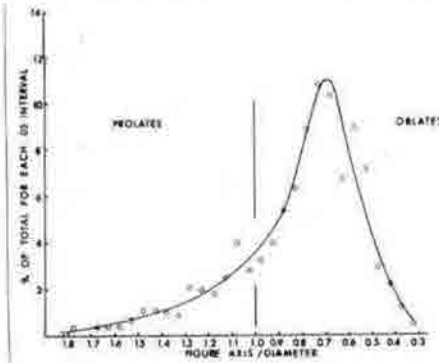

Fig. 4 Distributions of ellipsoids and spheres with figure axis/diameter

GROWTH AND ELECTRIFICATION

T. G. Owe Berg

T. G. Owe Berg, Inc., 14361 Deanann Place, Garden Grove, California 92640

It was generally thought at one time that electrostatic charges lack significant abundance and function in clouds other than thunderclouds. But data have continued to come forth, although sporadically, and it is now known that ice particles in partially glaciated clouds may be very strongly charged, that the collection of small particles by falling hydrometeors is affected by electrostatic charges, and that extensive collection of small particles by hydrometeors takes place in clouds. There is also evidence that electrification is part of the growth process and, more generally, of the exchange between a solid or liquid particle and its environmental atmosphere. Charged water droplets have been found to have peculiar properties, mainly due to reduced surface tension. A systematic study of this effect still remains to be conducted, but a few observations have been made. A review of our work is presented here.

We have developed techniques for the suspension of a charged particle in still air or an air current under controlled conditions, e.g. temperature and humidity, and the accurate measurement of charge, size, and fall velocity. (1-3) This technique has been used in investigations of charged droplets with respect to exchange of mass and charge (1) and heat (4) with the air, and of solid and liquid particles, e.g. AgI and ice (5), with respect to exchange of water and charge with the air. It has also been used in scavenging experiments (3), and in sampling of clouds (6).

When a charged water droplet evaporates, it loses relatively more mass than charge. Eventually its spherical shape becomes unstable, namely when its effective surface tension is zero. More generally, instabilities occur when

$$s = \frac{q^2}{2\pi\gamma d^3} = \frac{n+1}{2} \qquad (q \text{ charge, } d \text{ diameter, } \gamma \text{ surface tension})$$

n being the number of the harmonic of vibration. The drop becomes metastable for

$$s = \frac{1}{2}\,\frac{m - m^{2/3}}{m^{2/3} - 1}$$

and may then split into m equal fragments. Such metastability is shown only by drops larger than 150μ. Smaller metastable droplets behave as unstable droplets: they eject invisibly small droplets. Metastable droplets recover almost all the charge ejected, but unstable droplets recover only part of the charge. The recovery of charge may be a space-charge effect. Typical plots of q, d^2, and s against time are shown in Figure 1.

Evaporating charged droplets are not cooled by evaporation and do not exchange heat with the air; they retain the initial temperature.

Charged droplets of salt solutions lose solute as well as solvent in their evaporation. Such a case is shown in Figure 2.

The evidence thus indicates that charged droplets shrink by ejecting small droplets that then evaporate. The activation energy is compatible with evaporation, which indicates that the rate is determined by the removal of the ejected droplets, notably by evaporation and diffusion.

When charged solid or liquid particles are exposed to exchange of water with the air (sorption or desorption), they become charged and the air becomes ionized. This apparently applies generally and to growing ice in particular. Under circumstances the charge increases exponentially with time, and very large charges are then acquired. It appears that the rapid electrification takes place in thunderstorm clouds, and that the electrification in other clouds is slower. Plots of q and d^2 against time are shown in Figures 2 and 3 for a droplet and a solid particle.

The collision efficiency E for a falling uncharged drop of diameter D and velocity v_D with respect to a particle of terminal velocity v_{po} is (7)

$$E = E_o\, e^{-k\,\frac{E^D}{v_D v_{po}}},$$

where E_o and k are constants. For a charged drop the image force of the drop charge in the particle predominates over the aerodynamic force of repulsion when the drop charge is above a certain limit

$$Q_o = \left(\frac{3\pi}{4}\,\eta\, D^2 v_D\right)^{1/2} \qquad (\eta \text{ viscosity of air})$$

For drops charged above this limit the collision efficiency with respect to very small particles is unity or larger.

The mechanism of electrification of a single particle by exchange with the air has not yet been studied. A comparison with other cases of electrification, e.g. in friction (8), suggests an electrochemical process. The mechanism of charge separation, i.e. the transport of ions away from the particle has not been studied.

The growth of ice particles in a partially glaciated cloud is accompanied by electrification, and electrification promotes growth by collisions. Electrification is part of the growth process. The study of these phenomena, growth and electrification, appears as one of the most urgent tasks in clouds physics.

References

1. T. G. Owe Berg and D. C. George: Investigation of charged water drops. Monthly Weather Review 95 (1967) pp. 884-894.
2. T. G. Owe Berg and T. A. Gaukler: Apparatus for the study of charged particles and droplets. Amer. J. Physics 37 (1969) pp. 1013-1018.
3. T. G. Owe Berg, T. A. Gaukler and U. Vaughan: Collisions in washout. J. Atm. Sci. 27 (1970) pp. 435-442.
4. T. G. Owe Berg, T. A. Gaukler and R. J. Trainor, Jr.: The temperature of charged water drops. J. Atm. Sci. 26 (1969) pp. 558-559.
5. T. G. Owe Berg and T. A. Gaukler: Electrification experiments with AgI in the system water vapor, liquid water and ice. J. Atm. Sci. 26 (1969) pp. 675-683.
6. T. G. Owe Berg and T. A. Gaukler: Exploratory studies of charged ice particles in natural clouds. J. Appl. Meteor. 7 (1968) pp. 952-955.
7. T. G. Owe Berg: Collision efficiency in washout by rain. Paper submitted to Precipitation Scavenging Meeting, Richland, Washington, June 1970.
8. T. G. Owe Berg and T. A. Gaukler: Kinetics of exchange in the electrification of glass in friction. J. Chem. Engineering Japan, 1970.

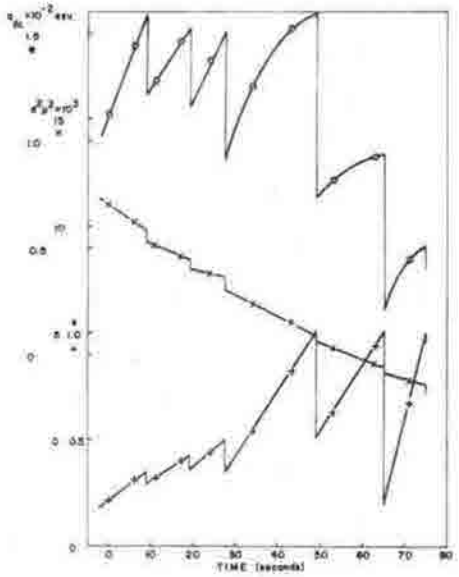

Figure 1. Plots of q, d^2, and s for a water droplet showing three "metastabilities" and three "instabilities".

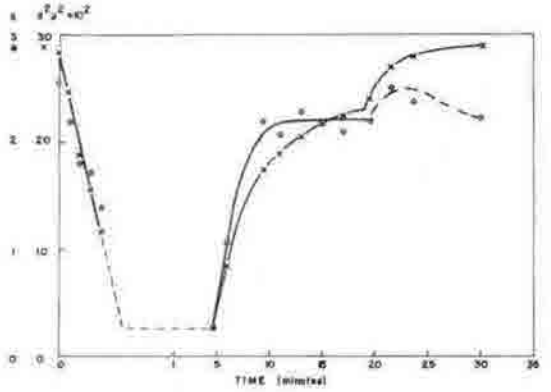

Figure 2. A droplet was made from NH_4NO_3-urea after dilution 5 times by water and suspended in a dry current of air. After reduction in volume by a factor of 30 it was exposed to a current of air at water vapor saturation. The plots show d^2 and q (arbitray units) as functions of time.

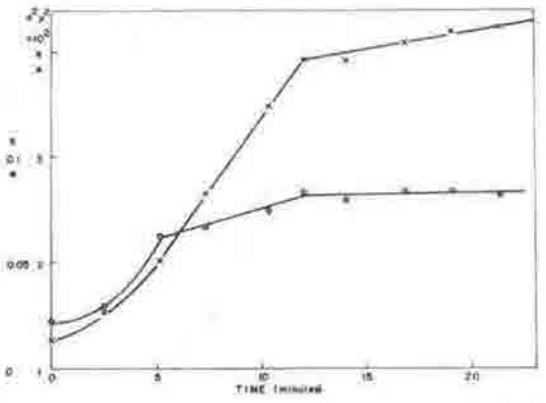

Figure 3. A dry CaCl particle was suspended in an air current of 33°C and 40% relative humidity. The plots show d^2 and q (arbitray units) as functions of time. The charge leveled off when the particle became liquid at time 5 minutes.

ICE CRYSTALS GROWN WITHIN THE NCAR ICE NUCLEUS COUNTER

by
John R. Middleton and August H. Auer, Jr.
University of Wyoming, Laramie, Wyoming

INTRODUCTION

The ability to detect the ice forming capability of the atmosphere is essential to many studies in cloud physics. In this regard, the NCAR ice nucleus counter has assumed a prominent role. This counter, developed at NCAR and made commercially by E. Bollay and Associates, Inc., is based on an acoustical particle counter as a detector. The principles and operation of the NCAR counter are described in (1, 2). The cloud chamber temperature profile has been investigated by (3), while a summary of cloud physics parameters describing the cloud at various chamber temperatures within the NCAR counter was given by (4). To date, however, there is no known published data concerning the characteristics of ice crystals grown within the NCAR counter.

The purpose of this paper is to examine the crystal types, sizes, and structures and compare these observed values with predictions from the appropriate temperature and humidity habitats, resident growth times and theoretical growth equations. In addition, concentrations of replicated crystals will be compared with concentrations of crystals detected by the acoustical counter.

PROCEDURES

A small insulated box containing a slide exposure mechanism was inserted through the observation port of the NCAR counter. This insulated box served to condition the Formvar coated (1-2% solution in methylene chloride) slides to the chamber temperature prior to and after exposure within the center of the NCAR cloud chamber. Ice crystal replicas were collected during exposure times of 60-90 seconds. This method of replication did not appear to disturb the normal operation of the counter.

Except at very cold temperatures (<-25C), infinitesimal amounts of silver iodide smoke (prepared with sodium iodide) from an acetone burner were introduced into the cloud chamber to increase ice crystal concentrations above background levels since the observed ice crystal concentration detection threshold for the Formvar slides was below the background concentration.

The reported deficiency (2) in the counting of ice crystals by the NCAR counter was rectified by improving the quality of the audible signal produced by the ice crystal passing through the acoustical sensor (5). Thus, the resulting ice crystals were replicated and the indicated concentrations as determined by the acoustical counter-rate computer system were noted.

RESULTS

Representative photographs of chamber crystals are presented in Figures 1-6. For indicated chamber temperatures between -10 to 20C, the principal type of crystals observed were hexagonal plates. This agrees with accepted habitats, with the possible exception of -15C, where dendritic crystals should be prominent. Some hexagonal plates found at -15C did exhibit dendritic extensions (Figure 4). This form may indicate that the crystal grew as a hexagonal plate in a warmer region in the upper part of the chamber (3) before falling into the dendritic growth region. Added support for the possibility of differing growth regimes due to varying temperature habitats within the chamber is also suggested by observations of columnar crystals and hexagonal plates with sector like extensions between indicated chamber temperatures of -10 to -20C.

Since, as a first approximation, the threshold detection size using the acoustical sensor is directly proportioned to air density (6), the threshold crystal diameter for the elevation at which the counter was operated (2200 m msl) is 18μ . The percentage of total replicated crystals with diameters greater than 18μ is presented in Table 1. Table 1 suggests that slightly over one-third of the crystals within the counter grow to a minimum detectable size at -10C while the percentage of crystals reaching the threshold size is a maximum (88%) at -15C. Ice crystals with double crystalline structures and frozen droplet centers (Figures 4-6), similar to those observed by (7, 8), were found within the NCAR chamber following small injections of silver iodide smoke. The percentage of detectable crystals ($d \geq 18\mu$) with frozen droplet centers is also shown in Table 1. These percentages are somewhat lower than those found by other cloud chamber nucleation studies (7). Thus it would appear that when AgI smoke is introduced into the NCAR cloud chamber, ice crystals growing to detectable size are nucleated by both deposition and droplet freezing modes.

Table 2 shows the average and maximum crystal sizes and respective calculated growth times for detectable ice crystals. These growth times are inferred from simple deposition growth theory at water saturation (9). These predicted residence times, as shown in Table 2, are slightly greater than the 20 seconds suggested by (1, 4) during measurements of first response to AgI seeding by the NCAR chamber. The data for maximum crystal sizes shown in Table 2 are in general agreement with the suggestion of (1) indicating a more reasonable residence time of 60 seconds. Thus, the observed ice crystal diameters appear in accordance with expectations of resident growth times between 20-60 seconds.

The observed concentrations of crystals of detectable size ($d \geq 18\mu$) were compared to concentrations indicated by the NCAR counter rate computer. The results presented in Figure 7, suggest agreement within a factor of two for the range of chamber temperatures and concentrations considered. Note that concentrations 1000 liter^{-1} were observed during periods when the rate computer indicated "overload".

TABLE 1

PERCENT OF TOTAL CRYSTALS $\geq 18\mu$ AND PERCENT OF THOSE $\geq 18\mu$ WITH FROZEN DROPLET CENTERS

Temp. C	No. of Observed Crystals	No. of Crystals with ($d \geq 18\mu$)	Percent	Percent Of Detectable Crystals ($d \geq 18\mu$)
-10	179	68	38	27
-12.5	128	82	64	35
-15	111	98	88	30
-17.5	248	174	70	30
-20	390	265	68	39

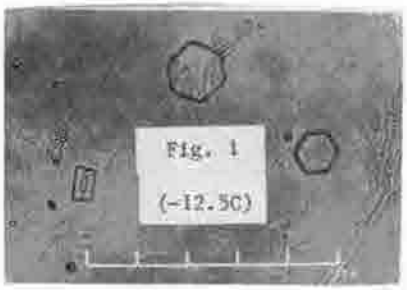

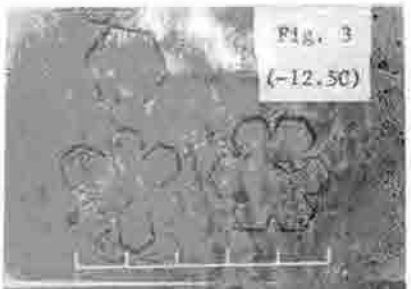

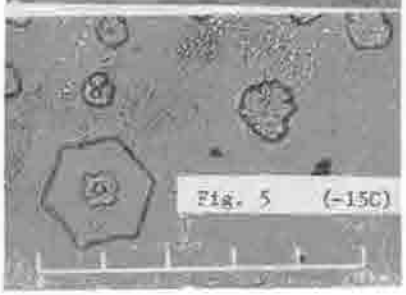

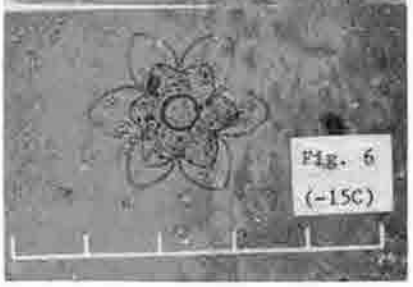

TABLE 2

AVERAGE CRYSTAL SIZE >18u, MAXIMUM CRYSTAL SIZE PREDICTED GROWTH TIME FROM THEORY

Temp. C	Average	Growth Time	Maximum	Growth Time
-10	28	25	35	30
-12.5	36	30	75	68
-15	36	27	80	60
-17.5	36	30	75	69
-20	38	31	85	79

Figure 7

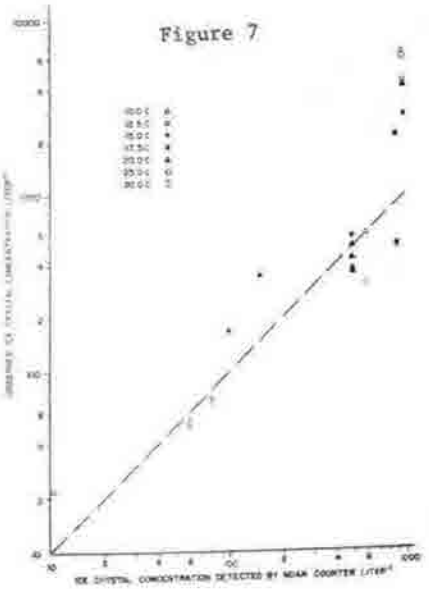

ACKNOWLEDGEMENTS

This research was made possible by the U. S. Department of Interior, Bureau of Reclamation, Office of Atmospheric Water Resources, under Contract No. 14-06-D-6801, (July 1, 1969) to the Natural Resources Research Institute, University of Wyoming, Laramie, Wyoming.

REFERENCES

(1) Langer, G., J. Rosinski and C. P. Edwards, 1967: A continuous ice nucleus counter and its application to tracking in the troposphere. J. of Appl. Met., 6(1), 114-125.

(2) Steele, R. L., C. P. Edwards, L. O. Grant and G. Langer, 1967: A calibration of the NCAR acoustical ice nucleus counter. J. of Appl. Met., 6(6), 1097-1107.

(3) Isaac, G. A., 1968: Variations in atmospheric ice nucleus concentrations. M. S. Thesis, Department of Meteorology, McGill University, Montreal, Quebec, Canada, 68 pp.

(4) Auer, Jr., A. H. and D. L. Veal, 1968: Characteristics of the cloud within the NCAR ice nucleus counter. J. R. A., 4(1-2), 155-165.

(5) Interim Progress Report, No. 1, July 1968, to the Office of Atmospheric Water Research, U. S. Bureau of Reclamation, Department of Interior, in fulfillment of Contract No. 14-06-D-6002 to the Natural Resources Research Institute, University of Wyoming, 36 pp.

(6) Rouse, H., 1946: Elementary Mechanics of Fluids. John Wiley and Sons, New York, 376 pp.

(7) Weickmann, H. K., U. Katz and R. L. Steele, 1970: AgI-sublimation or contact nucleus? Preprints of the Papers Presented at the Second National Conference on Weather Modification, Santa Barbara, California, 332-336.

(8) Auer, Jr., A. H. and D. L. Veal, 1970: Observations of ice crystal nucleation by droplet freezing in natural clouds. Extended Abstracts of Cloud Physics Conference, Fort Collins, Colorado.

(9) Byers, H. R., 1965: Elements of Cloud Physics. University of Chicago Press.

CHARACTERISTICS OF A LARGE NUMBER OF HAILSTONES FROM A SINGLE ALBERTA HAILSTORM

L.N. Rogers
Research Council of Alberta
Edmonton

INTRODUCTION

On August 4th 1969 a thunderstorm in Alberta produced hail of up to 7.5 cm diameter over a six mile wide swath extending more than forty miles from Pigeon Lake to northeast of the City of Edmonton. Some 300 samples of hailstones were collected by members of the public with a sample collection density of up to 40 per square mile. Analysis of these samples was divided into the study of the global properties of the whole stones and the study of their internal structure.

GLOBAL MEASUREMENTS

Global measurements were performed on 407 hailstones from 17 samples. Fifteen samples were from Edmonton, one from the beginning of the swath and one from east of Edmonton. Ten of the samples were reported to be biased towards the larger size of stone, 1 was said to be a representative sample and no information was available on the other samples.

Mass and density

The measured masses of the stones ranged from 0.521 g to 112.406 g and the densities, obtained from bouyancy measurements in varsol, ranged from 0.853 g/cc to 0.920 g/cc with a mean value of 0.884 g/cc. The samples from Edmonton showed no significant variation of density across the width of the swath and no variation was apparent along its length. The bias towards larger hailstones precluded the formulation of a size distribution of the stones.

Shape measurements

The lengths of the three perpendicular axes of the stones was measured and the shapes of the stones characterised by the shape factors $S_1 = 2c/(a+b)$ and $S_2 = c/a$ where a,b,c are respectively the lengths of the major, intermediate and minor axes. The factor S_1 is a measure of the sphericity of the stones and finds application in fall speed and growth studies, and S_2 is a measure of oblateness which is of importance in radar polarisation work. The values of S_1 ranged from 0.372 to 0.983 with a mean value of 0.744 and a modal value of 0.73. The values of S_2 had an extreme value of 0.26 and a modal value of 0.67 as taken from the smoothed histogram. The detailed histogram suggested a second peak at 0.8.

Cross-correlation of the parameters

The global data were punched onto IBM cards and a computer cross-correlation was performed. The results are shown in Table 1.

Table 1. Cross-correlation of global data

	Mass	Density	Major axis	Intermediate axis	Minor axis	Shape factor S_1
Mass	1	-0.093	0.807	0.904	0.904	0.165
Density	-0.093	1	-0.109	-0.116	-0.199	-0.231
Major axis	0.807	-0.109	1	0.972	0.844	-0.106
Intermediate axis	0.904	-0.116	0.972	1	0.893	-0.010
Minor axis	0.904	-0.199	-0.844	0.893	1	0.402
Shape factor S_1	0.165	-0.231	-0.106	-0.010	0.402	1

As expected the mass correlates highly with the axial lengths. The density has a small negative correlation with the mass and a negative correlation with the other parameters. The shape factor correlates positively with the mass.

Discussion of results

The measured masses were unexceptional but it is of interest to note that only one stone had an equivalent spherical radius of more than 3 cm despite the large number of reports of stones of this size. The measured densities were similar to those found by other workers, the lack of any low values being due to the absence of soft hail in the samples. The negative correlation with the mass is not thought to be significant because of the spread of values.

The values of the shape factors may be compared with those found by Barge and Isaacs [1] and by English [2]. Barge and Isaacs made measurements of S_2 on stones from 15 Alberta storms and found an extreme value of 0.3 and a modal value of 0.8. This modal value is significantly different from that of 0.67 found for the Edmonton storm, although it is the same as the secondary peak in the Edmonton storm. The radar depolarisation ratios appropriate to these modal values are 0.01 and 0.02 respectively. English made measurements of S_1 on stones from a single storm over Montreal and found the values to lie between 0.24 and 0.95 with a modal value of 0.63. English adjusted her mathematical model of a thunderstorm (English [3]) to take account of the shape of the stones and found that a stone with a shape factor of 0.8 could grow to twice the weight of a spherical stone starting its growth at the same point. The higher modal value for the Edmonton storm suggests that this effect was not so important as for the Montreal storm. Further, the positive correlation between shape factor and mass for the Edmonton storm shows that the larger stones tend to be more nearly spherical than the smaller stones and thus the growth enhancement due to shape does not apply to these stones.

INTERNAL STUDIES

One hundred hailstones were selected for study of their internal characteristics. Density measurements were not

performed on these stones so as to avoid varsol contamination. The emphasis in these studies was based on the nature of the growth embryos and the crystal structure of the stones.

Initial growth embryos

Of the 100 hailstones which were sectioned 40 were found to have growth centres of clear ice, 33 had conical graupel centres and the remainder had centres of opaque spheres or ellipsoids. The majority of the stones were sectioned perpendicular to the minor axis and generally the graupel centres were found to have the direction of growth lying in, or close to, this plane. The clear centres were spherical and ellipsoidal and between 1 mm and 8 mm diameter. On two occasions the stone was composed of clear ice up to 4 cm diameter with radial air bubbles of 1 mm or 2 mm diameter radiating from a spherical shell of about 1 cm diameter. The clear centres often showed rings of air bubbles similar to those observed by Kidder and Carte [4] in water drops frozen in the laboratory (their Fig 12a), and they often also showed central accretions of air bubbles. On three occasions diametrical chords of air bubbles were observed similar to those observed in the laboratory by Johnson and Hallett [5] (their Fig 3a,b). Kidder and Carte [4] state that their water drops were always supercooled below -5°C before freezing basing this statement on the criterion of Hallett [6] that large single crystals form at lesser degrees of supercooling.

These results may be compared with those of other workers. List [7] found that 80% of large hailstones in Switzerland originate as conical graupel; Carte and Kidder [8] found that in the Transvaal between 10% and 20% originated as clear embryos while Macklin, Strauch and Ludlam [9] observed over 90% clear centres in a storm over England.

Fractured embryos

Carte and Kidder [8] presented photographs of a stone which had broken in mid-air and then continued to grow. Browning [10] presented data from Oklahoma which showed that more than 10% of the stones from one storm had fractured and then continued to grow. In the present study 7 out of 100 stones had fractured and then continued to grow. As found by Browning breakage could occur at any stage in the growth, the limits for the Edmonton storm being a 4 mm diameter embryo and a 2 cm diameter stone. Fracture could occur along either a diameter or a chord of the stone.

Multiple and double embryos

In addition to the 100 stones mentioned above 5 other stones were sectioned. Of these 4 showed the presence of secondary growth embryos situated in one of the middle rings of the stones and 1 had a centre composed of two connected clear embryos. The multiple embryo stones came from two samples picked up within a mile of each other. The good sample density for the Edmonton storm has allowed this phenomenon to be isolated in this area.

Crystal structure

The crystal structures of the sectioned hailstones were observed under polarised light. Measurements of crystal area were made for 23 stones. In general changes in crystal structure correlated with changes in opacity, small crystals corresponding to opaque layers and large crystals to transparent layers. This was not always the case and, in particular, a sample from the beginning of the swath was found to be entirely composed of small crystals although the normal layer structure was apparent. A study of the clear-centred stones showed that in 21 out of 40 cases the centre was a large single crystal. According to Hallett this infers that these water drops were nucleated above -5°C.

Measurements of the average areas of crystals in the various layers showed the areas to range from 2.1×10^{-4} cm^2 to 2.7×10^{-1} cm^2. As pointed out by Schaefer [11] these sizes are generally larger than those of cloud drops. Kidder and Carte [4] have suggested an explanation of this in terms of the infiltration of liquid water into a low density region. Cantin [12] has observed a correlation between crystal area and layer density such that crystals of area less than 17×10^{-4} cm^2 are associated with opaque layers while larger crystals are associated with clear layers. This correlation has not been observed in the present work, probably because of the use of more than one sample.

Discussion of results

The most important result presented here is that 40% of the hailstone growth embryos were frozen raindrops of which half were nucleated above -5°C. If this is generally true for Alberta storms then it must be borne in mind in considering seeding of the storms.

REFERENCES

1. Barge B. and Isaacs G. Shape, size and surface characteristics of hailstones collected in Alberta. Submitted to AMS Conference on Cloud Physics Fort Collins, Colo. 1970.
2. English M. Private communication.
3. English M. Report MW-59, Stormy Weather Group, McGill University.
4. Kidder R.E. and Carte A.E. Structures of artificial hailstones. J. de Recherches Atmospheriques 1, 4, 1964.
5. Johnson D.A. and Hallett J. Freezing and shattering of supercooled water drops. QJRMS 94, 402, 1968.
6. Hallett J. Discussion of Douglas' paper. Met. Mono. 5, 1963.
7. List, R. Kenzeicher atmospharischer Eispartikeln. Z. Teil: Hagekorner. Z. arg Math. Phys. 9a, 1958.
8. Carte A.E. and Kidder R.E. Transvaal hailstones. QJRMS 92, 393, 1966
9. Macklin W.C., Strauch E. and Ludlam F.H. The density of hailstones collected from a summer storm Nubila 3, 1960.
10. Browning, K.A. Hailstones breaking in mid-air. Weather, August 1967.
11. Schaefer, V.J. Hailstorms and hailstones of the Western Great Plains Nubila 3, 1960.
12. Cantin, J.G. Structural properties of a hailstone sample. M.Sc. Thesis University of Toronto.

A CAMERA FOR PHOTOGRAPHING AIRBORNE ATMOSPHERIC PARTICLES

by

Theodore W. Cannon

National Center for Atmospheric Research
Boulder, Colorado 80302

One approach to obtaining information for studies of in-cloud water drops and ice crystals is to make in situ photographs of them. Photography is a desirable approach since it can give the particle size distribution as well as the special distribution and identity of the particles. If the components of the camera are sufficiently far removed from the in-focus volume, the sample should be relatively undisturbed and give a representative picture of the actual cloud.

The problem for the cloud particle case is made difficult by the fact that the in-focus volume is very small at the necessary magnifications. Furthermore at airplane speeds above stall speed some motion compensation as well as microsecond flash duration lights must be used to obtain sharp images. As low magnification as possible must be used in order to have enough in-focus particles to get meaningful information.

By using very fine grain film along with some recently developed high speed lights, a camera has been successfully demonstrated for photographing particles 15 microns in diameter and larger at reasonably low magnification. The camera uses very fine grain microfilm rated at 350 lines per millimeter at test-object contrast of 1000:1. A 135 millimeter focal length lens is used at 1:1 magnification, and in-focus particles about 360 millimeters in front of the lens are photographed. Lights with flash duration of 4.5 microsecond at 1/3 intensity level are used. Dark field illumination is employed. Two lights are normally used with their beams aimed from off the optical axis toward the in-focus volume and in the direction of the film plane. A light trap is placed beyond the in-focus volume so that light only enters the lens when a particle or particles are present. Images of transparent particles appear as the two refracted images of the lights, while translucent particles appear in their actual shape.

Photographs of particles in clouds at ground level near the hot pools in Yellowstone Park and in winter ground clouds near Boulder, Colorado, show particle distributions in space. The shallow depth of field has the advantage of showing only those particles which lie in a very thin slice of cloud. Photographs of clouds near the hot pools show very interesting swirls and clusters of droplets. Such special distributions would have a different effect on precipitation formation than the usually assumed random distributions if they exist in clouds in the free atmosphere.

The camera is calibrated for water droplet size determination by photographing transparent spheres of known size at known distances from some reference point in the camera. The refracted images of the two lights appear as two resolved dots on the film if the sphere is considered to be in focus. When the two dots merge or disappear they are considered to be out of focus. The calibrated camera has been used to photograph clouds in the laboratory and their drop size distributions measured from the negatives. Depth of field is dependent on drop size, being typically 500 microns for 25 micron diameter spheres.

Extreme care in installation of the camera and in processing the film and data must be used. The lights and optical system components should be precisely and rigidly fixed. The film should normally be handled in clean room conditions to avoid contamination by dust particles.

An interesting ground and laboratory application of the camera is determination of particle trajectories. Recently a series of lights has been developed which will generate microsecond duration pulses at rates up to 1000 Hz. These units have been used to make multiple exposure photographs of moving particles. Trajectories of the particles may be measured from these photographs and these are of interest to cloud physicists doing drop collection efficiency studies as well as determining charges on drops by electrostatic deflection.

At aircraft speeds, it is necessary to provide mechanical motion compensation since the high speed lights currently available do not have short enough light pulse durations to prevent blurring of the images. A version of the camera incorporating a rotating mirror with electronic speed control has been mounted in the NCAR sailplane and will be tested in flight in the near future.

A CONTINUOUS CLOUD SAMPLER

J. Pena, R. de Pena
R. L. Lavoie and J. Lease

The Pennsylvania State University
University Park, Pennsylvania

The most reliable and accurate technique for gathering cloud drop population data is still direct sampling by collection and replication. While there is increasing promise for fibre optics and laser scattering techniques, it appears that the conventional sampling methods will continue to fill an important need. In spite of the relatively tedious data reduction problems, the replicating devices have the potential of being simple, reliable and inexpensive.

We have recently expanded upon a device in use at Penn State for several years to sample clouds from aircraft. The previous system (1) used a modified 35 mm slide changer that exposed gelatin-covered glass slides briefly to an airstream. Water droplets impinging upon the slide dissolve the gelatin, leaving a crater about twice the size of the drop. Provided the slides are kept warm, ice crystals leave their own characteristic impressions upon the gelatin. However, the mechanical action of the changer and slide storage were limiting factors in collecting nearly continuous data over extended intervals. The new device uses a conventional 16 mm movie projector to transport gelatin-coated film over a cylindrical collector.

The drive motor and the supply and take-up reels (with 150 m capacity) are housed in a pod of volume of approximately 55 liters which is suspended from the aircraft wing as shown in Fig. 1. The film passes out through a 125 cm long aluminum tube to the cylindrical probe located well in advance of the wing. Exposure to the airstream takes place only as the film passes over the 0.8 cm diameter cylindrical roller at a speed of about 25 cm sec^{-1}. A cut-away view of the probe assembly can be seen in Fig. 2. A film transport distance of 340 cm is provided between the sampling point and the take-up reel to allow the collected droplets to evaporate before the film is stored. Collection efficiencies exceed 0.3 for cloud drops larger than 2 μm radius and reach 0.9 for 7 μm drops.

The instrument has been used with considerable success in maritime cumulus over the Caribbean. The most notable deficiency appears to be overexposure of the gelatin film in clouds of high liquid water content (LWC). Overexposure is achieved even before impacting droplets begin to overlap each other, and appears to result from a general softening of the gelatin coating by the absorbed water which makes crater walls less distinct. With the above-mentioned cylinder size and film speed, the cutoff LWC in maritime clouds is about 0.35 gm kgm^{-1}.

Figure 3 demonstrates the general agreement that was observed between LWC values computed from droplet populations measured on the gelatin film and values recorded from a Johnson and Williams hot-wire instrument. The response times of the two instruments are of course quite different. The film samples represent an average over 3.25 m of penetration distance through the cloud while the J & W instrument generates a value representative of a 100 m interval. The agreement between the two sets of data encourages the view that the cloud structure is reasonably homogeneous on a scale of tens of meters.

It can also be seen from Fig. 3 that no film samples could be studied in regions where the J & W device indicated LWC greater than about .35 gm kgm^{-1}. In these regions the film gave the appearance of being "washed out".

Figure 4 provides a more extensive comparison between the continuous sampler and the J & W measurements. The simultaneous data points were selected from three separate cloud penetrations in such a way as to provide a full range of LWC. The points have been plotted in order of increasing J & W values for convenience. The trend of the two sets of data agree reasonably well although calculations based on droplet populations produce somewhat lower LWC on the average. The discrepancy becomes quite marked at values greater than .35 gm kgm^{-1}.

The limitations imposed on the sampler at high LWC can be amerliorated in several ways. It could of course be flown on a slower aircraft, but given the airborne platform it is possible to baffle the air intake to the instrument, to speed up the film transport motor, or to decrease the cylinder size of the collecting probe. The latter modification is especially simple and is currently being tested.

In summary, the gelatin continuous sampler has proved to be a reliable instrument for the study of fogs and clouds. It is mechanically simple, remotely controlled, and has sufficient capacity for continuous sampling over path lengths exceeding 30 km. Droplets as small as 1.25 μm can be detected; the sampler could also be used as an aerosol sampler to collect particles larger than 1 μm radius. Dyes and specific chemical reagents can be easily added to the gelatin film for clearer replication of water drops or to facilitate special aerosol analysis.

ACKNOWLEDGMENT

This research is supported by the Atmospheric Sciences Section, National Science Foundation, NSF Grant GA-13818.

REFERENCE

1. Jiusto, J. E., 1965: Cloud particle sampling. Report No. 6, NSF G-24850, Dept. of Meteorology, Pennsylvania State University.

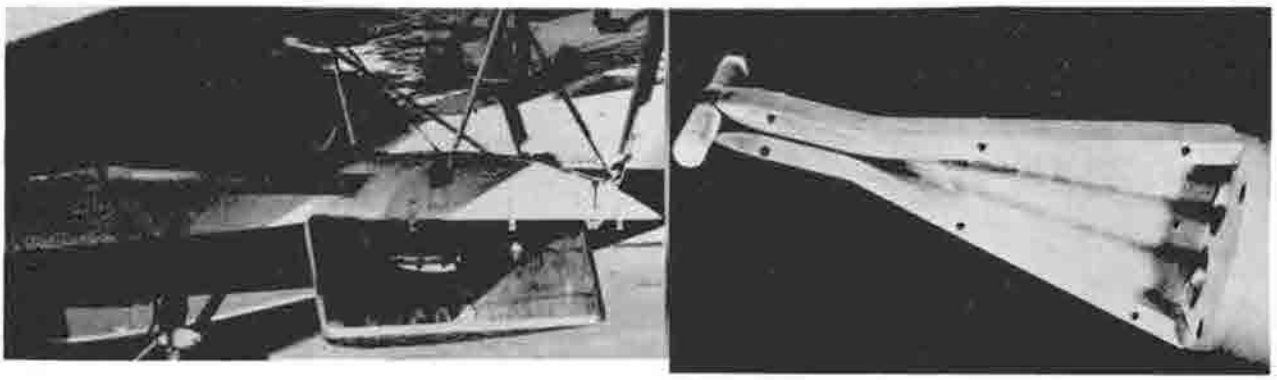

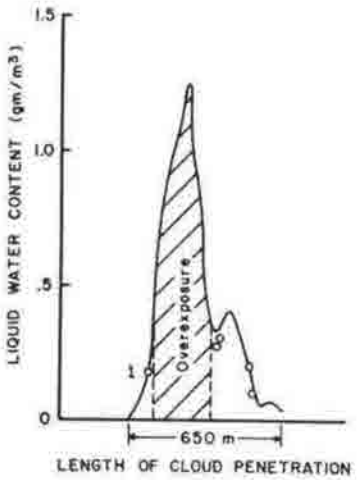

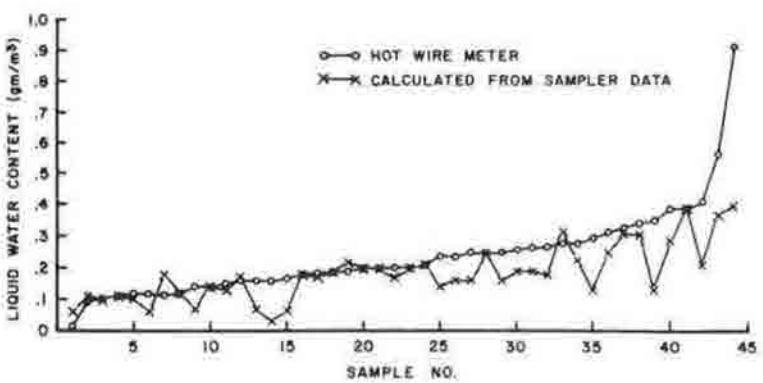

FOG DROP-SIZE DISTRIBUTIONS MEASURED WITH A LASER HOLOGRAM CAMERA

Bruce A. Kunkel
Air Force Cambridge Research Laboratories
Bedford, Mass.

INTRODUCTION

A laser hologram camera was developed by Silverman, Thompson & Ward (1964). This device in its final test design was capable of measuring droplets 4 μm diameter and larger. The sample volume varied from 0.8 cm^3 for 4 μm droplet to approximately 4.5 cm^3 for droplets greater than 40 μm. Initially, because of the imaging lenses and the film resolution, only droplets greater than 30 μm diameter were recorded. This paper presents some of the fog drop-size measurements obtained during a two-year test period at Otis AFB, Falmouth, Mass.

MEASURED DROP-SIZE DISTRIBUTIONS

Examples of the measured drop-size distributions are presented in the following manner: a)sample-to-sample variations; b)variations within an extended fog occurrence and c)variations between fog cases.

Sample-to-Sample Variation

Because of the small sample volume of the hologram camera, one must be concerned with the representativeness of the individual samples. It is, therefore, of interest to examine the sample-to-sample variation in the drop-size distribution. Table 1 shows the droplet concentrations for a series

	TIME (EDT)												
DIAM. (μm)	0539			0540					0541				
5													
10	2.0	1.3		1.3	0.7				1.3	1.3	1.3	1.3	
15	4.6	1.5	2.3		3.8	0.8	0.8	0.8	3.1	0.8	1.5	2.3	2.3
20	1.0	0.5	1.5	2.6	1.5	1.0	1.5	1.0		1.0	1.0	0.5	2.0
25	2.3	0.4	0.8	0.4	1.9	0.8	0.4	1.9	2.7	1.9	1.9	0.8	3.1
30	1.0	0.5	0.5	1.3	0.8	1.6	0.5	1.0	1.3	0.5	1.8	0.5	0.3
35	0.2		0.2	0.7	0.9	0.7	0.7	0.5	0.4	0.5	0.5	0.2	0.9
40			0.2	1.0	0.6	0.4		1.0	0.4	0.6	1.0	0.6	0.6
45	0.2		0.4		0.2		0.2	0.2	0.2		0.7		0.8
50				0.2		0.2			0.2	0.2			
55													
60									0.2				0.2
65													
70													
CONC. ($/cm^3$)	11.3	4.0	6.0	7.7	10.4	5.4	4.1	6.4	10.3	6.4	8.9	5.9	10.2
D (μm)	18.9	17.6	22.6	25.9	22.2	27.6	24.6	27.6	23.9	23.3	24.2	19.7	26.1
LWC (g/m^3)	.062	.021	.056	.110	.091	.077	.044	.090	.130	.071	.100	.045	.148

Table 1: Time variation in the number concentration ($\#/cm^3$) of fog droplets per size range as measured by the hologram camera. Total concentration, mean diameter and resulting liquid water content for each sample are also shown.

of measurements made with the hologram camera during a fog on 15 July 1965. As one might expect, because of the small sample volume, considerable variation is noted between samples. The peak number concentration occurs in either the 15, 20, 25 or 30 μm size ranges, and many bimodal and trimodal distributions are observed. Mean diameters vary from 17 to 26 μm and number concentrations vary from 4 to 11 cm^{-3}. The resulting liquid water contents vary from 0.02 to 0.15 g m^{-3}.

The mean droplet size generally shows the smallest sample-to-sample variation in all of the fog cases while the number concentration and liquid water content show the greatest variation. Undoubtedly, some of this variation is due to an insufficient sampling. However, continuous measurements from a J-W liquid water content meter, located about 50 feet from the hologram camera, also show considerable variation in the LWC, indicating that some of the variations in the hologram data are real. Correlations between liquid water contents measured with the hologram camera and the J-W were as high as .70.

Variation During the Life Cycle of a Fog

On the night of 29-30 August 1964, fog, which was preceded by drizzle, persisted for several hours. The rawinsonde data indicated the fog depth to be about 3000 feet at 2300 EDT with a gradual decrease in depth to around 800 feet at 0500 EDT. A SW wind blew at 2-5 knots throughout the night.

Drop-size measurements with the laser hologram camera were taken at various time periods throughout the life of the fog. The drop-size data from the hologram camera are shown in Fig. 1 for four different time periods. The data represents an average of many samples taken over a finite time period. Since this case occurred during the first half of our test program, droplets below 30 μm diameter were not detected by the hologram camera. To help fill the gap below 30 μm, mean drop size data from a light scattering cascade impactor (Schultz *et al* 1966) are shown in Fig. 1 for the size range from 0.5 to 16 μm. Because of the sampling difficulties with the cascade impactor this data should be regarded as only an indication of the actual concentrations. Because the impactor measures droplets in varying size ranges the concentrations in Fig. 1 are shown in terms of the number of droplets per cubic centimeter (ΔN) in diameter range (ΔD). The drop sizes, as measured by the hologram

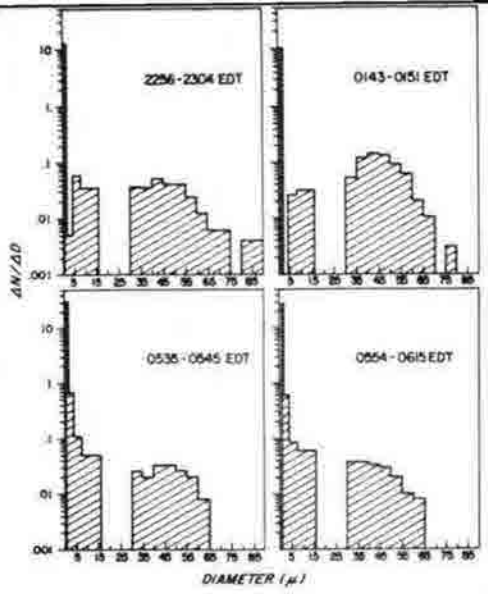

Fig. 1: Histograms of the mean drop-size distribution, measured by the hologram camera and cascade impactor, for various time periods during a fog on 29-30 Aug. 64.

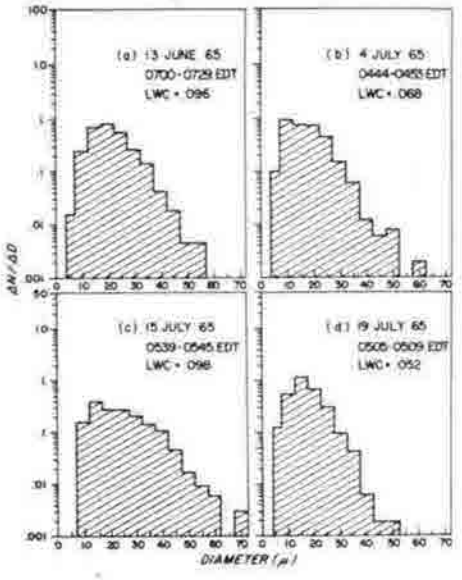

Fig. 2: Histograms of the mean drop-size distribution, measured by the hologram camera, for specific time periods during 4 fog cases.

camera, are generally quite large, with the highest concentration occurring around 40 μm. The large vertical extent of the fog and the occurrence of drizzle before the onset of the fog both lend support to these measurements. The average droplet size during the first two time periods is approximately the same, although a greater number concentration is observed during the second time period. The data from both the hologram camera and cascade impactor show a shift toward smaller droplet sizes in the latter 2 time periods. Continuous measurements with the cascade impactor showed that an increase in the number concentration of the smaller sizes occurred between 0400 and 0430. At this time the wind shifted about 30° toward the west. No change in the visibility or transmissivity was observed at this time. The radiational effects were not observed until one hour after sunrise ($\approx$ 0700) when again the number concentration of smaller droplets increased. This second increase in number concentration was accompanied by a gradual increase in visibility and transmissivity.

Variation Between Fog Occurrences

During the second half of the test program, samples of hologram camera data were obtained during 4 different fog cases. On 13 June 1965, a shallow radiation fog, 100-200 feet deep, developed during calm winds. On July 4th another shallow fog occurred but this time it was preceded by stratus and the winds were 3-6 knots from the west. A fog on the 15th of July was preceded by stratus and was roughly 800 feet deep. The winds were 5-8 knots from the southwest. A fog on the 19th of July was about 1500 feet deep occurring on southwest winds blowing from 5-10 knots and was also preceded by stratus.

Fig. 2 shows examples of the drop-size distributions, measured by the hologram camera for these 4 fog cases. Each histogram represents several minutes of data taken when the visibility was at a minimum, except in the 13 June case when the fog was in a dissipating stage and visibility was improving.

The shallower fogs, Fig. 2(a) and 2(b), contain a higher concentration of smaller particles than the deeper fog represented in Fig. 2(c). Very few droplets greater than 40 μm were observed in either of the shallow fogs while in the deeper fog, many droplets, representing 46% of the liquid water content, were observed in the 40 μm and higher size ranges. The fog shown in Fig. 2(d) has a rather narrow size distribution which is contrary to what we might expect for such a deep fog.

Conclusions

The two summers of testing the laser hologram camera proved the feasibility of using such an instrument in a foggy environment. Drop-size data from several fog cases were obtained. Some improvements were made in the instrument during the test period. However, there are many additional changes that could be made to improve the quality and reliability of the instrument.

REFERENCES

Schultz, E. J., R. A. Duffee and P. G. Andrus, 1966: Investigation of methods to measure size distribution of fog droplets and condensation nuclei. Final Report Cont. No. AF19(628)-344, AFCRL-65-724, 36 pp.

Silverman, B. A., B. J. Thompson and J. H. Ward, 1964: A laser fog disdrometer, J. Appl. Meteor., 3, 792-801.

AN ELECTROSTATIC CLOUD DROPLET PROBE

by

J. Doyne Sartor

and

C. E. Abbott

National Center for Atmospheric Research
Boulder, Colorado 80302

INTRODUCTION

An airborne probe has been described by D. P. Keily and S. G. Millen (1) which electrostatically measures cloud droplet sizes. The instrument, when coupled with the appropriate electronic circuitry, can be used to obtain droplet distributions over time periods as short as 0.5 sec. However, explanations of the physical processes involved remain unproven and indeed have been subjected to some criticism and comment by J. E. McDonald (2) and W. P. Winn (3). Because of the potential of this instrument, we have attempted to verify Keily and Millen's early results and advance our understanding of the electrostatic probe.

OBSERVATIONS

The probe operation as described by Keily and Millen proceeds as follows: The droplet to be sized is drawn quickly through an aspirated orifice subsequently striking a metallic electrode aligned on the axis of the inlet hole. The electrode is raised to a high potential and a short duration voltage pulse is observed when the droplet arrives at the electrode. The amplitude of the pulse plotted against the radius of droplets of known size produces a reproducible calibration curve.

To visually confirm this hypothesis we constructed a probe having viewing ports in the probe body normal to the electrode tip. Using stroboscopic light and dark field illumination photographs such as Fig. 1 were obtained. Air flow is from left to right towards the electrode which is visible as a dark object that forms the right hand boundary of the bright vertical band. In Fig. 1, a single 25 μ radius droplet entered a 1 mm diameter inlet hole and was shattered by the air stream to produce the fragments shown which then continued on to strike the electrode. Triggering the strobe flash at various times on the leading edge of the electrode voltage pulse determined that the pulse begins when the first fragments reach the electrode and that the peak of the pulse is reached as the last fragments arrive approximately 50 μ sec later. The fragments appear as horizontal streaks in the photo due to the strobe flash duration and indicate droplet velocities on the order of 100 m sec^{-1}.

The process has also been observed in a 1 mm glass capillary. Under sonic flow conditions, drops in the size range from 10 - 400 μ radius shatter producing a large number of smaller fragments. Shattering of 25 μ radius drop produces 30 - 40 fragments, an audible click and wetting of the capillary walls downstream from the event. Upon striking the electrode the droplet fragments are broken into still smaller particles, with an estimated 10^3 - 10^4 particles in the resulting atomized mist, visible as the bright vertical band. When large electrodes are used to insure that all incoming fragments strike the tip, the small particles are not adequately swept away by air flow and have been observed to fall back on the electrode resulting in an accumulation of water that causes erratic operation for subsequently approaching drops.

Based on these observations a probe was constructed having a 1.5 mm diameter hemispherical electrode. The electrode was placed 0.75 mm from the surface of a grounded hemispherical cavity and immediately behind a cylindrical inlet of 250 μ radius and 1 mm depth. These dimensions were chosen to prevent droplet breakup in the inlet channel, subsequent wetting of the walls and to restrict breakup to the volume inside the cavity.

A calibration curve of the completed probe, while approximating Keily's observation of an R^2 dependence for large droplets, approaches R^3 below 15 μ radius. Still present are variations in pulse height when the probe is supplied with a source of uniform size droplets. Variations of approximately 25% were attributed by Keily to instabilities in droplet production. However, by highly charging the droplets and observing the uniform pulses produced as they approach an electrode grounded through a large resistance, and by carefully controlling the production of uniform droplets, we have concluded that random variations in droplet breakup alone is responsible for the observed variations.

COMPARISON CHECKS WITH IMPACTOR SLIDES

Flight tests of the completed probe have been made. The output pulses were analyzed in a 10 channel pulse height analyzer and recorded with the ARIS system onboard the NCAR Queen Air. A MgO slide gun was used to obtain comparison data. Figure 2 is an example of the correlation between instruments. Unfortunately, agreement such as this was not obtained when the droplet population was large. This was due to inadequate storage capability, e.g. many analyzer channels were saturated, difficulty in maintaining full charge on the electrode during periods of high concentration, lack of accurate time correspondence

between the slides and probe data, and differences in sampling locations on the aircraft. Modification of the electronic components has been made to correct problems inherent in the probe and associated data recording systems. A double-headed probe is being constructed to minimize differences due to sampling locations during comparison checks between instruments.

REFERENCES

(1) Keily, D. P. and S. G. Millen, 1960: An Airborne Cloud-Drop-Size Distribution Meter, J. Meteor., 17, 349-356.

(2) McDonald, J. E., 1961: Comments on "An Airborne Cloud-Drop-Size Distribution Meter", J. Meteor., 18, 423-424.

(3) Winn, W. P., 1968: An Electrostatic Theory for Instruments which Measure the Radii of Water Drops by Detecting a Change in Capacity due to the Presence of a Drop, J. Appl. Meteor., 7, 929-937.

FIGURES

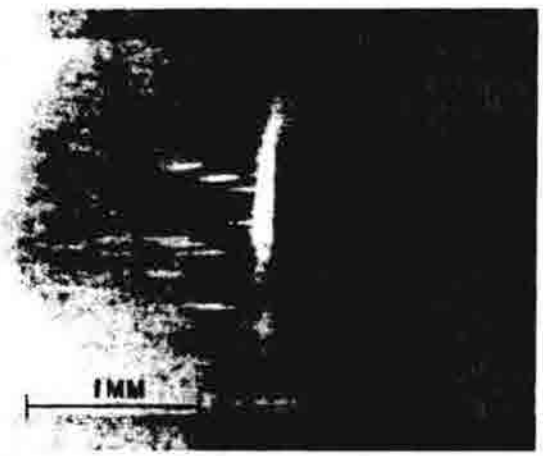

Fig. 1. Breakup of a 25 μ radius droplet inside the electrostatic probe.

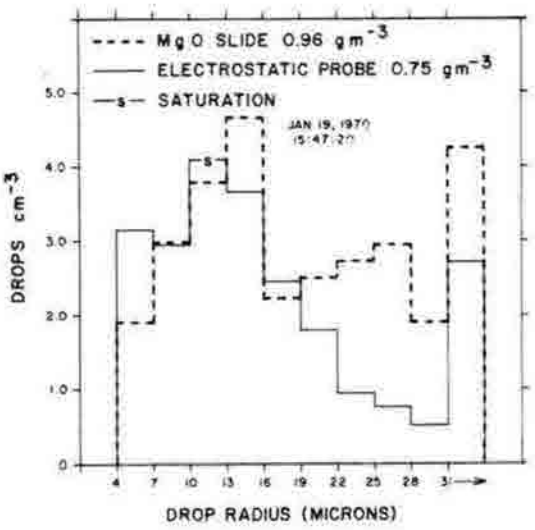

Fig. 2. Comparison of droplet distributions obtained from electrostatic probe and MgO coated slide.

AIRFLOW PATTERN AND DROPLET TRAJECTORIES ABOUT A CLOUD DROPLET PROBE

by

Ronald L. Drake

Theodore W. Cannon

William Briggs

National Center for Atmospheric Research
Boulder, Colorado 80302

In this study, NCAR's CDC-6600 computer was used to determine streamlines, droplet trajectories and collection efficiences for a cloud droplet probe. This electrostatic probe was originally developed at M.I.T. and recently has been improved and put into operation by the Cloud Physics Group at NCAR. In order to properly analyze the data collected by this probe, it is important to know its collection efficiency. That is, we must know the original location of those cloud droplets which actually enter the sampling hole at the forward "stagnation point" of the probe.

Since the forward part of the probe is an ellipsoid, the assumed shape of the probe for the above-mentioned computation is a prolate spheroid with dimensions consistent with the actual device. At the forward "stagnation point" there is a small sampling hole which is assumed to be along the entire major axis.

The external flow field is assumed to be steady, axisymmetric, irrotational and incompressible. This is a valid assumption if external boundary layer effects are ignored and if the speeds at which the probe is flown are well below compressibility effects. However, air is pumped through the sampling hole at an average speed equal to one-half sonic speed and thus there exists a compressible flow region near the hole inlet. But this region is sufficiently small and can be neglected as far as the streamlines and trajectories are concerned. This flow field is dependent upon several parameters, namely the sampling hole radius, the axial speed in the hole, the free stream velocity and the fineness ratio of the ellipsoid of revolution.

The droplet trajectory calculations are based on a three dimensional gravity field and the droplets are subjected to a fluid resistance based on the work of McDonald [1960]. From these trajectories we can compute collection efficiencies for the probe.

For the proposed flow field, the velocity components and the streamlines are obtained by two different techniques. One method is to transform the polar system into an elliptic coordinate system. Since ellipses are coordinate lines, this transformed flow field can be subdivided into a rectangular grid, thus simplifying the numerical computations. The inherent singularity in the elliptic differential equation for the stream function is handled by an iterative process. The first iterate is a solution of Laplace's equation and each new iterate, thereafter, is a solution of a Poisson equation. The right side of the Poisson equation contains the singular terms and is evaluated at the previous iterate. Thus, a very efficient ADI subroutine can be used for the solution of the flow field. In order to obtain maximum resolution in the numercial computations, the boundary farthest from the probe is only about 10 to 20 hole radii away, The flow on this boundary is assumed to be unaffected by the sampling hole and the stream function along the boundary is taken to be equivalent to that for flow around an ellipsoid without a sampling hole.

The other method of determining the flow field is based on a different transformation from polar coordinates into elliptic coordinates. Through the application of a generalized Fourier series approach, an exact solution of the boundary-value problem is obtained. In this case, the orthogonal functions are Geganbauer polynomials.

By applying these two methods of solution, flow fields about several different probes were obtained for free stream speeds varying from 1 to 100 miles per hour. With the resolution which we used, the effect of the sampling hole on the flow field and the presence of a stagnation ring on the probe were very vividly portrayed.

Using these flow fields, droplet trajectories were calculated from the particle equations of motion for droplet radii varying between 0.5 and 100 microns. As one would expect, the smaller droplets tend to follow the streamlines, while the inertia of the larger drops prevents them from "seeing" radical changes in the flow field. Thus, the collection efficiencies computed from these trajectory calculations have the following properties. If the collection efficiency is defined as the cross-sectional area of the cloud being sampled divided by the area of the sampling hole, the maximum collection efficiency is the speed of sound divided by two times the free stream velocity and the minimum value is one. Therefore, as the particle radius decreases, the collection efficiency approaches the maximum value; and as the particle radius increases, the efficiency approaches one.

Finally, the calculated trajectories were compared with trajectories photographed in a vertical wind tunnel. The comparison between theory and experiment appears to be good.

AN AIRBORNE MOMENTUM-SENSING RAINDROP SPECTROMETER

Joe L. Sutherland and D. Ray Booker

Weather Science, Inc.
Norman, Oklahoma

1. INTRODUCTION

To document possible seeding-induced changes in the rainfall characteristics of convective clouds, an airborne raindrop spectrometer has been developed. The instrument operates on piezoelectric principles. When a raindrop strikes the sensor head, a pressure is exerted on a quartz pressure transducer. Reacting to the pressure, the quartz pressure transducer emits a voltage pulse, the magnitude of which is proportional to the pressure. An electronic calibration relates the voltage pulse to drop mass or size.

The raindrop spectrometer probe is generally mounted on the side of the nose of a twin-engine aircraft. The probe consists of a circular sensor head connected to a shaft, with the base of the shaft resting against the face of a quartz pressure transducer. The voltage output from the quartz pressure transducer is fed into the spectrometer's electronics module. The processed voltage from the module is then recorded.

2. THE RR20 RAINDROP SPECTROMETER

The original raindrop spectrometer was designed chiefly to measure rainfall rates. This was accomplished by integrating the individual raindrop voltage pulses. The integrated voltage was converted to rainwater mass which, when multiplied by the terminal velocity of an assumed volume median raindrop and divided by the volume swept out by the probe, gave rainfall rate. The individual raindrop voltage pulses were also recorded; but the recorder, a light-beam oscillograph, was unable to respond at a speed and range sufficient to accurately record all of the pulses. Also, sizing the recorded individual drop pulses proved to be extremely slow and difficult. Sizing the integrated pulses was not required because the electronics was designed to reset the integrator to zero after a certain mass of water had been encountered. Simply counting the number of these folds in a unit of time and multiplying that number by the calibration factors gave rainfall rate.

The ability to measure the raindrop spectrum was achieved by using a 20-channel digital magnetic tape recorder. Sixteen of the 20 channels were used to record individual raindrop voltage pulses, one recorded the integrated voltage, one recorded the airspeed, and the remaining two channels recorded time. One channel was recorded each 0.02 seconds, so that the individual drop pulses had to be held 0.03 seconds to insure that they were recorded. Raindrops striking the probe during the 0.03 second hold were lost to the individual drop spectra measurement but were recorded by the integrator. Thus, only a sample of the total number of raindrops was recorded for drop spectra measurements. This sample was assumed to be representative of the total droplet population. It has been estimated that slightly more than 50% of the total droplet mass was not recorded in the individual drop channels. A flow diagram of this particular raindrop spectrometer (the RR20) is shown in Fig. 1.

3. THE RR40 RAINDROP SPECTROMETER

In order to measure the entire droplet population encountered by the probe, the electronics module of the raindrop spectrometer was redesigned to incorporate a quantizer. The quantizer sizes each individual drop pulse and, depending on the magnitude of the pulse, activates one of nine counters. Each counter is assigned to a particular voltage range, representing a particular raindrop diameter. Since small drops are more prevalent, the first three counters can count as many as 99 drops each, while the remaining six counters are limited to no more than 9 drops each. The number of counts in each of the 9 classes is recorded every 0.4 seconds by the digital magnetic recorder mentioned above. Since rainfall rate can be computed from the recorded raindrop spectra, the integrator used on the earlier raindrop spectrometer is no longer required.

The voltage pulse caused by a raindrop actually has the shape of a damped sine wave, having a duration of about 1.5 to 2 milliseconds. The quantizer sizes only the amplitude of the first peak of this damped sine wave. A fixed 2-millisecond delay prevents counting while the wave is damped. Calculations involving the Marshall-Palmer (1) raindrop concentrations have shown that, except in very heavy rain, there is a low probability of encountering a raindrop during the 2-millisecond delay.

A flow diagram for this spectrometer, designated the RR40, is shown in Fig. 2. The RR40 raindrop spectrometer also incorporates a larger sensor head, in order to sweep out more drops for each rain-measuring pass, and a more sensitive quartz pressure transducer. An example of the computer printout for a rain-measuring pass using the RR40 is given in Fig. 3.

4. CALIBRATION

The raindrop spectrometer is calibrated electronically by simulating the pressure transducer output. The force (pressure times area of transducer) exerted on the quartz pressure transducer by a drop of a certain diameter is related (by the sensitivity of the transducer) to the voltage emitted by the transducer. These voltages are then simulated and fed through the electronics module and recorded, giving a calibration relating recorded voltage and drop size.

5. CONCLUSIONS

Both of the raindrop spectrometers described above have been successfully used in field projects. The analysis of data collected by the original spectrometer, the RR20, has been given in Sutherland-Booker (2) and Sutherland-Booker (3). The RR40 raindrop spectrometer has been used in two projects since January 1970, but results of analyses of data collected by the RR40 have not yet been published.

6. REFERENCES

(1) Marshall, J. S. and W. M. Palmer, 1948: The distribution of raindrops with size. J. Meteor., 5, 165-166.

(2) Sutherland, J. L. and D. R. Booker, 1969: Airborne measurement of rain parameters. Technical Rept., Earth and Planetary Sciences Division, U.S. Naval Weapons Center, China Lake, California, 21 pp. (mimeo.)

(3) Sutherland, J. L. and D. R. Booker, 1970: Determination of seeding effects for Cloud Puff III and IV. Technical Rept., Earth and Planetary Sciences Division, U.S. Naval Weapons Center, China Lake, California, 16 pp. (mimeo.)

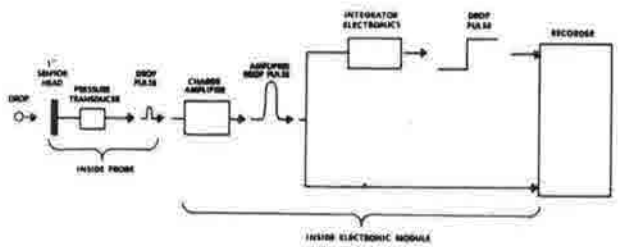

Fig. 1

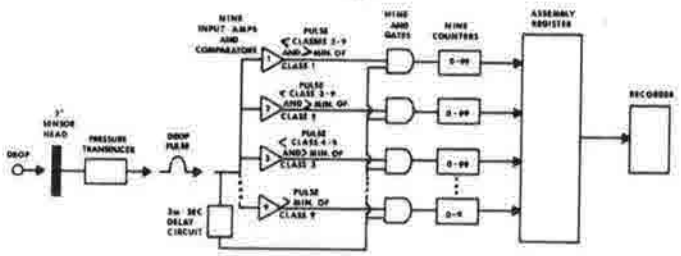

Fig. 2

AIRCRAFT DATA REDUCTION DATE = 30 A 1970 RR40 DATA

RIG RAINRATE

1-SECOND PD END (HHMMSS)	DROPS BY AVERAGE DIAMETER CLASS--(MM) (PLUS OR MINUS 0.25MM) 0.75	1.00	1.75	2.00	2.75	3.00	3.75	4.25	WATER CONTENT (GM/M3)	RAIN RATE (MM/HR)
190035	172	34	14	3	1	0	1	0	.03	4.06
190040	273	44	18	0	1	1	0	0	.33	4.00
190045	389	82	29	10	1	1	0	0	.48	8.14
190050	391	49	14	11	3	0	0	0	.33	6.71
190055	490	62	24	10	4	0	0	0	.48	9.37
190100	513	37	14	6	11	0	0	0	.42	9.28
190105	288	51	24	6	3	0	1	0	.45	9.90
190110	384	69	19	0	0	1	0	0	.24	5.67
190115	366	63	12	0	4	3	0	0	.43	9.35

PASS SUMMARY

DURATION OF SHOWER: 48 SECONDS

TOTAL NUMBER OF DROPS	PERCENTAGE DISTRIBUTION BY DROP DIAMETER CLASS (MM--PLUS OR MINUS 0.25) 0.75	1.00	1.75	2.00	2.75	3.00	3.75	4.25	AVG RWC (GM/M3)	AVERAGE FALLRATE (MM/HR)
3288.	77.7	13.9	8.0	2.4	.9	.2	.1	.0	.28	7.98

Fig. 3

ICE NUCLEATION EFFICIENCIES OBTAINED BY X-RAY DIFFRACTION

Briant L. Davis
Institute of Atmospheric Sciences, South Dakota School of Mines and Technology
Rapid City, South Dakota, 57701

EXPERIMENTAL APPARATUS AND PROCEDURE

The cloud chamber used in these experiments has been described previously by Davis[1] and the aerosol generator by Blair and Davis[2]. In these experiments the cloud was introduced into the front port of the chamber by means of a simple atomizer fog generator. This arrangement is shown in Fig. 1. Initial liquid water content in the interval between -15 and -25°C was determined from a commercial dew-point device to be 8.5 ± 1 gm m^{-3}.

The aerosol was produced by atomizing an AgI-NaI-acetone solution containing 3 per cent AgI by weight into the propane flame of the combustion chamber and by sampling with syringe at the exhaust line. Samples for runs GXX 20-36 were left undiluted whereas those for GXX 46-66 were diluted 1/40 immediately after sampling.

In a typical run the chamber was cooled to the desired temperature with x-ray system in operation. The fog device was then started and fog level established 1-5 minutes prior to sample injection. After injection the system was kept in a steady state in temperature and fog density until x-ray and photocell data indicated that all crystals had settled out. For the x-ray analysis MoKα radiation was used and the scanning oscillated within the interval containing the 002 and 100 ice diffraction. Data output consisted of integrated intensities printed on paper tape.

ABSORPTION AND CRYSTALLOGRAPHIC PARAMETERS

The relationship between volume of ice crystals deposited on the pedestal, V_p, and integrated x-ray intensities was found to be linear within 8 per cent up to a layer thickness of 50 microns, as determined from theoretical absorption relations. Experimental determination of the calibration curve for V_p verified this condition.

From structure-factor and absorption data and crystallography of the two dominant types of crystals present (plates giving 002 diffraction and prismatic forms giving 100 diffraction) the following equations have been derived to permit determination of the average crystal volume v_i for the precipitated crystals:

$$\Psi = 0.392 I_{002}/I_{100} \quad , \tag{1}$$

$$\frac{\bar{c}}{\bar{a}} = \sqrt{3}/2\Psi \quad , \tag{2}$$

$$\bar{D} = \bar{a}(1 + 0.866f) + \sqrt{\bar{a}^2 + \bar{c}^2/4}(1 - f) \quad , \tag{3}$$

and,

$$\bar{D} = \frac{\bar{a}(1 + 1.866\Psi + \sqrt{1 + 0.1875/\Psi^2})}{1 + \Psi} \tag{4}$$

where Ψ is a shape and volume factor determined from measureable integrated intensities I_{002} and I_{100}; $\bar{D}$, $\bar{a}$, and $\bar{c}$ are mean linear dimension through the center of the crystal, mean crystal half-width, and mean length parallel to the crystallographic c-axis of the crystal, respectively, for all crystals precipitated; f is the fraction of all crystals having the 002 orientation on the x-ray pedestal. $\bar{D}$ was obtained in these experiments by optical examination of replicas of the crystals taken during the seeding. From the crystal dimensions $v_i = (3\sqrt{3}/2)\bar{a}^2\bar{c}$, and the number of crystals N deposited is simply $N = V_p/v_i$.

The two most important assumptions of the theory include (a) no air cavaties within the crystal (less than 100 per cent error), and (b) equal volumes for both plates and prisms (less than 36 per cent error). X-ray and optical data actually demonstrate a prism volume twice the plate volume, in agreement with data of Mason[3]. These uncertainties have been neglected in view of the order of magnitude of the final efficiency numbers.

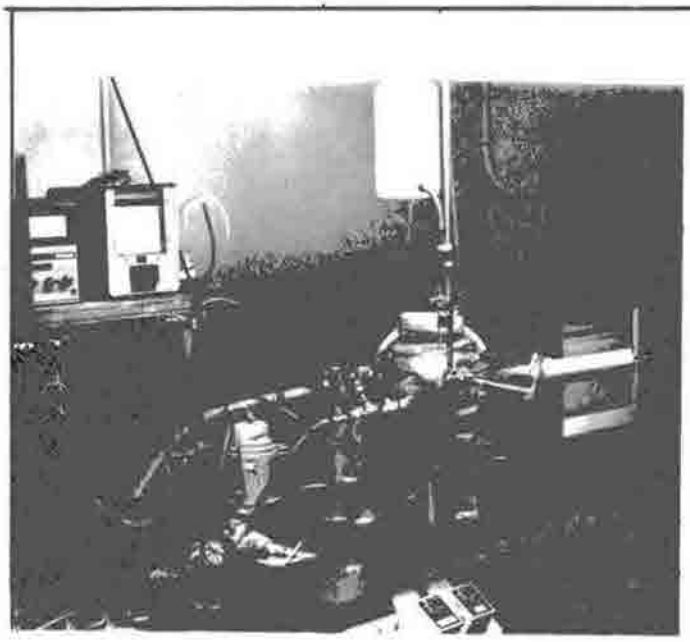

Fig. 1. X-ray diffraction cloud chamber with attached fog generator.

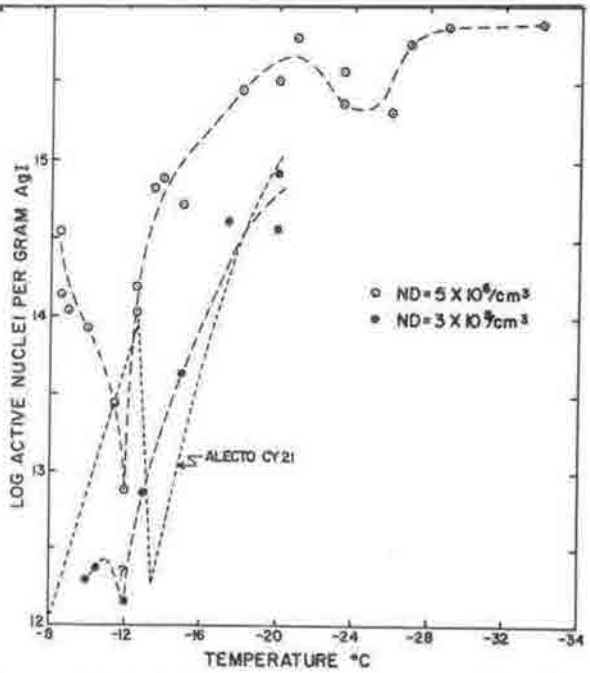

Fig. 2. Efficiency-temperature plot for 28 experiments. Alecto curve from St. Amand[4].

RESULTS

Figure 2 presents the final efficiency data for the 28 experiments and Fig. 3 presents the temperature variation of Ψ and $\bar{D}$. Experiments GXX 17, 37-44 were used only for these parameters and are not part of the data of Fig. 2.

The two experimental plots of Fig. 2 demonstrate the effect of sample dilution upon efficiency of such aerosols, ND being the particle number density of the aerosol as injected into the chamber.

We observe a major anomaly at -12°C in the activity curve, the rise at warm temperatures being due to larger counts from frozen droplets. This mechanism (condensation-freezing) requires more time for development than does the sublimation mechanism operative on the low-temperature side of the anomaly. We regard this anomaly as being related to this transition although the exact inhibitive process is uncertain. St. Amand[4] observed similar anomalies for certain pyrotechnics; one example is included in Fig. 2.

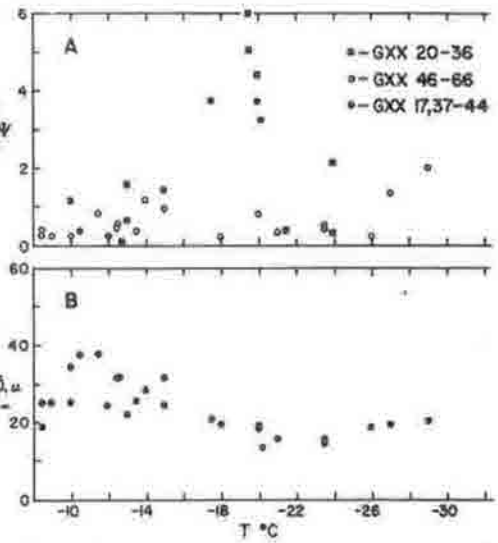

Fig. 3. Variation of Ψ (A) and $\bar{D}$ (B) with temperature.

Data of both Figs. 2 and 3 imply another anomaly at -18 to -22°C, this apparently being related to the change in crystal habit from large hollow columns above -18°C, to plates between -18°C and -22°C, to stubby prisms and columns below -22°C.

ACKNOWLEDGEMENT

This program was sponsored by the Office of Atmospheric Water Resources, Bureau of Reclamation, U.S. Department of the Interior, Contract No. 14-06-D-6796.

REFERENCES

1 Davis, B.L., 1969, Chemical complexing of AgI-NaI aerosols. J. Atm. Sci., 26, 1042-1048.

2 Blair, D.N., and Davis, B.L., 1969, Aging of silver iodide-sodium iodide generator effluent in moist and dry air. J. Appl. Meteor., 8, 551-555.

3 Mason, B.J., 1953, The growth of ice crystals in a supercooled water cloud. Quart. J. Royal Meteor. Soc., 79, 104-111.

4 St. Amand, P., 1967, Nucleation by silver iodide and similar materials. Project Skywater, Proceedings, Conference I, July 10-12, Denver, 305-346.

COUNTER FOR NUMBER OF SNOWFLAKES FALLING PER UNIT AREA

G. Langer
National Center for Atmospheric Research*
Boulder, Colorado 80302

In studies of ice nucleation it has become important to correlate ice nuclei counts with the number of ice crystals found in a cloud or falling from the cloud to the ground. The interesting ice nuclei counts are those found in the air mass that enters the cloud or storm system which produces the ice phase. This report concerns the development and evaluation of an instrument for counting individual snowflakes as they fall on a given area. The instrument is to be used in conjunction with presently available ice nucleus counters, which tend to give figures lower than the actual number of ice crystals foung. Data on the number of snowflakes vs ice nuclei are scarce, and one reason for this is the lack of convenient and suitably designed instrumentation to count individual snowflakes on a continuous basis. The instrument described below provides such data continuously over long periods of unattended operation with high resolution.

The device has a counting system based on the acoustic particle counter (Langer, 1966), which tallies all particles over 20 microns by an acoustic effect (Fig. 1). A 3 mm capillary is used to give a flow of about 20 lpm at 150 mm Hg suction; at the intake of the sensor, the flow is 65 cm/sec. The sensor intake is preceded by an entrance tube 12 cm diameter and 25 cm long. This tube eliminates wind noise that would develop if the air were allowed to blow at right angles over the sensor entrance. Also, it allows for quiescent settling of the snowflakes into the sensor. For data reduction it is assumed that only flakes falling over the projected area of the intake are counted, since the aspirating effect of the sensor may pull in additional small flakes from the sides. The associated electronics makes it possible to have a time resolution of 2 seconds for count rates over 1000/min.

This instrument was used in the winter months in Yellowstone (Schaefer 1969) and near Fraser, Colorado. In Yellowstone it was operated unattended for several hours, and at Fraser it ran continuously for two weeks in a period of heavy storms (1 m total snowfall). During the heaviest snowfall, the intake tube had to be cleared of snow every 6 hours; but the unit has since been modified to alleviate this problem.

Visual counts of large snowflakes falling in the sensor vs the actual count showed a one-to-one correspondence. It was expected that large flakes in the centimeter range, as they broke up and passed through the 3 mm capillary of the sensor, would give multiple counts. However, only one rather loud signal was produced for even the largest flakes. The warm pump exhaust air prevented freezing of drops, etc., in the capillary; and no plugging of the sensor was encountered even during wet snow.

Figs. 2 and 3 show the results of the field tests. Fig. 2 gives results from seeding experiments at Yellowstone with AgI flares. The reference to small ice crystsls on the graph alludes to visual observation of hexagonal crystals falling on a piece of black velvet. These crystals are obviously the result of the seeding 1/4 mile away since there was no natural snow during the first test; however, an hour later, light snow did fall. A day later at the same hour but during a period of light snow, a second test showed similar behavior, except that a change in wind shifted the AgI plume away from the sampling site giving less pronounced counts just after seeding. The second peak in snowfall rate was observed as before about an hour later, and the rate was approximately the same as in the first test. Presumably this second snow shower composed of much larger crystals was due to the seeding and was related to a return flow circulation in the Old Faithful Basin.

In Fig. 3 the data from Fraser cover a period of heavy snow storms. The snowfall rate shows a periodic nature with a fairly constant periodicity of 75 min, gradually decaying in amplitude over a period from 5 to 15 hours. Another storm system then moved in and decayed in a similar manner. As pointed out by Dyer (1970), a power spectrum analysis should show a persistence effect and thus could be a means of predicting storm duration and severity.

This work indicates the importance of carefully analyzing results of seeding operations during these types of storms. The periodicity of the snowfall may obscure or clarify seeding effects. It should be interesting to use this instrument to make snowfall rate counts in an unaffected control area vs the target area. In such an experiment seeding effects may be detected in considerable detail. With additional electronic instrumentation, a rough correlation between signal strength and flake size should be possible. This kind of measurement should help to resolve further any seeding effects.

The Fraser tests included some additional experiments to provide a quantitative calibration of the counter. Snow deposit on a small plate was recorded photographically, and in 15 comparisons between the visual count of ~ 5000 snowflakes and the acoustic count, the latter gave 5 times as many flakes on the average. Although this ratio ranged from 3 to 9, the agreement was as good as could be expected because the photographic system covered flakes down to only 100 microns while the acoustic sensor detected down to 20 microns. Moreover, a further discrepancy resulted from wind blowing flakes off the collection plates.

ACKNOWLEDGEMENT

J. Weickmann made the tedious snowflake counts from the photographs.

---

*The National Center for Atmospheric Research is sponsored by the National Science Foundation.

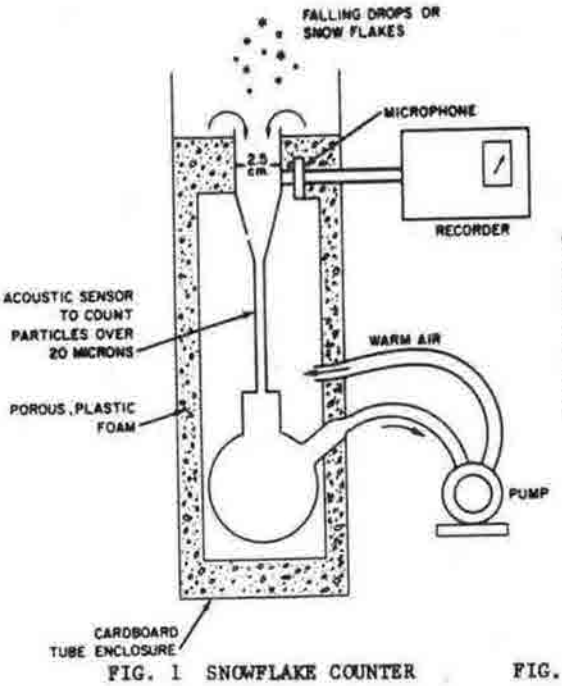

FIG. 1 SNOWFLAKE COUNTER

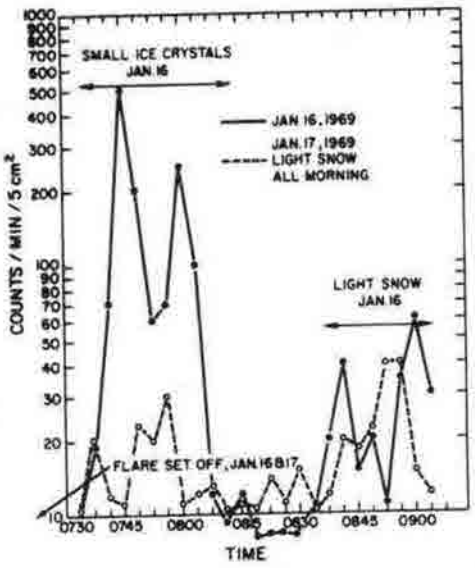

FIG. 2 SNOWFLAKE DEPOSITION RATE DUE TO SEEDING

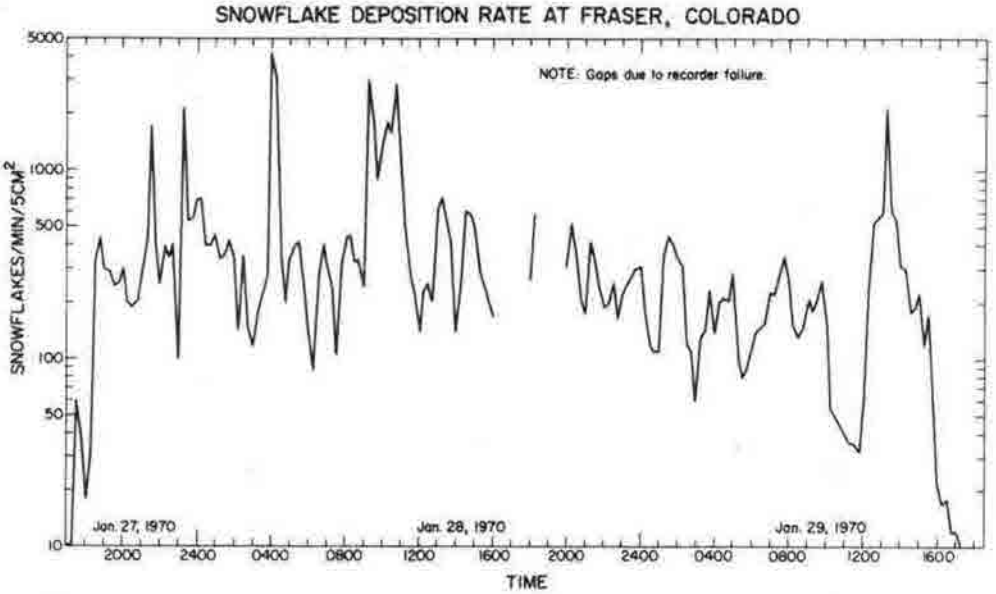

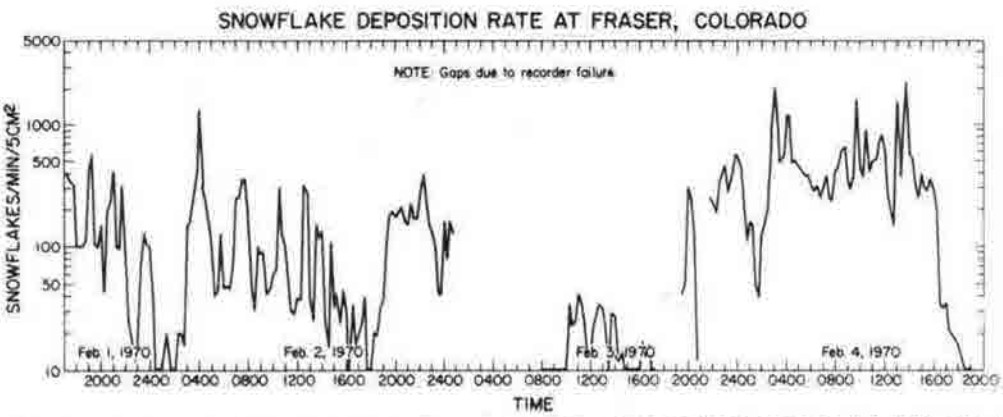

FIG. 3 VARIATION IN SNOWFLAKE DEPOSITION RATE DURING STORMS IN COLORADO FROM JAN 27 TO FEB 4, 1970

AN OPTICAL CHARACTER RECOGNITION TECHNIQUE FOR DETERMINING CLOUD DROPLET SIZES

W. M. Ketcham and H. W. Wold
Department of Meteorology, University of Utah
Salt Lake City, Utah 84112

CHARACTER RECOGNITION TECHNIQUE

An optical character recognition technique[1],[2] is an optical method of determining whether or not a specific character is contained in a group of characters. The purpose of this present work is to examine the feasibility of this technique in determining cloud droplet sizes.

To briefly and rather simplistically explain how this technique works, let us consider setting up a scheme to recognize a specific droplet size of 20 μ diameter. The first thing that must be done is to make a Fourier transform hologram[1],[2] of a 20 μ droplet. This hologram is a special type of photograph which is made by exposing a photographic plate to two beams of monochromatic light, one of which contains light diffracted by a 20 μ droplet. The other beam consists of plane parallel light and is called the reference beam (Fig. 1). This hologram possesses the useful property that if it is illuminated by a light beam which is identical to either of the beams that were used in making the hologram, beams nearly identical to the originals will be reconstructed.

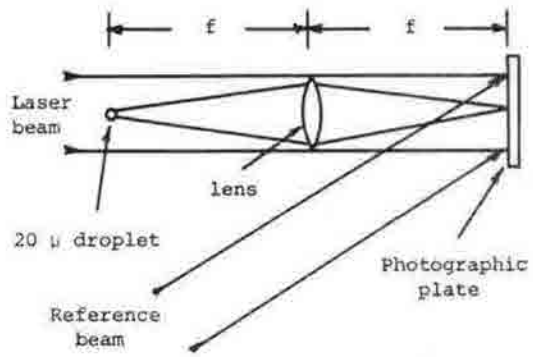

Fig. 1. Arrangement for making a 20 μ Fourier transform hologram. f is the focal length of the lens.

Let us now consider illuminating the hologram, which has just been made, with a beam that contains light diffracted by a 20 μ diameter droplet. Because this beam is identical to one of the beams that originally exposed the hologram, a reconstructed reference beam is generated which, as shown in Fig. 2, may be focused to a bright spot by lens 2. If the hologram were illuminated by light diffracted by a droplet of size different than 20 μ, no reference beam would be reconstructed, and consequently, no bright spot would be recorded in the back focal plane of lens 2. Thus, it is seen that the presence of a bright spot indicates a 20 μ diameter droplet, while the absence of this spot indicates no 20 μ diameter droplet in the input.

PROCEDURE

A computer program[3] was developed to simulate the character recognition technique. The procedure followed was first to compute the light distribution that would be recorded by a Fourier transform hologram of a square of specific size. Squares were selected as the objects to be recognized because they could be accurately represented on the rectangular data array of the computer. This computed hologram was then "illuminated" by the computed light intensity that would be diffracted by several squares in the size range 3 to 51 μ. Lastly, the intensity of light was computed in the back focal plane of lens 2, Fig. 2.

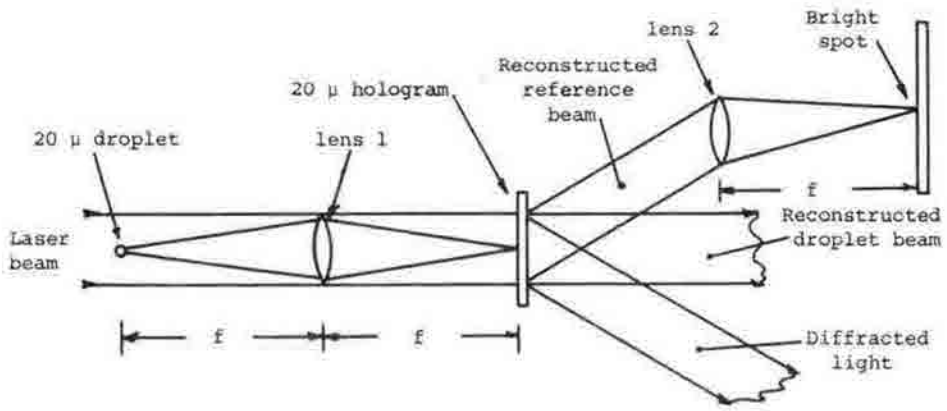

Fig. 2. Reconstructing reference beam by illuminating a 20 μ hologram with light diffracted by a 20 μ droplet.

RESULTS

The computer results for squares 3 to 51 μ are shown in Fig. 3. Each histogram represents a computer run in which the light diffracted by several squares of different size are "matched" to a hologram made from a square of specific size. For example, the upper left histogram in Fig. 3 represents a run in which a hologram made from a 3 μ square, was matched to squares 3, 5, 7, 9, 11, and 13 μ in size. Note that in each case, the intensity of light produced by a matched square is significantly greater than that produced by any of the mismatched squares.

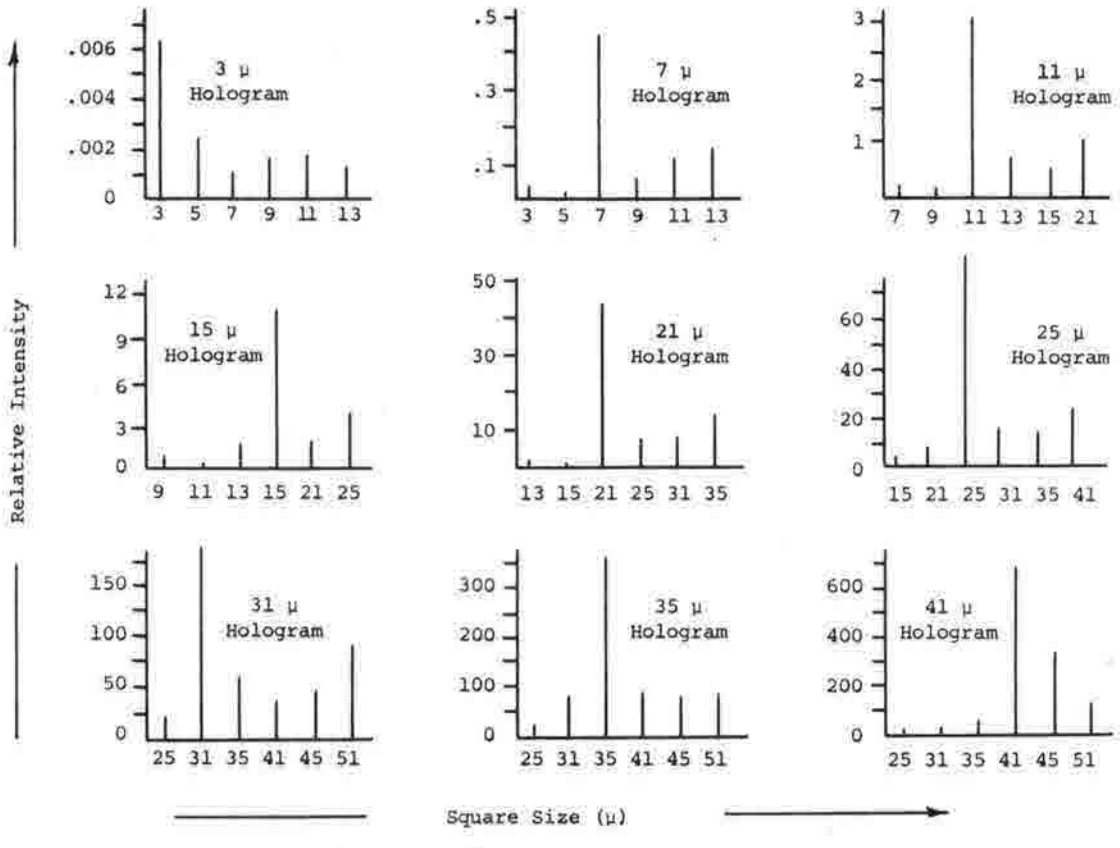

Fig. 3. Histograms of the relative intensity of squares of various sizes when matched to different holograms.

CONCLUSIONS

These results indicate that this method has promise of recording cloud droplet sizes in a range of 3 to 40 μ diameter to an accuracy of ±2 microns. Experimental work is progressing on an apparatus which utilizes the character recognition technique and which may be used in the field to record real time size distributions of cloud droplets.

REFERENCES

1. Goodman, J. W., 1968: Introduction to Fourier Optics, McGraw-Hill Book Co., New York, N.Y., 287 pp.

2. Smith, H. M., 1969: Principles of Holography, Wiley-Interscience, New York, N.Y., 239 pp.

3. Wold, H. W., 1970: An Optical Character Recognition Technique for Determining Cloud Droplet Sizes, Unpublished Master's Thesis, University of Utah, Salt Lake City, Utah.

AN INSTRUMENTED "HAILSTONE" FOR CLOUD PHYSICS RESEARCH

William D. Scott
Cloud Physicist, National Hurricane Research Laboratory, ESSA
Adjunct Professor, University of Miami, Florida

Probes of the atmosphere for meteorological data have taken many forms including the ordinary radiosonde and the dropsonde. (1,3) These devices are satisfactory only for measuring variables such as temperature, wind speed, and particle concentration, quantities that vary slowly and are, in a sense, 'passive'. With these instruments it is not possible to measure the rapidly varying quantities or 'active' quantities of importance in the formation of precipitation or in the electrification of clouds. These quantities include the number of particle collisions per unit time, the trajectory of a precipitation particle, and the electrical charge transferred when particles collide; they are altered beyond recognition by present measuring techniques. These particular variables require a simulation of actual happenings in the cloud and measurements during particle interactions. This paper describes perhaps the first attempt at such a measurement. The instrument used is a dropsonde the size of a hailstone, called herein a 'dropstone.'

INSTRUMENT DESIGN

The general instrument design is shown in Figs. 1 and 2. The dropstone transmits a vertically polarized FM signal to a remote receiver. The upper surface of the dropstone acts as the ground plane. A single wire trailing the dropstone in fall acts as the antenna.

This design makes possible the inclusion of ancillary data in the telemetered signal. These data might include the instantaneous acceleration of the dropstone or even its mass. The use of microcircuits and micropower signal conditioners (MOSFET) leaves sufficient room for a battery pack that should allow transmissions during most of the fall to ground.

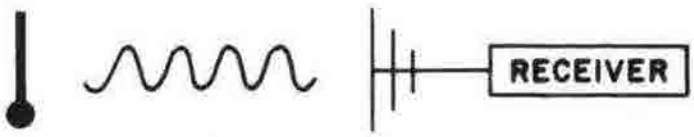

Fig. 1. Dropstone Transmitting "Active" Data to a Remote Receiver.

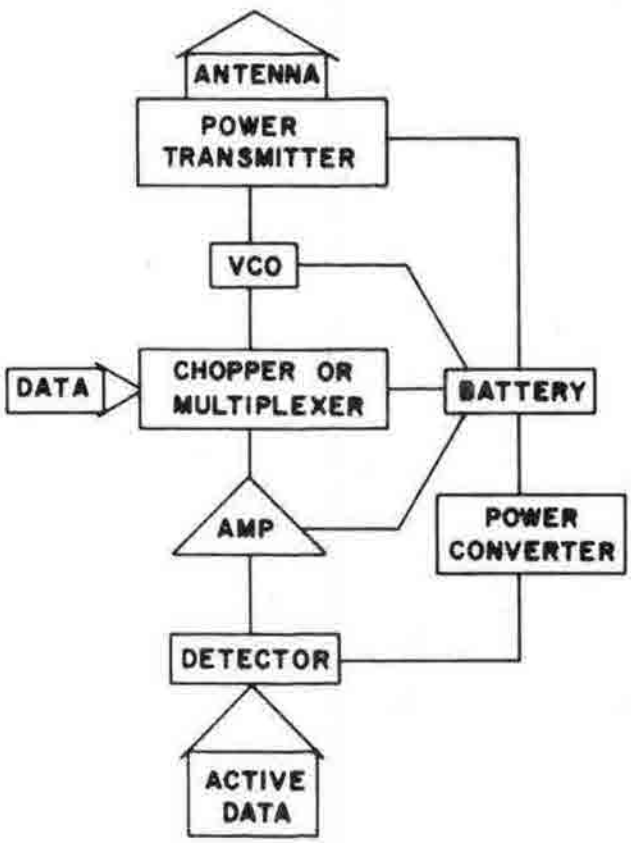

Fig. 2. Block Diagram of the Electronics Inside the Dropstone.

A picture of a prototype working dropstone is shown in Fig. 3 with a pictorial description. The prototype was built to detect the electrical charge exchange that occurs when a hailstone collides with ice crystals in a real cloud. The detector was a protected, insulated gate transistor; its gate was directly connected to the lower hemispherical portion of the dropstone. The transmitter was built from a single transistor and the upper, hemispherical portion of the dropstone served as the ground plane. The voltage difference between the two hemispheres was output at a transmitting frequency of 100 MHZ. A single, vertically inclined, elevated wire served as the receiving antenna for an ordinary FM receiver.

a.

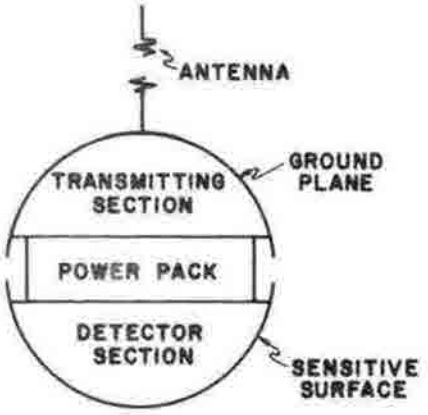

b.

Fig. 3. The Internal Construction of the Prototype Dropstone, a, with Description, b.

TESTING THE DROPSTONE

The transmitting efficiency of the instrument was low and the signal could only be detected up to 500 m. and a usable output could only be obtained to about 50m. This was a consequence of the necessity to transmit at low frequencies for long time periods to produce an operational instrument. After final development, of course, data would only be obtained for a minute or so at higher, more useful power levels. A major problem to the testing was the outside noise and local radio stations which made it essential to do the testing in remote locations. The Arctic proved to be the best testing ground; an actual trace during a short drop from a balloon is shown in Fig. 4.

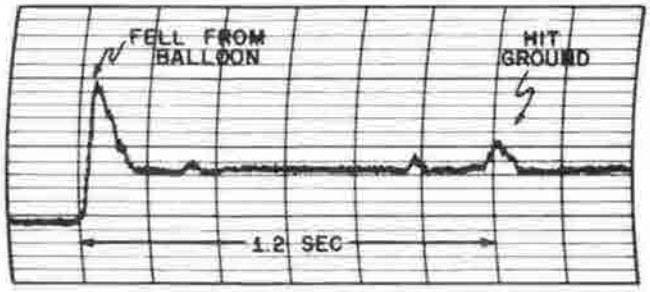

Fig. 4. Output during a Fall in Arctic Diamond Dust.

In this case diamond dust was present in the air and it appears that two collisions of the hailstone with the small ice particles were observed. This result agrees with the expected number of collisions; the sizes of the pulses indicate that the charges produced are of the same order as have been observed during simulated experiments on the ground in similar conditions.

FUTURE APPLICATIONS

The device is operational and, with a powerful, efficient transmitter and a high gain, directional antenna-receiver system, it should be able to transmit useful information several miles. (2) It is presently one inch in diameter and, with present state-of-the-art electronics, it probably could be made one centimeter or smaller. This should make it possible to make measurements of hydrometeor interactions in a realistic simulation. Also, the transmission itself will locate the trajectory of the hailstone in the real cloud. This ultimately should give an insight into active cloud processes, and hence become an invaluable tool in assessing cloud models.

REFERENCES

1. C. Magono and S. Tazawa, Design of Snow Crystal Sondes, J.A.S. 23; 618-625, 1966.
2. O.Z. Ray and J.S. Hart, A Multi-Channel Transmitter for the Physiological Study of Birds in Flight, Med. & Biol. Eng. 4. 457, 1966.
3. P. Squires, The NCAR Dropstone Development, NCAR Quarterly, Spring, 1966.

A RE-EXAMINATION OF THE CLASSICAL THEORY OF THE GROWTH OF A POPULATION OF CLOUD DROPLETS BY CONDENSATION

James W. Fitzgerald
The University of Chicago Cloud Physics Laboratory

INTRODUCTION

According to the simple classical condensation growth model droplets form on pure spherical hygroscopic nuclei contained in a parcel ascending at a prescribed rate with no entrainment through its boundaries [2,4,5]. This classical model has been criticized on the grounds that it predicts droplet distributions which are much narrower and which have smaller mean radii than those occurring naturally. It is argued that more realistic droplet distributions can be obtained only if the effects of entrainment and of a fluctuating updraft are considered.

The purpose of the present study is to recompute droplet growth by the classical model using data on cloud nuclei spectra which were unavailable at the time of the previous calculations [2,4,5] and to compare the resulting droplet distributions with published observations of the microstructure near cloud base as a test of the applicability of the model to natural cloud condensation processes.

CLOUD MODEL

Air containing a specified distribution of cloud nuclei is assumed to ascend at a uniform rate from cloud base where the temperature and pressure are taken to be 283K and 800 mb respectively. Accelerations arising from the buoyancy force are not considered. The parcel is closed with respect to the exchange of energy and matter with its environment. However, the "walls" of the parcel are not rigid and the parcel establishes a dynamic equilibrium with the environment.

EQUATIONS

Within the context of this cloud model the following set of equations governs the growth of a population of cloud droplets by condensation.

(a) Droplet Growth Equation. The growth equation for an individual droplet is expressed as

$$r\frac{dr}{dt} = \frac{e_s D' R_v T^2 K'}{\rho_w R_v^2 T^3 K' + D' e_s L^2 \rho_w}\left[\frac{xP}{e_s C(x+\varepsilon)} - \left(1 + \frac{A}{r} - \frac{B}{r^3}\right)\right] \tag{1}$$

where e_s is the saturation vapor pressure over pure water, ρ_w the density of water, x the water vapor mixing ratio, R_v the gas constant of water vapor, ε the ratio R_d/R_v, and C a correction factor for the departure of the mixture of air and water vapor from ideal gas laws. The modified diffusion and heat conduction coefficients, D' and K', are

$$D' = D\left[\frac{r}{r+\Delta} + \frac{D}{r\alpha}\sqrt{\frac{2\pi\varepsilon}{R_d T}}\right]^{-1}, \qquad K' = K\left[\frac{r}{r+\Delta_T} + \frac{4K}{r\rho_a c_p f}\sqrt{\frac{\pi}{8R_d T}}\right]^{-1}$$

where α is the condensation coefficient, f the accommodation coefficient, ρ_a the density of air, R_d the gas constant of dry air and Δ_T the temperature jump distance.

(b) Temperature Equation. The rate of change of temperature of the parcel may be formulated as the sum of the contribution due to adiabatic cooling of the ascending parcel plus a contribution due to warming by the release of latent heat of condensation.

$$\frac{dT}{dt} = -\frac{gV}{c_{pd}} + \frac{L}{c_{pd} + c_{pv}x + c_w w}\frac{dw}{dt} \tag{2}$$

where V is the vertical velocity, w the liquid water mixing ratio, c_{pd} the specific heat of dry air, c_{pv} the specific heat of water vapor and c_w the specific heat of water.

(c) Mass Conservation Equation. The equation for x as a function of t is obtained from a direct application of the mathematical statement of the conservation of mass. We have

$$\frac{dx}{dt} = -\frac{dw}{dt} = -\frac{4}{3}\pi\rho_w\frac{d}{dt}\left[\frac{1}{\rho_a}\int_0^\infty r^3 n(r)dr\right] \tag{3}$$

where n(r) is the droplet size distribution function.

The pressure-height relationship was obtained by assuming that the NACA Standard Atmosphere applies to the environment of the parcel.

The cloud nuclei supersaturation spectra used in this study were Twomey's[7] average continental spectrum ($N=945\ S^{.40}$) and Jiusto's[3] average Hawaiian spectrum ($N=53S^{.46}$). Under the assumption that cloud nuclei are pure spherical NaCl particles these N vs S spectra can be transformed into cumulative size distributions. Accordingly, we have $N(r_n)=66\ r_n^{-0.6}$ and $N(r_n)=2.5\ r_n^{-0.7}$. Here $N(r_n)$ is the number of cloud nuclei having a dry (crystalline) radius $> r_n$. The spectra were modified for supersaturations less than 0.05 per cent to provide a more realistic distribution of large and giant nuclei.

NUMERICAL PROCEDURE

The droplet growth equation was integrated numerically by the standard fourth-order Runge-Kutta method. Eq.(2) was integrated by the simpler Euler method. A small time increment in the range .006-.024 sec ensured that the smallest haze droplets grew stably.

The continuous distribution of cloud nuclei was approximated by a discrete distribution of 25 sizes. The integral in Eq. (3) was replaced by a summation over these 25 size classes.

The drop size distribution at cloud base was obtained by computing the radii attained by the nuclei at cloud base in rising from the 78 per cent R.H. level at the assumed V.

A simplified flow diagram of the computation is given in Fig. 1.

RESULTS AND DISCUSSION

Cloud droplet growth was computed up to a height of 200 m above cloud base for the continental and maritime cloud nuclei spectra, for updrafts of 1 and 2 m sec^{-1} and for values of α of 0.036 and 0.50. Four of the resulting droplet distributions are shown as the continuous curves in Fig. 2. For an updraft of 1 m sec^{-1} and an α of 0.036 the continental distribution at 100 m (curve b) is characterized by 500 droplets cm^{-3}, a mean diameter $\bar{d}$ of 8.4 μm and a dispersion coefficient $\sigma/\bar{d}$ of 0.35. In contrast, the maritime cloud (curve d) contains only 56 droplets cm^{-3} with a $\bar{d}$ of 19.1 μm and a dispersion of 0.06 at 100 m (for the same V and α). The maximum S attained in these two clouds was 0.24 and 1.10 percent respectively. The theory clearly shows that the cloud nucleus spectrum of an air mass has a pronounced effect on cloud microstructure.

In the continental case $\bar{d}$ increases from 6.4 μm at 50 m to 10.8 μm at a height of 200 m (curve c). The dispersion is essentially invariant with height. An increase in V to 2 m sec^{-1} increases the drop concentration in the continental cloud to 670 cm^{-3} (curve a). The effect of increasing α to 0.50 is to cause an increase in $\bar{d}$, a 15 percent decrease in droplet concentration and an increase in the value of the dispersion coefficient.

It can be seen from Fig. 2 that the shape, breadth, and mean diameter of the computed distributions compare favorably with these same properties of the measured distributions.

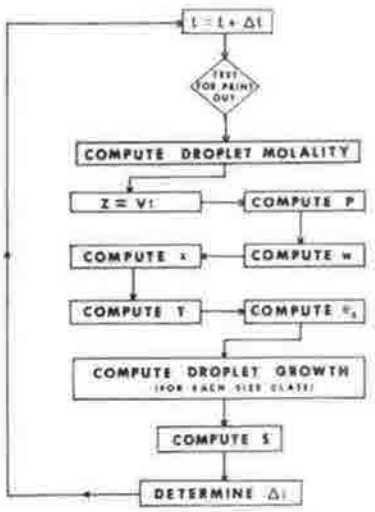

Fig. 1. Flow diagram for the computation.

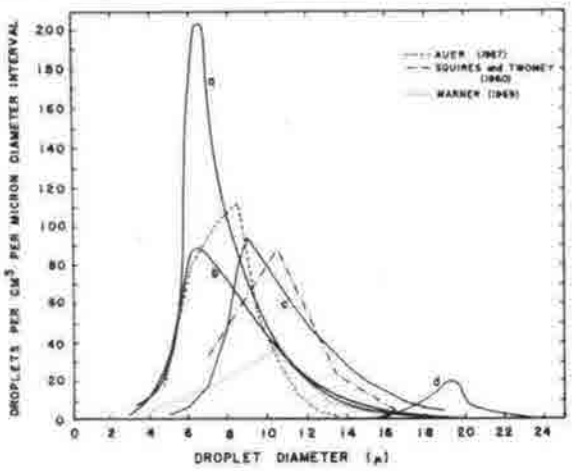

Fig. 2. Comparison between the computed droplet distributions (solid curves a, b, c, d) and those observed by several researchers near the base of continental clouds.

REFERENCES

1. Auer, A. H., 1967: J. de Rech. Atmos., 3, 91-100.
2. Howell, W. E., 1949: J. Met., 6, 134-149.
3. Jiusto, J. E., 1967: Tellus, 19, 359-368.
4. Mordy, W. A., 1959: Tellus, 11, 16-44.
5. Neiburger, M. and C.W. Chien, 1960: A.G.U. Monog. 5 Physics of Precipitation, 191-209.
6. Squires, P. and S. Twomey, 1960: A.G.U. Monog. 5 Physics of Precipitation, 211-219.
7. Twomey, S., 1959: Geofisica Pura e Applicata, 43, 243-249.

DROP GROWTH BY CONDENSATION IN THE ENTRAINING UPDRAFT

C. S. Chen

Department of Meteorology, University of California, Los Angeles

Previous computations of drop growth by condensation have ignored the mixing with the environment which is characteristic of actual cumulus convection. With entrainment the temperature of the rising parcel decreases faster than the pseudoadiabatic rate and the supersaturation on which the rate of drop growth depends is influenced by this difference in cooling rate as well as by the water vapor mixing ratio of the environmental air.

The physical processes, including drop growth and entrainment, are represented by seventeen differential equations in this model, seven for the physical parameters and ten for the growth of drops on different size nuclei. These equations were integrated numerically for a number of initial nuclei spectra, vertical velocities, and entrainment rates. The results are presented here for one particular variation of pressure, temperature, etc. for three different initial nucleus distributions, Case I, that used by Neiburger and Chien (1), Case II, that given by Warner (2), and Case III, a combination of I for radius $r \leq 0.1$ μm and II for $r > 0.1$ μm. The integration was carried out using Hamming's predictor-corrector method for 420 seconds of real time, beginning with the nuclei in equilibrium at 99% relative humidity.

In figures 1, 2, and 3 are shown the distribution of sizes of the dry nuclei, the nuclei at the starting point of the computation at 99% relative humidity, and at the end of 60 seconds and 420 seconds of growth. Because of the separation between the activated nuclei and those which are inactivated the distribution becomes bimodal, with a gap between the curve for the inactivated nuclei and the curve for the cloud drops. The mode of the cloud distribution occurs at larger radii in Case II than in Case I and Case III because the peak supersaturation attained is higher (0.39% compared with 0.24% and 0.27%). To attain one drop per liter larger than 20 μm requires less than 60 seconds in Cases II and III, compared with 420 seconds in Case I, because of the larger number of giant nuclei present in the initial distribution.

The temperature and dewpoint of the cloud and the environment computed in Case I are shown in Figure 4. The cloud is about 1°C warmer than the environment, resulting in continued upward bouyancy. For comparison, the average thunderstorm data in Ohio (3) on which the computed ambient conditions were based, are shown. It is seen that the computations reproduce these observed values closely. The corresponding data for Cases II and III are very close to those of Case I.

The computed vertical velocities increased continuously from 3 ms^{-1} to 10 ms^{-1} up to the 0°C level. Above this a deceleration is indicated. The entrainment did not decrease the vertical velocity materially, and since the rate of cooling produced by the vertical velocity dominates the drop growth, the condensation process was not slowed down by allowing for entrainment. However, the initial nucleus distribution was shown to be of primary importance in determining the number of large drops which develop.

REFERENCES

(1) Neiburger, M. and C. W. Chien, 1960: Computations of the growth of cloud drops by condensation using an electronic digital computer. Geophysical Monograph No. 5: Physics of Precipitation, American Geophysical Union (H. Weickmann, ed.), 191-210.

(2) Warner, J., 1969: The microstructure of cumulus cloud. Part II. The effect on droplet size distribution of the cloud nucleus spectrum and updraft velocity. J. Atmos. Sci., 26, 1272-1282.

(3) Byers, H. R. and R. R. Braham, 1949: The Thunderstorm. U.S. Department of Commerce, Washington, D.C.

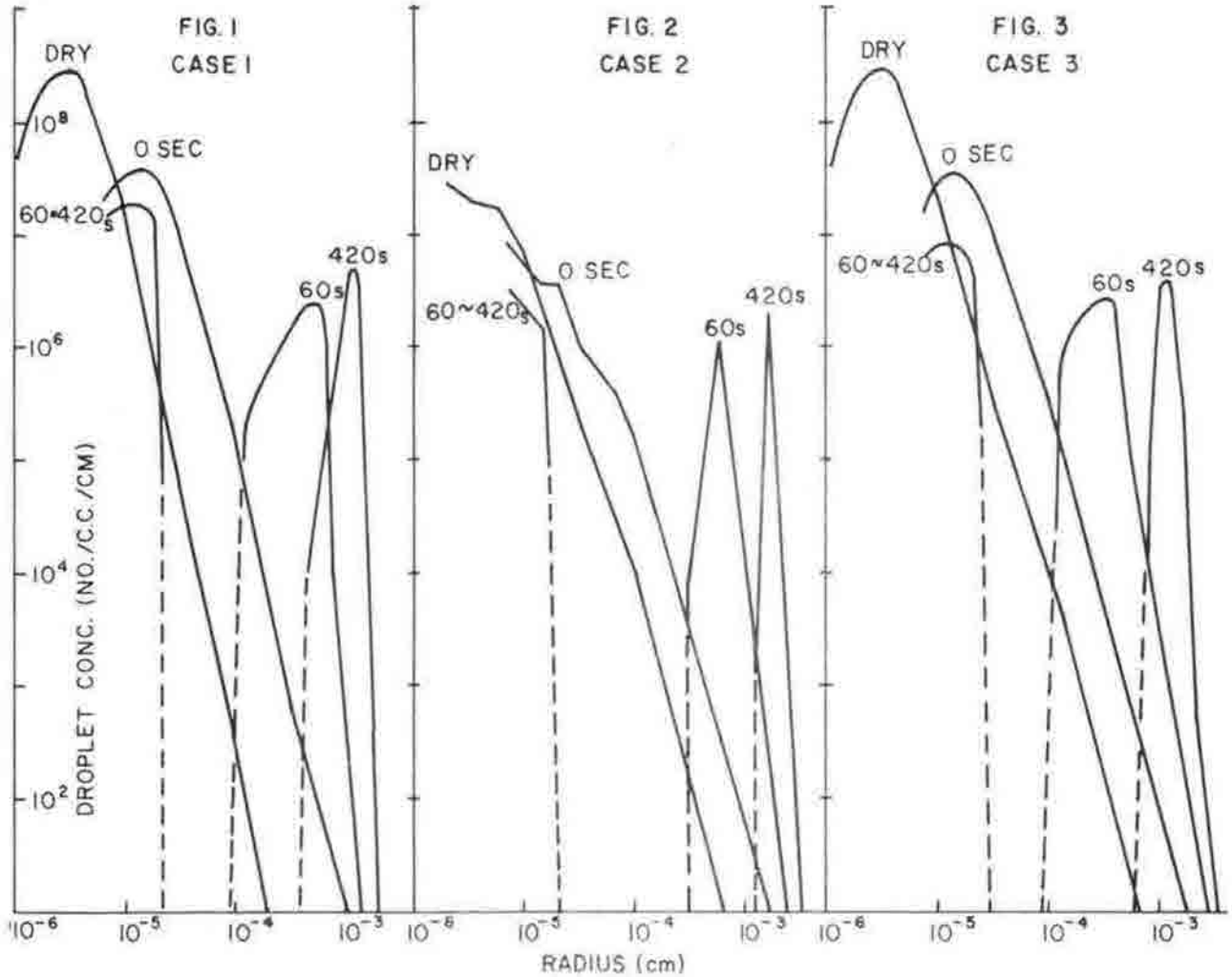

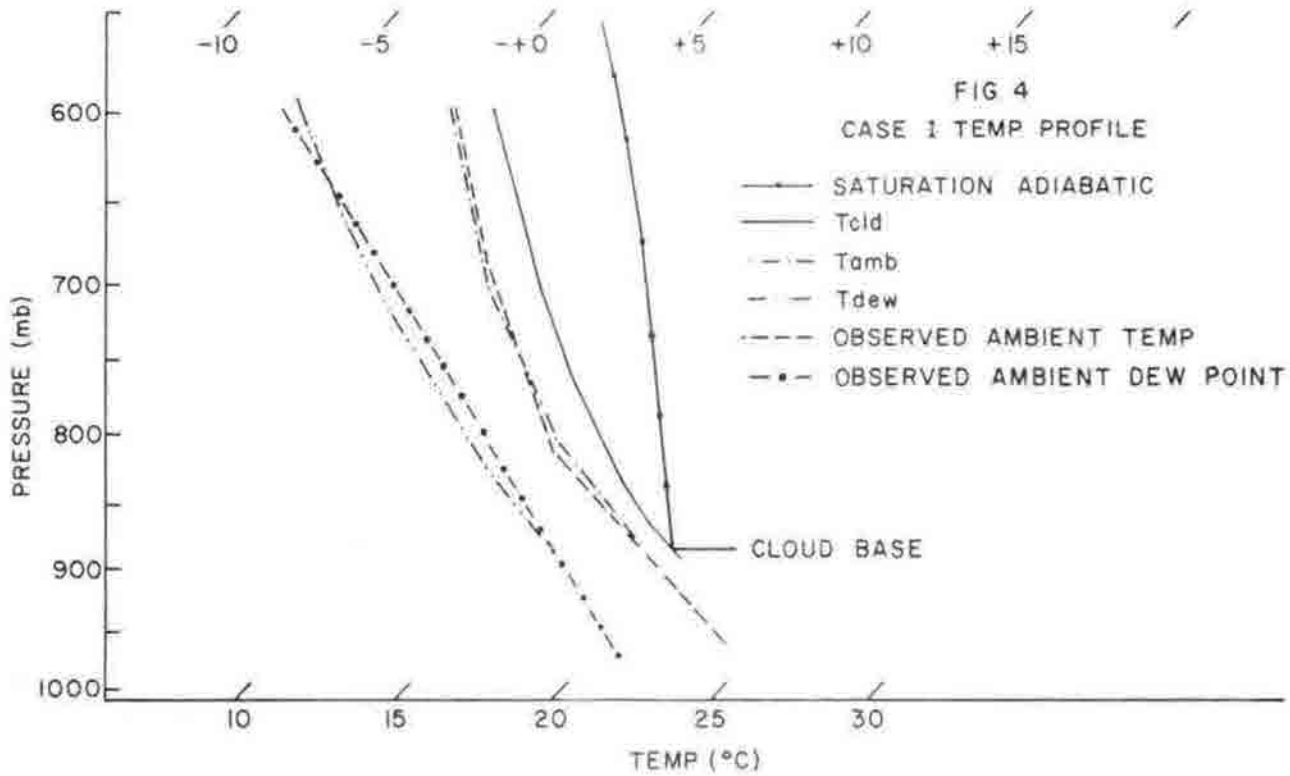

FIG 4
CASE 1 TEMP PROFILE

COLLISION EFFICIENCIES OF CLOUD DROPLETS AT SMALL REYNOLDS NUMBERS

By

M. H. Davis

National Center for Atmospheric Research
Boulder, Colorado

J. D. Klett

New Mexico Institute of Mining and Technology
Socorro, New Mexico

M. Neiburger

University of California, Los Angeles
Los Angeles, California

Accretion is a primary growth mechanism for cloud droplets after the initial condensation phase; its understanding requires knowledge of droplet collisional probabilities. The collisional probability depends upon the cross sectional areas of the droplets, their relative fall velocity, and the collision efficiency, here defined as the ratio of the square of the initial lateral offset distance for a grazing trajectory to the square of the sum of the droplet radii. If the collision efficiency vanishes, no collisions will occur, while if it exceeds unity, the probability of collision exceeds that of purely geometrical sweep-out.

In the present study collision efficiencies for spherical water droplets sedimenting in still air with no electrification were calculated according to a new hydrodynamic model due to one of us (JDK) (1). In this model at small but nonzero Reynolds numbers the drag forces are obtained by an approximate boundary value treatment of an assumed time-independent Oseen-type flow. These forces are then employed in a trajectory integration program to obtain collision efficiencies in the usual way using five iterations. A possible deficiency of the JDK forces is that at close separations they fail to reproduce certain of the force coefficients predicted from the Stokes theory, although under other conditions the two formulations check very well. In order to investigate the effect on the computed collision efficiencies, calculations were also carried out using a program that combines the forces derived by JDK with the Stokes coefficients (2) which are rigorous for time-independent flow at vanishing Reynolds number. Collision efficiencies computed using pure Stokes flow were also included for comparison (3).

None of the calculations exhibit a "cut-off" or zero collision efficiency for any droplet size or any size ratio. Those that involve the Oseen-type forces show a tendency to increase at size ratios very near unity--in contrast with the calculations using pure Stokes hydrodynamics. This tendency is presumably due to the fore-aft asymmetry introduced by the Oseen terms. Generally, the pure JDK forces produce collision efficiencies larger than those of JDK + Stokes, which are, in turn, larger than the pure Stokes values. Again, this is presumably the result of the Oseen asymmetry.

The present results are believed by the authors to be qualitatively sound. Since quantitative differences can be produced by small modifications in the forces used it appears likely that further refinement must await the results of suitable laboratory experiments.

References

(1) Klett, J. D., Thesis, UCLA (1968) Unpublished.
(2) Davis, M. H., Chem. Eng. Sci., 24, 1769-1776, (1969).
(3) Davis, M. H. and J. D. Sartor, Nature, 215, 1371, (1967).

THE INITIATION OF COALESCENCE: A THEORETICAL STUDY*

G. Brant Foote
Institute of Atmospheric Physics
The University of Arizona
Tucson, Arizona 85721

INTRODUCTION

Study of the coalescence problem seeks to examine the important question of whether two drops will actually combine and form a single drop upon collision. In discussing the coalescence problem it is helpful to break up the physical process into two distinct phases. The initial action of bringing the drops into close proximity is properly relegated to the collision problem, and not considered here. Once the drops are brought together the presence of the air serves as a cushion to keep them apart. The problem of getting rid of this air film and allowing the drops to make actual contact we will refer to as the coalescence problem of Type I. After contact has been made, coalescence (by which we here understand the formation of new molecular bonds between the two water surfaces) should proceed immediately. The problem once coalescence has started is that of stabilizing the subsequent motion of the now single drop to keep it from separating into two or more fragments. We will call this the Type II coalescence problem. It would be appropriate to call Type I the bounce-off problem, and Type II the disruption problem, for these are the general effects produced. While both bounce-off and disruption have been observed in laboratory experiments, the coalescence literature has not generally made a point of the distinction. It clearly seems of value to do so, for the physics involved in the two processes is quite different.

The Type I problem, which is the subject of this paper, depends on the dynamics of the colliding drops and the dynamics of the draining air film. Both have been theoretically estimated here. We limit consideration for the present, to a pair of nearly-equal size drops of diameter 1.2 mm, colliding along their line of centers. This geometry allows the governing equations to be formulated in two dimensions (axisymmetry).

DYNAMICS OF DROP COLLISIONS

The drop collision dynamics has been numerically simulated in the present work using a variation on the Los Alamos Marker-and-Cell Method (1), a computing technique designed to integrate the Navier-Stokes equations for a viscous incompressible fluid possessing a free surface. Capillary effects are included here with the aid of a spline interpolation curve to evaluate the surface curvature, a scheme first used by Daly and Pracht (2).

The accuracy of the computing technique has been evaluated by a variety of checks against an analytic solution, due to Lord Rayleigh, for the motion of a spheroid oscillating with small axial ratio about a spherical equilibrium shape. For example, at small axial ratio the computed period of oscillation approaches asymptotically the Rayleigh value, being within 0.2% at an axial ratio of 1.05. For oscillations of large amplitude the period increases to about a 10% excess for axial ratio 1.9.

The collision of equal-sized drops is simulated by allowing a single drop to collide with the rigid boundary of the finite-difference computing mesh. It is expected that the results should be valid when applied to drops which differ slightly in size, say by 10% in diameter. Such a size difference would lead to a difference in terminal velocity of about 50 cm/sec. We have here considered relative impact speeds, v_r, from 20 to 60 cm/sec.

Figure 1 shows a drop collision at speed v_r = 40 cm/sec (relative velocity between drop and wall of 20 cm/sec). The time is 1.5 msec after impact. The drop has not yet reached its maximum distortion, and the upper portion of the drop is still moving downward. The right hand side of Figure 1 shows the positions of marker particles which indicate where fluid is located (the interior region is treated as full). The left hand section through the drop shows velocity vectors drawn from the center of each occupied computing cell in the appropriate direction. A capillary wave induced by the impact has travelled around the drop and been reinforced at the top. The normalized pressure distribution within the drop is shown in Figure 2.

The time, t_b, for complete rebound of the colliding drops for the three relative velocities considered here are t_b = 4.4, 3.8 and 3.4 msec, for v_r = 20, 40 and 60 cm/sec, respectively.

FILM DRAINAGE PROBLEM

We seek to determine the time necessary for the trapped layer of air to escape. It has become well established that such a trapped film will drain relatively slowly until a critical film thickness is reached, whereupon the film will be suddenly bridged and coalescence will proceed rapidly (3, 4, 5). Most experimental work places the critical separation at about 0.1μ. Theories of this process generally follow a treatment due to Reynolds, in equating the work done pushing the two drop surfaces together to the

*The research reported in this paper was supported by the Atmospheric Sciences Section of NSF under Grant No. GA 1431.

viscous dissipation occurring in the intervening film. Plumlee (6) applied the treatment of Charles and Mason (3) to the meteorological coalescence problem, but did not provide numerical evaluation of any of his expressions for film drainage times. Explanation of the bounce-off (here termed Type I) coalescence problem is clearly concerned with the relation of drop rebound time to air film drainage time, so that it is desirable to refine the theory of the latter as much as possible. The Reynolds draining theory has been extended in the present work in the following ways: (1) the solution of the drop dynamics problem has provided important time-dependent parameters--the radius of the drop deformation and the dynamic force pushing the two near surfaces together during the collision; (2) the effect of drop internal circulation on the rate of film drainage has been evaluated; (3) the effects of net drop charge and external electric field have been considered; and (4) hitherto neglected consideration has been given to the effect on the air drainage of the finite mean free path of air molecules in this transition range of Knudsen numbers.

RESULTS AND CONCLUSIONS

The general results of this study for the case of 1.2 mm diameter drops impacting at the indicated speeds are:

(1) Film drainage times in the absence of charges and external fields are several hundred milliseconds, at least two orders of magnitude larger than the time for drop rebound. This agrees with laboratory results that no coalescence occurs under such conditions.

(2) Approximate theory indicates that charges of magnitude 5×10^{-11} coul, or external electric fields of 300-400 v/cm would be sufficient to effect coalescence.

(3) Consideration of drop internal circulation and finite Knudsen number of air drainage flow modifies the value of charge and field necessary for coalescence, but does not of itself provide a mechanism for significantly reducing predicted air drainage times.

REFERENCES

1. Welch, J. E., F. H. Harlow, J. P. Shannon and B. J. Daly, 1966: THE MAC METHOD. Los Alamos Scientific Lab. Rept. LA-3425, 146 pp.
2. Daly, B. J. and W. E. Pracht, 1968: Numerical study of density-current surges. Phys. Fluids, 11, 15-30.
3. Charles, G. E. and S. G. Mason, 1960: The coalescence of liquid drops with flat liquid/liquid interfaces. J. Colloid Sci., 15, 236-267.
4. Hartland, S., 1967: The coalescence of a liquid drop at a liquid-liquid interface. Part II: Film thickness. Trans. Instn. Chem. Engrs., 45, 102-108.
5. Lindblad, N. R., 1964: Effects of relative humidity and electric charge on the coalescence of curved water surfaces. J. Colloid Sci., 19, 729-743.
6. Plumlee, H. R., 1964: Effects of electrostatic forces on drop collision and coalescence in air. Charged Particle Res. Lab. Rept. CPRL-8-64, 101 pp.

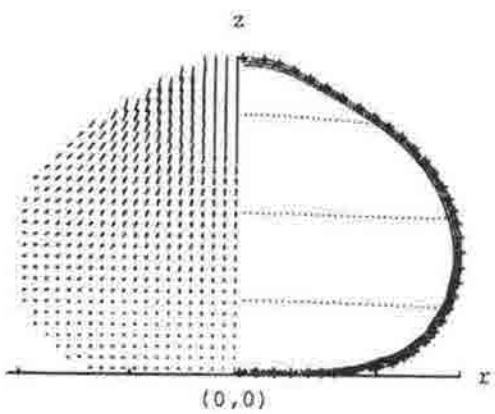

Figure 1

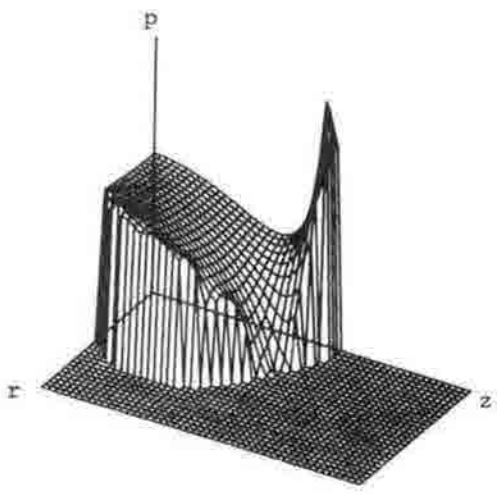

Figure 2

SIMULATION OF CLOUD DROPLET COLLECTION PROCESS

H. C. Chin

Department of Meteorology, University of California, Los Angeles

Previous investigations of the cloud droplet growth process were usually based on the assumption of a homogeneous and isotropic cloud. In this study this restriction is temporarily removed by introducing random positioning of cloud droplets within a liquid content distribution that is smooth in a scale of the order of 10 cm. The gravitational growth of large drops in such a heterogeneous cloud is considered.

In the interior of a warm cloud at 100% relative humidity composed of cloud drops represented by a steady-state spectrum in discrete size classes, the gravitational growth of a large drop with initial mass greater than that of any droplet in the spectrum, assuming a coalescence efficiency of unity, depends only on the present state of the drop and not its past behavior. Furthermore the one-step transitional probabilities are also independent of the time variable. The growth of the large drop then can be described by a Markov chain process with stationary transition probabilities.

We discretized the droplet spectrum by equal radius intervals with $\Delta r = 2\mu$, thus greatly reducing the number of required data points below those which would be needed using the smallest drop as the elementary mass, and considered one row vector of the transition matrix at a time. With the initial large drop radius given and the cloud spectrum assumed to be varying so slowly that it can be approximated as steady-state, we generated a realization of the Markov chain process which was equivalent to stimulating the life history of a large drop growing by collection in a heterogeneous cloud. The empirical Khrgian and Mazin spectrum with liquid water content $L = 1\ g/m^3$; average radius $R_{av} = 7.5\ \mu$ and droplet size range 3 to 29 μ was used (hereafter, K-M III). The initial large drop radius was 30 μ. The simulation procedure is described elsewhere (1). Thirty-two independent trial simulations of the growth for 1000 seconds of drops falling through the cloud were carried out. These constitute a random sample of growth histories for drops with initial radius of 30 μ in such an environment. The resulting sample means together with 95% confidence intervals are shown in Figures 1 and 2 as C.

For comparison the growth of a large drop in a polydisperse cloud due to gravitational coagulation as described by the continuous growth equation:

$$\frac{dR}{dt} = \frac{\pi}{3} \int_0^R n(r)\ r^3\ Y_c^2\ (U_R - U_r)\ dr \qquad [1]$$

was computed with the same initial large drop radius of 30 μ and the same cloud spectrum to yield growth curves B in Figures 1 and 2. The growth curves A were arrived at from equation [1] for a monodisperse cloud with the same liquid water content of 1 g/m^3 and the same mean volume radius of 10 μ as the K-M spectrum III used in the other cases.

It is apparent from Figures 1 and 2 that the drop growth rates in a polydisperse cloud are greater than that in a corresponding monodisperse one. The explanation is that although for the K-M III cloud the median droplet size is only 7 μ and about 75% of the droplets are actually less than 10 μ, the remaining droplets with size greater than 10 μ made such a major contribution to growth that an approximation with a monodisperse cloud with all droplets of 10 μ size would grossly underestimate the growth rate of a large drop. Because the growth simulations were conducted as independent trials the resultant radii (masses), $\{X_i\}$ $i = 1,2,\ldots,32$ constitute a sequence of independent identically distributed random variables which can be demonstrated to have the central limit property, so that Gaussian confidence intervals can be constructed. For drop mass at 1000 seconds, the standard value 3.85 obtained from [1] falls within the 95% confidence interval for the mean mass. For the case of drop radius, however, the 95% confidence interval with limits of 85.0 and 97.5 μ does not contain the standard value. This indicates that the sample mean radius is significantly smaller than that would result from uniform growth because of the spread in size distribution due to growth in a non-uniform cloud.

The average time required for the most fortunate one eighth of the large drops in the sample to reach 100 μ is 877 seconds compared with about 1020 seconds required by continuous growth. Under the same conditions if there are initially 80 drops of 30 μ size per liter, then after 15 minutes about 10 of these would reach 100 μ size. This is a result not predicted by the continuous growth equation.

To study the evolution of a whole cloud spectrum, the kinetic equation for particle coagulation has been used by many investigators, for example, see (2), to treat the cloud droplet collection process. While the Monte Carlo method does not enable such a computation, it is desirable to compare the two approaches. The kinetic equation for changes in drop size distribution has the familiar form:

$$\frac{\partial n(v)}{\partial t} = \frac{1}{2} \int_0^v n(u)\ n(v-u)\ K(u,v-u)\ du - n(v) \int_0^\infty n(u)\ K(u,v)\ du \qquad [2]$$

here $n(v)$, $n(u)$ are number densities of droplets of mass v and u respectively. $K(u,v)$ is the collection rate kernel describing rate of binary combinations between u and v sized droplets. The evolution of an initial K-M III spectrum computed from [2] using assumptions and methods described in reference (1) are shown in Figure 3.

To compare the results of the kinetic equation with the Monte Carlo sampling procedure we divide the spectrum into two non-overlapping parts and consider only the collection of the droplets in the small group by those in the large. For this situation equation [2] reduces to:

$$\frac{\partial n(v)}{\partial t} = -n(v)\int_0^{v_1} n_s(u)\,K(v,u)\,du + \int_{v_2}^{v} n(v')\,n_s(v-v')K(v',v-v')\,dv' \qquad [3]$$

Here v_2 (v_1) is the lower (upper) size limit of the large (small) droplet end of the spectrum with $v_1 \leq v_2$; n and n_s denote large and small droplet number densities respectively.

Computation was carried out with [3] under initial conditions similar to those of the sampling process. To make meaningful comparison of these two approaches, we converted the results into a non-dimensionalized representation. Define N_{ri} as the total number of droplets larger than a given size i, N_t as the total droplet number at time t and $p_i = v_i N_t/V$ where v_i is the volume of an i-sized droplet, and V is the initial total volume of large droplets under consideration. A graph of N_{ri}/N_t versus p_i then represents a dimensionless cumulative distribution of the spectrum at time t. In Figure 4, the smooth cumulative distribution curve obtained by computation with [3], is compared with the random sample computations represented by 32 discrete data points. The overall growth rate of random sampled drops is higher while the growth predicted by the kinetic equation is more "diffuse", with much of the mass remaining in relatively small drops. On the whole, the latter approach predicted a considerably lower rate of water mass transfer to the large drops.

REFERENCES

(1) Chin, H. C., 1970: Simulation of cloud droplet collection process. Ph.D. Dissertation, University of California, Los Angeles.

(2) Berry, E. X., 1967: Cloud droplet growth by collection. J. Atmos. Sci., 24, 688-701.

(3) Davis, M. H. and J. D. Sartor, 1967: Theoretical collision efficiencies for small cloud droplets in Stokes flow. Nature, 215, 1371-1372.

(4) Shafrir, U. and M. Neiburger, 1963: Collision efficiencies of two spheres falling in a viscous medium. J. Geophys. Res., 68, 4141-4148.

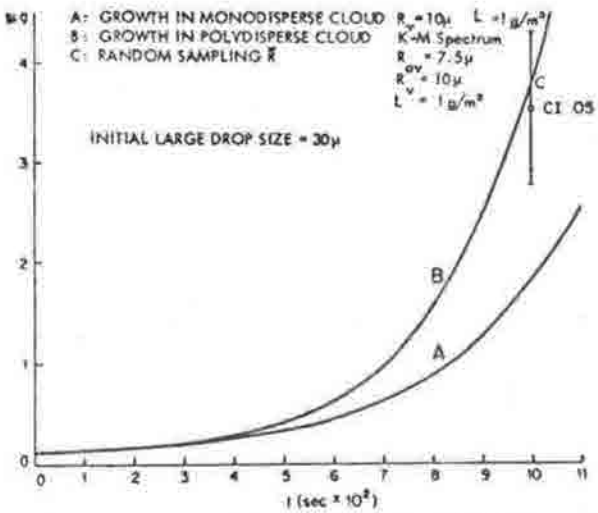

1. Comparison of mass growth, R_o = 30 μ, cloud L = 1 g/m³, (A) In a monodisperse cloud R_v = 10 μ. (B) In a cloud with K-M spectrum also with $\bar{R}$ = 10 μ, (C) Mean mass from random sampling, cloud same as B, n = 32, showing 95% confidence interval at t = 1000.

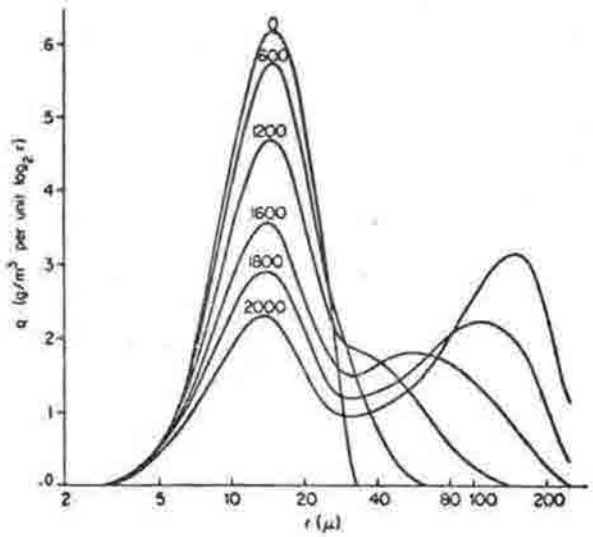

Figure 3. Evolution of spectrum III due to collection.

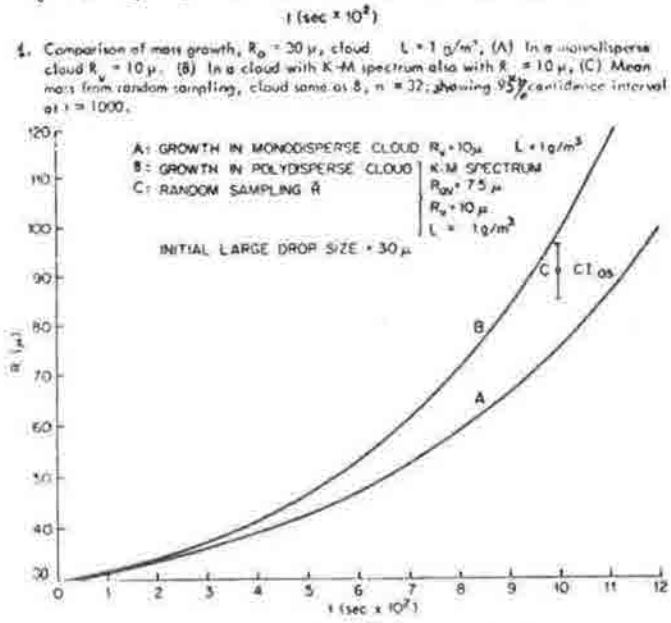

2. Comparison of radius growth, R_o = 30 μ, cloud L = 1 g/m³ (A) In a monodisperse cloud R_v = 10 μ. (B) In a cloud with K-M spectrum also with R_v 10 μ, (C) Mean radius from random sampling, cloud same as B, n 32, showing 95% confidence interval at t 1000.

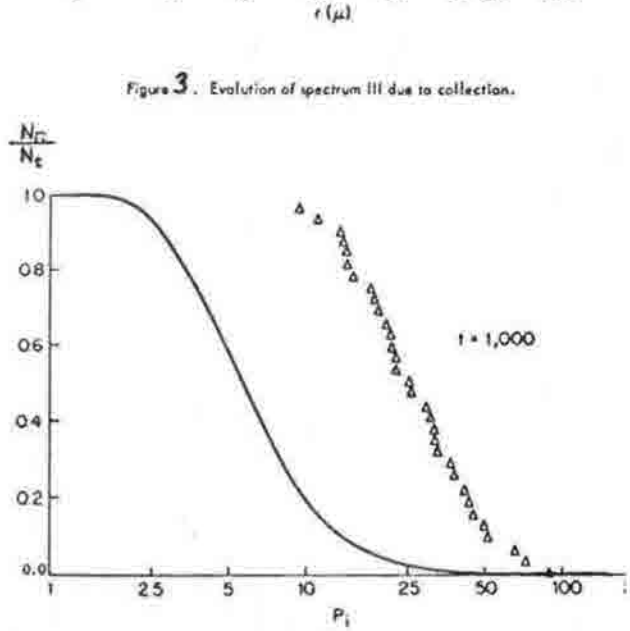

Figure 4. Comparison of dimensionless cumulative distributions at t = 1,000 between results computed from [3] and those obtained from random sampling.

THE ROLE OF COLLECTION IN DETERMINING RAINDROP SIZE DISTRIBUTIONS

John R. Adam
Illinois State Water Survey
Urbana, Ill.

INTRODUCTION

Raindrop size distributions have been measured at various locations around the world and attempts have been made to correlate their shapes and radar reflectivities with synoptic weather types and other physical parameters.(1) However, until now no theory has been found to explain the variability in drop distributions measured at the ground from even the most simple rain producing mechanisms, collision and coalescence in warm clouds. The shape of the raindrop size distribution for warm rain depends on the concentration and size of the cloud droplets, along with the physical properties of the cloud such as its thickness, and the ranges of temperature and humidity. These distributions are also modified by collection and evaporation between cloud base and the ground.

The raindrop size distributions from warm rain at Majuro Atoll, Marshall Island (Lat. 7 05' N, Long. 171 23' E), measured with a drop camera over a period from March 1959 to April 1960 have been reported by Mueller and Sims.(2) An examination of these distributions shows that for rates less than 10 mm per hour the shape of the distribution is constant, while the number of drops in the distribution increases linearly with rate. This indicates that the rate of rainfall depends most strongly on the rate of cloud droplet growth. For higher rates, the distribution broadens with a relatively higher concentration of large drops though the total number of drops in the distribution increases much less rapidly with rate. It can then be postulated that for warm rain, the shape of the size distribution at cloud base is independent of rate and that the number of drops in the distribution increases linearly with rate. Variations in the ground distributions are accounted for by the collision and coalescence of raindrops as they fall to the ground.

RAINFALL MODEL

To test this hypothesis, a rainfall model has been proposed which predicts the size distribution of raindrops as a function of rainfall rate and fall distance below cloud base. The model assumes that rain is being produced at a uniform rate and with a constant cloud base drop size distribution, independent of rate. There are no winds or updraughts below the cloud. The relative humidity is also assumed high enough below cloud base so the evaporation is negligible as is the case at Majuro. The drops are assumed to have unity collection efficiencies and are falling at their terminal velocities. Drops which collide grow into a new larger drop with no breakup or bounce. A numerical model, using these assumptions and the standard collection and fall equations was devised. A log-normal distribution was fitted to the lowest average rainfall rate (R = 0.3 mm/hr) at Majuro and was used as the initial distribution. When this distribution was used in the model, it did not change significantly in 1000 meters of fall, showing that collection is unimportant at this rainfall rate. Since the relative humidity was always greater than 80% below cloud base, evaporation is not appreciably. This should then be a good approximation to the actual cloud base drop distribution. To generate a greater rainfall rate, the total number of drops in the initial distribution was increased. Details can be found in Adam.(3)

RESULTS

A comparison of the theoretically predicted drop distributions may now be made with specific storms. The model is valid only if the rainfall has reached steady state with a constant rainfall rate at each level below the cloud. In the majority of instances of rainfall at the Majuro Atoll this was not true. Rainfall rates at the ground varied as much as 50% over successive one minute sample periods. This variation was most pronounced at very high rainfall rates. However, several storms did exist for which the rainfall rate did not vary more than 20% over a six minute period and four examples are listed below. The measured drop distributions for the last two minutes of these storms were averaged and the rainfall rate calculated.

Date	Time(GMT)	Rate(mm/hr)	Clouds(m)	Precip(m)	Date	Time(GMT)	Rate(mm/hr)	Clouds(m)	Precip(m)
25 July 59	1318-19	1.01	450	~	8 June 59	1145-46	29.3	390	890
8 June 59	1139-40	54.4	360	730	7 April 59	1100-01	100.0	390	630

Fig. 1 shows the predicted and measured drop distributions for these storms. For the lowest rainfall rate considered, the distribution does not change a great deal over the 1000 meters fall distance. The density of drops is not great enough for a significant amount of collection to occur. As the rainfall rate increases however, collection becomes more important as can be seen. The model is in reasonable agreement with these measured distributions for steady rains. Also, for each rainfall rate, the predicted liquid water contents and radar reflectivities agree with the measured value within 10%. The average distance below cloud base for best correlation between predicted and measured total number of drops, liquid water contents, and rainfall rates are shown in the table. In all cases, the lowest observable cloud cover was well below the level at which the model predicted the origin of precipitation. This indicates that the majority of precipitation produced by collection of cloud droplets originates well within the cloud.

Unfortunately, for more transient rains the agreement is not nearly as good and the distributions contain significantly more large drops than predicted. The extension of this model to predict rain produced by mechanisms other than the warm rain process is difficult. If ice is present in the clouds, the initial distribution will be broadened by the melting of large ice particles.

Acknowledgments: A portion of this work was performed as part of a Ph.D. thesis requirement in Electrical Engineering, University of Illinois under the direction of Prof. C. D. Hendricks. The work was supported by the NSF under grants GA-1614 and GA-4576.

REFERENCES

1. Cataneo, R., and G. E. Stout, 1968: Raindrop-Size Distributions in Humid Continental Climates, and Associated Rainfall Rate-Radar Reflectivity Relationships. J. Appl. Met., 7, 901-907.
2. Mueller, E. A., and A. L. Sims, 1967: Raindrop Distributions at Majuro Atoll, Marshall Islands Tech. Rept. ECOM-02071-RR1, Ill. State Water Survey, Urbana.
3. Adam, J. R., 1969: The Role of Collection in Determining Raindrop Size Distributions, Ph.D. Dissertation in Electrical Engineering, Univ. of Ill., Urbana.

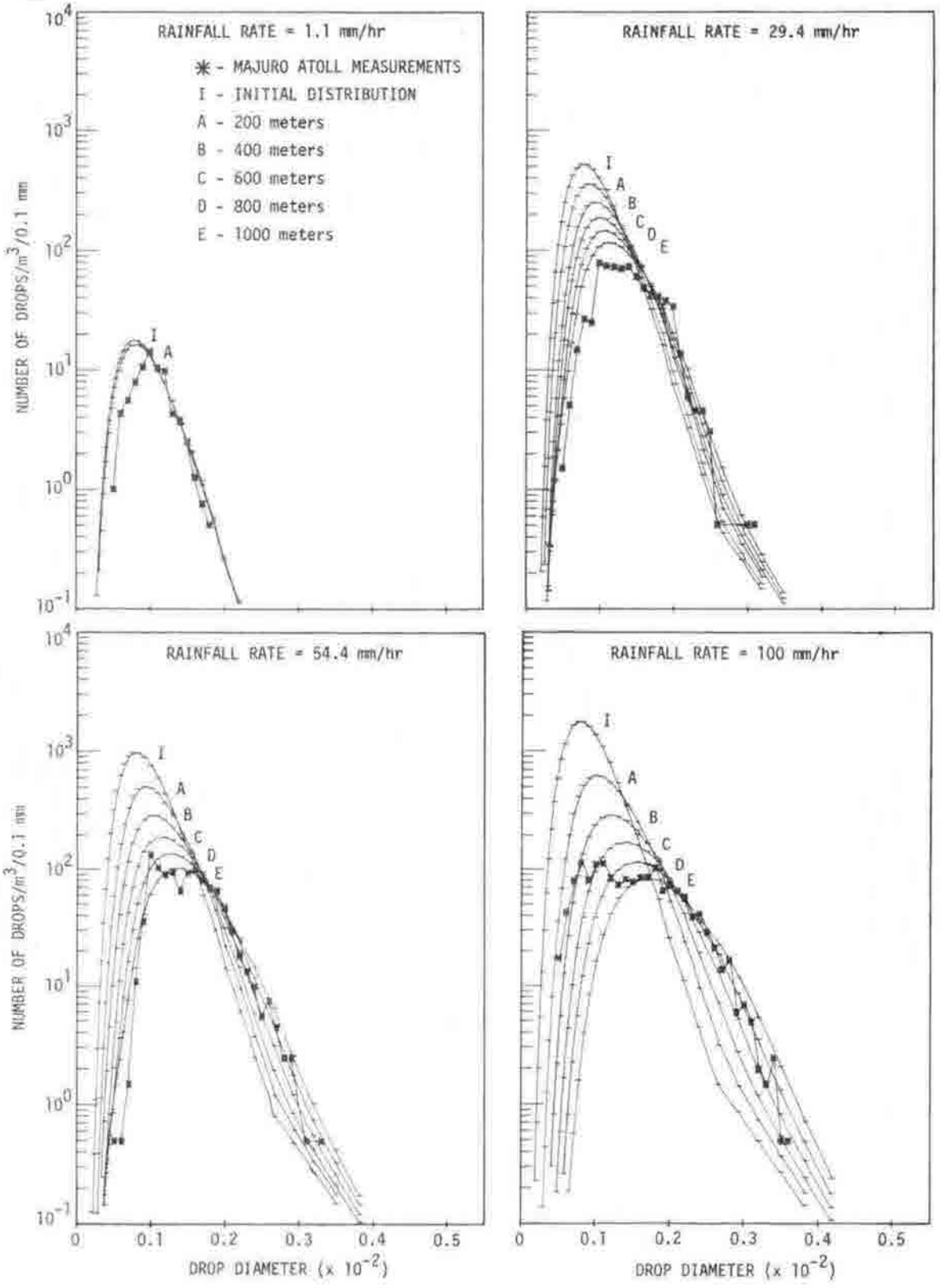

Figure 1. A comparison of predicted and measured raindrop size distribution

THE MUTUAL INFLUENCE OF EQUAL-SIZED DROPS DUE TO THE WAKE EFFECT

Robert Cataneo
John R. Adam
Richard G. Semonin

Illinois State Water Survey
Urbana, Ill.

INTRODUCTION

In early studies of the collision-coalescence process,[1,2] it was assumed that water droplets of nearly equal size in a cloud are in equilibrium with each other, and therefore coalescence would not take place unless larger droplets were present. Later experiments[3,4] indicated that collision efficiencies for equal-sized droplets were non-zero and in fact were unexpectedly quite large. These results brought out the importance of the asymmetric flow around a droplet in the collision-coalescence process for droplets of equal size. A recent empirical study[5] indicated that for Reynolds numbers as low as R = 0.06, which is the $\mathcal{N}_R$ of a 30-μm diameter droplet falling at terminal velocity, asymmetric flow exists around the droplet. Conceivably then, two 30-um droplets falling one above the other could approach each other if their vertical separation were sufficiently small, allowing the decreased drag force in the wake of the leading droplet to act upon the upper droplet. It becomes important then to determine the maximum vertical separation possible, as a function of droplet size, for equal-sized droplets to approach. In this paper we will describe the experimental procedure used to determine this distance, and the results.

EXPERIMENTAL APPARATUS AND PROCEDURE

The experimental apparatus is shown in Fig. 1. A stream of water droplets is produced by forcing water through a small opening of the desired size. A vibrating piezoelectric strip in the water supply upstream of the water exit point forces the exiting water jet to break up into uniform-sized, equally spaced droplets. Single, charged or uncharged droplets can be removed from the stream by applying a voltage pulse at controlled intervals to a charging ring placed around the jet breakup point, and then passing the stream through an electric field.[6] A pair of droplets may be produced in a similar way by applying a second, independent pulse to the ring after the first. The vertical separation between droplets in the pair can be controlled by varying the time between the first and second pulses. The horizontal position of the two droplets is determined by the pulse amplitude which controls the difference between droplet and stream charge. An automatic sawtooth amplitude sweep was incorporated in the circuitry to allow the upper droplet in the pair to move from one side of the lower droplet, over it, then to the other side in a sweeping fashion at a rate of 5 cycles per minute. The spacing between pairs was always set much greater than the distance between droplets in one pair.

When viewed under stroboscopic light, the droplets appear to stand in space with the upper one sweeping back and forth across the lower one as is shown in Fig. 1. If a wake effect is present, it is observed as a dip in the sweeping trajectory of the upper drop as it passes over and accelerates towards the lower drop. The droplets investigated were allowed to reach terminal velocity before the presence of a wake effect was determined. The distance at which terminal velocity is reached was calculated and was also measured for each pair.[7] The experimental apparatus permitted the droplets to be observed for wake effect a maximum distance of 1.5 m below the point at which they reached terminal velocity. If a wake effect was observed, the vertical separation was increased until the effect was no longer visible. The vertical separation at which the phenomenon visually disappeared was then measured at the terminal velocity point. The minimum detectable dip induced by the wake was approximately one droplet diameter. Charge on the droplets was varied from 10^{-12} to 10^{-16} coulombs and had no effect on the maximum separation measured. The experiment was carried out for four droplet sizes. The maximum separation as a function of droplet size is plotted in Fig. 2.

DISCUSSION

The results were indeed surprising. The wake effect was noted as far away as 11.5 cm for the 700-μm diameter droplets, the distances decreasing directly with droplet size. However, even for the 115-μm droplet, the distance was still quite sizable (1.15 cm, 100 diameters). The implications of these results with respect to precipitation physics are far reaching in regard to the warm rain production mechanism.

We observed the wake effect at the maximum vertical distance to be present at radial distances of 2-3 droplet diameters from the bottom droplet. There appears then to be a right circular cone of influence downstream of the leading droplet, which is the cone apex, whose radius at the maximum

vertical distance is 2-3 droplet diameters. If we consider that the number density of 100-μm diameter drops may be 3-4/cm^3 in a cumulus congestus cloud,[8] and if we consider the "wake cone" to be as described above, then the probability of any one of four 100-μm droplets in a cubic centimeter volume being influenced by the wake of one of the other three is ~1%; if we extrapolate this to a cubic meter, the probability of the number of drops being influenced by the wake effect becomes 10^4. Of course, the number density of larger size droplets in a cloud drops off sharply so the influence of the wake effect becomes increasingly small. However, the wake effect for smaller sizes where R <1 becomes important since their number density in clouds is greater. We are presently investigating these droplet sizes.

CONCLUSIONS

An experimental procedure has been devised to investigate the magnitude of the wake effect for equal-sized water droplets. From the data obtained to date, we conclude that this phenomenon has a large influence on the collision-coalescence process, and may be a major factor in the rapid growth of raindrops from cloud droplets.

Acknowledgments

Research sponsored by the AEC under contract AT(11-1)-1199 and by the NSF under grant GA-4576.

REFERENCES

1. Langmuir, I., 1948. J. Met., 5, p. 175.
2. Houghton, H. G., 1950. J. Met., 7, p. 363
3. Telford, J. W., Thorndyke, N. S., and Bowen, E. G., 1955. Q. J. R. Met. Soc., 81, p. 241.
4. Woods, J. D., and Mason, B. J., 1965. Q. J. R. Met. Soc., 91, p. 35.
5. Steinberger, E. H., Pruppacher, H. R., and Neiburger, M., 1968. J. Fluid Mech., 34, p. 809.
6. Lindblad, N. R., and Schneider, J. M., 1965. J. Sci. Instr., 42, p. 635.
7. Cataneo, R., and Semonin, R. G., 1969. J. Rech. Atmos., 4, p. 57.
8. Mason, B. J., 1957. The Physics of Clouds, p. 90.

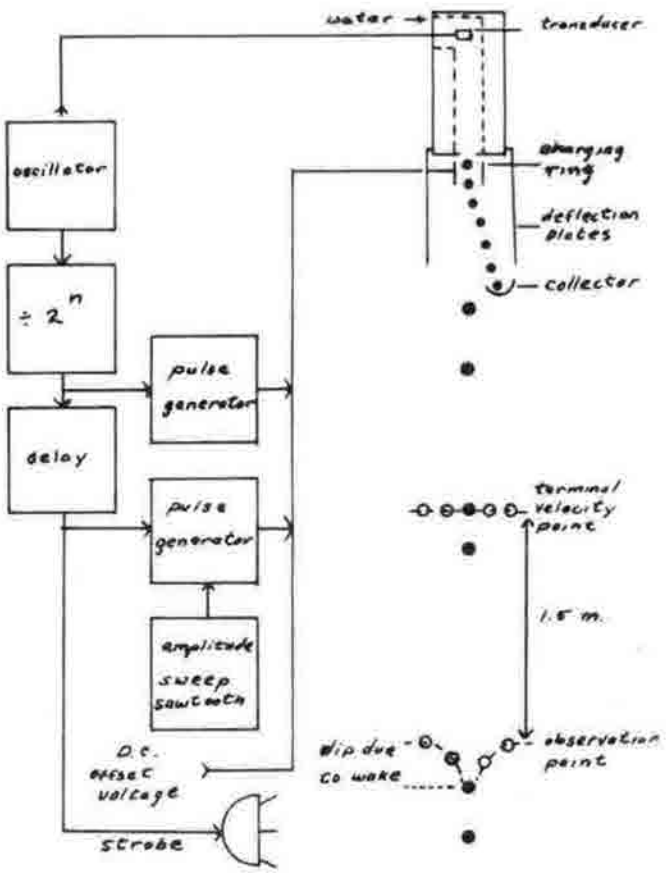

Fig. 1 Block diagram of apparatus to study wake effect.

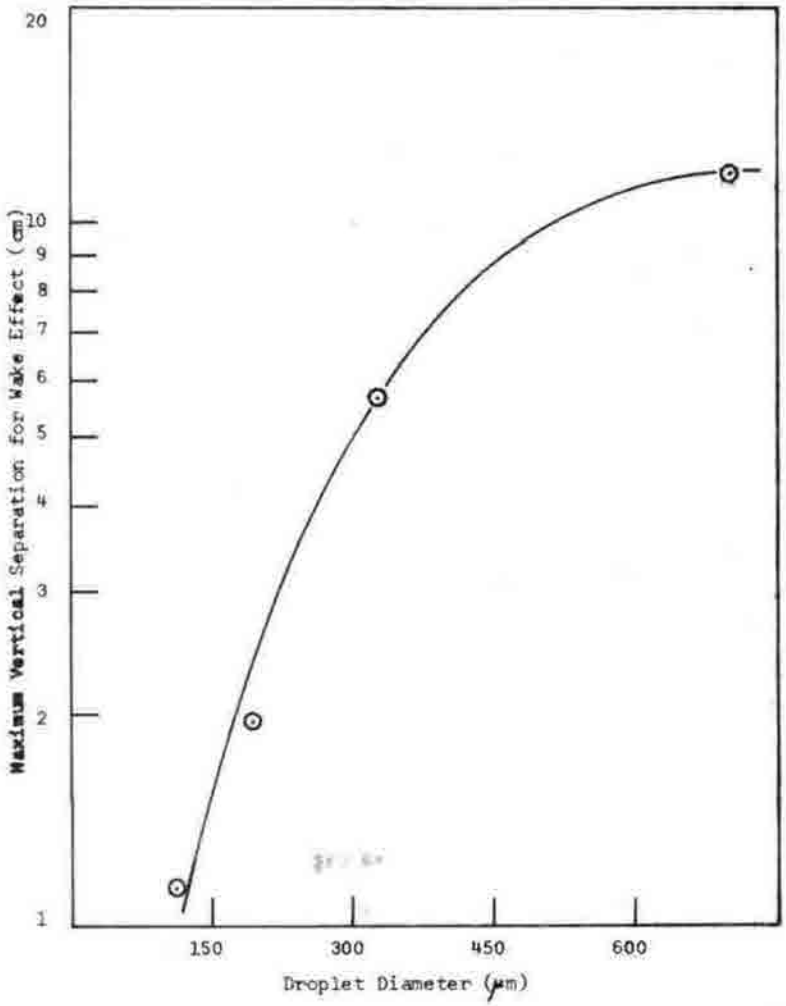

Fig.2. The maximum vertical separation for presence of a wake effect as a function of droplet size.

MODIFICATION OF DROP-SIZE DISTRIBUTION IN AN UNSATURATED DOWNDRAFT

Elizabeth L. Kintigh & Phanindramohan Das
Air Force Cambridge Research Laboratories
Bedford, Massachusetts

1. INTRODUCTION

All the theoretical studies of the unsaturated downdraft known to date have assumed the precipitation water to be divided into drops of a uniform size (1, 2, 3), although precipitation carried in a downdraft invariably consists of a population of drops of varying sizes. In many problems, especially those concerning radar measurements of rainfall, it is important to know how the drop-size distribution is modified as the precipitation descends from the cloud base. Rigby, Marshall and Hitschfeld (4), Mason and Ramanadham (5) and Hardy (6) have examined this question in a framework which is particularly meaningful for precipitation from layer-type clouds or for that falling into a stagnant subcloud layer. None of these studies, however, has incorporated the effect of an unsaturated downdraft, all their specifications of subcloud subsaturations being of an arbitrary nature. On the other hand, downdraft subsaturation is attained through a definite physical process so that any study made in its background is likely to be more definitive than those made under arbitrary specifications of the thermal and physical parameters.

The work of Das and Subba Rao (2) has set up a theoretical framework for studying the evaporation from drops carried in a subcloud downdraft. This study extends their method to the case of a steady (and constant) downdraft carrying a population of drops of varying sizes.

2. THE EQUATIONS

As in the study of Das and Subba Rao,(2) a one-dimensional, steady subcloud downdraft is assumed to have strength w_D. Then we have

the thermodynamic equation: $$dT/dz = -\Gamma_d + (L/c_p)\, d\xi/dz \; ; \qquad (1)$$

the moisture equation: $$d\xi/dz = (1/w_D) \sum_{i=1}^{I_{max}} N_i f_i \; ; \qquad (2)$$

the equation of drop concentration:

$$dN_i/dz = -(1/w_D \rho_a)\, d(\rho_a N_i V_i)/dz - \rho_a \pi \sum_{j=i+1}^{I_{max}} (r_i + r_j)^2 (V_j - V_i) N_i N_j / (w_D + V_j) + B_i \; ; \qquad (3)$$

and the equation of drop growth:

$$dm_i/dz = -f_i + \sum_{j=1}^{i-1} \pi \rho_a (r_i + r_j)^2 (V_i - V_j) N_j m_j / (w_D + V_i). \qquad (4)$$

In the above equations z is the vertical coordinate, T the temperature, ξ the humidity mixing ratio, N_i, m_i, r_i and V_i, respectively, are the concentration (per unit mass of air), mass, radius, and the terminal velocity of the drops belonging to the i-th size class. In addition, Γ_d is the dry-adiabatic lapse rate, L the latent heat of vaporization of water, c_p the specific heat of air at constant pressure and ρ_a is the air density. The functions f_i and B_i are of numerical nature, the first being obtained by a manipulation of the experimental observations of Kinzer and Gunn (7) on the evaporation of drops. B_i is a (numerical) transfer function which adjusts the drop concentration of the i-th class due to changes in the sizes of drops in the adjacent classes and break-up of the drops in the largest class. At the present moment, B_i changes the class of all the drops in a class when they meet certain criteria. This results in some empty classes at some levels. In addition, when the size of the drops falls below a certain predetermined minimum, they are made to evaporate completely adding the vapor to the air.

3. RESULTS

The results of some of the computations are summarized in Table I and a typical case of the modification of the drop-size distribution as the precipitation is carried from the cloud base to the ground is shown in Figure 1. From a study of the figure and the table, the following conclusions can be reached: (1) the evaporation in the downdraft removes the smallest drops although the nature of the distribution is not drastically changed by this cause alone; collision-coalescence effects more important changes to drop-size distribution and, by converting the population to one comparatively richer in larger drops, tends to augment downdraft subsaturation. By comparing the results of this study with those earlier studies with monodisperse precipitation and taking note of (b) above one can conclude that the presence of smaller drops in the population tends to keep the humidity in the downdraft higher.

TABLE 1

(Distribution, with height above ground (z), of liquid-water content (LWC), temperature (T) and relative humidity (H) in unsaturated downdrafts of magnitude w_D.)

w_D (m/sec)		5.0							10.0					
Z (km)		1.5	1.0		0.5		0.0		1.0		0.5		0.0	
Condition*		CLD BASE	E	EC	E	EC	E	EC	E	EC	E	EC	E	EC
LWC(gm^{-3})	I	.290	.241	.243	.152	.160	.081	.091	.262	.263	.196	.201	.127	.135
	II	.871	.733	.682	.492	.484	.282	.306	.790	.785	.613	.609	.411	.446
T (°C)	I	17.0	21.7	21.8	26.4	26.4	31.1	31.1	21.8	21.8	26.6	26.6	31.3	31.3
	II	17.0	21.4	21.5	25.6	25.7	29.8	30.1	21.6	21.7	21.0	26.1	30.4	30.5
H (%)	I	100	79.2	79.2	64.0	63.9	51.9	51.8	78.7	78.7	63.1	63.0	51.0	50.9
	II	100	81.5	81.1	68.7	67.7	57.7	56.7	80.1	79.9	66.1	65.6	55.0	54.3

*E - evaporation only; EC - evaporation and collision-coalescence

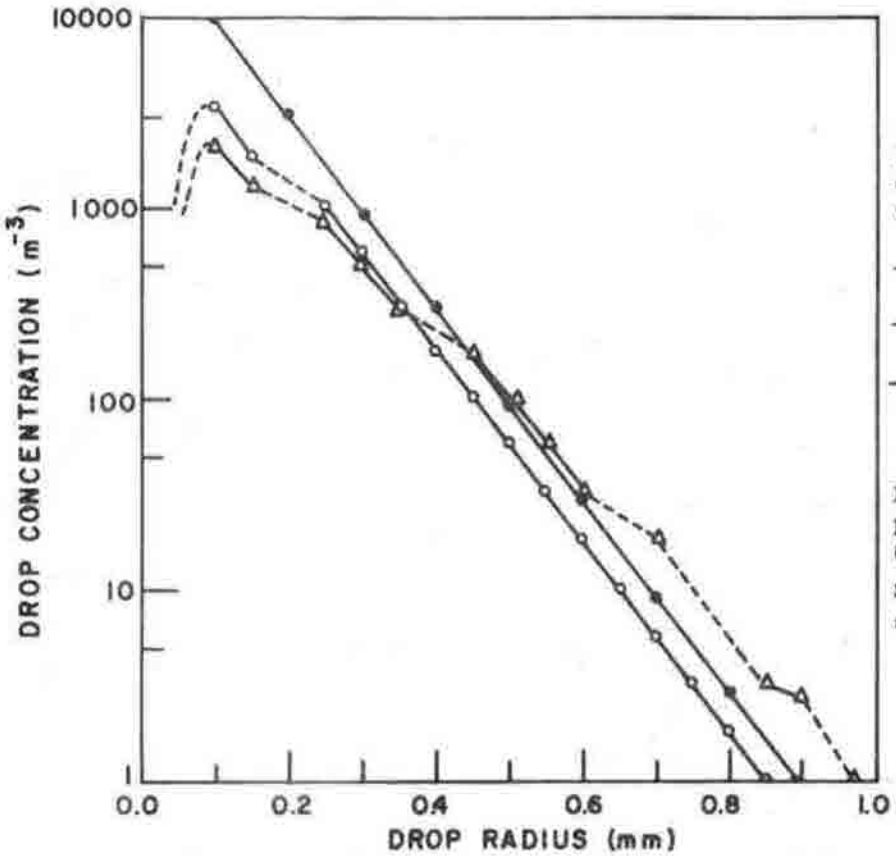

Figure 1. Modification of drop-size distribution in an unsaturated downdraft.

—●—●— Distribution at Cloud Base

—○—○— Distribution at Ground (Evaporation Only)

—△—△— Distribution at Ground (Evaporation and Coalescence)

Dotted sections of curves pass through empty classes (see text).

Speed of downdraft = 10.0 m sec^{-1}.

4. REFERENCES

(1) Kamburova, P.L, F.H. Ludlam, 1966: Rainfall evaporation in thunderstorm downdrafts. Quart. J. Roy. Meteor. Soc., 92, 510-518.

(2) Das. P., amd M.C. Subba Rao, 1968: The unsaturated downdraft. Proc. Intern. Conf. Cloud Physics, Toronto, Canada, 592-596

(3) Caplan, P.M., 1969: On thunderstorm downdrafts. Proc. Sixth Conf. Severe Storms, Chicago, 68-70

(4) Rigby, E.C., J.S. Marshall, and W. Hitschfeld, 1954: The development of the size distribution of raindrops during their fall. J. Meteor., 11, 363-372.

(5) Mason, B.J., and R. Ramanadham, 1954: Modification of the size-distribution of falling raindrops by coalescence. Quart. J. Roy. Meteor. Soc., 80, 388-394.

(6) Hardy, K.R., 1963: The development of raindrop-size distributions and implications related to the physics of precipitation. J. Atmos. Sci., 22, 299-312.

(7) Kinzer, G.D., and R. Gunn, 1951: The evaporation, temperature and thermal relaxation time of freely-falling water drops. J. Meteor., 8, 71-83.

MEASUREMENTS OF SOUND ATTENUATION BY A WARM AIR FOG

by

John E. Cole III, Tufts University, Medford, Massachusetts

and

Richard A. Dobbins, Brown University, Providence, Rhode Island

Measurements of the attenuation of sound by a warm air fog have been made at low dimensionless frequencies ($\bar{\tau} = \omega\tau_t/c_m$; τ_t = the thermal relaxation time for the droplet, ω = circular acoustic frequency, and c_m = liquid mass fraction) where the effects of mass transfer are dominant. Previous measurements of the attenuation of sound in fogs have been performed at higher frequencies where the loss mechanism is primarily the viscous interaction between the particle and the surrounding gas.

Experiments were performed in a Wilson cloud chamber of 15.2 cm inside diameter and initial length of 1.28 meters. The test volume of the chamber can be expanded to ratios as high as 1.8 in periods of about 200 ms. by the acceleration of the piston by a pressure differential. A fundamental longitudinal acoustic mode is excited during the cessation of the piston. A standing wave results when the piston motion ceases and the wave is attenuated by the various loss mechanisms. If the gas in the cloud chamber prior to the expansion is a water-saturated vapor, then the increased attenuation of the standing wave pattern is a measure of the acoustic damping owing to the cloud of droplets produced by the expansion. Measurements of attenuation are completed within about 150 ms. after cessation of piston motion. The effects of wall heat transfer are confined to a thin boundary layer region during this time and do not influence cloud or gas mixture properties.

Time-resolved measurements of spectral transmission at two appropriately selected wavelengths of light are made during the experiment. The spectral transmission curves display an oscillatory behavior that results from the variation of scattering coefficient K , with particle diameter D . The oscillations of the scattering coefficient curve indicate the cloud is a monodisperse. Particle size is measured by identifying an inflection point on the curve of transmission versus time as a particular feature of the curve of K vs. D . The calculation of droplet number density and size at any time during the subsequent growth of the droplets is made using the transmission law. Uniqueness is assured by the requirement for internal consistency of the measurements at the two different wavelengths of light. These time-resolved measurements of particle size and concentration are described in detail by Cole, Dobbins, and Semerjian.[1] The final particle size is controlled by varying the number of nucleation cites added by passing the air admitted to the test chamber over a spark.

Acoustic pressure is measured by a modified microphone connected to the fixed end of the chamber by flexible tubing which does not transmit mechanical vibrations. Wall losses are measured by exciting the fundamental mode when the piston is fully extended. This test is performed after each run and wall attenuation was found to be 20% to 100% greater than theoretical wall losses probably because of several small external cavities. Two other quantities measured on a time-resolved basis are chamber pressure and volume.

The thermodynamic state of the fog is determined by subtracting the pressure of the known mass of dry air from the measured final pressure to obtain the vapor pressure. This calculation is performed by trial and error until consistent values of final temperature and vapor pressure are obtained as would result when thermodynamic equilibrium is achieved. All thermodynamic quantities can then be determined.

For most fogs created in the cloud chamber $\bar{\tau} \approx 1$ and $c_m \approx 10^{-2}$. The simplified results of the theory due to Cole and Dobbins[2] for $c_m << 1$ are therefore applicable. In this limit the viscous effects are unimportant and the attenuation of acoustic energy results from heat and mass transfer processes. We compare $\alpha a_o/\omega$ (where α = spatial attenuation coefficient for acoustic energy, a_o = speed of sound in the gaseous water vapor mixture, and $\omega = 2\pi$ times the acoustic frequency) vs. $\omega\tau_t/c_m$. The experimental data shows a scatter amounting to $\pm 15\%$ and, on the average, the data is about 35% below the theoretical curve. The cause of this deviation is not apparent. Both theory and experiment show that the maximum value of $\alpha a_o/\omega$ occurs when $\omega\tau_t/c_m = 1$. We discuss the implications of these results on acoustic signaling.

References

(1) Cole, J. E., Dobbins, R. A., Semerjian, H., "Time-Resolved Measurement of Droplet Size and Concentration in Cloud Chambers," J. Appl. Meteor., August 1970.

(2) Cole, J. E., Dobbins, R. A., "Propagation of Sound Through Atmospheric Fog," J. Atmos. Sci., May 1970.

THE RATE OF EVAPORATION OF SMALL WATER DROPS FALLING AT TERMINAL VELOCITY IN AIR

by

K. V. Beard and H. R. Pruppacher
Cloud Physics Laboratory, Department of Meteorology
University of California, Los Angeles, California

INTRODUCTION

The effect of forced convection on the mass and heat transport from a spherical body has been the subject of numerous investigations in the fields of meteorology, physics and engineering. The theoretical approaches to this problem have met with only limited success because a complete description of the physical process which necessitates a simultaneous solution of the Navier-Stokes equation of fluid flow and the differential equations for heat and mass diffusion has so far proven intractable. Acrivos and Taylor[1] and Rimmer[2] used Proudman and Pearson's singular perturbation technique to find the effect of ventilation on the heat transport from an isothermal sphere valid for $N_{Re} \ll 1$, where N_{Re} is the Reynolds number based on the drop diameter. Preliminary numerical calculations by Wood[3] solving simultaneously the Navier-Stokes equation of fluid flow and the equation of heat conduction have given results for heat transfer by forced convection for $N_{Re} = 0.01$, 0.1 and 1.0. Froessling[4], Zikmundova[5], Baird and Hamielec[6] and Garner and Keey[7] have used boundary layer theory that ignores ventilation in the wake and seems most adequate only for $N_{Re} > 500$. In the intermediate region $1 \leq N_{Re} \leq 500$, Kinzer and Gunn[8] and Abraham[9] have developed a theory involving the transient transfer of packets of fresh environmental air to the drop surface. This theory remains tenuous because it is based on approximations of the terminal relaxation time between successive packets and ignores important characteristics of the flow field around the drop. A large number of experimental studies on heat and mass transport from a sphere embedded in a still or moving viscous medium have been reported in literature (for reference see Beard[10]). Unfortunately, most of these studies only apply to $N_{Re} > 100$ and yielded results which scatter strongly, especially in the range $N_{Re} \leq 200$ where the mass transport rates differ by as much as 50%. In previous studies for $N_{Re} \leq 200$ only Kinzer and Gunn have avoided the questionable procedure of studying evaporation by supporting drops on wires, fibres or capillaries. However, their results derived from evaporation rates of water drops falling freely in still air remain, in particular for small drops, somewhat suspect due to inaccuracies inherent in their experimental setup and due to questionable values used for the drop surface temperature. Our own experimental investigation was carried out by studying the effect of ventilation on the rate of evaporation of water drops using the UCLA Cloud Tunnel in which the drops were freely suspended in a vertical, low turbulence airstream. It was our objective to measure the ventilation coefficient for mass transfer from a water drop as a function of N_{Re} and to derive from that rates of evaporation of cloud and rain drops for a wide range of atmospheric conditions. In meteorological literature there are two formulations used for the non-dimensional ventilation coefficient associated with mass transfer. Firstly, the ventilation coefficients may be given as the ratio of the ventilated mass transfer rate to the stationary rate $dm/dt = f_1 (dm/dt)_o$. This ratio is referred to as the wind factor by Froessling and is related to the standard chemical engineering quantity, the Sherwood number by the equation $f_1 = (1/2)N_{Sh}$. Kinzer and Gunn defined another ventilation coefficient F_1 which is related to f_1 by the equation $f_1 = 1 + F_1 (N_{Sc} N_{Re}/4\pi)^{1/2}$, where $N_{Sc} = \nu/D$ is the Schmidt number given as the ratio of the kinematic viscosity to the diffusivity of water vapor in air. Numerous correlations between experimental values of f_1 and the quantity $N_{Sc}^n N_{Re}^m$ reported in literature for the case of forced convection around drops evaporating in a gas or solid spheres dissolving in a liquid suggest strongly that $n = 1/3$ and $m = 1/2$.

EXPERIMENTAL SETUP AND PROCEDURE

The evaporation experiments were carried out in the UCLA Cloud Tunnel described in detail by Pruppacher and Neiburger[11] and Beard and Pruppacher[12]. Water drops consisting of doubly distilled, deionized and filtered water and of sizes ranging between 375 to 100 microns were introduced into the tunnel airstream and there kept stationary on the tunnel axis at a calibrated position so that the known tunnel velocity U was equivalent to the terminal velocity V of the evaporating drop. The drops were allowed to evaporate to radii as small as 27 microns. By using the cloud physics laboratory as a plenum, the air drawn into the tunnel remained at a constant temperature and relative humidity over several experimental runs, but varied over longer periods with local meteorological conditions. The temperature T of the tunnel air was measured by a thermocouple while the dew point temperature T_d was continuously monitored by a Cambridge-Systems Dewpoint Hydrometer. The position of the tunnel velocity valve was recorded as a function of time to provide a measure for determining the drop size. The evaporation rates of ventilated water drops were measured for $22 \leq T \leq 24$C and for a relative humidity of the air stream between 27 and 65%. From the quantities T, T_d, the air pressure and the chart record of the velocity valve setting the ventilation coefficient f_1 could be calculated from the expression $f_1 = 2C_1 A\, dA/dt$, where C_1 is a complicated function depending on T, T_d, the air pressure and the drop temperature T_a. The drop temperature was determined by a semi-empirical method described in detail by Beard. The drop size corresponding to a particular air velocity was computed on the basis of the drag relations given by Beard and Pruppacher and Le Clair et al[13]. The rate of change of the drop size was determined from the records of the tunnel valve setting. In this way $A\, dA/dt$ could be calculated. For the relative humidity range tested we were able to demonstrate theoretically that the terminal velocity of an evaporating drop is for all practical purposes the same as its terminal velocity at water vapor saturation. A least squares fit to our data

gave the linear relation $f_1 = 0.78 + 0.308\, N_{Sc}^{1/3} N_{Re}^{1/2}$ for the range $1.43 \leq N_{Sc}^{1/3} N_{Re}^{1/2} \leq 12.0$. For $N_{Sc}^{1/3} N_{Re}^{1/2} \leq 1.43$ an equation was found that satisfied the theoretical requirements $f = 1$ and $f' = 0$ (where f' is the slope of f) for $N_{Re} = 0$ that agreed with our linear formula at the common point $N_{Sc}^{1/3} N_{Re}^{1/2} = 1.43$ in both f and f' and was consistent with our experimental data in that range. This relationship can be expressed by $f = 1.00 + .108(N_{Sc}^{1/3} N_{Re}^{1/2})^2$. The estimated error for these formulae is ±5% for $N_{Sc}^{1/3} N_{Re}^{1/2} \leq .5$ decreasing to ±3% for the range $1.5 \lesssim N_{Sc}^{1/3} N_{Re}^{1/2} \lesssim 12$. Although the experiment provided data only in the range $27 \leq A \leq 375$ microns it is probably justifiable to extend the range of applicability to A = 500 microns or larger when considering the linear results of previous engineering investigations. The range of our results may also be extended toward smaller drop sizes, at least to A = 10 microns, below which the effect of drop curvature on the vapor pressure over the drop has to be taken into account.

RESULTS

Some selected results of our measurements and computations are summarized in Figs. 1 and 2. In fig. 1 our ventilation coefficients are compared with those of Ranz and Marshall[14] and with those of Kinzer and Gunn. We suspect that the higher values of Ranz and Marshall have resulted from disturbances in the flow field of the drop by the support capillary and from the presence of turbulence. The results of Kinzer and Gunn, widely reported in literature, are higher in the range $1 \lesssim N_{Sc}^{1/3} N_{Re}^{1/2} \lesssim 7$ and lower for $N_{Sc}^{1/3} N_{Re}^{1/2} \gtrsim 7$. We feel that these discrepancies are caused by difficulties inherent in their experimental technique. Kinzer and Gunn measured the time it took a drop to fall through successive distances and determined the velocity by a finite difference method. Such a method constitutes a considerable source of error which we eliminated by measuring the velocity more directly. It is further seen from Fig. 1 that as N_{Re} approaches zero our results smoothly approach $f_1 = 1$ and $f_1' = 0$. This is in qualitative agreement with Acrivos and Taylor and Rimmer. Our investigations also show that in the range $N_{Sc}^{1/3} N_{Re}^{1/2} \leq 1.43$ our values for f_1 compare favorably with the numerical calculations of Woo. As an example of the application of our results to cloud physics we have computed the height Z of a hypothetical cloud base from which drops of various initial radii fall in a NACA standard atmosphere reaching sea level with A = 100μ. These calculations were carried out on the basis of our computed ventilation coefficients and, for comparison, on the basis of those given by Kinzer and Gunn. The comparison shows that the distances using Kinzer and Gunn's results are on the order of 50% shorter. These discrepancies indicate that the deviations between the ventilation coefficients determined by Kinzer and Gunn and by us for the range $1 \lesssim N_{Sc}^{1/3} N_{Re}^{1/2} \lesssim 7$ are of cloud-physical significance. Because of the presence of soluble and insoluble matter in atmospheric cloud and rain drops it should be kept in mind that our results given in Fig. 2 represent the minimum fall distance based on a maximum evaporation rate of pure drops. Significant changes from our values are, however, only expected for fog and clouds formed over heavily polluted areas.

1. Acrivos, A. and T. D. Taylor, Phys. Fluids, 5, 387 (1962).
2. Rimmer, P. L., J. Fluid Mech., 32, 1 (1968).
3. Woo, S. W., Ph.D. Thesis, McMaster U., Hamilton, Ontario, Canada (1969).
4. Froessling, N., Gerlands Beitr. Geophysik, 52, 170 (1938).
5. Zikmundova, J., Proceedings Cloud Physics Conference, Toronto, 364 (1968).
6. Baird, M.H.I. and A.E. Hamielec, Can.J.Chem.Engr., 40, 119 (1962).
7. Garner, F.H. and R.B. Keey, Chem.Engr.Sci., 9, 119 (1958).
8. Kinzer G.D. and R. Gunn, J. Meteorol., 8, 71 (1951).
9. Abraham, F. F., J. Atmos. Sci., 25, 76 (1968).
10. Beard, K. V., Ph.D. Thesis, U. Calif., Los Angeles (1970).
11. Pruppacher, H. R. and M. Neiburger, Proceedings Cloud Physics Conference, Toronto, 389 (1968).
12. Beard, K. V. and H. R. Pruppacher, J.Atm.Sci., 26, 1066 (1969).
13. LeClair, B., Hamielec, A. and H. R. Pruppacher, J. Atmos. Sci., 27, 308 (1970).
14. Ranz, W.E. and W.R. Marshall Jr., Chem.Engr.Prog., 48, 141 (1952).

Figure 1

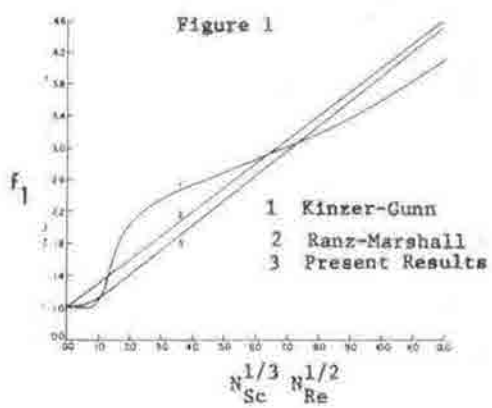

Figure 2

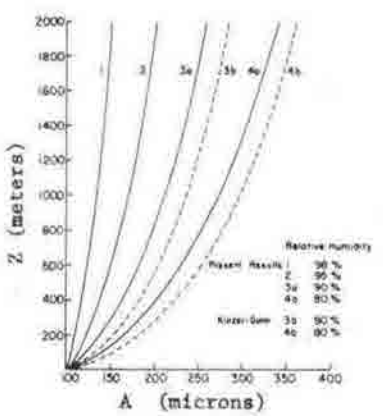

RETARDATION OF WATER DROP EVAPORATION WITH MONOMOLECULAR SURFACE FILMS

William D. Garrett
Naval Research Laboratory
Washington, D. C. 20390

There exists a large body of scientific literature concerned with the ability of monomolecular films to retard evaporation from plane water surfaces. Certain compounds, the n-alkanols, for example, have linear molecular configurations and form closely packed surface films which retard the passage of water molecules. An organic monolayer which has adsorbed at the surface of a water drop will assume a more closely packed orientation as the drop evaporates and the surface area contracts. In the case of hexadecanol-1, the surface film eventually becomes sufficiently compacted to retard the evaporation of the remaining water in the drop[1]. Other studies of water drop evaporation retardation by monolayers have been limited to the n-alkanols, fatty alcohols with linear molecular structures which can assume tightly packed, adlineated configurations under surface compression[2-4].

This property of surface films has been cited as justification for the hypothesis that airborne surface-active organic substances may stabilize sea fogs and haze through the formation of compressed films[5]. Film-forming material exists at the sea surface[6] and is transported into the marine atmosphere via bursting bubbles and spray[7]. A similarity in the ratios of specific fatty acids collected from the sea surface to those isolated from the ocean atmosphere strongly suggested that the sea is indeed a source of organic film-forming material[8]. However, a substantial portion of the recovered compounds had nonlinear molecular configurations or were weakly surface active. It was concluded that surface films formed from such mixtures might not exert a great influence in retarding the transport of water molecules across a water drop/air interface. Consequently, the goal of the present investigation was a controlled laboratory study of the effects of chemical structure on the ability of surface films to retard water drop evaporation. Both pure and mixed monolayers were applied to drops in controlled atmospheres to examine the influence of molecular configuration and nonlinear impurities on evaporation.

MATERIALS AND TECHNIQUES

Water drops (200-500 microns) were collected on 5 to 10-micron diameter spider webs and/or 15-micron diameter Teflon fibers mounted on a glass frame. The captured drops were produced as jet drops from air bubbles bursting at the surface of water contained in a glass-frit bubbler which produced 1-2 mm-diameter air bubbles. Pure monolayer-forming compounds spread at the air/water interface in the bubbler were effectively transferred onto the surface of the effected jet drops. For most compounds sufficient material was carried on the jet drop surface to immediately affect its evaporation rate without further concentration as the drop surface area decreased. The suspended drops were allowed to evaporate into open, quiet laboratory air at 25°C $\pm$ 0.2°C and 50 $\pm$ 2% relative humidity. Some experiments were performed at 30 $\pm$ 1% R.H. and the same temperature. Drop diameters were measured microscopically using a calibrated eye-piece. The pure compounds (Table I) were selected to provide a wide variety of molecular shapes, since molecular geometry as well as carbon chain length influences the ability of a close-packed monolayer to inhibit the evaporation and recondensation of water molecules. Essentially straight lines resulted when the square of the droplet radius (r) was plotted against time (t). This relationship was valid for both clean water and film-covered drops.

MONOLAYER EVAPORATION RETARDATION ON WATER DROPS

Average evaporation rates of at least 5 drops were determined for each monolayer system from the slope of r^2 vs. t plots (Table I) expressed as $-r\ dr/dt(10^7 cm^2/sec)$. The initial drop size did not influence the evaporation rate once the surface film had been compacted by the decreasing drop surface to a point where its molecules were packed tightly and evaporation was slowed. Molecules containing straight hydrocarbon chains were most effective in reducing the rate of evaporation (Table I). These included the n-alkanols, methyl heptadecyl ketone and glycerol tristearate. Structural deviations from linearity in the molecule which prevented adlineation gave expanded surface films which produced little decrease in the evaporation rate. Monomolecular films which did not effectively retard evaporation contained the following substituent groups: chemical unsaturation (cis or trans double bonds, e.g., oleic acid, oleyl alcohol, elaidic acid and glycerol trioleate), hydroxyl groups and any group which increased the cross-sectional area occupied per molecule over that for a vertically oriented $(CH_2)_n$ chain, i.e., about 20 A^2/molecule.

The most impermeable surface film, 1-docosanol, produced a 17-fold decrease in evaporation rate over that of distilled water. Cetyl alcohol (1-hexadecanol), the most widely used evaporation-reducing chemical, yielded a 9.1-fold reduction in rate at 25°C and 50% R.H. This value agrees well with the results of Deryaguin et al[1] who reported a 10-fold increase in drop lifetime in the presence of cetyl alcohol at about the same conditions of temperature and relative humidity.

The inclusion of nonlinear impurities into a monolayer which retards evaporation has been considered by La Mer[9]. Molecules such as benzene constituted molecular holes in the film and as little as one percent of this compound could reduce the retardation efficiency of a monolayer by 90 to 99 percent. For a mixed monolayer composed of two components, both of which retarded evaporation, the

specific evaporation resistance for the mixed film was best expressed by

$$\ln r_{12} = X_1 \ln r_1 + X_2 \ln r_2 \qquad \text{where}$$

X_1 and X_2 are the mole fractions of the constituents of the binary film and r is the specific evaporation resistance which was defined as proportional to $(t/m_f - t/m_w)$ with t/m being the reciprocal evaporation rate; the subscripts f and w referring to film-covered and clean water surface, respectively.

TABLE I

MONOMOLECULAR FILM	AVERAGE VALUE OF $-r\ dr/dt\ (10^7\ cm^2/sec)$
-----	19.4
9-Octadecen-1-ol (cis)	19.5
9,10-Dihydroxyoctadecanoic Acid	19.3
9-Octadecenoic Acid (cis)	19.3
Tri(cis-9-Octadecenoate) Glycerol	19.1
9-Octadecenoic Acid (trans)	18.6
12-Hydroxyoctadecanoic Acid	16.6
Tetradecanoic Acid	14.4
1-Tetradecanol	5.0
2-Octadecanone	4.8
1-Hexadecanol	2.2
1-Heptadecanol	2.0
Trioctadecanoate Glycerol	1.8
1-Docosanol	1.1

The influence of impurities which do not retard evaporation when present in a monolayer composed of linear alkanols was determined by measuring the evaporation of drops coated with monolayers composed of varying proportions of octadecanol-1 and 9-octadecen-1-ol. The former compound has a linear molecular structure, and its monolayer retards evaporation significantly (Table I) while the latter molecule is permanently bent, occupies a greater surface area, does not pack closely at high film pressure and does not affect the evaporation rate. The logarithm of the average evaporation characteristic (-r dr/dt) of the mixed monolayers are plotted against the mole fraction, X_b, of the 9-octadecen-1-ol. The resulting linear relationship is in accord with the La Mer equation even though the resistance of one of the two compounds is zero. Thus, the presence of a few percent of a branched-chain compound of the same carbon-chain length does not reduce the effectiveness of an alkanol monolayer significantly. This result contrasts with the dramatic effects of the benzene impurity cited by La Mer[9]. It can be estimated that the 40% unsaturated compounds (fatty acids) identified by Barger and Garrett[8] in marine aerosol samples would cause a 65% decrease in the specific evaporation rate over that for a monolayer composed of linear surface-active compounds.

CONCLUSIONS

Recently several authors[10,11] have considered the effects of surface films on small drop evaporation. These authors correctly assumed that adsorbed monomolecular films could alter evaporation rates but tacitly treated all such films as being equally effective. No consideration was given to the effects of chemical structure of the molecular constituents of the film, an effect made evident from the results of Table I. From the discussion in this paper on mixed films and the work of Barger and Garrett[8], we concluded that there are sufficient nonlinear impurities in natural surface films of marine origin to drastically interfere with their ability to retard evaporation, although some water might remain physically trapped in the thick-film portion of the remaining organic matrix.

In conclusion, the evaporation of water drops can be slowed by certain monomolecular films containing a preponderance of linear molecules. Natural films probably do not inhibit evaporation to a significant extent, but organic residues of low volatility possibly containing occluded water remain after evaporation of the major portion of the drop. However, the data in this paper indicate that fogs can be stabilized with artificial injections of specific film-forming agents which retard evaporation.

REFERENCES

1. Derjaguin, B. V., V. A. Fedoseyev and L. A. Rosenzweig, 1966: J. Colloid Interface Sci. 22, 45-50.
2. Eisner, H. S., B. W. Quince, and C. Slack, 1960: The Physical Chemistry of Aerosols, Aberdeen Univ. Press, Ltd., Aberdeen, pp. 86-95.
3. Jiusto, J. E., 1964: Cornell Aeronautical Laboratory Report RM-1788-P-4, 61 pp.
4. Snead, C. C. and J. T. Zung, 1968: J. Colloid Interface Sci. 27, 25-31.
5. Goetz, A., 1965: Proc. Int. Conf. on Cloud Physics, pp. 42-45, Tokyo and Sapporo, Japan.
6. Garrett, W. D., 1967: Deep-Sea Res. 14, 221-227.
7. Blanchard, D. C., 1964: Science 146, 396-397.
8. Barger, W. R. and W. D. Garrett, 1970: Accepted for publication in J. Geophys. Res.
9. La Mer, V. K., ed., 1962: Retardation of Evaporation by Monolayers, New York, Academic Press, 277 p.
10. Shih, Y. and D. R. Coughanowr, 1968: AICHE Journal 14, 502-504.
11. Smith, J. G., J. L. Kassner and A. H. Bierman, 1968: J. Recherches Atmospheriques 6, 41-44.

EVIDENCE FOR INCREASED EVAPORATION OF WATER DROPLETS DUE TO SURFACE CONTAMINATION

J.F. Stampfer, Jr., R.B. Hughes, H.A. Duguid
University of Missouri - Rolla
Rolla, Missouri

INTRODUCTION

The evaporation of droplets coated with insoluble films has been studied both experimentally[1,2,3] and theoretically[4,5,6,7]. All the direct experimental evidence has shown, as would be expected by comparison with plane surfaces (e.g. 8), a decrease in the rate of evaporation. However, both Rooth[5] and Derjaguin et. al[6,7] have noted that the rate might be greater if the condensation coefficient were greater for the coated drop than the pure drop. Indirect evidence for this effect may be found in Izmailova, Prokhorov and Derjaguin[9], Tovbin and Savinova[10], and Pueschel, Charlson and Ahlquist[11]. Leonov and Prokhorov[12] have demonstrated an increased evaporation rate for suspended droplets which had been treated with various soluble surface active materials (SAM).

With this brief background, we would like to present evidence for an increased rate of evaporation at 30°C for freely-falling, micron-sized water droplets which have been treated with an insoluble SAM, either dodecanol or hexadecanol. This increased rate appears to prevail for the life-time of the droplet (at least to the limit of our experimental capability which is approximately 6μ) and to be brought about by an amount of SAM which allows less than full surface coverage.

EXPERIMENTAL

Drops were allowed to form in a thermal diffusion cloud chamber on the nuclei present in room air which had been introduced into the chamber. They then fell into a drift tube, previously humidified to a known value, which was immersed in a constant temperature bath at 30°C. The drops were photographed at 0.5 second intervals and from the position in adjacent frames the average size was calculated from Stokes law. The room air was introduced either directly through an 8μ Millipore filter or through a train consisting of a trough, which could be heated, containing the SAM, a glass "equilibration" chamber and an "absolute" filter (MSA Ultra Filter Type "H").

For diffusion controlled evaporation, Maxwell's rate equation can be written in the approximate form $da^2/dt = k\Delta T + I$, where a is the radius of the drop, ΔT the dew point depression, and k and I constants for a given ambient temperature. Figure 1 shows the data for 300 "untreated" drops, which are considered to be those drops formed in air which passed through the Millipore filter only or through the train when it was at room temperature. The line marked "Maxwell" was drawn using the above equation and values for k and I of 17.8 μ^2/sec^oC and zero respectively. The line marked "These Data" was computed by the method of least squares.

Figure 2 shows the data obtained for 182 drops formed in air which had been passed through the trough containing dodecanol when it was heated to temperatures greater than 80°C. The line marked "these data" was again computed by the method of least squares. The other line is the data curve from figure 1. The data points indicated by triangles are those obtained when hexadecanol rather than dodecanol was used and the trough was at a temperature higher than 100°C.

DISCUSSION

Despite the scatter in these data, we believe it is evident that treatment of the air in which the drops formed increased the average rate of evaporation of the droplets. Under the conditions of these experiments, high relative humidities, the increase is relatively large and, within experimental error, independent of the dew point depression. Although a large number of questions, both experimental and theoretical remain unanswered, we would like to make the following observations.

The sizes of the particles which emerged from the absolute filter were measured with an optical particle analyzer. These results indicated that in the cloud chamber there would be fewer than two particles greater than 0.5μ. If it is assumed the nuclei on which the drops formed were 0.5μ and pure dodecanol, both apparent upper limits, and each dodecanol molecule provided 20 $Å^2$ coverage of the drop surface, then the surface of a 10μ drop would be about 10% covered. Although it is possible that some SAM could be adsorbed from the vapor, considering the data from (2), it is believed that this would be a small amount at best. Considering the small quantities of SAM which appear to be involved, the scatter in the data for contaminated drops is not unreasonable. Furthermore, if the atmospheric aerosol contains SAM, a reasonable assumption, the scatter in the "pure" data is also explainable.

Anytime the rate of evaporation of an object moving with respect to the medium is considered, there is the possibility of ventilation. It is usually considered that in the case of small water droplets moving with their terminal velocities, ventilation is not a significant factor. That the small amount of SAM present could change the surface characteristics enough to cause increased ventilation is improbable.[13,14].

The more modern theories of evaporation[15,16,17] predict that the evaporation rate is a function of both the droplet size and the condensation coefficient. The rate should decrease as the drop size and condensation coefficient decrease and should always be less than the rate calculated using the Maxwell equation. Our data for pure drops do not show this size dependence and, if anything, our rates exceed the Maxwellian rate. This again might be explained by contaminants introduced by the condensation nuclei. For the doped drops, the rates are higher still.

Assuming the evaporation is controlled by Fickian diffusion, the increased evaporation rates could be explained by a 0.06°C higher drop temperature. However, as increased evaporation should cool the drop even more, this appears to be an improbable explanation. A change in the thermal accommodation coefficient due to the presence of SAM might explain a higher temperature but this would require the coefficient for pure water to be less than one.

One factor which cannot be ignored, but the possible effect of which is unknown, is the manner in which the drops are formed. Assuming that the condensation nuclei are dodecanol, the drops must start out with the water covering the alcohol. Although it is further assumed that the alcohol quickly diffuses to the outside of the drop, leaving an interior composed of alcohol saturated water, this is not proven.

ACKNOWLEDGMENTS

This research was supported by the Atmospheric Sciences Section, National Science Foundation, NSF Grant GA-1509

REFERENCES

1. Eisner, H., B Quince and C. Slack, 1960: The stabilization of water mists by insoluble monolayers. Disc. Far. Soc., 30, 86-95.
2. Derjaguin, B.V., V.A. Fedoseyev, L.A. Rosenzweig, 1966: Investigation of the adsorption of cetyl alcohol vapor and the effect of this phenomenon on the evaporation of water drops. J. Coll. Sci., 22, 45-50.
3. Snead, C.C. and J.T. Zung, 1968: The effects of insoluble films upon the evaporation kinetics of liquid droplets. J. Coll. and Interface Sci. 27, 25-31.
4. Bradley, R.S., 1955: The rate of evaporation of micro-drops in the presence of insoluble monolayers. J. Coll. Sci., 10, 571-575.
5. Rooth, C., 1957: On a special aspect of the condensation process and its importance in the treatment of cloud particle growth. Tellus 9, 372-377.
6. Derjaguin, B.V., S.P. Bakanov and I.S. Kurghin, 1960: The influence of a foreign film on evaporation of liquid drops. Disc. Far. Soc. 30, 96-99. See also 1960, Dokl. Akad. Nauk SSSR, 135, 1417-1420; 1961, Kolloid Zhur., 23, 262-271.
7. Derjaguin, B.V., and I.S. Kurghin, 1964: Non-stationary evaporation of a droplet covered by an adsorbed layer. Dokl. Akad. Nauk SSSR 155, 644-646.
8. La Mer, V.K. (Ed), 1962: Retardation of Evaporation by Monolayers Academic Press, New York.
9. Izmailova, G.I., P.S. Prokhorov and B.V. Derjaguin, 1957: The possibility of surface activation and passivation of nuclei in water vapor condensation. Kolloid Zhur 19, 557-561.
10. Tovbin, M.V. Savinova, 1957: The kinetics of non-steady state processes at the liquid-gas interface. Zhur. Fiz. Khim., 31, 2717-2719.
11. Pueschel, R.F., R.J. Charlson and N.C. Ahlquist, 1969: On the anomalous deliquescence of sea-spray Aerosols. J. Appl. Met. 8, 995-998.
12. Leonov, L.F., P.S. Prokhorov, 1967: Influence of surface-active substances on the evaporation of five water drops. Izvestiya Akad, Nauk SSSR, 4, 735-742.
13. MacRitchie, F., 1968: Role of monolayers in retardation of evaporation. Nature 218, 669-670.
14. MacRitchie, F., 1969: Evaporation retarded by monolayers. Science 163, 929-931.
15. Fuchs, N.A., 1959: Evaporation and Droplet Growth in Gaseous Media. Pergamon Press, New York.
16. Monchik, L., and H. Reiss, 1954: Studies of evaporation of small drops. J. Chem. Phys. 22, 831-836.
17. Okuyama, M., and J.T. Zung, 1967: Evaporation-condensation coefficient for small droplets. J. Chem. Phys. 46, 1580-1585.

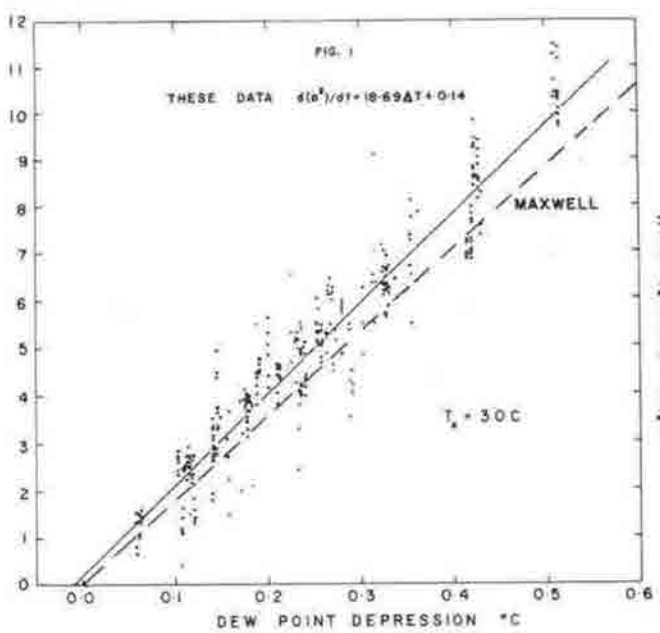

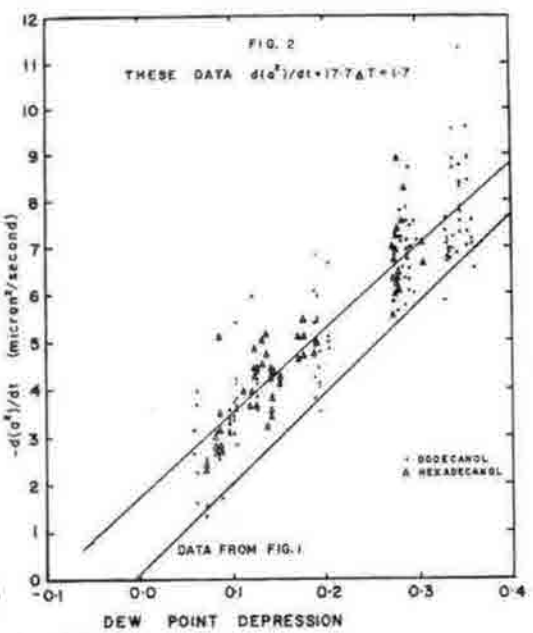

OBSERVATIONS OF STRATUS DROPLET SPECTRA*

By, F. L. Ludwig
Stanford Research Institute
Menlo Park, California 94025

Particle and droplet size distributions were obtained in stratus in the hills south of San Francisco using a light-attenuation type condensation nuclei counter for estimates of the numbers of small particles; a light-scattering particle counter (Royco Instruments, Menlo Park, Calif. Model PC 200A) for particle and droplet concentrations in 14 size ranges between 0.34 μ and 6.9 μ; and a horizontal gravimetric droplet elutriator for size distributions of droplets with $r > 8\,\mu$. The instrumentation and sampling procedures used on this program have been described in detail elsewhere.[1] Measurements were made at two ground level locations. One location, "Skyline," is on a ridge at an elevation of about 300 m about 8 km east of the coast. The "Bear Gulch" site is at almost 600 m elevation west of the crest of the hills and about 10 km inland. Sampling was generally limited to periods with westerly winds. Very little habitation is upwind. Skyline sampling was accomplished during the summers of 1968 and 1969, and Bear Gulch sampling, the summer of 1968. Because most data collection was done in the morning, we have more information from periods of cloud dissipation than during cloud formation.

Size distributions from Bear Gulch are shown in Figure 1. Small particle counts are included by assuming that they represent the particles with $0.01 \leq r \leq 0.1\,\mu$. (cf., Junge et al.[2]). The "cloud" curve shows the average of almost 8 hours of sampling; the "dissipating" and "forming" curves, about 3 hours and 1/2 hour, respectively. The forming data are for periods where stratus reappeared, rather than an initial onset. All the distributions show primary modes at condensation nuclei sizes. A secondary mode is found in the cloud and during its dissipation at about 6 μ radius, with a frequency of about 1.3 droplets $cm^{-3}\mu^{-1}$ in the cloud and about 1.8×10^{-1} during dissipation. Below 1 μ, there is little difference between the cloud and dissipating size distributions. The cloud formation curve does not show a distinct secondary mode, but does change slope substantially at $r \approx 1\,\mu$.

Skyline site size distributions are shown in Figure 2. About 2-1/2 hours of evening observations are averaged for the formation curve; about 7 morning hours for the dissipation; and about 36 hours for the cloud curve. The developed cloud size distribution has a secondary mode of about 3 droplets $cm^{-3}\mu^{-1}$ at $r \approx 5\,\mu$. The Skyline cloud dissipation average has a mode of about 0.8 droplets $cm^{-3}\mu^{-1}$ at a radius of about 8 μ. As expected, there are more small particles during cloud formation and more large droplets during dissipation.

Figure 3 shows Neiburger and Chien's[3] calculated distribution, using a 6° C/hr cooling rate. This is one of two stratus cases they simulated numerically; both give similar spectra. The initial particle size distribution is given for 0 seconds; it has fewer particles than found in this program. The observed and calculated distributions differ most at the secondary mode. The observed spectra show only a few percent as many droplets as the calculated distributions. At 20 μ, there is better agreement. Individual observations often had frequencies greater than 10 droplets $cm^{-3}\mu^{-1}$, and several 1-hour averages have shown values of about 50 $cm^{-3}\mu^{-1}$. Neiburger and Chien's cooling rate is greater than those observed, which could account for the high calculated numbers of droplets.

Time sections of the particle spectra were prepared to show temporal variability. In Figures 4 and 5, the isopleths of constant frequency are logarithmically spaced and the interpolation between nuclei counter data and Royco data is shown by dashed lines for $r < 0.3\,\mu$. The analysis for sizes larger than 7 μ is from elutriator data. Small particle counts and data from the Royco channels were collected at about 15 minute intervals; elutriator data at intervals of about 20 minutes to 2 hours.

Figure 4 shows the size distribution changes accompanying the onset of stratus on September 5, 1969. The numbers of small particles ($0.1 \leq r \leq 1\,\mu$) changed little, but the numbers for $r > 1\,\mu$ increased with the onset of saturation, marking the appearance of stratus at the site. A secondary mode (marked by +++) did not occur until about 1845; then it was short-lived. Another mode occurred from about 1905 until 2200, weakening at later times. Within 5 minutes after this observation period, the stratus suddenly withdrew toward the west and dropped below the level of the Skyline site.

On September 11, 1969, a partial solar eclipse occurred, obscuring about 2/3 of the sun's disc. Figure 5 shows the air was slightly unsaturated initially, and had a weak secondary mode at 5 μ. With saturation, a minimum of less than 1 droplet $cm^{-3}\mu^{-1}$ developed at 2 μ, making the 6 μ mode more

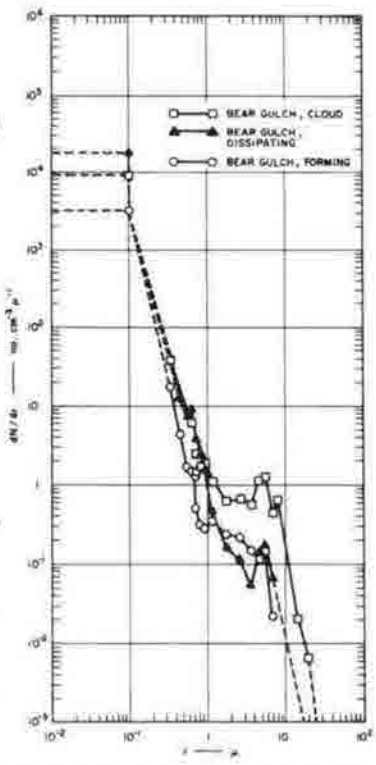

FIG 1 AVERAGE SIZE DISTRIBUTIONS AT VARIOUS STAGES OF STRATUS DEVELOPMENT AT BEAR GULCH

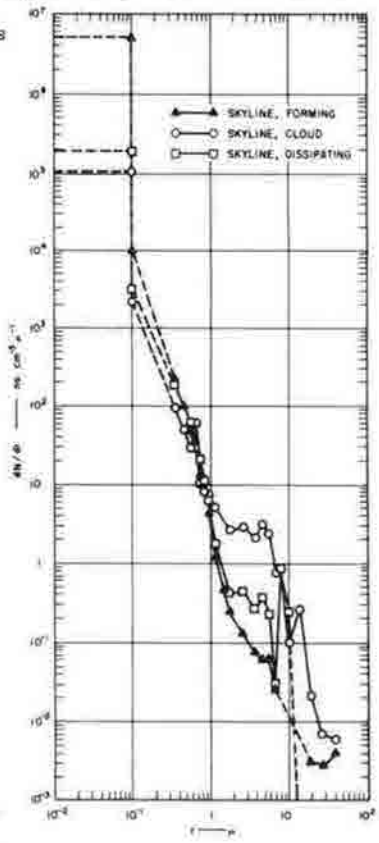

FIG 2 AVERAGE SIZE DISTRIBUTIONS AT VARIOUS STAGES OF STRATUS DEVELOPMENT AT SKYLINE

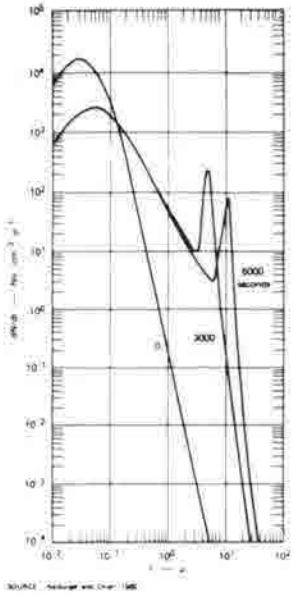

FIG 3 CALCULATED STRATUS DROPLET SIZE DISTRIBUTIONS

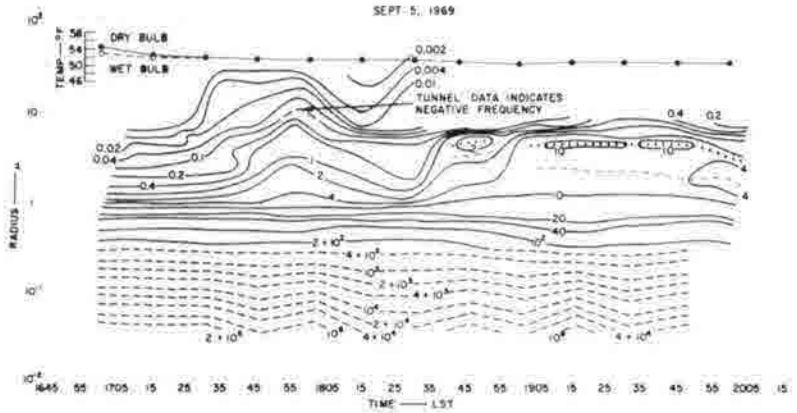

FIG 4 VARIATIONS OF THE SIZE DISTRIBUTION AT SKYLINE, SEPTEMBER 5, 1969, EVENING

pronounced. At 0915 the numbers of droplets larger than 5 μ began to decrease; this continued until the air temperature reached a maximum at 0945. With the eclipse-caused cooling, the numbers of droplets increased and weak secondary modes developed. Then the modal size decreased from about 4 to about 2.5 μ, the numbers of droplets with $r > 1$ μ declined, and the cloud disappeared as heating resumed toward the end of the eclipse.

In general, the analyzed cases have not shown the regular growth patterns during onset of stratus that Neiburger and Chien calculated. This may be because of the advective nature of the clouds, and the mixing that accompanies the advection. With mixing, all droplets in stratus do not have the same history;[4] droplets are removed and fresh nuclei introduced. This gives a broader secondary mode and stabilizes it so that it doesn't continue to grow to larger sizes.[4] This is consistant with the observations.

References

1. Ludwig, F. L. and E. Robinson, 1970: Observations of Aerosols and Droplets in California Stratus. Tellus, 22, pp. 94-105.
2. Junge, C. E., E. Robinson, and F. L. Ludwig, 1969: A Study of Aerosols in Pacific Air Masses. J. Appl. Meteorol., 8, pp. 340-347.
3. Neiburger, M., and C. W. Chien, 1960: Computations of the Growth of Cloud Drops by Condensation Using an Electronic Digital Computer. Geophys. Monograph No. 5, pp. 191-209.
4. Mason, B. J., 1960: The Evolution of Droplet Spectra in Stratus Cloud. J. Meteorol., 17, pp. 459-462.

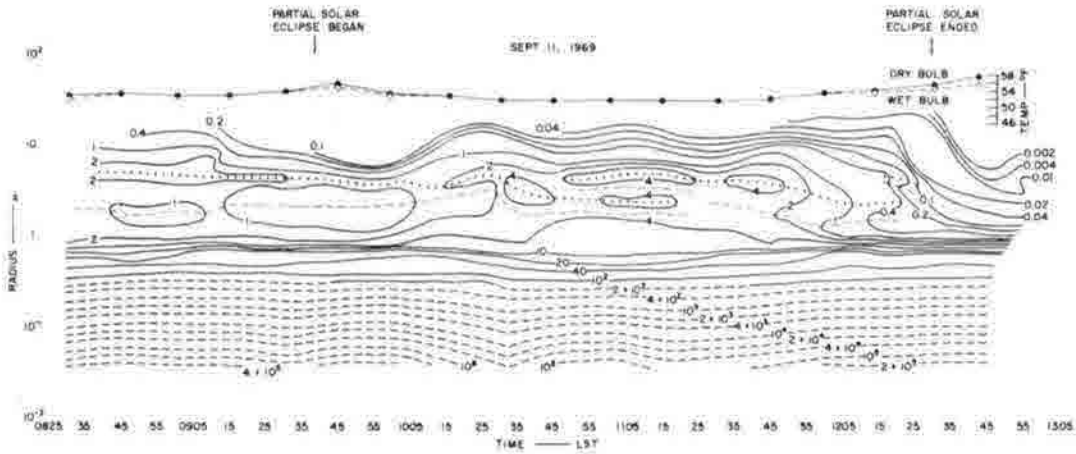

FIG 5 VARIATIONS OF THE SIZE DISTRIBUTION AT SKYLINE, SEPTEMBER 11, 1969, MORNING

* The work described in this paper has been supported by the Army Research Office-Durham under Contract No. DAHC04-67-C-0059.

DROPLET WAKE EFFECT

Larry R. Eaton

Desert Research Institute
Lab. of Atmospheric Physics
Univeristy of Nevada
Reno, Nevada 89507

INTRODUCTION

As the Reynolds number (Re) increases from zero, the flow around droplets becomes asymmetric. The effect due to the droplet extends further back from the droplet than forward. Thus, two droplets, one following the other, no longer experience equal and opposite effects for nonzero Re. The final result is that the back droplet moves faster than the forward droplet depending on the Re, drag coefficient, and interdroplet spacing.

Nonlinearity of the hydrodynamic equation has prevented complete analytical solutions of this two body problem while numerical techniques are unwieldy in space and time even for present computers.

This presentation is concerned with the experimental measurement of this wake effect on equal-mass fluid droplets in free fall for separations of 50 to 600 diameters.

The Reynolds numbers ranged from 20 to 80 ($300<d<500$ microns) for the ethylene glycol droplets in free fall at ambient room conditions.

EXPERIMENTAL ARRANGEMENT

Figure 1 is a flow diagram of the droplet generation, control, detection and data processing. Further description can be found in the paper by Eaton and Hoffer (1).

Ethylene glycol was used for the liquid droplets to minimize evaporation and thus permit accurate measurement of the effects due to the droplet wake.

At 20C, the fluid characteristics were; density 1.111g/ml, viscosity 21 centipoises, and specific heat 0.561 cal/g/c.

Evaporation and water absorption of ethylene glycol was measured to be less than 0.01% during the two seconds that the droplets were in free fall.

Temperature was continuously recorded at 60 cm intervals along the 3.5 meter insulated column.

PROCEDURE

Data was collected in the following way.

For a given droplet size, 36 single droplets were permitted to fall through the column at five second intervals (>6M separation) to obtain terminal velocities of single droplets which, from previous experiments, gave droplet size.

Droplet pairs were then released with known initial separation with more than five seconds elapsed time between the release of consecutive pairs. The data from eighteen such pairs were combined and fitted with polynomials to give position versus time for the front and rear droplet. These polynomials then gave the desired relative velocity as a function of droplet separation.

RESULTS

Figure 2 gives the results obtained for large separations of droplet.

Droplets with initial separations of less than 20 diamters were detected to coalesce giving a terminal velocity related to a single droplet but of double mass as compared with the original droplets.

For separations of 20 to 50 diameters, droplets either coalesced, moved horizontally out of the wake or actually passed each other then moved out of the wake influence.

The solid curve in Figure 2 (Reference 2) indicated that the theoretical results differ by a factor greater than two from the measured effect of the wake.

REFERENCE

1. Eaton, L.R. and T.E. Hoffer, 1970: Experiments on Droplets in free fall I: Terminal velocity and wall effects. J. Appl. Meteor., 9, pp. 269-275.

2. Happel, J. and H. Brenner, 1965: Low Reynolds Number Hydrodynamics. Englewood Cliffs, N.J., Prentice-Hall., pp. 553.

ACKNOWLEDGMENT

This research was made possible by the Office of Naval Research under Contract Nonr 4945(00) NRO 82 226.

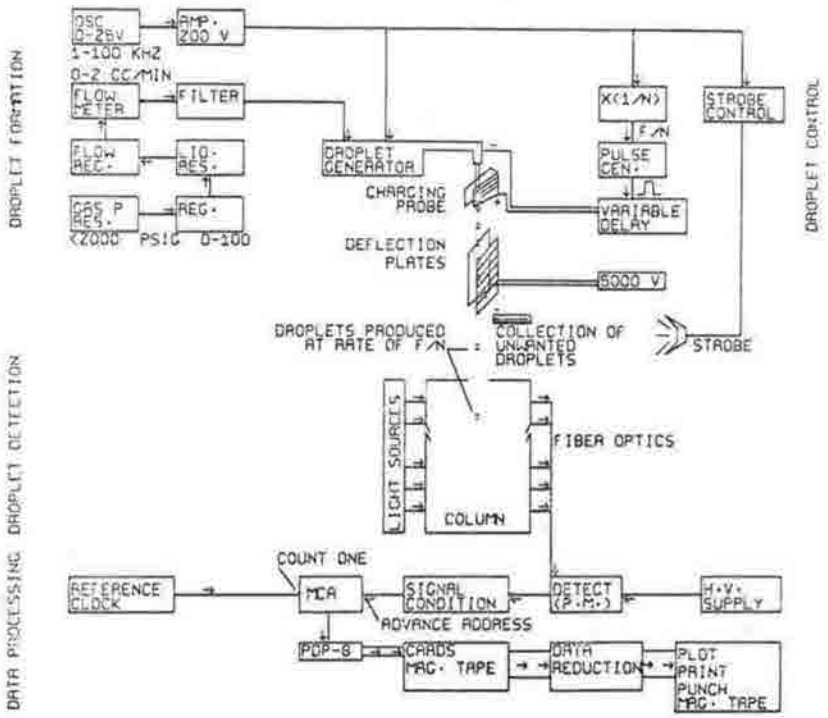

FIGURE I. Flow Diagram

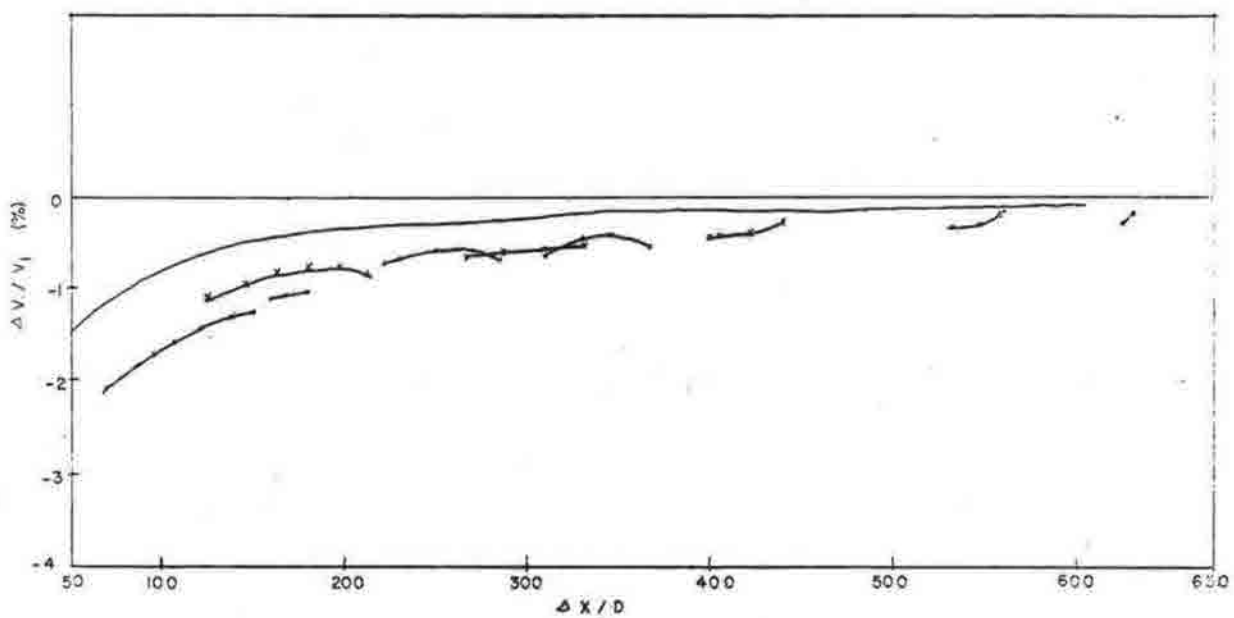

FIGURE 2. Relative velocity versus droplet separation. The continuous curve is from the equation due to Happel and Brenner (2) (After Dahl).

A TECHNIQUE FOR THE EXPERIMENTAL MEASUREMENT OF COLLECTION EFFICIENCY

J. R. Adam and R. G. Semonin
Illinois State Water Survey
Urbana, Ill.

INTRODUCTION

Aerosols are removed from the air by precipitation in three different ways: the impaction and capture, or collection, of particulates by raindrops; the consumption of particulates as condensation nuclei; and the attachment of particulates to cloud and raindrops by Brownian motion. It has been calculated theoretically[1] and determined experimentally[2] that impaction and capture is an efficient process for the removal of particles larger than a few microns diameter. However, extrapolation of these results to submicron size particles shows effectively zero removal by this method. In an attempt to extend the range of experimentally determined collection efficiency of a raindrop for particles below one micron, a new technique incorporating a biological aerosol of the type used by Sood and Jackson[3] to study scavenging by snow has been devised.

EXPERIMENTAL APPARATUS

The experimental apparatus, as shown in Fig. 1, consists of an aluminum raindrop acceleration tower 12.2 m tall and one meter in diameter. The lower two meters of the tower is sealed to form an aerosol chamber. The relative positions of the chamber trap doors, the aerosol atomizer, and the sampling tube are also shown.

A drop generator is mounted within the tower at a height chosen to insure that the drops achieve terminal velocity before entering the aerosol chamber. Drops larger than 2 mm diameter are dripped from a hypodermic needle. Smaller drops are blown from the tip of a capillary tube using the generator shown in detail in Fig. 1. The drop size is determined by both volumetric collections and direct optical measurement. The drops can be charged electrically by induction and the charge magnitude measured with a coulombmeter.

The amount of submicron particulate matter scavenged by a single simulated raindrop passing through the aerosol chamber is very small. Detection difficulties have been overcome by the use of bacteria spores as the aerosol constituent. After passing through the aerosol, the scavenging drop is collected on a petri dish, incubated, and the colonies originating from the individual spores are counted. Bacillus subtilis spores are presently being used. These spores are rod shaped, being 0.7 μm in diameter by 1.2 μm long. An aerosol of the spores is formed by atomizing a dilute aqueous solution of the spores with pressurized air. Extreme care is taken to insure that the spores are monodisperse. The aerosol concentration is determined at various times during an experimental run by passing a known volume of air through a midget impinger whose collection efficiency for the spores has been determined.

A typical experimental run proceeds as follows. The drop generator is positioned and adjusted to produce a specific size drop falling at terminal velocity within the aerosol chamber. The aerosol is then generated. The initial concentration is approximately 800 spores per cc and decays exponentially with a half-life of about 40 minutes. The next approximately 15-30 minutes of the highest aerosol concentration are divided into various series of drop collections. An aerosol concentration measurement is made at the beginning and end of each series. Within each series, a large number of drops with or without electrical charge are passed through the aerosol. Each drop is collected on a petri dish placed 1.2 m below the aerosol chamber. The dishes are then incubated long enough for each spore to develop into a colony of cells approximately 30 μm diameter. At this size the colonies are large enough to be easily counted optically with a microscope but do not overlap and lose their individual identities. The collection efficiency defined as the ratio of the number of particulates scavenged from the aerosol to the total number in the volume through which the drop falls is then calculated for each drop.

To obtain accurate experimental results, several precautions must be taken. To insure a clean environment before the experimental run begins, the area around the tower is cleaned and disinfected. The tower and aerosol chamber is ventilated with clean air to remove residual spores and dust. All glassware and agar, and the drop generator and its water are autoclaved. Control air samples are taken around the tower and chamber to obtain a background spore concentration. The concentrated spore solution is prepared and atomized by someone other than the experimenter to further reduce the possibility of contamination.

EXPERIMENTAL RESULTS

The collection efficiency for uncharged drops is shown in Fig. 2. The results shown are the average collection efficiency for over 50 drops of each size, produced, collected, and examined individually. The increase in collection of the uncharged aerosol by charged drops is shown in Fig. 3. The scavenging efficiency increases linearly with increasing charge from its value in the uncharged case (correlation coefficient greater than 0.95).

In all cases, the aerosol charge was monitored and no charge greater than 10^{-16} coulombs per spore was observed. Only for the 3.74-mm drops was there any tendency for increased collection with one sign of charge. This would indicate that possibly the aerosol had a small net charge for this run.

CONCLUSIONS

The experimental technique described is both accurate and sensitive for measuring collection efficiencies. The ease of generation, detection, and decontamination, the uniformity of size, and the ease of concentration determination makes bacteria spores well suited as the aerosol particulate. The only difficulty encountered is finding other suitable spores, smaller than 1 μm, which are viable after atomization and which have a relatively low natural occurrence.

Using the measured scavenging efficiencies, an estimate of the amount of material in the 1-μm size range removed by natural rain can be made. It is assumed that rainfall has a Marshall Palmer drop distribution for drops greater than 0.5 mm; they are uncharged, and they are falling at terminal velocity. A single calculation then shows that less than 1% of the particulates are removed per hour in a 5 mm per hour rain, and only 4.5% are removed in a 100 mm per hour rain.

Acknowledgments

The authors would like to thank Mr. Tony Rattonetti for his help in performing the experimental measurements reported. This research was sponsored by the AEC under contract AT(11-1)-1199 and by the NSF under grant GA-4576.

REFERENCES

1. Langmuir, I. and K. B. Biodgett, 1945: Mathetical Investigation of Water Droplet Trajectories. G. E. Research Lab. Rept. No. RL-225, 66 pp.
2. Engelmann, R. J., R. W. Perkins, D. I. Hagen, and W. A. Haller, 1966: Washout Coefficients for Selected Gases and Particulates, Battelle-Northwest Labs. Rept. No. BNWL-SA-657, 22 pp.
3. Sood, S. K., and M. R. Jackson, 1969: IIT Research Institute Rept. No. IITRI-C6105-6, 36 pp.

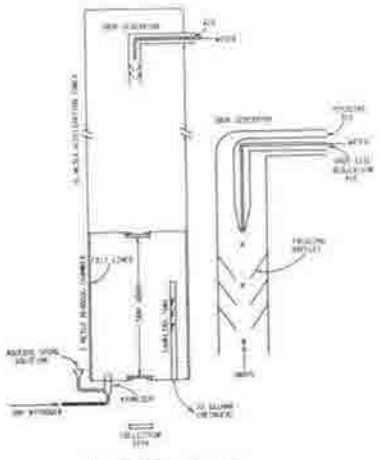

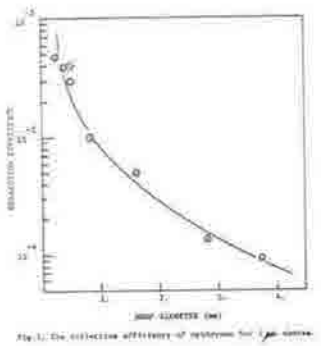

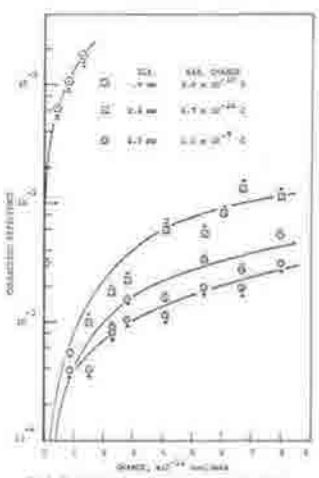

A WIND TUNNEL INVESTIGATION OF COLLECTION KERNELS

by

K. V. Beard and H. R. Pruppacher
Cloud Physics Laboratory, Department of Meteorology
University of California, Los Angeles, California

INTRODUCTION

The growth rate of cloud drops to rain drops by means of the collision-coalescence process has been studied theoretically on the basis of a continuous growth model, and more recently based on a stochastic model for discrete accretion by many investigators. Models of the type discussed by these investigators require a knowledge of the collection kernel $K = \pi(a+A)^2 E_1 E_2 (V-v)$, where a is the radius of the small drop falling with the velocity v, A the radius of the large drop falling with velocity V, E_1 the collision efficiency and E_2 the coalescence efficiency. Usually it is assumed that $E_2 = 1$. The collision kernel can then be written $K = \pi y_c^2 A^2 (V-v) = W\pi A^2$, where $W = y_c^2 (V-v)$ is the collision coefficient. An exact evaluation of W hinges on an exact knowledge of y_c which is difficult to determine in an exact manner either theoretically or empirically. Experimental determinations of the growth rates of cloud drops were made by Gunn and Hitchfeld[1], Kinzer and Cobb[2], Picknett[3], Woods and Mason[4]. With the exception of Kinzer and Cobb, these experiments were restricted to either very large or very small collector drops and to narrow size ranges of collector drops. For the size range $80 \leq A \leq 260$ the results of Kinzer and Cobb agree with collection coefficients based on the collision efficiencies given by Mason but remain to be checked carefully (Woods[5]) because of serious shortcomings in the experiments of Kinzer and Cobb resulting from the small size of their drop supporting apparatus which lead to erroneous results for $A > 260$ microns.

EXPERIMENT

The present experimental determination of collection coefficients was carried out in the UCLA Cloud Tunnel. This tunnel is fabricated out of aluminum and stainless steel and consists of a horizontal air conditioning system and a vertical flow control system which both were electrically grounded to prevent the presence of any stray electric fields in the tunnel The air is drawn through the tunnel by a vacuum pump while the air speed is controlled by a sonic velocity valve. Because of the use of a honeycomb, a screen and a contraction section the resulting air flow in the test section is laminar with a very low turbulence level and a flat velocity profile. Drops $10 \leq A \leq 425$ microns are freely suspended in the test section by matching the free stream air speed U to the drop velocity V so that $U = V$. Under these conditions a calibration of the tunnel air speed as a function of the sonic valve setting enabled us to find the terminal velocity of the collector drops. Details on the construction and calibration of the UCLA Cloud Tunnel are given by Pruppacher and Neiburger[6] and Beard and Pruppacher[7]. In the present study the air conditioning system allowed the temperature in the test section to be kept at 22°C and to be controlled to ± 1°C. A water cloud was produced by steam injection at the tunnel entrance of the airconditioning unit and was well-mixed when it arrived in the observation section. Drop size spectra were measured in the test section by using a sampling gun similar to that described by Squires and Gillespie[8]. The cylindrical sampling rods were coated with a solution of gelatin and Naphtol Green dye according to a method developed by Liddell and Wootten [9]. The droplets, after impinging on the rod, left stains that were 1.9 times their diameter. This size calibration was obtained by comparing our method with a method based on Magnesium Oxide coated rods (May[10]). Using this calibration, droplet size spectra were obtained from examining the coated glass rods under the microscope. The drop size distributions of liquid water content were fairly uniform throughout the experiment with a mode size near 4 or 5 microns radius and a dispersion of 8 micron with 95% of the liquid water within ± 2 micron of the mode. In Fig. 1, as an example, a typical size distribution has been plotted. The liquid water content of the cloud was determined from collision efficiencies found experimentally by Starr [11] after counting and sizing the drops on a movable stage microscope in at least 12 areas of the rod for a statistical evaluation. By this method the value of the total liquid water content L was determined to ± 20% at the 95% confidence level. Alternatively, the liquid water content was continuously measured with a Cambridge Systems dewpoint hygrometer using an aspirating probe with a carefully regulated intake velocity for isokinetic condition. The cloud droplets completely evaporated in a heated tube before reaching the hygrometer so that it became possible to calculate the liquid water content from the elevated vapor pressure. The results of the dewpoint hygrometer gave a value of L to ± 10%. The charge on the cloud droplets was measured by a method developed by Phillips and Kinzer[12] and was found to be on the order of a few electron charges. An electrometer was used to find the average charge for the collector drops as about 10^{-6} esu. By applying the criteria of Davis[13], Semonin and Plumlee[14], Woods, and List and Whelpdale[15] we concluded that there was not enough charge present to alter the collision efficiency, but probably enough to cause the coalescence efficiency to be unity. It was therefore assumed that our experimentally determined collection coefficients had the meaning of collision coefficients. For a typical experiment the tunnel was allowed to stabilize for several hours at constant velocity with a cloud of $0.8 \leq L \leq 1.2$ gr m^{-3}. A droplet sample was taken and, immediately afterwards, the tunnel velocity slightly reduced for the introduction of a collector drop with a hypodermic needle. The rate of change of tunnel velocity was recorded over an interval $A \cong 10$ microns of the collector drop size. Over this short run the cloud droplet spectrum remained constant. Several runs were made for collector drop sizes A = 73, 113, 155,

203, 250, and 299 microns. The average growth rate was obtained from our recorded velocity of the tunnel airstream which kept the suspended drop at a fixed position at the tunnel axis. The quantity dV/dt was then found from dU/dt. Values for dA/dV were calculated from the drag relations given by Beard and Pruppacher. The growth rate of a drop was determined from $dA/dt = (dA/dV)(dV/dt)$. Our theoretical considerations showed that for our case, where $dm/dt < 10^{-7}$ gr sec^{-1}, a growing drop could be assumed to fall at terminal velocity with no acceleration.

RESULTS

In order to compare our results with collection coefficients of other authors we used an approach outlined by Kinzer and Cobb for generalizing the continuous growth rate equation as $dA/dt = (1/4\rho_s)\overline{W}L$, where ρ_s is the drop density and $\overline{W}$ is the mean value of the collection coefficient obtained from summing over the individual droplet size categories and $\overline{W}L = \sum_i W_i L_i$. The recent results of Chin[16] substantiate such a generalization. Chin found that the average value of the final mass of 32 collector drops in a numerical experiment for a randomly distributed, polydispersed cloud was not significantly different from that obtained using the generalized continuous growth rate equation. The results of our measurements are presented in Fig. 2 where the collision coefficient $\overline{W} = W(\bar{a})$ is plotted as a function of the collector drop radius A for various cloud types which we characterized by $\bar{a}$. The quantity $\bar{a}$ is the liquid water content weightec mean value of the droplet size of an individual cloud. This characterization assumes that $dA/dt = (1/4\rho_s)\sum_i W_i L_i \approx (1/4\rho_s)W(\bar{a})L$ is a good approximation. It is seen from Fig. 2 that our measurements, with variance indicated by the vertical bars, and the results of Kinzer and Cobb, within the limited range chosen, are consistent with the collection coefficients derived from the collision efficiencies theoretically computed by Shafrir and Neiburger [17] as analytically described by Berry[18], and with the collision coefficients derived from the collision efficiencies theoretically computed by Mason[19]. It has to be stressed that this agreement only applies for $p = \frac{a}{A} \lesssim 0.1$, i.e. for the case of large cloud drops growing in a cloud of very small cloud drops. However, it is precisely for this range of p-ratios that, up to the present, experimental results quoted in literature scattered too much to test available collision efficiency theories (Woods and Mason). Our new results suggest that, for the range of p-ratios indicated, it is justified to compute values for the collision coefficient from the collision efficiencies of Shafrir and Neiburger as analytically given by Berry up to A = 136 microns and from the collision efficiencies given by Mason up to and possibly beyond A = 300 microns.

1. Gunn, R. and A. W. Hitchfeld, J. Meteorol., 8, 7 (1951). 2. Kinzer, G. D. and W. E. Cobb, J. Meteorol., 15, 138 (1958). 3. Picknett, R. G., Int. J. Air Pollution, 166 (1960). 4. Woods, J. D. and B. J. Mason, Quart. J. Roy. Meteor. Soc., 90, 373 (1965). 5. Woods, J. D., Ph.D. Thesis, Imperial College, London (1965). 6. Pruppacher, H. R. and M. Neiburger, Proc. Cloud Phys. Conf., Toronto, 389 (1968). 7. Beard, K. V. and H. R. Pruppacher, J. Atmos. Sci. 8. Squires, P. and C. A. Gillespie, Quart. J. Roy. Meteor. Soc., 78, 387 (1952). 9. Liddell, H. F. and N. W. Wootten, Quart. J. Roy. Meteor. Soc., 83, 263 (1957). 10. May, K. R., J. Sci. Instruments, 27, 128 (1950). 11. Starr, J. R., Ann. Occup. Hyg. (Great Britain), 10, 349 (1967). 12. Phillips, B. B. and G. D. Kinzer, J. Meteorol., 15, 369 (1958). 13. Davis, M. H., Proc. Int. Conf. Cloud Physics, Tokyo, 118 (1965). 14. Semonin, R. G. and H. R. Plumlee, J. Geophys. Res., 71, 4271 (1966). 15. List, R. and D. M. Whelpdale, J. Atmos. Sci., 26, 305 (1969). 16. Chin, H. C., Ph.D. Thesis, UCLA, Dept. of Meteorology (1970). 17. Shafrir, U. and M. Neiburger, J. Geophys. Res., 68, 4141 (1963). 18. Berry, E. X., J. Atmos. Sci., 24, 688 (1967). 19. Mason, B. J., The Physics of Clouds, Oxford Press, London (1957).

Figure 1

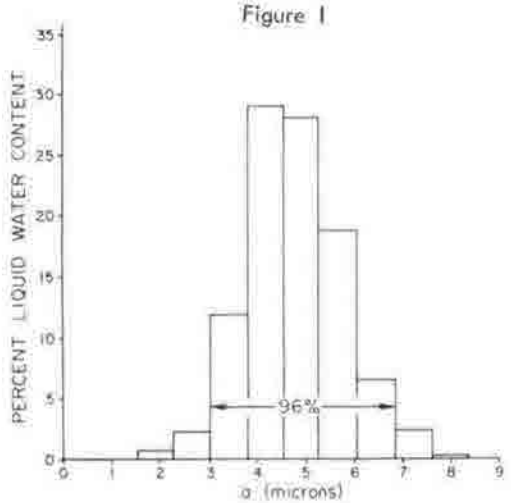

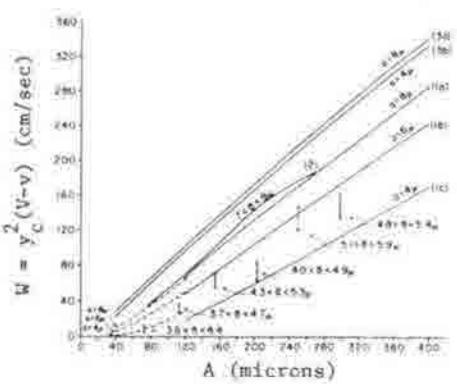

Figure 2

1a, 1b, 1c Mason (Theory)
2 Kinzer-Cobb (Experiment)
3a, b based on geometric collision efficiencies

I Present Results

---- Berry based on Shafrir and Neiburger

ELECTRIFICATION ASSOCIATED WITH BREAKUP OF DROPS AT TERMINAL VELOCITY IN AIR

J.V. Iribarne and M. Klemes

University of Toronto
Toronto, Canada

The electrification associated with the "bag bursting" of large drops has been studied by several authors. Both the experimental conditions and the results differed widely. In this research we have studied the charge separation between the fragments larger than about 0.1 mm and the finer spray produced in the process, in the absence of an electric field and varying the chemical composition of the liquid.

EXPERIMENTAL TECHNIQUE

Fig. 1 shows the experimental arrangement. Drops of about 7 mm equivalent spherical diameter were introduced in an updraught of 10 m/s. The updraught was produced in a closed circuit tunnel where the CO_2 content was maintained at a low level. The drops burst at the beginning of a decelerating expanding section, and the larger fragments fell onto metallic plates covering its lateral walls. The plates were connected to a vibrating reed electrometer provided with a recorder, and the charges were measured by the sudden changes in potential across the input capacitance. Pure water was obtained from ion-exchange resin, and used directly or to prepare solutions. Contamination from the air was avoided. The initial charge of the drops was $\sim -5 \times 10^{-4}$ e.s.u.

RESULTS

The measurements showed considerable scattering. Fig. 2 gives the charge distribution obtained for a series of experiments with pure water. A normal error curve could be reasonable fitted, except for an abnormal number of "zeros", sensitive to the location of the drop releasing needle. An investigation with a high-speed camera at 300 frames per second showed that most of these were not due to bag bursting Charges were associated with bag bursting, except for a small percentage associated with division of the drops into several fragments and satellite droplets. Therefore the following criterion was adopted. Averages of 150-200 breakup measurements were taken for each liquid composition, but only that number of zeros was considered as would correspond to a fitted normal error curve.

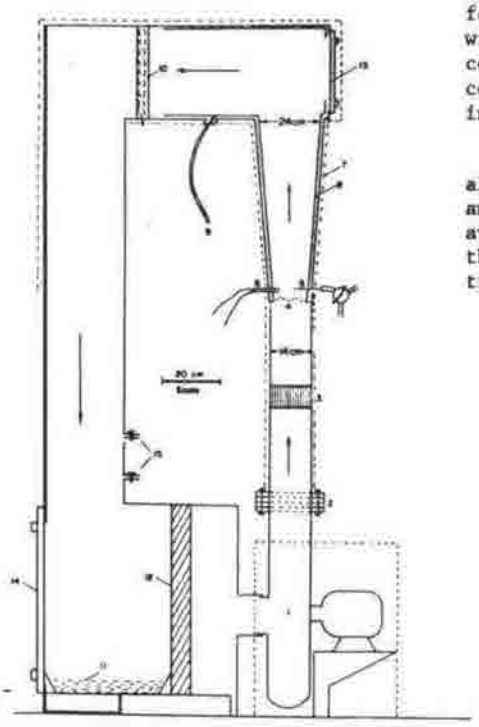

Fig. 1 - Tunnel. 1: blower; 2: wire screens; 3: honeycomb; 4: shaped wire screens; 5: needle; 6: conductivity cell; 7: external shielding; 8: copper plates; 9: connection to electrometer; 10: steel wool filter; 11: tray with concentrated sodium hydroxide solution; 12: cotton wool filter; 13: door with window; 14: door; 15: inlet and outlet.

Carbon dioxide and salt solutions. Experiments were performed with pure water (conductivity 0.1-0.3 μmhos/cm) and with solutions of CO_2, NaCl, KCl and $(NH_4)_2SO_4$ in variable concentrations, up to 0.1 M. The results (averages for each concentrations, with r.m.s. error $\sim 10^{-3}$ e.s.u.) are plotted in Fig. 3.

Surface active cations. Measurements (not plotted) were also done with solutions of tetrabutylammonium and tetrapentyl ammonium chloride. These substances reversed the sign of the average charge for dilute solutions ($\lesssim 10^{-5}$ N) and decreased the magnitude, without reversing the sign, for the concentrated solutions ($> 10^{-4}$ N).

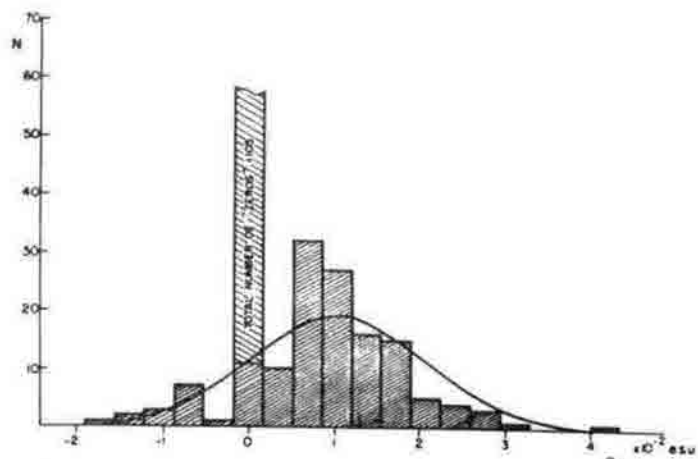

Fig. 2 - Distribution of separated charges. Pure water. N = number of breakups. Q = charge of large fragments. Curve is fitted normal error law.

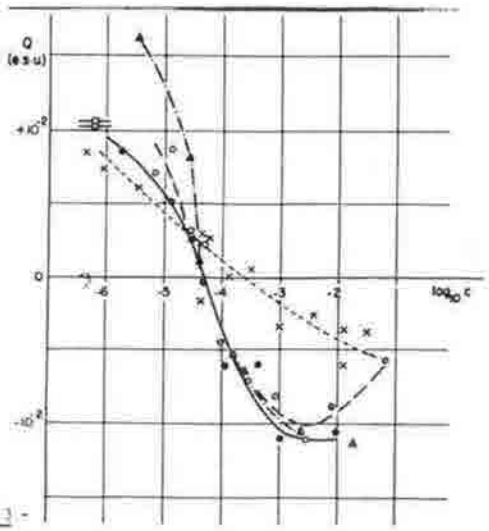

Fig. 3 -

Average separated charge per breakup (sign of large fragments), as a function of electrolyte concentration c (normality; for CO_2, molarity). —●: KCl; -- ⊖: NaCl; - • - Δ: $(NH_4)_2SO_4$; - - - x: CO_2; —□—: pure water, considered as CO_2 solution.

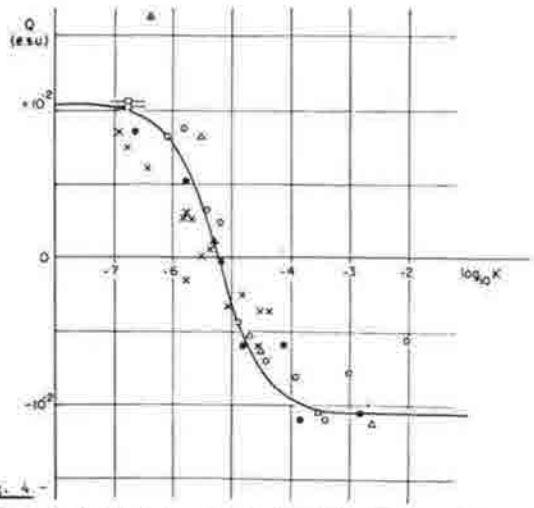

Fig. 4 -

Average separated charge per breakup (sign of large fragments), as a function of conductivity K (ohm^{-1} cm^{-1}). —●: KCl; - - ⊖: NaCl; - • - Δ: $(NH_4)_2SO_4$; - - - x: CO_2; —□—: pure water. Full line: theoretical curve.

DISCUSSION

Disregarding the action of surface active substances, the average results are very sensitive to the electrolyte concentration, but not to the particular compound. The non-specificity becomes apparent in Fig. 4, which strongly suggests that the average separated charge is only a function of the conductivity.

The electrification may be attributed to shearing effects on the electrical double layer at the water-air interface, and therefore linked with its value of the electrokinetic or zeta potential ζ. The fact that the sign reverses with concentration can neither be due to changes of the dynamics nor to changes of ζ. On the other hand, the surface active cations tested are known to change the sign of ζ, in agreement with the results of breakups of dilute solution drops.

Two competing processes have to be assumed in order to explain the behaviour shown in Fig. 4. We postulate that positive charges in the large fragments are due to the shearing effect on the internal surface of the bag blown up by the air. This would result in an accumulation in the upper part of the negative charges prodominant at the surface of the water, while a corresponding positive charge would remain in the toroid containing most of the liquid in the lower part. After the breakup the former will remain in the spray and the latter in the large fragments. An estimate of the shear stress at the surface and a calculation of the electrokinetic effect based in the theory of the double layer gives the correct order of magnitude. This process is counteracted by a neutralization or back current in the bag film. A theoretical computation, with adjusted parameters, would indicate a decay toward the larger concentrations such as shown by the curve of Fig. 4. The remaining negative value (~ -0.01 e.s.u.) would then be due to the second process, present throughout the whole range of concentrations, which we assume fast enough to be unaffected by a back current; this might perhaps occur during the separation of small droplets from filaments linked to the larger fragments, when the bag film collapses.

The range of electrical conductivity of raindrops at cloud levels may be roughly estimated between 10^{-6} and 10^{-4} mhos/cm. Thus practically any value between $\pm 10^{-2}$ e.s.u./drop or $\pm 6 \times 10^{-2}$ e.s.u./cm^3 could be expected, with positive values (on the large fragments)for purer air. These values are unlikely to make any significant contribution to thunderstorm electricity.

Acknowledgement. This research has been supported by a Meteorological Grant of the Department of Transport.

CHARGE SEPARATION DUE TO THE SPLASHING OF WATER DROPS

by
Zev Levin* and Peter V. Hobbs
Cloud Physics Group, Atmospheric Sciences Department
University of Washington, Seattle, Washington

INTRODUCTION

It is well known that when water drops break up electrical charges are separated (Lenard[1]). Our interest in this phenomenon is related to the possible role of the splashing of water drops on solid and partially melted hydrometeors in separating electrical charges in clouds and thunderstorms, and the generation of space charge near the ground due to the splashing of raindrops. To gain insight into the mechanisms responsible for splashing electrification, and to determine the magnitudes of the charges separated under various conditions, a detailed laboratory investigation has been carried out. A summary of the results of this study are presented in this paper.

HYDRODYNAMICS OF DROP SPLASHING

The electrical charges separated during splashing are intimately connected with the hydrodynamics of the splash. The latter was investigated by means of high speed photography at 5,000 frames per sec. Following the initial impact of a drop on a dry or a partially wetted solid surface a liquid "crown" is thrown up. As this "crown" grows jets emerge from its upper periphery. These jets become unstable and break up into a number of liquid fragments. For example, when a water drop 1.25 mm in radius collides with a solid surface with an impact velocity of 3.5 m sec^{-1}, over one hundred small fragments are ejected. The sizes of these fragments are log-normally distributed. As the impact velocity, or the size of the water drops, is increased both the number of liquid fragments and their velocity of ejection from the crown jets increase.

Direct superposition onto the photographs of the signal representing the charge transferred to the surface by a splash revealed that the charge is carried away on the liquid fragments which break away from the "crown" jets.

CHARGE SEPARATION IN THE ABSENCE OF AN ELECTRIC FIELD

Measurements of the charges separated by the splashing of individual drops onto various surfaces were carried out in the laboratory under controlled conditions. The water was distilled, deionized, and distilled again in a nitrogen atmosphere to prevent adsorption of carbon dioxide and other impurities. The drop splashing measurements were also carried out in an atmosphere of pure nitrogen. The net charge communicated to the surface by the splashing of a drop was measured with a solid-state electrometer which could detect charges down to 10^{-6} esu.

When drops consisting of pure water or dilute solutions of NaCl were splashed onto a copper surface at temperatures between 0 and 20°C a net positive charge was communicated to the surface. These charges were in the range 5×10^{-5} to 10^{-4} esu per splash. In the case of drops containing NaCl, the charge that was separated by splashing on a copper or ice surface at 0°C decreased with increasing concentration of the solution. For solution drops containing more than 10^{-3} moles of NaCl per liter, virtually no charge was separated (Fig. 1). The charges communicated to the copper and ice surfaces by splashing were approximately the same, however, the charge received by the ice surface was usually somewhat greater than that received by the copper surface. This was accounted for by the larger number of fragments ejected from the melted ice surface. The results shown in Fig. 1 can be partially explained by the disruption of the electric double layer during the break-up of the crown jets.

CHARGE SEPARATION IN THE PRESENCE OF APPLIED ELECTRIC FIELDS

When vertical electric fields were applied in the region where splashing occurred the charges separated by the splashing increased markedly (Fig. 3). This is a result of the polarization of the drop and the solid surface. However, the measured charges communicated to the surface under these conditions were greater than those predicted theoretically for the collision of rigid conducting spheres. This difference can be accounted for by the enhancement of the local electric fields around the jets and the wall of the "crown" which tends to increase the polarization of the jets. For impact velocities in excess of 4.5 m sec^{-1} the charges separated by splashing dilute NaCl solution drops in the presence of electric fields decreased with increasing impact velocity (curves c and d in Fig. 2). It is believed that this is the result of a reduction in the contact time between the small fragments that are ejected initially and the crown jets to a value comparable to the relaxation time of the charge carriers in the liquid.

It should be noted that the charges separated under identical experimental conditions were by no means unique. This is a result of the statistical nature of the break-up of the crown and the crown jets. Most of the distributions of charge were found to be log-normal.

APPLICATION TO CHARGING IN THE ATMOSPHERE

In the atmosphere splashing can occur due to the collision of cloud droplets or raindrops with solid hydrometeors (hailstones, graupel or other ice particles) or by the collisions of raindrops with the ground. The results described above show that for temperatures above 0°C, and in the absence of electric fields (or in the presence of fields less than 0.5V cm^{-1}), splashing will result in the solid surface receiving positive charge with the corresponding negative charge being ejected into the air on

*After August 1970 permanent address: Meteorology Department, University of California at Los Angeles

the small fragments. Subsequent gravitational separation of these charges will result in a build-up of the atmospheric electric field and this, in turn, will lead to increased charge separation during splashing. In clouds such a mechanism can explain the region of positive charge which is often observed just below the freezing level. The splashing of drops on solid hydrometeors will also change the drop size distribution in a cloud by generating large numbers of small droplets.

In the presence of moderate wind shears (e.g. a logarithmic wind profile) the charges separated by the splashing of raindrops on the ground can readily produce the negative space charge which is observed near the ground during heavy showers (Adkins[2]).

ACKNOWLEDGEMENTS

This research was supported by grants GA-11250 and GA-17381 from the Atmospheric Sciences Section, National Science Foundation.

REFERENCES

1. Lenard, P., 1892: "Über der Elektrizität der Wasserfälle." Ann. Phys. 46, 584-636.
2. Adkins, C.J., 1959: "The small ion concentration and space charge near the ground." Quart. J. Roy. Met. Soc., 85, 237-252.

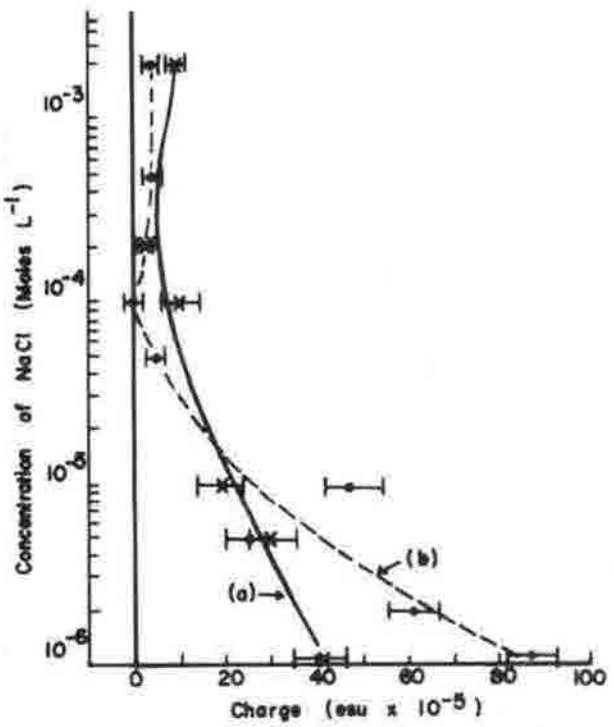

Fig. 1 Charge transferred to (a) copper sphere and (b) ice sphere by splashing 1.25 mm drops of various NaCl solutions at 4.1 msec^{-1} and at 0°C.

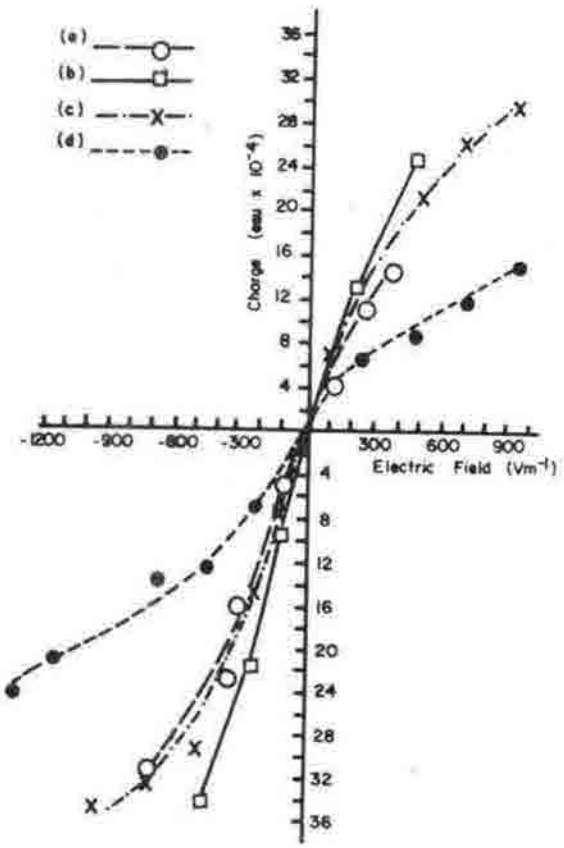

Fig. 2 Charge transferred to a copper sphere at 20°C, by splashing of 1.25 mm radius drops of 2 x 10^{-4} M NaCl at impact velocities of (a) 1.5 msec^{-1} (b) 4.1 msec^{-1} (c) 5.4 msec^{-1} and (d) 5.9 msec^{-1} as a function of the imposed electric field.

FIELD-ENHANCED PROPAGATION OF POSITIVE STREAMERS AND IMPLICATIONS TO ELECTRICALLY INFLUENCED DROPLET COALESCENCE

C. T. Phelps
State University of New York at Albany
Albany, New York 12203

INTRODUCTION

In order to understand the electrically influenced processes that take place in a thundercloud, it is necessary to know the effect of the lightning discharge on the droplet charge spectrum. In general, gross neutralization of a charge cell is accomplished by the discharge. The details of the change in the droplet charge spectrum, including its temporal development and spatial extent, however, are poorly understood.

Impulse corona processes and their interactions with cloud droplets are of particular interest, since these processes establish the extent and some aspects of the character of the discharge pattern in space. Recent experiments show that droplets can acquire substantial charges through interactions with impulse corona of either polarity (1). It is the purpose of this paper to report the results of experiments designed to determine the propagation characteristics of impulse coronas in uniform electric fields similar to those expected in highly electrified clouds. Theoretical arguments are advanced that relate to some of these results.

EXPERIMENT DESCRIPTION AND RESULTS

In the first set of experiments corona streamers were introduced into a parallel plate gap of 75 cm by applying a short rise time 200 kv pulse to a point electrode mounted perpendicular to, but insulated from, one of the plane electrodes. Photographs of the resulting luminosity in the gap indicate the range of these streamers. The ranges of positive streamers were dramatically increased for uniform field values above 5×10^5 v m^{-1} (field in the direction of streamer propagation). With a field of about 6×10^5 v m^{-1}, the streamers crossed the gap, and at about 6.5×10^5 v m^{-1}, the streamers triggered a spark discharge between the plane electrodes. These values are nearly independent of gap length. With the field direction reversed, streamer ranges decreased. The luminosity from negative streamers remained localized near the point with field values as high as 9×10^5 v m^{-1} (either direction).

In the second set of experiments the impulse corona was derived from field-induced hydrodynamic instability of falling water drops (2,3). Initially uncharged 1.5 mm radius drops were allowed to fall one at a time within the gap toward a hemisphere placed on the bottom plane electrode. The hemisphere had a small hole in its top, and the drops were aimed so as to pass through this hole and not splash. At a uniform field of about 7×10^5 v m^{-1}, directed away from the hemisphere, the drops each disrupted yielding upward advancing positive streamers, which crossed the gap and always triggered spark-over. With the field direction reversed, no luminosity was observed at values as high as 9×10^5 v m^{-1}. It should be noted that in these two sets of experiments the behavior of impulse corona, particularly positive streamers, in relatively strong uniform fields is remarkably similar considering the completely different sources of the corona.

DISCUSSION

The observed behavior of positive streamers in a uniform ambient field can be partially explained and predicted from the following analysis based in part on the streamer model advanced by Dawson and Winn (4). A positive streamer should be considered as a traveling wave of pulse nature characterized by a very high unipolar charge density and having certain elements in common with ordinary electromagnetic wave propagation including the intimate interplay of electric and magnetic fields. In the absence of a secondary streamer or other additional ionization in the channel, this wave is considered to be essentially isolated from its anode source. Calculations based on estimates of streamer electrical parameters indicate that the channel has insufficient conductivity to maintain the streamer head at anywhere near the anode potential during its propagation.

Energy is expended in ionization and excitation as the positive streamer progresses. This energy must be supplied either from the internal potential energy of the charge collection at the head of the streamer or from the interaction of this charge collection with the ambient field. If the energy is derived from the potential energy of the head, its radius and charge decrease, and the excess positive charge is deposited along the channel. With no external source of energy, a streamer dies out after advancing only a few millimeters (5). If an external electric field (having the same direction as the streamer propagation) is present, energy is supplied to the streamer as the charge collection falls down the "potential hill" created by that field. If the ambient field strength is sufficiently high, energy is supplied at the same rate as it is used and no attrition of the charge collection would be expected. This implies that for a critical ambient field, the range of a positive streamer is limited only by the spatial extent of the field. Calculations based on this energy balance give a critical field value in reasonable agreement to the value observed experimentally.

If the ambient field is greater than the critical value discussed above, the charge collection will grow. A direct consequence of this should be the deposition of negative charge along the channel. This concept was tested utilizing the Lichtenberg figure technique in which the streamers propagate in two dimensions over a dielectric surface. The surface is subsequently dusted with two

distinguishable powders that are attracted to the positive and negative regions respectively. A negatively charged electrode was placed under the dielectric surface well away from the point to provide a variable ambient field. Under suitable conditions it was often observed that as a streamer approached the negative electrode, the deposited charge on the channel smoothly changed from positive to negative. In the region of negative charge deposition, the radii of the channels increased slightly.

CONCLUSIONS

Electric field measurements made from aircraft flying near electrically active cumulonimbus cells yielded maximum values of about 1/3 of the experimentally observed critical field (6). The critical field in the cloud, however, is somewhat lower due to the reduced pressure. Also, the aircraft was unable to reach the locations where the highest fields exist. It is reasonable and probable, therefore, that the electric field, at least in a limited volume of the cloud, reaches the critical value. The results presented here, therefore, lead to the conclusion that of the possible corona processes that could be associated with a lightning discharge, only positive streamers are capable of charging great numbers of cloud droplets throughout a large volume.

The maximum positive charge a cloud droplet might acquire by interaction with a positive streamer is about an order of magnitude higher than the estimated charge held by a typical cloud droplet of the same size in a charge cell of an active cumulonimbus (1). Since the streamers must advance toward and into a negatively charged region, these droplets will always have the opposite polarity of the surrounding droplets. These positively charged droplets should be rapidly neutralized by coalescence with nearby negatively charged droplets. In this way the droplet size spectrum is suddenly altered in a fashion that should favor a more rapid growth of precipitation.

REFERENCES

(1) Phelps, C. T., and B. Vonnegut, Charging of droplets by impulse corona, J. Geophys. Res., to be published.

(2) Dawson, G. A., Pressure dependence of water-drop corona onset and its atmospheric importance, J. Geophys. Res., 74, 6859-6868, 1969.

(3) English, W. M., Corona from a water drop, Phys. Rev., 74, 179-189, 1948.

(4) Dawson, G. A., and W. P. Winn, A model for streamer propagation, Zeitschrift fur Physik, 183, 159-171, 1965.

(5) Dawson, G. A., The lifetime of positive streamers in a pulsed point-to-plane gap in atmospheric air, Zeitschrift fur Physik, 183, 172-183, 1965.

(6) Fitzgerald, D. R., Electric field and precipitation structure near convective cloud tops (abstract), Trans. Am. Geophys. Union, 50, 619, 1969.

ELECTRIFICATION ASSOCIATED WITH THE SPLASHING OF LARGE DROPS ON ICE

S.R. Shewchuk and J.V. Iribarne

University of Toronto
Toronto, Canada

In a previous investigation (1) we have studied the electrification associated with the splashing of large drops on different solid surfaces at room temperature. The present research extends the study to the case of drops at 0°C splashing on ice.

EXPERIMENTAL TECHNIQUES

The splashings were produced by letting the drops fall onto rotating metal spheres covered with a thin coating of pure ice. The initial negative charges of the drops were smaller than 4×10^{-4} e.s.u. Two spheres at the end of a shaft were made to rotate, in a plane slightly tilted from the vertical, by means of a variable speed motor. The spheres and shaft were insulated from the motor and connected through a needle spinning in a pool of mercury, to an electrometer provided with a recorder.

Flash photographs (3 μ sec flash duration) were obtained for high collision speeds by synchronizing photoelectrically the flash with the position of the sphere or of the drop.

The charge separations were measured by the sudden increases in voltage across the total input capacitance on the electrometer.

RESULTS

The photographs show a splashing process similar to that occurring at room temperature. Initially as the drop splashes, the liquid flows radially from the point of impact over the ice; its depth is of the order of 100 μ and speed is about 50 m/s (for impact speed of 20 m/s). The liquid separates from the surface as a film ~ 10 μ thick. The periphery of the film resolves into filaments, which emit droplets. Soon after all of the drop has passed to the film, holes appear in the surface which begins a rapid process whereby the film disintegrates into a fine spray (50-250 μ droplets).

Charge separation measurements.

Scatter of results and effect of roughness. The exact point of impact could not be controlled in our arrangement. Collisions varied from "head-on" to grazing, producing a considerable scattering in the individual results. Roughness of the surface had also some effect, giving smaller values for smoother ice. The reported values are averages of 15-20 consecutive readings taken after the first 10 splashes had given the surface an approximately constant roughness. The scatter can be estimated from the standard deviations represented by error bars in Fig. 1.

Influence of drop size. Fig. 1 shows the average charge transferred to the spheres for drops of 1 to 3 mm radius colliding at 25 m/s. Averages of the four largest charges for each set of measurements were about 50% higher than the overall averages.

Influence of collision speed. This is represented in Fig. 2 for several temperatures of the ice surface, using pure water and collision speeds of 25 m/s.

Influence of liquid composition. The pure water used was either from an ion-exchange resin column or distilled, with conductivities as it fell in drops of about 0.13 to 0.60 μmho/cm. The influence of a number of electrolytes was tested. Fig. 3 shows the results for varying concentrations of NaCl and $(NH_4)_2CO_3$. The results for pure water are also plotted for reference, at the conductivity equivalent NaCl concentration. Other electrolytes tested were $(NH_4)_2SO_4$, NaF, $NaOOCCH_3$, Na_2CO_3, $Pb(OOCCH_3)_2$. Only the ammonium compounds reversed the sign of the charging. At high concentrations the charge separation is approximately constant for different temperatures and electrolytes: $Q \cong + 0.015$ e.s.u. For dilute solutions there appears to be a maximum at about 10^{-4} M.

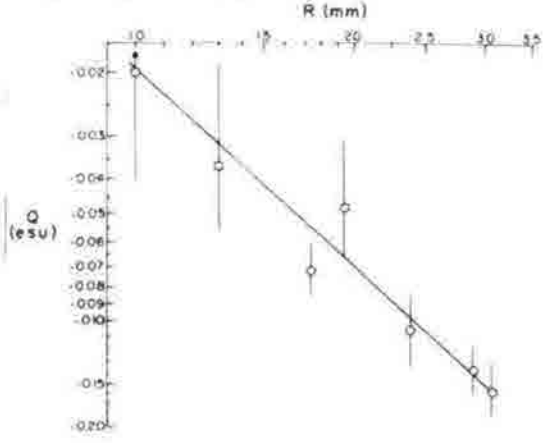

Fig. 1 - Charge vs. drop radius. 10^{-4} NaCl, -12°C, 25 m/s. Arrow indicates Q = 0.

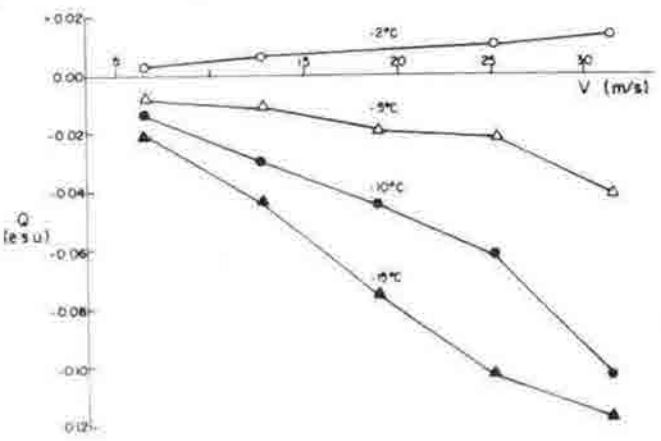

Fig. 2 - Charge vs. impact velocity. Pure water, R = 2.4 mm.

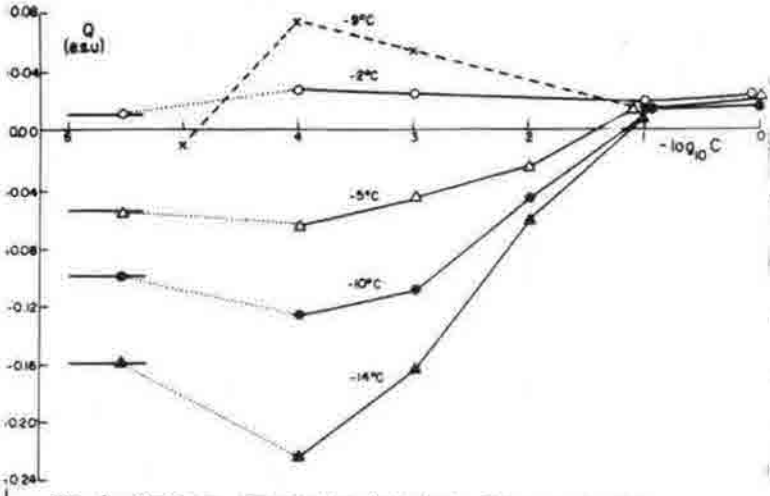

Fig. 3 - Charge vs. concentration (molarity). Points at the left correspond to pure water; bars indicate equivalent NaCl concentrations corresponding to conductivity range. O, Δ, ●, ▲: NaCl, R = 3.2 mm. x = $(NH_4)_2CO_3$, R = 2.9 mm. 25 m/s.

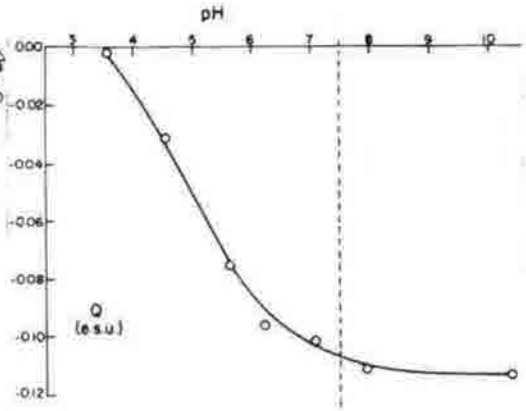

Fig. 4 - Charge vs. pH. 10^{-4} N NaOH + HCl. R = 3.2 mm, -12°C, 25 m/s. Dashed line indicates neutrality (0°C).

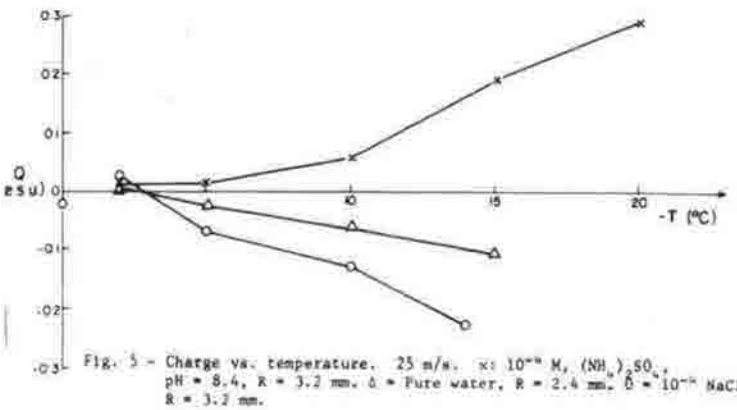

Fig. 5 - Charge vs. temperature. 25 m/s. x: 10^{-4} M, $(NH_4)_2SO_4$, pH = 8.4, R = 3.2 mm. Δ = Pure water, R = 2.4 mm. O = 10^{-4} NaCl, R = 3.2 mm.

Influence of pH. This was investigated by adding HCl in varying proportions to 10^{-4} N NaOH. As shown in Fig. 4 H^+ has a strong inhibiting effect. Small changes occur above neutrality (pH $\simeq$ 7.5 at 0°C). Occasionally we have observed a max. at pH 8.5-9 and small positive values at pH < 3.6.

Influence of ice temperature. Although implicit in several of the previous graphs, Fig. 5 shows more clearly the influence of the surface temperature. Above -3 to -4°C all observed charges become positive, while lowering the temperature has a marked effect, increasing the magnitude of charge transfer for both signs.

DISCUSSION

It was previously shown (1) that in the splashes at room temperature the main electrification mechanism is the shearing of the electrical double layer at the interface solid-liquid. The similarity of the dynamics allows us to assume that this also holds for the present case. Here, however, the process is further complicated by the growth of the ice and the preferential capture of ions of one sign into the ice. We interpret the strong variation with temperature as due to its influence on growth rate. Thus at temperatures close to 0°C, the surface potential ice-water is positive on the ice (2), and so presumably must be the electrokinetic or zeta potential. At lower temperatures the ion capture mechanism becomes predominant and determines the sign and magnitude of this potential. Apparent sign discrepancies between our measurements at low temperatures (< - 4°C) and freezing potential data (pure water and $Pb(CH_3COO)_2$ solutions (3)) disappear if the freezing potential is observed at freezing rates comparable with those of the experiments. This was shown by recording the transient potentials occurring when an ice coated metal bar at low temperature was brought into contact with water or solution at 0°C.

As in splashes at room temperature, the constancy of values at high conductivities suggest that a second process becomes dominant in this concentration range, perhaps linked with the final disruption of the liquid film attached to the sphere.

The values obtained for the splashing electrification indicate that significant charge separations might occur when hail falls through a cloud region containing raindrops.

Acknowledgement. This research has been supported by the National Research Council of Canada.

REFERENCES

(1) S.R. Shewchuk and J.V. Iribarne, Trans. Faraday Soc., 1970 (in press).
(2) T. Takahashi, J. Atm. Sci. 26, 1253, 1969.
(3) E.J. Workman and S.E. Reynolds, Phys. Rev. 78, 254, 1950; G.W. Gross, J. Geoph. Res. 70, 2291, 1965.

ESTIMATES OF THE PRECIPITATION GROWTH ENVIRONMENT IN THE UPDRAFT CORE OF ALBERTA HAILSTORMS

A.J. Chisholm
McGill University, Montreal, Canada

The Loaded Moist Adiabatic (LMA) Vertical Velocity Model

Recent aircraft observations of cloud base updrafts in Alberta (1) have shown conclusively that smooth, uniform updrafts of 4-6 m sec^{-1} and 5-15 km diameter persist in conjunction with hailstorms for periods up to several hours. Unsaturated air, entrained into such broad updraft regions by turbulent mixing processes at the cloud boundary, penetrates inward being successively diluted by saturated air. In order for this entrained air to reach the updraft axis, even in the upper reaches of the hailstorm, the effective horizontal velocity of the entrained air must be of the same order as the vertical velocity along the updraft axis. Even in this extreme case, the effect of the entrained air at the updraft axis in the upper reaches of the hailstorm must be extremely small due to dilution with saturated air. Consequently, it appears reasonable to assume that there exists within such hailstorms a central updraft core, either completely unaffected by entrainment or affected only slightly by entrainment in the upper reaches of the hailstorm. This updraft core region must have essentially moist adiabatic properties and can, therefore, be modelled to a reasonable degree of accuracy by moist adiabatic parcel theory. Traverse times for air parcels in the resulting high speed updraft core are typically less than 600 sec. As a consequence, the results of recent coalescence growth experiments (2) indicate that the major growth processes within the updraft core must be diffusion, which yields cloud droplets with diameters less than 40 μ. Droplets of this size and smaller effectively remain with the original air parcel, necessitating the inclusion of an adiabatic water loading effect. By integrating the buoyancy equation, the vertical velocity at any height can be obtained using:

$$W_z = \left(W_o^2 - 2R_d \int_{P_o}^{P_z} (T_{vp} - T_{ve} - m_l T_{ve})\, d\ln p\right)^{1/2}$$

Where
W_o = vertical velocity at cloud base
W_z = vertical velocity at height z
R_d = gas constant for dry air
T_{vp} = virtual temperature of a moist adiabatic cloud parcel
T_{ve} = virtual temperature of the environment
m_l = adiabatic water (per unit mass of air)
$m_l T_{ve}$ = adiabatic water loading term
P_o = pressure at cloud base
P_z = pressure at height z

This loaded moist adiabatic (LMA) model requires temperatures and relative humidities in the cloud environment as well as cloud parcel temperatures. Environmental conditions for use with this model were obtained by radiosonde, and cloud base temperatures and pressures were estimated using surface temperatures and dewpoints to compute the lifting condensation level. Moist adiabatic parcel temperatures above cloud base were calculated using a technique outlined by Stackpole (3). The additional energy source available due to freezing was neglected. Since the computed vertical velocity (see above eqn.) is a square root function of the energy, the maximum error incurred in the vertical velocity by neglecting freezing is less than 7%.

LMA Model Results vs. Radar Observations

Results of radar observations and LMA model calculations for the highest hailstorms in the Alberta Hail Studies (ALHAS) project area on 29 days during the summers of 1967 and 1968 have been compared. Radar-observed storm tops were obtained for each storm at 3 min intervals using the ALHAS 10 cm radar (1.15 deg beamwidth). At the time of maximum radar storm top, radiosonde data and surface data were used to obtain the maximum computed storm top as well as the vertical velocity, liquid water content and cloud temperature throughout the depth of the storm. The radiosonde data used for this purpose were generally available within 2 hr and 50 km of the time and location of the maximum radar storm top. Similarly, surface data were available within 30 min and 50 km of the maximum radar storm top. Figure 1 illustrates the maximum radar-observed storm tops plotted against the maximum computed storm tops for the 29 cases. The height used for the maximum computed storm top was the height at which W_z decreased to 10 m sec^{-1}, approximately the fallspeed of radar detectable particles at the height of the maximum radar storm top. Error bars in Fig. 1 indicate the vertical half-power radar beamwidth. In 75% of the cases, the computed storm tops agree within ± 0.8 km and only 25% of the computed storm tops fail to agree with the radar storm tops within the limits of the radar beamwidth. The degree of agreement exhibited between observations and computations suggests that the LMA model results yield reasonable estimates of the cloud environment within the updraft core of Alberta hailstorms.

Vertical Velocity and Liquid Water Content Estimates

Since the 29 vertical velocity and liquid water content profiles displayed variations related to the maximum available energy, they have been classified into Low, Medium and High Energy categories using cloud physical and dynamical considerations to specify boundaries as follows:

Low Energy ($0.0 - 0.2$ J gm^{-1}) - do not penetrate tropopause; storm top temperature >-40C.

Medium Energy ($0.2 - 0.45$ J gm^{-1}) - do not significantly penetrate the tropopause; -60C $<$ storm top temperature <-40C.

High Energy (>0.45 J gm^{-1}) - penetrate the tropopause significantly; storm top temperature <-60C.

Figure 2, which displays envelopes of the vertical velocity and liquid water content profiles, illustrates clearly that as the available energy increases, so does the maximum vertical velocity, maximum liquid water content and maximum storm top. Of particular relevance to the growth of hail are the cloud conditions between the 0C and -40C levels. In this hailgrowth region in Low Energy storms, the liquid water content averages $\simeq$1.8 gm m^{-3} with average vertical velocities of $\simeq$12 m sec^{-1}. Particularly important is the fact that Low Energy storms do not penetrate above the -40C level. This, in conjunction with updraft values not dissimilar to hailstone fallspeeds, permits hailstones to grow during both ascent and descent through the updraft core. The result is a highly efficient hail producing mechanism; surface hail observations taken in conjunction with Low Energy storms indicate that maximum hail sizes averaged from grape to walnut size. Medium and High Energy storms differed substantially in that they penetrate the -40C level with updraft values averaging $\simeq$20-40 m sec^{-1}. Due to these high vertical velocities, hailstones growing during ascent would not attain a fallspeed sufficiently large beneath the -40C level to permit them to descend back through the updraft core while continuing their growth. Instead, small hail particles would be swept upward through the -40C level and forced to descend external to the updraft core region. Surface observations of maximum size hail taken during Medium Energy storms revealed walnut to golfball size hail; High Energy storms were found to yield maximum size hail of golfball and larger than golfball size.

References

1. Chisholm, A.J., 1970: Alberta Hailstorms: A Radar Study and Model. Ph.D. Thesis. McGill University, Montreal, Canada

2. Phillips, B.B., and P.A. Allee, 1968: Experimental study of rain formation by coalescence. Proc. International Conference on Cloud Physics, Toronto, 102-106.

3. Stackpole, J.D., 1967: Numerical analysis of atmospheric soundings. J. Appl. Meteor., 6, 461-466.

Fig. 1

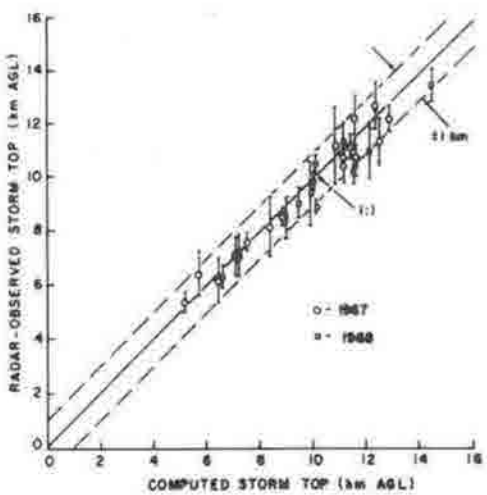

Fig. 2

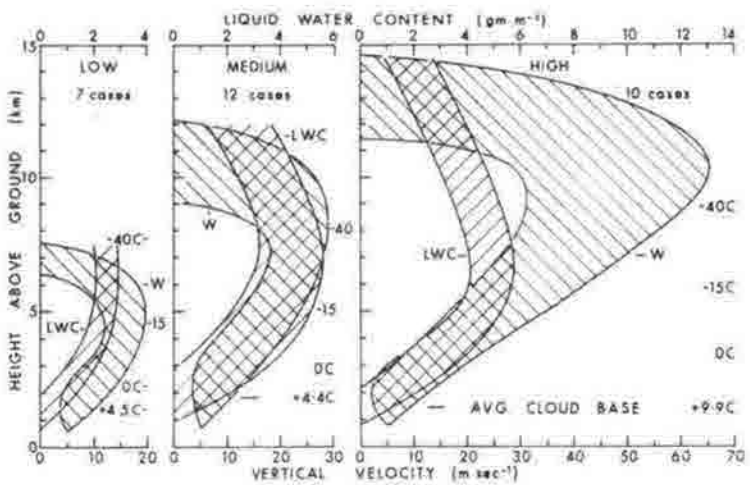

ON THE ROLE OF MICROPHYSICS IN CUMULUS DYNAMICS

Phanindramohan Das
Air Force Cambridge Research Laboratories
Bedford, Massachusetts

1. INTRODUCTION

Condensation of water vapor - a microphysical process - being its main driving mechanism, the cumulus should obviously experience an intimate interaction of cloud microphysics with its dynamical life. That this may indeed be the case has become increasingly obvious since the discovery, by the Thunderstorm Project, of the role of precipitation formation in the initiation of downdraft in and the subsequent dissipation of the cumulus. An important step in our understanding of how exactly this role is played was taken by Das (1) who constructed a simple one-dimensional precipitating model of the cumulus and showed how downdraft developed from an initially steady all-updraft cloud. This study was followed up by Srivastava (2) with a more realistic parameterization of the precipitation process. Precipitation effects have since been introduced, physically in a way similar to that of Das and Srivastava, by Arnason et al (3) and Liu and Orville (4).

It is noteworthy that all the studies mentioned used the classical thermodynamic equation which, in view of the unsaturated downdraft discovered by the Thunderstorm Project, is obviously inadequate. Studies of Kamburova and Ludlam (5) and Das and Subba Rao (6) have demonstrated that the downdraft, carrying most of its liquid water in the form of precipitation, does not get enough evaporated moisture to saturate it and thus becomes progressively more unsaturated as it descends. Thus, obviously, the classical saturation-adiabatic process is not sustained in the thunderstorm downdraft. Circumstances in which the saturation-adiabatic assumption may be inadequate even for an updraft have been revealed by the studies of McDonald (7) and Golovin (8). Taking the lead from these studies Das (9) has suggested a thermodynamic system in which the classical saturation assumption is obviated and has argued that the thermodynamics of the cloud is likely to depart appreciably from the classical picture when precipitation formation has advanced to such a stage as to consume most of the droplets which, in large numbers, are necessary for sustaining condensation at the near-classical rate. The study outlined below has been designed to examine the implications of this suggestion.

2. THE PHYSICAL MODEL OF A PRECIPITATING CUMULUS

The initial model is one of a steady-state, one-dimensional and non-precipitating cloud which is generated by the saturation-adiabatic process. This cloud is then treated as consisting of water nuclei and droplets, and subjected to a time-dependent treatment incorporating a microphysical condensation formula. A second steady state is then obtained with a vertical profile of droplet sizes and an attendant supersaturation of comparatively small magnitude. At this stage the concentration of nuclei and droplets per unit mass of the cloud air remains constant at $1.5\times10^{9}\,kg^{-1}$ (which is close to 1500 cm^{-3} at the cloud base).

Initial precipitation formation is handled by an autoconversion formula due to Berry (10), which gives a rate of conversion of a cloud into one with droplets having a sixth-moment radius of 40 μ. Assuming that the autoconverted fraction of the cloud water conforms to Golovin distribution, it is partitioned into the three classes of smallest precipitation drops, while returning a part to the droplet population. The hydrometeor spectrum is described by 13 classes of drops with their mean radii falling on an approximately logarithmic scale. The drop classes generated by autoconversion are then allowed to grow by accretion as well as condensation. The relative rates of growth of the classes are used to generate drops of larger sizes by way of a quasi-Lagrangian parameterization. Break-up of drops is incorporated by a scheme devised in accordance with the experimental results of d'Albe and Hidayetulla (11).

3. THE EQUATIONS

In numerical modelling the equations and procedures of computation are as important as the mathematical statements of the physical laws they simulate. Therefore we directly state the numerical forms of the physical equations.

The equations used in this study are

a momentum equation: $$w_i^{n+1} = w_i^n + \ell c_1 \overline{w}\,(w_{i-\ell}^{\,n} - w_i^n) + c_3 b; \qquad (1)$$

a thermodynamic equation: $$\theta_i^{n+1} = \theta_i^n + \ell c_1 \overline{w}\,(\theta_{i-\ell}^{\,n} - \theta_i^n) + \Delta t\,\overline{w}\,\overline{G} + \overline{H}_i^{\,n}; \qquad (2)$$

a moisture equation: $\xi_i^{n+1} = \xi_i^n + \ell c_1 \overline{w} (\xi_{i-\ell}^n - \xi_i^n) - \xi_i^n$; (3)

an equation for droplet concentration:

$$N_i^{n+1} = N_i^n + \ell c_1 \overline{w} (N_{i-\ell}^n - N_i^n) - A_i^n - C_i^n ; \quad (4)$$

an equation for the droplet mass:

$$m_i^{n+1} = m_i^n + \ell c_1 \overline{w} (m_{i-\ell}^n - m_i^n) + \mu_i^n ; \quad (5)$$

An equation for the concentrations of drops (written for the k-th class):

$$\nu_{k,i}^{n+1} = \nu_{k,i}^n + \ell' c_1 (\overline{w} - V_k) (\nu_{k,i-\ell'}^n - \nu_{k,i}^n) + p_k A_i^n m_i^n + \nu_{k-1,i}^n D_{k-1,i}^n / (x_k - x_{k-1}) - \nu_{k,i}^n D_{k,i}^n / (x_{k+1} - x_k) ; \quad (6)$$

where q_i^n is the value of a quantity q at the end of the n-th time step and at the i-th point of the (vertical) grid. In the above equations w is the vertical velocity, θ, the temperature part of buoyance ($\theta = \Delta T/T_e$ in customary symbols), ξ the water vapor mixing ratio, m the droplet mass, N the droplet concentration (per unit mass of air) and ν_k is the concentration of the precipitation drops of the k-th size. In addition $c_1 = \Delta t/\Delta z$, Δt being the time step and Δz the space-grid interval; $c_3 = g\Delta t$, where g is the acceleration due to gravity; $\ell = \text{sgn}(w_i^n)$, being +1 when $w_i^n > 0$ and -1 when $w_i^n < 0$; $\overline{w} = (w_i^n + w_i^{n+1})/2$; $\overline{G} = (\gamma_i - \gamma_d)/2T_{ei} + (\gamma_{i-\ell} - \gamma_d)/2T_{ei-\ell}$, where γ_i and T_{ei} are the environmental lapse rate and temperature at the i-th grid point and γ_d is the dry-adiabatic lapse rate; $\overline{H} = (L/2c_p)(1/Tei + 1/Tei-\ell)\mu_i^n$ = droplet growth by condensation = $\Delta t\, f_i (S_i^n - 1) r_i^n$, where f stands for an expression involving temperature, pressure, diffusivity, conductivity and saturation vapor pressure in Mason's formula for droplet growth, S is the saturation ratio, r is the radius of the droplet; χ_i^n = condensation-evaporation function = $N_i^n \mu_i^n + \Delta t\, f_i (S_i^n - 1) \sum F_k R_k \nu_{k,i}^n$, where F_k is the ventilation factor for and R_k is the radius of the drop of the k-th class; A_i^n and C_i^n are the numbers of droplets lost by autoconversion and accretion. V_k is the terminal velocity of the drops in the k-th class; $\ell' = \text{sgn}(\overline{w} - V_k)$, being +1 when $\overline{w} - V_k > 0$ and -1 when $\overline{w} - V_k < 0$; p_k is a partitioning factor and $D_{k,i}$ is the total growth (by condensation as well as collection) of the k-th class of drops.

4. RESULTS & REFERENCES

The results of the computation confirm that in a nonprecipitating cloud supersaturations are small and that the adiabatic approximation is quite adequate. As precipitation progresses supersaturation tends to increase and becomes very large especially in the later stages of the life of the cloud. This might be due to modelling conditions but one can confidently state that fairly high supersaturations - of the order of 10 to 20% - are a distinct possibility in a tall precipitating cumulus. - - - Being time-dependent, the present model shows all the characteristics of the earlier models of similar nature and, in addition, gives sharp accumulation zones of liquid water which changes its size and position with time. The subcloud downdraft, although accompanied with large amounts of liquid water, never gets saturated.

(1) Das, P., 1964: Role of condensed water in the life cycle of a convective cloud. J. Atmos. Sci., 21, 404-418.

(2) Srivastava, R.C., 1967: A study of the effect of precipitation on cumulus dynamics. J. Atmos. Sci., 24, 36-45.

(3) Arnason, G., R.S. Greenfield and E.A. Newburg, 1968: A numerical experiment in dry and moist convection including the rain stage. J. Atmos. Sci., 25, 404-415.

(4) Liu, J.Y., and H.D. Orville, 1969: Numerical modelling of precipitation and cloud shadow effects on mountain-induced cumuli. J. Atmos. Sci., 26, 1283-1298.

(5) Kamburova, P.L., and F.H. Ludlam, 1966: Rainfall evaporation in thunderstorm downdrafts. Quart. J. Roy. Meteor. Soc., 92, 510-518.

(6) Das, P., and M.C. Subba Rao, 1968: The unsaturated downdraft. Proc. Intern. Conf. Cloud Physics, Toronto, Canada, 592-596.

(7) McDonald, J.E., 1962: A note on anomalous adiabatic cooling rates in clouds. J. Atmos. Sci., 19, 309-312.

(8) Golovin, A.M., 1963: On the kinetic equation for coagulating cloud droplets with allowance for condensation. Izv. Akad. Nauk SSSR, Ser. Geofiz., 5, 1571-1580.

(9) Das, P., 1969: The thermodynamic equation in cumulus dynamics. J. Atmos. Sci., 26, 399-407.

(10) Berry, E.X., 1968: Modification of the warm rain process. Proc. First Nat. Conf. Wea. Modification, Albany, 81-85.

(11) d'Albe, E.M.F., and M.S. Hidayetulla, 1955: The breakup of large water drops falling at terminal velocity in free air. Quart. J. Roy. Meteor. Soc., 81, 610-613.

ON THE SOURCE OF CLOUD NUCLEI

J. E. Dinger and R. E. Ruskin
Naval Research Laboratory, Washington, D. C. 20390

INTRODUCTION

Previous measurements by Twomey and Wojciechowski[1] made on aircraft flights over the ocean in various parts of the world suggest that the cloud condensation nuclei (CCN) in the maritime atmosphere are produced by a widespread and relatively uniform source rather than resulting from an aerosol of continental origin which is depleted during its circulation over the ocean. They comment further that there is nothing in their measurements which requires that the marine cloud nuclei originate at the sea surface rather than within the atmosphere. Further evidences of an atmospheric source are found in the measurements in subsident marine atmospheres at Barbados and over the N. Atlantic as well as in a comparison with measurements over Florida in a convective situation.

MEASUREMENTS

The Florida measurements were made by the method described by Twomey[2]. The same basic method, extended as described by Dinger[3], was used for the measurements on Barbados and over the North Atlantic. In this method the air sample is divided and passed through six parallel tubes, one at room temperature and the other five heated to various temperatures, the highest being approximately 600 C. Discrimination between sea salt and other types of CCN is based upon the laboratory finding that sea salt nuclei are apparently unaffected by preheating to 600 C; whereas most other types of CCN are volatilized or by some mechanism become inactive after they have been preheated. Different types become inactive at different temperatures. Data on volatility were obtained by bubbling filtered air through a water solution of the particular salt in question. After the small droplets are formed and their water evaporated, the resulting aerosol contains particles of the former solute in sizes appropriate for use as CCN. By mixing a controlled proportion of filtered air with the aerosol from the bubble chamber a concentration of approximately 400 CCN cm^{-3} is introduced into the diffusion chamber with flow rates and other conditions similar to those used in making field observations. About half of the H_2SO_4 CCN were inactive after heating to a temperature of 150 C and all were apparently volatilized at 250 C. With $(NH_4)_2 SO_4$, heating to 150 C had no effect; but 80% were destroyed at 250 C and essentially all at 330 C. NaCl and oceanwater CCN were little affected by temperatures as high as 600 C. The latter measurement was further verified by measurements at Barbados using sea water within minutes after obtaining it from the surf.

Applying the results of these laboratory measurements to field observations makes it possible to determine that the CCN in an air sample are not composed of sea salt if all nuclei become inactive at the lower heating temperatures. Even though the CCN in the sample survive heating to 600 C it cannot be definitely stated that they are composed of sea salt, but they are definitely not any of a dozen or so other compounds which have been found to volatilize at the lower temperatures.

Aircraft Measurements

The first of the aircraft measurements presented here were made using a single channel to preheat the sample, which was then brought to approximate room temperature in a conditioning chamber. After the CCN had been photographically recorded in the diffusion chamber at a supersaturation of .75%, a new sample was introduced into the conditioning chamber without passing through the preheating channel, and the measuring procedure repeated. This method was used for the portion of the data in Fig. 1 labeled Florida. The sequential sampling required in this method introduced considerable spread in space and time between samples and hence reduced repeatibility. The N. Atlantic measurements were made with the multichannel sampling heaters, which permit simultaneous collection of the one unheated and five samples preheated to different temperatures to be accumulated in six separate conditioning chambers. The diffusion chamber measurements were then made sequentially. Occasional checks determined that the storage time in the conditioning chambers did not appreciably affect the measurements.

Aircraft Results

The right-hand curve of Fig. 1 presents measurements made over Florida on two days of 1968 on which the wind was from the north, resulting from circulation around a high pressure area in the Gulf of Mexico. The trajectory of the air had probably included crossing the Gulf states and flowing down the peninsula. The air at the cloud base had a typical continental type of cloud nucleus concentration averaging 1285 cm^{-3} with a decrease with altitude to about 200 at 17,000 ft. At the times of the Florida profiles the air was quite convective over the peninsula with cumulus clouds growing to 20 to 30,000 ft.[4]. After two days the wind shifted from north to generally west or south. During this period there was a tropical disturbance in the area. The CCN count at cloud bases appeared to have a mixture of continental and maritime concentrations (500 cm^{-3}). Cloud growth was generally faster and higher than on the two days represented by the right hand curve of Fig. 1. More mixing by convection produced considerably less drop in CCN concentration with altitude than had been the case during the period indicated in the figure as "continental". In both of these curves the concentrations of CCN at the higher altitudes were comparable to those in the next curve labeled N. Atlantic.

The CCN remaining after heating (sea salt) are shown in the three left hand curves. The concentration over Florida was almost constant with altitude, generally 25 to 50 CCN cm^{-3}. At the low altitude this concentration was comparable to that over the open ocean as shown in the left hand curve labeled N. Atlantic Subsident. The results here are markedly different from those shown in the sea salt curves in the convective Florida situation. Under the subsident conditions, mixing from the lower altitude apparently did not extend much above the temperature inversion. On the other hand the total CCN count decreased with altitude up to the temperature inversion and then increased markedly above that altitude, but with essentially no sea salt nuclei present.

Barbados Measurements

The same multichannel instrumentation which had been used on the aircraft measurements was set up near the beach on the upwind (east) side of Barbados. Here some samples were drawn from an inlet 20 m above the ground and others were drawn from a point near the water's edge. The average from 52 sets of measurements of total CCN was only about 5% greater at the waters edge than from the 20 m tower (389 vs. 374 CCN cm^{-3}). The fraction of sea salt CCN surviving after the heating was approximately 47% for the sample from the water's edge and 40% at the tower.

DISCUSSION

The data presented indicate that in the maritime air arriving at Barbados less than 50% of the CCN have a sea salt origin.

In a generally subsident situation the sea salt contribution to the total CCN decreased with altitude to essentially zero at the temperature inversion level. Above this altitude the total CCN increased with altitude for several thousand feet, reaching a concentration higher than had been present at cloud base.

The origin of these nonsalt nuclei at the higher altitude remains an open question. The likelihood that the higher altitude CCN found in subsident air were residue from a continental source is reduced by the further determination that the seasalt content above the inversion is far less than that found in convective air at the same altitude over Florida.

Under convective conditions the sea salt contribution to CCN extends to much higher altitudes, constituting 2 to 5% of the total at cloud base and increasing to possibly 20% at 17,000 ft. (the salt nuclei count remaining constant with altitude).

A likely source for the volatile component comprising most of the CCN at higher altitudes in the subsident maritime air masses is suggested by Dinger[3] to be by formation of sulfates or sulfuric acid by the oxidation of SO_2 or NH_4 over an extended area of the atmosphere.

ACKNOWLEDGEMENT

This work was sponsored by the U. S. Naval Air Systems Command.

REFERENCES

1. Twomey, S., and T. A. Wojciechowski, 1969; Observations of the geographical variation of cloud nuclei. J. Atmos. Sci. 26, 684-688.

2. Twomey, S., 1968; On the composition of cloud nuclei in the northeastern United States. J. Rech. Atmos., 3, 281-285.

3. Dinger, J. E., 1970; On the source and composition of cloud nuclei in a subsident air mass over the North Atlantic. J. Atmos. Sci., in press.

4. Simpson, J., W. Woodley, H. A. Firedman, T. W. Slusher, R. S. Sheffee, and R. L. Steele, 1970; An airborne pyrotechnic cloud seeding system and its use. J. Appl. Meteor., 9, 109-122.

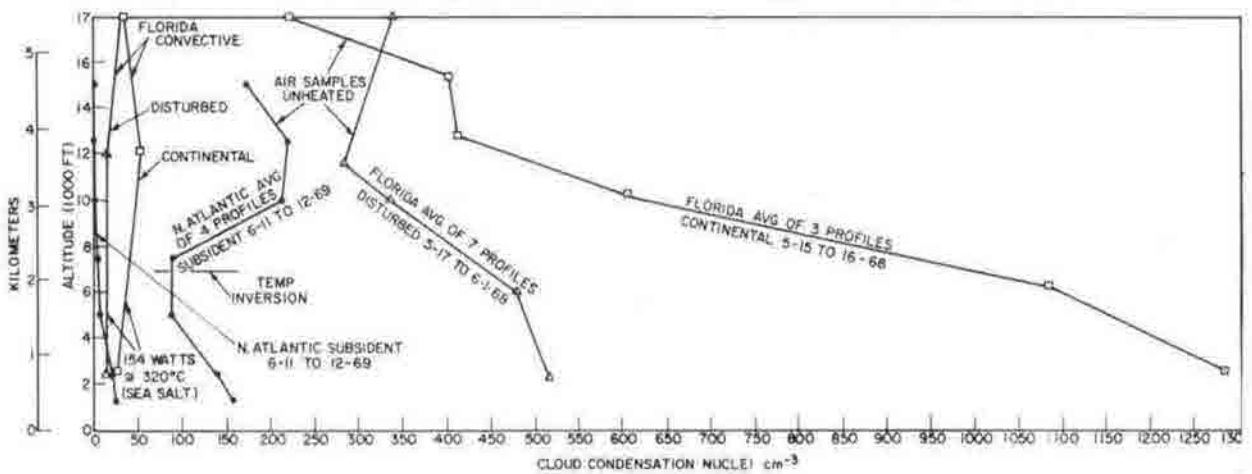

NUMERICAL SIMULATION OF THREE-DIMENSIONAL CONVECTIVE ELEMENTS

Douglas G. Fox
National Center for Atmospheric Research
Boulder, Colorado

INTRODUCTION

The simulation of thermals or convective elements by solving the appropriate equations of motion numerically has been accomplished by Lilly (1) and Ogura (2) among others. Ogura (2) solved a set of inviscid equations for an axisymmetric thermal. The solution was effected by artificial damping due to the particular finite difference scheme he chose. Nevertheless Ogura's results indicated an approach to the shape-preserving solution developed by Scorer (3). No confirmation of this solution could be made since the effects of boundaries were present in the numerical calculations. Lilly (1) avoided this difficulty by introducing a coordinate system which expanded in time at a rate governed by the similarity solution. Lilly's simulations were of a line (two-dimensional) thermal. They included a constant eddy viscosity. These two basic studies have received a great deal of attention largely because they showed that some of the essential dynamics of a convective system could be simulated numerically. It is not necessary to review the important numerical cloud models which are based upon mixing these dynamics with numerical solutions of cloud physics equations. There is, however, one strong limitation of all of these models which is linked to their two dimensionality (or axisymmetry). Since natural clouds are turbulent phenomena one must question the ability to model them with nonturbulent dynamics and, in particular, with a two-dimensional system which must suppress three-dimensional motions. In fact, recent work by Lilly (4) has shown that the hypotheses of Kraichnan and Leith concerning turbulence in two dimensions are correct, and that two-dimensional turbulence, while possible, is basically different from the three-dimensional variety on which clouds are based. One then must ask how essential is the simulation of turbulence to cloud modeling. Certainly it is clear that a turbulent model would be an improvement in principle over a nonturbulent one, and is therefore desirable.

Our purpose here is to present some preliminary results of a simulation of three-dimensional thermals. We use a system which is an extension of Lilly's earlier shape-preserving, two-dimensional solution. The results illustrate some of the difficulties in achieving turbulence in a numerical model while, at the same time, they indicate a steady transition toward this goal. The limitations of a constant eddy viscosity are clearly illustrated.

EQUATIONS

The Boussinesq system for an incompressible fluid is

$$\frac{\partial}{\partial t}\mathbf{V} + \mathbf{V}\cdot\nabla\mathbf{V} = \Delta T \propto g\mathbf{j} - \frac{1}{\rho}\nabla P + \nu\nabla^2\mathbf{V}, \tag{1}$$

$$\nabla\cdot\mathbf{V} = 0, \tag{2}$$

$$\frac{\partial}{\partial t}T + \nabla\cdot(\mathbf{V}T) = \kappa\nabla^2 T. \tag{3}$$

All the notation is conventional.

Dimensional analysis of a thermal (3) suggests that if F_o is the initial buoyancy, a constant defined as $\Delta_o R_o^3$, Δ is the density deficiency $g\propto\Delta T$, z is the height of the thermal above its source, $w\,(=dz/dt)$ the velocity of rise of the thermal, and R the width of the thermal, then the following proportionalities should be true:

$$R \sim z \quad ; \quad w \sim F_o^{1/2} z^{-1} \quad ; \quad \Delta \sim F_o z^{-3}$$

Introduction of this type of solution into equations (1)-(3) yields the following system, in terms of dimensionless variables:

$$\frac{\partial}{\partial s}\mathbf{V}' = -(\mathbf{V}'-\mathbf{X}')\cdot\nabla'\mathbf{V}' + \mathbf{V}' + T'\mathbf{k} - \nabla'\pi' + \nu'\nabla'^2\mathbf{V}' = \mathbf{R}' - \nabla'\pi', \tag{4}$$

$$\nabla'\cdot\mathbf{V}' = 0, \tag{5}$$

$$\frac{\partial}{\partial s}T' = -\nabla'\cdot(\mathbf{V}'-\mathbf{X}')T' + \kappa'\nabla'^2 T', \tag{6}$$

where

$$\mathbf{X}' = \frac{\mathbf{X}}{\ell} \; ; \; \mathbf{V}' = \frac{\mathbf{V}}{\dot{\ell}} \; ; \; T' = \frac{\Delta T}{\Theta} \; ; \; \pi' = \frac{P/\bar{\rho}}{\dot{\ell}^2} \; ; \; \begin{Bmatrix}\nu'\\ \kappa'\end{Bmatrix} = \frac{(\nu,\kappa)}{\ell\dot{\ell}} \; ; \; s \sim \ln(t) \tag{7}$$

and the length scale ℓ is proportional to $t^{\frac{1}{2}}$ and the temperature scale Θ is proportional to $t^{-3/2}$. Notice that a logarithmic relationship exists between dimensionless time and real time so that in our typical numerical experiments which run for 2-3 dimensionless time units, the grid volume increases on the order of 10 times its original size. In order to insure incompressibility and solve for the pressure field, we form a Poisson equation for π' by taking the divergence of (4) yielding

$$\nabla'^2 \pi' = \nabla' \cdot \mathbf{R}' - \frac{\partial}{\partial t}(\nabla' \cdot \mathbf{V}') \tag{8}$$

The numerical methods used are those which have become nearly standard for three-dimensional solutions of the Navier-Stokes equations(Deardorff (5)). They are based upon using an Arakawa second-order accurate scheme for the spatial discretization on a staggered space grid and a centered time step. The Arakawa scheme can be shown to conserve energy and other square quantities.

A test of the numerical scheme, in fact of the entire procedure, is to consider the balances resulting from integrating the kinetic energy equation, the potential energy equation, and the temperature and temperature variance equations over the entire volume. Performing these integrations suggests the following relationships:

$$E_K \,(K) = -E_P \,(P) - \epsilon_K \,(\epsilon) = \{E_K : E_P\}\,(X) - \epsilon_K \,(\epsilon)$$
$$T^2/2 \;\; (T) = \frac{1}{3}\,\epsilon_T \,(\theta) \tag{9}$$

Figure 1 illustrates the time history of these various terms. As is obvious a steady state is achieved, and the various relationships of (9) are held.

RESULTS

Because of the nondimensionalization there are only two parameters of the equations, namely ν' and κ'. It is important to realize that ν' really represents the inverse of a Reynolds number since

$$\nu' \equiv \nu / \ell \dot{\ell} = \nu / \sqrt{g\alpha\theta\ell^3}$$

where the relationship between the length velocity product and the buoyancy comes from the second of the similarity relationships. Clearly then the parameter represents a measure of the strength of the thermals in the solution. It is of further interest to note that the product of length and velocity is constant and therefore the local Reynolds number is constant. This indicates that the flow in a thermal will remain stable (laminar) if the Reynolds number is subcritical and will be unstable (turbulent) if that parameter is made supercritical. The second parameter of the solution is a Prandtl number (ν'/κ') and will be unity for all the work described herein.

Figures 2, 3 and 4 show the results of calculations with Reynolds numbers of 10, 50 and 75, respectively. The change in the solution is obvious; as the Reynolds number increases the thermal rises to a higher position and becomes narrower. At the same time gradients tighten up and the front becomes more defined. Figure 5 shows the ratio of $\mathbf{Z}/\mathbf{R}$ for a number of experiments as a function of Reynolds number. Shown also are Scorer's experimental results. Reynolds number 100 is the largest which can be calculated without excessive numerical errors on the present grid (approximately 10,000 grid points). Clearly our solution is not turbulent, however, is approaching turbulence. Were one able to increase the grid sufficiently to achieve a supercritical Reynolds number, then the solution presumably would be turbulent. Indications are that the critical Reynolds number for a thermal is of order 100, however, the precise number is not known. It is obvious that considerably more grid points are needed to achieve turbulence. Since the number of grid points required increases at least as the third power of the Reynolds number, these results are not encouraging.

Figure 5 shows further that with a Reynolds number of 40-50 we reproduce at least one of the statistics of laboratory thermals quite well. In fact figure 3, the Re = 50 case, compares very well with the laboratory realizations. Thus if one desired mean motions one could consider this value of 50 an eddy Reynolds number. A precise comparison of this case with the laboratory results is quite good since the only laboratory results available for comparison are essentially averaged data. Thus with the eddy viscosity concept one is able to reproduce the mean motions of a thermal quite well except for some sharpness of the thermal boundaries which is rather diffuse in the numerical case compared to laboratory results. However, it must be realized that there is no explicit turbulent mixing going on in this thermal, but rather all is occurring on a subgrid scale. If the nature of the turbulent interaction is of interest and need be simulated, the constant eddy viscosity concept is of limited use. An improvement of this procedure may be to use a nonconstant eddy viscosity. This is under investigation.

The author wishes to acknowledge that this work has been strongly aided and improved from advice and insights given him by D. K. Lilly, J. W. Deardorff and S. A. Orszag.

REFERENCES

1. Lilly, D. K. 1964: J. Atmos Sci., 21, pp. 83-98.
2. Ogura, Y. 1962: J. Atmos Sci., 19, pp. 492-502.
3. Scorer, R. S. 1947: J. Fluid Mech., 2, pp. 583-594.
4. Lilly, D. K. 1969: Phys. Fluids Supplement II, pp. II-240 - II-249.
5. Deardorff, J. W. 1970: J. Fluid Mech., 41, pp. 453-480.

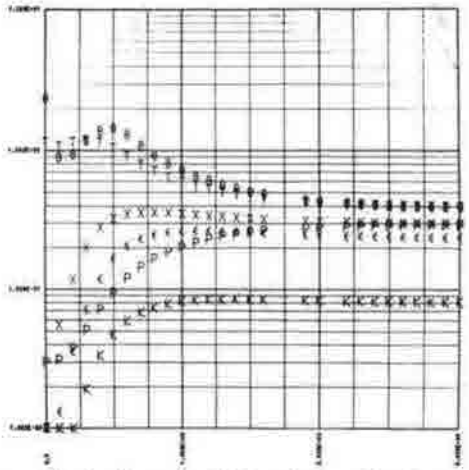

Fig. 1. Integrals of the motion as a function of dimensionless time. X is the total kinetic energy, P the negative potential energy, x the exchange between kinetic and potential energy, T the temperature variance, ϵ the dissipation of kinetic energy and θ the thermal dissipation.

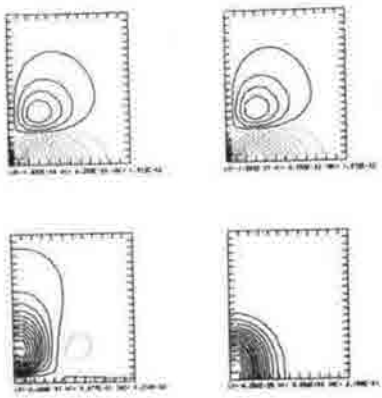

Fig. 2. Reynolds number 10 contours (clockwise from upper left, u horizontal velocity, v horizontal velocity, T temperature difference, and w vertical velocity) on an r-z plane at 45° from u and v axes.

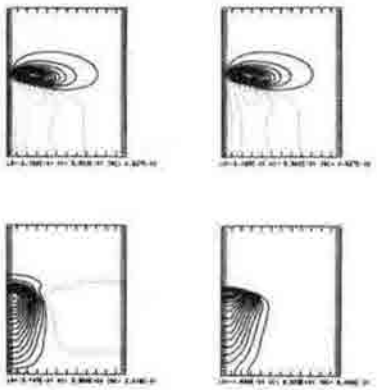

Fig. 3. Reynolds number 50 contours (see figure 2).

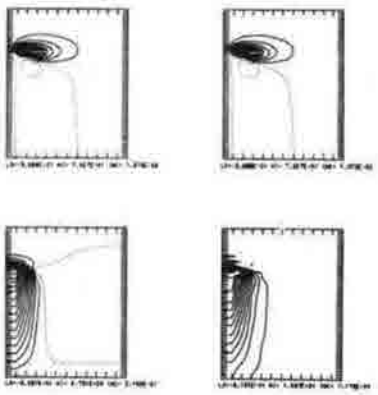

Fig. 4. Reynolds number 75 contours (see figure 2).

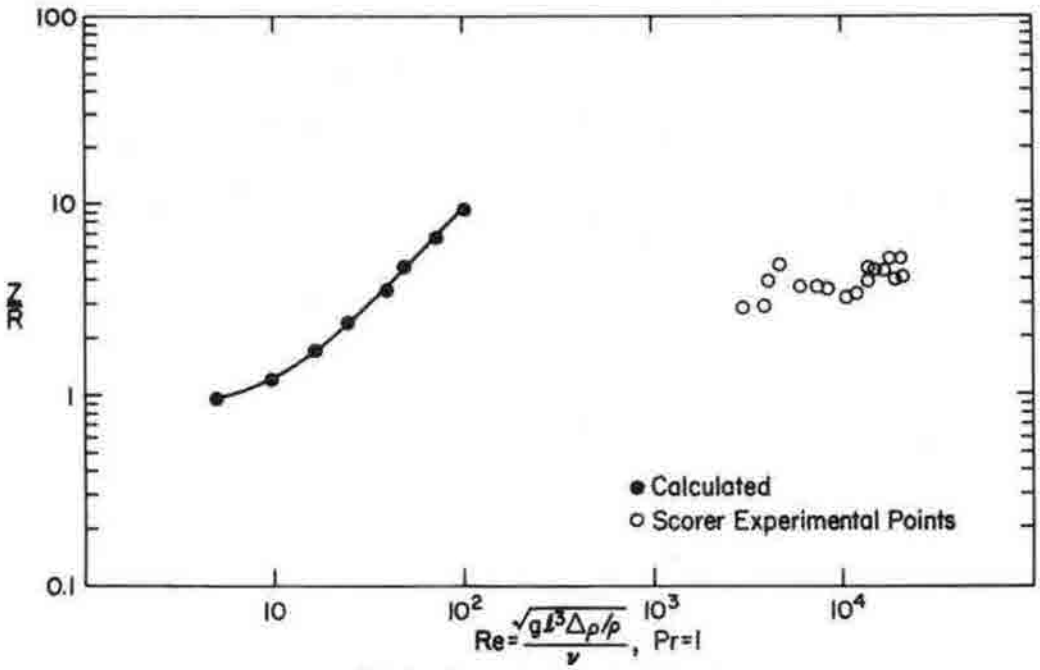

Fig. 5. z/R as a function of Reynolds number.

SOME RESULTS OF MEASUREMENTS OF THE LATENT HEAT RELEASED FROM SEEDED STRATUS

Robert G. Knollenberg
The University of Chicago Cloud Physics Laboratory

INTRODUCTION

Experiments were conducted during February 1968 in northern Wisconsin to study the latent heat released during glaciation of seeded stratus. Experiments were designed to measure the temperature increase during glaciation. From such thermal mapping it was hoped to gain insight into the mechanism(s) responsible for the spread of glaciation.

A comprehensive theory describing the spread of a glaciated region has been developed by Kolesnikov and Belyaev (1) assuming the mechanism for spread is turbulent diffision. It has not been tested with field data and may not be satisfactory. In particular the model is quite sensitive to initial ice crystal concentrations while field results often indicate indistinguishable results with seeding materials which give vastly different ice crystal concentrations. See Knollenberg (2) Kidney (3).

The only reference to convective activity induced by seeding in stratus is an observation by aufm Kampe (4). However, in light of the present findings prior work was reexamined and the author finds considerably greater support for cellular development.

EXPERIMENTAL DESIGN

The aircraft used in these experiments was an NCAR Queen Air instrumented to make state parameter, logistics, radiative and cloud parameter measurements. As a minimum the experiement required knowledge of aircraft position with respect to the cloud, temperature, liquid water content, and extent of glaciation. These measurements were obtained with a doppler navigational system, liquid water content meter, three independent temperature sensors, and an optical array particle measuring system Knollenberg (5).

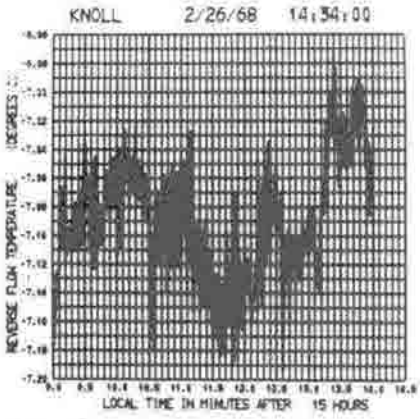

Fig. 1. Raw temperature record from Experiment #2.

In order to measure anticipated heating effects of only 0.5 to 1.0C extreme lateral temperature homogeniety with less than 0.1C variation is desirable. Fig. 1 shows that over a few miles these clouds meet this criterion. Seeding was accomplished with dry ice at a release rate of 10 pounds per mile over a straight line track (overseeding was intended). The dry ice was in large aggregates to insure seeding throughout the vertical depth. The targeting procedure required standard rate turns at constant altitude intersecting the seed line at least once per revolution (see Fig 2).

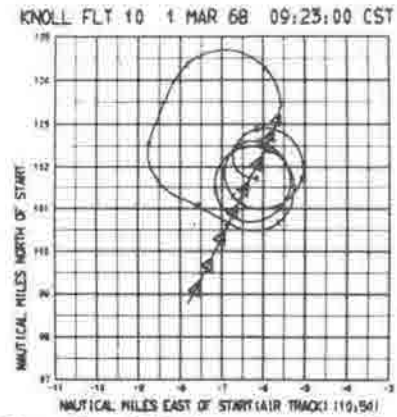

Fig. 2. Flight pattern of Experiment #3. Arrows indicate seed line.

RESULTS OF MEASUREMENTS

The results of these measurements are given in Table I. The measurements were all made at seeding altitude. The measured temperature increases of 0.6 to 1.1 C are consistent with vapor reduction to near ice saturation. The overwhelming latent heat contribution results from ice crystal growth from the vapor density excess. The latent heat of fusion released during freezing of cloud water alone would hardly be measurable.

It is important to emphasize that these measurements represent the maximum heating observed. In the course of these experiments the observed ΔT nearest the seed line usually reaches a maximum within 10 minutes after seeding and then decreases steadily and may become negative. It was found in Experiment 4 that the temperature increased 0.6C in about 10 minutes and then decreased over a degree after 40 minutes (Figure 3). It appears from the measured temperature profiles that glaciation produced vertical motions resulting in a steeper, less stable lapse rate. These results suggest that while the immediate

TABLE I

SUMMARY OF MEASUREMENTS OF TEMPERATURE INCREASE FOLLOWING SEEDING

Experiment #	Cloud Top/ Cloud Base (1000 ft)	LWC ($gm\ m^{-3}$)	Seeding Altitude (1000 ft)	Pre-seed Temperature (C)	Maximum Post-seed Temperature (C)	Temperature Increase (ΔT) (C)	Temperature Increase Attributable to (L_f) (C)	(L_s)
1	9.3/8.0	0.8	9.1	-14.0	-12.9	1.1	0.3	0.7
2	4.8/3.0	0.6	4.2	- 7.1	- 6.5	0.6	0.2	0.5
3	5.0/1.5	0.2	4.5	-11.1	-10.2	0.8	0.1	0.6
4	8.5/6.5	0.5	8.2	-15.3	-14.7	0.6	0.2	0.6
5	6.2/4.5	0.2	6.1	- 6.1	- 5.5	0.6	0.1	0.5

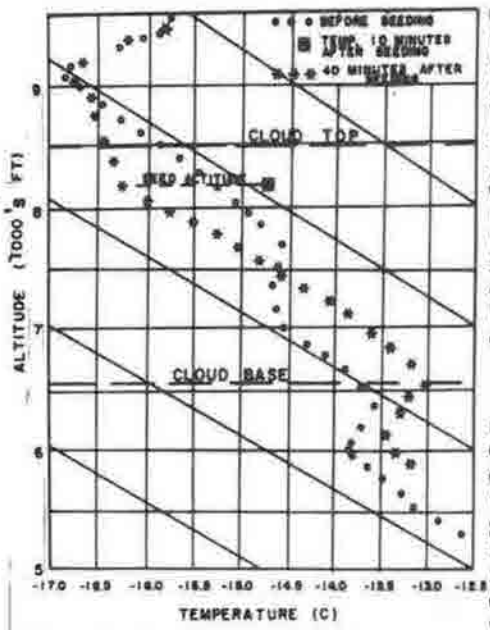

Fig. 3. Vertical profiles before and after seeding in Experiment #4. Note heating below cloud base and steeper lapse rate following seeding.

effects of seeding are simply an increase in local temperature of 0.5 to 1.0C, the temperature structure nearer "equilibrium" is determined by the heating and ascent history of parcels at much lower levels or even below cloud base. Heating in this experiment was observed below cloud base and is attributed to ice crystal growth in an envrionment subsaturated with respect to water but above ice saturation. It has been observed that the entire region from cloud base to ground is often above ice saturation and may provide more water for ice crystal growth than the cloud itself! Observations of snow virga immediately following seeding are attributable to nucleation and growth of ice in the sub-cloud region.

DISCUSSION

The usual temperature profile in these clouds is slightly less steep than moist adiabatic with a subsidence or radiative inversion at cloud top. The strength of the inversion is important in capping vertical motions and inducing horizontal divergence. The divergence near cloud top provides an attractive mechanism for spreading glaciation at more rapid rates than diffusion processes alone. For instance, a lateral spread of 17 miles in 2½ hours was observed in one of our experiments.

Without such an inversion cloud puffs become visible above the seed line. Observations by aufm Kampe (4) of growth to 300 feet above cloud tops were not uncommon (see Figures 36,43,50). It is interesting to point out that within minutes aufm Kampe observed these puffs to subside into a smooth glaciated hole. Still later he observed water clouds appearing in the glaciated hole. This writer suggests that the latter observations are of the upwelling of moist air below cloud base. Convergence of moist air below and near cloud base is thus implied. Kidney (3) suggested the transfer of water into the glaciated region was necessary to explain the computed snowfall. The convergence of moist air below cloud base upwelling into the glaciated region provides such a mechanism.

The writer also suggests that the "closing in" of glaciated regions, frequently cited in the literature, is not incompatable with convergence near cloud base. Examinations of available photographs from seeding experiments definitely do not support a closing in near cloud top. In fact, glaciation is invariably more extensive at cloud top than near base. Furthermore, there is some evidence in the horizontal temperature profiles (30 to 40 minutes after seeding) of subsidence near the boundaries of the glaciated region. The temperature drops by a few tenths of a degree. Also the boundaries of glaciated regions are noticeably more clear than the interior. See aufm Kampe (4),Figures 33, 39, 40, 41.

CONCLUSIONS

These experimental observations and analyses suggest that a small convective cell is often initiated from the release of latent heat during stratus glaciation. Kinematically this cell appears to be of a Bénard type. The Cellular development observed during stratus glaciation is attractive in explaining a more rapid spread of glaciation than by turbulent diffusion alone. It is also helpful in explaining the persistence of snow showers by establishing an important source of moisture below cloud base. Previously unrecognized ice crystal growth and heating below cloud base have been established.

REFERENCES

1. Kolesnikov, A G. and V. I. Belyaev, 1965: The basis of the theory of the propagation of the crystallization process in super-cooled clouds. Proc. Int. Conference on Cloud Physics (Tokyo), 1965.
2. Knollenberg, R. G., 1967: Ice nucleation by soluble compounds: A study of the effects of endothermic heats of solution. Ph. D. thesis, the University of Wisconsin.
3. Kidney, John B., 1965: Winter 1965 field tests of urea, ion incorporated silica,and hydrophobed silica as seeding reagents. University of Chicago Cloud Physics Laboratory, Technical Note No. 31.
4. aufm Kampe, H. J., H. K. Weickmann & J. J. Kelly, 1953: Seeding experiments in super-cooled stratus clouds, Signal Corps Engineering Labs. Tech. Memorandum No. 1576.
5. Knollenberg, R. G., 1970: The Optical Array: An Alternative to Scattering and Extinction for Airborne Particle Size Determination. J. Appl. Meteor., 9, 86-103.

STUDY OF WIND FIELD IN A CONVECTIVE STORM BY DUAL DOPPLER RADAR

Roger M. Lhermitte
Environmental Science Services Administration
Research Laboratories
Boulder, Colorado

The paper presents and discusses observations of convective storm circulation derived from the probing of particle motion inside a storm by use of a dual-Doppler radar system. A single Doppler radar provides information on the spectrum of radial velocity of precipitation particles, which is the particle velocity projected onto the axis of a radar beam. If two radars are installed at different locations and both are scanning the same storm, the two radial velocity fields obtained from the radars can be combined to provide two-dimensional velocity information.

The measurements reported in this paper were derived from such a method and concern observations of the mean air flow estimated from the mean Doppler speed within the assumption that precipitation particles move horizontally at wind speed. The observations were made at the low levels of a convective storm with a low radar beam elevation angle, thereby minimizing the contribution to the Doppler velocity due to the vertical speed of the particle. The observational data are presented in the form of two-dimensional horizontal motion fields at different altitudes, as well as the echo intensity pattern, showing the distribution of precipitation intensity in the same region. An example of such results is shown in Figure 1 which illustrates the well-organized structure of the motion field observed at a mean altitude of 300 meters. One sees that there is a strong dependence between the echo intensity and certain features of the wind field, such as vorticity and convergence. There is a strong vorticity region in the southwest part of the radar cell and there is noticeable convergence between the two cells which can be identified in the figure. Note that the storm was moving steadily at a speed of about 10 m sec^{-1} to the north-northeast direction.

The data obtained at other altitudes show systematic variations of the horizontal motion field, explained by a significant tilt of the vorticity and convergence zones in the direction of the storm's movement. Also, by applying the equation of continuity, the vertical air motion was estimated and showed a significant updraft located slightly ahead of the stronger cell.

The paper also discusses the use of computer processing and data assembling which should enhance the capability of the method and its applicability to the observation and study of three-dimensional convective storm circulation, which should result in drastic advances in the understanding of storm dynamical processes.

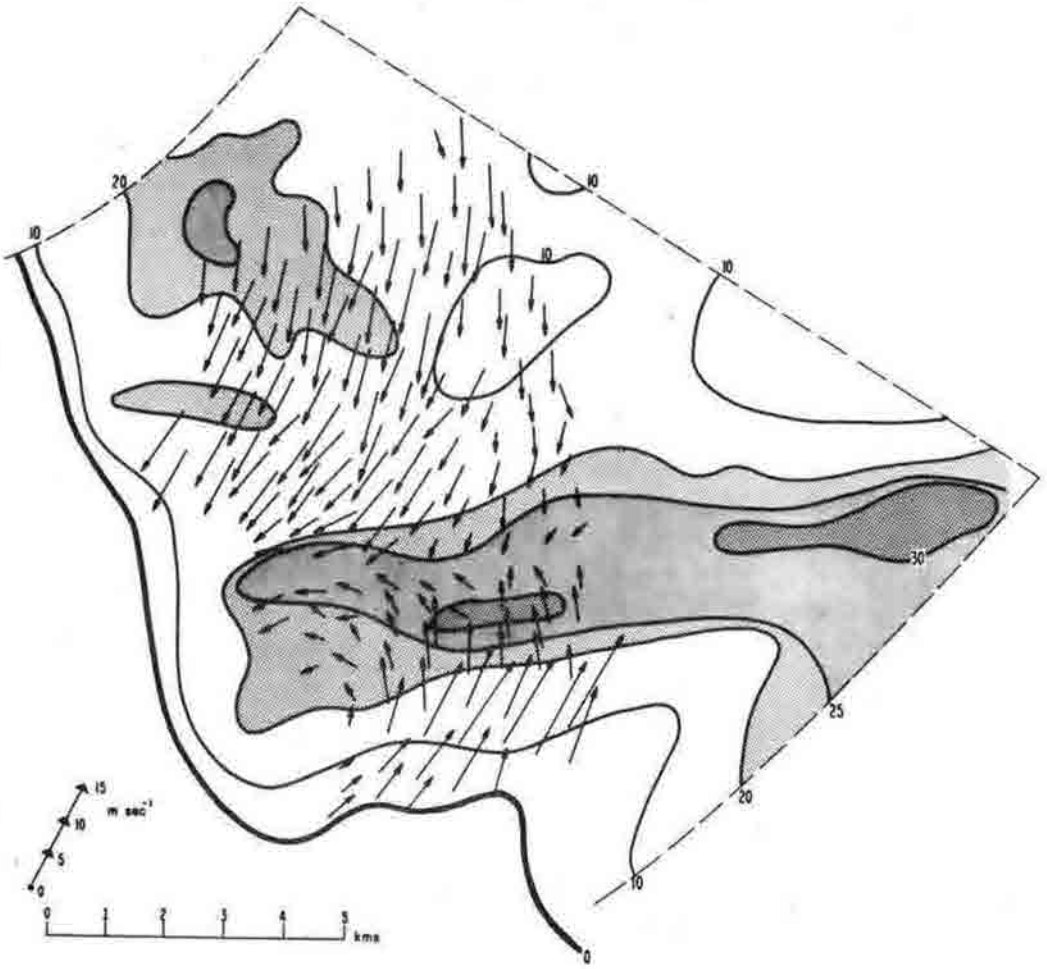

Figure 1. The figure shows the particle horizontal motion field inside a convective storm observed at a mean altitude of 300 meters by a dual-Doppler radar system. Although there is a more extensive region which is covered by one of the radars, the dual-Doppler observations are limited to regions covered by both radars. The echo intensity is also shown by contour lines in the figure. The contour labeled 30 refers to precipitation intensity of 15 mm hr^{-1}. Note the strong vorticity in the southwest part of the storm and the convergence between the two radar cells.

A MORE REFINED GROWTH EQUATION FOR STUDYING CONDENSATION NUCLEI

Richard D. H. Low

Atmospheric Sciences Laboratory, U.S. Army Electronics Command,
White Sands Missile Range, New Mexico

In cloud physics as well as in weather modification, one equation of fundamental importance is that for the growth rate of an isolated immobile liquid solution droplet in a stationary medium of moist air. Several versions thereof may be found in the literature, but they are physically defective in one way or another, all ignoring the lowering of the vapor gradient as a consequence of the release of the latent heat of condensation and most neglecting the hygroscopicity of a condensation nucleus. Neglecting the latter would be tantamount to treating all condensation nuclei alike, and ignoring the former would result in an overestimate of the growth or evaporation rate. This paper chooses to deal alone with these two important processes without regard to such other factors as vapor diffusivity, thermal conductivity, local circulation, and moving boundaries in the hope of placing this basic equation of cloud physics on a more firm physical basis.

The hygroscopic term can be easily incorporated, as will be shown later. To include the effect of vapor gradient lowering, we may visualize that covering the droplet there exists a thin layer, some 10^{-5} cm in thickness, of moist air, which is assumed to be in thermal equilibrium with the droplet temperature. Thus, the droplet experiences a humidity somewhat lower than the ambient, and its growth rate is retarded. So will be its evaporation rate in a low humidity environment. This should be more pronounced during the early stage of growth where the rate is most rapid. In evaporation, the reverse is true. Then, the vapor diffusion equations inside and outside the layer may be written down, respectively, as

$$r\frac{dr}{dt} = \frac{D}{\rho_d}(\rho_\Delta - \rho_r) \quad , \quad \text{and} \quad r'\frac{dr'}{dt} = \frac{D'}{\rho_d'}(\rho - \rho_\Delta) \quad , \tag{1}$$

where ρ_d' is the combined layer and droplet density; $r' = r + \Delta$, Δ being the thickness of the layer; ρ, ρ_r, and ρ_Δ are vapor densities in the ambient air, in equilibrium with the droplet, and in the layer; and D' is the vapor diffusivity outside the layer. Notations which are obvious will not be defined. These two equations can now be combined to eliminate ρ_Δ. Dividing and multiplying the resulting equation by the saturation vapor density $\rho_o(T_r)$ at the droplet or layer temperature T_r, we arrive at the following expression:

$$r\frac{dr}{dt} = \frac{D\rho_o(T_r)}{\rho_d}\left[\left(\frac{\rho}{\rho_o(T_r)} - \frac{\rho_d'}{D'\rho_o(T_r)}\, r'\frac{dr'}{dt}\right) - \frac{\rho_r}{\rho_o(T_r)}\right] \quad . \tag{2}$$

We, then, make use of the Clapeyron-Clausius equation and that for thermal conductivity in a slightly different form as follows:

$$T_r = T + \frac{L\rho_d'}{K}\, r'\frac{dr'}{dt} = T(1 + \xi') \quad , \quad \text{where} \quad \xi' = \frac{L\rho_d'}{KT}\, r'\frac{dr'}{dt} \quad . \tag{3}$$

$$\rho_o(T_r) = (1 + \xi')^{-1}\rho_o(T)\exp\left[\frac{L\xi'}{R_v T(1 + \xi')}\right] \quad , \text{ by using (3)} \quad . \tag{4}$$

Substitution of (3) and (4) into (2) enables the growth equation to be expressed as a function of the ambient temperature, except for $\rho_r/\rho_o(T_r)$, which is still at the droplet temperature. Noting that these density ratios are equivalent to saturation ratios, let us put $S = \rho/\rho_o(T)$, which expresses the ambient saturation ratio, and $S_r(T_r) = \rho_r/\rho_o(T_r)$, the equilibrium saturation ratio over the droplet. An expression for the growth rate is now obtained:

$$r\frac{dr}{dt} = \frac{D\rho_o}{\rho_d}\left\{(S - \varphi') - (1 + \xi')^{-1}S_r(T_r)\exp\left[\frac{L\xi'}{R_v T(1 + \xi')}\right]\right\} \quad , \tag{5}$$

$$\text{where} \quad \varphi' = \frac{\rho_d'}{D'\rho_o}\, r'\frac{dr'}{dt} \quad .$$

The equilibrium saturation ratio at the droplet temperature, $S_r(T_r)$, can be best dealt with by separating it into two factors, hygroscopic and curvature, the former being the water activity, a, of a condensation nucleus and rather insensitive to moderate temperature changes. Thus, we have

$$S_r(T_r) = a\exp\left[-\frac{2\sigma'}{r\rho_d R_v T(1 + \xi')}\right] \quad , \tag{6}$$

which can be substituted into (5). To solve this equation, we have to resort to some approximations; $r' \approx r$, $\rho_d' \approx \rho_d$, $(1 + \xi')^{-1} \approx (1 - \xi)$, and $D' \approx D$. For large and giant nuclei, these approximations are quite reasonable, except, perhaps, the last one, on which there has been considerable discussion. Here, it should be noted that the exponential factor in $S_r(T_r)$ now splits into two exponential terms one of which, when combined with the water activity, will give the equilibrium saturation ratio, S_r, at the

ambient temperature. Finally, Eq. (5) becomes

$$r\frac{dr}{dt} = \frac{D\rho_0}{\rho_d}(S - \xi) - S_r(1 - \xi)\exp\left(\frac{2L\sigma' + \rho_d L^2 r}{KR_v T^2}\frac{dr}{dt}\right). \qquad (7)$$

This is the equation to be used for studying the various condensation nuclei. In the beginning of growth, neither ξ nor ξ is negligible. However, as the droplet grows larger, ξ becomes smaller, and it may be dropped. Now we have Neiburger and Chien's expression (1960). As the droplet grows still larger, $(1 - \xi)$ may be discarded, and the exponential term expanded in series. Noting that $2L\sigma'$ is much smaller that $\rho_d L^2 r$ and that S_r may be approximated, we can easily obtain Fletcher's expression (1962) and then Mason's (1957) upon dropping the higher order terms.

A computer program was written to solve this equation for the growth rate and time. They were compared with published theoretical and experimental values, and two figures are presented in this summary, one for each case.

As may be expected, the new expression generally gives a lower rate of growth and hence a longer growth time, when compared with other theoretical values. In the case shown in Fig. 1, Neiburger and Chien's rate, given the same size, varies from 52% higher in the beginning to less than 1%, when the solution droplet has reached a nearly pure water state. A comparison in growth time is not quite realistic in that the accumulative effect of time increments, since the larger droplets take longer and longer time to grow from one size to the next, has completely masked the initial growth time. Nevertheless, Jiusto's values (1967), not shown here, average about 11% faster. It may be remembered that while Jiusto adequately took into account the hygroscopicity of NaCl, Neiburger and Chien, perhaps, did not.

Comparisons with Dennis' (1960) and Ye's (1962) experimental data are not entirely convincing. In the cases studied, the results are not consistent; that is, the theoretical equation either overestimates or underestimates the growth times, if we accept their data as valid. In the example illustrated in the other figure, the comparison, however, looks unbelievably excellent, the percentage difference, even at equilibrium, being less than 6%. Despite that Dennis' equilibrium sizes are generally smaller by about 3% to 25%, the lengths of their growth times match the calculated values rather well. The same appears to hold true for Ye's data, although by a greater percentage. In view of the great difficulty and formidability of these experiments, particularly in Ye's case, it would indeed be surprising if the experimental and theoretical values fit rather nicely, as in Fig. 2.

In conclusion, the fact that the percentage differences between the experimental and calculated values are both positive and negative and vary by a reasonable amount in most cases may well indicate that the refined equation has adequately taken into account the important physical processes in the growth of an isolated immobile liquid solution droplet despite the uncertainty of the vapor diffusion coefficient.

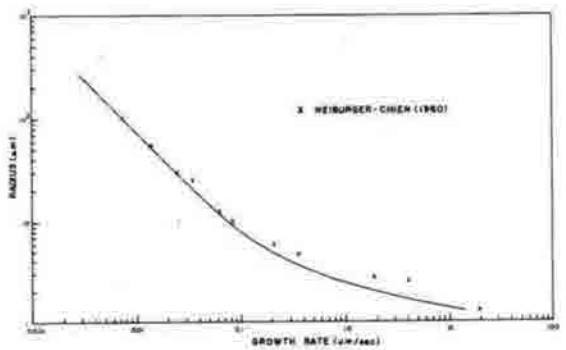

Figure 1. Comparison with Neiburger and Chien's calculated growth rate of 2.656×10^{-12} gram NaCl nucleus at 1% supersaturation and 5°C.

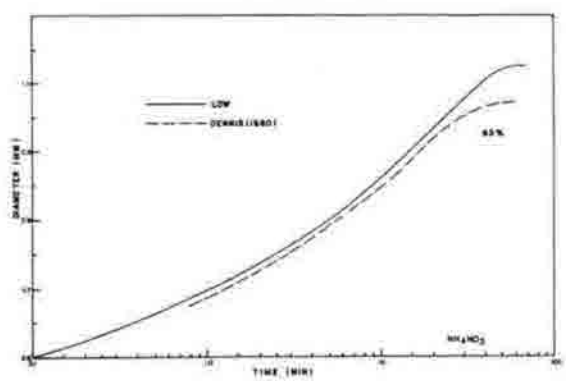

Figure 2. Comparison with Dennis' experimental growth time of 1.19×10^{-4} gram NH_4NO_3 nucleus at 93% relative humidity and 25°C.

A COMPARISON OF EXPERIMENTAL AND THEORETICAL CONDENSATION GROWTH RATES OF HYGROSCOPIC NUCLEI

Loren D. Nelson
Air Force Cambridge Research Laboratories
Bedford, Mass.

INTRODUCTION

Hygroscopic particle seeding has been shown by many researchers (Houghton & Radford (1), Juisto et al (2), Silverman & Kunkel (3)) to be effective in dissipating warm fog. The technique, however, is currently impractical for commercial use over heavily traveled airfields since most commonly used hygroscopic materials (e.g. NaCl) are very corrosive. It is thus desirable to find a hygroscopic chemical which performs well and is at the same time non-corrosive and non-toxic. Kunkel and Silverman(4) presented theoretical evaluations for inorganic chemicals based on published data. Cress(5) investigated the fog clearing potential of organic chemicals. Because of a lack of published data on vapor pressure reduction for these materials he was forced to determine this quantity experimentally before he could determine their fog clearing capability. St. Amand (6) has discussed the use of binary mixtures of ammonium nitrate and urea as fog-seeding agents. He was also forced to an experimental method of obtaining the necessary vapor pressure reduction data. Many organic compounds and binary mixtures are very hygroscopic, non-corrosive, and non-toxic. Vapor pressure reduction data is not available for many of these chemicals. A relatively quick experimental evaluation method is required if the fog clearing capabilities of such materials are to be compared and tested.

This paper will present such a method: photomicrographic observation of single, thermally and physically isolated crystals growing by water uptake in a closed, controlled humidity environment.

EXPERIMENTAL METHOD

The droplet growth chamber is a glass box 2.5 cm wide by 1 cm deep placed on a microscope stage. Provision is made for a horizontal air flow through the chamber at velocities variable over the range of droplet free-air fall speeds. Saturation can be achieved either by evaporation from a layer of distilled water on the chamber floor or by a flow of previously saturated air through the chamber. This air source is provided by bubbling compressed air through a 30 inch path length of distilled water in a constant temperature bath. Subsaturated conditions can be achieved either by maintaining this temperature bath at a lower temperature than the chamber or by the use of a layer of known solution on the chamber floor. Wet and dry bulb temperature are measured by precision thermistors inside the chamber and the dew-point in the chamber is provided by a Cambridge Systems Dew Point Hygrometer.

The growing droplet is suspended from a 10μ diameter glass fiber stretched across the center of the chamber. Solutions of the chemical to be investigated are first produced by weighing the material to $\pm$ .1 mg and then adding distilled water in a 50 ml volumetric flask. Small droplets of these solutions of accurately known molality are dispensed through a micrometer syringe to a repeatable accuracy of .00001 cm^3. The syringe needles are hand pulled from glass tubing to an O.D. slightly smaller than the 10μ diameter glass fiber. Thus when the drop on the end of the needle is moved into contact with the fiber by a micromanipulator and then pulled away, surface tension pulls the drop off the needle onto the glass fiber. The drop is then evaporated to leave a single crystal of accurately known mass attached to the fiber. This procedure proved necessary since the volume of an irregular crystal cannot be determined accurately by a cross-sectional view in one plane.

As the crystal is regrown in a controlled humidity environment the size of its droplet as a function of time is given by frequent photomicrographs taken through a long working distance objective at an optical magnification of 258X. Drop size is then reduced from the photomicrographs. The long working distance objective permits the drop under observation to be in thermal and physical isolation: suspended only from a 10μ diameter fiber of low thermal conductivity and with no other solid surface within 5000μ of its location. "Free Air" conditions are thus closely simulated in the chamber.

COMPARISON WITH THEORY

Figure I shows sample comparisons of droplet growth determined by the above method and the numerical theory of Silverman and Kunkel(3). All the particles shown in Fig.I were grown from single sodium chloride crystals initially dry at t=0 minutes. The points shown at t=0 are thus equivalent spherical diameters. Saturation was maintained at 100% R.H. by a distilled water layer on the chamber floor and the flow velocity was zero throughout the experiments. Chamber temperature was maintained at 22 degrees Centigrade.

As shown by Fig.I the experimental and theoretical values agree very well, lending support to the accuracy of both.

CONCLUSIONS

The inherent accuracy of the photomicrographic method has been demonstrated and it may thus be used to determine the relative efficiencies of various hygroscopic warm-fog seeding materials. Comparisons

can be made among many chemicals for which relevant data on vapor pressure, etc. is not available. The method is relatively fast, permitting several compounds to be evaluated in a day's experiments and is accurate enough to give meaningful comparisons on an equal mass, equal molality or equal volume basis. Experiments are now being conducted to provide such comparisons for a wide variety of materials.

REFERENCES

1. Houghton, H.G., and Radford, W.H., 1938: On the Local Dissipation of Natural Fog, M.I.T. Papers on Oceanography and Meteorology, Vol. VI, No. 3
2. Juisto, J.E., et al, 1968: Fog Modification with Giant Hygroscopic Nuclei, J. Appl. Meteor., 1, 860-869
3. Silverman, B.A., and Kunkel, B.A., 1970: A Numerical Model of Warm Fog Dissipation by Hygroscopic Particle Seeding, J. Appl. Meteor., Aug. 1970
4. Kunkel, B.A., and Silverman, B.A., 1970: A Comparison of the Warm Fog Clearing Capabilities of Some Hygroscopic Materials, J. Appl. Meteor., Aug. 1970
5. Cress, Ted S., 1970: Factors in Warm Fog Dissipation, M.S. Dissertation, Colorado State Univ.
6. St. Amand, Pierre, Unpublished Paper.

FIG. I

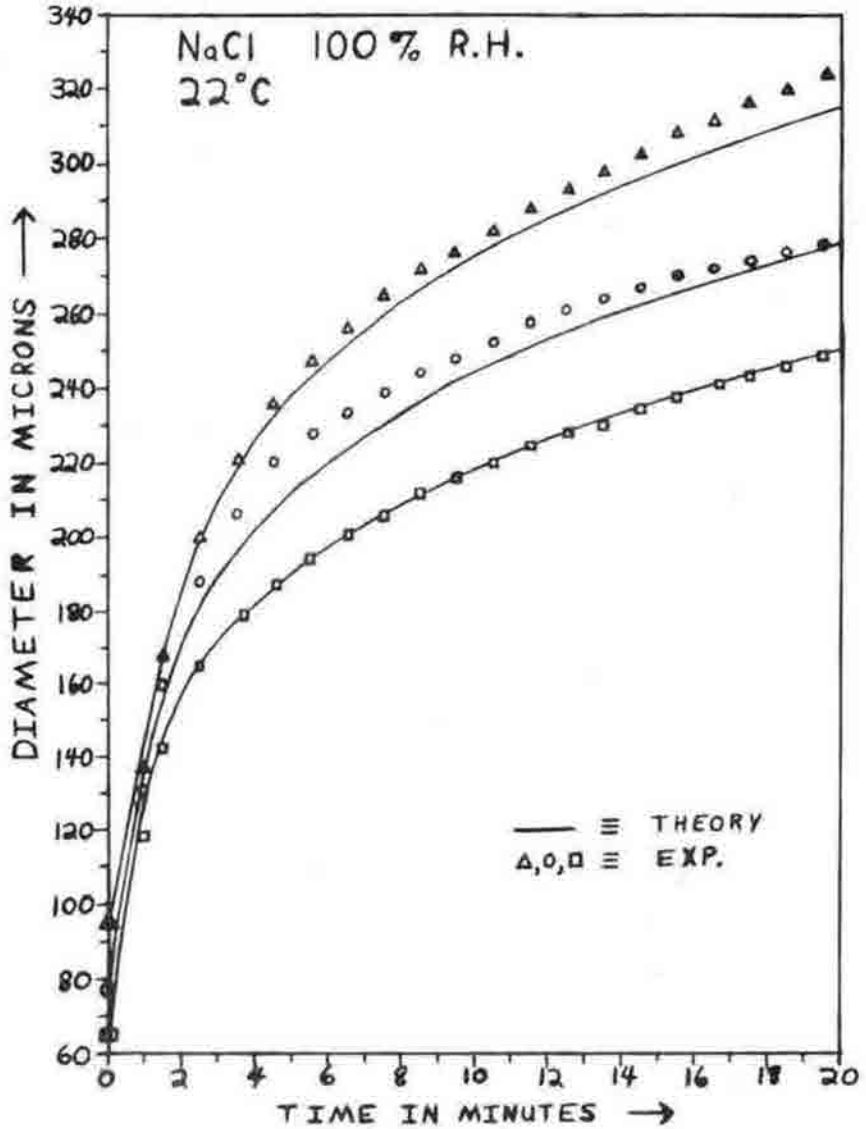

ON A PROBLEM OF RANDOMIZED CLOUD-SEEDING EXPERIMENTS *

J. Neumann

Department of Meteorology
The Hebrew University
Jerusalem, Israel

The main objection against the use of historical rainfall data for the evaluation of results of cloud-seeding experiments is in the great variability of rainfall: A regression relation valid for the past may be invalid with respect to present or future rain data. Consider now a randomized seeding experiment involving randomly alternating time units such as the 24-hour day. One would expect that on such a design the averages of 'natural' rain per time unit for the two randomly constituted groups would show little or no difference provided that the experiment is conducted for a number of years. However, certain features of rain data for the 1961-67 Israeli randomized cloud-seeding experiment and some features of Project Whitetop have prompted this writer to scrutinize the soundness of the foregoing anticipation. In the Israeli experiment, for instance, on the days allocated to seeding in the Center experiment area but not actually seeded the rainfall was heavier than on the days allocated to the North area but not actually seeded. Additionally, in the Buffer area, lying in-between the North and Center experiment areas (the Buffer was not supposed to be seeded; in practice, it was contaminated though, apparently, only for a relatively small fraction of the seeding hours), also on days when the Center was actually seeded the rainfall was heavier than on days actually seeded in the North.

In order to study the variations in 'natural' , unseeded rain, we have analyzed the rain data for Acre, Israel, for a period of 36 years prior to the beginning of the 1961-67 experiment. The days involved are those between 1 December and 30 March (29 March in leap years), i.e. 120 days in each rain season. The dates were paired with random numbers, and, then, six-year running averages of rainfall were computed for the 'odd' and for the 'even' days (meaning days associated with odd and even random numbers, respectively). The number of years chosen for averaging is close to the number of years representing the duration of the Israeli experiment and that of Project Whitetop.

It will be seen in Fig. 1 that for most of the time of the above desk experiment the even rainfall was heavier than the odd one. Over two extended periods (11 and 15 years) the even rainfall was 15 to 40 per cent greater than the odd rainfall. If we would identify the even (odd) days as 'seeded', we would conclude a high positive (negative) 'effect' of seeding - unless we make proper precautions for possible natural differences of substantial magnitude between two nearly simultaneously running sequences of relatively short time units. Simple statistical considerations indicate that long sequences of positive or negative excesses will occur for extended periods of time with high probability .

Gabriel's (1) Monte Carlo experiments with the double ratio for the Israeli trial take note of the above type of great variability between the averages of two random sequences. Nevertheless, some problems remain to be understood. As to Project Whitetop, it would be worthwhile to study in randomized desk experiments possible fluctuations of rainfall in the past in what subsequently became plume and non-plume areas.

REFERENCES

(1) Gabriel, K.R. and P. Feder, 1969: On the distribution of statistics suitable for evaluating rainfall stimulation experiments. Technometrics, 11: 149-160.

* Dr. Neumann will also present cloud physics data obtained from this project.

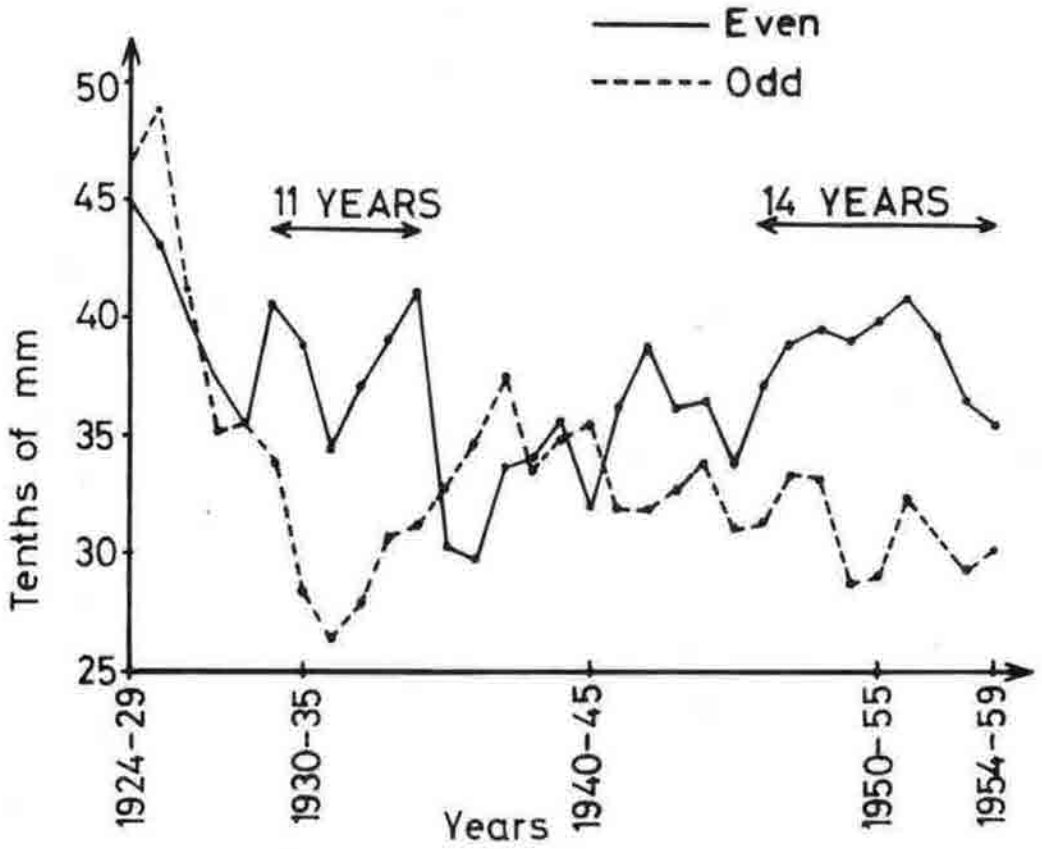

Fig. 1. Running six-year averages of mean daily rainfall, for even and odd random units, at Acre, Israel. Period: 1 December to 30 March (29 March in leap-years) of the years 1924/25 to 1959/60. In the diagram 1924-29 stands for 1924/25 to 1929/30 and so on. Each pair of odd and even points represents 720 days.

A PRELIMINARY INVESTIGATION INTO THE ELECTRICAL STRUCTURE OF A SEVERE STORM

J.E. Pakiam and J. Maybank
Saskatchewan Research Council
Saskatoon, Canada

INTRODUCTION

The charge separation process in a thunderstorm is dependent upon both the microphysical and macrophysical properties of the cloud and the environment; on the one hand, electrical effects are associated with different physical states of the hydrometeors while, on the other, the hydrodynamic and thermodynamic aspects of a storm are responsible for different temperatures, updraft speeds and wind flow patterns, all of which affect the state and spatial position of the hydrometeors. While the electrical structure of the classical thunderstorm model of Byers and Braham has received much attention and a profusion of laboratory and field measurements and theories exists, it is only recently that attention has been called to observations made on severe storms, i.e. those producing large hail and/or tornadoes. The relationship between the occurrence of hail and lightning has proved to be especially curious. The results of Sansom(1) in Kenya, Blevins and Marwitz(2) in Colorado and Smith(3) in Nebraska showed that large hail was associated with infrequent or no lightning while frequent lightning was generally not accompanied by hail.

FIELD MEASUREMENTS

During the summers of 1968 and 1969, "field mills" (electrostatic voltmeters) were set in operation at various localities in Alberta as part of a project designed to study the relationship between hail production and electric fields beneath thunderstorms. In addition, the field mill records were supplemented by visual observations. The data obtained were analysed with the aid of the Alberta Hail Studies 10.4 cm radar located at Penhold and hail reports supplied by farmers.

THE ALBERTA STORM OF 28 JULY 1968

A case study of this storm has provided some useful results.

The storm evolved at the foothills of the Rocky Mountains near Nordegg, developed into a steady state storm and broke loose from the foothill region. At Rocky Mountain House (RMH), the storm was transformed into a vigorous, multicellular complex and finally weakened considerably at localities east of Lacombe.

Maximum hailstone size at the ground was 2½ inches diameter from the foothills to RMH, with gradually decreasing hailstone size past RMH. At Lacombe and to the east, no hail was reported.

Lightning flash rate was 1-2 per minute at the foothills (visual reports), gradually increased past RMH (visual reports) and attained a value of 40-60 per minute at Lacombe (field mill records).

Figure 1 shows these results diagrammatically.

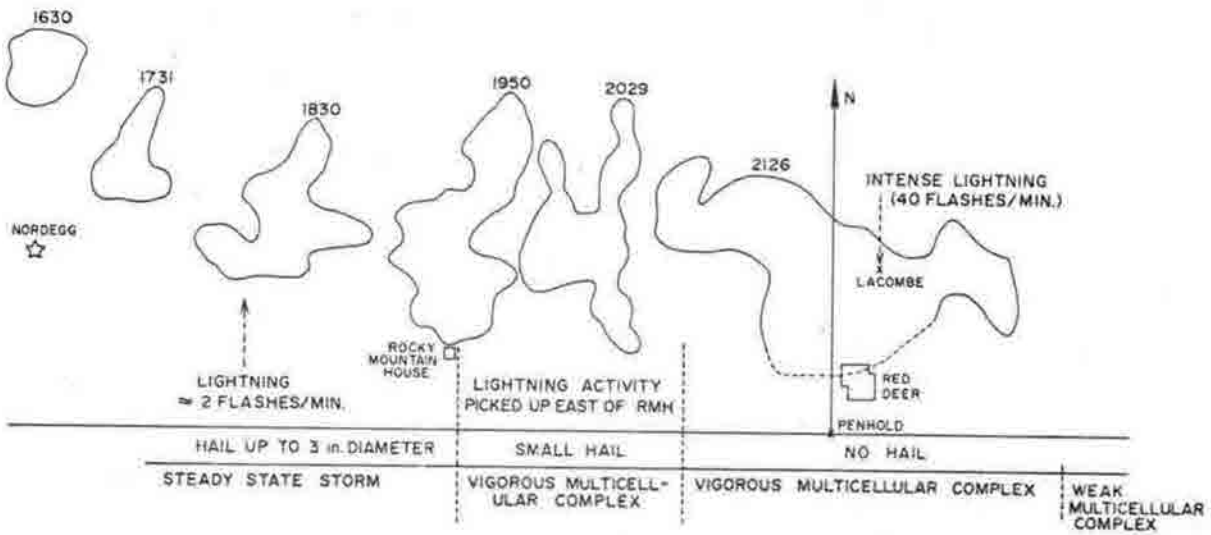

Fig. 1. Lightning-hail-radar echo relationships of the storm of July 28, 1968. Times shown above radar echoes are in Local Standard Time.

DISCUSSION OF RESULTS

The electrical behaviour of this storm seems to bear out some of the earlier findings of others. With very large hail, little lightning activity is observed; as the hailstones produced by the storm diminish in size, lightning activity increases. However, the very high rate of lightning flashes at Lacombe does not appear to have been due to single cells alone but to groups of cells with a good likelihood of many cloud-to-cloud flashes between cells.

CONCLUSIONS

The preliminary results obtained from the storm of the 28th of July 1968 are not sufficient to provide any physical severe-storm model incorporating electrical structure. At Lacombe and the other stations to the east, a positive bipolar electrical structure (corresponding to the Byers and Braham thunderstorm) was evident but no actual quantitative measurements were made at the foothills on the steady state storm.

REFERENCES

(1) Sansom, H.W., 1966: "A possible effect of lightning on hail" Weather, 21, 315.

(2) Blevins, L.L. and J.D. Marwitz, 1968: "Visual observations of lightning in some Great Plains Hailstorms" Weather, 23, 192-194.

(3) Smith, M.D., 1968: "A correlation study of hail and lightning" Proc. Int. Conf. Cloud Physics, Toronto, 460-463.

OBSERVATIONS OF MICROSTRUCTURE IN TWO CUMULI

Paul A. Spyers-Duran

Cloud Physics Laboratory

The University of Chicago, Chicago, Illinois

INTRODUCTION

Observations of cloud microstructure variation with height are few in the literature because of the difficulty involved in making such measurements. The earliest detailed and systematic data on cumulus cloud microstructure variations with height were made by Zaitsev (5). Recently, the continuous replicating device allowed MacCready and Takeuchi (3) to follow the droplet evolution with height in convective cloud cores. The study made in this paper gives additional evidence on microstructure changes with height.

DATA COLLECTION

An instrumented twin engine Beechcraft D-18 was used to make the cloud penetrations. Cloud droplet collections were made with a continuous replicator, Spyers-Duran and Braham (4) and precipitation size particles were obtained with a lead impactor, Brown (2). A continuous record of liquid water content was obtained with a hot wire device*.

In northern Minnesota on July 31, 1965, a series of measurements was made through two cumuliform clouds in a step-down manner at approximately 300 m intervals starting in the upper portions of convective turrets which had grown out of stratocumulus clouds.

DATA PRESENTATION

Figure 1 shows the physical properties of Cloud A, Flt. 663, as a function of height. Cloud base was at 1520 m with a top of 3480 m. The liquid water content (maximum) increased with height, reaching a value of 3.0 gm^{-3} at the upper portion of the cloud. The liquid water content (LWC) trace shows a highly cellular structure. Cloud droplets increased in size upward from the base; the volume median diameter, $\tilde{D}_v$, ranged from 9.5 μm at 240 m to 23 μm diameter at 1500 m above the base. Cloud droplet concentrations (maximum) decreased with height from 970 cm^{-3} to 280 cm^{-3}. That the average droplet distribution with height shows a broadening and shifting toward larger diameters is clearly shown. Precipitation size particles were

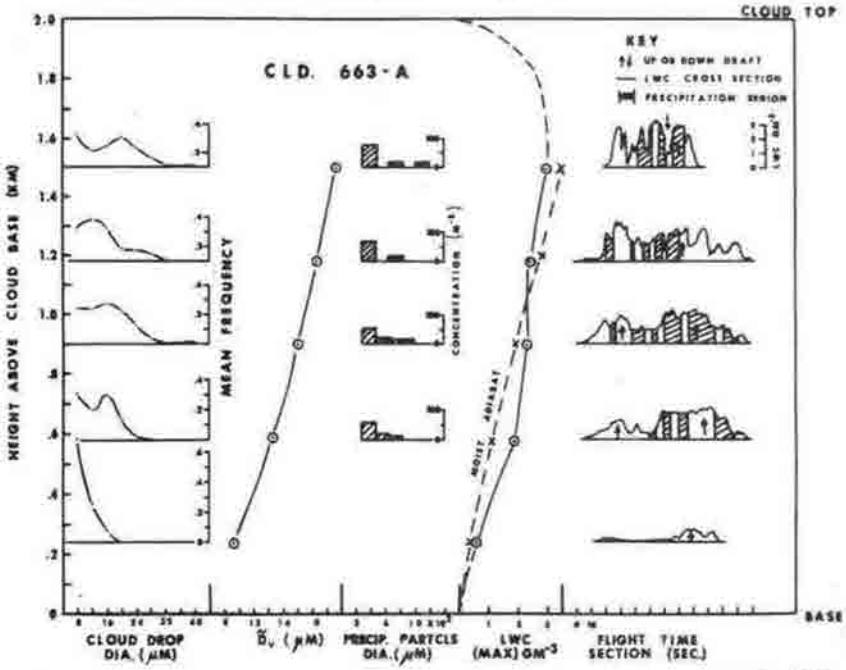

Fig. 1 shows the physical properties of Cloud A, Flt.663 as a function of height. The mean frequency represents the average droplet spectra along a segment of the flight pass.

*Manufactured by Johnson-Williams, Inc., 2300 Leghorn Ave., Mountain View, Calif.

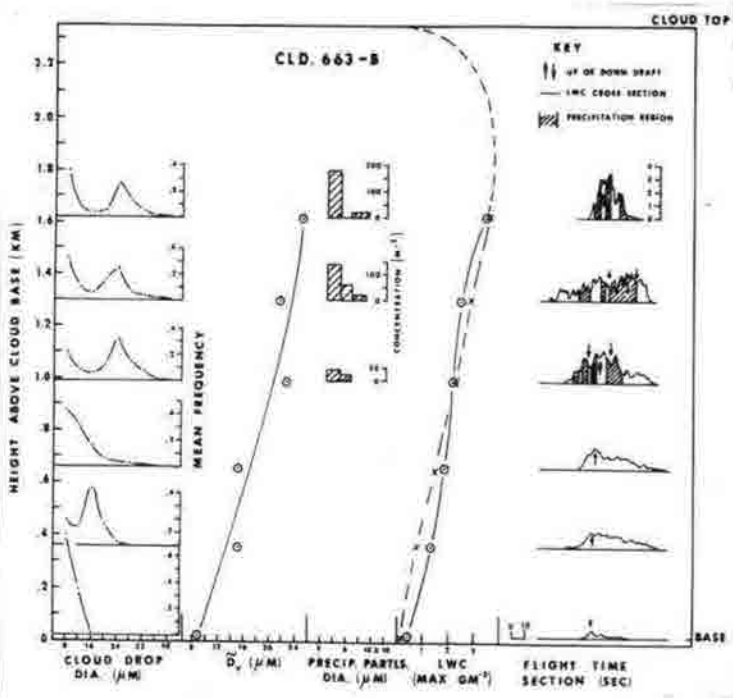

Fig. 2. Variation of droplet distribution and precipitation particle data from Cloud B, Flight 663.

observed first at 600 m level above the base and the largest size droplets were captured near the top of the cloud. Precipitation particles were found in shafts during the penetrations.

Fig. 2 shows that the physical properties of Cloud B, Blt. 663, are very similar to Cloud A. The base is noted at 1520 m, with a top of 3870 m. Liquid water content increased with height with a measured maximum value of 3.4 gm^{-3} near the top. The calculated adiabatic LWC value is about 3.5 gm^{-3}, indicating that in the core very little mixing was taking place with its environment, again the LWC trace shows highly cellular structure. Just above the base we measured volume median diameter of 8μm, increasing to 25μm at the upper portion 1620 m above the base Precipitation particles were measured 1 km above the base and upward, with the tendency to increase in size and frequency with height. The drop size distribution shows that the droplet diameter is displaced toward larger sizes with increasing height, while a frequency decrease with height is also noted. The bimodal droplet spectra appears to be a real phenomenon, not due to sampling difficulties, and most likely explained in terms of recent studies of stochastic coalescence by Berry (1).

REFERENCES

1. Berry, E. X., 1965: The effect of collection efficiencies on droplet growth. Desert Research Institute, Reprint #12.
2. Brown, E. N., 1961: A continuous recording precipitation particle sampler. J. Meteor. 18, 815-818.
3. MaCready, P. B., Jr., and Takeuchi, D. T., 1968: Precipitation initiation mechanism and droplet characteristics of some convective cloud cores. J. Appl. Meteor. 7, 591-602.
4. Spyers-Duran, P., and Braham, R. R., Jr., 1967: An airborne continuous cloud particle replicator. J. Appl. Meteor. 6, 1108-1113.
5. Zaitsev, V. A., 1948: Site and distribution of droplets in cumulus clouds. Trudy GGO, No. 13 (81).

D. M. Takeuchi
Meteorology Research, Inc., Altadena, California

INTRODUCTION

To insure maximum seeding effectiveness in supercooled cumulus clouds, it is required that the precipitation mechanisms in natural as well as in seeded clouds be understood. Besides being able to evaluate the effects of seeding from the understanding of the natural precipitation processes and its relation to the clouds' time history, this knowledge can provide one with possible clues to seeding techniques which lead to beneficial results. Since the microsphysical processes of the liquid and solid phases are interrelated with the dynamics of the cloud, the understanding of the precipitation mechanisms necessitates the discernment of the interactions of the dynamics, thermodynamics, and microphysics of the cloud and with the environment.

This paper presents results of precipitation mechanisms occurring primarily in isolated convective cumulus clouds (seeded and unseeded) from Flagstaff, Arizona. The observations were gathered during MRI's summer field programs of 1967 to 1969.

RESULTS AND DISCUSSION*

Precipitation development in a total of 24 test clouds at temperature levels ranging from about -7 to -12C has been investigated (Table I). This sample includes 9 control (C) and 15 seeded cases. The seeded cases include experiments employing three seeding techniques (ST): (1) cloud base seeding by means of high-output AgI-acetone solution (2 percent) generators (AgI-A), (2) cloud base seeding with aircraft-mounted pyrotechnic devices (fusees), and (3) vertical-fall pyrotechnic cartridges discharged from about the -8 to -10C levels of the cloud (VFP). Heavy aircraft icing prevented the instrumented research aircraft from obtaining the complete history (initiation→ dissipation) of hydrometeor development at a given (±1C) cloud level in 16 of the 24 test clouds. Clouds A, G, and Q were parts of large complex cloud systems and thus are not classified as being isolated clouds.

Findings (Takeuchi, 1970b) based upon information collected during the 1967 and 1968 Flagstaff summer programs have been substantiated by the addition of test clouds from the 1969 program.

1. Of the 24 test clouds, 17 contained large (1-3 mm) liquid drops. All 9 control clouds contained large liquid drops prior to the appearance of ice particles. This indicates that the coalescence or "warm rain" process initiates precipitation in summer convective clouds at Flagstaff.

2. Initially sampled graupel particles which were as large as the previously sampled raindrops were located in downdraft or inactive cloud regions in all the natural cloud cases. These observations imply that the ice phase results from the freezing of the large liquid drops.

3. Observations of increases in both ice hydrometeor mass concentrations (IC) and number concentrations of even larger sized particles during periods of incomplete glaciation, and decreases in both once glaciation was complete, denote that the primary hydrometeor growth mechanism of the ice phase is by the riming process. Ice phase growth by riming occurred over durations (t_r) averaging about +12 min in natural isolated clouds. During this growth period, time weighted averages of liquid water content ($\overline{LWC_r}$) and of ice hydrometeor mass concentrations ($\overline{IC_r}$) amounted to 0.24 and 0.12 gm/m^3, respectively.

4. Measurements and observations of cloud motion revealed that the majority of the natural isolated clouds were decaying or inactive during the ice phase hydrometeor growth periods. This infers that ice phase precipitation mechanism occurs during much of the dissipating stages of natural cloud development. Updrafts were recorded in about one-tenth of the cloud penetrations during periods of hydrometeor growth. In general, the larger and more complex clouds remained active for longer time periods and therefore had longer periods of incomplete glaciation.

5. Natural clouds which do form precipitation eventually do glaciate completely and do eventually contain ice number and mass concentrations as high as 500/ℓ and 0.7 gm/m^3, respectively.

The development (initiation →) of the ice phase in the clouds' decaying stages discloses that the additional heating caused by the riming process is not sufficient enough to rejuvenate the dynamics of the natural isolated clouds (top temperatures $\gtrsim$ -20C) and that it is the interaction of the microphysics of the liquid phase with the environment which determines how large these clouds grow. Support to later contention is given by numerical cloud models (e.g., Weinstein and Davis, 1968) which assume

*Due to space limitations, details of the experimental, data collection, and data handling procedures are not presented here but can be found elsewhere (Takeuchi, 1970a).

no thermodynamic contributions from the ice phase to the dynamic process but which yet successfully predict natural cloud top heights warmer than about -25C. The effect of the interaction of the environment (stability and moisture conditions) with the cloud processes is apparent from the observations of wide variations in t_r, $\overline{LWC}_r$, and $\overline{IC}_r$ between clouds with slightly varying diameters (CD).

These observations of the natural precipitation mechanisms in summer Flagstaff cumuli are similar to those reported by Braham (1964) and Koenig (1963) for summer convective clouds in Missouri.

The observations of precipitation development in natural clouds suggest that successful (increase rainfall) seeding techniques should prolong the riming growth periods and occur during the active growth stages of cloud development. The additional heat release by the ice phase in the cloud's growth stage increases cloud buoyancy and thereby invigorates the dynamic structure of the cloud. The increased buoyancy leads to higher vertical velocities and, in some stable environmental conditions, lead to significant vertical cloud growth. In so doing, the onset of cloud decay is delayed thereby resulting in increasing the duration of the primary growth period of hydrometeors. This seeding effect is evident when one notes (Table I) that during ice phase development, seeded clouds remained active for longer periods and experienced longer durations of incomplete glaciation than the natural clouds.

The prolonged duration of cloud activity and of the primary hydrometeor growth period leads to additional beneficial effects. The increase in both $\overline{IC}_r$ and $\overline{LWC}_r$ for longer periods of t_r results in more total water being processed by the seeded clouds. Since hydrometeors grow during riming conditions, increases in IC and therefore rainfall intensity ensue. The extension of t_r also enlarges the areal coverage of precipitation. Thus these increases in rainfall intensity and areal coverage for longer durations lead to a desired effect of seeding, increase of total rainfall (TR).

Table I. CLOUD SUMMARY

Cloud	ST	CD (km)	Cld. Temp. Level (°C)	t_r (min)	$\overline{LWC}_r$ (g/m^3)	$\overline{IC}_r$ (g/m^3)	Cld. Activity (%)	TR (acre-ft)
*A	C	3.3	- 8.5	+22	0.79	0.14	100	+ 3.7
B	C	3.5	-10.5	9	0.09	0.05	0	15.1
C	C	3.0	- 7.5	7	0.18	0.07	0	2.2
D	C	3.0	- 8.0	18	0.41	0.03	0	0.6
E	C	2.9	- 7.0	12	0.15	0.08	0	0.8
F	C	2.9	- 7.5	13	ND	0.11	ND	3.6
*G	C	7.4	- 8.0	+23	0.28	0.02	60	+ 1.2
H	C	5.1	- 9.0	+19	0.36	0.27	17	+29.2
I	C	2.1	-11.0	+ 6	ND	0.30	33	+ 5.1
Average		3.1	- 8.5	+14	0.32	0.12	26	+ 6.8
Av. Iso. Cld.		2.8	- 8.6	+12	0.24	0.12	8	+ 7.5
J	AgI-A	2.4	- 7.5	22	0.49	0.10	50	1.5
K	AgI-A	3.0	-10.0	11	0.41	0.20	33	4.7
L	AgI-A	3.0	-10.0	+21	0.30	0.24	67	+11.0
M	AgI-A	2.6	- 9.0	+13	0.44	0.04	33	+ 0.3
N	AgI-A	3.2	- 9.0	28	0.68	0.29	67	+23.9
O	AgI-A	3.0	- 9.5	56	0.58	0.57	55	40.2
P	VFP	3.9	- 8.0	+10	0.38	0.49	100	+13.7
*Q	VFP	7.8	- 8.0	+17	0.19	0.02	40	+ 2.9
R	VFP	3.8	- 9.5	19	0.22	0.35	67	+39.7
S	VFP	4.0	-10.0	33	0.33	0.82	43	+179.0
T	VFP	4.8	-11.0	+24	ND	1.47	100	+264.0
U	VFP	5.2	- 9.0	+15	0.51	0.11	25	+ 1.1
V	Fusee	3.7	-10.0	+19	0.40	0.64	50	+72.7
W	Fusee	3.5	-10.0	17	ND	0.08	ND	2.9
X	Fusee	3.2	- 8.0	+34	0.42	0.13	67	+13.0
Average		3.8	- 9.2	+22	0.41	0.37	57	+44.7
Av. Iso. Cld.		3.5	- 9.3	+23	0.43	0.39	58	+47.7

*Complex cloud. + Sampling incomplete. ND No data.

ACKNOWLEDGMENTS

The author would like to express his appreciation to Dr. Theodore B. Smith for his encouragement and helpful conversations throughout this study. The work reported was done under Contract No. 14-06-D-6581 to MRI from the U. S. Bureau of Reclamation.

REFERENCES

Braham, R. R., Jr., 1964: What is the role of ice in summer rain showers? J. Atmos. Sci., 21, 640-645.

Koenig, L. R., 1963: The glaciating behavior of small cumulonimbus clouds. J. Atmos. Sci., 20, 29-47.

Takeuchi, D. M., 1970a: Evaluation of Flagstaff seeding techniques. Report in Final Report to Bureau of Reclamation, Cont. 14-06-D-6581.

Takeuchi, D. M., 1970b: Precipitation development in seeded and natural cumulus clouds. AMS Second Natl. Conf. on Weather Modification, Santa Barbara, Calif., April 6-9.

Weinstein, A. I., and L. G. Davis, 1968: A parameterized numerical model of cumulus convection. Rept. 11 to National Science Foundation under Grant GA-777 by Dept. of Meteor., Penn State Univ.

TEMPERATURE AND HUMIDITY CONDITIONS IN CUMULUS MEDIOCRIS

Helmut K. Weickmann, ESSA Research Laboratories, Boulder, Colorado
Albert R. Tebo, U.S. Army Electronics Command, Fort Monmouth, New Jersey
Frank R. Jones, National Bureau of Standards, Washington, D. C.

BACKGROUND

Using a Barnes infrared thermometer sensitive in the CO_2 band, and a barium fluoride humidity sensor mounted in a C-47 aircraft, a program of measurements was carred out at Flagstaff, Arizona, in July 1966. The program was designed to determine the horizontal profiles of temperature and humidity through fair weather clouds (cumulus humilis to cumulus mediocris), and to study the variation of these profiles at several vertical levels through the clouds. In the summers of 964 and 1965 comparisons were made between the remote sensing Infrared Atmospheric Thermometer and a direct reading vortex thermometer. The conclusion reached from these comparisons is that the radiation thermometer is superior. In warm clouds the vortex thermometer registers somewhat colder (evaporation effect), in supercooled cloud it can be several degrees warmer (heat of fusion!).

DISCUSSION

It was most surprising to find that all clouds, almost without exception, were colder than ambient and yet apparently buoyant. Great care was taken in the determination of the ambient temperature from the original flight records. It is important to emphasize here that the criterion for selection of a cloud was that it be an actively growing cloud with well defined and bulging cumulus contours and no evaporating tops. The cloud depth was usually between 1.5 and 2.0 km.

Table I has been condensed from the data and shows an average cloud cross section from base to top. The cloud is coldest at middle levels by $1/2^{\circ}$ below ambient. This mean cloud is a composite from numerous individual cloud penetrations, yet all clouds are consistent among themselves by being colder than ambient. This result at first sight is most puzzling, and it must be assumed that gross over simplification of the cloud process has entered in the straight forward averaging. Certainly many clouds were traversed at different times in their life history. It is therefore necessary to consider the individual temperature and humidity trace separately.

The outstanding typical case in this series is represented in Fig. 1a to g. This cloud was encountered on 20 July 1966 from 1507 until 1542 local time. General conditions of base and top levels and temperatures are well represented by the data in Table I. During the first penetration at 4.0 km a characteristic temperature oscillation was observed. Here, the visible cloud had a virtual average temperature difference of + 0.26°C, with + 0.8°C maximum difference. This warm cloud corresponds to a sharp rise in humidity from which the humidity sensor did not fully recover, probably due to flooding. Note the symmetric temperature fluctuations on both sides of the center peak. These fluctuations extended about 3 km from center peak to both sides while the cross section of the visible cloud was only one kilometer. Similar temperature and humidity responses have been observed repeatedly, they are however for space considerations not shown here.

The temperature variation recorded, probably reflects the accidental encounter with the active buoyant cloud stage which has all the characteristics of a buoyant rising vortex element as it has been analyzed in numerical models. This element is short-lived. After it has passed through, the cloud readily breaks up into much smaller eddies. While the scale size in the initial element is of the order of one kilometer, after three to four minutes at the same level elements of the size of .2 to .3 km appeared on the original records. Simultaneously the cloud becomes colder than the environment, not only sensible but virtually and yet it appears to remain buoyant in the wake of the initial pulse. Also beginning with the second pass the cloud expands laterally and assumes the width of the initial pulse which extended beyond the visible cloud. In the third pass this width is already nearly 5 kilometers whereby visibly the cloud had separated in two parts which are shown by the heavy hatching. The fourth pass was through the cloud edge which is especially cold probably due to evaporation of the liquid water. Here additional kinetic energy is generated which keeps the cloud alive even in absence of an active warm updraft. The 5th, 6th and 7th passes were made at a 600 m higher level. Here the picture appears to change with the 6th pass in which the virtual temperature becomes again warmer than environment apparently through the occurrence of a new active pulse. The new pulse is also reflected in the humidity which reaches 100 percent after which the meter again does not fully recover as was the case in the first pass. This pulse is barely apparent in the 7th pass. It so appears that the cloud "coasted" along for 1/2 hour feeding on the potential energy created in the original pulse through the lifting of cloud water. This energy is liberated unorganized through evaporation and a negative buoyancy term. Sometimes particularly in warm clouds with higher liquid water contents, the coasting stage of cloud life may become organized into a general downdraft. If this happens the cloud virtually collapses before one's eyes and it is difficult to follow the cloud top downward with aircraft. While the active lifetime of the cloud lasts only a few minutes, the subsequent coasting stage lasts of the order of 1/2 hours. It is conceivable that the coasting stage still exhibits healthy cauliflower

appearance which makes it almost impossible to distinguish between the initial pulse and the coasting stage. Most penetrations take place in the latter episode which explains why the "average" cloud turns out to be colder than environment. It is also conceivable that in this stage the cloud is very susceptible to outside influences so that a slight additional impulse or momentum may initiate total collapse. Such impulse could be aircraft downwash; particularly the more organized helicopter downwash or the discharge of a few pounds of sand or cement as has been observed by Soviet scientists.

CONCLUSION

We believe to have shown that cumulus mediocris clouds exhibit two important stages in their life history: one active formative pulse which is shortlived and which generates potential energy in the form of cloud liquid water and through lifting it and one inactive coasting stage during which this energy is dissipated by turbulence. This stage is much longer in duration, the cloud is virtually colder, but the dissipating character is not necessarily visible from the exterior appearance of the cloud.

TABLE I

Flight level km msl	Cloud Level	Ambient temp T_E	ΔT	No. Cases
3.25	Under cloud base UB	10.4	-.06	(2)
3.3	In cloud base IB	9.4	-.17	(9)
3.7	In cloud IC	6.0	-.51	(12)
4.0	In cloud IC	4.8	-.29	(4)
4.6	In cloud IC	-.1	-.1	(3)
4.6	In cloud top IT	+.1	0.0	(3)

Mean temperature conditions during penetrations of cumulus mediocris clouds on 20 July 1966.

Fig. 1a-f(Fib. 1g not shown): History of 7 penetrations through cloud B, July 20, 1966, 1507 to 1542 MST

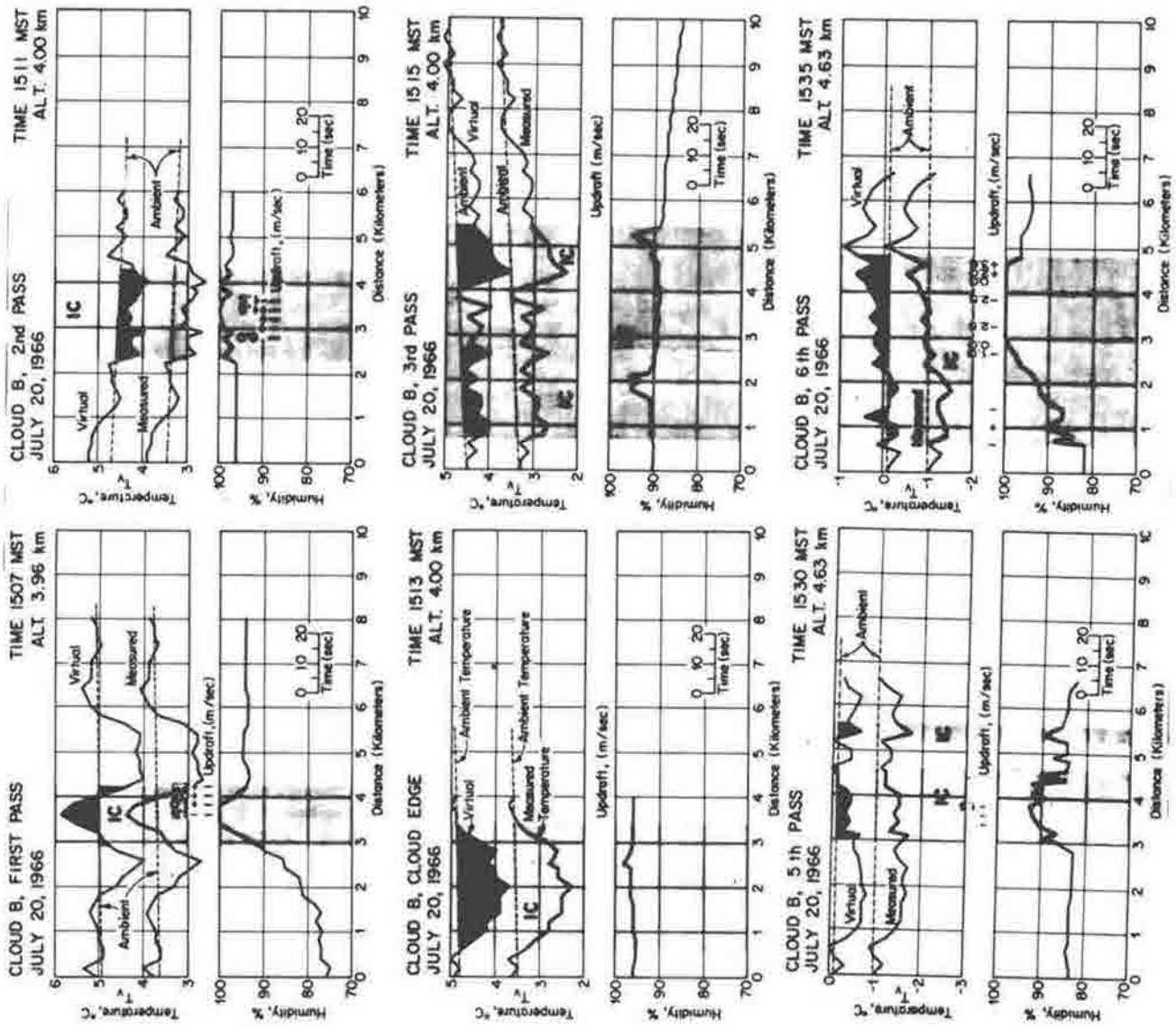

CALCULATIONS OF THE GROWTH OF GRAUPEL PARTICLES WITHIN THE UPDRAFT CORE OF ALBERTA HAILSTORMS

A.J. Chisholm
McGill University, Montreal, Canada

The Precipitation Growth Environment in the Hailstorm Updraft Core

An accompanying paper (1) presented in this Proceedings outlines a loaded moist adiabatic (LMA) updraft model which has been used to compute estimates of the cloud temperature, liquid water content, and vertical velocity within the hailstorm updraft core. Specifically, LMA model estimates of the precipitation growth environment will be utilized in this paper for two specific cases - a Low Energy storm (27 June 1967) and a High Energy storm (28 July 1967).

The liquid water content, as computed by the LMA model, specifies neither phase nor distribution with size. The rapid traverse (< 600 sec) of an air parcel through the updraft core results in the growth of a narrow cloud droplet distribution mainly by diffusion. Thus, a monodisperse cloud droplet spectrum has been assumed for the purposes of the graupel growth model described herein. The cloud droplet number density (typically 200 - 600 cm^{-3}) is prescribed at cloud base and adjusted with height according to air density considerations. Cloud droplet diameters are determined from the number density and LMA model liquid water content. Using this computation scheme the cloud droplet diameter increases with height to a maximum between 25 and 35 μ. Measurements by Vali (2) of the ice nucleus content of Alberta hailstorm precipitation have been used to describe the fraction of cloud droplets which remain supercooled at temperatures warmer than -40 C. In essence, the supercooled droplet fraction decreases rapidly from a value near 1.0 at -35 C to 0.0 at -40 C. Thus, the estimates from the LMA model in conjunction with a monodisperse cloud droplet spectrum and the cloud droplet freezing characteristics constitute a description of the growth environment for graupel particles in the updraft core.

The Graupel Growth Model

Observations taken by MacCready and Takeuchi (3) in unmixed updraft cores at Flagstaff indicate the existence of giant cloud droplets 100 μ diameter and larger at -5 C. Since the breadth of a typical hailstorm updraft excludes the possibility of entraining graupel particles inward to the updraft axis, it appears that giant cloud droplets may indeed constitute the original graupel embryo. Toward this end, a model was designed to compute graupel growth beginning with particles as small as 100 μ diameter at -5 C.

The initial particles are considered frozen at -5 C (D=100,300 and 600 μ; ρ=0.917). At all times they are assumed to be smooth spheres and the drag coefficient (variable) and fallspeed are computed using the Goldstein empirical equation. Graupel growth due to both accretion (using Langmuir collection efficiencies) and sublimation is calculated. A heat balance is maintained (neglecting the finite heat capacity of the graupel) and the density of the accreting ice is calculated from the graupel surface temperature, droplet size and fallspeed using experimental data due to Macklin (4). Radar reflectivity factor values are also computed accounting for particle density and wet and dry surfaces.

Graupel Growth Model Results and Weak Echo Regions

The growth of graupel particles will first be considered in a Low Energy storm (27 June 1967). LMA model results indicated that this storm was based at 2 km (+3.1 C) and topped at 7.8 km (-37.0 C) with a vertical velocity maximum of 16.4 m sec^{-1} at 5 km and a liquid water content maximum of 3.19 gm m^{-3}. As illustrated in Fig. 1, the graupel particles ascend in the updraft region growing to 5 - 7 mm diameter by the time they reach the top of the trajectory. Since supercooled water still exists at this point they continue to grow while descending back through the one-dimensional updraft. After 12 - 14 min the hail has reached the 0 C level having attained a diameter of 1.8 - 2.0 cm. Accounting for melting, the final hailstone diameter at the surface is in good agreement with the grape and walnut maximum size hail observed at the ground during this storm.

This storm was observed continuously by the Alberta Hail Studies 10 cm radar from a range of 68 km; the minimum detectable Z_e at this range being +35 dBz ($Z_e(dBz) = 10 \log_{10}(Z_e(mm^6m^{-3}))$). Assuming a number density of 1 m^{-3}, the computed Z values reach radar detectability only after 7 - 8 min at a size of 6 mm diameter. Prior to this time a weak echo region (or echo-free vault) would be observed in the lower portions of the storm. However, this weak echo region would be short-lived (9 - 12 min) as the descending hailstones would bring about the demise of the weak echo region. This

behaviour pattern was observed by radar. The storm consisted of a series of small, almost vertical cells in a weak wind flow; each cell displaying a weak echo region during development but decaying to be replaced by another cell on the RH flank of the storm in 25 - 35 min.

The growth of graupel particles will now be considered in a High Energy storm (28 July 1967). This storm was based at 2.2 km (+6.3 C), topped at 11.8 km (-66.0 C) with a maximum vertical velocity of 31.2 m sec^{-1} at 9.1 km and a maximum liquid water content of 3.7 gm m^{-3}. As a result of the high vertical velocities (15 m sec^{-1} at -5 C and 31 m sec^{-1} at -40 C) the graupel particles are swept to the -40 C level reaching sizes of 1.5 - 8.0 mm diameter as shown in Fig. 2. These graupel particles are unable to descend back through the updraft core while continuing to grow. Consequently, it would be anticipated that the low calculated Z values (100 μ <-35 dBz, 300 μ <0 dBz, 600 μ <+19 dBz at 7 km) would appear as a weak echo region reaching upward into the storm from its base. A weak echo region (bounded by radar echo) was observed to persist in association with this storm for approximately 2 hr to a height of 8.3 km. During this period, the storm was in its most intense phase, reached its maximum height and yielded hail at the surface larger than golfball size.

In summary, it is apparent that weak echo regions observed within severe storms can be comprised of cloud droplets and graupel particles in an updraft region. The development and persistence of such weak echo regions is most likely in deep, highly energetic storms.

References

1. Chisholm, A.J., 1970: Estimates of the precipitation growth environment in the updraft core of Alberta hailstorms. Proc. Cloud Physics Conference, Ft. Collins, Colo.

2. Vali, G., 1968: Ice nucleation relevant to formation of hail. Sci. Rep. MW - 58, Stormy Weather Group, McGill University, Montreal 51 pp.

3. MacCready, P.B. and D.H. Takeuchi 1968: Precipitation initiation mechanisms and droplet characteristics of some convective cloud cores. J. Appl. Meteor., 7, 591-602.

4. Macklin, W.C. 1962: The density and structure of ice formed by accretion. Quart. J. Roy. Meteor. Soc., 88, 30-53.

Fig. 1

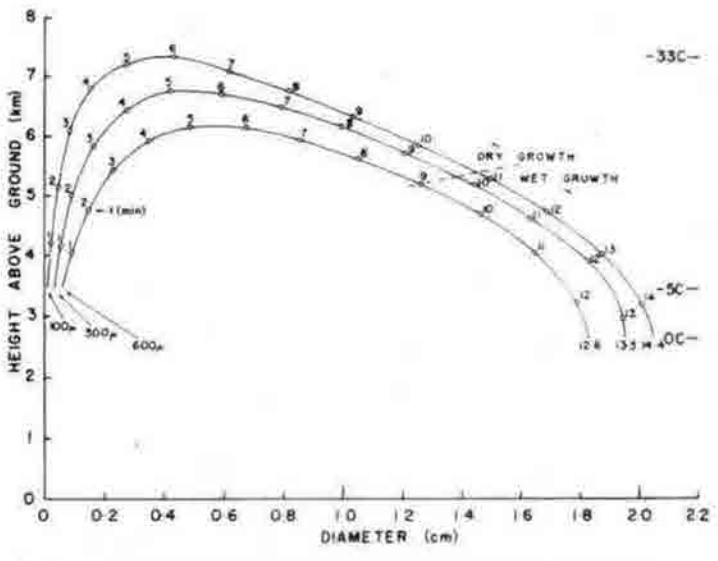

Fig. 2

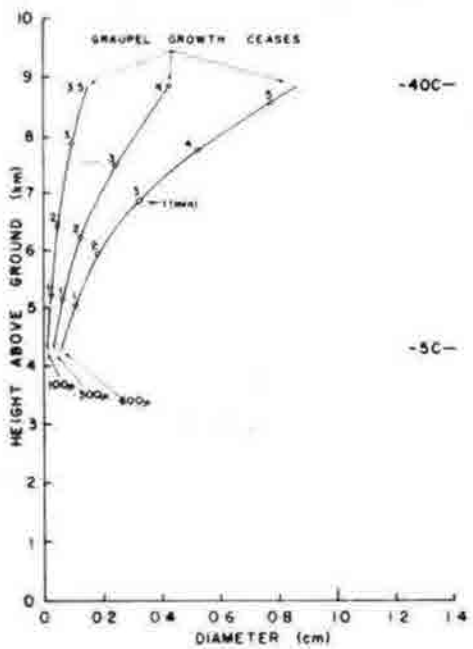

SEVERE STORM SFERICS: STROKE RATE HISTORY

William L. Hughes
School of Electrical Engineering
Oklahoma State University
Stillwater, Oklahoma

Emmett J. Pybus
School of Electrical Engineering
Oklahoma State University
Stillwater, Oklahoma

Electromagnetic radiation of severe storms has been received and recorded on magnetic tape from an Oklahoma State University airplane flying within 25 miles of the storms. Radiation is received, detected and recorded at six discrete frequencies from 10 KHz to 250 KHz. Samples of R.F. radiation are also recorded at five minute intervals in the band 2 KHz to 300 KHz. Two identical receiving systems are used, one horizontally polarized, the other vertically polarized. This system is more fully described in a Themis Project Annual Report. (1)

From the recorded data, sferic rate histories are made by counting the number of received strokes on each of the six frequencies and on each of the two receiving systems. The data processing system is described in a Themis Project Annual Report.(2)

Results from two storms are presented here to illustrate the technique and to help substantiate a growing belief that storm sferics are closely related to either or both the vertical velocity within a storm and wind shear.

Figure 1 shows data reduced from a hail and tornado storm which occurred near Rapid City, South Dakota on 17 July 1969. The continuous but jagged line represents a running weighted average of the number of detected energy impulses per minute at 100 KHz received from the storm. Superimposed upon the sferic rate history are dashed lines representing the Institute of Atmospheric Sciences radar indicated cloud top heights. Also shown are times of occurrence of hail and funnel cloud as well as later hail and a verified tornado. It can be shown from time-lapse radar data (not given here) that the overall sferic rate history reflects the areal extent of the storm, while it is seen here that perturbations of the sferic rate history show discrete events (hail, tornado) which in turn are related to vertical cloud growth (given by radar cloud heights).

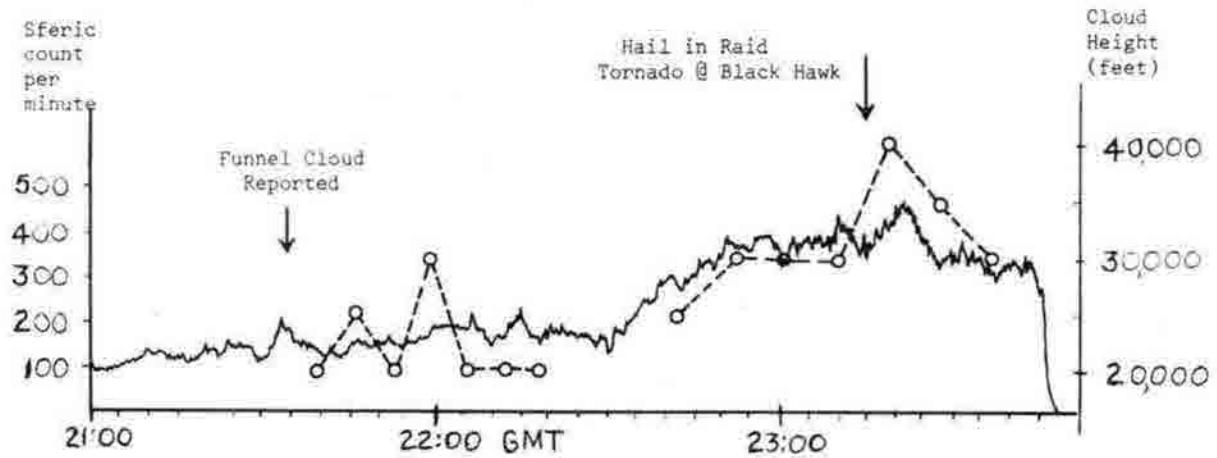

Figure 1 - Sferic Rate History - Rapid City, South Dakota, 17 July 1969

O.S.U Flight #10 I.A.S. Hail Cases #7, #8

Similar results were noted from a tornadic storm near Fairview, Oklahoma on 11 June 1969 as shown in Figure 2. In that case radar cloud top heights were provided by the National Severe Storms Laboratory (ESSA) at Norman, Oklahoma and show a growth of cloud heights at the same time at which the sferic rate was increasing. The tornado event corresponded to an increased sferic rate but radar information was not available at that particular time.

Although radar cloud heights are not available for the earlier portions of the storm, it is evident that the tornado at Fairview occurred during the peak of sferic activity at 03:10 G.M.T. It is conjectured that the peaks of sferic rate prior to that time represent earlier periods of cloud building.

It must be mentioned, however, that the tornado event does not appear to have occurred during the time of maximum cloud height. A similar situation held during the early tornado of Figure 1 at Rapid City, South Dakota. There also, the first reported funnel occurred while cloud heights were relatively low. In both cases, nevertheless, the tornado was accompanied by increased sferics. From this, one

must conclude that wind shear or vertical velocity are more important to sferic generation than is absolute cloud height.

Still to be correlated are relative freezing levels and other meteorological parameters surrounding these storm events.

/

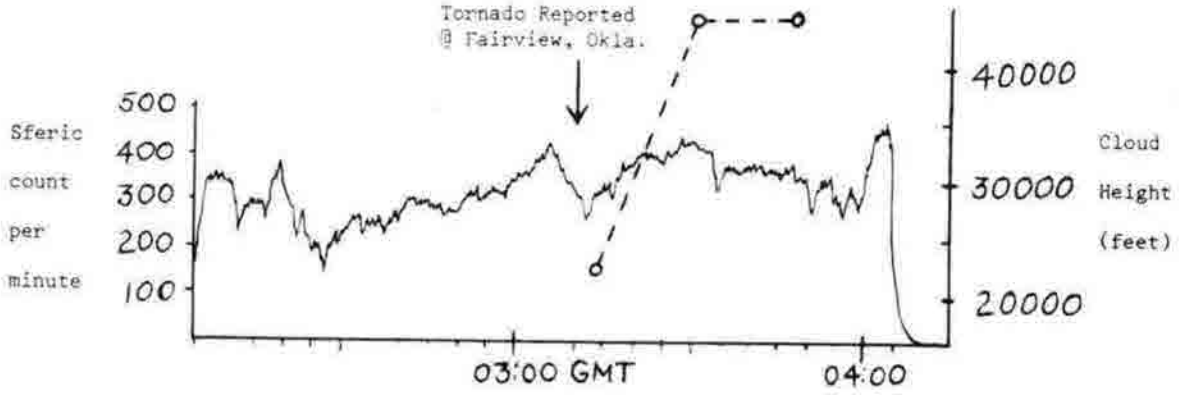

Figure 2 - Sferic Rate History - Fairview, Oklahoma, 11 June 1969

O.S.U. Flight #5 NSSL Radar

In view of these data and others presently being obtained it is strongly felt that storm sferics are an indicator of vertical velocity within a storm as well as an indicator of wind shear. The detailed nature of the sferics are now being studied to relate the changing type of discharge (cloud to ground compared to intercloud) with the age and progress of a storm.

The goal of these studies at Oklahoma State University is to be able to diagnose the state of a severe storm as well as to forecast the probable actions of the storm.

References.

(1) A Center for the Description of Environmental Conditions - Weather Phenomena - Annual Report - October 1968, U.S. Army ECOM - Contract #DAAB 07-68-C-0083 by Oklahoma State University, Stillwater, Oklahoma.

(2) A Center for the Description of Environmental Conditions - Weather Phenomena - Annual Report - December 1969, U.S. Army ECOM - Contract #DAAB 07-68-C-0083 by Oklahoma State University, Stillwater, Oklahoma.

NUMERICAL SIMULATION OF THE LIFE CYCLE OF A THUNDERSTORM CELL

Yoshimitsu Ogura and Tsutomu Takahashi
Laboratory for Atmospheric Research
University of Illinois
Urbana, Illinois

1. PARAMETERIZATION OF MICROPHYSICAL PROCESSES

Models of cumulus clouds are presented which combine the equations of motion, the equation of mass continuity, the first law of thermodynamics and the following cloud microphysical processes: condensation of water vapor to produce cloud droplets, conversion of cloud droplets to raindrops, glaciation, sublimation of water vapor, melting of ice crystals, evaporation of cloud droplets, evaporation of ice crystals and evaporation of melting ice crystals.

It is assumed that all water vapor over the saturation level condenses instantaneously into small cloud droplets which share the velocity with the surrounding air. The conversion process from cloud droplets to raindrops is incorporated into the model by the parameterization which does not depend upon the details of how coalescence and collection are achieved. It simply states that the conversion is achieved at a given rate and that the rate is proportional to the mixing ratio of cloud droplets. It is written as

$$\frac{dQ_r}{dt} = C_0 Q_c$$

where Q_r and Q_c are the mixing ratio of raindrops and cloud droplets.

Similarly the glaciation process is assumed to take place whenever the air temperature is below the freezing point and is expressed as

$$\frac{dQ_i}{dt} = G Q_r$$

where Q_i is the mixing ratio of ice crystals.

The terminal velocities for raindrops and ice crystals are expressed in terms of Q_r and Q_i respectively, with the assumption that the size distributions of raindrops and ice crystals follow always the Marshall-Palmer distribution. In some cases, the Gunn-Marshall distribution is applied for ice crystals.

2. ONE DIMENSIONAL MODEL

The cloud is modeled as a circular air column with a time-independent radius in an environment at rest. All equations are formulated along the line taken by Asai and Kasahara[1] as far as the dynamic terms are concerned. The effect of compensating downward motions in the environment is not considered however. The equation for the vertical velocity is written as

$$\frac{\partial w}{\partial t} = -\frac{w\partial w}{\partial z} - \frac{2\alpha^2}{a} w|w| + \frac{2}{a}(w - w_a)u_a + g\frac{T_v - T_{vc}}{T_{vc}} - g(Q_c + Q_r + Q_i)$$

Here the subscript a denotes the quantities at the edge of the cloud whose radius is a. The second term in the right-hand side represents the lateral eddy exchange and the third term represents the dynamic entrainment which is required to satisfy the mass continuity between the cloud and environment. Other prognostic equations are not produced here.

This set of equations were integrated numerically as an initial value problem. As was discussed by Weinstein[2], the solution attains a steady state when no cloud microphysical processes are included. Fig. 1 shows an example of the height-time cross sections of vertical velocity (in m/s) by our model for Co = 0.005 and G = 0.005. Byers and Braham[3] divided the life cycle of a thunderstorm into three stages: developing stage, mature stage and dissipating stage. The typical duration times for each stage are roughly 10-15 minutes, 15-30 minutes and 30 minutes respectively. These features are well simulated in Fig. 1. The strong downdraft observed in the dissipating stage at approximately 3 km height is caused by melting of ice crystals.

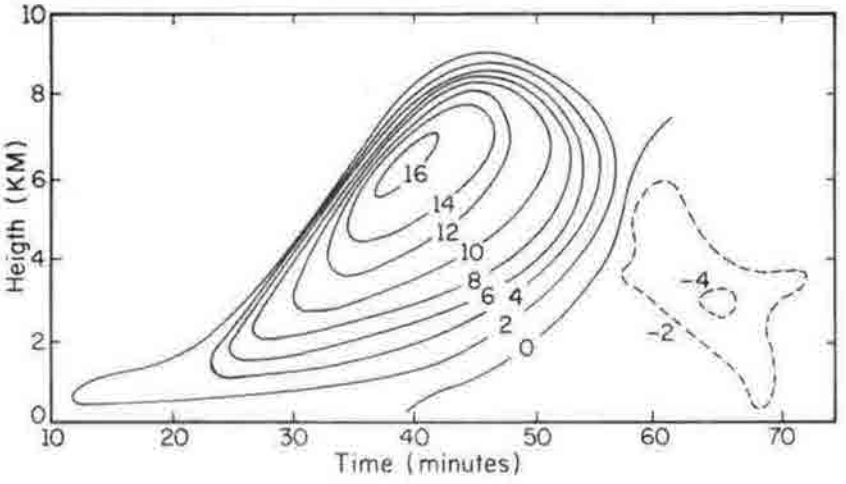

Fig. 1. Time-height cross section of vertical velocity (in m/s).

The computations were then repeated for various values of Co. The results indicate that the motion is rather sensitive to the variation of Co: the motion undergoes the life cycle when Co is larger than 0.005 and the larger Co is the shorter the life time of the cloud becomes. The result also indicates that, although the inclusion of the drag force provided by the weight of liquid and solid water is essential for the dissipation of the cloud, it is not sufficient for it. For example, in the case with Co = 0.001, the total amount of water was calculated as high as 8 gr kg^{-1} and yet the motion attained a steady state.

The effect of the large scale vertical motion upon the development of a thunderstorm cell was also investigated. Within the framework of the one-dimensional treatment, the large scale vertical motion was represented by imposing a non-vanishing vertical velocity (wo) at the ground surface. The result of computation for parameters applied in the case of Fig. 1 and for various values of wo show that there is no appreciable change from Fig. 1 when wo is smaller than 20 cm/s. When wo is 30 cm/s the cloud does not reach the dissipation state until 80 minutes and when wo is 50 cm/s, the cloud attains a steady state.

3. TWO DIMENSIONAL MODEL

The study is being extended to two-dimensional modeling to study the effect of the mean flow on the development and maintenance of a thunderstorm cell and the interaction between clouds. The computation was made with = 2 km, = 400 m and over the grid points of 64 (horizontal) x 30 (vertical). An example shows that, when initial conditions are such that two cumulus clouds are separated with a distance of 15 km, the cell in the upstream side develops faster than the other and eventually there is only one intense cell of the size of approximately 10 km. In another case where an initial cloud has a horizontal dimension of 40 km, the cloud breaks up into two cells and these two cells undergo the changes described above.

REFERENCES

1. Asai, T. and A. Kasahara, 1967: A theoretical study of compensating downward motions associated with cumulus clouds. J. Atmos. Sci., 24, 487-496.

2. Weinstein, A. I., 1970: A numerical model of cumulus dynamics and microphysics. J. Atmos. Sci., 27, 246-255.

3. Byers, H. R. and R. R. Braham, 1949: The Thunderstorm. U.S. Government Printing Office, Washington, D.C., 297 pp.

THE INTERACTION BETWEEN CUMULUS DYNAMICS AND MICROPHYSICS

Alan I. Weinstein
Meteorology Research, Inc., Altadena, California

INTRODUCTION

Recent precipitation (Haman, 1968, and Iribarne, 1968) and hail (Gokhale and Rao, 1969) development models have hypothesized the existence of a steady-state, parabolic, updraft profile. This shape of updraft profile leads to the production of a water accumulation zone above the level of maximum vertical velocity. It is in this accumulation zone that the precipitation and/or hail particles grow.

The present paper shows how and where this accumulation zone develops and how non-steady-state conditions lead to the dissipation and then redevelopment of the zone.

THE MODEL

The model equations are given elsewhere (Weinstein, 1968). Suffice it to say here that the model is a one-dimensional, time-dependent solution of the first law of thermodynamics, the third equation of motion, and the paramaterized equations of moisture balance explained by Kessler (1969). The solution is similar to that presented by Srivastava (1967) except that the development stage of the cloud is also modeled.

RESULTS AND DISCUSSION

Figure 1 shows the time-height cross sections of a sample calculation. The points to note in the figure are: (1) the updraft maximum is concentrated near the top of the cloud and occurs during the first growth stage of the cloud's lifetime; (2) the downdraft starts at cloud base and spreads vertically (Srivastava found the same development); (3) the liquid water content maximum occurs below the level of maximum vertical velocity; and (4) the updraft and liquid water content maxima are out of phase.

The last point is shown more clearly in Fig. 2. It can be seen that at two sample levels in the cloud, near the level of maximum vertical velocity and just below the level of maximum liquid water content, the parameters undergo periodic, damped oscillations in time. The oscillations of the two parameters are almost 180° out of phase.

Srivastava found similar oscillations in his model calculations of the decay of cumuli. His Fig. 7 is very similar to the present Fig. 2. The physical reason that he gave for the coupled oscillations is also valid for the present case. The updraft increases in response to the buoyancy generated by latent heat of condensation. This condensate (liquid water) becomes a drag on the updraft until eventually it equals the buoyancy. If the liquid water were constrained to remain with its original parcel (i.e., the drops had no terminal velocity), the buoyancy and drag terms would remain equal and the cloud would become steady state (see Weinstein, 1968, for a sample calculation of this case). If the liquid water is allowed to move with its terminal velocity but there is no drag on the updraft, the water will accumulate in some zone, and the updraft profile will still remain in a steady state.

If there is both movement of the liquid water and drag, the steady-state condition cannot be maintained. As the liquid water content increases, its terminal velocity as well as its drag increases. Eventually, the increasing terminal velocity exceeds the decreased updraft speed, and the water starts to fall relative to the ground. As soon as the water leaves any level, it frees the updraft and the condensation-fallout cycle starts again. The resulting periodic oscillations are damped because the levels never completely unload their water. The updraft always starts with some drag which it did not have when the cloud started.

A THREE-DIMENSIONAL CLOUD

The sequence of events described above must occur in a one-dimensional time-dependent framework. In the three-dimensional framework of a real cloud, precipitation particles are not constrained to fall or rise; they may move horizontally. In this case, a storm may maintain a steady updraft with a radar echo that has the appearance of an accumulation zone. This radar echo cannot be thought of as an area of collection of liquid water, since any collection at one level would have to result in a drag on the updraft and a subsequent unloading as has been described for the one-dimensional case. A more physically realistic explanation for the steady radar echo is to consider the accumulation zone as being similar to a lenticular cloud. The echo maximum is being constantly formed from the bottom and evacuated out the sides.

Precipitation particles and/or hailstones growing in this zone must either be carried out the sides or drag down the updraft. In either case, it is physically unrealistic to model a steady-state updraft in which liquid water remains fixed in the accumulation zone.

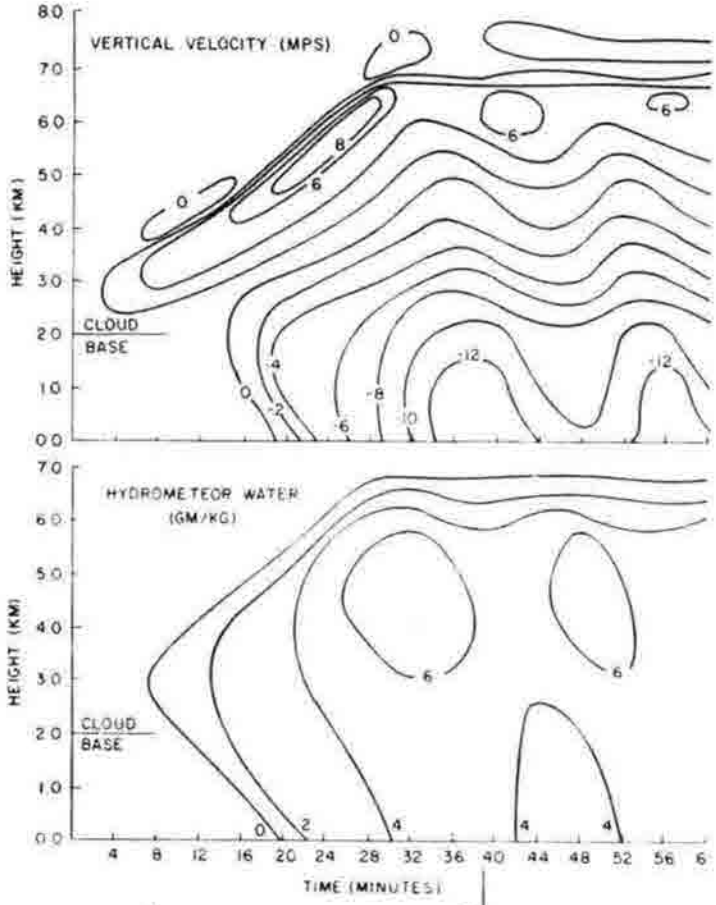

Fig. 1. TIME-HEIGHT CROSS SECTIONS WITH THE CLOUD MICROPHYSICS PARAMETERIZATION

References

Gokhale, N.R., and K.M. Rao, 1969: Theory of hail growth. J. Rech. Atmos., IV, 4, 153-178.

Haman, K., 1968: On the accumulation of raindrops by Langmuir chain reaction in an updraft. Proc. Intl. Conf. on Cloud Phys. Toronto, Canada, 26-30 Aug., 345-349.

Iribarne, J.V., 1968: Development of accumulation zones. Ibid., 350-355.

Kessler, E., 1969: On the distribution and continuity of water substance in atmospheric circulation. Meteor. Monogr., 10, 32, AMS, 84 pp.

Srivastava, R.C., 1967: A study of the effects of precipitation on cumulus dynamics. J. Atm. Sci., 24, 422-434.

Weinstein, A.I., 1968: Ph.D. Thesis, Dept. of Meteor., Penn State Univ., University Park, Pa., 75 pp.

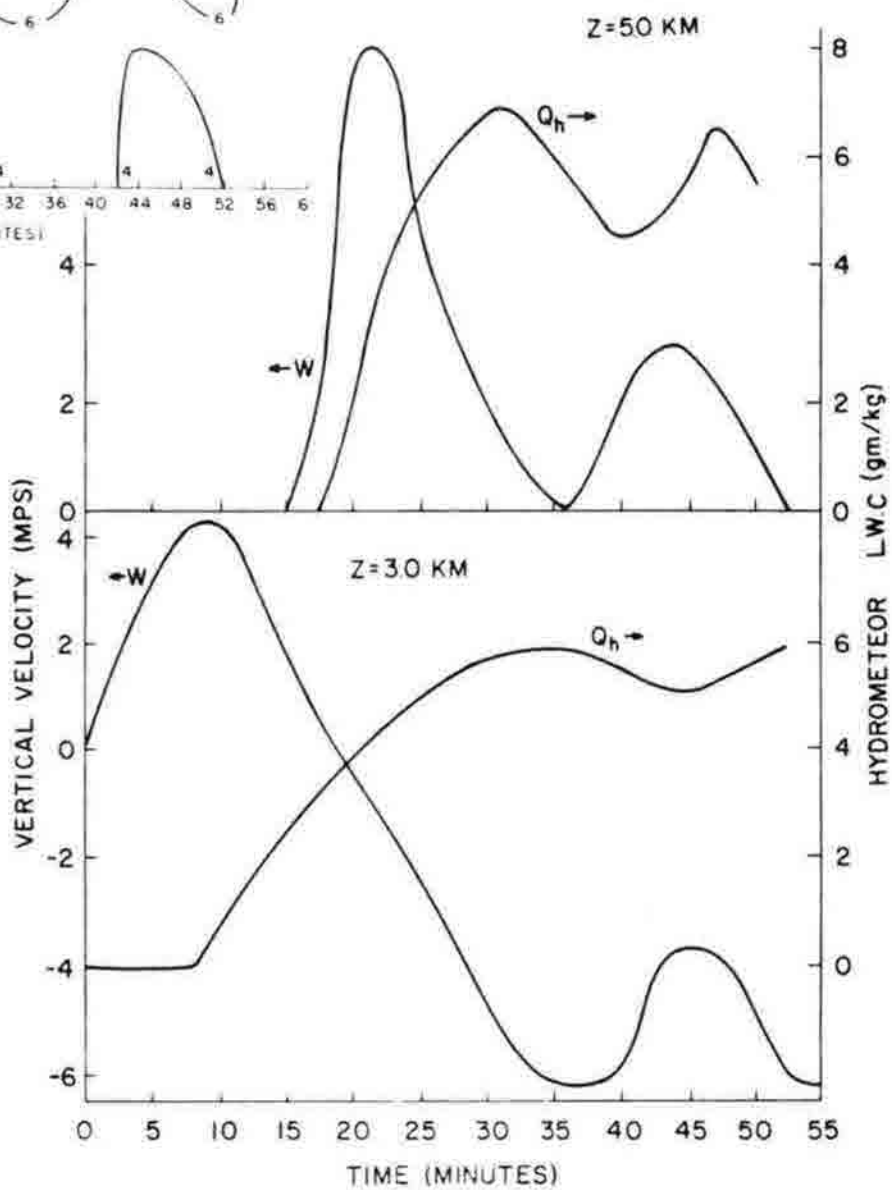

Fig. 2. TIME HISTORY OF VERTICAL VELOCITY (W) AND HYDROMETEOR WATER (Q_h) AT 5.0 AND 3.0 KM IN THE CLOUD

A NUMERICAL MODEL OF HAIL-BEARING CONVECTIVE STORMS

Chester Wisner
Institute of Atmospheric Sciences, Rapid City, South Dakota*

A numerical model was developed which allows investigation of the interactions between the dynamical, thermodynamical, and hydrometeor processes which are active in the core of a cumulus cloud. A brief description of the model and some representative results are presented here. A more complete presentation is available elsewhere. (1)

The model is time-dependent and one-dimensional in space. The dependent variables are vertical velocity, temperature, radius, and the mixing ratios of water vapor, cloud water, rain water and hail. The environment is assumed to be static and is specified by the pressure, temperature, and water vapor mixing ratio at each grid point.

Fig. 1 shows in schematic fashion the processes involved in the formation of the various categories of water substance. Water vapor in excess of the saturation value is immediately converted to cloud water, and saturation is maintained whenever cloud water is present. Cloud water is converted to rain water at a rate specified by the parameterization of the coalescence process suggested by Berry. (2) Kessler's method of treating the accretion of cloud water by rain water is utilized. (3) Evaporation of the rain water in subsaturated air is included by integrating the rate of evaporation from one raindrop over the raindrop size distribution. The raindrop size distribution is assumed to be a Marshall-Palmer distribution. Hailstone growth in the model is by two processes, the freezing of raindrops and the accretion of supercooled cloud water and rain water. Raindrops are frozen according to the Bigg equation, and the accretion of cloud water and rain water is treated in a fashion similar to Kessler's treatment of the accretion of cloud water by rain water. The size distribution of hailstones is assumed similar to the Marshall-Palmer distribution but with a different constant, i.e., Marshall and Palmer's N_0 of 0.08^{-4} cm^{-4} is replaced by 5×10^{-4} cm^{-4}.

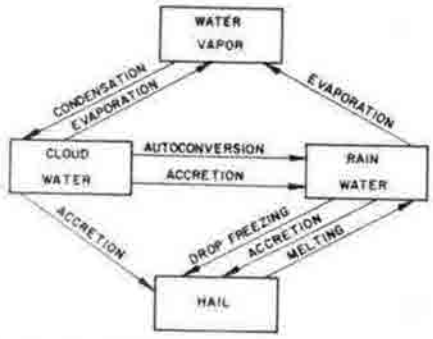

Fig. 1. Schematic of microphysical processes.

The numerical method of solution was based on upstream differencing. Numerical instabilities were encountered in the solution to such an extent that it would be adviseable to investigate other techniques prior to further use of the model.

In the cases presented here, the environment has a temperature of 300K at the surface, decreasing according to the dry adiabatic lapse rate to 1.5 km, then decreasing by 6.5C km^{-1} to 9 km, and decreasing by 2C km^{-1} from 9 km to the top of the grid. (All references to altitude are given in terms of height above ground level.) The melting level is at about 3.4 km, and -20C is found at about 6.5 km. The water vapor mixing ratio is 10 g kg^{-1} at the surface and decreases at 2 g kg^{-1} km^{-1} to 5 km. The initial perturbation of the core consists of a constant water vapor mixing ratio of 11.9 g kg^{-1} (which is the saturation value at 1.5 km) for the region below 1.5 km and a sinusoidal variation in the vertical velocity in the same region with the vertical velocity reaching a maximum of 1 m sec^{-1} at 0.75 km.

Figs. 2a and 2b show the results when hail was not allowed to form. Note that a steady state is attained. Figs. 3a through 3d show the results for the same situation with hail formation allowed. We may observe the following from the results: 1) Hail plays a very important role in the chain of events leading to precipitation at the ground. It provides a mechanism for transporting water down through the updraft, and in the lower levels, its weight and the cooling due to its melting are important factors in the initiation of a downdraft. 2) The steady-state assumption is appropriate until appreciable amounts of hail are formed in the cloud. 3) The downdraft begins at the melting level and propagates downward, but not upward.

REFERENCES

1. Wisner, C. E., 1970: A numerical model of a cumulus cloud. Masters thesis available from the Institute of Atmospheric Sciences, South Dakota School of Mines and Technology, Rapid City, South Dakota 57701
2. Berry, E. X., 1968: A parameterization of the collection of cloud droplets. Presented at the First Conference on Weather Modification, Albany.
3. Kessler, E., 1969: On the distribution and continuity of water substance in atmospheric circulations. Meteor. Monogr., 10, No. 32, 84 pp.

ACKNOWLEDGEMENTS

I thank Dr. Harold D. Orville for functioning as an exceptionally competent and devoted teacher throughout this study.

The research was supported by the National Science Foundation (Grant GA 11749) and the State of South Dakota. The computations were performed on the Control Data Corporation 6600 computer at the National Center for Atmospheric Research, which is sponsored by the National Science Foundation.

*Present affiliation, San Luis Valley Weather Engineering, Inc., Alamosa, Colorado.

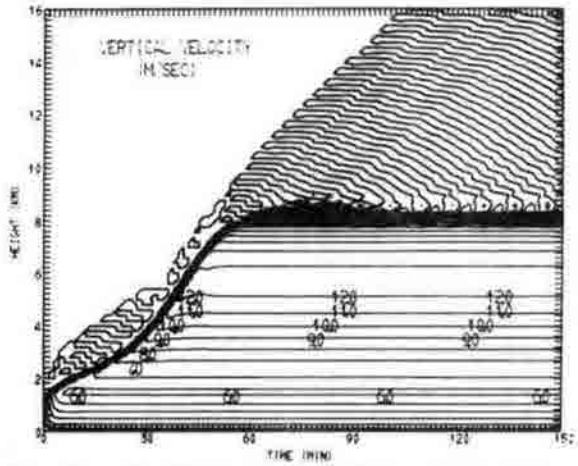

Fig. 2a. Vertical velocity for no hail case. The contour interval is 1 m sec^{-1}.

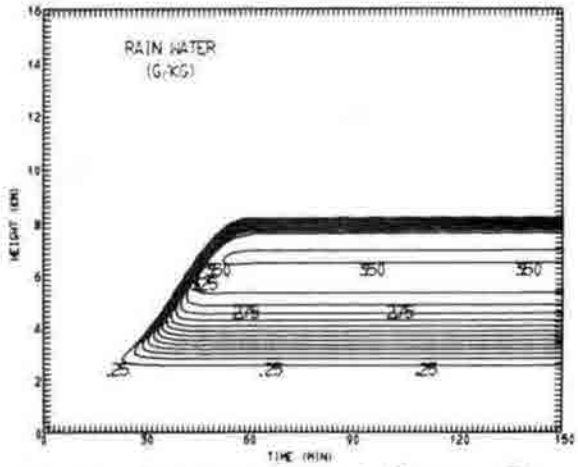

Fig. 2b. Rain water for no hail case. The contour interval is 0.25 g kg^{-1}.

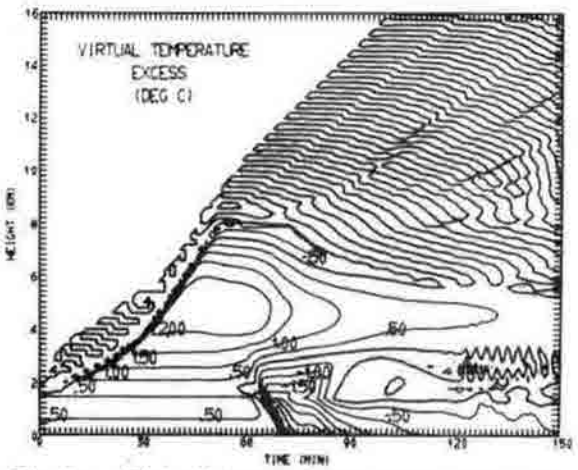

Fig 3a. Virtual temperature excess for hail case. The contour interval is 0.5C.

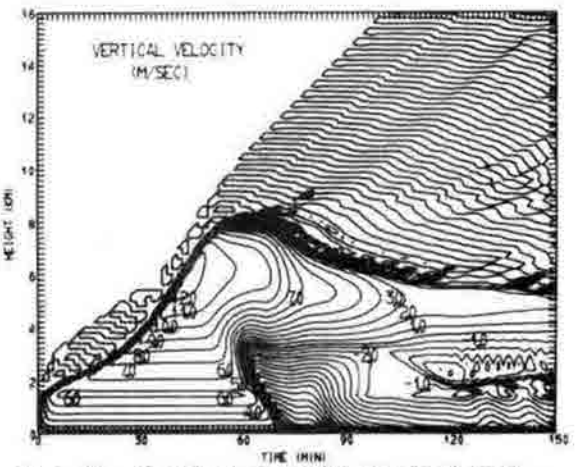

Fig. 3b. Vertical velocity for hail case. The contour interval is 1 m sec^{-1}.

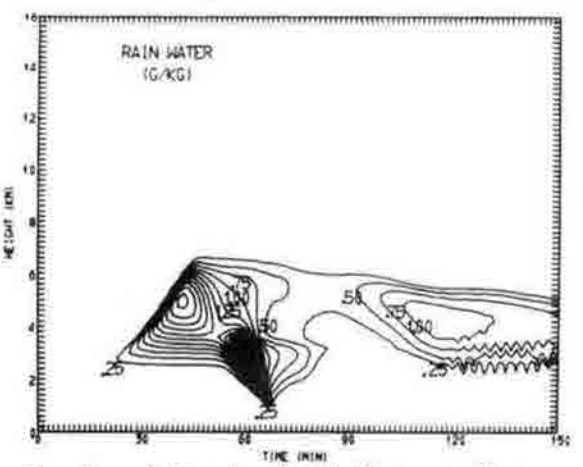

Fig. 3c. Rain water for hail case. The contour interval is 0.25 g kg^{-1}.

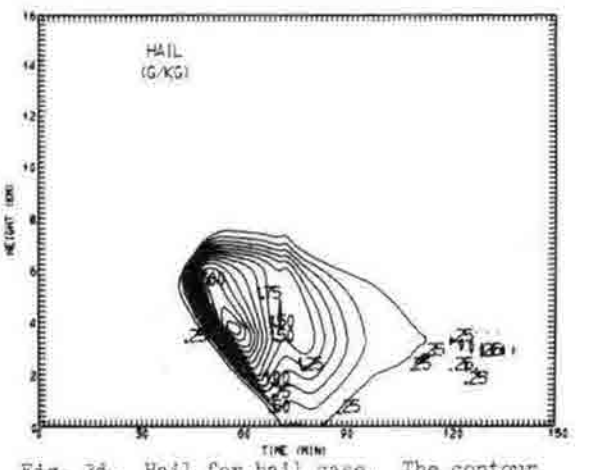

Fig. 3d. Hail for hail case. The contour interval is 0.25 g kg^{-1}.

USE OF THE ATMOSPHERIC WATER BALANCE TECHNIQUE TO INFER THE RATES OF CONDENSATION IN A CYCLONE AND IN AN OROGRAPHIC CLOUD SYSTEM

James L. Rasmussen
Department of Atmospheric Science, Colorado State University
Fort Collins, Colorado 80521

The purpose of this paper is to report some results of synoptic-scale atmospheric water balance studies carried out at CSU that would be of particular interest to cloud physics problems. Because of the space restrictions, the material, background and bibliography are incomplete. I refer the reader to the articles Rasmussen, et.al. 1969, Rasmussen 1970, and Parisi and Rasmussen for the details of the studies.

Computation of the atmospheric water balance yields the exchange of water and vapor at the earth's surface (precipitation minus evaporation) through the observation of the spatial and time distributions and fluxes of water vapor in an atmospheric volume. The volume extends over the area of interest from the earth's surface to a level where water vapor is negligible. It is assumed that the neglect of the water in the form of clouds does not significantly affect the computation (Palmen 1967, Rasmussen, 1968). The water balance may be written

$$P-E = \frac{1}{g}\int_{p_{min}}^{p_{max}} \int_A \frac{\partial q}{\partial t}\, dA\, dp + \frac{1}{g}\int_{p_{min}}^{p_{max}} \int_l c_n q\, dl\, dp \qquad (1)$$

where P-E is precipitation rate minus evaporation rate, g is acceleration of gravity, p is pressure, t is time, A is an increment of area on a pressure surface, Cn is the component of the horizontal wind normal to the sides of the volume and l is a line increment defined by the intersection of the isobaric surface and the sides of the volume. If the situation chosen is one where evaporation is negligible equation (1) is evaluated to yield precipitation rate alone. allowing

The rate of condensation may be estimated by the mass flow in the atmospheric volume to be governed by the thermodynamic constraint of constant equivalent potential temperature, θe. Masses then would follow a thermodynamic path depending upon their initialconditions of temperature, pressure and humidity upon entering the volume and their successive motion within the volume. Accumulating the condensate over the sum of the masses then leads to the determination of the condensate production within the volume. The reader is encouraged to read the more detailed account of the technique in Rasmussen et.al. (1969). Complications to the analysis of course arise for atmospheric systems in which there is much turbulent mixing or where the physical cloud process can not be either specified as an ice or water process.

The experiments described herein are chosen because they are results of a rather comprehensive study of the atmospheric water balance. The following sketches will serve as a background for the results described in Tables I and II and Figures 1

Cyclone Case

The atmospheric water balance was determined for a cyclone that crossed the central United States from the Texas Panhandle to the Great Lakes during the period February 17-19, 1961. The storm may be characterized as an "average" winter time cyclone that developed and began to occlude during this time span. The coordinate system over which the computations were done moved with the storm system. Table I gives the total precipitation computed from the water balance, the condensation determined from the θe analysis and the precipitation deduced from the records of about 150 hourly rain gauges. The agreement between precipitation determined by the two different techniques is exceedingly good. The condensation for the middle time period appears low. Perhaps this is a reflection of a large change in storage of cloud water in the volume as the storm moved northward and occluded (Rasmussen et.al. 1969).

Figure 1 shows the percent of total rate of condensate occurring at various temperatures in the cloud mass. The result shows that as the cyclone matures the shift in condensate formation is toward colder temperatures.

Orographic Cloud Case

We asked whether or not we could evaluate the water balance of a large orographic cloud system using an approach similar to that described above. We searched for days when such a cloud existed over climax, Colorado, when the wind direction was quite invarient with height and from about 260°. These restrictions were necessary to do a two dimensional analysis using Grand Junction as the upwind station, Chalk Mountain as the crest station and Denver as the downwind station.

Table I: The calculated precipitation P and condensate C for each time period and the corresponding gauge precipitation P_G. (Cm/12 hrs)

Time	C	P	P_G
18/00Z	1.4	1.0	1.0
18/12Z	0.9	1.1	1.0
19/00Z	0.6	0.5	0.5

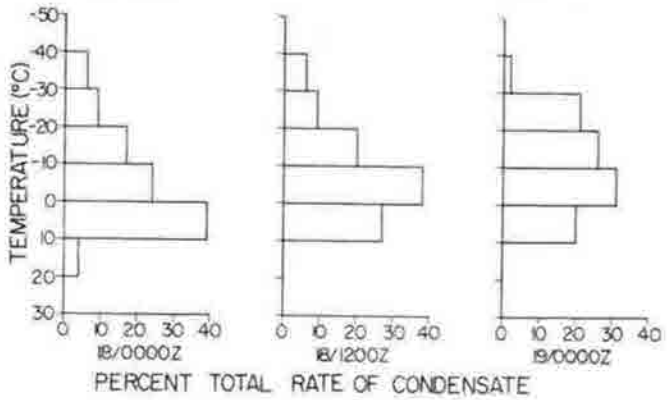

Figure 1. Percent of total rate of condensate within the cyclone system for each period classed according to temperature.

Table II: Condensate values for parcels above Grand Junction lifted over Chalk according to the $_e$ trajectories.

Pressure above Grand Junction (mb)	Pressure over Chalk (mb)	Condensate (gm/kgm)	(%)	Cloud Temperature Range (°C)
725	643	.00	0	
650	600	.24	34	-20 to -25
590	530	.26	37	-25-to -30
545	485	.18	26	-30 to -35
495	455	.02	3	-35 to -40
485	450	.00	0	

Table II shows the details of the cloud determined from the analysis. The precipitation derived from the Grand Junction - Denver water balance yielded .01" per two hours, the length of time the cloud precipitated is as evidenced from the precipitation records. Currently more cases of this nature are being evaluated in order to determine if such techniques could be used in the control and monitoring of cloud seeding experiments.

References

Palmen, E. 1967: Evaluation of Atmospheric Moisture Transport for Hydrological Purposes. Rept. No. 1, WMO International Hydrological Decade Projects, Geneva, 63 pp.

Parisi J. and J. Rasmussen, Water Balance of Orographic Cloud Systems. Atmospheric Science Paper, Colorado State University. In preparation.

Rasmussen J., R. Furman and H. Riehl, 1969. Moisture Analysis of an Extratropical Cyclone, Arch. Met. Geoph. Biokl. Ser. A. 18, 275-298.

Rasmussen J. 1970: Atmospheric Water Balance and Hydrology of the Upper Colorado River Basin, Water Res. Research, Vol. 6, No. 1, 62-76.

SYNOPTIC VS. MICROSCALE INFLUENCES ON GREAT LAKES SNOWSTORMS

By

Douglas A. Paine and James E. Jiusto

State University of New York
Albany, New York

A low level trough, initially positioned beneath a 500 mb low, often propagates southeastward behind a strong cold front crossing the Great Lakes during the early winter season. Its position is most noticeable from the surface to 850 mb, usually becoming indistinct above the 700 mb level. This secondary trough often undergoes a slight intensification because of the favorable diabatic effects induced by the lakes' presence; namely, surface heating resulting from the passage of cold air over warm water and the release of latent heat during the ensuing cloud formation and outbreak of snowshower activity.

Relative vorticity maximums associated with the feature normally lie within a +4 to +8 x 10^{-5} sec^{-1} range. Unlike the main frontal trough, colder air advection is slight and the resulting omega (ω) field is primarily a consequence of this vorticity advection.

Trajectories computed from isentropic analyses have given a valuable insight into the trough's imposed field of vertical motion. These computations were restricted to layers above the 850 mb surface, and care was also exercised to avoid those regions of convective mixing of momentum, energy and moisture over the lakes which violate the assumptions employed by the trajectory technique.

The trough's presence produces two distinct fields of vertical motion. The weak ridging behind the main cold front is associated with negative relative vorticity advection where air parcels undergo a gentle descent of 1000 to 2000 ft/12 hrs below 500 millibars. This is often sufficient to form a capping inversion (near 700 mb) over the convective activity induced by a particular lake. Closer to the secondary trough, trajectories show its positive vorticity advection to be associated with 1000 to 6000 ft ascents of air parcels in 12 hrs.

The importance of such a feature to mesoscale and microscale development of Great Lakes snow-squall activity is as follows:

(1) The passage of a secondary trough typically shifts the prevailing wind below 5000 ft from a southwest and west-southwest direction to that of west-northwest and northwest. Other studies have shown that the most intense snow bands covering a relatively small area occur when the prevailing wind parallels lakes Erie or Ontario, with less intense snowfalls of greater areal extent under a northwest flow.

(2) One case studied showed convective cloud depths doubling (8,000 to 17,000 ft) with the passage of a fast-moving trough across Lake Erie. Its short-lived influence, lasting only three to six hours at a particular point, produced intense snow showers, irregular and conical shaped graupel, and lightning discharges.

(3) Three-hourly soundings reveal that thermal heating and destabilization of the air by the warm lake water remains effective in both the region of synoptically induced descent and ascent in the lowest 5,000 to 10,000 ft of the atmosphere. However, the moistening of the lapse rate becomes efficient only when significant positive vorticity advection occurs. This near-saturation at low levels promotes vertical cloud development and presumably augments precipitation.

(4) Finally, there is some evidence to suggest that the strength of a secondary trough may not be as important in determining the intensity of Great Lakes mesoscale snowstorms as its length of stay over a particular body of water. Indeed, the most severe of these storms in the past four years occurred when such a trough had become nearly stationary over Lake Erie. The total water equivalent of that storm's snowfall over land exceeded 1/20th the capacity of Lake Mead, one of man's largest reservoirs.

Point four has led to attempts to forecast the movement and associated vorticity advection of secondary troughs. The NWP synoptic-scale grid spacing of 381 km commonly misses or loses this feature within 12 hrs of the initial data. A mesoscale grid length of 127 km has given initial encouragement to predicting the feature's movement at its equivalent barotropic level--the 850 mb surface.

Analyzing Great Lakes snowstorms from the micro and mesoscale, it soon becomes evident that the lakes constitute a primary force in supporting the phenomenon. The strong vertical flux of thermal energy, momentum and water vapor at low levels stem directly from these large source reservoirs. For example, as the winter season progresses and the lakes cool, the total precipitation generated by lake (Erie and Ontario) storms decreases by a factor of 5. This largely reflects the direct impact of the lakes on storm intensity.

Updrafts stemming from the local convective process vary from a few tens of centimeters per second to a few meters per second in intense cell regions. Water budget calculations indicate that an overall average updraft of approximately 50 cm/sec over a typical 3 km cloud depth is required to produce the intense snowfalls of 1-3 inches per hour. Note that the synoptic scale updrafts induced by the secondary trough are of the order of a few centimeters per second (6000 ft/12 hr) averaged over a 12 hour period, or approximately an order of magnitude less than the mesoscale convective updrafts.

Thus, it is believed that even in an unfavorable synoptic environment, i.e. absence of a secondary trough, some lake-induced snow could be generated. The less intense NW flow cases appear to substantiate this hypothesis. However, in order to produce the intense lake storm (SW-W flow), we feel that the presence of a slowly-moving secondary trough with its associated positive vorticity advection field is essential. This phased coupling of synoptic and mesoscale events then can produce the "classic" Great Lakes snowstorm, of which there are few rivals.

Acknowledgment

This work was supported by [illegible] under grant [illegible] and by the State University of New York at Albany.

STRUCTURE OF WEAK SNOWBAND IN RELATION WITH PROPAGATION MECHANISM AS REVEALED BY RADAR

Z. Yanagisawa and M. Fujiwara

Meteorological Research Institute
Tokyo, Japan

1. OBSERVATION

A modified marine radar RHI (8kw, 1.5° vertically X 13° horizontally, Antenna: 17 turn/min in vertical plane, 0.3 turn/min in horizontal plane), a vertically pointing 3-cm Doppler radar, and a conventional PPI radar were used (1).

Several snowbands, which were formed in a continental out break, were observed at a coast of the Japan Sea by the three radars. The snowbands brought mostly snow pellets or mixture with flakes, but fewer cases was associated with flakes alone depending on the developing stage. The cloud tops were about 3,300 m in height (-20C) and the surface temperatures were 1 to 3C.

2. RESULTS

It was found from the several observations by reducing the receiver gain about 3 dB that the laterary extent of the snowband is about 10 km and composed of 2 or 3 small (bubble type) echoes, the dimension of which is about 1 km in diameter. The advancement of the band is achieved by an updraft at the immediate rear of the leading edge of the band.

In Fig.1, a sequential RHI picture taken in a vertical plane which is parallel to the moving direction of the band, 100 deg., illustrates the behavior of the bubble echoes A, B and C. Echo A which had been moving by 12 m/s at about 2 km in height started to descend as it got the radar site. The descending speed increased from 1.5 m/s for 8 to 11 min to 3.5 m/s for 11 to 14 min in average. Thus, a bubble echo once generated in the rear edge of the band gets over the precede one near the leading edge.

It is also found by similar illustrations that the first bubble echo used to fall immediately after it passes the radar site. Whereas the pursue gains energy by updraft (2-3 m/s from Doppler data which are shown in Fig.3 for Echo B.) from the underneath and the precipitation is suspended further to reach more extended distance forward. This instance is shown in Fig.2 by E and F.

Comparing the horizontal velocity of the bubble echo with the wind speed (see also Fig.2) it is indicated that the echo speed is almost equivalent to the wind speed at the echo base, suggesting an effect of momentum transport from lower levels. It is interesting to see in Fig.2 that when active updraft was observed underneath the bubble echo its horizontal speed was reduced considerably by the momentum exchange.

In spite of the slowing, this activated parcel reached the distance further than 5.8 km on Echo B and 7.1 km on Echo F. This distance seems to increase with the energy supply near the leading edge.

3. DISCUSSION

The bubble echo B precipitated the mixture of snowpellets and snowflakes on the ground station at about 5 km leeward but snowflakes alone, on the stations about 9 and 14 km leeward. From the analysis of the Doppler spectrum, in terms of v_{min} at the cut-off of S(v) and mean velocity $\overline{v}$, it was found that snowflakes develop within the circumstances where updraft is less than 70 cm/sec, while snowpellets or the mixture, where the updraft is more than -70 cm/sec.

It was also found that very narrow sharp spectrum showing snowflakes or tiny pellets prevails in the region immediately after (0.5 to 1 minute) the updraft. Therefore the energy supply by an updraft would serve the rather persistent boyancy at first by latent heat of condensation and later by that of graciation.

When the updraft core of the band is far behind the leading edge the updraft may not be effective for speeding the propagation of the band. This coincides with the facts that a traveling band has its active convective core is biased toward the extreme front.

4. REFERENCE

(1) Aoyagi J., N. Kodaira, M. Fujiwara, and Z. Yanagisawa, 1966: Doppler radar observation of snow showers. 12th Weath. Radar Conf. Norman, Oklahoma, pp 112-116.

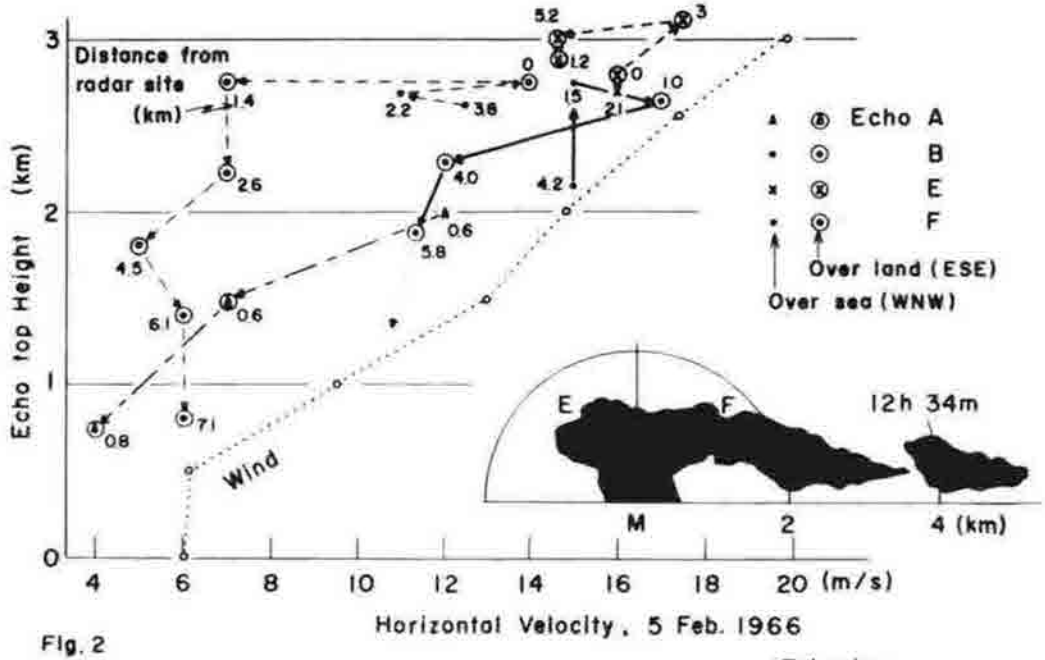

Fig. 2

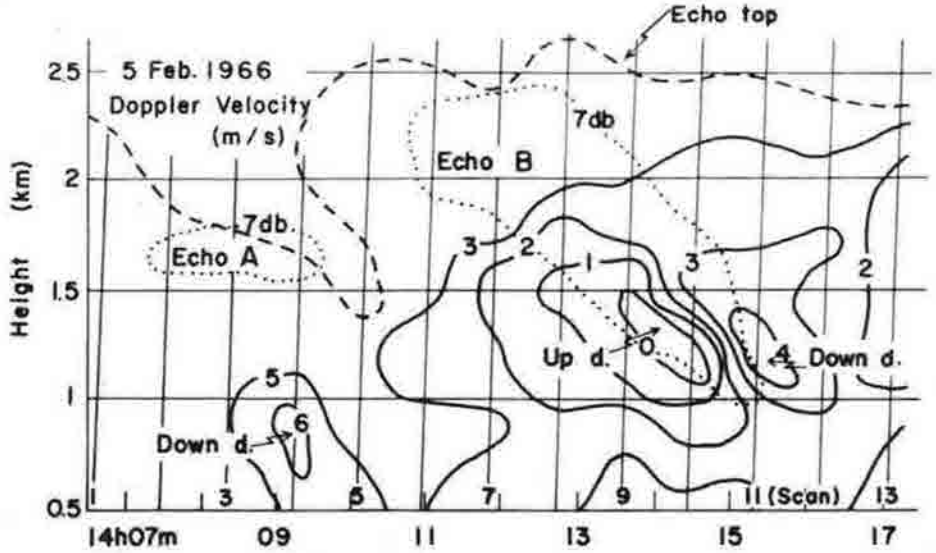

Fig. 3

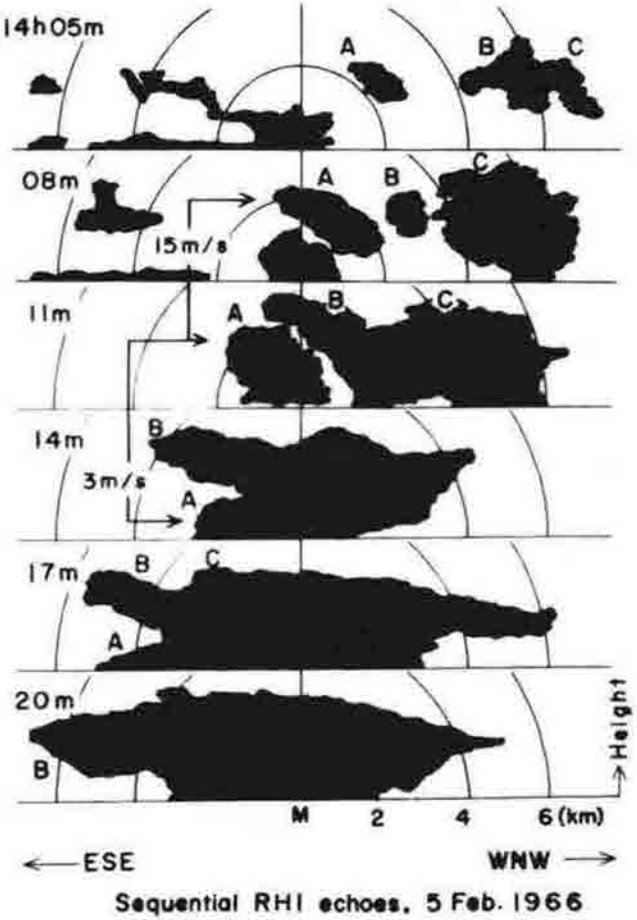

Sequential RHI echoes, 5 Feb. 1966

Fig. 1

THE INFLUENCE OF A COLD FRONT ON THE DROP SIZE DISTRIBUTION

by A. Waldvogel and J. Joss

Osservatorio Ticinese Locarno-Monti, Switzerland

The influence of an air mass change on the precipitation mechanism is illustrated with an example. The example shows a drastic change of the drop size distribution during an orographic wide spread rain at the time when a cold front passed the area.

Instruments

The rain drop size distributions are measured with a distrometer for raindrops by Joss and Waldvogel (1). Drops with diameters between 0.3 mm and 5.3 mm can be measured continuously and automatically. The data of the distrometer are fed into an analog computer to produce real time registrations. In addition the data are recorded on magnetic tape to be evaluated later with a digital computer.

The radar reflectivity is measured with a vertically pointing radar ($\lambda = 4.6$ cm). The time vs. height profile of the radar reflectivity factor is recorded in real time with a facsimile recorder, see Joss et al. (2).

Data processing

The analog computer calculates from the measured distribution N(D): the liquid water content W [$g\,m^{-3}$], the rainfall rate R [$mm\,hr^{-1}$] and the radar reflectivity factor Z [$mm^6\,m^{-3}$]. The quantities W and Z of the distribution are transformed into two new parameters N_o and Λ to give a better idea of the distribution. The transformation is also done by the analog computer in real time.

$$N_o = \frac{1}{\pi}\left|\frac{6!}{\pi}\right|^{4/3}\left|\frac{W}{Z}\right|^{4/3} W \qquad ; \qquad \Lambda = \left|\frac{6!}{\pi}\,\frac{W}{Z}\right|^{1/3}$$

If the distribution is an exponential one, the parameters N_o and Λ get the same meaning as those proposed by Marshall and Palmer (3).

In addition to the quantities mentioned above, the digital computer calculates the median drop diameters D_W, D_R and D_Z, where W, R and Z respectively reach 50 % of their total value. To get an idea of the character of the distribution we also calculate the quotient $D_W/D_{W'}$. ($D_{W'} = 3.67/\Lambda$ is the meadian drop diameter for W for an exponential distribution, for which $D_W/D_{W'} = 1$).

All quantities and parameters which are calculated originate from samples with an exposing time of 1 minute, thus the errors due to sampling size are small enough, see Joss and Waldvogel (4).

Example

The example given below, shows the registrations of the radar reflectivity factor profile, the parameters N_o, Λ, R and $D_W/D_{W'}$, of the drop size distribution and a table with the mean values and the standard deviations of the parameters for different time intervals with a duration of ca. 30 minutes each.

The meteorological situation was first an orographic wide spread rain starting at ca. 09.30 in a warm air mass with a pseudopotential wet-bulb temperature $\theta = 14.3^o$ (this θ is the mean value between 950 mb and 500 mb). A colder and less humid air mass arrived at ca. 15.00, with a pseudopotential wet-bulb temperature $\theta = 12.2^o$. The change of the air masses resulted at our station in a change of temperature, humidity, pressure, wind, radar reflectivity profile as well as the drop size distribution.

References

(1) J. Joss and A. Waldvogel, 1967 : Ein Spektrograph für Niederschlagstropfen mit automatischer Auswertung
Pure and Applied Geophysics, Vol. 68, 240-246

(2) J. Joss, K. Schram, J.C. Thams and A. Waldvogel, 1970 : On the quantitative determination of precipitation by radar (to be published)

(3) J.S. Marshall and W. McK. Palmer, 1948 : The distribution of rain drops with size, J. Meteor, Vol. 5, 165-166

(4) J. Joss and A. Waldvogel, 1969 : Raindrop Size Distribution and Sampling Size Errors
J. Atmos. Sci., Vol. 26, 566-569

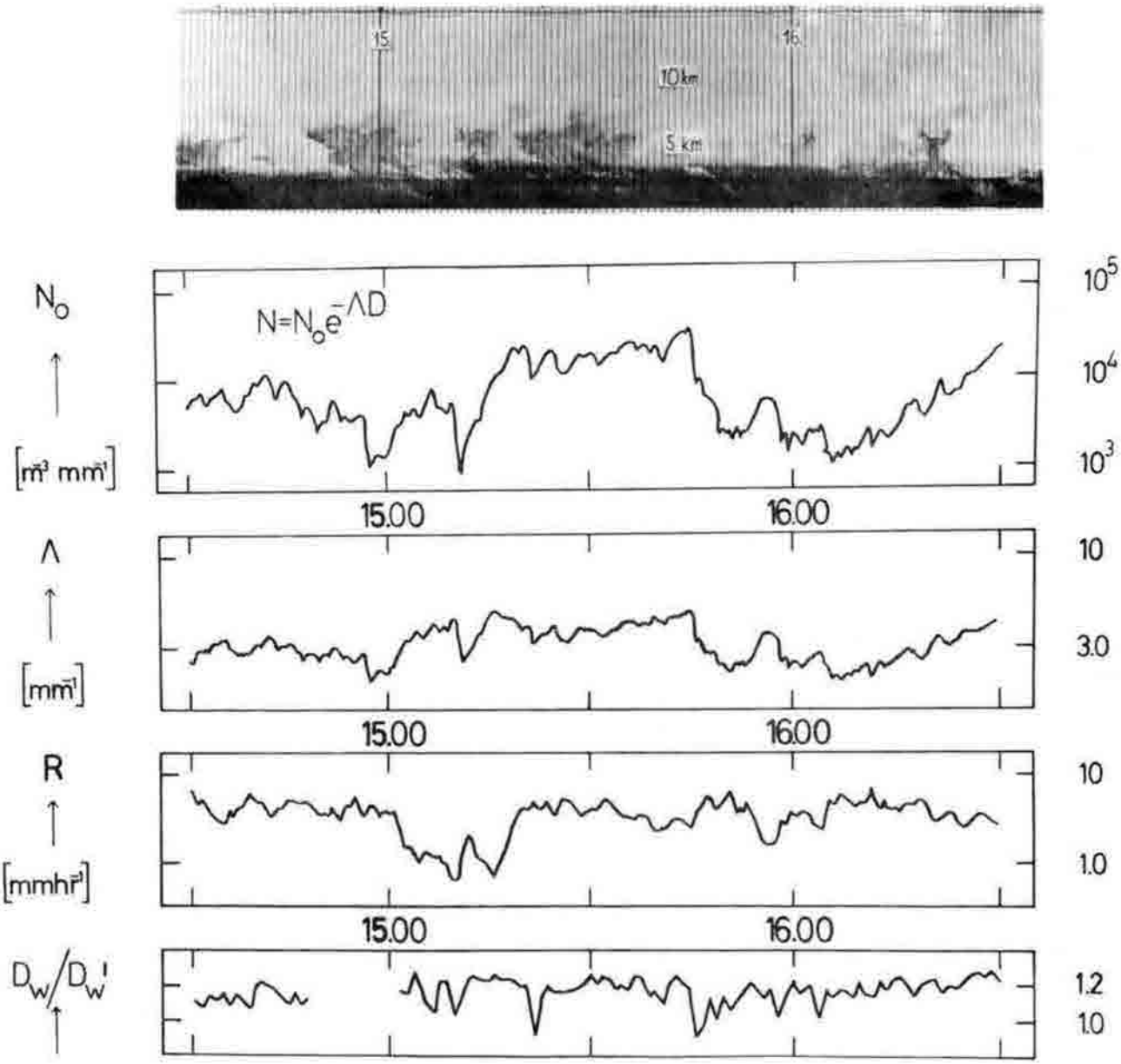

$\overline{N_o}$	6887	16220	3364	$[mm^{-1}m^{-3}]$
s (N_o)	24 %	35 %	44 %	
$\overline{\Lambda}$	2.8	3.56	2.57	$[mm^{-1}]$
s (Λ)	9.2 %	10 %	15 %	
$\overline{R}$	6.75	5.51	4.81	$[mm\ hr^{-1}]$
s (R)	26 %	43 %	33 %	
$\overline{D_W/D_W'}$	1.14	1.20	1.17	
s (D_W/D_W')	3.9 %	6 %	5 %	

Registrations of a precipitation period on 18 September 1969 from 14.30 till 16.30 at Locarno-Monti. The radar reflectivity profile is at the top, below the registrations of the parameters N_o, Λ, R and D_W/D_W', and a table showing the mean values $\overline{N_o}$, $\overline{\Lambda}$, $\overline{R}$ and $\overline{D_W/D_W'}$ and the quotients s of the standard deviation devided by the corresponding mean value.

A MESOSCALE NUMERICAL MODEL OF AIRFLOW OVER THE BLACK HILLS

Chia Bo Chang and H. D. Orville
Department of Meteorology, SDSM&T, Rapid City, S. D. 57701

INTRODUCTION

The Lavoie model for Lake-effect Storm has been modified to simulate the disturbance of the air motion in the Black Hills area. In Fig. 1, layer I, 50 m deep in contact with the surface of the earth, is characterized by a superadiabatic lapse rate to represent a condition of upward heat and water vapor flux. Layer II with homogeneous distribution of potential and mixing ratio of total water content vertically is well-mixed. Layer III is assumed to be stable.

ASSUMPTIONS

1. The atmosphere is modeled as consisting of three layers in z-direction and two-dimensional in the x, y plane. 2. Determination of the distribution of the time-dependent variables is restricted to the well-mixed layer. 3. The Coriolis parameter is assumed uniform throughout the entire region. 4. The effect of the curvature of earth is neglected. 5. There is no heat and water vapor exchange between the well-mixed layer and the upper stable layer.

BASIC EQUATIONS

The first and second equations of motion are

$$\frac{\partial u}{\partial t} = -u\frac{\partial u}{\partial x} - v\frac{\partial u}{\partial y} - fv - \frac{1}{\rho}\frac{\partial P}{\partial x} - \frac{1}{\rho}\frac{\partial \tau_x}{\partial Z} \quad (1)$$

and

$$\frac{\partial v}{\partial t} = -u\frac{\partial v}{\partial x} - v\frac{\partial v}{\partial y} - fu - \frac{1}{\rho}\frac{\partial P}{\partial y} - \frac{1}{\rho}\frac{\partial \tau_y}{\partial Z} \quad (2)$$

In the above equations u, v are the components of the wind velocity along the x,y axes respectively, f is the Coriolis parameter, ρ is the density of dry air, P is atmospheric pressure, and τ_x, τ_y are the components of eddy stress vector along the x,y axes, respectively. The water conservation equation is

$$\frac{\partial Q}{\partial t} = -u\frac{\partial Q}{\partial x} - v\frac{\partial Q}{\partial y} - \frac{1}{\rho}\frac{\partial F_r}{\partial Z} \quad (3) \quad \text{where} \quad F_r = -\rho K_r \frac{\partial Q}{\partial Z}$$

represents a vertical flux of water vapor. Q is the mixing ratio of total water content (vapor plus liquid) in g/kg. Also K_r is the eddy coefficient for water vapor. The thermodynamic energy equation is

$$\frac{\partial \theta}{\partial t} = -u\frac{\partial \theta}{\partial x} - v\frac{\partial \theta}{\partial y} - \frac{\theta}{T\rho}\frac{1}{c_p}\frac{\partial q}{\partial Z} - \epsilon\frac{L}{c_p}\pi^{-1}\frac{1}{\rho}\frac{\partial F_r}{\partial Z} + \text{Source} \quad (4)$$

where $\pi = (P/P_*)^K$ and $q = -c_p \rho K_q \partial\theta/\partial Z$

represents a sensible heat flux, θ is the potential temperature of the dry air, T is Kelvin temperature, c_p is the specific heat for dry air at constant pressure, q is the vertical sensible heat flux, K_q is the eddy coefficient for sensible heat and L is the latent heat of condensation. In equation (4) the fourth term gives the latent heat flux and the Source term is used to account for phase change occurring due to the disturbance of an air column. ϵ is the ratio of cloud depth to the thickness of the well-mixed layer. The continuity equation is

$$\frac{\partial u}{\partial x} + \frac{\partial v}{\partial y} + \frac{1}{\rho}\frac{d\rho}{dt} = 0 \quad (5)$$

which is employed to estimate the deformation of the inversion height.

BOUNDARY AND INITIAL CONDITIONS

There are 58 grid points along the y-axis and 35 grid points along the x-axis. The y-axis is selected nearly parallel to the ridge line of the Hills, with an azimuth of 340 deg. to 160 deg. The x-axis is perpendicular to the y-axis. A 4-km grid distance between each point is set along both the x and y direction in the central part of this model. An exponential expansion of the grid distance is used around the outer limits of the model. The total area covered by this model is about 8500 km^2. The surface potential temperature is taken to be a constant and water vapor mixing ratio is made a function of the surface temperature. Model input values come from the adjustment of a real sounding (shown in solid line, Fig. 1). Dashed and dotted line in layer III incorporating the solid line in layer II represents a thermal structure of zero order temperature inversion.

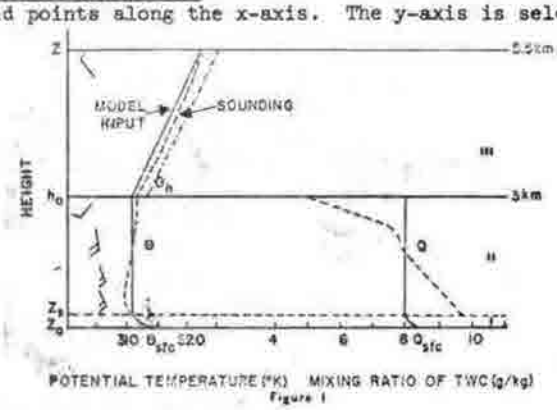

Figure 1

COMPUTATIONAL PROCEDURE

A finite difference method has been used to solve the equations. Upstream differencing is utilized to approximate any spatial derivative involved in the advection term. All other spatial derivatives are replaced by central differences. A 9 point weighting operator is used for smoothing the elevation.

PRINCIPAL RESULTS

The principal results of four cases are shown in Table 1, where Δh, $\Delta\theta$, and ΔQ are the deviations of inversion height, potential temperature and total water content, respectively. LWC stands for the liquid water content inside the cloud. All numerical values are taken when the solutions are steady state. "The case of VAPOR EFFECT" in Table 1 means that we consider no phase change but only the change of air density because of the addition of water vapor.

PARTIAL RESULTS OF SOUTHERLY FLOW (CASE I IN TABLE I)

The real sounding and model inputs for this case are shown in Fig. 1. Fig. 2 shows that the maximum deviation of h, θ, Q after 560 minutes of integration. Fig. 3 gives the perturbation of the inversion surface at 560 minutes as the results of temperature, water vapor, and terrain influences. The largest deformation of the inversion surface is on the downwind side of the mountain. Also there is an upwind maximum forming because of the airflow lifted by mountains. Reflecting patterns at the fixed inflow boundary are shown.

TABLE 1. PRINCIPAL RESULTS

Case	1. Wet	2. Dry	3. Wet	4. Vapor Effect
Order of Inversion	first	first	zero	first
Initial wind speed (knots)	15	15	15	15
Direction (deg.)	179	179	179	179
Max. Δh(m)	1300 downwind 28 km from ridge line	850 downwind 28 km from ridge line	810 downwind 28 km from ridge line	870 downwind 28 km from ridge line
Max. Δθ(°K)	1.85 downwind 28 km from ridge line	1.02 downwind 24 km from ridge line	1.47 downwind 28 km from ridge line	1.01 downwind 24 km from ridge line
Max. ΔQ(g/kg)	2.8	0	3.0	2.73
Max. LWC (g/kg)	1.13 downwind 30 km from ridge line	0	0.71 downwind 28 km from ridge line	0.79 downwind 28 km from ridge line
Max. cloud depth (m)	1300	0	820	920
Min. time to steady state (minutes)	544	400	400	400

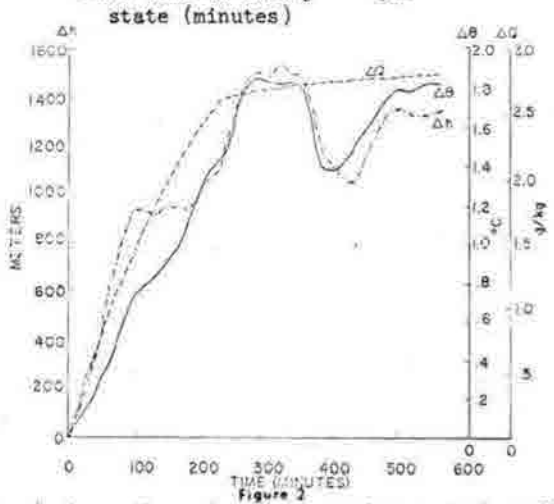

Figure 2

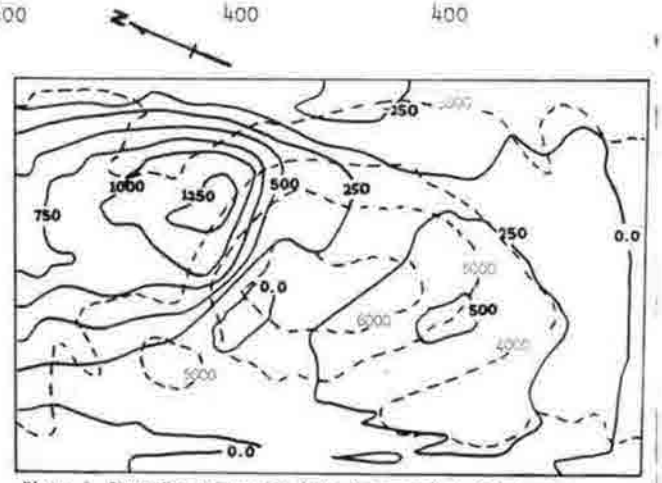

Figure 3. Inversion deformation (unit in meters) at 560 minutes. Dashed lines are topographic contour (unit in feet)

Fig. 4 shows the radar echo envelopes at four different times from 2 to 5 PM indicated by the solid lines around a vertical cross-hatching area, a horizontal cross-hatching area, a larger open area and the two close-dashed curves, respectively. There is little change in position with time. The thinner solid lines in Fig. 4 represent the contour of topography. Since the precipitation comes from thicker clouds which are associated with greater inversion deformation, the maximum inversion deformation should be close to the radar echo in location. But the comparison of Fig. 3 and Fig. 4 reveals that the correlation between them is not good. Some refinements have been considered. For instance, a precipitation scheme or the elevation effect on the surface mixing ratio of water vapor will be added.

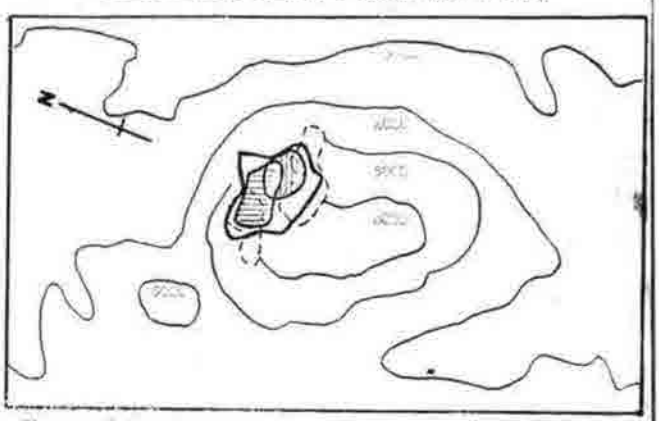

Figure 4. Radar echo envelopes at four different times.

CONCLUSIONS

1. From the results of Case 1, 2, and 4 in Table 1 we can find that the thermal effect of water (via condensation or evaporation) is much more important than the dynamic effect of water vapor through the density changes. 2. A zero order temperature inversion gives a stronger damping result with a decrease of inversion deformation and temperature deviation (see Case 3 in Table 1). 3. Wind direction and topography are two very important factors in determining the location of the maximum deformation of inversion.

ACKNOWLEDGEMENTS

The computations were done on the CDC 6600 at the National Center for Atmospheric Research. The NCAR computing facility has been most cooperative. The research is sponsored by the Bureau of Reclamation, U. S. Department of the Interior, under Contract No. 14-06-D-6796.

REFERENCES

Chang, Chia Bo, 1970: A Mesoscale Numerical Model of Airflow over the Black Hills. M.S. Dissertation, Department of Meteorology, South Dakota School of Mines and Technology, 63 pp.

Lavoie, R. L., 1968: A Mesoscale Numerical Model and Lake-effect Storms. Ph.D. Dissertation, The Penn. State Univ., 102 pp.

THE TIME VARIATION OF THE WATER BUDGET OF A SEVERE SUMMER STORM

Clifford D. Holtz
Meteorological Service of Canada, Toronto, Canada

The purpose of this paper is twofold: 1) to indicate the time varying water budget (partitioning amongst vapour, cloud and precipitation) of an observed thunderstorm; and 2) to develop a theoretical model that simulates numerically the budget during the storm's life cycle by parameterizing the rates of the various sources and sinks. The budget is expressed in terms of the bulk or total masses for the storm-as-a-whole. Figure 1 is a schematic of the time rate of change (denoted by a dot over the symbol) of the various components and their sources and sinks (subscripted by g). Time dependence is implicit.

The main source of air and water into a storm is that due to inflow of moist air through the base (their rates given by $\dot{A}_{1gs}$ and $\dot{V}_{1gs}$); a secondary source is that due to entrainment through the sides ($\dot{A}_{2gs}$ and $\dot{V}_{2gs}$). A storm is visualized as consisting of two regions: 1) a core where air is ascending or decending without mixing, and 2) a shell consisting of mixed entrained air at rest. Moisture entering the base is continuously both stored as saturated vapour in the core ($\dot{V}_1$) and condensed ($\dot{C}_g$) in the updraft. Then part of the cloud is stored in the core ($\dot{C}_d$) and evaporated later ($\dot{V}_{1gd}$) when downdrafts develop; a second part is stored in the shell ($\dot{C}_e$) and converted to vapour by evaporation ($\dot{V}_{2ge}$) when drier air is horizontally mixed into the storm through the sides; and a third part is stored ($\dot{C}_p$) and converted into precipitation ($\dot{P}_g$) which is in turn temporarily stored ($\dot{P}$) and then falls out $\dot{F}_g$.

The observed water budget

Figure 2 gives the partitioning: the total masses of Vapour V(t), precipitable-cloud $C_p(t)$ and Precipitation P(t) existing at time t, and the accumulative masses of the various sources and sinks for the large severe storm of 18 July 1964 observed by the McGill radar. Its output consists of a time-series of CAPPI maps at 6 heights with grey scale to indicate spatial distribution of precipitation intensity (density or flux). In Figure 2, $F_g(t)$ the accumulative mass of fallout to time t was obtained by integrating, using the lowest maps, the flux in the horizontal and in time. Using the remaining upper maps, P(t) the total mass of precipitation existing aloft within the storm is obtained by spatial integration of density. Addition of P and F_g gives $P_g(t)$ the accumulative mass of precipitation that has been generated. Interestingly it was found that the fallout rate $\dot{F}_g$ is proportional to $\dot{P}$ at all t.

Although radar cannot detect cloud, it was recognized that precipitation is converted or generated from cloud. The following equation was derived empirically and describes the interaction: $\dot{P}_g(t) = K\ P(t)\ C_p(t)/A(t)$ Using this equation in reverse gives C_p; then addition to P_g gives C_g the accumulative mass of cloud generated by condensation.

Calculations of A(t) and V(t) the total masses of Air and saturated Vapour requires knowledge of the storm's volume. Since the true cloud volume is not known, the radar-observed volume is used along with the spatial distribution of saturation vapour density. Adding V to C_g gives $V_g(t)$ the accumulative mass of water taken into the storm. Using this and the mixing ratio r_{1b} at the base gives $A_{1gb}(t)$ the accumulative mass of inflow air. Calculations indicate this inflow was less than the observed mass of air within the storm. To account for this discrepancy, environment air is incorporated into the shell by horizontal mixing. If the mixture does not rise, then evaporation of cloud is required to saturate this entrained air. Computations indicate that as the storm develops, less and less air enters by entrainment (i.e. at 1900 about half of the total air intake has come in through the sides; by 2100, the fraction is one-quarter.

The theoretical water budget

In developing a model to simulate the water budget, the viewpoint is taken that each of the physical processes associated with the sources and sinks can be described by a parameterization whereby simple functions replace the complicated physical relationships that actually exist. In this model, all the sources and sinks are given by the following equations with a very brief explanation of their derivation.

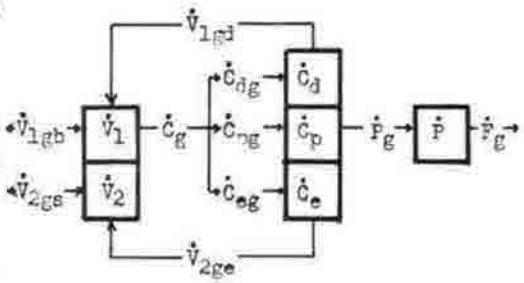

Fig 1. Schematic Water Budget

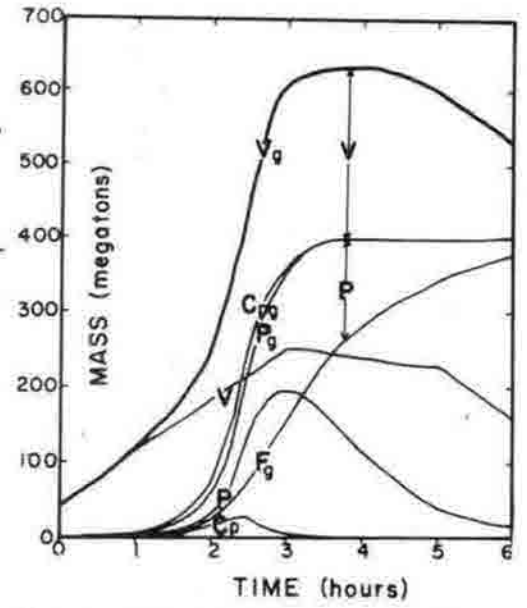

Fig 2. Radar-derived water budget for 18 July '64 storm observed by McGill CPS-9 radar.

The flux of air into the core through the base given by $\dot{A}_{1gb} = K_1 A_1 W_b$ is derived assuming the core base area is proportional to A_1 the mass of air in the core. Empirical studies support this near exponential growth characteristic. To compar the theoretical results with those observed, the vertical velocity W_b is prescribed to vary sinusoidally in time with a period of six hours.

The flux of moisture in (or out) through the base is $\dot{V}_{1gb} = r_{1b} \dot{A}_{1gb}$ where r_{1b} is the mixing ratio at the base. To ensure that vapour intake during updrafts exceeds vapour output during downdrafts (and so allow for condensed products) a smaller value of r_{1b} is used in the latter stage. The ratios used are .010 g/g and .0047, applicable for 18 July '64.

Following the development suggested by Kessler (1969), part of the incoming moisture is used to saturate the expanding core (with mean mixing ratio r = .0033) and the remaining fraction of input (f = .67) to provide for condensation, its rate is given by $\dot{C}_g = f \dot{V}_{1gb}$

This cloud generation is then partitioned into 3 classes depending on the phase the cloud is next converted (its sink).
$\dot{C}_{dg} = f_1 \dot{C}_g$; $\dot{C}_{pg} = f_2 \dot{C}_g$; $\dot{C}_{eg} = f_3 \dot{C}_g$
f_2 = .6 is chosen so final accumulative fallout is equal to that of 18 July '64; f_1 = .2 and f_3 = .2 are arbitrary.

Next the sinks for cloud and their rates are described: When downdrafts develop in the latter half of the life cycle it is assumed that cloud evaporates to maintain the down draft in saturation. This source of core vapour is given by $\dot{V}_{1gd} = f_- \dot{V}_{1gb}$ where f_- depends on r_{1b-} (and so equal to .28).

Following empirical findings (Holtz, 1968) and microphysical theory (Kessler, 1969), the generation rate of precipitation is given by
$\dot{P}_g = K_3 P C_p / A$ where $A = A_1 + A_2$. Although the reasonable assumption is made that cloud density is spatially uniform, no restriction is placed on precipitation density.

The third sink results when cloud is converted to vapour during the entrainment or detrainment process. When dry outside air is mixed with saturated shell air (with mixing ratios r_3 and r_2) shell air will increase in mass if there is sufficient cloud not only to saturate the mixture but also to have some cloud left over. Shell expansion ($\dot{A}_{2gs} > 0$) occurs when cloud mixing ratio $m = C_e/A_2$ exceeds the critical value $\Delta r = (r_2 - r_3)$. The rate of vapour entrained is then $\dot{V}_{2gs} = r_3 \dot{A}_{2gs}$; and the rate at which additional shell vapour is generated by evaporation is $\dot{V}_{2ge} = \Delta r \dot{A}_{2gs}$.
When $m < \Delta r$, cloud is still evaporated but saturation is not attained so that air and moisture are ejected, their rates are $\dot{V}_{2ge} = m \dot{A}_{2gs}$ and $\dot{V}_{2gs} = (m + r_2) \dot{A}_{2gs}$.

The rate at which air is entrained into (or detrained out of) the storm is still rather speculative. The flux should be proportional to the surface area and the horizontal speed of the walls. The most reasonable results were attained when speed was also assumed proportional to surface area with its sign determined by the sign of $(m - \Delta r)$. If it is assumed the surface area is proportional to the square root of total mass A then the flux through the sides can be parameterized by
$\dot{A}_{2gs} = \pm K_2 A \qquad \pm$ if $(m - \Delta r) \gtrless 0$.

The rates of change of V, C and P, given by the boxes (Figure 1), were rewritten in terms of the above parameterized equations for their sources and sinks and were then integrated in time. The theoretical results are given in Figures 3 and 4. Strictly speaking, only the precipitation curves can be compared with the observed results, since mass values of C_d and C_e could not be calculated and values of V were based on radar volume and not cloud volume. However the differential equations formulated here, indicating the gross interactions, do appear to give a reasonable simulation of the water budget for the whole storm and its variation during the life cycle.

Holtz, C.D. 1968: McGill University, MW-55, May 1968.
Kessler, E: 1969: Amer. Meteor. Soc., Met. Monograph 10, 32.

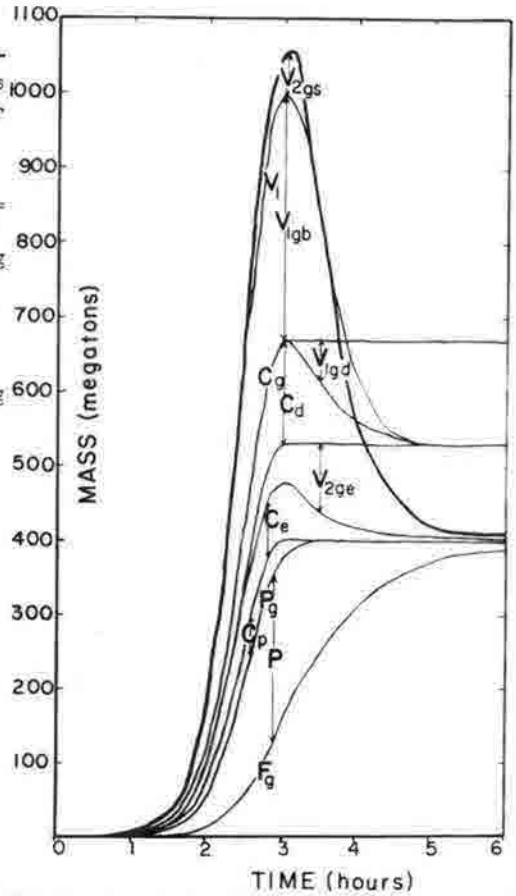

Fig 3. Model results of accumulative values of sources and sinks.

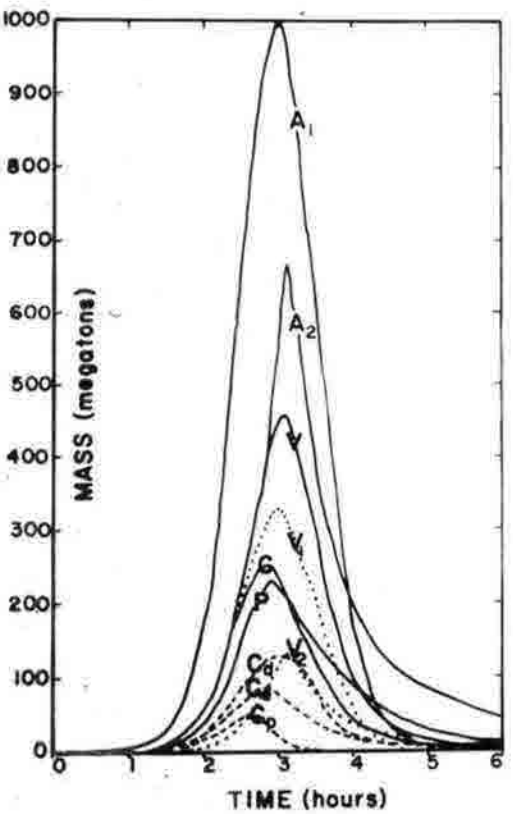

Fig 4. Model results of partitioning into V, C and P and their components.

A NUMERICAL SIMULATION OF THE LIFE HISTORY OF A RAIN SHOWER

by

Harold D. Orville
Institute of Atmospheric Sciences
South Dakota School of Mines and Technology
Rapid City, South Dakota

and

Lansing J. Sloan
University of California
Livermore, California

I. Introduction

The numerical simulation of a localized region of the atmosphere has resulted in the formation of a multi-element cloud that develops into a rain shower. The life history of the shower cloud resembles many of the observations reported in the Thunderstorm Project[1]. A cumulus stage with updrafts predominant, a mature stage with both updrafts and downdrafts, and a dissipation stage with downdrafts predominant are illustrated. The effects of rain drag and surface heating on the shower are seen by comparing results of the model with various effects such as these eliminated in reruns of the model from the time of cloud initiation.

II. General Description of the Model

The first and third equations of motion, the thermodynamic energy equation, and various water mass and air mass conservation equations are integrated numerically. The equations and background information are presented in much previous work.[2,3,4,5,6,8]

The numerical model is 2-dimensional (in the x-z plane) and illustrates the development of clouds above a mountain ridge. The region of integration is 10 km on a side with 100 m grid intervals used in both the x- and z-direction.

The stability of the atmosphere is initially specified in three layers. Potential temperature increases of 1.8 C km^{-1}, 3.5 C km^{-1} and 10 C km^{-1} are specified in the layers 0 to 3 km, 3 to 8 km and 8 to 10 km, respectively. This simulates instability in the lower atmosphere and large stability in the upper two kilometers of the atmosphere. The mixing ratio is initially 10 gm kg^{-1} at the plain surface decreasing by 2 gm kg^{-1} km^{-1}.

Two stream functions are superimposed for the initial airflow. The first stream function models potential flow about a cylinder, the radius of the cylinder equal to the height of the mountain. The second imposes a linearly increasing airflow from 8 km to 10 km. The potential flow about the cylinder at infinity is 1.5 m sec^{-1} while the linear shear flow aloft increases from 0 to 10 m sec^{-1}. This results in speeds of 3 to 4 m sec^{-1} around the mountain ridge decreasing to 1.5 m sec^{-1} in the middle atmosphere and then increasing to 11 m sec^{-1} near the top of the grid.

Whenever a cloud forms, the heating and evaporation at the surface directly beneath the region with finite cloud liquid water contents are decreased exponentially with a time constant of 2 minutes to one half of their original amplitude. After a cloud moves past a grid point, the original amplitudes for heating and evaporation are approached exponentially.

III. Sample Results

Fig. 1 shows three successive printouts of the vertical velocity field and the corresponding rainwater content field. The broad updraft at 153 minutes in the upper part of the cloud (cloud outline is not shown but is given roughly by the zero rainwater content line) is associated with the storage aloft of rainwater into a T-shaped pattern. The updraft narrows and intensifies increasing to 35 m sec^{-1} at 156 minutes. At 159 minutes the updraft maximum has decreased to 25 m sec^{-1}. The rainwater content is now in a tulip-shaped pattern, the appendages of the "T" having fallen into the lower atmosphere. The updraft continues to weaken after its penetration into the "stratosphere." A rain shaft forms, evident at 168 minutes, which results in a shower of approximately 7 mm depth. A downdraft of 10 m sec^{-1} is associated with the rain. More complete discussion of these results are given in Orville and Sloan.[7]

Two reruns from the time of cloud initiation in this model have been completed to test the effects of rainwater drag and continuous surface heating on the rain shower development. The no drag case is not greatly different from the standard. The cloud penetrates 1.5 km further into the stratosphere and at an earlier time (by 3 minutes). The downdrafts to the sides of the updraft maxima are weaker, and the rain shaft are much less than in the drag case. The weaker downdraft results in less rain at the ground ($\sim$4.5 mm), leading to the speculation that there may be an optimum evaporation rate (excludir zero) for the maximum rainfall.

The continuous surface heating case, i.e., no cloud shadow is simulated, leads to completely different results from the standard case. The lower atmosphere becomes unstable. Flow over the ridge becomes strong, advecting all lower clouds and rain off the grid.

IV. Acknowledgements

Mr. Ray Bryant has aided greatly in several programming aspects of the problem. Personnel of the Computing Facility at the National Center for Atmospheric Research, which is sponsored by the National Science Foundation, have been most cooperative in all phases of the computational work.

The work has been supported by the U. S. Department of the Interior, Bureau of Reclamation, Office of Atmospheric Water Resources, under Contract No. 14-06-D-6796 and the Office of Naval Research under Themis Contract No. N00014-68-A-0160.

V. References

1. Byers, H. R. and R. R. Braham, Jr., 1949: The Thunderstorm. Washington, D. C., Gov't Printing Office, 287 pp.

2. Kessler, E., 1969: On the distribution and continuity of water substance in atmospheric circulations. Meteor. Monogr., 10, No. 32, 84 pp.

3. Liu, J. Y., and H. D. Orville, 1969: Numerical modeling of precipitation and cloud shadow effects on mountain-induced cumuli. J. Atmos Sci., 26, 1283-1298.

4. Ogura, Y., and N. A. Phillips, 1962: Scale analysis of deep and shallow convection in the atmosphere. J. Atmos. Sci., 19, 173-179.

5. Orville, H. D., 1965: A numerical study of the initiation of cumulus clouds over mountainous terrain. J. Atmos. Sci.. 22. 684-699.

6. _____, 1968: Ambient wind effects on the initiation of cumulus clouds over mountains. J. Atmos. Sci., 25, 385-403.
7. _____, and L. J. Sloan, 1970: A numerical simulation of the life history of a rain shower. Submitted to J. Atmos. Sci., May 1970.
8. Srivastava, R. C., 1967: A study of the effects of precipitation on cumulus dynamics. J. Atmos. Sci., 24, 36-45.

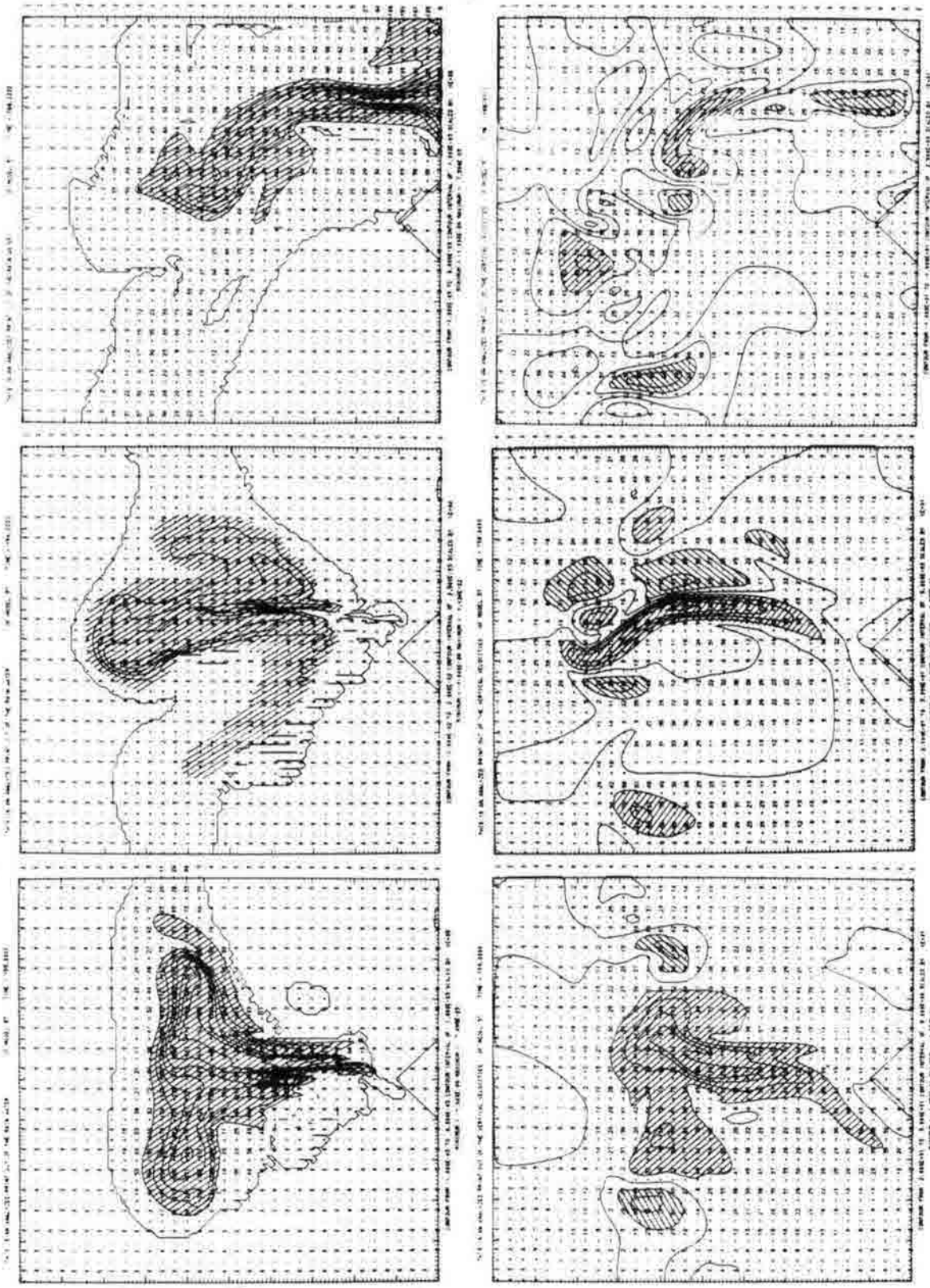

Fig. 1. Computer printouts on bottom and top are of vertical velocity and rainwater content, respectively. Real time is given above frames. Rainwater contents greater than 1 gm kg^{-1} and vertical velocities greater than 5 m sec^{-1} (absolute values) are shaded (left slanting depicts updrafts, right slanting downdrafts).

SOME RESULTS OF MICROWAVE MESOSCALE STUDYING OF ATMOSPHERIC WATER

A. E. Bashatinov, A.S. Gurvich, B.I. Kutusa, L.M. Mitnik
Institute of Radiotechnics and Electronics Academy Science
Moscow, U.S.S.R.

The method of microwave satellite observations, connected with the studying of atmospheric humidity and clouds have been considered in the paper.

The characteristics of humidity and clouds from data of the microwave experiment on "Cosmos 243" in September 1968 are given.

The latitudinal variations of humidity and clouds and correlation characteristics of the humidity and water contents with the variations of meteorological parameters have been discussed.

This page left blank intentionally.

COMPUTER AND OBSERVATIONAL STUDY OF DIFFERENTIAL EFFECTS OF LAKE MICHIGAN UPON VARIOUS SIZES OF SUMMER CONVECTIVE SYSTEMS

Walter A. Lyons
Department of Geography, and Center for Great Lakes Studies
University of Wisconsin--Milwaukee

INTRODUCTION

The Great Lakes often markedly suppress warm season convection, especially in spring when air flowing over the cold lake may be as much as 30°C warmer than the water. Yet there is no immediately apparent explanation as to why certain convective systems are totally dissipated or absent on one day and then seem totally oblivious to the lake on another[1]. It has been found that the answer must consider both (a) the type of convective systems (cumulus, "air mass" thundershower, squall line, frontal showers, etc.), and (b) the detailed mesosynoptic conditions induced by the cold lake water.

MESOSCALE REGIMES AND OBSERVED CLOUD PATTERNS OVER LAKE MICHIGAN IN SUMMER

On about half of all summer days, gradient winds flow relatively undisturbed from shore to shore. During the day, air, superadiabatically stratified within about 100 m of the surface, advects off the upwind shore and rapidly loses heat by conductive cooling. Wiresonde observations and calculations have shown that while intense inversions form after just several kilometers fetch, the cooling effect rarely extends above the 100 m level[2]. The air in the sub-cloud layer above the shallow cold dome, while not cooled by the lake, ceases to heat after passing offshore. The result is a lake mesohigh of some 2 or 3 mb. Pibal observations indicate a small mean divergence of 3×10^{-5} sec^{-1} producing a weak subsidence of 3 cm sec^{-1} at 1500 m. Thus cloud suppression is more likely thermal than dynamic in nature.

On the remaining summer days, a lake breeze circulation cell is found on the west and/or east shores. An inflow layer, typically 500 m deep, has a narrow (2 km) convergence zone at its leading edge with vertical motions often exceeding 100 cm sec^{-1} [3]. Complex moisture and thermal fields develop. There is a broad area of subsidence offshore where dry air from aloft sinks down close to the surface. One finds multiple inversions over water due to heat conduction and subsidence. Typical mean divergence values run $15 \times 10^{-5} sec^{-1}$, associated with a subsidence of 8 cm sec^{-1} at 1500 m[4].

During periods of gradient flow, advecting cumulus and "air mass" thundershowers dissipate a short distance offshore and almost never form over the lake. Yet sometimes thunderstorms associated with middle level phenomena (short wave troughs, etc.) and organized squall lines appear to survive and/or form over the water. Clouds respond to lake breezes in a complicated manner dependent on the direction of the large scale flow. With zero gradient winds, time lapse photographs show cumulus above the surface convergence zone small and short lived. If the flow is normal to the shore, clouds form inland, advect over the surface convergence zone, grow momentarily, and then collapse rapidly as they move toward the lake. In one case, a mature squall line intersected a well organized lake breeze on the western shore and totally dissipated within a distance of 30 to 40 km[5].

A THERMODYNAMIC DIAGNOSTIC PROGRAM

Thermodynamic diagrams are used operationally to assess an air mass's potential for convection. If adequate temperature and dewpoint data exist, such techniques should be applicable to mesoscale variations in convective potential. A computerized Stüve diagram was developed having data inputs at 25 levels from the surface to 400 mb, analyzing up to 58 soundings in any geometric pattern. The program accounts for the variations in atmospheric moisture content when calculating the various parcel lapse rates. Initial outputs include such environmental parameters as potential and virtual temperature, relative humidity, mixing ratio, hydrostatic pressure, and density. The Showalter and lifted indices are then evaluated at each point. Also the 500 mb buoyancy of parcels originating at any selected level of interest can be found as well as the level containing the potentially most unstable air (the best lifted level). For each sounding, the LCL, LFC, adiabatic liquid water content, cloud buoyancy (in virtual temperature), and potential parcel vertical motion are also found.

Data representative of a day when moist, southwesterly gradient flow covered the lake were run. Neither the Showalter nor lifted index were significantly affected by the cold, shallow surface layer (Fig. 1a). However, the 500 mb buoyancy of a parcel originating at the 23 m level was drastically reduced. As Fig. 2 reveals, potential parcel vertical motions corresponding to the lifted index (a good indicator for large convective storms drawing in air from a deep layer) were barely affected, whereas extreme forced lifting would be necessary to raise a parcel from near the lake surface. On this day, cumulus and small "air mass" thundershowers (presumably with their updraft roots at very low levels) neither formed over water nor survived advection offshore. By contrast, range normalized radar data indicated little or no weakening of a large squall line crossing the lake during the late afternoon of the same day. Lake breeze input data on a zero gradient wind day were obtained by an NCAR Queen Air (Figs. 3 and 4a). Figure 4b shows calculated buoyancies for parcels originating at the 45 m level. The observed short lifetimes of these cumulus are felt to be due to the fact they were colder than their environment, being maintained by a region of forced convection above the lake breeze front. The program (which assumes all parcels rise vertically) does not appear to confirm this (Fig. 4b). However, tetroon studies on this day showed the air in these clouds began ascending near the shoreline. Thus they would have indeed been colder than their environment. For the case of a large squall line hitting the lake breeze cell, the program indicated the thunderstorms were destroyed due to the injection of dry air present over the lake after many hours of continuous subsidence offshore. In that case (not shown) maximum parcel updrafts over land were calculated as 44 m sec^{-1}, whereas a -25 m sec^{-1} value was found over the lake for a lifted index computation.

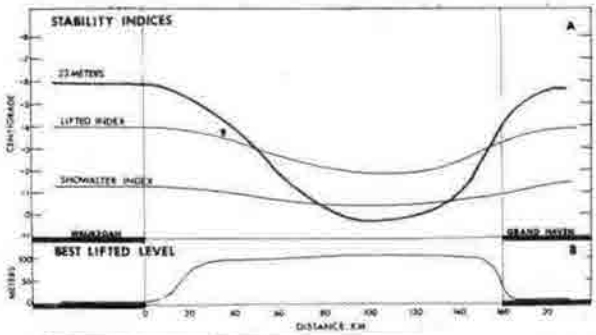

Fig. 1--(a) Various 500 mb parcel buoyancies computed along a northeast-southwest cross section through the southern basin of Lake Michigan, 1400 CST, 26 July 1966. Data in the lowest 100 m were calculated from a modified form of the heat conduction equation. From 100 to 2000 m, after air left shore, it was assumed no further heating occurred, and $D\theta/Dt = 0$ (θ is the equivalent potential temperature). Corrections were assumed for adiabatic warming due to slight subsidence. (b) The level of the most unstable layer of air rose from the surface over land to only 100 meters over water.

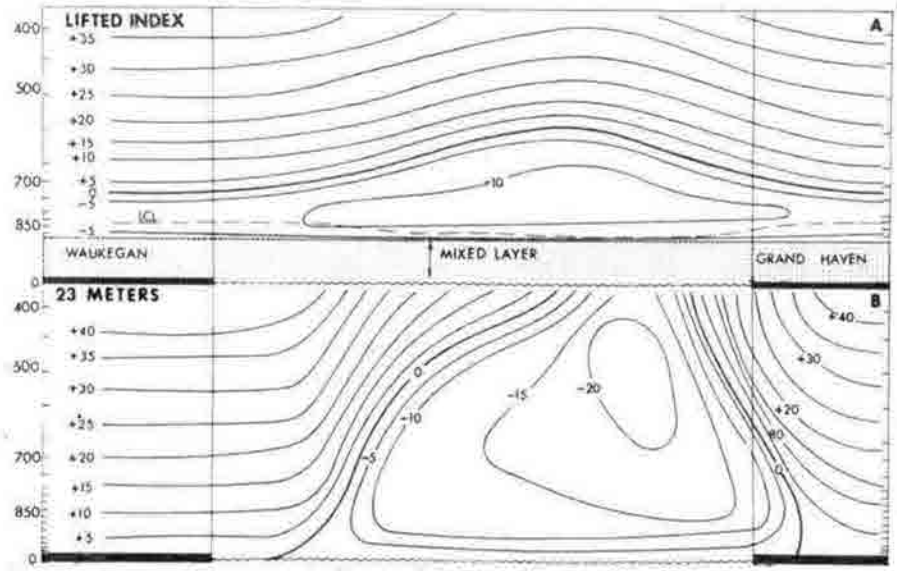

Fig. 2--The maximum vertical motions obtainable by release of instability. Input data are the same as in Fig. 1. Updrafts in meters per second. Liquid water drag not accounted for. (a) Updrafts resulting from parcels with a mean potential temperature and mixing ratio of the lowest 1000 meters, appropriate to squall line thunderstorms with a mesocold front injecting a deep layer of air into cells. (b) Integrated vertical motions for parcels originating at 23 m, within the superadiabatic layer over land and the onduction inversion over water.

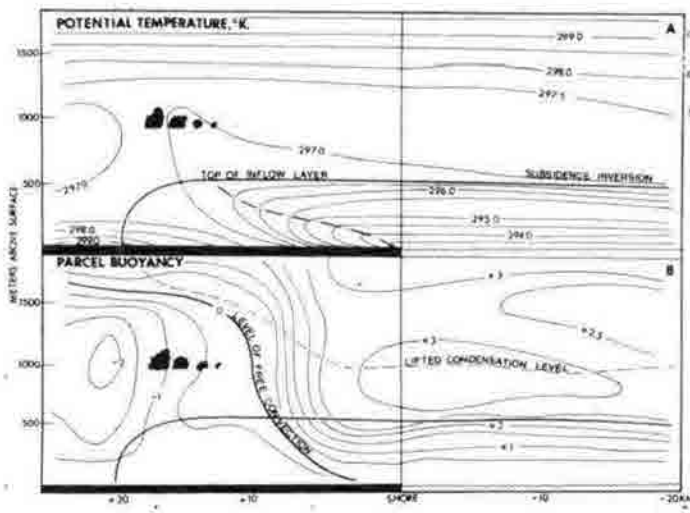

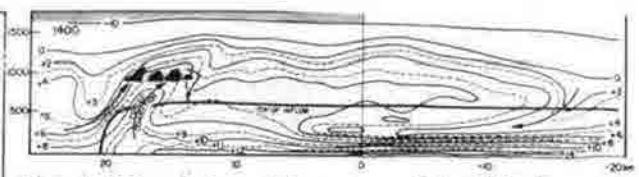

Fig. 3 (above) Dewpoints measured by NCAR Queen Air in east-west section through lake breeze in Chicago, 1400 CST, 13 August 1967. The boundary of the onshore wind flow marked by heavy line. Observed cumulus clouds indicated.

Fig. 4--(a) Potential temperatures derived from Queen Air data (see Fig. 3). (b) Buoyancy for parcels leaving the 45 m level. Here positive numbers indicate thermals colder than environment.

REFERENCES

(1) Stout, G.E. and K.E. Wilk, 1962: Influences of Lake Michigan upon Squall Line Rainfall, Proc. 5th Conf. Great Lakes Res., University of Michigan, 111-115.

(2) Lyons, W.A., 1970a: Numerical Simulation of Great Lakes Summertime Conduction Inversions, Proc. 13th Conf. Great Lakes Res., Intl. Assoc. Great Lakes Res., (in press).

(3) Olsson, L.E. and W.A. Lyons, 1969: Air Pollution Dispersion in a Lake Breeze Regime; Trajectory Study Using Tetroons, Smoke Photography, and Aircraft Measurements of Aerosols, presented at Annual Meeting, Air Pollution Control Association, New York, paper 69-29.

(4) Lyons, W.A., 1970b: Mesoscale Regimes over the Southern Basin of Lake Michigan and Their Effect upon Summertime Convective Clouds, Ph.D. dissertation, Department of the Geophysical Sciences, the University of Chicago, 255 pp.

(5) Lyons, W.A., 1966: Some Effects of Lake Michigan upon Squall Lines and Summertime Convection, Proc. 9th Conf. Great Lakes Res., University of Michigan, 259-273.

AUTHOR INDEX